A Computational Analysis of the Platinum-Water-Vacuum Interface

Dissertation
zur Erlangung des Doktorgrades
des Fachbereichs Chemie
der Universität Hamburg

vorgelegt von

Timm Lankau
aus Hamburg

Hamburg 2000

Gutachter
Prof. Dr. K. Nagorny, Hamburg
Dr. I. L. Cooper, Newcastle
P.D. Dr. K. Dräger, Hamburg

Tag der letzten mündlichen Prüfung: 14. Dezember 2000

To my mother

> Die Quanten sind doch eine hoffnungslose Schweinerei.
>
> Max Born to Albert Einstein

Abstract

The simple bilayer model of the platinum-water-vacuum interface can explain most experimental results, but fails on details. Our work suggests that cooperative effects are very important for the fine-structure of the interface. The platinum-water (chapter 6) and the hydrogen bond (chapter 3) have been found to be very much alike. Intermolecular electron transfer as observed in the water trimer has a strong influence of the interface structure and can move the water molecules out of their ideal positions (chapter 8).

Our new water-water interaction potential (chapter 4) has been used to explore the potential energy surfaces of the water trimer (chapter 4) and hexamer (chapter 8). The results on the hexamer suggest that a seamless transition between the platinum surface and the ice crystal is not possible. Structures similar to the QLL (**Q**uasi **L**iquid **L**ayer) have been observed, which can explain the low vertical dipole moment of surface water, while cooperative forces can be used to explain the second desorption peak (165 K) in TDS (**T**hermal **D**esorption **S**pectroscopy) experiments.

The weak bond between water and platinum is controlled by two opposing forces: the Coulomb repulsion between the 6s electrons of the platinum cluster and the oxygen atom and the bonding interaction between a platinum 5d orbital and the free electron pair of the water molecule. A high 6s population, which repells the water molecule, creates at the same time a strong bond among the platinum atoms. It is therefore impossible to create a surface model with strong intermetallic bonds and a strong platinum-water bond at the same time.

The quality of the surface model depends strongly on the 6s population and so on the electronic state of the metal cluster. The analysis of the platinum-water bond would have been impossible without a modification of the Hückel theory (chapter 5), which was used to select suitable candidates as surface models and to understand the electronic structure of the platinum cluster and electron movements during the formation of the platinum-water bond.

The intermetallic bond in the platinum cluster is dominated by the 6s orbitals and the 5d orbitals have to be considered in full detail only at active surface atoms. This assumption was finally proofed by the development of a new 1 valence electron ECP (**E**ffective **C**ore **P**otential) for bulk and passive surface atoms (chapter 7), which can be used to reduce the computational costs for the analysis of larger platinum clusters.

Zusammenfassung

Ein einfaches Doppelschicht-Modell für das Grenzsystem Platin-Wasser kann die meisten experimentellen Ergebnisse erklären, versagt aber bei der Interpretation von Details. In dieser Arbeit werden wir nachweisen, daß cooperative Effekte sehr wichtig für die Feinstruktur der Grenzschicht sind. Die Platin-Wasser Bindung und die Wasserstoffbrückenbindung sind einander sehr ähnlich (Kapitel 6) und intermolekularer Ladungstransfer, wie er auch im Wassertrimer beobachtet wird, kann einzelne Wassermoleküle aus ihrer idealen Position bringen (Kapitel 8).

Unser neues Wasser-Wasser-Wechselwirkungspotential (Kapitel 4) wurde benutzt, um die Energiehyperfläche des Wassertrimers (Kapitel 4) und des Wasserhexamers (Kapitel 8) zu untersuchen. Die Ergebnisse für das Hexamer lassen vermuten, das ein nahtloser Übergang zwischen der Platinoberfläche und einem Eiskristall wie bisher angenommen nicht möglich ist. Strukturen, ähnlich einer zweidimensionalen Schicht flüssigen Wassers auf Eis (engl. QLL, **Q**uasi **L**iquid **L**ayer), wurden an der Grenze zwischen Metall und Eis beobachtet. Solch ein Strukturmodell erklärt den kleinen Anteil des Dipolmoments eines Wassermoleküls in der Grenzschicht senkrecht zur Metalloberfläche, während die oben erwähnten cooperativen Kräfte erstmals eine Deutung für den zweiten Desorptionspeak (165 K) in TDS Experimenten (**T**hermal **D**esorption **S**pectroscopy) bieten.

Die schwache Bindung zwischen Platin und Wasser kann mit zwei einander widersprechenden Kräften erklärt werden: Die Coulomb-Abstoßung zwischen den 6s Elektronen des Platins und dem negativ geladenem Sauerstoff im Wassermolekül ist die erste Kraft und die zweite bindende folgt aus dem Überlappen eines freien Elektronenpaars des Wassermoleküls mit einem Platin 5d Orbital. Eine hohe 6s Besetzungsdichte, die das Wassermolekül abstößt, ezeugt aber gleichzeitig eine starke Platin-Platin Bindung. Es gibt entweder eine starke Platin-Platin Bindung im Metallcluster oder eine starke Metall-Wasser Bindung, aber nie beides gleichzeitig.

Die 6s Elektronendichte erwies sich als Schlüssel zu einem realitätsnahen Oberflächenmodell. Eine Modifikation der Hückel-Theorie (Kapitel 5) half uns, die elektronische Struktur des Platinclusters und die Bewegung der Elektronen während der Wasseradsorption zu verstehen. So war es uns möglich, gezielt nach geeigneten Kandidaten für die Oberflächenmodellen zu suchen.

Die Metall-Metall Bindung im Platincluster wird von den 6s Orbitalen dominiert, während die 5d Orbitale nur wichtig sind für die Bindung des Wassermoleküls an ein aktives Oberflächenatom. Diese Annahme führte zu der Entwicklung eines funktionierenden 1 Valenzelektronen ECP (**E**ffective **C**ore **P**otential), daß in Zukunft die Untersuchung großer Oberflächenmodelle ermöglichen wird.

Contents

List of Figures

List of Tables

Chapter 1

Introduction

1.1 General Introduction

Water is probably one of the most common and best analysed chemical substances on this planet. The oceans, which cover 70.8% of the planet's surface, store 97.3% of all water ($1.385 \cdot 10^9$ km^3). Platinum on the other hand is very rare (0.01 ppm [1]). This work so focuses on the interaction between the common and the noble.

Platinum is a very important catalysist. The first reaction studied in detail, which served for the definition of a catalysis, was the hydrogen combustion ($2\ H_2 + O_2 \rightarrow 2\ H_2O$) [2–5]. A stoichometric mixture of hydrogen and oxygen does not react until a small dose of platinum powder is added. Then, the mixture reacts vividly and an explosion can be observed. The platinum dust lowered the barrier of activation effectively for the reaction to start.

Today, one of the most important applications of platinum is the purification of exhaust fumes from motor vehicles [6]. Platimum catalysis the oxidation of carbon monoxid and hydrocarbons to carbon dioxide, but more important is the reduction of nitrogen oxides.

$$2\,\mathrm{CO} \;+\; 2\,\mathrm{NO} \;\longrightarrow\; \mathrm{N_2} \;+\; 2\,\mathrm{CO_2}$$

Water is next to carbon dioxide the most important product of the combustion and large amounts of water are also at the surface of the platinum catalysist.

$$\mathrm{C_xH_{2x+2}} \;+\; \frac{3\mathrm{x}+1}{2}\,\mathrm{O_2} \;\longrightarrow\; \mathrm{x\,CO_2} \;+\; (\mathrm{x}+1)\,\mathrm{H_2O}$$

These water molecules compete with the other oxides in the exhaust fumes for active surface sites on the catalyst and have so a major impact on the quality of the cleaning process. Electrochemical experiments showed, that the rate of the O_2 reduction and H_2 ionisation reaction on platinum electrodes depends stongly on the orientation of the water molecules [7].

Regarding the economical and environmental importance of the platinum-water interaction it is not surprising, that the work on this topic started early and first results have been published by General Motors [8].

Theoretical work as published within this thesis will help us to understand the interaction between platinum and water better, which will hopefully end in the development of better catalysists in the future. Computational chemistry can help so to fight air polution in the long term.

1.1.1 Properties of Water

Bernal and Fowler showed, that the structure of an individual water molecule does not change much with the phase of the substance [9]. The free water molecule has C_{2v} symmetry and the structure of the molecule can be explained well with the VSEPR model (**V**alence **S**hell **E**lectron **P**air **R**epulsion) [10–12]. The oxygen atom (sp^3 hybridisation) has a tetrahedral environment: Two sp^3 hybrid orbitals form the bonds to the hydrogen atoms (r_{OH}) while the remaining two hybrid orbitals from the lone electron pairs. The lone electron pairs, needing slightly more space than the chemical bonds, force the hydrogen atoms closer to eachother and the bond angle ω is therefore smaller than that found in an ideal tetrahedreon (109.47°).

property	value		ref.
M	18.0151	g/mol	[1]
r_{OH}	0.9572	Å	[16]
ω	104.52	deg	[16]
μ	1.85	D	[17]
I_X	2.9376	$10^{-40} g^{-1} cm^{-2}$	[16]
I_Y	1.0220	$10^{-40} g^{-1} cm^{-2}$	[16]
I_Z	1.9187	$10^{-40} g^{-1} cm^{-2}$	[16]
α	1.45	$Å^3$	[15]
E_{ION}	11.53	eV	[15]
E_{AFF}	1.07	eV	[15]
ΔE_{HO-H}	498	kcal/mol	[15]
ΔE_{O-H}	427.5	kcal/mol	[15]
T_F	0.0	°C	[1]
T_B	100.0	°C	[1]

Table 1.1: Properties of water.

Water is a chemical substance with extraordinary physical properties (table 1.1). The boiling (T_B) and the freezing point (T_F) are much higher than the values for the other hydrogen chalcogenids (eg H_2S: -85.6 °C and -60.3 °C). The high transition temperatures are caused by strong hydrogen bonds among the water molecules [13]. Different electronegativities for oxygen (3.5) and hydrogen (2.1) cause polar oxygen-hydrogen bonds and so create a large dipole moment (μ). Coulomb forces can be used for a first attemp to explain the strong hydrogen bond between a positively charged hydrogen atom and a lone electron pair on the oxygen, but quantum chemistry provides far better methods (chapter 3, page 45).

The covalent hydrogen bonds [14] can form a rigid, tetrahedral network and so the basis of ice. This network keeps the water molecules further apart than in the liquid phase, where thermic motions allow the water molecules to collide and form so distorted micro cluster. The density of the low pressure ice phases Ih and Ic (table 1.2) is therefore smaller than the density of the liquid ($\rho = 0.99978$ g cm^{-3} at the triple point [15]). The structure of these two ice phases can be explained well with a set of rules originally developed by Bernal, Fowler and Pauling (BFP rules or ice rules) [9, 13]:

- The water molecule in ice resembles the water molecule in the gas phase.
- Each water molecule is oriented so that its two hydrogen atoms are directed approximately toward two of the four oxygen atoms which surround it tetrahedrally, forming hydrogen bonds.
- Only one hydrogen atom is positioned between each neighbouring oxygen-oxygen pair.
- Under ordinary conditions the interaction of non-adjacent molecules is not such as to stabilize appreciably any one of the many configurations satisfying the preceding conditions with reference to the others.

The hexagonal ice Ih is the 'normal' ice. Figure 1.1 shows the structure of the ice crystal. Only the oxygens of the water molecules are drawn and different grey shades in figure 1.1 mark differnt layers of water molecules in the crystal. The structure of ice Ih can be visilized by the condensation of water hexamers. These water hexamer are rings in the chair conformation. One hexamer is marked light grey as an example in the centre of the figure.

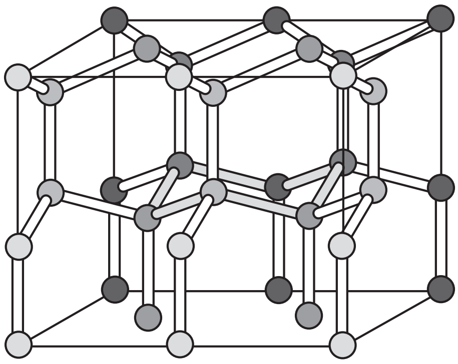

Figure 1.1: Structure of ice 1h. [18]

PAULING suggested 1935, that next to the hexagonal ice phase (ice Ih) with another ice phase with a cubic crystal system (ice Ic) should be possible [13]. Ice Ic can created by the condensation of water vapors between −120° C and −140° C [1]. Table 1.2 shows a compilation of the strctural characteristics of both low pressure ice phases.

In both ice phases Ic and Ih are the positions of the hydrogens disordered. The hydrogen is attached to either water molecule sharing a hydrogen bond. The bonds among the water molecules oscilate therefore between hydrogen bonding and covalency, depending on the distance of the hydrogen from the oxygen atom[1]. If the ice crystal is cooled to very low temperatures, the movement of the hydrogens freezes and the hydrogens stay in random positions.

ice phase	Ih	Ic
crystal system	hexagonal	cubic
space group	P63/mmc	Fd3m
cell dimensions^a [pm]	a=450 c=732	a=635
molecules per unit cell	4	8
nearest neighbours	4	4
distance to the next neighbour [pm]	275	275
O−O−O angle [deg]	109.3, 109.6	109.6
hydrogen position	disordered	disordered
Density^a [g cm^{-3}]	0.93	0.94

^{a} 110 K, athmospheric pressure

Table 1.2: Properties of ice. [18]

Proton ordered ice phases are possible and still subject of current research [19, 20]. A complete ordering of protons can be used to align the dipole moments of the water molecules parallel to eachother (ferroelectricity) [1, 21]. Ferroelectric ice phases show a spontaneous polarisation and strong electric fields can be observed between opposite sides of the ice crystal.

One of the many ways to obtain ferroelectric ice is the epitaxial growth on Pt(111) [20, 22]. The platinum surface is belived to order the protons in the first layer of water. Careful condensation of

---

[1] Proton transfer similar to the GROTTHUS mechanism [23, 24] is impossible in ice between 30 to 190 K [25]. The potential, in which the proton moves, is not periodic, since the proton structure in ice is disordered, and long distance proton tunneling for the GROTTHUS mechanism demands a perodic potential. Proton transfer in ice is the movement of a D defect (two hydrogen atoms are on one oxygen-oxygen bond) in the crystal.

additional water layers should then continue to grow with orientated hydrogens until a metastable, ferroelectric bulk ice phase has been reached. Witek and Buch showed, that only the first bilayer gowths with orientated hydrogens and that the protons in the second layer are not orientated to minimize the electrostatic energy [26] and break so the standard rules for hydrogen bonds [27].

1.1.2 Properties of Platinum

Three countries cover 98% of the worlds demand for platinum metals (South Africa 45%, former UdSSR 45%, Canada 8%). Only the Merensky-Mine in South Africa (South Africa covers 65% of the worlds platinum demand.) is exploited for platinum solely, in every other case is the platinum refined from impurities of other ores [1].

property	value
number	78
isotopes	6
mass	195.08 g/mol
configuration	[Xe] $4f^{14}5d^{9}6s^{1}$
electronegativity	2.2
$d_{\mathrm{Pt-Pt}}$	2.77 Å
T_F	1769 °C
T_B	4170 °C
E_{ION}	9.0 eV

Table 1.3: Properties of platinum [1].

Platinum is a silver white, ductile metal with a cubic closed structure and can be dissolved easily in aqua regia and slowly in hydrochloric acid in the presence of air.

$$\mathrm{PtCl_4^{2-}} + 2\mathrm{e} \rightarrow \mathrm{Pt} + 4\,\mathrm{Cl^-} \qquad E^0 = 0.75\,\mathrm{V}$$

$$\mathrm{PtCl_6^{2-}} + 2\mathrm{e} \rightarrow \mathrm{PtCl_4^{2-}} + 2\,\mathrm{Cl^-} \qquad E^0 = 0.77\,\mathrm{V}$$

Platinum dissolves also readily in fused alkali oxides and specially in alkali peroxides. It is also attacked by fluorine and chlorine at red heat and reacts also with elemetal P, Si, Pb, As, Sb, S and Se under reducing conditions.

Pt(0) compounds are well known and the synthesis of many cluster compounds with direct platinum-platinum bonds starts from $\mathrm{Pt(PPh_3)_4}$ [28]. Huge amounts of molecular hydrogen can be solved in platinum and the metal activates the hydrogen-hydrogen bond, which explains its catalytic activity in hydrogenation reactions.

Platinum is chemically much more reactive than commonly asumed: More than 70 oxidation-reduction reactions are catalyzed by platinum and it is now possible to predict catalytic activities from the thermochemical properties of the reacting couples [29].

1.1.3 Literature Survey

The platinum-water interface has been examined with various experimental techniques ranging from UHV (**U**ltra **H**igh **V**acuum) to electrochemical experiments. Both experiments differ principally in the number of water molecules. But, it is possible to vary the electric field at the surface systematically in electrochemical experiments and not in UHV experiments. The electric field at the surface is varied in UHV experiments by the coadsorption of polar or ionic species, which makes the fine tuning of the field strength difficult. On the other hand, UHV experiments give informations on the microscospic scale, whereas electrochemical experiments give integral values for the double layer [30]. Various structure models have been proposed for the electrochemical bilayer to explain the value of the differential capacity as a function of the excess charge, but the number of experimental parameters adjusted to reproduce experimental data quaestions the validity of the model [24, 30–33].

Weaver et al. exploited the similarity of both experimental methods for the analysis of the platinum-carbon monoxide interface and tried to model the electrochemical interface by UHV

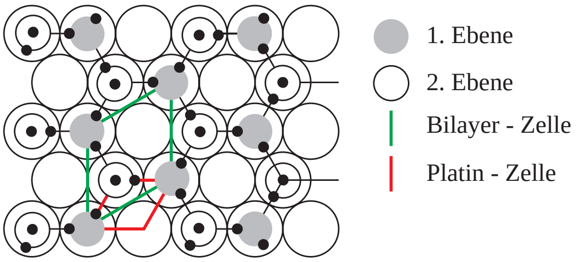

Figure 1.2: Ideal bilayer structure.

means ("UHV electrochemical modeling") [34, 35]. They showed, that both methods complete eachother very well.

Early UHV experiments [36, 37] on the adsorption of water on platinum(111) reported a p($\sqrt{3} \times \sqrt{3}$) R30° surface structure of adsorbed water molecules and suggested the formation of ice ordered in domains of $30 - 40$ Å in lenght.

A water bilayer structure [38, 39] (figure 1.2) has been proposed as the basis of the growth of ice on hexagonal metal latices. The ice phase on platinum is believed to have the same hexagonal symmetry as the surface and the water hexamer marked in figure 1.1 forms the basis of the bilayer structure [40]. The structure of this water bilayers is generally explained in terms of an extension to surfaces [39] of the Bernal-Fowler-Pauling rules (ice rules) [9, 13]. Specifically [39], each water molecule is assumed bound by at least two bonds (which may be hydrogen bonds to other water molecules or oxygen lone pair bonds to the surface) while maintaining a tetrahedral bonding configuration. The water is assumed bound to the surface via one lone pair orbital on the oxygen and all free lone pair orbitals on oxygen stay nearly perpendicular to the surface. In an ideal infinite bilayer, all water molecules have their dipole moments pointing away from the surface ("flip up"), whereas in a finite cluster, water molecules whose dipole moments point toward the surface ("flip down") may occur at the edge of the cluster [39, 41, 42]. Experimental results [43] suggest that the edges of ice-like clusters on Pt(111) are constructed from flip up molecules together with water molecules with one OH bond parallel to the metal surface, in contrast to the flop down geometry predicted at the edges by the BFP rules. Such a water species has been observed on Pt(100) [44] and experimental evidence suggests that such a species may also exist on Pt(111) [45, 46]. It has not been possible to rule out such a structure by application of ultraviolet photoelectron spectroscopy (UPS) to Pt[6(111)×(100)] [37].

Doering and Madey [39] concluded using the surface extended ice rule set, that the smallest stable water cluster on a hexagonal metal surface should be the water nonamer. Such an $(H_2O)_9$ cluster has been observed on Ru(0001) as part of p($6\sqrt{3} \times 6\sqrt{3}$) R0° superstructure [39, 47], whereas experimental results suggest, that the smallest cluster possible on platinum(111) is a three-dimensional water trimer [45].

In the initial stages of growth, a water molecule has two possible adsorption sites: attached either directly above a platinum on the surface or to a water molecule already bound to the surface [46, 48]. The coexistence of both species (i.e. a water molecule directly bound to the surface and a water molecule attached to another water molecule) is commonly explained in terms of the energy of isolated bonds, although the importance of cooperative forces has been suggested previously [42, 45, 49]. The strength of the platinum-water bond corresponds to that of two to three hydrogen bonds, so either type of bonding is possible.

TDS spectra (**T**hermal **D**esorption **S**pectroscopy) [38, 43, 46, 48, 50–56] of water from the platinum(111) surface allow us to distinguish different water species, but the discussion remains controversial. The most recent data from OGASAWARA et al. [56] shows three prominent peaks at 155 K, 165 K and 200 K. The first peak (at 155 K) was assigned to ice sublimation, the second (at 165 K) to water in the second adsorption layer and the third (at 200 K) to water directly bound to the surface. While the first two peaks have been positively identified, the origin of the third remains a matter of discussion [53, 54]. The formation of the second peak at 165 K can be observed at coverages as low as 0.13 to 0.27 monolayer (ML), where 1 ML refers to one ideal bilayer [39]. These TDS results are consistent with other experimental results [43, 45, 46, 48, 57, 58], which also support the formation of water clusters at low surface coverage.

The second peak[2] (165 K) is the multilayer peak in the TDS spectrum. A water molecule from the top should therefore be in a chemical environment similar to an ice Ih crystal. Differences in the desorption temperature have to be therefore the result of the lattice distortion of the ice crystal, because this molecule has no direct contact with the metal underneath. A measure for this distortion is the lattice-mismatch (ltm) (table 1.4). A negative value indicates the contraction of the ice lattice and a positive its expansion. The highest desorption temperature should therefore be found for the metal with the smallest value for the lattice-mismatch (copper), but was found for ruthenium. This shift of the maximum peak position and the higher bonding energy compared with ice sublimation suggest, that the simple bilayer model from DOERING and MADEY may need further refinement [42, 59].

surface	ltm [Å]	T [K]
Ni(111)	+0.19	170
Cu(111)	+0.08	150
Rh(111)	−0.16	190
Ru(0001)	−0.19	212 - 220
Re(0001)	−0.28	180
Pt(111)	−0.30	170
Ag(111)	−0.50	150

Table 1.4: Multilayer Peaks data from refs. [38, 47]

The theoretical work published on the metal-water interface can be seperated into two main groups: The first group focuses on electrochemical aspects of the subject. Molecular mechanics (MC) and molecular dynamics (MD) calculations are used to model the platinum-electrolyte interface. The second approach concentrates more the UHV aspects. Quantum chemical calculations on various level of theory examine the interaction of one water molecule with a metal cluster [54, 60–72].

Both quantum chemistry and experiment agree that the water molecule is only slightly disturbed upon adsorption on Pt(111) [41, 45, 46, 48, 58, 73–75] and dissociation has so far only been observed experimentally on pre-covered surfaces [76–79], which allows us to use rigid water geometries within the computational simulations.

First quantum chemical results have been publihed by HOLLOWAY and BENNEMANN using the EHT (**E**xtended **H**ückel **T**heorie) for the calculation (1980, [64]). They used a Pt_5 pyramid to model the surface and reported a bonding energy of 0.5 eV with the water molecule in an on-top position with a platinum-oxygen distance of 2.3 Å. These calculations served as the basis for the development for classical platinum-water interaction potential used for MD calculations.

Eight years later ESTIU et al. [65] reported a new set of EHT calculations with a differnt set of Hückel parameters and larger metal clusters (Pt_{18}, Pt_{19} and Pt_{25}). The platinum-water distance

---

[2] The precise value of the desorption temperature depends slightly on the experimental conditions (heating rate, coverage), which explains the difference of 5K between OGASAWARA [56] and HOFFMAN [47].

was fixed at 1.7 Å as a result of earlier calculations (bonding energy = 0.94 eV [60]). They reported bonding energies of 0.42 eV for the Pt(111) surface and 0.57 eV for Pt(100). In both cases was the water molecule in an on-top position with its molecular plane perpendicular to the surface.

MÜLLER et al. used the KOHN-SHAM sheme with a local density approximation [70] to perform cluster calculations ($Pt_{10}-H_2O$) on the adsorption of water on Pt(111) [54, 63, 68]. This group reported a bonding energy of 0.53 eV with a platinum-oxygen distance of 2.5 Å. MÜLLER proposed also a quantum chemical model for the platinum-water bond [68] basing on his work on the aluminium-water interaction [70], which was later used by RIBARSKY et al. for the copper-water bond [71]: The $3a_1$ and the $1b_1$ orbitals, which do not contribute much to the bonds within the water molecule, interact with filled platinum 5d orbitals. The low lying LUMO interacts then with both filled orbitals resulting from the platinum-water overlap and lowers so the total energy. The occupation of the former empty LUMO leads to an charge transfer from the water molecule to the metal cluster. This interaction model is the quantum chemical equivalent to the electrostatic polarisation and the authors therefore call the LUMO a polarisation function. They give the following equation for the polarisation energy ΔE

$$\Delta E = \frac{\langle\, POL \,|\, \hat{V} \,|\, L \,\rangle^2}{\epsilon_{POL} - \epsilon_L} \tag{1.1}$$

$|\, POL \,\rangle$ is the LUMO, which acts as a polarisation function, and $|\, L \,\rangle$ the free electron pair of the water molecule. Two principal features of the platinum-water bond follow from equation 1.1, which are not mentioned in reference 68:

1. The binding energy of the water molecule depends on its orientation relative to $|\, POL \,\rangle$, since ΔE is proportional to the square of the overlap between the platinum 5d orbitals and the free electron pair of the water molecule $\langle\, POL \,|\, \hat{V} \,|\, L \,\rangle$.
2. ΔE is inversely proportional to the energy difference between both orbitals. The larger the cluster becomes, the smaller becomes the HOMO-LUMO gap and so the energy difference between $|\, POL \,\rangle$ and L , because ϵ_L is independent of the cluster size.

The importance of polarisation for the platinum-water bond suggests, that cooperative forces are important for the structure and energy of the platinum-water interface. The significance of hydrogen bonding and polarisation effects has been discussed previously [45, 56, 64, 68, 71, 75], but, to our knowledge, has not been studied in great detail. KUTNETSOV et al. published 1989 CNDO/2 (**C**omplete **N**eglect of **D**ifferential **O**verlap) for water clusters bonded to 1b (Cu, Ag, Au) and 2b group (Zn, Cd, Hg) elements [67].

Modern quantum chemical calculations on the platinum-water interface suggest that the molecular plane of the water molecule lies parallel to the surface [54, 63, 68]. These results agree with workfunction measurements [45, 52, 58, 73] on water-covered platinum surfaces, which show that that a contribution of about 0.2 D of the water dipole moment (free water molecule 1.84 D) is normal to surface [58], but contradict the ice rules for surfaces, which explain very well other UHV data like the LEED (**L**ow **E**nergy **E**lectron **D**iffraction) results. The orientation of the hydrogens in water molecule with a direct bond to the metal surface underneath should therefore be regarded as unsetteled.

The number of atoms and molecules in the electrochemical interface inhibits the application of quantum chemical methods and other have to be used. Monte Carlo simulations (MC) [80–83] and molecular dynamics (MD) have been used for theese calculations.

A. A. Gardner and J. P. Valleau [82, 83] used a simple interaction pontential basing on mirror images for the simulation of the metal-water interaction. They assumed an ideal, highly polarizable metal surface. The image charges had therefore the same size as the charges on the water molecules (TIPS2 potential for bulk water), but were different in sign. These calcualtions for an uncharged metal wall resulted in erroneous water orienations close to the wall. The first layer water molecules bonded with one hydrogen atom to the metal surface while the other pointed into the bulk water. Despite this principle problem these calculations indicate that polarisation and many body effects within the metal have a significant influence on the structure of the metal-water interface, while Kohlmeyer et al. [84] published molecular dynamics calculations showing that the inclusion of polarisation into the water-water interaction potential has only little influence on the results of the siumulation. MC calculations with a more elaborate set of potential energy functions [80, 81] reproduce correctly the orientation of the first layer water molecules close to an uncharged copper wall.

MD calculations [84–102] form the second group of computational methods applied to the electrochemical metal-water interface. The potential energy functions used for the metal-water interaction can be subdivided into two groups: First, potentials exploiting electrochemical effects such as mirror charges and second, potentials trying to mimic chemisorption data from quantum chemical calculations.

Hautman et al. [91] published MD calculations for uncharged metal walls using the first group of metal-water potentials with a peculiar result: Although the first peak of the hydrogen density lies 0.2 Å closer to the metal surface than the first peak of the oxygen density (ref. 91 fig. 2) the dipole moments of the water molecules point preferentially away from the surface (ref. 91 fig. 3). The authors explain this effect with the larger charge (factor -2) on the oxygen atoms than on the hydrogen atoms resulting in an overall negative charge at the metal surface.

Zhu and Robinson [92] reported MD calculations of water between two solid, insulating walls. The interaction between the wall and the water molecules is described with a gas-crystal potential excluding mirror charges. They conclude form their calculations that the water molecules close to the surface orientate the hydrogen atoms towards the solid and not into the bulk water. In a second paper Zhu and Philpott [93] showed, that the orientation of the water molecules towards the surface depends strongly on the chosen potential energy functions now including mirror charges. They compare two potential energy functions for a variety of metal surfaces differing in an anisotropic Lennard-Jones energy term (V_{an}) acting on the hydrogens. The potential energy functions containing V_{an} result in water molecules bonding to a Pt(100) surface via one hydrogen atom similar to the bonding geometries reported by Gardner et al. [82, 83] whereas the potential energy function without V_{an} produces no platinum-hydrogen bonds.

The second class of MD calculations uses individual potential energy functions for the hydrogen atoms and the oxygen atom to calculate the metal-water binding energy. The parameters of these fuctions have been chosen by Heinzinger and Spohr [94–96] to reproduce Extended-Hückel results [64] and experimental data. Later, these potential energy functions have been extended by Berkowitz et al. about a surface term, which includes the symmetry of the metal surface [97, 98].

Spohrs [94–96, 99–101] results for the uncharged platinum-water interface may be summarized as follows:

- The oxygen and the hydrogen atom density show strong oszilations close to the surface, but approach bulk values for the center of the model.

- The oxygen atom density shows at least two strong peaks indicating two defined layers of water molecules close to the surface. These two peaks suggest the existence of water layers similar to the bilayer structure observed for water in UHV experiments.

- The water moelcules, which cause the first peak in th oxygen atom density profile (directly attached to the surface), stay at their position during the MD run, whereas molecules from the second peak are less tight bound and move freely within the layer [102].

- At low coverages of water (θ) the water molecules in the first layer are orientated in a tilted position with their dipole moment pointing away from the surface ($\vartheta = 75°$, ϑ is the angle between the surface normal and the dipole moment). Both hydrogen atoms of the water molecule are at the same distance from the surface [95]. Such an orientation of the water molecules is expected for a bonding bonding mechanism via a lone electron pair, which is surprising, since the platinum-water potential favours an adsorption geometry with the water molecules dipole moment perpendicular to the surface[3]. A strong hydrogen bonding network is assumed to stabilize this geometry. The same principle geometry effects have been observed by SPOHR [100, 101] also for Hg(111).

  As θ increases from 0.2 to 0.8 move the hydrogen atoms closer ot the surface until finally the molecular plane of the water molecule is parallel to the surface.

The electrochemical results suggest, that hydrogen bonding within the interface is essential for a valid description of the platinum-water interface. The transition between both electrochemistry and UHV experiments is done by the reduction of the water molecules used for the simulation. Instead of bulk water come now small water clusters into focus. LIU et al. [103] pointed out, that water-water interaction potentials, which reproduce well the properties of bulk water tend to fail on small water clusters.

The water dimer is probably the best analysed water cluster of all. It was not only the first water cluster subject of *ab initio* calculations [104] but is also commonly used as benchmark test for new calculations. It is therefore possible to find reference values in the literature for the water dimer on every possible level of theory [105–131]. The global minimum has a linear geometry with C_S symmetry with the nonbonding hydrogens on opposite sites of the oxygen-oxygen bond. The optimized oxygen-oxygen distance is about 3 Å and the bonding energy about 5 kcal/mol.

SCHÜTZ et al. suggested a namening system for the non-bonding hydrogens in the cyclic water trimer, which fully describes the geometry of the cluster [132]: The nonbonding hydrogen can be either above (up, "u"), parallel to (planar, "p") or under (down, "d") the oxygen plane, while the bonding hydrogens rest in the oxygen plane. If the oxygen plane bisects the water molecule, the geometry is marked with an "b". The global minimum of the potential energy surface of the water trimer has a cyclic geometry. Early calculations on the water trimer suggest, that the {uuu} water trimer is less stable than the ideal linear structure [133], but already the {ppp} trimer is more stable than the linear one. The linear trimer again transforms smoothly into a cyclic {uud} geometry, which marks the global minimum [128, 131, 132, 134–150]. The geometry of the water

---

[3] This orientation reflects the results of the Hückel calculations used for the creation of the potential energy functions. The Hückel calculations for Pt_5-H_2O favour the same geometry and the observed equilibrium geometry may be the result of the missing interactions between surface atoms and the hydrogens of the water molecule [64].

trimer is very flexible and tunneling facilitates rapid changes between the 96 isoenergetic isomers ($2^n \times n! \times 2$, where n is the number of water molecules in the cluster) [103, 150–156].

18 stationary points have been found on the potential energy surface of the water trimer [142, 145]. The {ppp} trimer has a slightly smaller bonding energy than the {uud} ($\Delta E < 0.5$ kcal/mol) [132] and is a stationary point with a Hessian index of 3. Most of the published results focuses on the {uud} trimer and only few articles concentrate on the {ppp} [132, 140, 142, 144, 157–159], despite the fact, that the {ppp} and the {udp} trimer are possible intermediates in the movement of the hydrogens [132].

The computational analysis of water cluster gained more interest recently, because these microcrystals can be used to investigate phase transitions [160]. But, the transition from small water cluster to larger is not straight forward and the water hexamer seperates the water clusters into two domains.

Two principles control the structure of water clusters: First, the number of hydrogen bonds in the cluster should be as high as possible for a maximum energy gain. And second, repulsive interactions between nonbonding hydrogens and geometrical strains within the water rings should be as low as possible at the same time. Small water cluster $(H_2O)_n$ with $n \leqq 5$ are therefore commonly assumed to be cyclic planar [103, 128, 133, 161–170], while large clusters with $n \geqq 7$ have three dimensional structures [160, 170–178]. The water hexamer marks the border between both regions and is the smallest water cluster with a three dimensional equilibrium structure. Several geometries with similar energies ($\Delta E < 1$ kcal/mol) have been found for the water hexamer [128, 148, 149, 179–182]. The multitude of energetically similar isomers makes the water hexamer a new benchmark system for methods, which are going to be applied to larger clusters.

Although the cyclic water hexamer forms the basis of the ice structure [18, 183, 184] and has been observed as a structural element in liquid water [185], has the most stable water hexamer in the gas pase a cage structure [186, 187]. The energy difference between the cyclic and the cage hexamer is small and it has not been possible to observe the free hexamer experementaly until recently [187].

Quantum chemical calculations [128, 148, 149, 179–182, 188] on the cyclic water hexamer agree reasonably well on the geometry of the cluster, but disagree heavily on the total energy of the cluster. The most stable ring has a "chair"conformation (S_6 symmetry) with straight hydrogen bonds and the oxygen-oxygen distance between direct neighbours varies between 2.708 Å and 2.855 Å. The main properties of the cluster's geometry can be reproduced with simple methods, whereas reliable energy calculations require sophisticated ones. Published values for the bonding energy of the cyclic water hexamer vary between −37.99 kcal/mol and −56.00 kcal/mol (with one exception: −66.66 kcal/mol [181]) depending on the level of computation.

1.2 This work

Two computer experiments are used commonly for the simulation of the platinum-water interface: First, quantum chemical calculations with a single water molecule and second, molecular dynamics simulations with various potential energy functions. Between theese two extremes is this work placed: A computational analysis of water clusters attached to a platinum surface.

Figure 1.3 shows, how the calculation of water clusters on a platinum surface ($Pt_n-(H_2O)_m$ in the center of the sketch) is embeded in its scientific environment. As mentioned in section 1.1 molecular dynamics simulation of the electrochemical interface give physically reasonable results

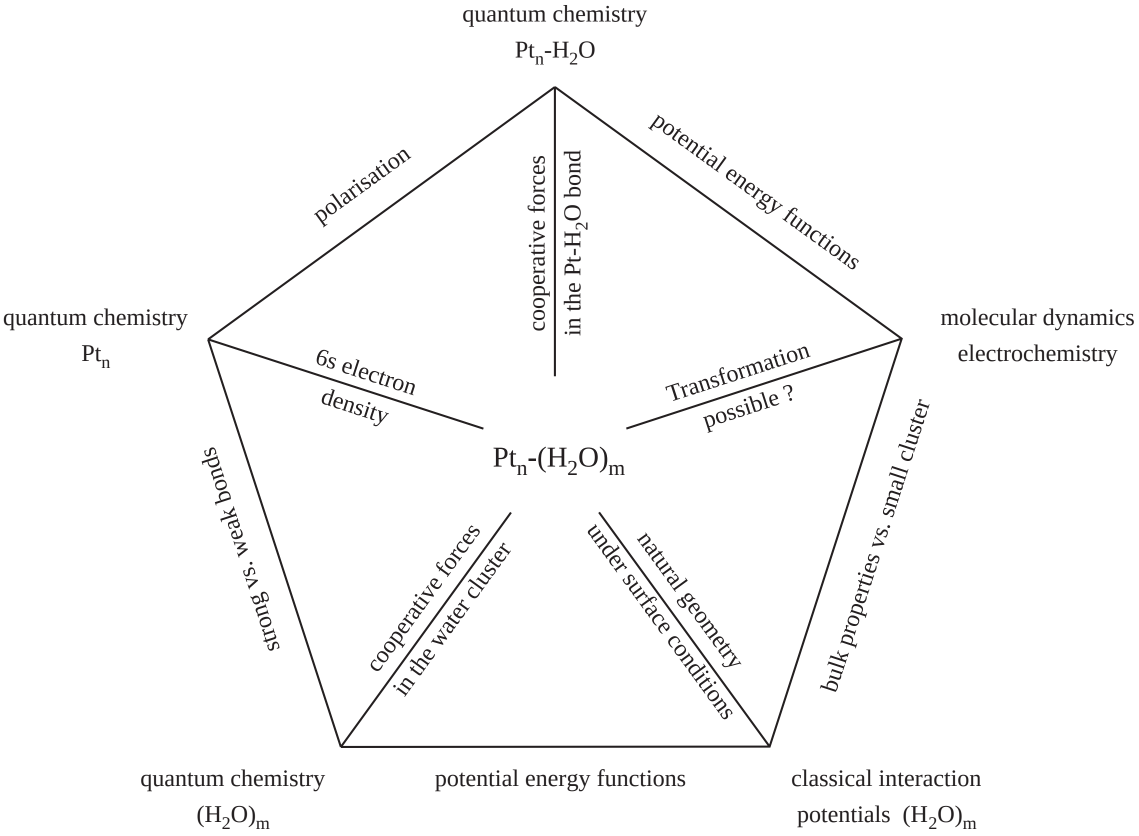

Figure 1.3: Scientific environment of this work.

[101]. The potential energy function used for these calculations base on extended Hückel calculations using a Pt_5-H_2O pyramid with the water molecule at the top as surface model (Pt(100)). Such a cluster has no other surface atoms than the one bonding the water molecule and the representation of the interactions between the water molecule and the non-bonding surface atoms seems to be poor for the equilibrium geometry. Another problem arises from the water-water interaction potential used for the simulation. Most of the used potentials have been optimized to reproduce properties of bulk water. Many-body forces are important for bulk water, where an individual water molecule is evenly surrounded by other water molecules and the water molcule can therefore be thought captured in a homogenous matrix. Simple, pair wise additive interaction potentials can simulate a great share of these forces by their parametrisation and good bulk values can so be easily computed. In a small cluster is a water molecule not evenly surrounded by its peers and 'bulk potentials' fail therefore to reproduce the properties of small water cluster.

This work started with a quantum chemical revision of the water dimer and trimer to obtain a set of basis data for small water cluster. A selection of clasical water-water interaction potentials, used by other groups for molecular dynamics simulations, was unable to reproduce the quantum chemical results.

Quantum chemical calculations on large water clusters are computationally expensive and a classical water-water interaction potential would allow us to find good starting geometries for the quantum chemical analysis. Therefore, we created a new water-water interaction potential, which inludes partially cooperative forces by its parametrisation.

Next, we started a quantum chemical investigation of small platinum clusters (LanL2DZ ECP, 18 valence electrons [189]). The platinum-platinum bond strength depends strongly on the electronic state of the cluster, as the bond between the metal atoms is formed mainly via the 6s orbitals, who interact with the partially filled 5d band.

The quantum chemical investigation of the platinum-water bond showed, that this bond depends also on the 6s population in the metal cluster, but in the other direction: A strong platinum-platinum bond and a strong platinum-water bond exclude eachother. The construction of a working surface model proofed therefore to be much more complicated than expected. Polaristion effects caused by the electric dipole field of the water molecule can lead to a sudden redistribution of the 6s electrons and change so the electronic structure of the cluster as well as the total energy.

At this point we started the development of our own 1-valence electron ECP for platinum. The aim was not so much the reduction of the computational costs but to minimize the number of electronic states close to the ground state. As the density of electronic states becomes smaller, sudden changes of the electronic structure of the cluster become less likely and the scanning of the potential energy surface easier.

Both, the 1- and the 18 valence electron ECP calculations, would have been much more difficult without the application of the Hückel theory to the platinum 6s orbitals. Hückel theory allowed us to identify suitable electronic states for the surface model and to understand the electron movements within the cluster.

The platinum-water bond was found to be similar to the hydrogen bond in water clusters and cooperative effects are therefore likely to be found in the interaction between water and the platinum surface. Inspired by OGASAWARA we used $Pt_3-(H_2O)_3$ as model for the adsorption of water on Pt(111) [42, 56]. These calculations showed that cooperative effects, similar to the effects observed in the water trimer, have a strong influence on the geometry and the energy of the water cluster.

Cooperative forces in the platinum-water bond can turn a water molecule out of its ideal orientation. DOERING and MADEY suggested a water bilayer similar to the structure of ice Ih to grow on the metal surface [39]. In this model every water molecule is tetrahedraly surrounded by bonding partners and the hydrogens of the water molecules directly attached to platinum point away from the surface. Our quantum chemical calcualtions on the other hand showed, that the energy to move the hydrogens up or down is very small and the prefered angle between the molecular plane of the water molecule and the platinum-oxygen bond depends strongly on the chosen method for the computation. We used therefore our own clasical water-water interaction potential to analyse the preferd geometry of a water hexamer under surface conditions.

The following list sumarizes the individual chapters of this work and their contents.

Chapter 1	contains the literature survey as well as an introduction to this work.
Chapter 2	compiles brief summaries of the methods used for this work. Theories, who are not described in standard quantum chemistry text books, are described in greater detail than procedures and formulae, which are part of those text books.
Chapter 3	focuses on the quantum chemistry of small water clusters. The water dimer served as benchmark test for the computational method (DZP basis set, MP3, full BSSE correction), which was later used for the analysis of cooperative forces in the water trimer.

Chapter 4	describes the development of a new water-water interaction potential from cuts through the potential energy surface of the water dimer and selected points from the trimer surface (chapter 3) and first applications of the new potential.
Chapter 5	demonstrates the application of the Hückel theory to the analysis of small platinum clusters. The results of these calculations are later used in the chapters 6 and 7.
Chapter 6	is a compilation of the quantum chemical calculations for Pt_n and Pt_n-H_2O (n = 1, 2, 3, 5, 9) using the LanL2DZ ECP (18 velence electrons) from Hay and Wadt [189]. This chapter examines the correlation of the platinum-water bond strength and the electronic state of the metal cluster.
Chapter 7	summarizes the development of a new 1 valence electron ECP for platinum and its application for the analysis of Pt_5-H_2O.
Chapter 8	combines all results obtained so far and focusses on water clusters on the platinum surface. The first section of Chapter 8 combines the results from chapter 3 and 6 for the analysis of cooperative effects in $Pt_3-(H_2O)_3$ while the second section uses the results from the chapters 4, 6 and 7 to investigate the water hexamer on a virtual metal surface.
Chapter 9	is the summary of summaries and suggests further proceedings.
Chapter 10	lists the literature references and programs used for this work
Chapter 11	Appendix

Attention: The atomic energy unit *Hartree* is abbreviated with 'H' within the whole text mainly to sqeeze it into small table columns.

Chapter 2

Theory

This chapter summarizes the theory of the methods used for this work. Theories, who are not described in standard quantum chemistry text books, are described in greater detail. Procedures and formulae, which are part of those standard text books are only briefly paraphrased.

The longest part of this chapter is a description of the effective core potentials. They are of vital importance for all calculations with heavy metal atoms. Although many papers have been published on this subject, no paper, explains a given potential in detail. The authors generally cite each other and considerable work has to be done to unravel the citations.

2.1 Hartree-Fock Calculations

The Hartree-Fock theory is broadly discussed in the literature [17, 190–192]. Therefore, this report only contains a short summary.

The time independent nonrelativistic Hamiltonian operator $\hat{\mathrm{H}}_{\mathrm{mol}}$ of a molecule can be written as the sum of different interactions in the molecule:

$$\begin{aligned} \hat{H}_{mol} &= \hat{T}_e + \hat{T}_N + \hat{V}_{NN} + \hat{V}_{Ne} + \hat{V}_{ee} = \hat{H}_e + \hat{H}_N \\ \hat{H}_e &= \hat{T}_e + \hat{V}_{Ne} + \hat{V}_{ee} \equiv \hat{\mathcal{H}} \\ \hat{H}_N &= \hat{T}_N + \hat{V}_{NN} \end{aligned} \tag{2.1}$$

For ease of reading the 'e' in $\hat{\mathrm{H}}_{\mathrm{e}}$ will be further omited.

$\hat{\mathrm{T}}$ is the operator of the kinetic energy of the electrons and of the nuclei while $\hat{\mathrm{V}}$ describes the interactions between the nuclei ($\hat{\mathrm{V}}_{\mathrm{NN}}$), between the electrons ($\hat{\mathrm{V}}_{\mathrm{ee}}$) and between nuclei and electrons ($\hat{\mathrm{V}}_{\mathrm{Ne}}$). The Born-Oppenheimer separation [192, 193] allows the separation of the motion of the electrons from the motion of nuclei, because the light electrons in a molecule move much faster than the heavy nuclei. This procedure leads to an equation which only describes the motion of the electrons and asumes the nuclei at fixed positions $\vec{\mathbf{R}}$.

$$\hat{\mathcal{H}}\,\Psi(\vec{\mathbf{R}},\vec{r}) = E(\vec{\mathbf{R}})\,\Psi(\vec{\mathbf{R}},\vec{r}) \tag{2.2}$$

While the wavefunction Ψ depends on the positions of the electrons $\vec{\mathrm{r}}$ at specified nuclear positions $\vec{\mathbf{R}}$ the electronic energy E depends only on the position of the nuclei as a parameter.

For a given molecule consisting of n electrons and N nuclei with the charge Z_α $\hat{\mathcal{H}}$ has the following form (in atomic units, neglecting relativistic effets):

$$\hat{\mathcal{H}} = -\sum_{i=1}^{n} \frac{1}{2}\nabla_i^2 - \sum_{i=1}^{n}\sum_{\alpha=1}^{N} \frac{Z_\alpha}{r_{i\alpha}} + \sum_{i=1}^{n-1}\sum_{j=i+1}^{n} \frac{1}{r_{ij}} \tag{2.3}$$

The last sum in equation 2.3 describes the electron-electron interaction and prohibits an analytic solution of equation 2.3. In a first attempt to solve equation 2.3 the electron-electron interaction may be neglected (model of independent electrons, equation 2.4). $\hat{\mathcal{H}}$ may then be written as the sum ($\hat{\mathrm{H}}$) of n one electron operators $\hat{\mathrm{h}}_\mathrm{i}$ which allows us the separation of (2.3) in n one-electron equations (2.4). The solution for Ψ in this case is the product of one electron wavefunctions φ_i.

$$\begin{aligned} \hat{h}_i &= -\frac{1}{2}\nabla_i^2 - \sum_{\alpha=1}^{N} \frac{Z_\alpha}{r_{i\alpha}} \quad \Rightarrow \quad \hat{h}_i\varphi_i(\vec{\mathbf{R}},\vec{r}) = e_i(\vec{\mathbf{R}})\ \varphi_i(\vec{\mathbf{R}},\vec{r}) \\ \hat{H} &= \sum_{i=1}^{n} \hat{h}_i \qquad \Psi(\vec{\mathbf{R}},\vec{r}) = \prod_{i=1}^{n} \varphi_i(\vec{\mathbf{R}},\vec{r}_i) \qquad E(\vec{\mathbf{R}}) = \sum_{i=1}^{n} e_i(\vec{\mathbf{R}}) \end{aligned} \tag{2.4}$$

This solution does not consider the Pauli-Principle, the interexchangeability of electrons and the spin. Those disadvantages could be overcome if not the direct product of the φ_is is used as a solution for Ψ but a Slater determinant (antisymmetrized product) built of the φ_is after normalisation.

$$\Psi(\vec{\mathbf{R}},\vec{r}) = \frac{1}{\sqrt{n!}} \begin{vmatrix} \varphi_1(\vec{r_1})\alpha & \varphi_1(\vec{r_1})\beta & \dots & \varphi_{\frac{n}{2}}(\vec{r_1})\beta \\ \varphi_1(\vec{r_2})\alpha & \varphi_1(\vec{r_2})\beta & \dots & \varphi_{\frac{n}{2}}(\vec{r_2})\beta \\ \vdots & \vdots & \ddots & \vdots \\ \varphi_1(\vec{r_n})\alpha & \varphi_1(\vec{r_n})\beta & \dots & \varphi_{\frac{n}{2}}(\vec{r_n})\beta \end{vmatrix} = \frac{1}{\sqrt{n!}} \begin{vmatrix} \chi_1(\vec{r_1}) & \chi_2(\vec{r_1}) & \dots & \chi_n(\vec{r_1}) \\ \chi_1(\vec{r_2}) & \chi_2(\vec{r_2}) & \dots & \chi_n(\vec{r_2}) \\ \vdots & \vdots & \ddots & \vdots \\ \chi_1(\vec{r_n}) & \chi_2(\vec{r_n}) & \dots & \chi_n(\vec{r_n}) \end{vmatrix} \tag{2.5}$$

χ_i are the spin orbitals built by the multiplication of φ_i with the appropriate spin eigenfunction (α or β). The Slater determinant (2.5) and the full electronic Hamiltonian operator (2.3) allow us to calculate the expectation value for the electronic energy E.

$$E = \frac{\langle\Psi|\,\hat{\mathcal{H}}\,|\Psi\rangle}{\langle\Psi|\Psi\rangle} \tag{2.6}$$

Assuming the χ_is form a set of orthonormal functions yields the following expression for the energy:

$$\begin{aligned} E &= \sum_{i=1}^{n} h_{ii} + \frac{1}{2}\sum_{i=1}^{n}\sum_{j=1}^{n}(J_{ij} - K_{ij}) \qquad h_{ii} = \left\langle \chi_i \left| -\frac{1}{2}\nabla_i^2 - \sum_{\alpha=1}^{N}\frac{Z_\alpha}{r_{i\alpha}} \right| \chi_i \right\rangle \\ J_{ij} &= \left\langle \chi_i(\vec{r})\chi_j(\vec{r}\,') \left| \frac{1}{|\vec{r}-\vec{r}\,'|} \right| \chi_i(\vec{r})\chi_j(\vec{r}\,') \right\rangle \quad K_{ij} = \left\langle \chi_i(\vec{r})\chi_j(\vec{r}\,') \left| \frac{1}{|\vec{r}-\vec{r}\,'|} \right| \chi_i(\vec{r}\,')\chi_j(\vec{r}) \right\rangle \end{aligned} \tag{2.7}$$

h_ii is the one electron integral similar to the one in equation (2.4). J_ij is the coulomb integral and describes the interaction between the electron densities $\varphi_\mathrm{i}(\vec{\mathrm{r}})^*\varphi_\mathrm{i}(\vec{\mathrm{r}})$ and $\varphi_\mathrm{j}(\vec{\mathrm{r}})^*\varphi_\mathrm{j}(\vec{\mathrm{r}})$. The exchange integral K_ij cannot be explained in classical terms[1]. Since the spin eigenfunctions are orthogonal, the exchange interaction is only non zero between electrons of the same spin.

---

[1] If instead of the Slater determinant (2.5) the direct product of the φ_is (2.4) is used to calculate the energy expectation value, the expression for the energy (2.7) does not contain the exchange integrals. The exchange integral is a truly quantum mechanical effect.

A better approximate wavefunction for Ψ can be found by minimizing[2] $\mathrm{E}(\Psi)$ by varying χ with the constraint that the χs stay orthogonal $\langle\chi_\mathrm{i}|\chi_\mathrm{j}\rangle = \delta_\mathrm{ij}$ [17, 192, 194a].

$$F(\Psi) = E(\Psi) - \sum_{i=1}^{n}\sum_{j=1}^{n} \epsilon_{ij}\,\langle\chi_i|\chi_j\rangle \qquad \frac{\partial F}{\partial \chi_i} = 0 \tag{2.8}$$

The solution of (2.8) leads to n Hartree-Fock equations. The orbital energies ϵ_i derive from the Lagrangian multiplicators ϵ_ij in (2.8).

$$\begin{gathered} \left\{\hat{h} + \sum_{j=1}^{n}(\hat{J}_j - \hat{K}_j)\right\}\chi(r) = \hat{F}\,\chi(r) = \epsilon\,\chi(r) \\ \hat{J}_j\,\chi(r) = \int \frac{\chi_j^*(r')\,\chi_j(r')}{|r-r'|}\,d\tau'\,\chi(r) \qquad \hat{K}_j\chi(r) = \int \frac{\chi_j^*(r')\,\chi_j(r)}{|r-r'|}\,d\tau'\,\chi(r') \end{gathered} \tag{2.9}$$

Equation (2.9) can be solved by iteration. A first guess for Ψ allows us to calculate the Fock Operator $\hat{\mathrm{F}}$ thus to determine the electrical field in which the i-th electron is moving. This enables the calculation of an improved Ψ. This Ψ will be used again as the starting point for a new cycle. The cycles of repetition will be stopped, if the change in the electrical field drops below a preset limit.

The sum of the energy of all occupied orbitals does not yield the energy of the system (2.7).

$$\sum_{i=1}^{n}\epsilon_i = \sum_{i=1}^{n} h_{ii} + \sum_{i=1}^{n}\sum_{j=1}^{n}(J_{ij} - K_{ij}) \tag{2.10}$$

While the expectation value for energy contains (2.7) the electron-electron interaction once in comparison with the model of independent electrons (2.4), this expression contains the electron-electron interaction twice. KOOPMAN's theorem [192] allows us to interpret the orbital energies ϵ_i as the negative of the ionisation energy.

The symmetry of the Fock operator depends on the symmetry of the first guess for Ψ, because Ψ is used to construct the operator. Therefore, the Hartree Fock wavefunction Ψ^HF does not necessarily have the full symmetry of the molecule. Ψ^HF is antisymmetric towards electron exchange, but Ψ^HF is not necessarily an eigenfunction of the total spin operator $\hat{\mathrm{S}}^2$ or the operator of the total spin's orientation $\hat{\mathrm{S}}_\mathrm{Z}$. The introduction of additional symmetry restrictions into equation 2.9 and, if necessary, the construction of linear combinations of Ψs for different configurations assures the right symmetry for Ψ^SHF, the result of this procedure. The final energy will be slightly higher for Ψ^SHF than for Ψ^HF, obtained without any further constrains. The solution for Ψ has either the right symmetry or the lowest energy.

In closed shell molecules all orbitals are doubly occupied. This allows us to use only the spatial part of the χ_is to solve equation 2.9. After the calculation the obtained orbitals are filled with two electrons. While this RHF (restricted Hartree Fock) calculations usually yields good results for closed shell molecules, problems arise together with the calculations for open shell molecules or excited states. During those UHF (unrestricted HF) calculations equation 2.9 divides into

---

[2] The definition of such a deviation is:

$$\frac{\partial F[\chi_i(x')]}{\partial \chi_j(x)} = \lim_{\epsilon \to 0} \frac{F[\chi_i(x') + \epsilon\delta_{ij}\delta(x'-x)] - F[\chi_i(x')]}{\epsilon} \qquad \text{and} \qquad \frac{\partial \chi_i(x')}{\partial \chi_j(x)} = \delta(x'-x)\delta_{ij}$$

two subsets of equations for each spin state. The exchange operators in the Fock operators are different for both sets, since exchange interactions exists only between electrons with the same spin. This leads to different spatial wavefunctions for spin up and spin down, the so called exchange polarisation.

For an average molecule with low symmetry the calculation of Ψ is far too expensive and nearly impossible. ROOTHAAN and HALL suggested independently 1951 [192] to construct the one electron wavefunctions χ_i as a linear combination of M different basis functions γ_k (LCAO method, linear combination of atomic orbitals).

$$\chi_i = \sum_{k=1}^{M} c_{ik}\,\gamma_k \tag{2.11}$$

The LCAO approach simplifies the calculation of (2.8). Instead of the complicated functional differentiation the easer differentiation to a constant $\mathrm{c_{ik}}$ can be done.

The more basis functions are used for the linear combination, the better the description of χ_i and the lower the electronic energy. The total energy of a molecule obtained by an infinite number of wavefunctions is called the Hartee-Fock limit.

$$\begin{gathered} E = \sum_{j=1}^{n}\sum_{i,j=1}^{M} c^*_{ik}\,c_{jk}\,h_{ij} + \frac{1}{2}\sum_{k=1}^{n}\sum_{l=1}^{n}\sum_{i,j=1}^{M}\sum_{p,q=1}^{M} c^*_{ik}\,c_{jk}\,c^*_{pl}\,c_{ql}\,\Big(V_{ijpq} - V_{iqpj}\Big) \\ h_{ij} = \langle\gamma_i(r)|\,\hat{h}_i(r)\,|\gamma_j(r)\rangle \qquad V_{ijpq} = \left\langle \gamma_i(r)\,\gamma_j(r')\,\middle|\,\frac{1}{|r-r'|}\,\middle|\,\gamma_p(r)\,\gamma_q(r')\right\rangle \end{gathered} \tag{2.12}$$

The expression for the energy (2.12) is not a functional of χ_i anymore but a function of $\mathrm{c_{ik}}$. The differentiation of (2.12) with respect to c yields a set of M independent nonlinear algebraic expressions that can be solved to get coefficients. The general procedure of this method is the same as for the Hartree Fock method. A first guess for the coefficients $\mathrm{c_{ik}}$ the electric field of the molecule can be calculated. This leads to an improved set of coefficients that will become the starting point for another cycle.

Modern quantum chemical programs no longer use a single function for a certain atomic orbital. They usually use a sum of gaussian functions with different exponents.

$$\gamma_k = \sum_{\nu}^{G} g_\nu e^{-\alpha_\nu r^2} \qquad\qquad \chi_i = \sum_{k=1}^{M} c_{ik}\sum_{\nu}^{G} g_\nu e^{-\alpha_\nu r^2} = \sum_{k,\nu}^{M,G} a_{ik\nu} e^{-\alpha_\nu r^2} \tag{2.13}$$

Now are the new constants $\mathrm{a_{ik\nu}}$ optimized. This procedure allows the atomic orbitals to vary during the calculation. This extra flexibility enables the introduction of polarisation into the calculation of molecular orbitals, if cartesian gaussians (section 2.4, page 23) are used.

Sometimes the basis of the Hartree-Fock calculation γ_k of a supermoelcule is formed by the monomers molecular orbitals. Those calculations simplify the analysis of the chemical bond between the monomers. On the other hand is such a basis more rigid then the other and the interaction energies inferior.

The occupied orbitals give usually a good description of the molecule's electronic structure. The virtual orbitals on the other hand cannot be explained physically. This can be shown by rearranging the Fock equations 2.9. The electrons move in an effective potential $\mathrm{V_{eff}}$.

$$V_{\text{eff}} = \sum_{j}^{occ} \hat{J}_j - \hat{K}_j = \int \frac{\gamma(r'|r')}{|r-r'|}\,dr' - \int \frac{\gamma(r|r')\,\hat{P}_V(r\to r')}{|r-r'|}\,dr'$$

$$\hat{P}_V(r\to r')\,\chi(r) = \chi(r') \tag{2.14}$$

$\gamma(\mathrm{r}|\mathrm{r}')$ is the first order density matrix[3] and the operator $\hat{\mathrm{P}}_{\mathrm{V}}$ exchanges the variables r and r′ of the function χ. The potential energy of an electron χ_{i} can be calculated straight forward.

$$\int \chi_i^*(r)\, V_{eff}\, \chi_i(r)\, dr = \iint \frac{\chi_i^*(r)\, \gamma(r'|r')\, \chi_i(r)}{|r-r'|}\, dr\, dr' - \iint \frac{\chi_i^*(r)\, \gamma(r|r')\, \chi_i(r')}{|r-r'|}\, dr\, dr' \qquad (2.15)$$

Equation (2.15) can be interpreted as the coulomb interaction of the charge distribution $\chi_{\mathrm{i}}^*\chi_{\mathrm{i}}$ with a model charge distribution $\rho(\mathrm{r}')$.

$$\rho(r) = \gamma(r'|r') - \frac{\chi_i^*(r)\, \gamma(r|r')\, \chi_i(r')}{\chi_i^*(r)\, \chi_i(r)} \qquad (2.16)$$

To obtain (2.16) the exchange part of equation (2.15) has to be reduced to higher terms with $\chi_{\mathrm{i}}^*\chi_{\mathrm{i}}$. The model charge distribution $\rho(\mathrm{r}')$ depends on the orbital χ_{i}. The number of electrons $\mathrm{N_e} = \int \rho(\mathrm{r})\,\mathrm{dr}$ described by $\rho(\mathrm{r})$ therefore depends also on the chosen orbital χ_{i}. The trace of the density matrix $\int \gamma(\mathrm{r}|\mathrm{r})\,\mathrm{dr}$ equals the total number of electrons N. The second term of (2.16) has to compensate one electron to avoid self interaction.

$$\begin{aligned} N_e &= \int \rho(r')dr' = N - 1 \qquad i \leq N \\ N_e &= \int \rho(r')dr' = N - 0 = N \qquad i > N \end{aligned} \qquad (2.17)$$

The exchange charge density is zero for virtual orbitals (i > N), since all virtual orbitals are orthonormal to the occupied orbitals used for the construction of the Fock operator. For an occupied orbital (i ≤ N) the integral contains a non vanishing part $\chi_{\mathrm{i}}^*\chi_{\mathrm{i}}$ and the number of electrons described by $\rho(\mathrm{r})$ is physically correct N-1.

Virtual orbitals are therefore not suitable to describe excited states correctly. For the correct description of an excited state several virtual orbitals are usually necessary.

2.2 Møller-Plesset Perturbation Theory

The Hartree Fock method does not take the correlated movement of the electrons into full account. The energy difference between the 'exact', which takes the full account of the electron correlation, and the Hartree Fock Energy is called the correlation error [195]. Since the exact value of the correlation error is usually not known, the correlation energy as the difference between the Hartree Fock energy and the energy obtained by any post Hartee Fock procedure is reported in the literature.

The electrons can avoid each other more easily, if the possibility to occupy unoccupied orbitals for short 'time' is permitted [195]. This is achieved by mixing excited states with the ground state. The additional energy gain is called correlation energy. One of the most common methods is the Møller Plesset procedure.

The Møller-Plesset Theory (MP) [196] is often also called Many Body Perturbation Theory (MBPT) [190, 191]. An additional figure denotes the level of perturbation. The second name describes much better the underlying theory.

---

[3] The first order density matrix $\gamma(\mathrm{r}|\mathrm{r}')$ of an N electron wavefunction Ψ is defined as follows:

$$\gamma(r|r') = N \int\int \cdots \int \Psi(r, r_2, r_3, \ldots, r_N)\, \Psi^*(r', r_2, r_3, \ldots, r_N) dr_2 dr_3 \ldots dr_N$$

The principal idea is based on the Hartree-Fock-Approximation. If the assumptions of the Hartree-Fock theory are right, the difference between the Hartree-Fock-wavefunction and the eigenfunction of the original Hamiltonian $\hat{\mathcal{H}}$ (2.3) should be small. This allows the use of the Rayleigh-Schrödinger method [190, 192, 193] to improve the wavefunctions and energies. The unperturbed Hamiltonian is taken to be the sum $\hat{\mathrm{G}}$ of the Fock operators $\hat{\mathrm{F}}$ (2.9) and the perturbation operator $\hat{\mathrm{V}}$ the difference between the original Hamiltonian $\hat{\mathcal{H}}$ and $\hat{\mathrm{G}}$ (2.18).

$$\hat{H} = \hat{G} + (\hat{\mathcal{H}} - \hat{G}) = \hat{G} + \hat{V} \qquad \rightarrow \qquad \hat{H}\,\Psi_\mu = E_\mu\,\Psi_\mu \tag{2.18}$$

$$\Psi_\mu = \Psi_\mu^{(0)} + \Psi_\mu^{(1)} + \Psi_\mu^{(2)} + \ldots \qquad E_\mu = E_\mu^{(0)} + E_\mu^{(1)} + E_\mu^{(2)} + \ldots \tag{2.18 a}$$

$\Psi_\mu^{(0)}$ and $\mathrm{E}_\mu^{(0)}$ are the solutions for the energy-state E_μ of the unperturbed system (2.7). Introducing the expansions (2.18 a) into expression (2.18) and collecting terms of equal order in the usual way [193] yields the following set of equations:

$$\hat{G}\,\Psi_\mu^{(0)} = E_\mu^{(0)}\,\Psi_\mu^{(0)} \qquad \text{0. order} \tag{2.19}$$

$$(\hat{G} - E_\mu^{(0)})\,\Psi_\mu^{(1)} = (E_\mu^{(1)} - \hat{V})\,\Psi_\mu^{(0)} \qquad \text{1. order} \tag{2.19 a}$$

$$(\hat{G} - E_\mu^{(0)})\,\Psi_\mu^{(2)} = E_\mu^{(2)}\,\Psi_\mu^{(0)} + (E_\mu^{(1)} - \hat{V})\,\Psi_\mu^{(1)} \qquad \text{2. order} \tag{2.19 b}$$

$$(\hat{G} - E_\mu^{(0)})\,\Psi_\mu^{(3)} = E_\mu^{(3)}\,\Psi_\mu^{(0)} + E_\mu^{(2)}\,\Psi_\mu^{(1)} + (E_\mu^{(1)} - \hat{V})\,\Psi_\mu^{(2)} \qquad \text{3. order} \tag{2.19 c}$$

Equation (2.19) is already solved during the Hartree-Fock calculation. It can be easily separated into the set of one-electron-equations (2.9). To solve the rest (2.19 a - 2.19 c) the functions $\Psi_\mu^{(1)}$, $\Psi_\mu^{(2)}$ and $\Psi_\mu^{(3)}$ are developed in terms of the complete set of functions $\Psi_{\mu\nu}^{(0)}$.

$$\Psi_\mu^{(1)} = \sum_{\nu\neq\mu} a_{\mu\nu}^{(1)}\Psi_{\mu\nu}^{(0)} \qquad \Psi_\mu^{(2)} = \sum_{\nu\neq\mu} a_{\mu\nu}^{(2)}\Psi_{\mu\nu}^{(0)} \qquad \Psi_\mu^{(3)} = \sum_{\nu\neq\mu} a_{\mu\nu}^{(3)}\Psi_{\mu\nu}^{(0)} \tag{2.20}$$

The introduction of (2.20) into (2.19) allows a stepwise solution of (2.19)[4]. The procedure starts with the calculation of the first order perturbation:

$$E_\mu^{(1)} = \left\langle \Psi_\mu^{(0)} \middle| \hat{V} \middle| \Psi_\mu^{(0)} \right\rangle \qquad a_{\mu\nu}^{(1)} = \frac{\left\langle \Psi_{\mu\nu}^{(0)} \middle| \hat{V} \middle| \Psi_\mu^{(0)} \right\rangle}{E_\mu^{(0)} - E_\nu^{(0)}}_{\text{for } \mu\neq\nu} \tag{2.21}$$

Møller and Plesset showed that $\mathrm{E}_\mu^{(1)}$ equals zero. The Hartree-Fock energy is therefore correct to the first order of perturbation. On the other hand $\mathrm{a}_{\mu\nu}^{(1)}$ allows us to figure out the non vanishing second order energy correction:

$$\begin{aligned} E_\mu^{(2)} &= \sum_{\nu\neq\mu} \frac{\left\langle \Psi_\mu^{(0)} \middle| \hat{V} \middle| \Psi_{\mu\nu}^{(0)} \right\rangle \left\langle \Psi_{\mu\nu}^{(0)} \middle| \hat{V} \middle| \Psi_\mu^{(0)} \right\rangle}{E_\mu^{(0)} - E_\nu^{(0)}} = \sum_{\nu\neq\mu} a_{\mu\nu}^{(1)} \left\langle \Psi_\mu^{(0)} \middle| \hat{V} \middle| \Psi_{\mu\nu}^{(0)} \right\rangle \\ a_{\mu\nu}^{(2)} &= \frac{1}{E_\mu^{(0)} - E_\nu^{(0)}} \left(\sum_{i\neq\mu} a_{\mu i}^{(1)} \left\langle \Psi_{\mu\nu}^{(0)} \middle| \hat{V} \middle| \Psi_{\mu i}^{(0)} \right\rangle - a_{\mu\nu}^{(1)} E_\mu^{(1)} \right)_{\text{for } \mu\neq\nu} \end{aligned} \tag{2.22}$$

The second order energy correction yields on average already 90% of the total correlation energy [195] and $\Psi_\mu^{(0)}$ makes usually more than 95% of the total wavefunction.

---

[4] Møller and Plesset emphazise, that their description of the development of the perturbation method for molecules is strictly only valid for electronic systems without any degeneracies ($\mathrm{E}_\mu^{(0)} \neq \mathrm{E}_\nu^{(0)}$ for $\mu \neq \nu$) [196]. The problem of degeneracy can be overcome by other derivations of the perturbation theory, which are described elsewhere in the literature [192].

According to the Brillounin theorem [192, 197] the integral $\langle\Psi_\mu^{(0)}|\hat{\mathrm{V}}|\Psi_{\mu\nu}^{(0)}\rangle$ vanishes for singly excited $\Psi_{\mu\nu}^{(0)}$. It also vanishes for more than doubly excited wavefunctions. The influence of the second order perturbation is therefore controlled by double excitation (ij → ab). This can be used to simplify (2.22) and (2.21) [190].

$$
\begin{gathered}
a_{\mu\nu}^{(1)} = -\frac{(ij||ab)}{\epsilon_i+\epsilon_j-\epsilon_a-\epsilon_b} \qquad E_\mu^{(2)} = \frac{1}{4}\sum_i^{occ}\sum_j^{occ}\sum_a^{virt}\sum_b^{virt}\frac{(ij||ab)(ab||ij)}{\epsilon_i+\epsilon_j-\epsilon_a-\epsilon_b} \\
(ij||ab) = \left\langle \chi_i(1)\,\chi_j(2)\left|\frac{1}{r_{12}}\right|\chi_a(1)\,\chi_b(2)\right\rangle - \left\langle \chi_i(1)\chi_j(2)\left|\frac{1}{r_{12}}\right|\chi_a(2)\,\chi_b(1)\right\rangle
\end{gathered}
\tag{2.23}
$$

χ_i, χ_j, χ_a and χ_b are one-electron functions, which satisfy (2.9) and the ϵ's are the corresponding orbital energies. i and j denote occupied orbitals while a and b designate virtual orbitals.

Although the calculation of the third order perturbation is logically straightforward, numerical efforts set a limit in practice; especially the calculation of the wavefunction (2.24). Since (2.24) contains the same type of integrals than (2.23), the third order of perturbation is also controlled by double excitation. This shows the equivalence of a MP3 and SD-CI (Single and Double excitations Configuration Interaction) calculation.

$$
\begin{gathered}
E_\mu^{(3)} = \sum_{\nu\neq\mu} a_{\mu\nu}^{(2)}\left\langle\Psi_\mu^{(0)}\left|\hat{V}\right|\Psi_{\mu\nu}^{(0)}\right\rangle = \sum_{\nu\neq\mu}\frac{1}{E_\mu^{(0)}-E_{\mu\nu}^{(0)}}\left(\sum_{i\neq\mu} a_{\mu i}^{(1)}\left\langle\Psi_\mu^{(0)}\left|\hat{V}\right|\Psi_{\mu\nu}^{(0)}\right\rangle - a_{\mu\nu}^{(1)}E_\mu^{(1)}\right) \\
a_{\mu\nu}^{(3)} = \frac{1}{E_\mu^{(0)}-E_{\mu\nu}^{(0)}}\left(\sum_{i\neq\mu} a_{\mu i}^{(2)}\left\langle\Psi_{\mu\nu}^{(0)}\left|\hat{V}\right|\Psi_{\mu i}^{(0)}\right\rangle - a_{\mu i}^{(1)}E_\mu^{(2)} - a_{\mu i}^{(2)}E_\mu^{(1)}\right)_{\text{for } \mu\neq\nu}
\end{gathered}
\tag{2.24}
$$

The dominant computational step in MP2 scales as nN^4, in MP3 as $\mathrm{n}^2\mathrm{N}^4$ and in MP4 as $\mathrm{n}^3\mathrm{N}^4$ [123]. Here is n the number of occupied molecular orbitals and N the number of basis functions. This increase in the computational efforts is the reason for limitations of the configuration space in MP4 calculations [124, 198].

One big advantage of MP calculations is the correct dissociation behaviour of supermolecules. A supermolecule AB dissociates into two fragments A and B. At an infinite distance between the fragments, the integral (ij||ab) equals zero, if the functions χ are located on different fragments. To the sum $\mathrm{E}_\mu^{(2)}$ contribute at an infinite difference only terms, on which all four orbitals are located on the same fragment. In this case $\mathrm{E}_\mu^{(2)}$ is the same as the sum of the MP2 energies for two isolated molecules A and B.

A similar argument holds also for the Hartree Fock energy. If distance between A and B gets bigger, the interaction $\hat{\mathrm{H}}_\infty$ between both molecules becomes neglible. This allows us to separate the hamiltonian into two hamiltonians for A and B. In this case the total energy equals the sum of the individual molecular energies.

$$
\hat{H}_{AB} = \hat{H}_A + \hat{H}_B + \hat{H}_\infty \qquad \underset{r_{AB}\to\infty}{lim}\ \hat{H}_{AB} = \hat{H}_\infty = \hat{H}_A + \hat{H}_B \qquad E_\infty = E_A + E_B
\tag{2.25}
$$

Bartlett has proved that MP calculations are not only size consistent but also size extensive [195, 198].

2.3 Configuration Interaction and Multiconfiguration SCF Theory

Another way to incorporate electron correlation into the calculation is via configuration interaction (CI) calculations. Unlike the Møller Plesset calculations configuration interaction calculations are not based on perturbation theory. This allows the use of configuration interaction calculations, when the influence of the electron correlation on the wavefunction is large. Electron correlation is particularly important for platinum compounds. For clusters with nearly degenerate states this type of calculation is especially important.

The exact wavefunction for an N-electron system Ψ can be written in an expansion of antisymmetrized products of one electron functions.

$$\Psi(1,2,3,\ldots,N) = \sum_k d_k \Phi_k(1,2,3,\ldots,N) \tag{2.26}$$

Φ_k is called a configuration or a configuration state function and is a Slater determinant (please refer to equation 2.5) or a sum of Slater determinants to describe an electronic state. The expansion coefficients $\mathrm{d_k}$ can be calculated with the linear variation method [115, 199], which leads to the secular determinant.

$$det\{\mathbf{H} - E\mathbf{S}\} = 0 \qquad \mathbf{H}_{st} = \left\langle \Phi_s \middle| \hat{H} \middle| \Phi_t \right\rangle \qquad \mathbf{S}_{st} = \left\langle \Phi_s \middle| \Phi_t \right\rangle = \delta_{st} \tag{2.27}$$

The configurations will be orthonormal if the molecular orbitals used for their construction are orthonormal. The configurations are formed by promoting one or more electrons into an unfilled "virtual"orbital. The configurations obtained by the promotion of one electron are called singly excited configurations. The terminology is extended to the excitation of more electrons: double, triple, quadruple and higher. Usually those excitations are abbreviated by a capital letter: S, D, T and Q. The number of configurations increases rapidly with the number of spin orbitals. The highest possible number of configurations T regardless of the constraints due to spin und spatial symmetry is given by [197]:

$$T = \binom{M}{N} = \frac{M!}{N!(M-N)!} \tag{2.28}$$

M is the number of spin orbitals and N the number of electrons. The number of configurations increases rapidly with the number of spin orbitals. To limit the computational effort without reducing the basis is usually the manifold of excitations truncated. According to the Brillouin theorem [192, 197] singly excited states do not mix with the Hartree Fock ground state. But, singly excited states still mix with higher excited states. Therefore, the contribution of the singly excited states to final wavefunction is small. The dominant part of the correlation wavefunction next to the ground state is formed by double excitations. Saxe et al. examined the influence of the manifold of excitation on the energy of a water molecule (double zeta basis set) [200]. Their results are summarized in table 2.1. 94.7% of the total correlation energy is already covered by single and double excitations. The addition of triple excitations only gains little in the correlation energy but multiplies the computational effort by nearly a factor of 10.

The lowest root $\mathrm{E_0}$ of (2.27) is the ground state. The higher roots $\mathrm{E_N}$ describe excited states of the molecule. As shown in section 2.1 (page 15) several virtual orbitals are necessary to form a single excited state. The orbitals used to construct the excited state can be extracted from the

		SCF	D-CI	SD-CI	SDT-CI	SDTQ-CI	full CI
config.		1	342	361	3203	17678	256473
$-\mathrm{E}$	[H]	76.009838	76.149178	76.150015	76.151156	76.157603	76.157866
$-\mathrm{E}_{\mathrm{CORR}}$	[H]	0.0	0.139340	0.140177	0.141318	0.147765	0.148048

Table 2.1: Influence of the excitation on the correlation energy of water. [200]

configurations used to build the wavefunction (2.26). The excited states that can be formed by this procedure have the same multiplicity and symmetry as the ground state. Otherwise would the matrix elements $\langle \Phi_\mathrm{s}|\hat{\mathrm{H}}|\Phi_\mathrm{t}\rangle$ vanish. The excitation energy $\Delta\mathrm{E}_\mathrm{N}$ equals $\mathrm{E}_\mathrm{N} - \mathrm{E}_0$.

During multiconfiguration self consistent field calculations (MCSCF) not only the configuration coefficients d_k (2.26) but also the atomic orbital coefficients $\mathrm{a}_{\mathrm{ik}\nu}$ (2.13) are optimized. This is done iteratively in two steps. First, the configuration interaction problem (2.26) is solved. Second, the atomic orbital coefficients $\mathrm{a}_{\mathrm{ik}\nu}$ are optimized. Those cycles are repeated until the convergency criterion is reached. During those calculations two different states are allowed to mix. This might be necessary for a continuous description of the dissociation of a molecular complex. The computational efforts are tremendous. To keep the efforts at a reasonable limit, the configuration space has to be as small as possible.

During complete active space calculations (CASSCF) the orbitals are separated into three different groups. The first group contains low lying double occupied orbitals, and from those no excitation is allowed. The second class contains the virtual orbitals, which are never populated. The third group, the active space, contains occupied and virtual orbitals, which are used to construct the different states for the configuration interaction. Modern quantum chemistry codes today can handle more than 10^5 states during CASSCF calculations. Due to the limited configuration space CASSCF calculations cannot usually cover the complete electron correlation. A systematic improvement can be achieved by a combination of CASSCF and Møller Plesset calculations CASMP2. This method allows the combination of multi reference calculations and electron correlation and therefore offers a powerful tool for the theoretical analysis of dissociation processes.

The quality of CASSCF and MCSCF calculations depends strongly on the orbitals chosen for the active space. If the orbitals necessary for the correct description of the important states are not included, the calculations cannot describe the process. In this work SD-CI calculations are used to get information of states close to the ground state and are therefore likely to mix.

2.4 Basis Sets and Basis Set Superposition Error

The quantum chemistry program GAMESS UK uses cartesian gaussian orbitals (2.29) for the calculations [133, 190, 201, 202].

$$\begin{array}{llll} g_s = N_S\, e^{-\alpha r^2} & & & N_S = \left(\dfrac{2\alpha}{\pi}\right)^{\frac{3}{4}} \\ g_x = N_P\, x\, e^{-\alpha r^2} & g_y = N_P\, y\, e^{-\alpha r^2} & g_z = N_P\, z\, e^{-\alpha r^2} & N_P = \left(\dfrac{128\alpha^5}{\pi^3}\right)^{\frac{1}{4}} \\ g_{xx} = N_D\, x^2\, e^{-\alpha r^2} & g_{yy} = N_D\, y^2\, e^{-\alpha r^2} & g_{zz} = N_D\, z^2\, e^{-\alpha r^2} & N_D = \left(\dfrac{2048\alpha^7}{\pi^3}\right)^{\frac{1}{4}} \end{array} \tag{2.29}$$

$$g_{xy} = N_D\, xy\, e^{-\alpha r^2} \qquad g_{xz} = N_D\, xz\, e^{-\alpha r^2} \qquad g_{yz} = N_D\, yz\, e^{-\alpha r^2} \qquad N_D = \left(\frac{2048\alpha^7}{\pi^3}\right)^{\frac{1}{4}} \tag{2.29}$$

The function g_{xx}, g_{yy} and g_{zz} are used to construct the d_{zz} and the d_{xx-yy} orbitals. This procedure yields also an additional Gauss orbital with s-symmetry g_{rr} (2.30).

$$\begin{gathered} g_{3zz-rr} = \frac{1}{2}(2g_{zz} - g_{xx} - g_{yy}) \qquad g_{xx-yy} = \sqrt{\frac{3}{4}}(g_{xx} - g_{yy}) \\ g_{rr} = \frac{1}{\sqrt{5}}(g_{xx} + g_{yy} + g_{zz}) = \frac{N_S}{\sqrt{5}} r^2 e^{-\alpha r^2} \end{gathered} \tag{2.30}$$

During the construction of the molecular orbitals this pseudo-s-orbital (g_{rr}) may be used as an additional s orbital, if the exponential coefficients of the s-orbitals are not well chosen and the s-orbitals have a lack of electron density where this pseudo-s-orbital electron density has its maximum. This may cause 'overcompleteness' if two orbitals overlap.

The maximum d_{max} of the radial electron density of the pseudo-s-orbital P_{rr} can be found the following way:

$$\begin{aligned} P_{rr} &= r^2 g_{rr}^2 = N_D^2 r^6 e^{-2\alpha r^2} & \left(\frac{\partial P_{rr}}{\partial r}\right)_{r=d_{max}} &= 0 \\ d_{max} &= \sqrt{\frac{3}{2\alpha}} & P_{rr}"(d_{max}) &= -\frac{87}{\alpha^2} e^{-3} \end{aligned} \tag{2.31}$$

Analogous to this the maximum s_{max} of the radial electron density of a s-orbital P_s can be figured out the same way:

$$\begin{aligned} P_s &= r^2 g_s^2 = N_S^2 r^2 e^{-2\alpha r^2} & \left(\frac{\partial P_s}{\partial r}\right)_{r=s_{max}} &= 0 \\ s_{max} &= \frac{1}{\sqrt{2\alpha}} & P_s"(s_{max}) &= -2e^{-1} \end{aligned} \tag{2.32}$$

The total energy of a wavefunction depends on the number of functions in the basis set. The more functions used the lower is the total energy. This is a serious problem for the quantum mechanical description of reactions, in which the number of molecules changes.

A good example of this is any dimerisation. The dimer contains twice as many orbitals as a single monomer. Therefore, its basis is much more flexible. This additional flexibility leads to a further decrease of the dimer's energy. This additional decrease is called the basis set superposition error (BSSE). The BSSE is still subject of research and discussion in the scientific community and regularly discussed at the Computational Chemistry Mailing List [203].

Boys and Bernardi introduced the counterpoise method (CP) to handle this problem 1970 [204]. After the calculation of the dimers energy the energies of the monomers are recalculated using ghost orbitals to simulate the presence of the other monomer. This increase of the basis yields a further decrease in the monomers' energy. This energy change can be regarded as the BSSE. Figure 2.1 shows the influence of the BSSE on the complete interaction energy. If the monomers basis is complete, no further increase in the number of orbitals by the other monomer can induce a further decrease in energy and the BSSE equals zero. This allows the conclusion that an increase in the number of orbitals in the basis set should give a smaller BSSE.

The CP method was believed to overestimate the BSSE slightly. To correct this Daudey et al. suggest using only the virtual orbitals of the other monomer (VCP method) [205]. To emphasize the difference between these two methods, the CP method of Boys and Bernadi is

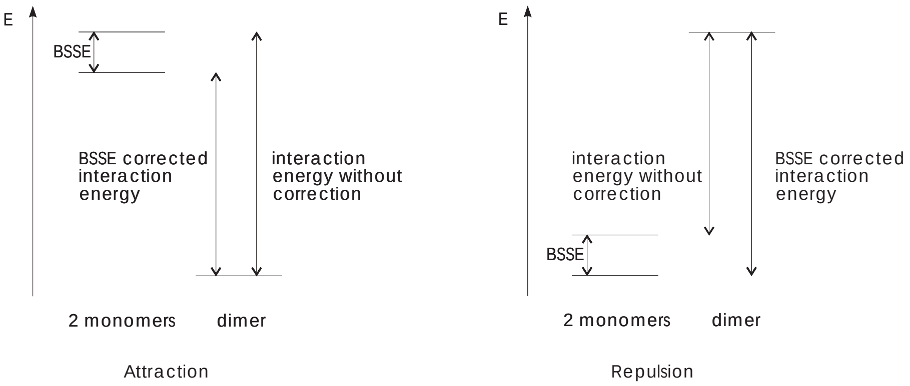

Figure 2.1: Influence of the BSSE on the interaction energy.

often abbreviated as FCP (full counterpoise). Both methods have been compared in the literature [105, 106, 206, 207]. The use of those methods (FCP or VCP) seemed to depend on the interaction energy of the monomers. The overestimation of the BSSE by the FCP method seemed to be a lesser problem than the underestimate of the VCP method regarding water-water interactions [105, 106]. For very weak interactions it is vice versa [207]. Nowadays, it is generally believed that the FCP method is the theoretically correct method [208a]. A simplified argument starts with a Heitler-London approach towards the supermolecule. The wavefunction of the complex AB is the antisymmetrized product of the monomers' wavefunctions, $\hat{\mathrm{A}}\Psi_0^{\mathrm{A}}\Psi_0^{\mathrm{B}}$.

$$E_{AB}^{HL} = \frac{\left\langle \hat{A}\Psi_0^A\Psi_0^B \middle| \hat{H} \middle| \hat{A}\Psi_0^A\Psi_0^B \right\rangle}{\left\langle \hat{A}\Psi_0^A\Psi_0^B \mid \hat{A}\Psi_0^A\Psi_0^B \right\rangle} \tag{2.33}$$

The antisymmetrization operator $\hat{\mathrm{A}}$ causes exchange interaction between the two fragments. This exchange interaction between occupied orbitals again causes a short repulsion of the fragments [17a, 194c].

$$\Delta E_{HL} = E_{AB}^{HL} - E_A - E_B \tag{2.34}$$

For the calculation of the Heitler-London interaction energy $\Delta\mathrm{E}^{\mathrm{HL}}$ the choice of the basis for the calculation of the free monomers energies $\mathrm{E_A}$ and $\mathrm{E_B}$ is important. The VCP method would not permit the occupied orbitals of fragment A to mix with occupied orbitals of B. The overlap controls the exchange interaction and therefore the short range repulsion. The VCP method would give a wrong estimate of the BSSE. This reasoning proves only that the FCP method give better estimates of the BSSE than the VCP method, but does not show that the FCP method describes the BSSE correctly. The later argument can be found in VAN DUIJNEVELDT's text [208a] and cited literature therein.

The assumption that the total BSSE can be extrapolated only from ghost orbital calculation of the electron donor has been proven inaccurate. Since the BSSE is large in comparison with the small interaction energy of two water molecules, even changes of a tenth of a kcal/mol should be considered to get a better description of the interaction energy. The interaction energy on the other hand is not a good measure of the absolute size of the BSSE, since the BSSE is a result of the inadequate description of the monomers. The decision whether the BSSE is small or large should therefore be made in comparison with the monomer energy.

As important as the selections of the orbitals used for the calculation of the BSSE is the selection of the fragments, from which the complex is built [208a]. There is only one chemically sensible way to build a dimer from a monomer, but there are four equivalent ways to construct a trimer (figure 2.2).

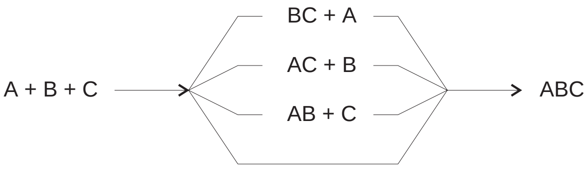

Figure 2.2: Formation of a trimer.

The first three paths are chemically more sensible, because the addition of a third party to an existing dimer is generally more likely than the formation of a trimer in a single step [187]. The calculation of the BSSE during the formation of the first dimer can be done with the FCP method without any problems. The dimer is then taken as a monomer for the next step and the BSSE is then calculated again. The last way shown in figure 2.2 is the formation of the trimer in a single step. To calculate the BSSE of A the basis functions of the B and C were added to the basis of A. The same basis is used to calculate the BSSE of the reminding monomers B and C. All four ways would yield a different BSSE and therefore different interaction energies for the formation of a trimer. This finding is in contradiction to the laws of thermodynamics. The energy of a compound should be independent of the way of formation. To achieve consistency the full basis of ABC should be used to calculate the monomers' energies regardless of the chosen way.

The BSSE not only influences the dimerisation energy but also bond lengths and angles, because it changes the curvature of the energy hypersurface. Since most quantum chemical programs do not take the BSSE into account for geometry optimizations, the energy hypersurface has to be probed manually by single point calculations. Those points are then used to find the minimum of the BSSE corrected energy surface. This procedure allows us to estimate the BSSE for geometry changes.

2.5 The Morokuma Energy Decomposition Scheme

The supermolecular approach usually does not allow the decomposition of the total interaction energy into physically important energy terms. This disadvantage [209] can be overcome by the Morokuma's energy decomposition scheme [127, 129, 210, 211]. This part of the thesis follows the very clear explanation from Kitaura and Morokuma [212].

The Hamiltonian of a van der Waals complex AB can be written in the following way:

$$\hat{H} = \hat{H}_A + \hat{H}_B + \hat{H}_{AB} \tag{2.35}$$

$\hat{\mathrm{H}}_{\mathrm{A}}$ and $\hat{\mathrm{H}}_{\mathrm{B}}$ are the Hamiltonians for the isolated molecules and $\hat{\mathrm{H}}_{\mathrm{AB}}$ is the interaction term. The total energy of the unperturbed state is the sum of the Hartree Fock (HF) ground state energies.

$$E^0 = \left\langle A^0 \middle| \hat{H}_A \middle| A^0 \right\rangle + \left\langle B^0 \middle| \hat{H}_B \middle| B^0 \right\rangle \tag{2.36}$$

A^0 and B^0 are the HF wavefunctions of the molecules A and B. The HF wavefunctions ψ_i of the dimer AB are built from the monomers' molecular orbitals.

$$\psi_i = \sum_k C_{ik}\, \phi_k^A + \sum_\mu C_{i\mu}\, \phi_\mu^B \tag{2.37}$$

The subscripts k, l, m are employed for the HF molecular orbitals of the isolated molecules A, while μ, ν and γ are used for B, and i and j for the complex. The redundant superscripts A and B emphasize the molecular origin of the orbitals. On this basis the Hartree Fock equation for the dimer can be written in the following manner[5]:

$$(\mathbf{F} - \boldsymbol{\epsilon}\mathbf{S})C = 0 \tag{2.38}$$

F is the Fock matrix, **S** the overlap matrix, **C** the coefficient matrix and $\boldsymbol{\epsilon}$ the diagonal matrix of orbital energies.

The total interaction energy (positive for attraction) is[6]:

$$-\Delta E = \sum_i^{occ} C_i^+ (\mathbf{F} + \mathbf{H}) C_i - \mathbf{E}^0 \tag{2.39}$$

H is the kinetic energy and nuclear attraction part of **F**. To describe molecular interactions the total energy $(\mathbf{F} - \boldsymbol{\epsilon}\mathbf{S})$ is split into two terms.

$$(\mathbf{F} - \boldsymbol{\epsilon}\mathbf{S}) = (\mathbf{F}^0 - \boldsymbol{\epsilon}\underline{\mathbf{1}}) + \boldsymbol{\Sigma} \tag{2.40}$$

$\mathbf{F}^0$ is the Hartree Fock matrix of the unperturbed system (infinite separation) and $\underline{\mathbf{1}}$ the unit matrix, while $\boldsymbol{\Sigma}$ contains the molecular interaction. The matrix elements are defined as follows:

$$F_{kl}^0 = \epsilon_k \delta_{kl} \qquad F_{\mu\nu}^0 = \epsilon_\mu \delta_{\mu\nu} \qquad F_{k\nu}^0 = 0 \tag{2.41}$$

$\mathbf{F}^0$ is build only from the monomers' orbital energies, which are calculated in the first step. The molecular interaction matrix $\boldsymbol{\Sigma}$ contains the following elements:

$$\begin{aligned}
\Sigma_{jk} &= \langle k | V^B | l \rangle + \left\langle k \left| \sum_i^{occ} (2J_i - K_i) \right| l \right\rangle - \left\langle k \left| \sum_m^{occ} (2J_m^0 - K_m^0) \right| l \right\rangle \delta_{kl} \\
\Sigma_{\mu\nu} &= \langle \mu | V^A | \nu \rangle + \left\langle \mu \left| \sum_i^{occ} (2J_i - K_i) \right| \nu \right\rangle - \left\langle \mu \left| \sum_\gamma^{occ} (2J_\gamma^0 - K_\gamma^0) \right| \nu \right\rangle \delta_{\mu\nu} \\
\Sigma_{k\nu} &= -\epsilon S_{k\nu} + \langle k \mid \hat{T} + V^A + V^B \mid \nu \rangle + \left\langle k \left| \sum_i^{occ} (2J_i - K_i) \right| \nu \right\rangle
\end{aligned} \tag{2.42}$$

---

[5] Starting point is the equation, which describes the energy of the i-th molecular orbital (compare with (2.8))

$$\left\langle \psi \middle| \hat{F} \middle| \psi \right\rangle = \epsilon\psi \quad \text{with} \quad \psi = \sum_\alpha C_\alpha\, \phi_\alpha$$

Minimizing ϵ by varying C_α with non orthogonal wavefunctions ϕ_α yields the following equation for C_α:

$$\sum_\beta C_\beta (F_{\alpha\beta} - \epsilon S_{\alpha\beta}) = 0 \qquad F_{\alpha\beta} = \left\langle \phi_\alpha \middle| \hat{F} \middle| \phi_\beta \right\rangle \quad S_{\alpha\beta} = \langle \phi_\alpha \mid \phi_\beta \rangle$$

Doing this for all Cs and rearranging the equations into matrix form yields (2.38)

[6] This follows directly from (2.9) and (2.10) for closed shell molecules.

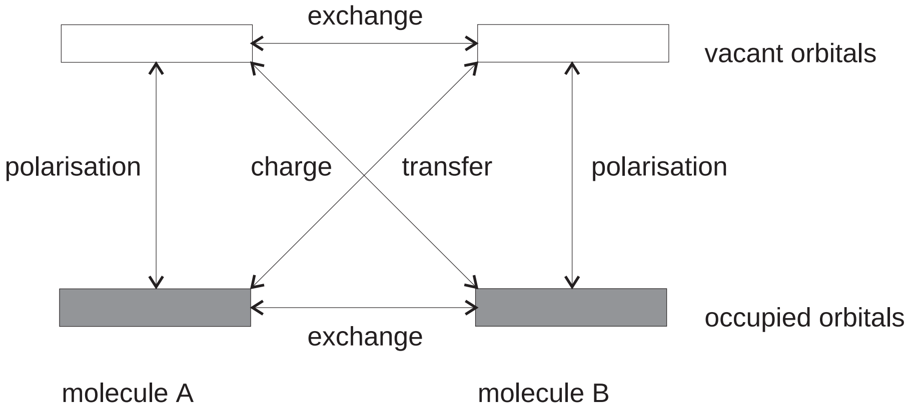

Figure 2.3: Interaction and mixing of the monomer's orbitals.

V^A and V^B are the nuclear attraction potentials of A and B and $\hat{T}$ is the kinetic energy operator. J^0_m and K^0_m are the coulomb and exchange operators for the orbital ϕ^A_m of the isolated molecule A. J^0_γ and K^0_γ are similar operators for ϕ^B_γ. The molecular interaction term also includes the off diagonal elements $S_{k\nu}$ of $\mathbf{S}$.

This approach allows us to distinguish between four different types of interactions (please refer to figure 2.3):

1. Electrostatic: The classical electrostatic interaction operates between the occupied molecular orbitals without mixing them.

2. Polarisation: The polarisation causes the mixing of the occupied and the vacant orbitals of each molecules due to the presence of the other.

3. Exchange: The interaction between both molecules leads to an exchange of electrons between the molecules and an extension of the delocalisation.

4. Charge transfer: The interaction causes a mixing of occupied orbitals of one molecule with vacant molecules of the other and vice versa. This mixing allows a charge transfer from one molecule to the other.

Those four basic principles allow us to subdivide the molecular interaction matrix $\mathbf{\Sigma}$ into different regions:

	A, occ	A, vac	B, occ	B, vac
A, occ	ESX	PLX	EX'	CT
A, vac	PLX	ESX	CT	EX'
B, occ	EX'	CT	ESX	PLX
B, vac	CT	EX'	PLX	ESX

The blocks **ESX** contain parts of the exchange and the electrostatic interaction energy as a comparison with equation (2.42)[7] proves. The **PLX** areas contain the polarisation and part of the

---

[7] The first term $\langle k \,|\, V^B \,|\, l \rangle$ represents the electrostatic interaction with the nuclei of the other molecule. The second half describes how the coulomb and the exchange interaction with all electrons, and therefore with the electrons of the other molecule, affect the orbitals of A.

exchange energy, while the **CT** and **EX'** fields describe only charge transfer and exchange interactions.

Setting all blocks of $\mathbf{\Sigma}$ to zero apart from one type ($\mathbf{\Sigma}^{\mathrm{X}}$) enables the formulation of a model Hartree Fock equation with only one dominant interaction. These model Hartree Fock equations allow us to determine individual interaction energies.

$$0 = (\mathbf{F}^X - \boldsymbol{\epsilon}\mathbf{S}^X) \equiv (\mathbf{F}^0 - \boldsymbol{\epsilon}\underline{\mathbf{1}} + \mathbf{\Sigma}^X)\,\mathbf{C}^X \qquad E^X = \sum_i^{occ} C_i^{X+}\,(\mathbf{F}^X + \mathbf{H}^X)\,C_i^X \tag{2.43}$$

H^{X} is the one electron operator, which is included in F^{X}. The interaction energy E_{X} due to the interaction X is therefore:

$$-E_X = E^X - E^0 \tag{2.44}$$

The first interaction energy to calculate is $\mathrm{E}^{\mathrm{ESX}}$ (diagonal blocks). By definition electrostatic interactions do not change the monomers' molecular orbitals ($\mathrm{C}^{\mathrm{ESX}} = 1$). Neglecting intermolecular exchange terms allows also to figure out the pure electrostatic interaction energy E_{ES}.

The remaining values are calculated together with $\mathrm{E}^{\mathrm{ESX}}$ (i.g. $\mathrm{E}^{\mathrm{ESX}}$ + E^{CT}), since the ESX-blocks are the diagonal blocks and a calculation without them is meaningless. The reminding blocks are set to zero and equation (2.43) solved. The resulting wavefunctions are of the following structure.

$$\phi_i^{ESX+CT} = \sum_k^{occ} C_{ik}\phi_k^A + \sum_\nu^{vac} C_{i\nu}\phi_\nu^B \quad \text{or} \quad \phi_j^{ESX+CT} = \sum_\mu^{occ} C_{\mu k}\phi_\mu^B + \sum_l^{vac} C_{jl}\phi_l^A \tag{2.45}$$

The charge transfer energy itself can be easily determined.

$$-E_{CT} = E^{ESX+CT} - E^{ESX} \tag{2.46}$$

This procedure allows the calculation of the following energies:

E_{ES}	electrostatic interaction energy
E_{PL}	polarisation energy
E_{EX}	exchange energy
E_{CT}	charge transfer energy
$\mathrm{E}_{\mathrm{EXPL}}$	exchange polarisation energy
E_{MI}	coupling term $= \Delta\mathrm{E} - (\mathrm{E}_{\mathrm{ES}} + \mathrm{E}_{\mathrm{PL}} + \mathrm{E}_{\mathrm{EX}} + \mathrm{E}_{\mathrm{CT}} + \mathrm{E}_{\mathrm{EXPL}})$
$\mathrm{E}_{\mathrm{MIX}}$	$= \mathrm{E}_{\mathrm{MI}} + \mathrm{E}_{\mathrm{EXPL}}$ (GAMESS US does not calculate the individual terms but only the sum [213])

Since the procedure by Kitaura and Morokuma uses the monomers' molecular orbitals for the calculation rather than the individual atomic orbitals the complete interaction energy ΔE should be smaller than the interaction energy of an ordinary supermolecular SCF calculation. This is caused by the reduced flexibility of the basis.

2.6 Pseudopotentials

The chemical nature of an element is governed by its outer electrons. This rule is most beautifully displayed in the periodic system of elements, where elements with the same number of valence electrons are joined into groups of similar chemical reactivity. The inner core electrons do not participate in the chemical bonds. Since the amount of computational work increases rapidly with the number of electrons, it might be economically sensible to replace those core electrons by an additional potential, which keeps the valence electrons away from the nucleus and provides the correct energetic and angular behaviour.

The electrons "get faster"as the charge of the nucleus increases and the relativistic corrections of the quantum chemical results have to be made. Relativistic influences of the core electrons onto valence electrons and vice versa has to be simulated by the core potential (RECP, **R**elativistic **E**ffective **C**ore **P**otentials). The incorporation of the relativistic effects into the core potentials is briefly described in the second part of this chapter. The first and more detailed part explains the development of non relativistic core potentials (NRECP). For the better understanding of the ECP from HAY and WADT [189, 214, 215] used in this work brief notes on the historical development are also made in both parts.

2.6.1 Non Relativistic Core Potentials

The development of modern pseudopotentials started with the basic paper by PHILLIPS and KLEINMAN [216]. WEEKS and RICE [217, 218] generalized their approach. This generalized Phillips-Kleinman-potential (V^{GPK}) is the basis of the ECP from HAY and WADT [189, 214, 215] and they refer to the paper of KAHN, BAYBUTT and TRUHLAR [219] as a principal description of the underlying theory.

The next section summarizes the development of the V^{GPK} for a single valence electron. The energy expectation value E of this valence electron's wave function ϕ_V is the minimum of the functional (2.47a) under the constraints of normalisation (2.47b) and orthogonality (2.47c) with the core functions ϕ_C.

$$(a) \quad \left\langle \phi_V \middle| \hat{H} \middle| \phi_V \right\rangle \qquad (b) \quad \langle \phi_V \mid \phi_V \rangle = 1 \qquad (c) \quad \langle \phi_V \mid \phi_C \rangle = 0 \tag{2.47}$$

The core part of any function could be obtained with the idempotent, hermitian projection operator $\hat{P}$.

$$\hat{P} = \sum_C |\phi_C\rangle\langle\phi_C| \qquad \hat{P}^2 = \hat{P} \qquad \hat{P}\phi_C = \phi_C \qquad (1-\hat{P})\phi_C = 0 \tag{2.48}$$

The valence function ϕ_V could be obtained from any function χ with the help of the projection operator $\hat{P}$.

$$(1-\hat{P})\chi = \chi_V = \phi_V \qquad \hat{P}\chi = \chi_C = \sum_C a_C\,\phi_C \qquad a_C = \langle \phi_C \mid \chi \rangle \tag{2.49}$$

$\hat{P}$ takes every bit of χ in the core region out of χ. Hence ϕ_V and ϕ_C cannot overlap and therefore the integral 2.47c vanishes. Equation 2.49 allows us to rewrite (2.47a) and (2.47b).

$$\left\langle (1-\hat{P})\chi \middle| \hat{H} \middle| (1-\hat{P})\chi \right\rangle \qquad \left\langle (1-\hat{P})\chi \middle| (1-\hat{P})\chi \right\rangle = 1 \tag{2.50}$$

Arbitrary variation of χ^* with ϵ as a Lagrange multiplier leads to:

$$\left\langle \delta\chi \left| (1-\hat{P})\,\hat{H}\,(1-\hat{P}) \right| \chi \right\rangle - \epsilon \left\langle \delta\chi \left| (1-\hat{P}) \right| \chi \right\rangle = 0 \tag{2.51}$$

Since $\delta\chi^*$ is arbitrary follows from this equation:

$$[(1-\hat{P})\,\hat{H}\,(1-\hat{P}) - \epsilon(1-\hat{P})]\,\chi = 0 \tag{2.52}$$

The rearrangement of (2.52) leads directly to the expression of generalized Phillips-Kleinman-Potential $\mathrm{V}^{\mathrm{GPK}}$ [218].

$$\begin{aligned} \hat{H}\,\chi - \hat{H}\hat{P}\,\chi - \hat{P}\hat{H}\,\chi + \hat{P}\hat{H}\hat{P}\,\chi - \epsilon\,\chi + \epsilon\hat{P}\,\chi = 0 \\ (\hat{H} + \hat{P}\hat{H}\hat{P} - \hat{H}\hat{P} - \hat{P}\hat{H} + \epsilon\hat{P})\,\chi = \epsilon\,\chi \\ (\hat{H} + V^{GPK})\,\chi = \epsilon\,\chi \\ V^{GPK} = \hat{P}\hat{H}\hat{P} - \hat{H}\hat{P} - \hat{P}\hat{H} + \epsilon\hat{P} \end{aligned} \tag{2.53}$$

In the next step the Lagrange multiplier ϵ (2.51) is set equal to the energy eigenvalue E of the valence function (2.47a). By construction E is then the extreme value of (2.50) subject to the constraints (2.47b) and (2.47c). The test function χ may now have an arbitrary core part. This can be proved by a rearrangement of the first equation of (2.53) and combination with (2.49).

$$\begin{aligned} [(1-\hat{P})\,(\hat{H}-E)\,(1-\hat{P})]\,\chi &= 0 \\ (1-\hat{P})\,(\hat{H}-E)\,\phi_V &= 0 \\ (E-E)\,\phi_V &= 0 \qquad \text{q.e.d.} \end{aligned} \tag{2.54}$$

A similar argument applies to the core part of the test function χ_C.

$$\begin{aligned} (\hat{H} + V^{GPK})\,\chi_C &= (\hat{H} + \hat{P}\hat{H}\hat{P} - \hat{H}\hat{P} - \hat{P}\hat{H} + E\hat{P})\,\chi_C \\ &= \hat{H}\,\chi_C + \hat{P}\hat{H}\hat{P}\,\chi_C - \hat{H}\hat{P}\,\chi_C - \hat{P}\hat{H}\,\chi_C + E\hat{P}\,\chi_C \qquad |\hat{P}\,\chi_C = \chi_C \\ &= E\,\chi_C \end{aligned} \tag{2.55}$$

E is therefore the lowest possible eigenvalue of (2.47a). Also, every core function is degenerate with the eigenvalue E in this approach.

$\mathrm{V}^{\mathrm{GPK}}$ is a nonlocal potential. Further simplification could be obtained by the localisation of $\mathrm{V}^{\mathrm{GPK}}$. This is described in the paper of Kahn, Baybutt and Truhlar [219]. In the case of a single electron circling round a closed shell core $\hat{\mathrm{H}}$ equals the Fock operator $\hat{\mathrm{F}}$.

$$\begin{aligned} (\hat{F} + V^{GPK})\,\chi = E\,\chi \qquad & \hat{F} = \hat{h} + \sum_C (2\hat{J}_C - \hat{K}_C) \\ [\hat{h} + \sum_C (2\hat{J}_C - \hat{K}_C) + V^{GPK}]\,\chi = E\,\chi \qquad & \\ (\hat{h} + U^{core})\,\chi = E\,\chi \qquad & U^{core} = \sum_C (2\hat{J}_C - \hat{K}_C) + V^{GPK} \end{aligned} \tag{2.56}$$

c counts the number of doubly occupied orbitals[8]. If the effective potential $\mathrm{U}^{\mathrm{core}}$ is used in an analytical form, the potential in which the valence electron moves is local and the integrals are easy to compute.

---

[8] This form of the Fock operator (2.56) differs from (2.9) by the way of counting. In the form of (2.9) are all electrons counted, in (2.56) only the double occupied orbitals are counted. While the coulomb integral has a non-vanishing value among all electrons vanishes the exchange integral for electrons with different spins.

The orbital ϕ_{V} and the eigenvalue E are solutions of the exact hamiltonian $\hat{\mathrm{H}}$ and are used numerically during the following calculations. The next step in the evaluation of an ECP is to fix the pseudo orbital χ_{l}. At this point of the calculation it is no longer possible to neglect the angular momentum of the valence electron. The construction is done in such a way that χ_{l} is smooth and nodeless in the core region and similar to the original valence orbital ϕ_{Vl} in the valence region. Such a nodeless wave function has the lowest energy eigenvalue applied to the pseudo potential hamiltonian [219]. Originally the pseudo orbital is formed by a linear combination of ϕ_{V} and the core orbitals ϕ_{C}.

$$\chi_{nl} = \sum_{C} b_{Cl}\, \phi_{Cnl} + \phi_{Vnl} \tag{2.57}$$

The arbitrary coefficients $\mathrm{b_C}$ are chosen in such a way, the χ has the right form under certain constraints. HAY and WADT used this form [220] until CHRISTIANSEN et al. [199] proved, that this form causes too strong bonds and too short bond lengths. CHRISTIANSEN et al. suggested constructing χ_{l} from two parts. HAY and WADT followed their suggestion for the ECP used in this work. The first part is a polynomial $\mathrm{p_{nl}}$ (2.58) and the second part is the original orbital ϕ_{Vl}. At a point $\mathrm{r_C}$ close to the outermost maximum the polynomial turns into ϕ_{Vl}.

$$p_{nl}(r) = r^b\,(a_{n0} + a_{n1}\,r + a_{n2}\,r^2 + a_{n3}\,r^3 + a_{n4}\,r^4) \tag{2.58}$$

l is the quantum number of the angular momentum of the electron. In the non relativistic case b = l + 3. The remaining five coefficients $\mathrm{a_{ni}}$ are determined in such a way, that

1. $\mathrm{p_{nl}(r)}$ and its first three derivatives match ϕ_{Vl} and its first three derivatives at $\mathrm{r_C}$.
2. χ_{nl} remains normalized.

The precise criteria to which the coefficients of the pseudo orbitals are optimized differ from paper to paper. The contribution of the original HF orbitals to the pseudo orbitals of the type (2.57) is about 80% to 95%[9]. It may be higher for pseudo orbitals of the second type (2.58). A change of the criteria did not much alter the pseudo orbitals. Only the swapping between the two forms (2.57) and (2.58) makes a significant difference.

After the determination of the pseudo orbitals in a numerical form starts the extraction of $\mathrm{U^{core}}$.

$$(a)\quad U_l^{core}(r) = E_{nl} - \frac{\hat{h}\,\chi_{nl}}{\chi_{nl}} \quad l < L \qquad\qquad (b)\quad U_l^{core}(r) = E_{nl} - \frac{\hat{h}\,\phi_{Vnl}}{\phi_{Vnl}} \quad l \geq L \tag{2.59}$$

L is defined as $\mathrm{l_{max}} + 1$, where $\mathrm{l_{max}}$ is the maximum angular quantum number of the core electrons. HAY and WADT [214] use for their pseudo potentials a combination of (2.59a) and (2.59b).

$$U_l^{core}(r) = E_{nl} - \frac{l(l+1)}{2r^2} + \frac{Z}{r} + \frac{\chi_{nl}"}{2\phi_{Vnl}} - \frac{\hat{V}_{nl}\,\chi_{nl}}{\phi_{Vnl}} = E_{nl} - \frac{l(l+1)}{2r^2} + \frac{Z}{r} + \frac{\chi_{nl}"}{2\phi_{Vnl}} \tag{2.60}$$

$\hat{\mathrm{V}}_{\mathrm{val}}$ contains the electron electron interaction of the valence electrons. Since the theory described here considers only one valence electron, this term may be omitted. The rest follows from the definition of $\hat{\mathrm{h}}$.

$$\hat{h} = -\frac{1}{2}\nabla^2 - \frac{Z}{r} + \frac{l(l+1)}{2r^2} \tag{2.61}$$

---

[9] Figures calculated from table I in the basic paper of KAHN et al. [219]

The last term of (2.61) is the centrifugal energy, which may be regarded as a result of the separation of the radial and the angular part of the atomic wavefunction. The combination of (2.59a) and (2.59b) is done in the fourth term of (2.60), where the second derivative of the pseudo orbital is divided by the original valence orbital.

For wavefunctions with l < L the pseudo orbitals have to be used to ensure the right nodal behaviour in the core region. Electrons with l $\geq$ L have automatically the right behaviour and the original HF orbitals ϕ_V are used for the construction of $\mathrm{U^{core}}$.

The ECP strongly depends on the angular momentum of the electrons while l < L. For l $\geq$ L the difference between different $\mathrm{U_l^{core}}$ is negligible [219, 221].

$$(a) \quad U_{l+1}^{core}(r) \ncong U_l^{core}(r) \quad l < L \qquad\qquad (b) \quad U_l^{core}(r) \cong U_L^{core}(r) \quad l > L \tag{2.62}$$

For l < L contains $\mathrm{U_l^{core}}$ the coulomb and the exchange potentials and $\mathrm{V^{GPK}}$. For l > L $\mathrm{U_l^{core}}$ does not contain $\mathrm{V^{GPK}}$ as the orthogonality of those angular states to the core states is ensured automatically by their spatial parts. The spatial dependencies of the coulomb and exchange part are small and can be ignored.

The different forms of $\mathrm{U_l^{core}}$ can be unified by using angular momentum projection operators.

$$U^{core} = \sum_{l=0}^{\infty} \sum_{m=-l}^{l} U_l^{core}(r)\, |lm\rangle\langle lm| \tag{2.63}$$

The combination of (2.62) and (2.63) with the standard closure property $\sum\sum |\mathrm{lm}\rangle\langle\mathrm{lm}| = 1$ leads finally to the form of $\mathrm{U^{core}}$.

$$U^{core}(r) = U_L^{core}(r) + \sum_{l=0}^{L-1} \sum_{m=-l}^{l} |ml\rangle[U_l^{core}(r) - U_L^{core}(r)]\langle lm| \tag{2.64}$$

The first term $\mathrm{U_L^{core}}$ provides a basic potential in which all valence electrons move. It contains the coulomb and exchange potentials, which are rather angular independent. This is expressed in (2.62b). The second term provides the repulsive term $\mathrm{V^{GPK}}$ which is strongly angular dependent. The coulomb and exchange parts with small angular dependence cancel each other out.

The last step is an analytic expression for the pseudo orbitals and potentials. The ECP is fitted with a set of gaussian functions.

$$r^2[U_l^{core}(r) - U_L^{core}(r)] = \sum_k d_k\, r^{n_k}\, exp[-\zeta r^2] \qquad l = 0, 1, \ldots, L-1 \tag{2.65}$$

$$r^2\left[U_L^{core}(r) - \frac{N_C}{r}\right] = \sum_k d_k\, r^{n_k}\, exp[-\zeta r^2] \qquad l = L$$

$\mathrm{N_C}$ is the number of core electrons. At an infinite distance from the nucleus the spatial arrangement of the core electrons is irrelevant. The valence electron moves in a repulsive field caused by the coulomb interaction between the valence electron and all core electrons gathered together at the nucleus.

$$(U_l^{core}(r))_{r\to\infty} = \frac{N_C}{r} \tag{2.66}$$

Gaussian functions are useful, because nearly all quantum chemical codes today use gaussian orbitals and therefore have the facilities to handle gaussian functions.

The choice of L is interesting. Some authors do not choose the value suggested by the theory [eg 221]. They argue that in a molecular environment usually only s-, p- and d- electrons are involved in a chemical bond. Therefore, it is not necessary to include f-type repulsive functions in the ECP. The potentials used in this work [189, 214, 215] use the full range. For platinum L equals four (g-type) and therefore f electrons are handled correctly.

The ECP would force any basis set into orbitals of the right shape. So in theory any basis set could be used in theory. But this would be a waste, since those basis sets are expected to reproduce the correct nodal behaviour of the HF wavefunctions in the core region. To keep the computational efforts at a minimum, the pseudo orbitals χ are also fitted to gaussian functions and published with the ECP. The basis set used for this work uses the original exponents [189, 214, 215] but has a double zeta quality [222] by rearranging the functions into new groups.

2.6.2 Relativistic Quantum Mechanics and Core Potentials

As the charge of the nucleus increases, the electrons move faster. For heavy atoms like platinum relativistic corrections of the quantum mechanical results have to be made. The basis of relativistic quantum mechanics is given by the Dirac equation. While most textbooks discuss only the results of this approach [192, 194] very few books [197, 223, 224] discuss the equation itself. This section of the thesis summarizes the chapter of CHRISTOFFERSEN's book [197] to show the origin of the different effects.

The force acting on a particle with the mass m, moving with the velocity v can be described with Newton's laws of motion.

$$F = \frac{d}{dt} p = \frac{d}{dt}(mv) \tag{2.67}$$

The mass is allowed to vary with its velocity according to the relativistic mass correction, where m_0 denotes the particle's rest mass.

$$m = \frac{m_0}{\sqrt{1-(v/c)^2}} \tag{2.68}$$

While the particle moves in an electromagnetic field, two forces are acting on the particle. First, the coulomb interaction with the electric field q·E and second the Lorentz force (q/c)(v × B).

$$\frac{d}{dt}\left\{\frac{m_0\, v}{\sqrt{1-(v/c)^2}}\right\} = F = q\,E + \left(\frac{q}{c}\right)\,(v \times B) \tag{2.69}$$

E is the strength of the electric field and B is the density of the magnetic flux. Rearrangement converts equation (2.69) into its final form for the construction of the Dirac equation.

$$\begin{gathered} E = -\nabla\phi - \frac{1}{c}\frac{\partial A}{\partial t} \qquad\qquad B = \nabla \times A \\ \frac{d}{dt}\left\{\frac{m_0\, v}{\sqrt{1-(v/c)^2}} + \left(\frac{q}{c}\right) A\right\} = -q\,\nabla\phi + \left(\frac{q}{c}\right)\,(v \cdot \nabla A) \end{gathered} \tag{2.70}$$

The Hamiltonian is built from equation 2.70 via the Lagrangian function L including interparticle interactions V.

$$\begin{gathered} p_i = \frac{\partial L}{\partial \dot{q}_i} = \int F_i\, dt \qquad\qquad H = \sum p_i\, \dot{q}_i - L \\ H = \sqrt{c^2\left[\hat{p} - \left(\frac{q}{c}\right) A\right]^2 + m_0^2\, c^4} + q\,\phi + V \end{gathered} \tag{2.71}$$

The Hamiltonian (2.71) is difficult to use due to the square root. The factorisation of the Hamiltonian into a product of two four-component vectors forms the basis of the actual Dirac equation. For a hydrogen atom A equals zero and the potential in which the electron moves is given by $-\mathrm{e}^2/\mathrm{r}$. The tedious rearrangement of the corresponding Dirac equation is omitted here for the sake of brevity and the results of the calculation are taken from SCHWABL's book [194].

From the solution of the Dirac equation for the hydrogen atom three correction terms for the single electron follow directly:

1. The relativistic energy momentum correlation (square-root of (2.71)) introduces a correction to the electron's kinetic energy.

$$E = \sqrt{c^2\,\hat{p}^2 + m_0^2\,c^4} = m_0\,c^2 + \frac{\hat{p}^2}{2m_0} - \frac{1}{8}\,\frac{(\hat{p}^2)^2}{m_0^3\,c^2} + \dots \tag{2.72}$$

The first term of the expansion is the energy mass relation, the second the non relativistic kinetic energy and the third the relativistic correction to the kinetic energy. The Hamiltonian of the hydrogen atom would be:

$$\hat{H}_0 = \frac{\hat{p}^2}{2m_0} - \frac{e_0^2}{r} \qquad \hat{H}_1 = -\frac{1}{8}\,\frac{(\hat{p}^2)^2}{m_0^3\,c^2} \qquad \hat{H} = \hat{H}_0 + \hat{H}_1 \tag{2.73}$$

. The rest energy $\mathrm{m}_0\,\mathrm{c}^2$ is constant and can be separated from the energy expression.

2. The electron orbiting around the proton can be regarded as the source of a magnetic field B $= -(\mathrm{v} \times \mathrm{E})/\mathrm{c}$. This field interacts with the electron's spin S. The interaction is called the spin orbit coupling.

$$\begin{aligned}\frac{-e}{m_0\,c}\,\hat{S}\cdot\hat{B} &= \frac{e}{m_0\,c^2}\,\hat{S}\cdot(\hat{v}\times E) = \frac{e}{m_0\,c^2}\,\hat{S}\cdot\left(\frac{\hat{p}}{m_0}\times E\right) = \frac{-e}{m_0^2\,c^2}\,\hat{S}\cdot(\hat{p}\times\nabla\phi) \\ &= \frac{1}{m_0^2\,c^2}\,\hat{S}\cdot\left(\hat{p}\times\frac{\vec{r}}{r}\,\frac{dV(r)}{dr}\right) = \frac{1}{m_0^2\,c^2}\,\hat{S}\cdot\hat{L}\,\frac{1}{r}\,\frac{dV(r)}{dr}\end{aligned} \tag{2.74}$$

After the introduction of the magnetogyric ratio for an electron $\mathrm{g_e} = \frac{1}{2}$, equation 2.74 and the solution of the Dirac equation become equivalent. The correct expression for the hydrogen atom would be:

$$\hat{H}_2 = \frac{1}{2\,m_0^2\,c^2}\,\hat{S}\cdot\hat{L}\,\frac{1}{r}\,\frac{d}{dr}V(r) = \frac{1}{2\,m_0^2\,c^2}\,\hat{S}\cdot\hat{L}\,\frac{Ze^2}{r^3} \tag{2.75}$$

The expectation value $<\mathrm{H}_2>$ of the spin orbit coupling has the following value:

$$\left\langle\hat{H}_2\right\rangle_{n,\,j=l\pm\frac{1}{2},\,l} = \frac{m_0\,c^2(Z\alpha)^4}{4\,n^3\,l\,(l+\frac{1}{2})\,(l+1)}\begin{pmatrix} l \\ -l-1\end{pmatrix} \tag{2.76}$$

α is the fine structure constant. Since l appears in the denominator of (2.76), spin orbit coupling is only possible for electrons with $\mathrm{l} \geq 1$.

3. The last term H_3 from the Dirac equation of the hydrogen atom is the Darwin term.

$$\hat{H}_3 = \frac{\hbar^2}{8\,m_0^2\,c^2}\,\nabla^2 V = \frac{\pi\,\hbar^2\,e^2}{2\,m_0^2\,c^2}\,\delta(r) \tag{2.77}$$

A physical interpretation of the Darwin term is found few text books. They all take H_3 as a result of the Dirac equation for the hydrogen atom. According to SCHWABL [194b] the position of a localized electron is uncertain $\delta\mathrm{r} = \frac{\hbar}{\mathrm{m\,c}}$, which looks like a combination of the

Heisenberg uncertainty relation and Einstein mass energy equivalent. Due to this uncertainty feels the electron an average field from the nucleus.

$$\langle V(r+\delta r)\rangle = V(r) + \frac{1}{6}\,(\delta r)^2\,\nabla^2 V(r) \tag{2.78}$$

The second term of the right-hand side of equation 2.78 has the same form as H_3 (2.77). The Darwin term is purely relativistic.

Due to the delta function in the far right term of (2.77) the Darwin term is only relevant for s-electrons. Since only the wavefunctions of s electrons have a non vanishing value at the nucleus. The expectation value of H_3 has the following value:

$$\left\langle \hat{H}_3 \right\rangle_{n,\,j,\,l} = \frac{m_0\,c^2\,(Z\alpha)^4}{2\,n^3}\delta_{l,0} \tag{2.79}$$

The value is formally identical with the expectation value of H_2 (2.76) with $\mathrm{j} = \frac{1}{2}$ and $\mathrm{l} = 0$.

All three relativistic corrections are about the same size and $(\mathrm{Z}\cdot\alpha)^2$ times $(1.9\cdot 10^4$ for hydrogen) smaller than the coulomb interaction. The relativistic effects are small in comparison with other quantum effects and a perturbation approach for relativistic effects is appropriate.

The next relativistic correction[10] is the Lamb shift. The Lamb shift is caused by the quantisation of the electromagnetic field and has the same structure as the Darwin term, but again is $\alpha \log{(1/\alpha)}$ times smaller (about 64 for hydrogen). The hyperfine structure is caused by the interaction of the electrons with the spin of the nucleus. The hyperfine interaction is even smaller.

The development of relativistic pseudopotentials [189, 214, 215] starts with introduction of the mass-energy ($\hat{\mathrm{H}}_1$) and the Darwin operator ($\hat{\mathrm{H}}_3$) into the nonrelativistic Hartree-Fock atomic equation [221].

$$\begin{aligned}\Bigg(-\frac{1}{2}\frac{d^2}{dr^2}+\frac{l(l+1)}{2r^2}+\hat{V}_{nl}-\frac{\alpha^2}{2}\left[\epsilon_{nl}-\hat{V}_{nl}^{lo}\right]^2 &-\\ \frac{\alpha^2}{4}\delta_{l,0}\left\{1+\frac{\alpha^2}{2}\left[\epsilon_{nl}-\hat{V}_{nl}^{lo}\right]\right\}^{-1}\frac{\partial V_{nl}^{lo}}{\partial dr}\left(\frac{d}{dr}-\frac{1}{r}\right)\Bigg)P_{nl} &= \epsilon_{nl}\,P_{nl}+\sum_{n'l}\epsilon_{nl,n'l}\,P_{nl}\end{aligned} \tag{2.80}$$

$\mathrm{V_{nl}} = -\frac{\mathrm{Z}}{\mathrm{r}} + \mathrm{V_{nl}^{HF}}$ is the potential, in which the electron moves and $\mathrm{V_{nl}^{lo}}$ its localized version. To obtain radial wavefunctions, which are independent of a j quantum number, the spin orbit term has been omitted by KAHN et al. [221]. Although the spin-orbit coupling term H_2 has been omitted, the relativistic Hartree Fock approach (HFR) describes correctly the enlargement of the d and f orbitals and the shrinking of the s and p orbitals. The influence onto orbitals with l $\neq$ 0 is only indirect, since the Darwin operator works only with s orbitals. Table 2.2 shows the expectation values for $\langle \mathrm{r}^2\rangle$ for the uranium and the corresponding values of pure Hartree-Fock (HF) and Dirac-Hartree-Fock (HFD) calculations.

Table 2.2 demonstrates how well the approach given by equation 2.80 reproduces the j-averaged results of the Dirac-Hartree-Fock calculation (av. HFD). The data also justify the use of the Darwin operator instead of the spin orbit coupling operator, since the changes of the 7s orbital are by far the greatest in the table. Non relativistic wavefunctions based on equation 2.80 can be described by three component vectors, while relativistic wavefunctions from Dirac-Hartree-Fock calculations need four component vectors.

---

[10] Please refer to [192, 194, 224] for details.

	$5f_-$	$5f_+$	$6d_-$	$6d_+$	7s	$6p_-$	$6p_+$
HF	1.94		9.63		28.8	4.11	
HFR	2.57		12.4		21.5	3.73	
HFD	2.53	2.67	11.1	13.7	21.8	3.13	4.08
av. HFD	2.61		12.7		—	3.76	

Table 2.2: Expectation value of $\langle r^2 \rangle$ in bohr for different uranium orbitals [221]

The relativistic pesudopotentials by Hay and Wadt [189, 214, 215] are based on HFR calculations (equation 2.80). The determination of relativistic pseudopotentials is the same as the calculation of the nonrelativistic potentials once the pseudo orbitals χ_{nl} are known. The difference between both orbitals is the exponent b of the orbital's core part (2.58). For orbitals with $l \neq 0$, $b = \lambda + 2$.

$$\lambda + 1 = \sqrt{l(l+1) + \frac{1}{4}(l + \delta_{l,0})^2 + (\alpha Z)^2} \tag{2.81}$$

For s orbitals a 6th degree polynomial is used instead of the fifth degree polynomial and b is set equal to $\lambda + 3$. Since the pseudo orbitals and potentials are based on HFR calculations the mass-energy and the Darwin term are incorporated into any calculation which uses those potentials. If spin orbit coupling is important for the calculation, spin orbit coupling has to be introduced later into the calculation as a perturbation. The coupling constants might be taken from HFD calculations or spectroscopic data.

Ermler et al. [225] used a j-averaged pseudopotential basing on a Dirac-Hartree-Fock calculation of xenon for the quantum chemical analysis of Xe_2 and Xe_2^+. Wadt et al. [226] did an analysis of the same molecules using their approach based on equation 2.80. Both groups obtained nearly the same results for interaction energies and bondlengths. This result is hardly surprising, since calculations at an atomic level (table 2.2) showed how well the nonrelativistic approach reproduces the values of j-averaged HFD calculations. The simplification does not cause any additional errors during molecular calculations. The difference between the theoretical and the experimental values is caused by two effects.

1. Comparison with all electron calculations showed the ECP calculations to predict too short bond distances and too high bonding energies. Those differences are caused by the poor description of the inner core part of the pseudo orbitals χ_{nl} [199].
2. Additional spin orbit calculations improve the overall performance of the ECP calculations. The improvements of the results are too small to overcome the error due to the incorrect form of the pseudo orbitals. The small differences between calculations with relativistic and nonrelativistic ECP suggest, that for xenon compounds relativistic effects are negligible and the main relativistic effect is the spin orbit coupling.

Similar investigations of AuH, AuCl, HgH and HgCl were done by Hay et al. [227]. For heavy metal atoms relativistic effects of the core electrons are important. The calculations show that the correct relative energies of different atomic states are impossible to determine without relativistic corrections. The calculations show that further improvement could be achieved by correlation calculations. Additional spin orbit calculations improve the performance and good reproduction of the experimental value is possible. Without spin orbit coupling, calculations with relativistic ECP give good j averaged results.

The use of relativistic ECPs by HAY and WADT [189, 214, 215] in combination with correlation calculations should form a good basis for the calculation of platinum clusters as surface models, because the largest error caused by the poor description of the pseudo orbitals core part has been corrected. The analysis of the gold and mercury compounds also showed that even a qualitative analysis of heavy metal compounds would be impossible without the use of relativistic core potentials. Spin orbit coupling could only be achieved by perturbation of the final results. The coupling constants are usually taken from spectroscopic experiments.

2.7 Interactions between different electronic states

The problems of intersections and intersystem crossings are widely covered by basic quantum mechanics text books. This section follows the reasoning of LANDAU and LIFSHITZ [228] and GILBERT and BAGGOT [229].

2.7.1 Intersection of Potential Energy Curves

E_1(r) and E_2(r) describe the total energy of an adduct as a function of the distance r between the components of the binary complex. To decide whether an intersection can occur, it is convenient to start the examination at a point r_0, where E_1 and E_2 are very close but not similar. E_1 and E_2 are eigenvalues of Ψ_1 and Ψ_2 with the hamiltonian $\hat{H}_0$ at r = r_0. The new hamiltonian after a small movement of δr towards the possible intersection has the following form:

$$\hat{H} = \hat{H}_0 + \hat{V} \qquad\qquad \hat{V} = \delta r \frac{\partial \hat{H}_0}{\partial r} \tag{2.82}$$

The energies at this new point can be regarded as eigenvalues of the new hamiltonian (2.82). The according wavefunction Ψ_T is built from the eigenfunctions Ψ_1 and Ψ_2 of the unperturbed hamiltonian $\hat{H}_0$.

$$\begin{gathered} \Psi_T = c_1\Psi_1 + c_2\Psi_2 \\ (\hat{H}_0 + \hat{V})\Psi_T = E\Psi_T \quad \text{and} \quad \hat{H}_0\Psi_1 = E_1\Psi_1 \quad \text{and} \quad \hat{H}_0\Psi_2 = E_2\Psi_2 \\ c_1(E_1 + \hat{V} - E)\Psi_1 + c_2(E_2 + \hat{V} - E)\Psi_2 = 0 \end{gathered} \tag{2.83}$$

The multiplication of this equation on the left by Ψ_1^* and Ψ_2^*, integration and rearrangement directly lead to the secular determinant and an expression for E.

$$\begin{vmatrix} E_1 + V_{11} - E & V_{12} \\ V_{21} & E_2 + V_{22} - E \end{vmatrix} = 0 \tag{2.84}$$

$$E = \frac{1}{2}(E_1 + E_2 + V_{11} + V_{22}) \pm \sqrt{\frac{1}{4}(E_1 - E_2 + V_{11} - V_{22})^2 + |V_{12}|^2}$$

If the energy values of the two terms become equal at the point r_0 + δr (the two curves intersect) both values of E have to be the same. This happens as the square root term in equation (2.84) vanishes.

$$E_1 - E_2 + V_{11} - V_{22} = 0 \qquad\qquad V_{12} = 0 \tag{2.85}$$

$V_{12} = \langle \Psi_1 | \hat{V} | \Psi_2 \rangle$ vanishes as Ψ_1 and Ψ_2 have different symmetries. $\hat{V}$ is always totally symmetric, since no symmetry operation can alter the energy of the perturbation. This integral only has a non vanishing value, if the function to be integrated transforms totally symmetrically. This is only possible, if both wavefunctions Ψ have the same symmetry. Once V_{12} has vanished, the term on the left side of (2.85) can be set equal to zero by a suitable choice of δr. Therefore, two terms can only cross if they have different symmetries including the spin.

2.7.2 Photoexcitation and Intersystem Crossings

Photoexcitation can alter the electronic state of a molecule. A photoexcitation is possible, if the transition moment is not equal to zero. The transition moment is one result of the time dependent perturbation theory of the transition.

The interaction of light with a molecule's dipole moment can be described as a perturbation of the molecule. Since the vector of the electric field of the light changes with the time, the perturbation analysis has to be time dependend. $\hat{H}_0$ is the time independent hamiltonian of the molecule and Ψ_1^0 and Ψ_2^0 are stationary eigen functions of $\hat{H}_0$.

$$\begin{aligned} i\hbar \frac{d}{dt}\Psi &= \hat{H}_0\,\Psi & \hat{H}_0\,\Psi_1^0 &= E_1\,\Psi_1^0 & \Psi_1 &= \Psi_1^0\,e^{-(i/\hbar)E_1 t} \\ & & \hat{H}_0\,\Psi_2^0 &= E_2\,\Psi_2^0 & \Psi_2 &= \Psi_2^0\,e^{-(i/\hbar)E_2 t} \end{aligned} \tag{2.86}$$

The interaction with the light is described with the perturbation operator $\hat{H}^S$ and the wavefunction Ψ_T is a linear combination of Ψ_1^0 and Ψ_2^0.

$$i\hbar \frac{d}{dt}\Psi_T = (\hat{H}_0 + \hat{H}^S)\,\Psi_T \qquad \Psi_T = c_1\,\Psi_1^0 + c_2\,\Psi_2^0 \tag{2.87}$$

$$i\hbar\left(\Psi_1\frac{dc_1}{dt} + \Psi_2\frac{dc_2}{dt}\right) + i\hbar\left(c_1\frac{d\Psi_1}{dt} + c_2\frac{d\Psi_2}{dt}\right) = c_1\hat{H}_0\Psi_1 + c_2\hat{H}_0\Psi_2 + c_1\hat{H}^S\Psi_1 + c_2\hat{H}^S\Psi_2$$

$$i\hbar\left(\Psi_1\frac{dc_1}{dt} + \Psi_2\frac{dc_2}{dt}\right) = c_1\,\hat{H}^S\,\Psi_1 + c_2\,\hat{H}^S\,\Psi_2$$

Multiplication with Ψ from the left side and integration lead to two expressions for the constants c.

$$\frac{dc_1}{dt} = \frac{1}{i\hbar}\left[c_1\left\langle\Psi_1\left|\hat{H}^S\right|\Psi_1\right\rangle + c_2\left\langle\Psi_1\left|\hat{H}^S\right|\Psi_2\right\rangle\right] \tag{2.88}$$

$$\frac{dc_2}{dt} = \frac{1}{i\hbar}\left[c_1\left\langle\Psi_2\left|\hat{H}^S\right|\Psi_1\right\rangle + c_2\left\langle\Psi_2\left|\hat{H}^S\right|\Psi_2\right\rangle\right] \tag{2.88a}$$

At the beginning ($t = 0$) is Ψ_T equal to Ψ_1, since nothing has happened and therefore $c_1 = 1$ and $c_2 = 0$. Shortly after the start of perturbation c_1 remains close to one and c_2 is still so small, that c_2 can be neglected safely. This line of reasoning leads to the following expression for c_2 (2.88a).

$$\frac{dc_2}{dt} = \frac{1}{i\hbar}\left\langle\Psi_2\left|\hat{H}^S\right|\Psi_1\right\rangle \tag{2.89}$$

At the end of transition c_2 equals one and c_1 equals zero. Therefore, c_2 has to change its value during the transition and $\frac{dc}{dt}$ can not be zero. The time derivative does not vanish, if the integral does not vanish.

$$\left\langle\Psi_2\left|\hat{H}^S\right|\Psi_1\right\rangle = \left\langle\Psi_2^0\,e^{-(i/\hbar)E_2 t}\left|\hat{H}^S\right|\Psi_1^0\,e^{-(i/\hbar)E_1 t}\right\rangle = e^{-(i/\hbar)(E_2-E_1)t}\left\langle\Psi_2^0\left|\hat{H}^S\right|\Psi_1^0\right\rangle$$

$$\hat{H}^S = -\mu\,E = -\mu\,E_0\,\cos(2\pi\nu t) \tag{2.90}$$

$$\left\langle\Psi_2^0\left|\hat{H}^S\right|\Psi_1^0\right\rangle = -E_0\,\cos(2\pi\nu t)\,\langle\Psi_2^0\,|\,\mu\,|\,\Psi_1^0\rangle = -E_0\,\cos(2\pi\nu t)\,H_{21}^S$$

The problem of the vanishing integral can be reduced to a integral $\mathrm{H}^{\mathrm{S}}_{21}$, which contains only stationary wavefunctions Ψ^0 and the molecule's dipole moment μ. $\mathrm{H}^{\mathrm{S}}_{21}$ is called the transition moment and allows a quick decision whether a transition is possible or not.

The components of μ transform like a translation along the axis of the coordinate system. Only if the product $\Psi^0_2 \cdot \mu \cdot \Psi^0_1$ transforms totally symmetrically, has the transition moment a non vanishing value.

The wavefunctions in the transition moment $\mathrm{H}^{\mathrm{S}}_{21}$ may be separated into their spatial ψ^0_{i} and their spin parts χ_{i}:

$$\left\langle \Psi^0_2 \,|\, \mu \,|\, \Psi^0_1 \right\rangle = \left\langle \psi^0_2 \,|\, \mu \,|\, \psi^0_1 \right\rangle \left\langle \chi_2 \,\middle|\, \chi_1 \right\rangle = \left\langle \psi^0_2 \,|\, \mu \,|\, \psi^0_1 \right\rangle \delta_{ij} \qquad i,j = \alpha, \beta \tag{2.91}$$

The transition moment vanishes as the ground and the excited state have different spins. Photoexcitation does not allow a change of the molecule's multiplicity.

A change of a molecule's multiplicity is still possible. Intersystem crossing is usually observed after photoexcitations of organic molecules with substituents, which contain heavy atoms. The molecule relaxes in a non radiative way from the first excited singlet state into the lowest lying triplet state.

Only the total angular momentum has to be conserved. The multiplicity of a wavefunction may change, if the angular momentum of the spatial part changes simultaneously. A coupling between the spin and the electron's angular momentum may be achieved with the relativistic spin-orbit-coupling operator[11] $\hat{\mathrm{H}}^{\mathrm{SO}}$. The spin-orbit interaction can be introduced into the calculation as a perturbation of the non-relativistic part. During the calculation a mixing term $< {}^3\Psi \,|\, \hat{\mathrm{H}}^{\mathrm{SO}} \,|\, {}^1\Psi > \equiv \mathrm{H}^{\mathrm{SO}}_{31}$ arises, which is the direct equivalent of the transition moment. Since $\hat{\mathrm{H}}^{\mathrm{SO}}$ transforms as a rotation, a conclusion whether $\mathrm{H}^{\mathrm{SO}}_{31}$ vanishes or not can be reached quickly with the help of a character table.

The possibility of an intersystem crossing is usually rather small. As $\hat{\mathrm{H}}^{\mathrm{SO}}$ behaves as Z^4 [229] a change of the molecule's multiplicity is likely for a platinum compound.

2.8 Dipole-Dipole Interaction and Polarisation

The theory of electric polarisation is well understood [23, 230]. Since it includes a large part of the nonadditive contributions to the water-water interaction potential, it is important to understand its background beginning with the dipole moment.

A set of point charges $\mathrm{q_i}$ is scattered around the origin. The calculation of the electrostatic potential φ at a point $\vec{\mathrm{r}}$ is straight forward.

$$\varphi = \frac{1}{4\pi\epsilon_0} \sum_i \frac{q_i}{r - r_i} = \frac{1}{4\pi\epsilon_0} \sum_i \frac{q_i}{\sqrt{(x-x_i)^2 + (y-y_i)^2 + (z-z_i)^2}} \tag{2.92}$$

---

[11] The first part of the multi electron spin-orbit coupling operator [192] describes the interaction between the electron's angular momentum and its spin. The second part represents the same interaction between one electron and the remaining electrons.

$$\hat{H}^{SO} = \sum_k \frac{g_k\,\beta_k}{2\,m_k\,c\,\hbar} \left(\frac{\nabla_k V}{e_k} \times \hat{p}_k \right) \cdot \hat{s}_k + \sum_k \sum_{\neq l} \frac{g_k\,\beta_k\,e_l}{m_l\,c\,\hbar}\,\frac{1}{r^3_{kl}} \left((\vec{r}_k - \vec{r}_l) \times \hat{p}_l \right) \cdot \hat{s}_k \qquad \beta_k = \frac{-e_0\,\hbar}{2\,m_e\,c}$$

$\mathrm{g_e} = 2.0023$ is the gyromagnetic factor of an electron.

As long r_i is small in comparison with r the potential φ can be described by a Taylor series $\varphi(r - r_i) = \varphi(r) - r_i \cdot (d\varphi/dr)$.

$$\begin{aligned} \varphi &= \frac{1}{4\pi\epsilon_0}\left\{\sum_i \frac{q_i}{r} + \frac{1}{r^3}\left[x\sum_i q_i\, x_i + y\sum_i q_i\, y_i + z\sum_i q_i\, z_i\right]\right\} \\ &= \frac{1}{4\pi\epsilon_0}\left\{\frac{q}{r} + \frac{1}{r^3}(\vec{r}\cdot\vec{\mu})\right\} \qquad \vec{\mu} = \sum_i q_i \vec{r}_i \qquad q = \sum_i q_i \end{aligned} \tag{2.93}$$

q is the total charge of the cluster and μ its dipole moment. Further expansion of (2.93) yields higher multipole moments. Only if the cluster carries no net charge (q = 0) is the dipole moment independent of the chosen coordinate system. All higher multipole moments depend on the chosen frame.

The electrostatic potential φ_μ and the strength of this field E_μ can be derived directly from (2.93).

$$\varphi_\mu = \frac{1}{4\pi\epsilon_0}\frac{(\vec{\mu}\vec{r})}{r^3} \qquad E_\mu = -\nabla\varphi_\mu = \frac{-1}{4\pi\epsilon_0}\frac{1}{r^3}\left[\vec{\mu} - 3\frac{(\vec{\mu}\cdot\vec{r})\vec{r}}{r^2}\right] \tag{2.94}$$

The energy ϵ_i of a point charge q_i in an electric field φ by other point charges q_j and dipoles μ_k is:

$$\epsilon_i = q_i\varphi = \frac{q_i}{4\pi\epsilon_0}\sum_{j=1}^{N}\frac{q_j}{r_{ij}} + \frac{q_i}{4\pi\epsilon_0}\sum_{k=1}^{M}\frac{(\vec{\mu}_k\cdot\vec{r}_{ik})}{r_{ik}^3} \tag{2.95}$$

and the energy ϵ_i of a dipole μ_i in an electric field depends on the field's strength E.

$$\epsilon_i = \mu_i\vec{E} = \frac{\mu_i}{4\pi\epsilon_0}\sum_{j=1}^{N}\frac{q_j}{r_{ij}^2} + \frac{1}{4\pi\epsilon_0}\sum_{k=1}^{M}\left(\frac{(\vec{\mu}_i\cdot\vec{\mu}_k)}{r_{ik}^3} - 3\frac{(\vec{\mu}_i\cdot\vec{r}_{ik})(\vec{\mu}_k\cdot\vec{r}_{ik})}{r_{ik}^5}\right) \tag{2.96}$$

Equations (2.95) and (2.96) allow us to determine the interaction energy V between two molecules ($r_{12} = -r_{21}$) with charges q_1, q_2 and dipole-moments μ_1 and μ_2.

$$\begin{aligned} V(\vec{r}) &= \frac{1}{4\pi\epsilon_0}\left(\frac{q_1 q_2}{r^2} + q_1\frac{(\vec{\mu}_2\cdot\vec{r})}{r^3} - q_2\frac{(\vec{\mu}_1\cdot\vec{r})}{r^3} + \frac{1}{r^3}\left[(\vec{\mu}_1\cdot\vec{\mu}_2) - 3\frac{(\vec{\mu}_1\cdot\vec{r})(\vec{\mu}_2\cdot\vec{r})}{r^2}\right]\right) \\ V_{(H_2O)_2}(\vec{r}) &= \frac{1}{4\pi\epsilon_0}\frac{1}{r^3}\left[(\vec{\mu}_1\cdot\vec{\mu}_2) - 3\frac{(\vec{\mu}_1\cdot\vec{r})(\vec{\mu}_2\cdot\vec{r})}{r^2}\right] \end{aligned} \tag{2.97}$$

Since the water molecule does not carry any charge, the water-water interaction consists only of dipole-dipole and higher multipole interactions.

Since the dipole moment of a neutral molecule is independent of the chosen origin of the coordinate system, the dipole moment may be placed anywhere in the molecule. As long as the initial boundary condition ($r \gg r_i$) is fulfilled and the distance between the two molecules is much bigger then a single molecule, is the precise position unimportant. As the distance gets shorter the total interaction energy depends on the position of dipole moment. Figure 2.4 demonstrates this effect. To calculate the figures for the plot two AB molecules are placed in an antiparallel position with separation d. The molecules are assumed to be 1 Å long (r) and each centre carries a charge (q) of 1 e. The dipole moment μ of the molecule is 1 Åe = 4.8 D [17b].

$$V_A = 2K\left[\frac{q^2}{\sqrt{d^2+r^2}} - \frac{q^2}{d}\right] \qquad V_B = -K\frac{\mu^2}{d^3} \qquad V_C = K\frac{2\,\mu^2\,r^2 - \mu^2\,d^2}{(d^2+r^2)^{\frac{5}{2}}} \qquad K = \frac{1}{4\pi\epsilon_0} \tag{2.98}$$

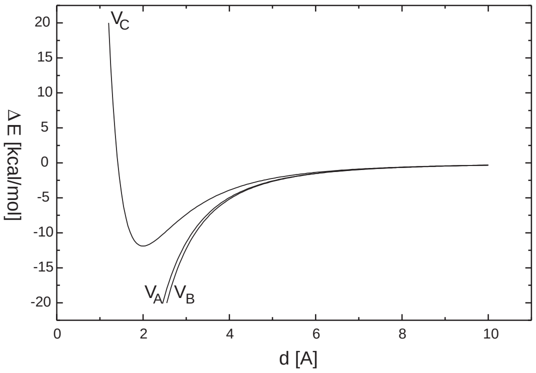

Figure 2.4: Dipole-dipole interaction.

V_A is the interaction between both molecules calculated by the summation of the coulomb interaction between the individual charges. V_B and V_C are calculated with the help of (2.97). For the calculation of V_B the dipole moment was placed at the molecule's centre and for V_C onto the negative charge. V_B is good description of the exact coulomb interaction (V_A), while V_C is only suitable for long distances ($d \geq 5r$).

The position of the dipole moment on the negative charge seems to be a good guess, since the dipole moment points from the negative charge to the positive charge. On the other hand it is physically impossible to explain the minimum at $d = 2r$ of V_C with the point charge model. The positioning of the dipole moment at the centre of the molecule is closer to the initial idea, where the individual charges are clustered around the origin. Therefore, the Taylor series is merely a projection of the electrostatic characteristics into the centre of the molecule. This demonstrates that although the size of the dipole moment is independent of the chosen coordinate system, the interaction energy of two dipoles depends strongly on the position of the dipole moment in the molecule.

The interaction energy of the two AB molecules in a linear head to tail orientation (V_D) is twice as large as in an antiparallel position (V_B).

$$V_D = -K\frac{2\mu^2}{d^3} \tag{2.99}$$

In such an orientation two opposite charges can get very close to each other. The exploding coulomb energy overpowers everything else. A prototype of such an AB molecule is hydrogen fluoride. The dimer has a bent head tail orientation. The experimental FFH angle is 116° and theory predicts an angle between 110° and 120° [208b]. The general description of the relatively simple HF hydrogen bond by dipole moments describes only the basic orientation. For a better description the chemical bond has to be considered either by quantum chemical calculations or by the introduction of higher multipole terms. The hydrogen cyanide dimer is linear with a head tail orientation [208b, 231]. The orientation of the free electron pairs controls the details of the hydrogen bond while the dipole dipole interaction only allows a rough estimate.

The electric field induces an additional dipole moment. The net dipole-moment of a molecule in an electric field is the sum of its static dipole-moment μ and the induced dipole-moment p.

$$\vec{\mu}_{net} = \vec{\mu} + \vec{p} = \vec{\mu} + \alpha'\vec{E} \qquad \vec{p} = \alpha'\vec{E} \tag{2.100}$$

α' is the polarisation ($\alpha' = (4\pi\epsilon_0)\ 1.45\ \text{Å}^3$ for water) [15]. For the ease of reading the polarized volume $\alpha = \alpha'/(4\pi\epsilon_0)$ is used for the following equations[12].

An induced dipole moment causes an electric field, which induces other dipole-moments. Therefore all induced dipole moments are coupled together. The polarisation between two charged molecules can be described by the following set of equations:

$$\vec{p}_1 = -\frac{\alpha_1 q_2 \vec{r}}{r^3} - \frac{\alpha_1}{r^3}\left(\vec{\mu}_2 - \frac{3(\vec{\mu}_2 \cdot \vec{r})\vec{r}}{r^2}\right) - \frac{\alpha_1}{r^3}\left(\vec{p}_2 - \frac{3(\vec{p}_2 \cdot \vec{r})\vec{r}}{r^2}\right) \tag{2.101}$$

$$\vec{p}_2 = +\frac{\alpha_2 q_1 \vec{r}}{r^3} - \frac{\alpha_2}{r^3}\left(\vec{\mu}_1 - \frac{3(\vec{\mu}_1 \cdot \vec{r})\vec{r}}{r^2}\right) - \frac{\alpha_2}{r^3}\left(\vec{p}_1 - \frac{3(\vec{p}_1 \cdot \vec{r})\vec{r}}{r^2}\right) \tag{2.101a}$$

Böttcher [230] published the most elegant solution for this problem. In the first step $\vec{\mathrm{p}}_2$ in equation 2.101 is replaced by equation 2.101a. Then (2.101) is used to figure out $(\vec{\mathrm{p}}_1 \cdot \vec{\mathrm{r}})$. This result is used to replace $(\vec{\mathrm{p}}_1 \cdot \vec{\mathrm{r}})$ in the result of the first step. Tedious rearrangement leads to the following equation for $\vec{\mathrm{p}}_1$:

$$\begin{aligned}
\vec{p}_1 &= -\frac{\alpha_1}{r^3}\left[\frac{q_2}{A_4}\vec{r} + \frac{1}{A_1}\vec{\mu}_2 - \frac{A_2}{A_1 A_4}\frac{3(\vec{\mu}_2\vec{r})\vec{r}}{r^2}\right] + \frac{\alpha_1\alpha_2}{r^6}\left[\frac{2q_1}{A_1}\vec{r} + \frac{1}{A_1}\vec{\mu}_1 + \frac{1}{A_1 A_4}\frac{3(\vec{\mu}_1\vec{r})\vec{r}}{r^2}\right] \\
\vec{p}_2 &= -\frac{\alpha_2}{r^3}\left[\frac{-q_1}{A_4}\vec{r} + \frac{1}{A_1}\vec{\mu}_1 - \frac{A_2}{A_1 A_4}\frac{3(\vec{\mu}_1\vec{r})\vec{r}}{r^2}\right] + \frac{\alpha_1\alpha_2}{r^6}\left[\frac{-2q_2}{A_1}\vec{r} + \frac{1}{A_1}\vec{\mu}_2 + \frac{1}{A_1 A_4}\frac{3(\vec{\mu}_2\vec{r})\vec{r}}{r^2}\right] \\
A_n &\equiv 1 - \frac{n\alpha_1\alpha_2}{r^6}
\end{aligned} \tag{2.102}$$

In an analogous fashion $\vec{\mathrm{p}}_2$ can be determined. This allows the calculation of an improved value for V(r) and therefore to get an estimate for the nonadditive interactions.

Two models for water are widely used:

1. The water molecule is a homogeneous particle with no charge and a dipole-moment.

$$\vec{p}_1 = -\frac{\alpha_1}{r^3}\left[\frac{1}{A_1}\vec{\mu}_2 - \frac{A_2}{A_1 A_4}\frac{3(\vec{\mu}_2 \cdot \vec{r})\vec{r}}{r^2}\right] + \frac{\alpha_1\alpha_2}{r^6}\left[\frac{1}{A_1}\mu_1 + \frac{1}{A_1 A_4}\frac{3(\vec{\mu}_1 \cdot \vec{r})\vec{r}}{r^2}\right] \tag{2.103}$$

2. The water molecule consists of independent charges and only the oxygen is polarizable. No atom has a dipole-moment on its own. Now a calculation with a single charge is not possible. The charges in (2.96) have to be replaced by the sum of all charges in the system.

$$\vec{S}_i = \sum_{i \neq j} \frac{(\vec{r}_{ij} q_j)}{r_{ij}^3} \tag{2.104}$$

$$\vec{p}_1 = \frac{\alpha}{A_1}\left[-\vec{S}_1 - \frac{\alpha}{r^3}\left(-\vec{S}_2 + \frac{3\alpha}{r^5 A_4}(\vec{S}_1\vec{r})\vec{r} + \frac{3A_2}{r^2 A_4}(\vec{S}_2\vec{r})\vec{r}\right)\right]$$

---

[12] For a quantum chemical description of polarisation of molecular orbitals and the calculation of the polarizability please refer to ref. 232, while ref. 233 describes the quantum chemical approach towards multipole interactions.

Chapter 3

Quantum Chemistry of small Water Clusters

Water is one of the best analysed substances. The work started with an investigation of a single water molecule, since experimental values are readily available from the literature. The water dimer allows us to test the method's reliability and to obtain information about the water water interactions. The water trimer finally gives additional insight into non additive effects and the formation of small water clusters. Calculations on larger clusters (up to the hexamer) [180] and ice [130] show, that higher cooperative effects than three body forces are not important for the water water interaction.

The clustering of water molecules on metal surfaces is commonly observed [38]. Understanding the mechanism is important for the description of the water metal interface. Additional data on the undisturbed water cluster are therefore necessary to recognise the influence of the metal onto water cluster. Quantum chemical calculations on solvation of ions show that the ordering influence of the ions also controls the water water interaction in the solvation shell. To recognize similar effects at the platinum water interface additional data on the undisturbed water water interactions are also necessary.

3.1 The Water Molecule

The work started with a broad test of different basis sets and methods to calculate the properties of water. Section 11.3 (page 319) of the appendix displays a selection of those experiments.

Most papers on the water dimer start with a short reexamination of water to test the chosen method [110, 113, 115, 118]. Table 3.2 displays the final results for water in comparison with various values taken from the literature. The most useful basis sets to predict the properties of water seems to be the DZP and the TZVP base in combination with MP2 / MP3 calculations (h2o_18 and h2o_9). A combination of a small basis set with a high correlation level obtains usually results of the same high quality as a combination of a large basis set with a low level of correlation. Table 3.1 shows the dfifference between the experimental values and the best GAMESS UK results.

At first sight h2o_9 seems to yield the best results, since the geometry is slightly better than that of h2o_18. On the other hand, the electronic properties of h2o_18 are much better. The quantum chemical dipole moment μ_{QC} (equation 3.1a) is a sensitve measure of wavefunction quality.

		experiment	h2o_9	h2o_18	h2o_18
basis set		—	TZVP	DZP	6-311++G**
method		—	MP2	MP3	MP2
ω	[deg]	104.5	104.84	104.89	104.05
r_{OH}	[Å]	0.9572	0.9576	0.9590	0.9588
μ	[D]	1.85	2.2354	2.1512	1.8988
q_O^b	[e]	-0.66^a	-0.58	-0.65	-0.57
q_H^b	[e]	$+0.33^a$	$+0.29$	$+0.325$	$+0.29$

[a] point charge model [b] Mulliken population analysis

Table 3.1: Optimized water geometries.

Although the dipole moment of h2o_18 is higher than experiment it is still better than h2o_9. As a further test the charges of the bonded atoms were calculated. The quantum mechanical charges are calculated by Mulliken population analysis [190] of the MP2/MP3 density matrices. The experimental charges were calculated from the experimental dipole moment μ assuming a fixed geometry (r_{OH} = 0.9572 Å, ω = 104.52°) and a simple point charge model (μ_{PC}, equation 3.1b).

$$\text{(a)}\quad \mu_{QC} = e\,\langle\Psi|\,r\,|\Psi\rangle \qquad\qquad \text{(b)}\quad \mu_{PC} = q_0\,r_{OH}\,\cos\left(\frac{\omega}{2}\right) \tag{3.1}$$

Together with a conversion factor of 1 D = 3.336·10^{-30} C m and an experimental dipole moment μ = 1.85 D [17] equation (3.1) yields an oxygen charge of 0.66 e. The charges calculated for h2o_18 (DZP MP3) are much better than those calculated for h2o_9 (TZVP-MP2).

The best values for geometry and electronic properties were found with 6-311++G** MP2 calculations. Sadly those calculations are too costly to be used for bigger clusters. The reproduction of the experimental dipole moment is excellent. The charges found by quantum chemistry are smaller than expected. Two things should be considered when discussing charges:

1. Localized charges at the atoms are not the best model of a water molecule. Basic chemical theory expects a tetrahedral oxygen atom with two nonbonding electron pairs. Molecular orbital theory describes the same effect with a nonbonding ($3a_1$) and another bonding orbital ($1b_1$). In both cases electron density is moved away from the oxygen nucleus and the hydrogen atoms. This movement increases the distance between negative and positive charges. The same dipole moment could be achieved with smaller charges than the point charge model predicts. The point charge model therefore predicts only an upper limit for the charges.

   The molecule's geometry is an experimental well-established fact. Any model, which is based on something else has to make considerably more assumptions about the electron distribution. The point charge model is therefore a sound basis for the exploration of the dipole moment.

2. The charge of an atom in a molecule is not a physical observable and cannot be calculated directly from the molecule's wavefunction. Assumptions of the distribution of the electrons between the atoms have to be made. The quantum chemically calculated charges therefore depend on the model used for their computation and are difficult to compare.

The problems with the quantum chemical calculation of charges are shown by a comparison of the Hartree Fock (HF) charges with MP2 charges. Using the 6-311++G** basis set the dipole moment

		experiment	Kim[d]	h2o_17	h2o_18	h2o_9	h2o_12	h2o_28	h2o_46	h2o_47
method		—	MP2	MP2	MP3	MP2	MP3	MP2	MP2	MP3
basis set		—	DZP[b]	DZP	DZP	TZVP	TZVP	6-311++G**	TZVP+1[e]	TZVP+1[e]
functions		—	25	26	26	32	32	83	33	33
ω	[deg]	104.5	104.7	104.71	104.89	104.84	105.21	104.05	104.84	104.95
r_{OH}	[Å]	0.957	0.963	0.9621	0.9590	0.9576	0.9532	0.9588	0.9576	0.9535
dipol.	[D]	1.85	2.161	2.1653	2.1512	2.2354	2.2085	1.8988	2.2355	2.2129
q_O	[e]	−0.66[a]	−0.65[c]	−0.66	−0.65	−0.58	−0.57	−0.57	−0.58	−0.57
q_H	[e]	+0.33[a]	+0.32[c]	+0.33	+0.325	+0.29	+0.285	+0.29	+0.29	+0.295
E_{ELEC}	[H]	—	—	−85.1935	−85.2228	−85.2457	−85.2872	−85.2399	−85.2457	−85.2850
E_{NUC}	[H]	—	—	+9.1474	+9.1765	+9.1904	+9.2316	+9.1802	+9.1904	+9.2294
E_{RHF}	[H]	−76.0675[f]	—	−76.0461	−76.0463	−76.0553	−76.0556	−76.0596	−76.0554	−76.0556
E_{MP2}	[H]	—	—	−0.2110	−0.2107	−0.2356	−0.2353	−0.3054	−0.2360	−0.2357
E_{MP3}	[H]	—	—	—	−0.0063	—	−0.0036	—	—	−0.0036
E_{TOTAL}	[H]	−76.4802[d]	−76.25484	−76.2571	−76.2634	−76.2910	−76.2945	−76.3650	−76.2913	−76.2948

[a] Charges calculated from the experimental dipolmoment (pointcharge model)

[d] [118]

[b] Kim uses one basis function less than GAMESS UK (section 2.4, page 23).

[e] TZVP basis set from GAMESS UK plus additional s-orbital

[c] Kim did not mention the method of calculation.

[f] Hartree Fock limit [113]

Table 3.2: Compilation of the main results for water in comparison with results from experiments and literature.

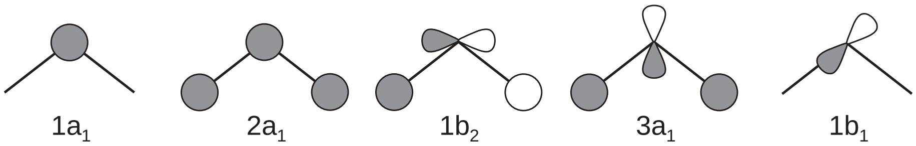

Figure 3.1: Sketch of the molecular orbitals of water.

changes form 1.9677 D (HF) to 1.8998 D (MP2) and the oxygen charge from −0.62 e (HF) to −0.57 e (MP2). The changes of the geometry and the charges would suggest a rise of about 2.11% of the dipole moment. Actually is the dipole moment 3.57% larger. The charges and the dipole moment are not well correlated and the charges therefore do not form a good basis for comparison. Consequently the quantum chemical dipole moment μ_{QC} was chosen as the main criterion.

According to general expectation the wavefunction's quality should increase with the number of basis functions. The row 'functions' of table 3.2 displays the numer of basis functions for each calculation. As the number of basis functions increases from 26 to 32 on changing the basis from DZP to TZVP an improvement of the wavefunction's quality should be expected, but the opposite was found.

An error of GAMESS UK is very unlikely, since the calculations reproduce very well the results of Kim for DZP-MP2 computations (table 3.2, [118]). In the next step the eigenvectors for each calculation were checked carefully. The main difference can be observed for the polarising d-type orbitals on oxygen. In DZP calculations those orbitals contribute mainly to the $3a_1$ orbital of water (figure 3.1). In TZVP calculations they contribute significantly to the $1a_1$ and the $2a_1$ orbitals. This indicates, that the TZVP basis set might not be well balanced. To check this, equation 2.31 and 2.32 (section 2.4, page 23) were used to add an additional s-type function to the TZVP basis set. The radial maximum of the electron density of this function was at the same place as the maximum of the d-orbitals. This basis set was used for full geometry optimizations at MP2 and MP3 levels (h2o_46 and h2o_47). The geometry and the electronic properties did not change during the MP2 calculation while those values improved on a MP3 level. On the electronic level the relative contributions to the $3a_1$ orbital increased while the relative contributions to the $1a_1$ and the $2a_1$ orbitals decreased. At the same time the contributions of the original s-type orbitals to the the $1a_1$ and $2a_1$ orbitals decreased slightly while their contribution to the $3a_1$ increased. This increasing s character of the $3a_1$ orbital might be the reason for the shrinking of the bonding angle in the water molecule.

The introduction of the additional s orbital did not change the geometry at MP2 level, but lowered the energy about 0.0003 H (0.188 kcal/mol). The Hartree Fock energy changed only slightly (0.0001 H) but the MP2 energy is about 0.0003 H lower. The extra orbital increases the flexibility of the basis set and therefore lowers the Hartree Fock energy. The jump in the MP2 energy is causes by the enlargement of the correlation space.

The TZVP basis set seems to be not well balanced and therfore yields poorer results than the smaller DZP basis set. Dunning, Jr [234] made similar conclusions in his work on Gaussian basis sets in correlated molecular calculations. He suggests that a DZ basis set for first row elements should at least contain one d-type function as polarisation function. A TZ basis set should contain at least two d-functions and one f-function. They are necessary to give a reliable description of the lone electron pairs. The DZP and the TZVP basis sets of GAMESS UK only contain one d-function as polaristion function. The DZP basis is therfore much closer to the suggested optimum than the

	B_2 / ν_3 [cm^{-1}]		A_1 / ν_1 [cm^{-1}]		A_1 / ν_2 [cm^{-1}]		
	ω_{harm}	diff[a]	ω_{harm}	diff[a]	ω_{harm}	diff[a]	⟨diff⟩[f]
exp.[c]	3942	—	3832	—	1648	—	—
exp. N_2[bc]	3913	—	3808	—	1649	—	—
Kim - RHF[c]	4290	+348	4165	+333	1753	+105	262
Kim - MP2[c]	4056	+114	3906	+ 74	1663	+ 15	68
Kim - MP4[c]	4038	+ 96	3903	+ 71	1675	+ 27	65
RHF[d]	4290	+348	4166	+334	1753	+105	262
MP2[d]	4052	+110	3905	+ 73	1664	+ 16	66
MP3[e]	4037	+ 45	3875	+ 53	1611	- 37	61

[a] experimental value - calculated value [b] isolated in a nitrogen matrix [c] [118] [d] calculated with Gaussian 94 - analytic frequencies [e] calculated with GAMESS UK - numeric frequencies
[f] mean of the absolut values

Table 3.3: Harmonic vibrational frequencies of water calculated with a DZP basis set.

TZVP basis.

The optimized geometries were the starting point for the calculation of the vibrational frequencies.

The analytic MP2 frequency calculations have the same reliability as the expensive MP4 calculations of Kim. The calculation of the frequencies at higher correlation level than MP2 has to be done numerically. It is therefore difficult to gain additional accuracy by increasing the correlation level from MP2 to MP3. The quality of the frequencies depends strongly on the quality of the optimized geometry [190, 235, 236] and the chosen method. Sadly Kim does not give any information about these topics. The frequencies are therefore difficult to compare, although the data suggest that the frequencies at the HF and MP2 level published by Kim were calculated analytically. The importance of correlation calculations is evident from tables 3.3 and 3.4. The quality of the frequency calculation greatly improves with the introduction of electron correlation. Also the entropy S^0 improves with introduction of electron correlation. The results of the MP2 calculation are in reasonable agreement with the experimental values. Again the numerical value is poorer than the analytical one. Analytical MP2 frequencies form a sound basis for the thermochemical analysis of water clusters. At a reasonable price the frequencies are of similar quality and the MP2 entropy is even better than the MP3 value. The MP3 frequencies are not shifted in the same direction. A shift in the same direction is desirable, since it facilitates the comparison of different results. The value of heat capacity is not a well chosen indication, since gaseous water is not an ideal gas and $C_P - C_V = R$ is therefore not strictly true. The zero point vibrational energy of 13.757 kcal/mol found with the MP2 calculation is therefore the most reliable value.

	S^0 [cal/mol/K]	C_V [cal/mol/K]
RHF[a]	44.955	5.992
MP2[a]	45.095	6.003
MP3[b]	45.071	6.012
exp.[c]	45.104	6.039

[a] Gaussian 94 - analytic
[b] GAMMESS UK - numeric
[c] [15] $C_V = (C_P - R)$

Table 3.4: Thermodynamic properties of water.

Table 3.5 displays the effect of the basis set's size on the Hartree Fock energy during pure RHF calculations. The biggest influence on the total energy is the addition of polarisation functions to the DZ basis. This indicates that polarisation functions are more important than the actual size of the basis set. The basis set closest to Hartree Fock limit (6-311++G**, 83 functions), the only one which yielded excellent geometrical and electronic properties simultaneously (table 3.2, h2o_28), is already so large, that it was impossible to perform any correlation calculations on the dimer with HP 710 and HP 730 workstations at Newcastle.

Table 3.6 shows the ground state coefficient c_0 for various correlation calculations. In all cases c_0 equals 0.974 to three significant figures. The small figure indicates the importance of correlation calculations for water. The close similarity of c_0 for DZP MP2 and the DZP CI calculations prove that single and double excitations significantly contribute to the ground state. This justifies the use of MP calculations instead of CI calculations for correlation effects.

basis set	E_{RHF} [H]	num
DZ	−76.0110	14
DZP	−76.0469	26
TZVP	−76.0560	32
6-311++G**	−76.0604	83
HF limit[a]	−76.0675	infty

[a] [113]

Table 3.5: RHF results for water.

basis set	DZP	DZP	TZVP	6-311++G**
method	MP2	CI	MP2	MP2
c_0	0.974381	0.974129	0.974202	0.974129

Table 3.6: Ground state coefficients from different correlation calculations.

3.2 Water Dimer

The water dimer and the hydrogen bond are still matters of interest [125], as the water dimer is also a good starting point to analyse proton transfer reactions [237, 238].

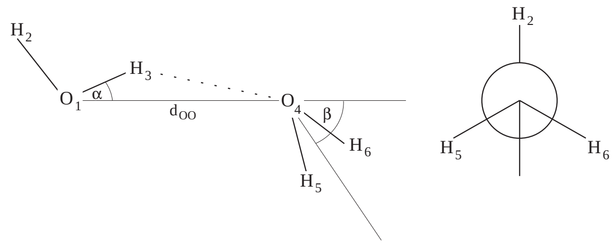

Figure 3.2: Geometry of the water dimer.

According to the literature [125] the configuration shown in figure 3.2 is the most stable configuration of the dimer. The relative positions of the monomers A (O_1, H_2, H_3) and B (O_4, H_5, H_6) can be described by the three variables d_{OO}, α and β. d_{OO} is the distance between the oxygen atoms, α the bending angle of the hydrogen bond and β the angle between the molecular plane of monomer B and the extension of d_{OO}. The dihedral angles $H_2O_1O_4H_5$ and $H_2O_1O_4H_6$ were always kept equal to conserve C_S symmetry.

3.2.1 Single Point Calculations

Table 3.7 displays a short compilation of previous results from the literature. The oxygen-oxygen distance tends to be too short and the basis set error corrected energies too small. Only the bending

ref.	basis	method	d_{OO} [Å]	α [deg]	β [deg]	ΔE [kcal/mol]	ΔE^{b}_{BSSE} [kcal/mol]
[118][a]		experiment	2.967 ± 0.03	1 ± 10	57 ± 10	-5.44 ± 0.7	
[118][a]		experiment	2.98 ± 0.01	1 ± 6	58 ± 6	-5.50 ± 0.5	
[118]	DZP	RHF	2.9851	1.6	45.5	−5.03	−4.73
[118]	DZP	MP2	2.9009	3.1	54.6	−6.36	−5.03
[118]	DZP	MP4	2.9161	3.1	44.3	−6.17	−4.80
[113]	ccp VDZ	MP4	2.911	4.5	56.8	−7.10	−3.73
[113]	aug ccp VDZ	MP4	2.911	4.5	56.8	−5.20	−4.27
[113]	aug ccp VQZ	MP2	2.911	4.5	56.8	−5.05	−4.81
[112]	DZP'	MP2	3.04	4.7	55.99		−4.35
[131]	6-31G*	SCF	2.971	5.18	62.42	−5.62	
[107]	STO	SCF	2.73	0.735	58.0	−6.09	
[119]		HF	3.00	0	30	−4.6	
[124]	ba1	MP2	2.970	0	60	−6.21	−4.25
[124]	ba1	MP3	2.970	0	60	−6.21	−4.20
[121]	DZP	SCF	3.01	−7.2		−4.55	
[121]	DZP	CI	2.98	−7.2		−5.63	
[110]	ba2	HF	2.980	0	58	−3.612	−3.609
[110]	ba2	MP2	2.980	0	58	−4.781	−4.529
[110]	ba2	MP3	2.980	0	58	−4.728	−4.533
[115]	[531|21]	RHF	3.00	0	40	−4.72	
[130]	ba3	RHF	2.98	2.448	52.26	−7.18	

ba1 : (11,7/6) → [4,3/2] + s,p
ba2 : 7s8p6d1f / 4s2p1d
ba3 : (6111/311/2)(31/2)

[a] Energies and geometries from different references.
[b] BSSE corrected interaction energies
[c] [239]

Table 3.7: Results for the water dimer from previous works.

angle seems to be close to the experimental value. β is usually close to the experimental value, but varies strongly between different calculations.

Figure 3.3 displays the variables optimized for the dimer. Table 3.8 summarizes the main results of single point calculations for the water dimer.

One main feature of the hydrogen bond is the bend of the bond itself (W3 ≠ 90°). Although the importance of this bend for the hydrogen bond is obvious from theoretical and experimental results, the underlying physics are still a matter of discussion. This work started with an examination of the dimer with a linear hydrogen bond. The other variables of the dimer were optimized at different level of theory.

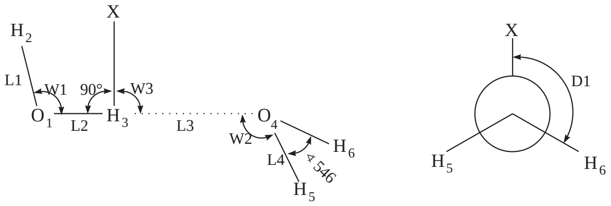

Figure 3.3: Variables of the dimer.

For weak interactions the basis set superposition errors are very important. To get an estimate about this error the counterpoise method of Boys and Bernardi [204] with the full basis set of the second monomer was used. Since the BSSE alters the energy, it also changes the equilibrium geometry. To check the BSSE's influence on the monomer geometry and energy, the combined basis sets were used for a full geometry optimisation of the monomers, while the relative positions of the water molecules were fixed. Table 3.10 shows a compilation of the results for the DZP-MP2 calculation. The energy differences between the calculations with fixed and flexible geometries were very small, usually between 50 and 200 nH. Such a small energy difference is negligible in comparison with an overall interaction energy about 10 mH and an average BSSE about 1 to 2 mH. However, the method has to be used to calculate the influence of the BSSE on the monomers' geometries in the dimer during the analysis of dimer's geometry.

The main quest of quantum mechanical calculations with small basis sets for weak hydrogen bonds is the bond length [125]. Table 3.7 shows how the bond length varies with the chosen method of calculation. The length of the oxygen-oxygen distance is therefore a good measure of the quality of a calculation. The best values were obtained by RHF-MP3 calculations with a DZP basis (dim_10, table 3.8). The angles α and β are still in the experimental range. The BSSE corrected interaction energy of 4.9 kcal/mol for this conformer is at the lower limit of the experimental value but still of a reasonable size. Extended calculations [208e] suggest, that 4.9 kcal/mol is the correct value for the interaction energy. This limit is reached with increasing basis set size. While BSSE uncorrected calculations approach this value from higher interaction energies BSSE corrected calculations approach this limit from the other side.

In the next step the angle W3 was allowed to change during the optimisation. Again the DZP-MP3 calculation gave the best results. The energy difference between the bent and the straight conformation is very small, only 0.014 mH (0.009 kcal/mol), although α changes about 2.5°. This result heralds a major problem: The potential surface of the water dimer is so flat that the geometry optimisation algorithm might stop too early, since the energy becomes approximately constant. To check the geometry the potential energy surface around the optimized geometry was sampled manually. Since all calculations were done with a full BSSE correction, the sampling allows us also to calculate the BSSE of the dimer's geometry (section 3.2.4, page 70).

The influence of the bend seems to negligible, because all changes are of the order of 2%. The bond length to the bonding hydrogen atom in monomer A (L2) slightly increases while simultaneously the hydrogen bond itself (L3) decreases. In summary H3 of monomer A moved away from O1 slightly towards O4 and therefore underlines the importance of bending for proton transfer reactions [237, 238]. The influence of the bending is much stronger in the hydrogen donor (monomer A) than in the hydrogen acceptor (monomer B). The geometry of B hardly changes. This bending also shows how sensitive the dipole moment reacts towards changes in the wavefunction. It changes by about 3% while the charges and the electron transfer do not change at all.

Since all observed changes are very small, the reliability of those changes was checked with the extended BSSE correction for dim_16. The results of this test are displayed in table 3.10.

Table 3.10 shows, that all changes are larger than the BSSE. The increase Δd_{OHb} and the decrease Δd_{OHn} indicate the tightening of the bond to the non bonding hydrogen and the loosening of the bonding hydrogen atom. The charge transfer from B to A is displayed in the increasing bond angle of B. According to the VSEPR model [12] the loss of electrons from the free electron pairs of B reduces the repulsion between them and therefore increases the bond angle towards the value of a tetrahedron (109.47°). The increasing polarisation of the dimer can be deduced from two independent features:

file	exp	[118][d]	dim_7[a]	dim_10[a]	dim_26[b]	dim_16[b]	dim_29[c]	dim_30[c]	dim_19[b]
method		RHF-MP2	RHF-MP2	RHF-MP3	RHF-MP2	RHF-MP3	RHF-MP2	RHF-MP3	RHF-MP2
basis		DZP	DZP	DZP	DZP	DZP	DZP	DZP	TZVP
L1 [Å]	0.9572[e]	0.962	0.9613	0.9584	0.9613	0.9584	0.9572	0.9572	0.9564
L2 [Å]	0.9572[e]	0.9695	0.9686	0.9638	0.9687	0.9640	0.9572	0.9572	0.9637
L3 [Å]			1.9452	1.9717	1.9446	1.9685	1.9575	1.9805	1.9194
L4 [Å]	0.9572[e]	0.9644	0.9635	0.9601	0.9635	0.9600	0.9572	0.9572	0.9582
W1 [deg]	104.52[e]	104.8	104.38	104.89	104.53	105.02	104.52	104.52	104.96
W2 [deg]			111.66	114.07	110.82	114.00			118.68
W3 [deg]			90.0	90.0	93.39	93.85	95.64	94.87	89.9
D1 [deg]			121.42	119.43	121.97	119.48			114.84
∠546 [deg]	104.52[e]	104.98	104.95	105.34	104.92	105.36	104.52	104.52	105.53
d_{OO} [Å]	2.97 ± 0.03[f]	2.9009	2.9138	2.9355	2.9122	2.9311	2.9116	2.9354	2.8832
α[deg]	1 ± 10[f]	3.1	0.0	0.0	2.26	2.59	3.79	3.28	−0.07
β [deg]	57 ± 10[f]	54.8	52.71	47.73	55.44	49.13	55.94	54.57	37.49
q_{O1} [e]		−0.717	−0.70	−0.69	−0.67	−0.69	−0.69	−0.69	−0.61
q_{H2} [e]		+0.323	+0.32	+0.32	+0.32	+0.32	+0.32	+0.32	+0.28
q_{H3} [e]		+0.376	+0.35	+0.36	+0.35	+0.36	+0.35	+0.35	+0.32
q_{O4} [e]		−0.689	−0.66	−0.67	−0.66	−0.67	−0.66	−0.66	−0.61
$q_{H5/H6}$ [e]		+0.353	+0.35	+0.34	+0.35	+0.34	+0.35	+0.34	+0.32
Δq[h] [e]		0.017	0.028	0.021	0.029	0.021	0.028	0.022	0.015
μ [D]	2.6-2.64[f]	3.092	3.2353	3.3082	3.0792	3.1879	2.9265	3.0018	3.6634
E_{RHF} [H]			−152.1000	−152.1006	−152.1000	−152.1006	−152.1008	−152.1009	−152.1187
E_{CORR} [H]			−0.4243	−0.4358	−0.4243	−0.4358	−0.4233	−0.4354	−0.4732
E_{TOT} [H]		−152.5198	−152.5243	−152.5364	−152.5243	−152.5364	−152.5241	−152.5363	−152.5919
ΔE	-5.44 ± 0.7[e]	−6.36	−6.34	−5.96	−6.36	−5.97	−6.2	−5.9	−6.27
ΔE_{BSSE}		−5.03		−4.9	−5.1	−4.89	−5.19	−4.82	−4.9
BSSE		1.33		1.094	1.278	1.08	1.28	1.111	1.339
$\Delta E_{BSSE}(A)$[g]				0.27[i]	0.302[i]	0.248[i]	0.280	0.237	0.399
$\Delta E_{BSSE}(B)$[g]				0.824[i]	0.976[i]	0.832[i]	1.005	0.874	0.94

Table 3.8: Optimized geometries for the water dimer.

All interaction energies in kcal/mol, if not mentioned differently	
a	fixed, straight hydrogen bond
b	free, bended hydrogen bond
c	fixed water geometry, flexible hydrogen bond
d	calculated from given changes
e	no values found, assumed to be close the monomer's values
f	[118], first set, since the bigger error margin included the second set
g	influence of the BSSE onto the monomers
h	charge transfer
i	full monomer geometry optimisation in the presence of ghost orbitals

Table 3.9: Remarks to table 3.8

		free	A_{DIM}	A^{a}_{BSSE}	B_{DIM}	B^{a}_{DIM}
$\sphericalangle_{\mathrm{HOH}}$	[deg]	104.89	105.02	104.92	105.35	104.92
$\Delta\sphericalangle_{\mathrm{HOH}}$	[deg]		+0.13	+0.03	+0.46	+0.03
d_{OHn}	[Å]	0.9590	0.9584	0.9591	0.9600	0.9592
Δd_{OHn}	[Å]		−0.0006	+0.0001	+0.0010	+0.0002
d_{OHb}	[Å]		0.9640	0.9589		
Δd_{OHb}	[Å]		+0.0050	−0.0001		
q_{O}	[e]	−0.65	−0.69	−0.65	−0.67	−0.64
Δq_{O}	[e]		−0.04	0	−0.02	+0.01
q_{Hn}	[e]	+0.325	+0.32	+0.32	+0.34	+0.325
Δq_{Hn}	[e]		−0.005	−0.005	+0.015	0.0
q_{Hb}	[e]		+0.36	+0.33		
Δq_{Hb}	[e]		+0.035	+0.005		

The indices n and b refer to bonding and non bonding hydrogen atoms.

[a] Geometry optimisation with a full set of ghost orbitals.

Table 3.10: Influence of the BSSE onto the monomer's geometry.

1. Electrical charges are transferred from H_3 to H_2 and O_1 as indicated by Δq of monomer A. This might be interpreted as a sign of a possible heteropolar cleavage of the O_1H_3-bond (autoprotolysis).
2. The polarisation of H_3 induces an electron transfer from H_4 and H_5 to O_4. Because of the smaller polarisibility of hydrogen in comparison with oxygen the charge transfer on B is much smaller than on A.

A much better insight into the physics of the hydrogen bond is offered by the analysis of the molecular orbitals and the eigenvectors of the system. Figure 3.4 displays the composition of the bonding orbitals.

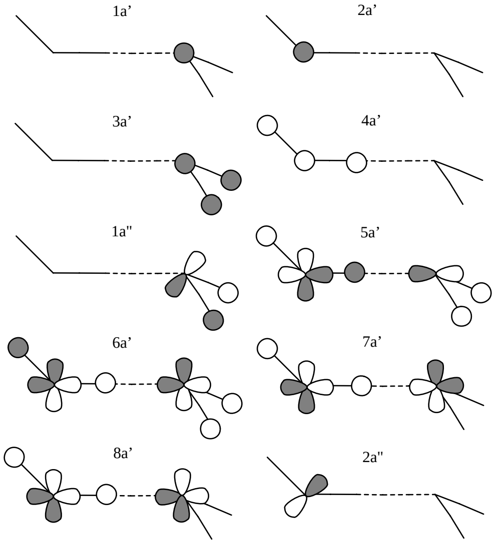

Figure 3.4: Composition of the dimer's MOs.

Only two orbitals, apart of the oxygen 1s orbitals, do not contribute to the molecular orbitals of the water dimer. The donor's $1b_1$ and the acceptor's $1b_2$ orbital transform according to a" in the environment of the water dimer. They are too far away from each other to overlap and therefore do not contribute to the hydrogen bond. The hydrogen bond is formed by the overlapping of inner orbitals. The positively polarised hydrogen atom H3 next to O4 of monomer B leads to a general lowering of the orbital energies. At the same time the close neighbourhood of a lone electron pair of monomer B increases the orbital energies of monomer A (For example the two $2a_1$ orbitals in figure 3.11.). This movement of the orbitals facilitates the combination of the donor's $1b_2$ orbital with the acceptor's $3a_1$ and the overlapping of the $3a_1$ orbital of the donor with the $3a_1$ orbital of the acceptor. Those interactions cause the hydrogen bond. This movement also explains the surprising position of the energy levels of the molecular orbitals. For both interactions the energy of the bonding combination is higher than the energies of the contributing orbitals. The energy of the antibonding combination of the orbitals is lower than the energy of the highest contributing orbital. Figure 3.5 shows a simplification of this movement and the resulting orbitals.

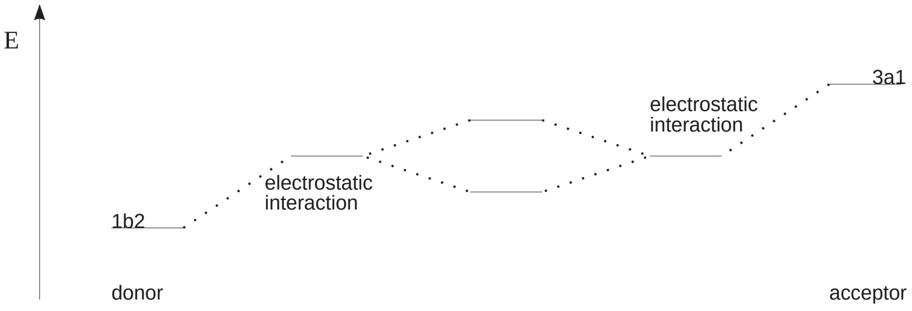

Figure 3.5: Influence of the electrostatic interactions on the orbital energies.

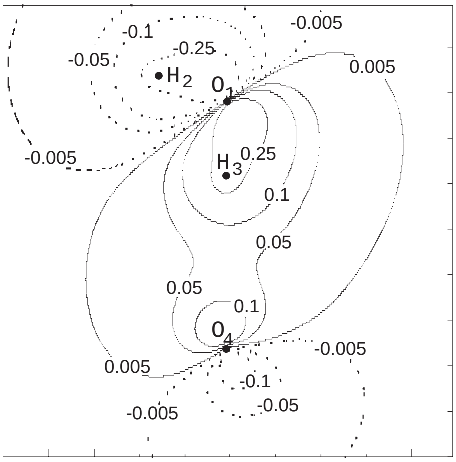

Figure 3.6: MO 5a' of the water dimer.

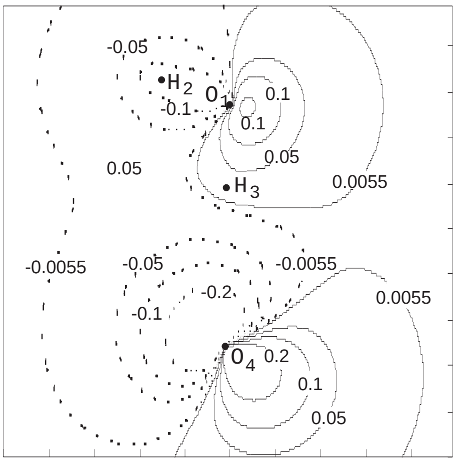

Figure 3.7: MO 6a' of the water dimer.

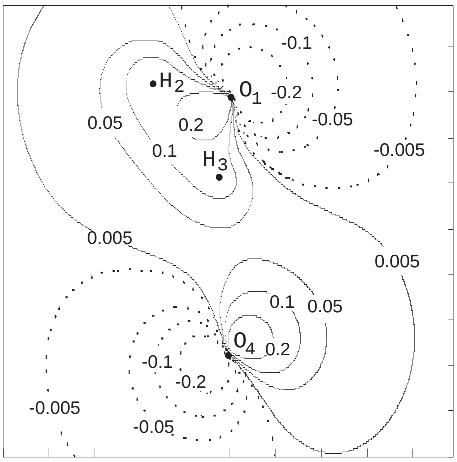

Figure 3.8: MO 7a' of the water dimer.

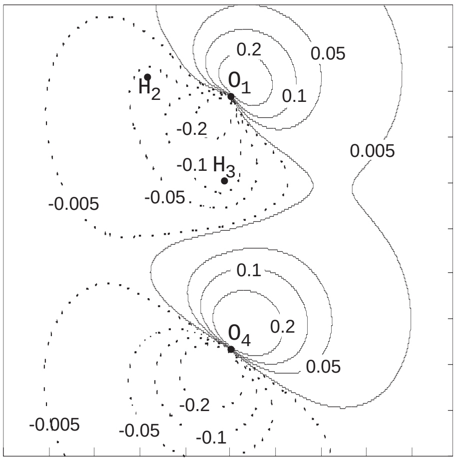

Figure 3.9: MO 8a' of the water dimer.

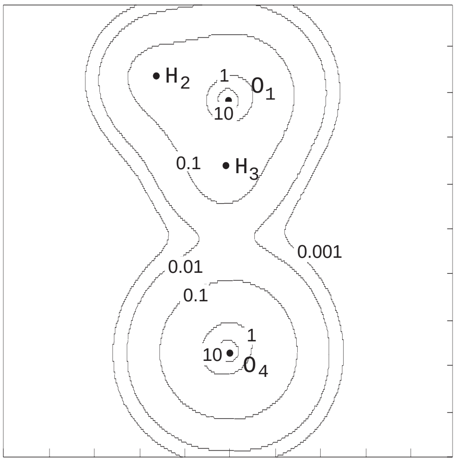

Figure 3.10: Electron density in the symmetry plane.

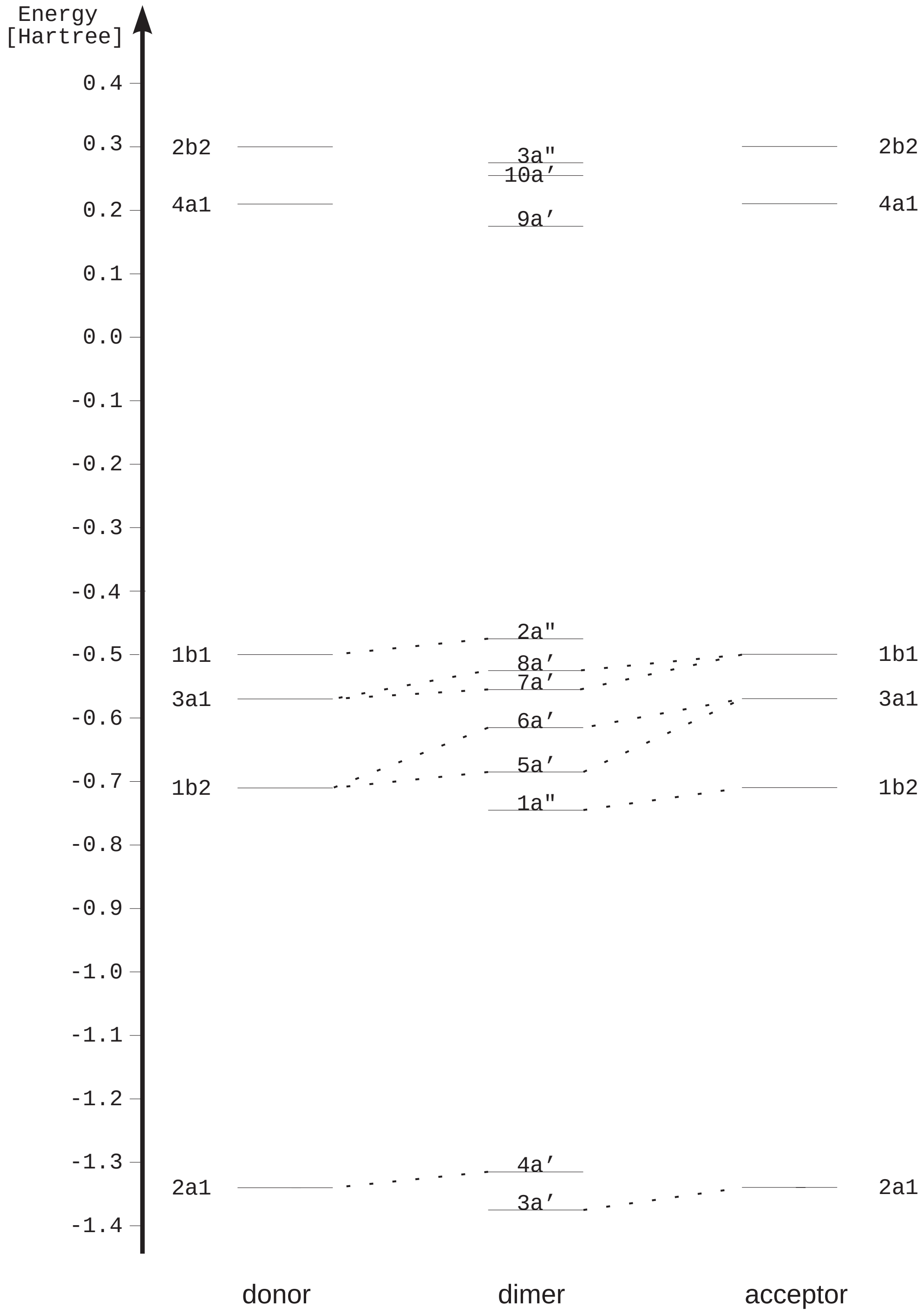

Figure 3.11: Formation of the water dimer.

The bonding orbitals cut along the symmetry plane are displayed in the figures 3.6 to 3.9. Figure 3.10 shows the electron density in the plane of symmetry. The precise movement of the different orbitals during the formation of the dimer is shown in figure 3.11. The analysis of the molecular orbitals can be summarised as follows: ***The formation of hydrogen bonds is not only controlled by electrostatic interactions. The mutual polarisation of the molecules in each others electric field leads to a rearrangement and overlapping of inner molecular orbitals of the monomers.***

CHAKRAVORTY et al. [110] arrived with a similar calculation to the same conclusions. The $1b_2$ and the $3a_1$ orbitals of the donor can be easily identified in the figures 3.6, 3.8 and 3.9. The strong distortion of the $1b_2$ orbital in figure 3.7 makes an identification difficult. Figures 3.6 and 3.7 show the p-component in the symmetry plane of the acceptor's $3a_1$ orbital. Figures 3.8 and 3.9 show a crossection of the free nonbonding p orbital. This interpretation of the figures correlates well with the analysis of the eigenvectors.

An alternative, but inferior, interpretation at an atomic level would be a two-electrons-two-centres (2e2c) bond [29]. Orbital 5a' may be regarded as the bonding interaction of two oxygen 2p-orbitals with a hydrogen 1s. The nonbonding and the antibonding combinations are not populated. In this model the overlap of the hydrogen donor's $3a_1$ with the acceptors $1b_1$ orbital would be neglected. The orbitals 6a', 7a' and 8a' would be regarded as representations of the monomers orbitals. This model could be improved by assuming a four-electron-two-centre (4e2c) bond. Such a bond would be formed between the OH bond of the donor and the lone electron pair of the acceptor. In this model the orbital 6a' would be the nonbonding overlap of the OH bond and the free electron pair. Both models are not satisfactory, since at least two molecular orbitals are unexplainable. On the other hand such a model explains the directionality of the free electron pairs. The MO explanation cannot form anything like a free electron pair, since the monomer's $1b_1$ and $3a_1$ orbitals cannot mix due to their symmetry. The only hint directly given by MO theory for a free electron pair is the small distortion of the electron density (figure 3.10) towards the lower left corner of the plot. YOUNG et al. [240] showed that the electron density is actually not a sensitive quantity to observe lone pairs. The distortion of the electron density by the lone pair is usually small. A better tool for the detection of lone pairs is the molecular electrostatic potential (MEP), which will be used later.

Figure 3.10 also shows how electron density is moved away from the monomers into the dimer's centre to form the hydrogen bond.

The geometry of the bond dimers seems to be reliable. It is not only close to the experimental values but also a good reproduction of calculations reported in the literature [118]. Although the absolute values between KIM et al. and GAMESS UK differ slightly, the changes of the monomers' values due to the formation of the hydrogen bond are a good match as shown in table 3.10.

Sadly KIM does not mention how they calculated the charges. This missing information inhibits a careful examination of the difference between both calculations. The changes in the individual charges calculated with GAMESS UK are smaller than the changes published by KIM (Gaussian 90). At the same time the charge transfer calculated with GAMESS UK is bigger than KIM's value. Contrary to KIM's work our calculations favour charge transfer to polarisation. The difference between the calculations is also reflected by the dipole moment.

All the other parameters except ΔW1 fit nicely. The absolute energy calculated with GAMESS UK is a little lower than the one reported in the literature. This is likely to be the result of the additional two carthesian d-orbitals of the GAMESS basis set.

		[118]	GAMESS UK
E	[H]	−152.51982	−152.52432
ΔE	[kcal/mol]	−6.36	−6.36
ΔE_{BSSE}	[kcal/mol]	−5.03	−5.1
d_{OO}	[Å]	2.9009	2.9121
α	[deg]	3.1	2.3
β	[deg]	54.8	49.12
ΔL3	[Å]	+0.0065	+0.0066
ΔL2	[Å]	−0.0010	−0.0008
ΔL4	[Å]	+0.0014	+0.0014
ΔW1	[deg]	+0.10	−0.18
$\Delta\sphericalangle_{456}$	[deg]	+0.28	+0.21
Δq_{O1}	[e]	−0.071	−0.038
Δq_{H3}	[e]	+0.53	+0.22
Δq_{H2}	[e]	0	−0.012
Δq_{O4}	[e]	−0.043	−0.006
$\Delta q_{\mathrm{H5/6}}$	[e]	+0.030	+0.17
Δq	[e]	0.017	0.029
μ	[D]	3.092	3.188

Table 3.11: Comparisson with [118].

The third part of the single point calculations involved the calculations with a fixed, experimental geometry for the monomers. Table 3.8 displays the results for the DZP-MP2 (dim_29) and for the DZP-MP3 (dim_30) calculations.The values of d_{OO}, α and β are close to the experimental values. The difference between the geometry obtained by calculations with a flexible and a fixed water molecule are smaller than the experimental uncertainties. The angle between the molecular plane of B and the oxygen-oxygen axis is even closer to the experimental value. The BSSE corrected interaction energy differs only 0.07 kcal/mol (1.4 % of the value with a flexible water geometry). These results justify the calculation of the water interaction energy with a fixed water geometry. The advantages of a faster and easier computation outweigh the disadvantage of the slightly higher interaction energy.

All calculations displayed in table 3.8 have a similar BSSE corrected interaction energy close to 4.9 kcal/mol and are therefore close to the true theoretical value [208e]. This shows clearly the benefits of the counterpoise method of Boys and Bernardi for calculations with small basis sets. This value is low in comparison with experiment, but good in comparison with other calculations. At a correlated level calculations even with larger basis sets tend to a BSSE corrected interaction energy about 4.8 to 5.0 kcal/mol. Reliable results with an interaction above 5.0 kcal/mol are rarely reported [125].

The bent dimer calculations were repeated at a TZVP-MP2 level to check the results discussed earlier (section 3.1) regarding the poor balance of the TZVP basis set. For the water monomer the combination of the TZVP basis with RHF-MP2 calculation proved to yield good results. The results for the dimer are much worse than those from DZP-MP3 calculations. The oxygen-oxygen

	experiment[a]	[118][b]		DZP-RHF[c]		DZP-MP2[c]		DZP-MP3[d]	
ν_3 a"acc	3881	4039	(+158)	4279	(+398)	4034	(+153)	4068	(+187)
ν_3 a' don	3899	4021	(+122)	4263	(+364)	4017	(+118)	4051	(+152)
ν_1 a' acc	3797	3897	(+100)	4160	(+363)	3896	(+ 99)	3956	(+156)
ν_1 a' don	3718	3826	(+108)	4116	(+398)	3825	(+107)	3909	(+191)
ν_2 a' don	1669	1700	(+ 31)	1783	(+114)	1701	(+ 30)	1721	(+ 52)
ν_2 a' acc	1653	1665	(+ 12)	1757	(+104)	1667	(+ 14)	1692	(+ 39)
op bending		679		614		668		697	
ip bending		396		352		397		380	
OO stretch		194		170		193		188	
ip bending		167		145		164		164	
op bending		156		144		151		156	
torsion		142		134		141		141	

[a] values from [118] assignment from [239]   [b] DZP - MP2 calculation
[c] analytic frequencies   [d] numeric frequencies
in brackets () the deviation from the experimantal value

Table 3.12: Calculated haronic frequencies of the water dimer [cm^{-1}].

distance is far too small, the hydrogen bond still straight, or bent slightly negative[1] and the tilt of B's molecular plane (β) too small. The BSSE of the TZVP-MP2 calculation is 2.13984 mH and for the DZP MP2 2.03691 mH. More important than the actual size is the ratio between the BSSE and the monomer energies. This ratio for TZVP MP2 calculations is $1.40\cdot10^{-5}$ and for DZP-MP2 is $1.33\cdot10^{-5}$. The BSSE has a stronger impact on the monomers in TZVP-MP2 calculations than in DZP-MP2 calculations. The BSSE of 1.34 kcal/mol of the TZVP-MP2 interaction energy is the largest of the series. This again is a result of the inbalance of the basis set. The s-function of hydrogen has its radial maximum at 2.2216 a.u. and the fifth s-function of oxygen at 1.3981 a.u.. The distance between H3 and O4 is 3.6227 a.u. (1.9197 Å). Along this bond both functions have their maximum at nearly the same place. This results in a strong contribution of the corresponding ghost orbital during the BSSE calculations and therefore in a large value of BSSE. The attempt to minimize simultaneously the oxygen-oxygen repulsion leads to a straight hydrogen bond.

		experiment	[118][a]	DZP-RHF[b]	DZP-MP2[b]	DZP-MP3[c]
$\Delta\nu_3$	[cm^{-1}]	- 14	- 17	- 11	- 18	- 31
$\Delta\nu_3$	[cm^{-1}]	- 32	- 35	- 27	- 35	- 14
$\Delta\nu_1$	[cm^{-1}]	- 11	- 9	- 7	- 9	- 81
$\Delta\nu_1$	[cm^{-1}]	- 90	- 80	- 50	- 80	- 34
$\Delta\nu_2$	[cm^{-1}]	+ 20	+ 37	+ 30	+ 35	- 110
$\Delta\nu_2$	[cm^{-1}]	+ 4	+ 2	+ 4	+ 3	- 81

[a] DZP-MP2   [b] analytical frequencies   [c] numerical frequencies

Table 3.13: Frequency shifts caused by the dimerisation of water.

---

[1] The calculation was repeated with a different start geometry to be sure.

Although there is considerable literature on the infrared spectroscopy of water [139] the harmonic frequencies have proved to be difficult to find [118]. The analytic Gaussian 94 calculations reproduce the frequencies published by KIM et al. (table 3.12), but the absolute values in comparison with experiment are not so good. The similarity of the empirical scaling factors defined by HONNEGER et al. [131] for water (1.023364) and the dimer (1.025363) suggest a high reliability for DZP-MP2 frequency calculations. The experimental frequency shifts due to the hydrogen bond as shown in table 3.13 are well reperoduced. The high frequencies from Hartree Fock calculations suggest a hard force field. Frequency shifts from HF calculations are therefore too small. The shifts are so small, that an error of a few wavenumbers leads to a large scaling factor. Scaling factors are therefore not useful for the analysis of frequency shifts in water polymers. The numerical DZP-MP3 calculation cannot describe the absolute frequencies and frequency shifts, and are unsuitable for the thermochemical analysis of the dimerisation.

The zero point vibrational energy found with the DZP-MP2 calculation is 29.814 kcal/mol. The zero point vibrational energy correction for the formation of the bond is therefore 2.299 kcal/mol. The standard entropy of the complex is 69.278 cal/mol/K. The formation of a dimer is entropically disfavoured by 20.912 cal/mol/K. A reasonable value is 21 cal/mol/K, since a simplified estimate by the equation of SACKUR and TETRODE predicts an entropy decrease about 15 cal/mol/K. The data suggest that the dimerisation of water is primarily energetically driven.

3.2.2 Potential Curve with a Flexible Geometry

This section only covers the quantum chemical aspects of the interaction potentials. Any fits or comparisons of those curves with previously published potentials will be discussed later in section 4.2 (page 88).

The graphs of this section are based on geometry optimisations to include relaxation effects. The distance L3 in figure 3.3 (page 51) was set to a fixed value. This procedure allows a simultaneous description of the water water interaction and the autoprotolysis of water - the main relaxation pathway. The values of L3 spanned a range from 10 Å (essentially infinite separation) to 0.95 Å (roughly r_{OH} in water). The smallest physically sensible oxygen-oxygen distance reached by this way is about 2.2 Å. This distance is close to the oygen-oxygen distance in a linear ion contact pair. All other variables were allowed to vary during the optimization. The chosen level of computation was a RHF-MP3 calculation with a DZP basis set.

Figure 3.12 shows the interaction energy as a function of d_{OO} and figure 3.13 an enlargement of the area around the equilibrium. The BSSE corrected potential curve has its minimum at a different value of d_{OO} than the uncorrected curve. The BSSE corrected minimum is at the point $d_{OO} = 2.9625$ Å with $\Delta E = -5.0$ kcal/mol. The enlargement of the oxygen oxygen distance is directly caused by the BSSE correction. Since the influence of the second monomer's orbitals is eliminated from the curve, the orbitals of the hydrogen atom H3 can no longer compensate for any deficiencies of the oxygen basis set. The unphysical overlap of orbitals caused by the BSSE pulls the monomers closer to each other.

These BSSE corrected values are much closer to the experimental ones and can compete with the results from sophisticated calculations with extended basis sets. This result also emphasises the importance of BSSE correction. To search for the minimum with ordinary algorithms and then do a single point BSSE correction at the resultant optimum is not sufficient. The whole surface has to be scanned near the minimum at a BSSE corrected level [241] (Please refer for details to

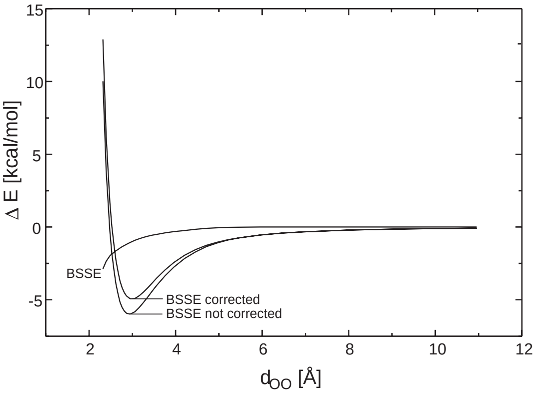

Figure 3.12: Interaction energy and BSSE.

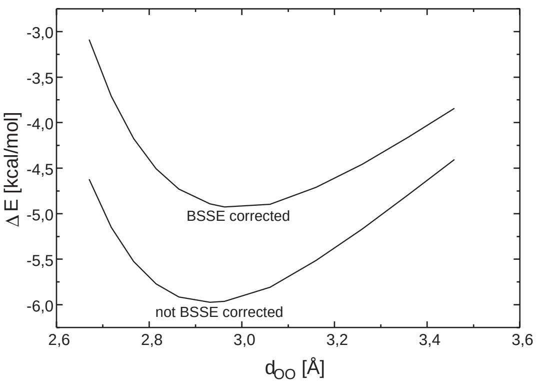

Figure 3.13: Minima in figure 3.12.

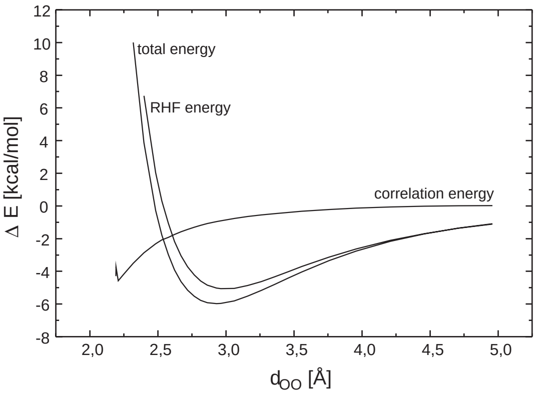

Figure 3.14: Energy composition, not BSSE corrected.

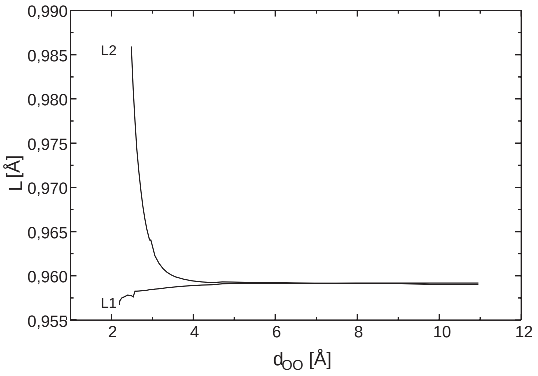

Figure 3.15: Changing of r_{OH} with d_{OO}.

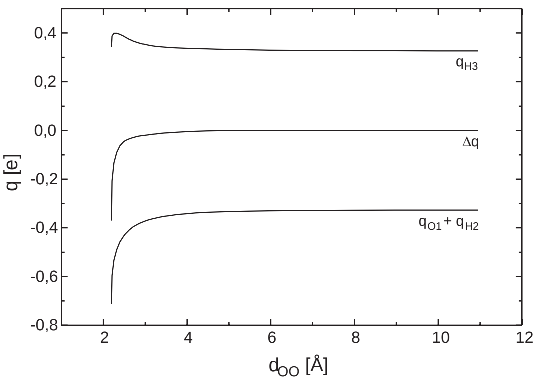

Figure 3.16: Changing of charges during dimerisation.

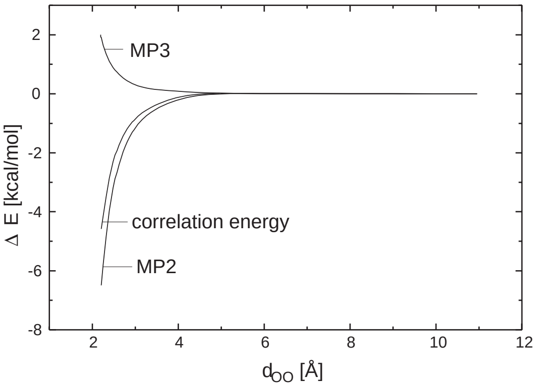

Figure 3.17: Correlation energy vs. d_{OO}.

subsection 3.2.4, page 70).

The composition of the total interaction energy (figure 3.14) shows an interesting feature. The minimum of the correlation energy is at a much smaller oxygen-oxygen distance. Table 3.13 shows how this distance varies with the level of correlation without BSSE correction for different basis sets.

The oxygen-oxygen distance shrinks if the level of calculation changes from RHF to MP2 and increases again with the change from MP2 to MP3. The initial shrinking is not surprising because correlation calculations allow the electrons to avoid each other. This improved description of the electron motion produces a smaller distance between both monomers, since the electrons can now use the wide extensive orbitals to avoid each other. More interesting is the second rise of d_{OO}.

	d_{OO} [Å]		
basis	DZ	DZP	TZVP
RHF	2.836	2.9834	2.9624
MP2	2.834	2.9138	2.8836
MP3	2.855	2.9355	2.8948

Table 3.14: Correlation level and d_{OO}, $\alpha = 0°$

Figure 3.17 shows the composition of the MP3 correlation energy as a function of d_{OO}. As in table 3.14 all values are calculated without BSSE correction. The MP3 part of the correlation energy increases steadily as d_{OO} gets smaller. The opposing effect enlarges the equilibrium distance again. If correlation effects are considered for the water water interaction calculations, the correlation level has to be as high as possible to get a good equilibrium distance.

As the oxygen-oxygen distance gets smaller, L2, the donor's OH bond (figure 3.3, page 51) increases. This indicates a proton transfer and so an autoprotolysis proces. Meanwhile L1, the OH bond in the future hydroxide ion decreases. This shrinkage is in contradiction to chemical expectation, since the the bond lenght of an free hydroxide ion is calculated as 0.9696 Å (table 3.15). The sudden drop of L1 at d_{OO} = 2.529 Å is currently regarded as an artefact of the calculation caused by an extra loop of the geometry optimizer. The whole gap is only 0.0004 Å; a distance well below physical significance.

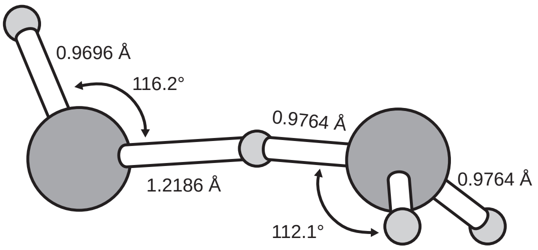

Figure 3.18: Geometry of a possible ion pair.

At small distances the formation of a contact ion pair is possible. Such a pair is energetically unstable, since in the vacuum no solvent can stabilize the charges. Any attempt to optimize the geometry of such a pair without additional constraints ended with a perfect reproduction of the water dimer optimisation. The best possible pair, which looks like a water dimer (d_{OO} = 2.9103 Å, $\alpha = 3.40°$, $\beta = 47.56°$) with the proton moved along the hydrogen bond, is shown in figure 3.18. The optimized structure was generated is several steps:

1. Optimisation of hydroxide ion's geometry at DZP / RHF-MP3 level (table 3.16).

2. Optimisation of the hydronium ion's structure under a C_{3V} symmetry constraint at DZP / RHF-MP3 level (table 3.16).

3. The fixed structures of steps 1 and 2 were assembled to form a pair with C_S symmetry as shown in figure 3.18. The monomers' structures were fixed. Only the pair distance and the two bonding angles were allowed to vary during the optimisation. The result of this

	L1 [Å]	L2 [Å]	L3 [Å]	$\sphericalangle H_2O_1H_3$ [deg]	q_{H3} [e]	Δq [e]	$q_{O1} + q^a_{H2}$ [e]
dimer	0.9569	1.25	1.0	116.15	+0.358	0.310	−0.673
ion pair	0.9696	1.22	0.9764	116.12	+0.363	0.328	−0.686
linear pair	0.9696	1.21	0.9764	180.0	+0.378	0.356	−0.735

[a] hydroxide ion

Table 3.15: Comparison of different ion pairs and dimer at L3 = 1.0 Å.

calculation is displayed above. Any optimisation with an increased number of degrees of freedom led to a structure similar to the equilibrium structure of the water dimer.

Table 3.15 contains a short compilation of those results for the dimer with L3 = 1.0 Å. This point is closest to the optimized ion pair. The pair's bond lengths differ from the dimer's. This is hardly surprising, since L1 and L3 were fixed to the monomer's values. Remarkably good is the agreement of the L2 values. The calculations on the dimer also showed that the distance between both fragments is hardly affected by the monomer's geometry. The calculation about the ion pair allows us to estimate the charge transfer and the charge of the hydroxide ion after the proton transfer. The electronic values of both calculations are similar.

	OH^-	H_3O^+
symmetry	$C_{\infty V}$	C_{3v}
charge [e]	−1	+1
r_{OH} [Å]	0.9696	0.9765
∠HOH [deg]		112.131
q_O [e]	−1.14	−0.40
q_H [e]	+0.14	+0.47
μ [D]	1.5379	1.6344
E_{RHF} [H]	−75.3723	−76.3289
E_{CORR} [H]	−0.2141	0.2179
E_{TOT} [H]	−75.5864	−76.5468

Table 3.16: Results for H_3O^+ and OH^-

Table 3.15 contains also the data of a linear ion pair (d_{OO} = 2.2053 Å, α = 0°, β = 47,56°), because a linear approach of the hydroxide ion was assumed to be more likely for an ionic interaction based purely on electrostatic forces. The increased charge of the hydroxide ion is in good agreement with this assumption, but the charge of the moved proton is still smaller than the charge of a proton in a free hydronium ion (table 3.16). Figure 3.16 suggests a possible explanation. During the proton transfer the proton's charge rises and falls again, as the proton is built into the hydronium ion and gets bound to the free electron pair of the hydrogen acceptor.

To check this theory, the hydrogen atom of a linear hydrogen bond (dim_10, table 3.8) was moved along the bond. The remaining variables of the dimer geometry were kept at their optimized values. Figure 3.19 shows that the energy increases steadily during the motion. No second minimum in the region of the hydronium ion can be observed. Such a second minimum is unlikely for the water dimer in the gas phase rather than in a polar solvent. The solvent stabilizes the ion pair and therefore facilitates the formation of the pair. The electrochemically observable tunneling of protons in water can be explained by such a mechanism. In the gas phase the ion pair cannot be stabilized by the environment. The lowest energy electronic state of the dimer is therefore uncharged. The second minimum for proton transfer in gas phase reactions is often an artifact of the calculation. The only clue of the second oxygen atom is the steep rise at the right edge of the plot. Figure 3.20 displays the charge on the moving proton during the transfer. The mark ”hydronium ion” was set at the point, where all three OH bonds of the ion are of equal length. The mark ”water molecule” is set at the equilibrium bond length of the water dimer. The charge of the protons increases steadily

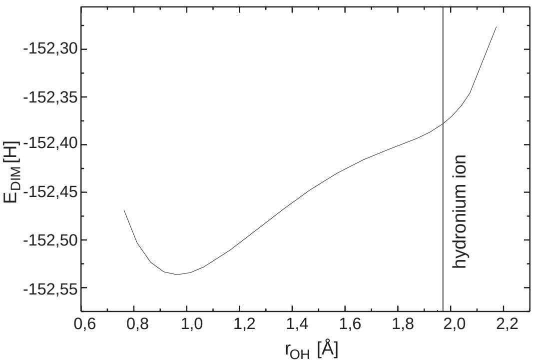

Figure 3.19: Energy during the proton transfer.

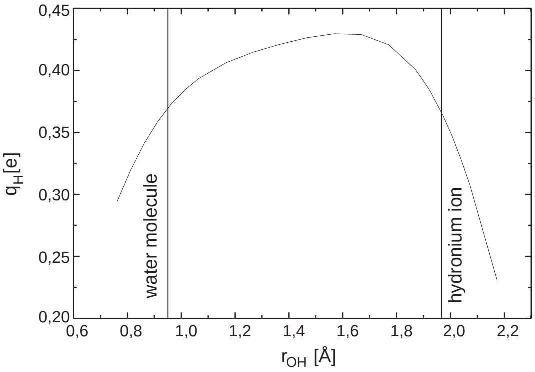

Figure 3.20: Proton charge during proton transfer.

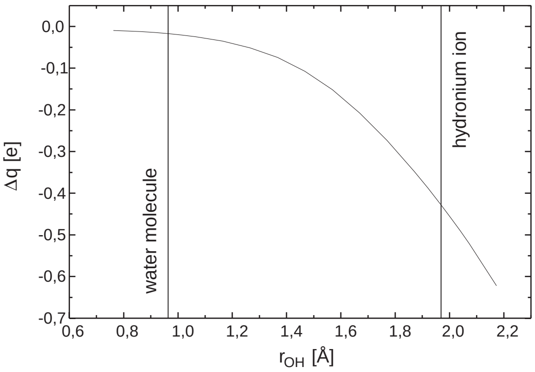

Figure 3.21: Chargre transfer Δq during proton transfer.

until the second water molecule captures the proton. At the same distance the slope of the energy rise decreases (figure 3.19).

It is difficult to define the subunits between which the charge is moved during the proton transfer. To be compatible with the previous part of this work the water moelcules were defined as the units, although this definition loses its credibility at the right end of figure 3.21. Figure 3.21 shows that the influence of the proton position on the charge transfer may be neglected in physically sensible regions (close to the equilibrium geometry).

3.2.3 Potential Curve with a Fixed Geometry

A comparison of the DZP MP3 calculations (table 3.8, 53) with a flexible (dim_16) and a fixed (dim_30) monomer geometry shows that the influence of monomer relaxation is very small. This part of the work tests the utility of such a simplification for the analysis of the energy hypersurface on a larger scale.

Figure 3.22 and 3.23 show the interaction energy as a function of the oxygen-oxygen distance d_{OO}. Figure 3.23 is a close up of figure 3.22 to demonstrate the effect of the BSSE. Again the BSSE correction increases the oxygen-oxygen distance and moves the dimer structure closer to the experimental.

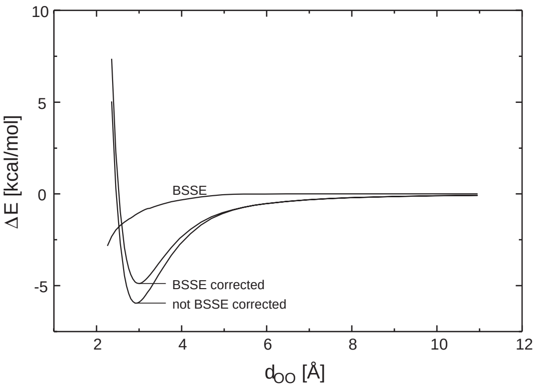

Figure 3.22: Interaction energy with rigid geometries.

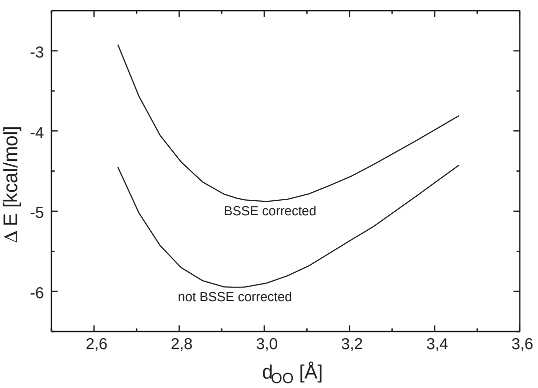

Figure 3.23: Details from figure 3.22.

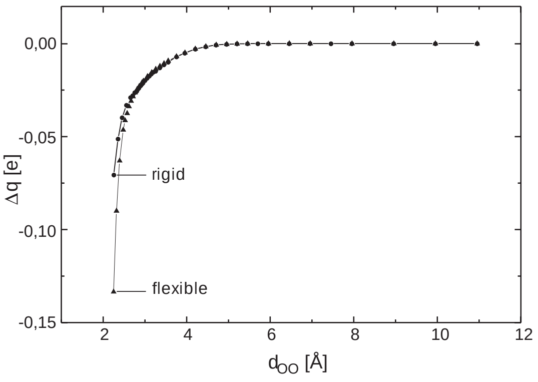

Figure 3.24: Comparison of the charge transfer.

Figure 3.25 shows a superposition of the interaction potential curves with a rigid and a flexible water geometry. The curves are nearly indistinguishable. Only a close up (figure 3.26) shows the difference.

The interaction energy is slightly smaller and the oxygen-oxygen distance also slightly enlarged. However, the differences are so small that they may be safely neglected.

This result allows us to use the fixed experimental water geometry to scan the potential surface. The biggest disadvantage of such a simplification can be seen in figure 3.24. The charge transfer of the rigid dimer agrees nicely with that from calculations with a flexible water geometry at large distances. At small distances the charge transfer is much smaller. As shown in section 3.2.2 the charge transfer is coupled with proton transfer. It is impossible to describe such a reaction with rigid water molecules. Charge transfer is one of the main forces of the dimerisation (please refer to section 3.3, page 72).

The inability of calculations with rigid monomer geometries to describe the charge transfer correctly is therefore the reason for the increasing difference between the two models at small distances.

The influence of the angles α, β (figure 3.2, page 50) and W3 (figure 3.3, page 51) on the energy of the dimer with equilibrium structure was also analysed. The angles were changed systematically, while the remaining variables were fixed at the previously optimized values. Results for α and β of this analysis are shown in the figures 3.27 and 3.28. The minimum for β is shifted about 1.25°

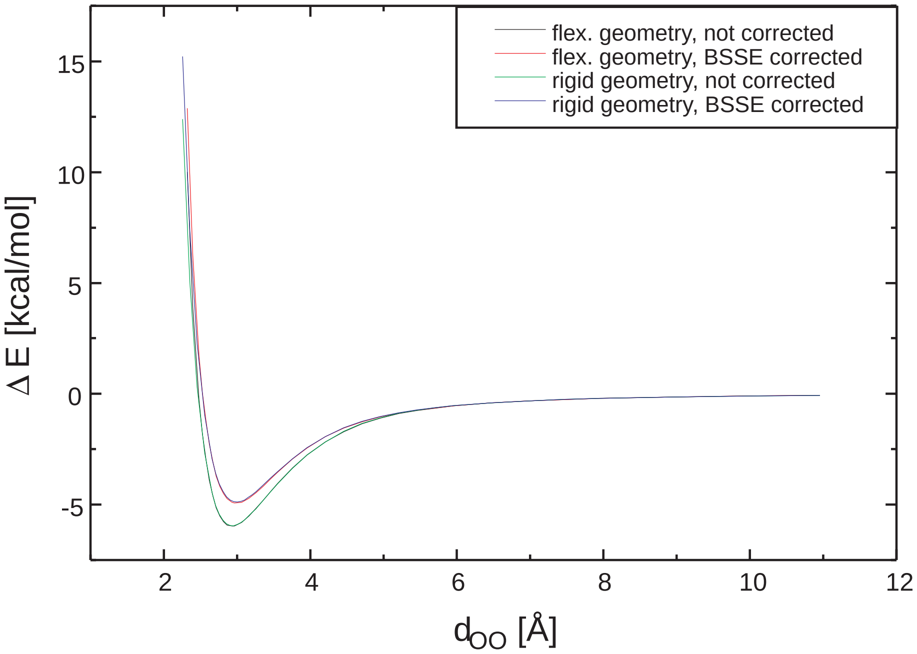

Figure 3.25: Difference between a flexible and a rigid monomer geometry.

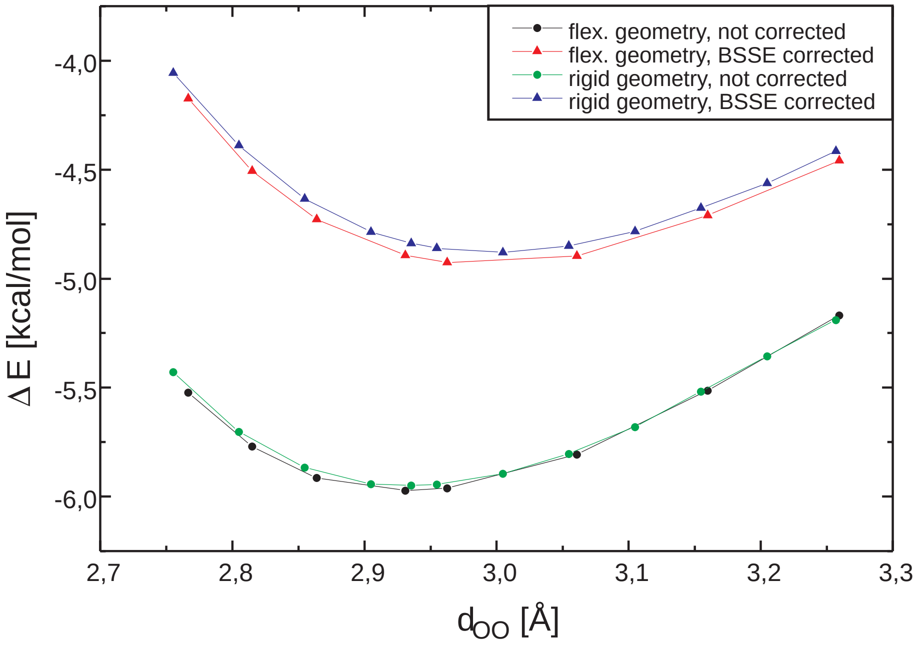

Figure 3.26: Details from figure 3.25.

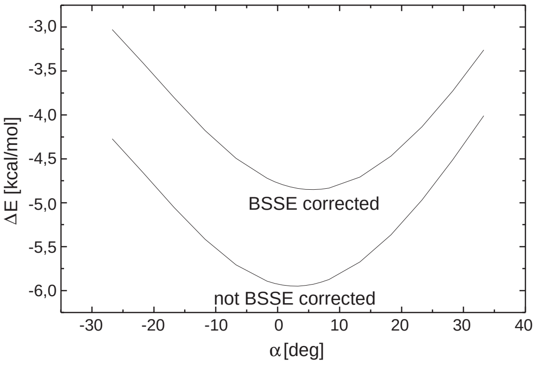

Figure 3.27: Bending of α.

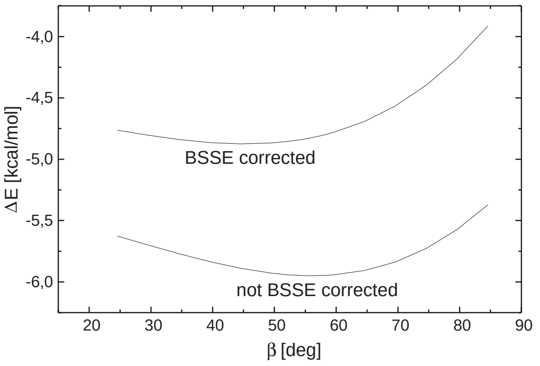

Figure 3.28: Bending of β.

from the value found by the geometry optimisation. This failure of the optimisation algorithm may be explained with the corresponding force constants. To calculate the force constants, the vertex and two neighbouring points of the quantum mechanical curves were taken to find the corresponding parabola. The second derivative of the parabola was taken as the force constant. The force constants for the geometry controlling angles W3[2] and beta are:

W3 : $3.8 \cdot 10^{-6}$ H/deg^2 = 2.4 cal/deg^2 not BSSE corrected

β : $1.7 \cdot 10^{-6}$ H/deg^2 = 1.1 cal/deg^2 not BSSE corrected

The force constants are close to zero like the values of the hessian in the GAMESS UK printout (only to six decimal places). The energy difference between the optimized geometry and the minimum of figure 3.28 is 0.001 kcal/mol. Following the optimisation in the print out proved, that the algorithm stopped too early, since the force to change β vanished.

The influence of the BSSE on the geometry of the water dimer is large. β is changed by 10° by the BSSE. Table 3.17 displays the minima of the BSSE corrected curve. All variables are changed. The BSSE corrected curves allow the calculation of the BSSE corrected dimer geometry with a rigid water monomers (section 3.2.4, page 70).

curve	d_{OO} [Å]	α [deg]	β [deg]	ΔE [kcal/mol]	ΔE_{BSSE} [kcal/mol]
geo optimisation	2.9354	3.28	54.57	−5.949	−4.838
d_{OO}(Potential)	3.0049	3.31	54.57	−5.896	−4.880
W1	2.9304	5.72	54.57	−5.927	−4.844
W2	2.9354	3.28	44.57	−5.840	−4.875
W3	2.9354	5.78	54.57	−5.927	−4.851

Table 3.17: Influence of the BSSE on the variables of the water dimer with a fixed water geometry.

---

[2] A combination of L3 and W3 (figure 3.3) is much better for a geometry optimisation than a combination of d_{OO} and α. α might become zero or negativ during the optimisation. In such a case the algorithm would stop, since a transformation between internal (z-matrix) and cartesian coordinates is not possible anymore. The curve is displayed in the appendix (section 11.6, page 326).

To get a good description of the potential surface an examination of the repulsive force is also necessary. To do so the configurations shown in figure 3.29 were analysed. Both conformers have D_{2h} symmetry.

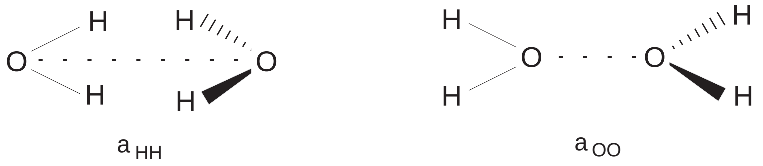

Figure 3.29: Repulsion between water molecules.

The only variable of the system is the distance between the pair of oxygen atoms. The geometry of the water molecules is fixed at the experimental value. Figure 3.30 and 3.31 display the results. The importance of repulsive terms for a good description of the energy hypersurface will be discussed in detail in chapter 4 (page 85).

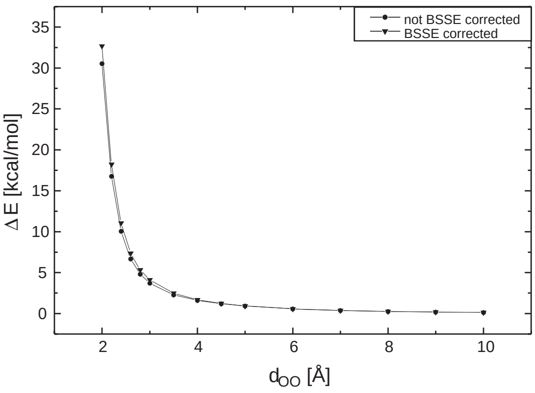

Figure 3.30: Oxygen-oxygen repulsion a_{OO}.

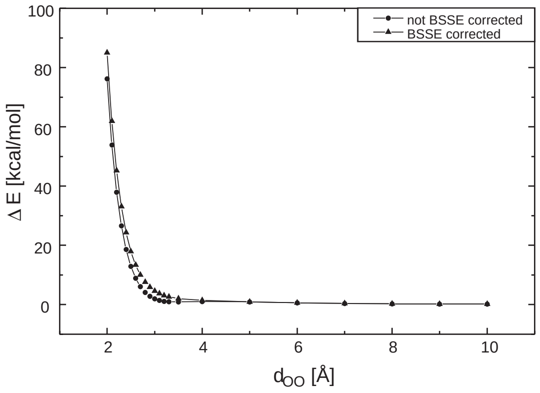

Figure 3.31: Hydrogen-Hydrogen repulsion a_{HH}.

The potential energy curve of the oxygen-oxygen repulsion shows no additional features. According to chemical expectation the interaction potential becomes more repulsive as the oxygen atoms get closer to each other. The curve of the hydrogen-hydrogen repulsion has a shallow local minimum at 3.5 Åwithout a BSSE correction. Figure 3.32 displays a close up of the minimum

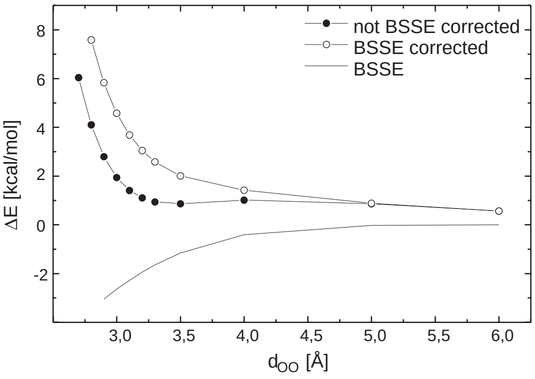

Figure 3.32: Local minimum of H-H repulsion.

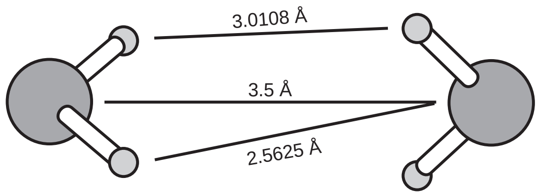

Figure 3.33: Artificial BSSE minimum of a_{HH}.

and figure 3.33 a plot of its molecular geometry. The BSSE corrected curve (figure 3.32) does not have this minimum. The BSSE is caused by a non physical overlap of oxygen and hydrogen orbitals from different molecules. In the minimum geometry all four hydrogen atoms are in ideal positions for such an overlap. In the minimum's regions the BSSE increases faster than the short range exchange repulsion and causes the local minimum.This proves again the importance of BSSE correction for calculations on the water-water interaction.

Those extended interaction curves, especially for α, β and W3, will help to develop a simple analytical description of the water-water interaction potential (chapter 4, page 85). This potential can be used to find the other extrema of the surface [131].

3.2.4 Calculation of the BSSE corrected geometry of the water dimer

A first guess for a harmonic interaction potential close to the minimum (d_0, α_0, β_0) would be:

$$V_{TEST}(d,\alpha,\beta) = K_0 + D_2(d-d_0)^2 + A_2(\alpha-\alpha_0)^2 + B_2(\beta-\beta_0)^2 \tag{3.2}$$

The constants A_2, α_0, B_2, β_0 are taken directly from the BSSE corrected interaction energy curve of the corresponding angles (figure 3.27, 3.28). Only the vertex and the two neighbouring points were used for the calculation. Afterwards, the values of $A_2(\alpha-\alpha_0)^2$ and $B_2(\beta-\beta_0)^2$ were subtracted from the BSSE corrected potential energy curve (figure 3.26), since α and β were allowed to change during the optimisation. This procedure allowed the calculation of K_0, D_2 and d_0.

$$\begin{aligned}\frac{V_{TEST}(d,\,\alpha,\,\beta)}{kcal/mol} &= -4.9296 + 9.6194\left(\frac{d}{\text{Å}} - 2.9991\right)^2 \\ &\quad + 2.56\cdot10^{-3}\left(\frac{\alpha}{deg} - 5.624\right)^2 + 3.8\cdot10^{-4}\left(\frac{\beta}{deg} - 44.894\right)^2\end{aligned} \tag{3.3}$$

The minimum of the function is: $V_{TEST}(2.9991\text{Å}, 5.624°, 44.894°) = -4.9296$ kcal/mol. A quantum mechanical calculation (DZP basis set, RHF-MP3, full counterpoise BSSE correction) gave for the same geometry an interaction energy of -4.8903 kcal/mol. Although all values agree well with experiment (2.967 ± 0.03 Å, 1 ± 10°, 57 ± 10°), a difference of 0.0393 kcal/mol between the prediction and the actual quantum chemical interaction energy is disappointing.

To achieve further improvement the potential energy surface around the minimum of equation 3.3 was sampled with a fine mesh (144 points). To get an estimate of the coupling between the variables, for 60 points two variables were changed simultaneously.

$$\begin{aligned}V_{TEST}(d,\,\alpha,\,\beta) = {} & x_1\,d + x_2\,d^2 + x_3\,d^3 + a_1\,\alpha + a_2\,\alpha^2 + a_3\,\alpha^3 + b_1\,\beta + b_2\,\beta^2 + b_3\,\beta^3 + \\ & k_1\,d\,\alpha + k_2\,d\,\beta + k_3\,\alpha\,\beta + K_0\end{aligned} \tag{3.4}$$

V_{POL} was fitted with the help of a linear least squares algorithm [242] to the 144 quantum chemical points (root mean square (rms) = 0.00126913 kcal/mol). Next a simple search algorithm sampled V_{POL} over the quantum chemical geometries to find the starting point for a local minimum search. From this point the program followed the gradient of V_{POL} to find the local minimum. The minimum was reached when the value of the gradient was smaller than $1{\cdot}10^{-9}$. The minimum geometry and energy E_0 allow us transcribe V_{POL} into a more chemical form V_{CH}.

$$\begin{aligned}V_{CH}(d,\,\alpha,\,\beta) = {} & X_2(d-d_0)^2 + X_3(d-d_0)^3 + A_2(\alpha-\alpha_0)^2 + A_3(\alpha-\alpha_0)^3 + \\ & B_2(\beta-\beta_0)^2 + B_3(\beta-\beta_0)^3 \\ & K_1(d-d_0)(\alpha-\alpha_0) + K_2(d-d_0)(\beta-\beta_0) + K_3(\alpha-\alpha_0)(\beta-\beta_0) + K_0\end{aligned} \tag{3.5}$$

The coefficients X_n to K_n are the results of a rapid transformation.

$$K_0 = E_0 \tag{3.6}$$

$$K_1 = k_1 \qquad K_2 = k_2 \qquad K_3 = k_3 \tag{3.6 a}$$

$$X_3 = x_3 \qquad A_3 = a_3 \qquad B_3 = b_3 \tag{3.6 b}$$

$$X_2 = x_2 + 3X_3 d_0 \qquad A_2 = a_2 + 3A_3\alpha_0 \qquad B_2 = b_2 + 3B_3\beta_0 \tag{3.6 c}$$

To check the transformation the following expressions were used.

$$\begin{aligned} x_1 &\overset{?}{=} x_0(3D_3x_0 - 2D_2) - K_1\alpha_0 - K_2\beta_0 \\ a_1 &\overset{?}{=} \alpha_0(3A_3\alpha_0 - 2A_2) - K_1x_0 - K_3\beta_0 \\ b_1 &\overset{?}{=} \beta_0(3B_3\beta_0 - 2B_2) - K_2x_0 - K_3\alpha_0 \end{aligned} \tag{3.7}$$

To increase the reliability of any prediction an upper energy limit of −4.75 kcal/mol was used. The rms of the reminding 136 points was 0.000953. Table 3.18 shows a compilation of the minima associated with the different steps.

	points	rms [kcal/mol]	d_0 [Å]	α_0 [deg]	β_0 [deg]	E [kcal/mol]
V_{TEST}	9	0.0	2.9991	5.62	44.89	−4.9296
V_{CH}	145	0.001269	2.9926	2.46	44.57	−4.9147
V_{CH}	136	0.000953	2.9926	2.44	44.53	−4.9145

Table 3.18: Minimum geometry and energy at the different steps.

Table 3.18 shows how well the simple estimate V_{TEST} actually describes the influence of the BSSE on the dimer's geometry, but the reliability increases with effort. A quantum chemical check of the final minimum geometry gave a interaction energy of −4.91496 kcal/mol. The difference between the calculations is 0.00042 kcal/mol and therefore neglible. The BSSE has a value of 0.95 kcal/mol and is the smallest found during this work. A geometry optimization with a full BSSE correction is therefore a minimization of the BSSE at the same time. Figure 3.34 displays the BSSE corrected geometry of the water dimer.

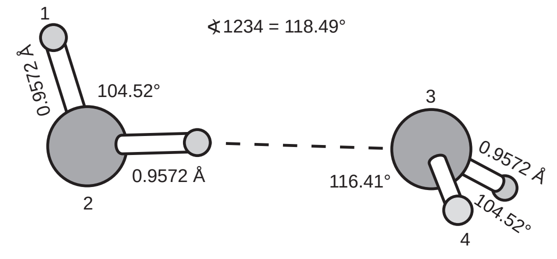

Figure 3.34: BSSE corrected minimum geometry.

Table 3.19 displays the parameter of V_{CH} of the last step. The anharmonicity X_3 of the oxygen-oxygen distance is at first sight larger than the harmonic part X_2. By definition Δd is much smaller than one. The actual anharmonic correction is therefore much smaller than the harmonic value. The anharmonicities in the angle are negligible ($B_3 < A_3 \leq 6{\cdot}10^{-6}$ kcal/mol/deg^3). The high quality of the prediction for the angles α and β of the test function V_{TEST} is now understandable. The predictions for the distance d are poorer due to the strong anharmonicity and the coupling of α and d (K_1). K_1 indicates that α becomes bigger as the hydrogen bond gets shorter. The hydrogen atom H_3 and the oxygen atom O_4 seem to avoid each other at short distances. The underlying physics of this phenomenon is discussed in section 3.3. The coupling of β and d is straight forward.

As the bond length increases, increases in β help to turn the extensive $1b_1$ water orbital into the right direction. The coupling of α and β is negligible.

The force constant for β (1.1 cal/mol/deg^2) without BSSE correction (section 3.2.2, page 61) is about three times larger than the BSSE corrected value B_2. This difference cannot be caused by the method of computation, since the corresponding values of V_{CH} and V_{TEST} agree well and the same simple three-point-parabola approach was used in both cases. The large BSSE in the frequencies is disturbing at first glance, since the basis set does not change during the calculation. Nonetheless this is commonly observed [208a]. The pointwise BSSE correction changes the curvature of the energy surface. This change alters the force constatnts. A correction of the BSSE in frequency calculations is tedious and difficult. Frequency calculations therefore should be done with large basis sets with a small BSSE.

X_3	−15.087	kcal/mol/Å^3
A_3	0.0000060	kcal/mol/deg^3
B_3	0.0000056	kcal/mol/deg^3
X_2	9.94145	kcal/mol/Å^2
A_2	0.0022851	kcal/mol/deg^2
B_2	0.0003302	kcal/mol/deg^2
K_1	0.0352951	kcal/mol/Å/deg
K_2	−0.0085391	kcal/mol/Å/deg
K_3	−0.0010564	kcal/mol/deg^2
d_0	2.99261	Å
α_0	2.43594	deg
β_0	44.534	deg
K_0	−4.91454	kcal/mol

Table 3.19: Final parameter for V_{CH}

3.3 Energy Decomposition

The analysis of the Hartree-Fock energy according to MOROKUMA (section 2.5, page 26) helps us to understand the underlying physics of the water dimerisation and so the formation of water clusters. The answers to this question will help to develop an analytical water-water interaction potential.

The importance of d_{OO} and β for the hydrogen bond can be explained with the VSEPR model [12]. While d_{OO} governs the orbital overlap and therefore the strength of the bond, β controls the orientation of the free electron pair. The bend of the hydrogen bond α is not explained by the VSEPR model and the small value for β only with difficulty.

	Variation of d_{OO}		Variation of α		Variation of β	
d_{OO} [Å]	3.0049	3.0548	2.9354	2.9354	2.9354	2.9354
α [deg]	3.32	3.32	0.28	4.28	3.32	3.32
β [deg]	54.57	54.57	54.57	54.57	49.43	54.57
ES	−7.75	−7.13	−8.77	−8.72	−8.704	−8.744
EX	4.28	3.52	5.71	5.58	5.533	5.622
CT	−1.19	−1.06	−1.43	−1.41	−1.375	−1.417
PL	−0.54	−0.48	−0.64	−0.64	−0.649	−0.637
HO	0.07	0.06	0.08	0.10	0.110	0.099
ΔE	−5.11	−5.08	−5.04	−5.08	−5.085	−5.076

Table 3.20: Energy composition near the minimum in kcal/mol.

The analysis started with an examination of the dimerisation curve for rigid water geometries (fig. 3.22) using the MOROKUMA algorithm analysis for the Hartree Fock interaction energy. The minimum of the curve is therefore moved to a larger oxygen-oxygen distance (3.0049 Å, table 3.14, page 63). This movement is in good agreement with the results from table 3.14 and figure 3.17, since the inclusion of the correlation calculations into the geometry optimization allows the oxygen-oxygen distance to shrink. Table 3.20 displays the energy composition close to the minimum. The same abbreviations as in section 2.5 (page 26) are used for the different energy terms (ES: eletrostatic, EX: exchange repulsion, CT: charge transfer, PL: polarisation, HO: high order coupling).

An analysis of table 3.20 shows that the dimerisation is controlled by the electrostatic interaction and the exchange repulsion. Charge transfer and polarisation play only a minor role while the high order coupling terms can be safely neglected. The flatness of the energy surface close to the minimum is due to a cancellation of the main three components: electrostatic interaction, exchange repulsion and charge transfer ($\Delta E_{ES} + \Delta E_{EX} + \Delta E_{CT} = +0.01$ kcal/mol). The energy gain in the last 0.05 Å is caused by the polarisation term ($\Delta E_{CT} = -0.06$ kcal/mol).

Table 3.20 also provides a reasonable explanation for the bending of the hydrogen bond. The energy gain (0.04 kcal/mol) of the bend is caused by the reduction of the exchange repulsion ($\Delta E_{EX} = -0.13$ kcal/mol). Simultaneously, there are reductions in the electrostatic interaction and the charge transfer ($\Delta E_{ES} + E_{CT} = +0.07$ kcal/mol). As shown in section 3.2.1 / figure 3.11 (page 57) is the hydrogen bond formed by an interaction of occupied orbitals. The exchange repulsion is also caused by the interaction of occupied orbitals (section 2.5 / figure 2.3, page 28). The bend of the hydrogen bond α may be regarded as the solution of the dilemma to form a bond of occupied orbitals and to minimize the exchange repulsion at the same time. The conflict is also reflected by the coupling constant K_1 between d_{OO} and α (section 3.2.4). An enlargement of the oxygen-oxygen distance decreases the exchange repulsion and therefore allows α to decrease. At larger distances between the monomers linear hydrogen bonds are formed.

An *ad hoc* model of the water molecule would be a tetrahedron. A water dimer built from such tetrahedra would be linear ($\alpha = 0°$) and β would be 54.73°. The minimum of the MOROKUMA curve is between 49.57° and 50.57°. Both points (49.57° and 50.57°) are not distinguished by GAMESS US because the energy differences are too small. Such a minimum shift has been observed previously in section 3.2.3 and is caused by the optimisation algorithm and its control parameter. While the VSEPR model would explain the shift by a stronger repulsion between free electron pairs than bonds, table 3.20 gives the quantum chemical answer. The energy gain (0.009 kcal/mol) caused by the decrease of β is caused by the reduction of the exchange repulsion ($\Delta E_{EX} = -0.089$ kcal/mol). The weakening of the electrostatic interaction and charge transfer cannot compensate for this energy gain ($\Delta E_{ES} + \Delta E_{CT} = 0.082$ kcal/mol). The reduction of the exchange repulsion explains the coupling between d_{OO} and β in greater detail. The enlargement of the oxygen-oxygen distance decreases the exchange repulsion. This reduction allows an increase of β. Together with this rotation the hydrogen acceptor's $1b_1$ orbital moves closer to the hydrogen atom. Such a movement reinforces the electrostatic interaction between both molecules and the charge transfer. The $1b_1$ orbital is more extensive than the $3a_1$ orbital and this reduces the reduction of the exchange repulsion. A change of α decreases the exchange repulsion about 0.052 kcal/mol/deg while the same movement of β decreases the exchange repulsion only about 0.018 kcal/mol/deg. The greater extension of the $1b_1$ orbital explains, why B_2 and K_2 are much smaller than A_2 and K_1.

At the minimum geometry (3.0049 Å) the ratios for the individual interaction energies are as follows: ES : EX : CT : PL : HO = 1 : 0.55 : 0.15 : 0.07 : 0.01. ***It is therefore more important to find a good description of the electrostatic interaction (ES) and the exchange repulsion (EX) for a classical model than to introduce a polarisation term.*** The charge transfer (CT) plays only a minor, but still important, role and cannot be described adequately by a rigid water molecule model as shown in subsection 3.2.2 and 3.2.3.

All MOROKUMA calculations were done with GAMESS US. The basis set generated by the input line "`$BASIS GBASIS=DZV NPFUNC=1 NDFUNC=1 $END`" is the same as the GAMESS UK DZP basis set.

3.4 Water Trimer

Calculations on water trimers at an RHF/MP3 level with a DZP basis need considerable computational resources. Therefore, only four different geometries with rigid monomers were examined.

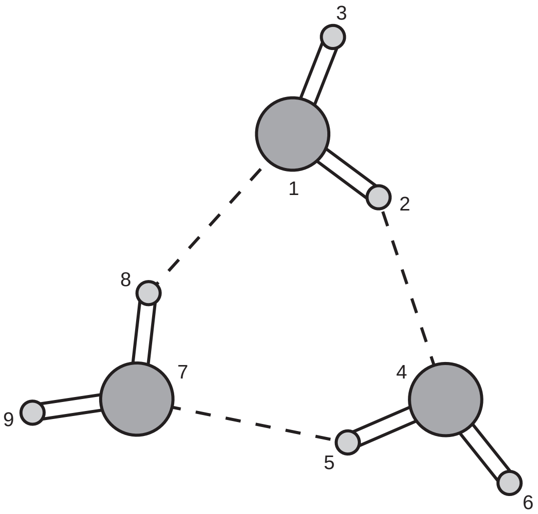

Figure 3.35: Geometry of trimer I.

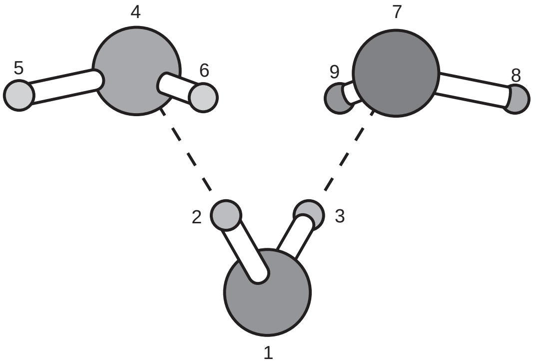

Figure 3.36: Geometry of trimer II.

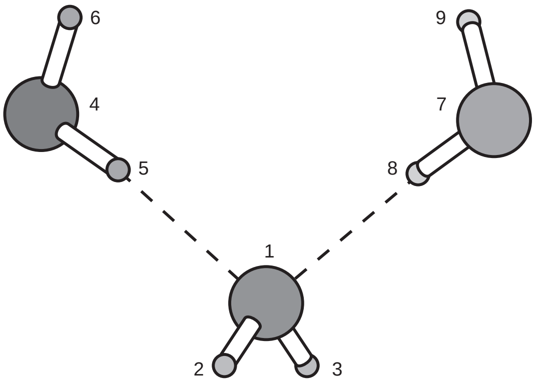

Figure 3.37: Geometry of trimer III.

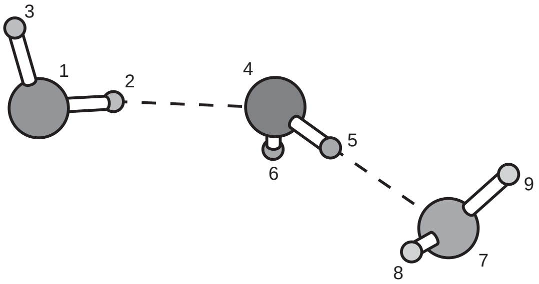

Figure 3.38: Geometry of trimer IV.

Figures 3.35 to 3.38 display pictures of the examined trimers. The three variables are the same as in the water dimer. d_{OO} is the distance between the two oxygen atom of a hydrogen bond, α is the bend of the hydrogen bond and β the angle between the acceptor's symmetry plane and d_{OO}. For details please refer to table 3.21.

d	d_{OO}	α	β
I	1-4	2-1-4	—
	4-7	5-4-7	—
	7-1	8-7-1	—
II	1-4	2-1-4	1-4-(5,6)
	1-7	3-1-7	1-7-(8,9)
III	1-4	5-4-1	4-1-(2,3)
	1-7	8-7-1	7-1-(2,3)
IV	1-4	2-1-4	1-4-(5,6)
	4-7	5-4-7	4-7-(8,9)

(x,y) sum of the corresponding OH vectors

Table 3.21: Definition of the trimer geometries.

There is only one principal way to construct a cyclic trimer (figure 3.35) but three different linear combinations, which can be distinguished by the function of the central water monomer. In trimer II as shown in figure 3.36 the central water molecule donates both hydrogen atoms to the hydrogen bond. Trimer III (figure 3.37) is built vice versa. In both cases the central water molecule accepts the hydrogen atom from the other water molecules. Finally, the central water molecule acts in trimer IV (figure 3.38) as an acceptor as well as a hydrogen donor. Experimental data only exist for trimers I and IV. All experiments on the free trimer suggest, that the most stable water trimer is cyclic with C_1 symmetry. A twisted head-tail chain like trimer IV is commonly observed on metal surfaces (e.g. Pt(111)) [38].

All calculations (GAMESS UK) were done with a rigid monomer geometry. Only the geometries of trimer I and II were fully optimized. The geometries of the trimers III and IV were constructed from ideal hydrogen bonds with a BSSE corrected oxygen-oxygen distance (table 3.18). Table 3.22 lists the geometries and energy compositions of the four trimers.

	trimer I	trimer II	trimer III^{+}	trimer IV^{+}
method	DZP-MP3	DZP-MP3	DZP-MP3	DZP-MP3
d [Å]	2.8014	2.9761	3.0049	3.0049
α [deg]	23.54	9.70	3.31	3.31
β [deg]	not defined	70.745	54.57	54.57
dipole moment [D]	0.0	0.4830	1.2963^{SCF}	3.7546^{SCF}
E_{ELEC} [H]	−312.0214	−301.3425	−302.4546	−301.9393
E_{NUC} [H]	83.8604	73.1893	74.3017	73.7817
E_{RHF} [H]	−228.1610	−228.1532	−228.1529	−228.1575
E_{MP2} [H]	−0.6372	−0.6357	−0.6354	−0.6355
E_{MP3} [H]	−0.0178	−0.0182	−0.0183	−0.0182
E_{TOT} [H]	−228.8161	−228.8071	−228.8066	−228.8111
ΔE^{*}_{TOT} [kcal/mol]	−16.213	−10.578	−10.286	−13.112

^{SCF} calculated from the SCF matrix $^{+}$ geometry not optimised

* not BSSE corrected

Table 3.22: Geometrical details of the trimers.

The three possible orientations (figure 3.39) of the hydrogen atoms (both hydrogens inside, both hydrogens outside, one inside and the other outside) of the terminal water molecules of trimer III were checked with a rapid RHF-MP2 calculation (GAMESS US). The geometry with both hydrogens inside had the lowest total energy of −228.75199 H. The geometry with both hydrogens outside the inner area yields an energy of −228.74796 H while the geometry with one hydrogen inside and the other outside gave a total energy of −228.7511 H. These results show that the Coulomb repulsion between the nonbonding hydrogen atoms of a single hydrogen bond is more important than the repulsion between the hydrogen atoms at separated water molecules.

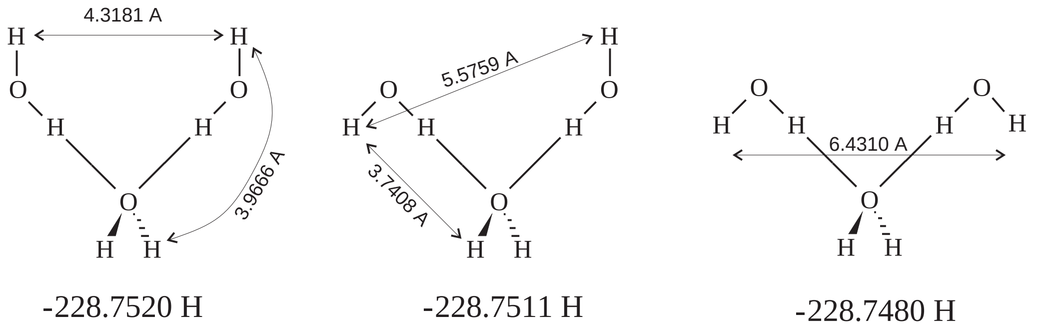

Figure 3.39: Three possible conformers of trimer III with their MP2 energies in Hartree.

In the literature (eg [157]) the conformation with both hydrogen atoms inside the molecular centre is commonly used. It is therefore difficult to relate to previously published results.

The water trimer (still subject of the current research) has been examined both experimentaly [139, 141, 150, 154, 243, 244] and theoretically [107, 108, 119, 131–133, 140, 142, 145, 147, 157, 159, 245, 208d (review on nonadditivity)]. The theoretical papers provide a wide range of results and depend heavily on the used technique. The experimental results can be summarized as follows:

The most stable water trimer is cyclic with C_1 symmetry. The three oxygen atoms form nearly an equilateral triangle (2.97 Å, 2.97 Å and 2.94 Å). The hydrogen atoms of the hydrogen bond are slightly tilted out of the oxygen plane. Two of the remaining three hydrogen atoms are above and the third hydrogen atom is below this plane. The eight different conformers (including only the non binding hydrogens) interchange rapidly by quantum tunneling. All clusters larger than the dimer have a small or vanishing dipole moment.

The theoretical analysis of this minimum is very difficult. The low symmetry and the flatness of the potential energy surface make quantum chemical calculations costly, since it is no longer possible to reduce the number of integrals by symmetry operations and the geometry optimisation algorithmen converges only slowly. Also the flat potential energy surface has 96 isoenergetic minima [132] around the minimum. Despite those problems the work published in the literature focuses on the global minimum. Table 3.23 displays a short compilation of results for related geometries.

	trimer I			trimer II	
	this work	[140]	[142]	this work	[145]
basis set	DZP	ESPB	DZP	DZP	6-311+G(2d,2p)
method	MP3	MP2	CCSD	MP3	MP4SDQ
d [Å]	2.801	2.80	2.799	2.9761	2.9496
α [deg]	23.54	25.0	23.28	9.70	6.2
β [deg]	not defined	not defined	not defined	70.745	69.0
E_{TOT} [H]	-228.8161		-228.7757	-228.8071	-228.8257
ΔE^{*}_{tot} [kcal/mol]	-13.789^{a}	-13.659	-15.695	-8.281^{a}	-5.3

[a] BSSE corrected

Table 3.23: Previously published results for the water trimer.

		trimer I	trimer II	trimer III*	trimer IV*
$\Delta \mathrm{E}_{\mathrm{ABC}}$		−16.213	−10.578	−10.286	−13.112
$\Delta \mathrm{E}_{\mathrm{ABC}}$	(BSSE)	−13.789	−8.281	−8.242	−11.071
BSSE		2.424	2.297	2.044	2.041
$\Delta \mathrm{E}_{\mathrm{BC}}$		−4.802	+0.724	+1.112	−5.899
$\Delta \mathrm{E}_{\mathrm{BC}}$	(BSSE)	−3.644	+0.724	+1.163	−4.882
$\Delta \mathrm{E}_{\mathrm{AC}}$		−4.802	−5.859	−5.899	−0.613
$\Delta \mathrm{E}_{\mathrm{AC}}$	(BSSE)	−3.644	−4.724	−4.882	−0.586
$\Delta \mathrm{E}_{\mathrm{AB}}$		−4.802	−5.859	−5.899	−5.899
$\Delta \mathrm{E}_{\mathrm{AB}}$	(BSSE)	−3.644	−4.724	−4.882	−4.882
$\Delta \mathrm{E}_{\mathrm{Pair}}$		−14.406	−10.994	−10.686	−12.411
$\Delta \mathrm{E}_{\mathrm{Pair}}$	(BSSE)	−10.923	−8.724	−8.602	−10.351
$\Delta \mathrm{E}_{\mathrm{NPA}}$		−1.807	+0.416	+0.400	−0.701
$\Delta \mathrm{E}_{\mathrm{NPA}}$	(BSSE)	−2.866	+0.443	+0.360	−0.720
nonadd. BSSE		−1.050	+0.027	−0.040	−0.019
$\Delta \mathrm{E}_{\mathrm{H-BOND}}$		−5.404	−5.289	−5.143	−6.556
$\Delta \mathrm{E}_{\mathrm{H-BOND}}$	(BSSE)	−4.596	−4.140	−4.121	−5.535
$\Delta \mathrm{E}_{\mathrm{MONO}}$		−5.404	−3.578	−3.429	−4.371
$\Delta \mathrm{E}_{\mathrm{MONO}}$	(BSSE)	−4.569	−2.760	−2.747	−3.690

(BSSE) : BSSE corrected NPA : not pair wise additive
H-BOND : per hydrogen bond MONO : per monomer
* : geometry not optimized A = 1,2,3 B = 4,5,6 C = 7,8,9

Table 3.24: Analysis of the interaction energy.

Table 3.24 displays the analysis of the trimerisation energy. For the calculation of the BSSE ghost orbitals were placed at the position of the two water molecules (section 2.4, 23 - trimerisation in a single step, [145]). The BSSE is roughly the same for all trimers regardless of the number of bonds. The BSSE has a strong nonadditive component ($\mathrm{BSSE}_{\mathrm{TRIM}} - \sum \mathrm{BSSE}_{\mathrm{DIM}}$). Trimer I with the strongest nonadditive forces ($\Delta \mathrm{E}_{\mathrm{NPA}}$) has also the largest nonadditive contributions to the BSSE.

At the first glance at table 3.24 trimer I is the most stable trimer, because it is made of three binding hydrogen bonds while the other three trimers contain only two binding bonds. Trimer I has the highest interaction per monomer, but the weakest hydrogen bond in pair interactions. The hydrogen bond in the cyclic trimer is heavily distorted ($\alpha = 23.54°$). Since α is the bond breaking angle, the energy gain has to be small. The energy gain per hydrogen bond ($\Delta \mathrm{E}_{\mathrm{H-BOND}} = \Delta \mathrm{E}_{\mathrm{ABC}} \div \mathrm{n}$, where n is the number of bonds) is not a reasonable quantity to explain the strong interactions in trimer I, since it also contains the non pairwise interactions (−4.802 kcal/mol versus −5.404 kcal/mol). The weakness of a single hydrogen bond is not only compensated by the number of bonds but also by very strong cooperative effects ($\Delta \mathrm{E}_{\mathrm{NPA}}$). The BSSE corrected value for $\Delta \mathrm{E}_{\mathrm{NPA}}$ is calculated with the BSSE corrected pair interaction energies and the corrected trimerization energy $\Delta \mathrm{E}_{\mathrm{ABC}}$. The BSSE of $\Delta \mathrm{E}_{\mathrm{NPA}}$ is therefore by construction the nonadditive part of the BSSE. The only other trimer with a negative value for $\Delta \mathrm{E}_{\mathrm{NPA}}$ is trimer IV, which is build out of optimised dimers (C_{S}) and has the highest binding energy per hydrogen bond. This is not only caused by the dimers' geometries. The interaction between the monomers A and C is attractive, while the similar interaction in the trimers II and III is repulsive. Trimer IV is also the only linear trimer with binding cooperative effects. According to Mó's [145] quantum chemical calcaltions changes trimer IV without a barrier of activation into the global minimum (C_1). Our own calculations with a classical pairwise additive potential (please refer to section 4.3.2, page 109) gave the same result: trimer IV transforms without a barrier of activation into the global minimum. The cyclisation is in good agreement with the experimental findings for the dipole moment of the water cluster. Cyclic oligomers have naturally a small or vanishing dipole moment. The correlation of the dipole moment with the cluster's stability is observable in table 3.22. The trimers II and III, which cannot transform easily into a cyclic version have dipole moments and a smaller interaction energy. The increase of α and β in trimer II results in a more arrangement position of the dipole moments and in smaller overall dipole moment.

The correlation between cooperative effects and charges has been examined previously [107, 145]. With increasing cluster size $(H_2O)_n$ (n = 1, 2, 3) the average charge on the oxygen atom increases from 0.65 (n=1) via 0.68 (n=2) to a value in the range from -0.68 to -0.76 e for the different trimers. This general increase is caused by polarisation. The differences of the stabilisation energy of the four trimers may be explained with a simple acid-base model on the basis of the atom charges. Atomic charges are a much better tool to determine the relative acidities than classic proton affinity or acidity calculations. The protonation of the dimer (rigid monomer geometry, C_S symmetry) of O_4 (figure 3.2, $\sphericalangle(H^+O_4O_1H_2) = 0°$) for example leads directly to the dissociation of the water dimer. Protonated water molecules are ions and the mechanism of the water water interaction changes from covalency to electrostatic interaction. Protonated dimers are only stable if the oxygen of the second water molecule points directly to a hydrogen atom of the protonated species.

The most likely place for a nuclophilic attack would be the hydrogen atoms H_5 and H_6 (q_H = 0.34 e) and the most likely place for an electrophilic attack would be O_1 ($q_O = -0.69$ e) (figure 3.2 and tables 3.8, 3.10). The corresponding attacks at these places lead directly to the formation of trimer IV. The less favourable attacks at H_2 and O_4 would lead to the formation of the trimers II and III. The formation of trimer IV is therefore not only favoured by energy (Coulomb energy for the formation of the transition state and total energy of the final trimer) and by the number of places for a succesful attack. Since trimer IV transforms immediately into the cyclic trimer the observation of an open chain water trimer is very unlikely.

	E [H]	ΔE [eV]	ΔE^*_{EXP} [eV]
H_2O	−76.04639400	0.00	0.00
H_2O^-	−75.84941915	5.36	1.07
H_2O^+	−75.64330432	10.97	11.53

Table 3.25: Electron affinity and ionisation energy of water.

Further insight into the bonding mechanism of a water trimer than a pure analysis of acidity [eg. 145] allows a detailed comparison of the charges on the oxygen atom and the total charge on the monomers. Table 3.25 displays the Hartree-Fock results for the electron affinity and the first ionisation energy of single water molecule with rigid geometry. The energy for the cation is much better than the energy of the anion, since in the anion the antibonding $3a_1$ orbital is populated and major changes of geometry are therefore likely. The most stable molecule is the uncharged water molecule. Since a water dimer/trimer cannot be built without charge transfer, the most stable water cluster should therefore be built from water molecules, which give and receive electrons simultaneously. This happens with cyclic polymers and trimer IV. The central water molecule of trimer IV is simultaneously hydrogen donor and acceptor. The net charge change of -0.001 e due to the trimerisation is small and slightly negative, since the water molecule bonds electrons better than it gives them away. The charge on O_4 is -0.724 e, while the charge on the electron donor O_7 is -0.695 e and on the electron acceptor O_1 is -0.716 e. The charges on the oxygen atoms also show that not only charge transfer but also polarisation controls the charge distribution in the trimers. If charge transfer was the only cause for the charge distribution in the trimer, the charge on the central oxygen O_4 in trimer IV should be closer to the free water value of -0.69 e and smaller than the charge of the pure electron acceptor O_1 -0.716 e. This disagreement can be explained by polarisation. The electrical field of the other water molecules polarises the oxygen of the water molecule and so causes an additional electron shift. Investigation of the water trimer with SAPT calculations (**S**ymmetry **A**dapted **P**erturbation **T**heory) show, that close to equilibrium structure the cooperative forces are dominated by polarisation.

The difference between the abilities to give and to receive electrons is reflected by the charge on the central water molecules in the trimers II and III. In trimer III both water molecules pull electron density away from the centre molecule. The total charge of the centre molecule is $+0.028$ e and the charge of the central oxygen O_1 is -0.709 e. The charge on the other oxygen atoms O_4 and O_7 is -0.706 e. Although the two water molecules pull electrons away from O_1, O_1 is more negative than O_4 or O_7. Since the water molecule and therefore oxygen receives more electrons than it donates, electron density is moved from the hydrogens H_2 and H_3 to O_4 in order to compensate the electron drag. The second reason is polarisation. The hydrogens H_8 and H_5 pull electron density along the direction of the dipole moment and therefore enhance the dipole moment. An increase of the dipole moment enhances the charge separation as long the geometry is fixed (equation 3.1). In trimer II the oxygen atoms O_4 and O_7 donate electron density to O_1. The charge on O_1 is -0.722 e while the charge on the oxygen atoms O_4 and O_7 is -0.655 e, even lower than the charge on oxygen in the free water molecule. Table 3.26 summarizes the correlation of charge transfer and stability.

trimer	electron transfer to central oxygen	q_{H2O} [e]	q_{O4} [e]	E* [kcal/mol]
IV	donate - receive	-0.001	-0.724	-13.112
II	receive - receive	-0.043	-0.722	-10.578
III	donate - donate	$+0.028$	-0.709	-10.286

* not BSSE corrected

Table 3.26: Correlation of charge transfer and stability.

Since the charges are not BSSE corrected the uncorrected interaction energies are displayed in table 3.26. The table examplifies an extremly simplified model of coopeative effects in water trimers and therefore for water cluster growth: ***The next water molecule is attached to an existing water cluster in such a way that the target water molecule in the cluster donates and receives electrons simultaneously. The net change of charge at the attacked water molecule is thereby kept to a minimum.***

The hydrogen bonds in the trimers are formed by an overlap of the occupied orbitals similar to the bond in the water dimer. Figure 3.40 displays the 3a' orbital from trimer I. The bond is formed by a bonding overlap of the $1b_2$ orbitals of the monomers. An analysis of the moleculear orbitals of the global minimum shows (please refer to section 4.3.2 (page 109) for details on the

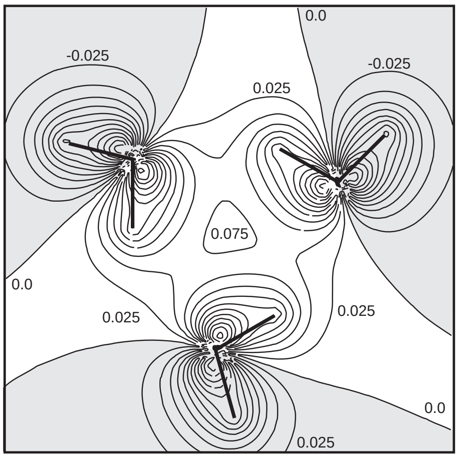

Figure 3.40: 3a' orbital of trimer I.

$$\begin{array}{rcll} 6H_2O & \longrightarrow & 3(H_2O)_2 & \Delta E = -13.98\text{kcal/mol} \\ 6H_2O & \longrightarrow & 2(H_2O)_3 & \Delta E = -16.48\text{kcal/mol} \\ 3(H_2O)_2 & \longrightarrow & 2(H_2O)_3 & \Delta E = -2.50\text{kcal/mol} \end{array}$$

Figure 3.41: Formation of trimer III from dimers.

global minimum structure), that the corresponding orbital has the same shape. The distortion of the molecule reduces the Coulomb repulsion of the two cis hydrogens by increasing the dihedral angle. The molecules get closer to each other and the overlap increases. Meanwhile the orbital energy decreases and the trimer stabilizes. The distortion of the water trimer not only reduces the Coulomb repulsion but also increases the overlap of the $1b_2$ orbitals. Therefore, any model which is used to explain the distortion of the trimer has to take orbital effects as well as cooperative forces into account as showed by SAPT calculations [159].

The energy difference between trimers II and III at a BSSE corrected level is very small (0.039 kcal/mol) and may be neglected. Since the geometry of trimer III was not optimized, the geometries are difficult to compare. The optimization of trimer III lowers the energy even further. Energy and geometry optimisations at DZP/MP3 level proved to be tedious with the available computers. The geometry optimisations were done with a classical pairwise interaction potential (chapter 4, page 85). Further refinement was done at MP2 level. Those results are discussed in section 4.3.2 (page 109).

Figure 3.41 displays the formation of trimer III from a set of dimers. All trimers are energetically favoured in comparison with the dimer. This is also displayed by the mean binding energy per monomer (table 3.22 / ΔE_{H-BOND}). All values are lower than that for the dimer (−2.44 kcal/mol). In contrast to trimer I, the cooperative forces (ΔE_{NPA}) for trimer II are repulsive. The repulsion leads to a lengthening of the oxygen-oxygen bond in trimer II, despite the stronger hydrogen bond (3.644 kcal/mol versus 4.724 kcal/mol).

The cooperative forces change from attraction to repulsion between the different trimers. Most classical water water interaction potentials describe three body forces with polarisation terms. Since the energy gain from polarisation should always be negative, a second force of equal strength or stronger has to contribute to the cooperative effects. The nature of the cooperative forces can be analysed with SAPT [208c]. Tachikawa et al. [159] and Chałasiński et al. [157] examined the cyclic planar trimer (trimer I). Both papers show that the trimer's geometry is controlled by the two centre forces. The three body forces have a shallow minimum at the equilibrium geometry and are strongly repulsive at other regions of the potential energy surface. The attractive part of the three body forces is the polarisation interaction while the repulsive part is governed by three body exchange repulsion and second order exchange induction [159]. A good water-water interaction potential should therefore find a suitable expression for the changing three body forces to reproduce the balance of the three body forces.

The sign and value of the energy gain from cooperative forces not only change with the molecule's geometry but also with the basis set and method used for the calculation. Therefore, it is difficult to compare the results of this work with other values published in the literature. According to Mó [145] only the cyclic trimer has a negative value for ΔE_{NPA}, while Lentz [133] concluded that the cyclic trimers are not favoured in comparison with the linear trimers. Xantheas [147] and Van Duijneveldt [140] found three-body terms (2.3 kcal/mol / 2.0 kcal/mol) for the cyclic trimer (C_1 symmetry), that agree with the value found in this work. Del Bene and Pople [107, 108] investigated the linear trimers in greater detail. Their findings agree qualitatively with the results from this work.

	trimer I	trimer II	trimer III	trimer IV
[107]		+1.87	+0.957	−2.055
[108]	−2.94[a]	+1.87[b]	+2.05[b]	−2.06[b]
this work[c]	−2.866	+0.443	+0.360	−0.720

[a] 4-31G Basis [b] STO-4F Basis [c] BSSE corrected

Table 3.27: ΔE_{NPA} in kcal/mol

Sadly it was not possible to analyse the global minimum of the water trimer potential energy surface at DZP/MP3 level. The calculation of four selected points at different levels of geometry optimisation showed that the cyclic trimer is favoured. Such a trimer cannot be part of a three-dimensional ice like lattice. This will be important, if the structure of the different water layers on a metal surface is examined. The stabilisation of linear trimers has to be caused by the interaction with the platinum and/or lattice effects. The calculations showed also, that all trimers are energetically more favourable than dimers. In two cases (trimers II and III) the cooperative forces are repulsive and therefore reduce the interaction energy. This change of sign gives a reasonable clue that at least one force other than polarisation controls the cooperative effects. It is also reported in the literature that a classical polarisation model yields only up to 60% of the cooperative forces in a trimer [209]. SAPT [159] calculations show, that the other dominat repulsive cooperative forces are three body exchange repulsion and second order exchange induction. The repulsive cooperative forces are important for the development of a classical interaction potential. If only polarisation (always bonding) is taken into account, trimers are stabilized, which should decay by the nonadditive interactions.

3.5 Summary of the Quantum Mechanical Calculations

1. GAMESS UK offers a selection of internal basis sets. The DZP basis set was the most useful set for calculations. The basis set is small enough to keep the computational cost low but at the same time flexible enough to yield good geometries and energies. The bigger TZVP basis set is not well balanced. The TZVP basis set of GAMESS UK not flexible enough, since it does not contain the necessary polarisation functions. The BSSE of the results obtained with the TZVP basis set is much bigger than the BSSE of the DZP results. Ghost orbital calculations with the TZVP basis showed that s-electron density is moved from the bonding

hydrogen atom (H_3) to s-orbitals of the accepting oxygen atom (O_4). The pseudo-s d-orbital of the TZVP basis set helps the oxygen's s-orbitals during the calculation. The TZVP basis set loses its flexibility. The DZP basis set has a s-orbital with a maximum at the same place as the pseudo-s d-orbital. The d-orbitals are much less used to describe s-orbitals.

2. The MP3-method includes correlation effects into the calculations. The optimized geometries and energies for the water dimer agree very well with other published experimental and theoretical results. SCHEINER claims in his review [125] that the MP and coupled cluster (CC) methods are the best ones to analyse the interaction, because both are size consistent. Both methods CC and MP3 gave nearly the same results for planar water trimer (C_{3h} symmetry).

   MP2 includes already most of the correlation effects. MP3 only contributes small but subtle changes. More important changes are reached at MP4 level according to the literature, but those calculations are too costly. Since the MP3 calculations reproduce reasonably well the CC results, a further increase of the perturbation level seems not to be necessary and is, considering the increasing size of the system, unwise.

3. The correction of the interaction energy with the method of BOYS and BERNARDI yields very good energies close to experiment. The geometry of the water dimer with fixed monomer geometries was optimized with a full CP correction. Those values ($\Delta E = -4.914$ kcal/mol) are not only closer to the experimental values but also to the theoretical limit of -4.9 kcal/mol.

4. Numerical frequencies and frequency shifts at MP3 level are of the same quality as those of the costly MP4 method. Analytical MP2 frequencies are very reliable and allow thermochemical predictions such as the zero point energy. Further improvement might be achieved by scaling.

5. The hydrogen bond is not only formed by electrostatic forces but also by the rearrangement and interaction of inner orbitals of the water molecules. Energy decomposition according to MOROKUMA shows that the dimer is formed by electrostatic interaction and exchange repulsion. The bend of the hydrogen bond leads to a relaxation of the exchange repulsion. The energy gain by this relaxation is larger than the price paid by electrostatic interaction. The formation of the hydrogen bond is accompanied by a small but important charge transfer. Within a chosen method of computation the binding energy is proportional to the charge transfer. Test calculations showed that the correlation between charge and proton transfer is small at equilibrium geometry. Calculations with fixed water geometries therefore give reliable results for the charge transfer during hydrogen bond formation.

6. The error obtained by fixing the water geometry at the experimental value is small and negligible compared with the interaction energy. This allows us to scan vast areas of the potential surface in a reasonable amount of time. A BSSE correction of the energy during this scan is necessary to distinguish between real minima and BSSE induced minima.

   The potential energy surface around the dimers minimum (C_S symmetry) is very flat. The energy decomposition showed that changes in the electrostatic interaction and the exchange repulsion energy cancel each other in this region. The surface is even flatter around the trimer's minimum.

7. Calculations for four different water trimers at MP3 level suggest that cooperative effects are important for the formation of small water clusters. The cooperative forces change their sign

for the different trimers. This indicates that at least another antibonding three body force is involved.

Stable hydrogen bonds cause charge transfer. Calculations of the electron affinity and the ionization potential show that the most stable water molecule is uncharged. Stable trimers therefore are built from water molecules which donate and receive electrons at the same time.

The most stable water cluster is cyclic. Such a cluster cannot be part of a three-dimensional ice-like lattice. The formation of linear water clusters on metal surfaces is therefore caused by the direct interaction of the water molecules with the surface.

Chapter 4

Classical Water-Water Interaction Potentials

A quantum chemical simulation of an extended metal surface with several water molecules is unrealistic at the chosen level of computation. The dynamics of large systems can be easily simulated with a molecular dynamics code. Such a program utilizes the interaction potentials between the different molecules in analytical form. Various water-water interaction potentials have been used for the simulation of liquid water or ice [246–253]. Those potentials differ in their computational complexity. A suitable potential should be simple and easy to calculate and also describe the quantum chemical results well.

Such a potential also simplifies the examination of the water trimer's potential energy surface. The structure of the trimers is optimized using the classical potential in the first step. The preoptimized geometry is then used for a quantum chemical geometry optimisation. This procedure reduces the computational efforts and helps us to distinguish between quantum chemical and electrostatic forces in the trimerisation.

Successful descriptions of the metal-electrolyte interface use simple water-water interaction potentials [95–98], so the comparison started with these simple potentials.

4.1 Classification of the Different Potentials

Various potentials have been published and used in simulations (see section 1.1.3, page 4). They are most easily distinguished by the number of points necessary to describe the monomer. Figure 4.1 displays the four basic water geometries. Geometry I with five points (**BNS** [126], **ST2** [126]) is a tetrahedron with two negative charges representing the free electron pairs. The monomer geometries of the two potentials differ only by the distance between the charges and the oxygen atom. Close related to geometry I is ROWLINSON's geometry (II) (**Row** [126]). The negative charges are perpendicular to the molecular plane like the B_1 molecular orbital (figure 3.1, page 48). Geometry III (**BF** [9, 116], **TIPS2** [116, 117], **TIP4P** [116, 249, 250]) using four points for the description of the monomer is the oldest found during the literature search [9]. The negative charge is moved on the bisector of the bond angle ω to simulate the polarisation of the oxygen atom by the hydrogens. The whole monomer keeps its C_{2v} symmetry. Since the distance between the charges is smaller for geometry I and II than for geometry III, the charges have to be higher to get a dipole moment of a similar size. Geometry IV using only three points (**SPC** [116], **SPC/E** [97, 98, 109, 254, 255], **TIPS** [248, 256], **TIP3P** [116], **CFMS** [257], **NCC** [258, 259]) is closest to the experimental geometry with no additional assumptions. Geometry IV is the only geometry with the negative charge placed at the oxygen atom. The geometries of type IV monomers found in the literature vary between the experimental values and a simplified tetrahedron. The geometry of water in potentials with flexible bonds is usually of type IV.

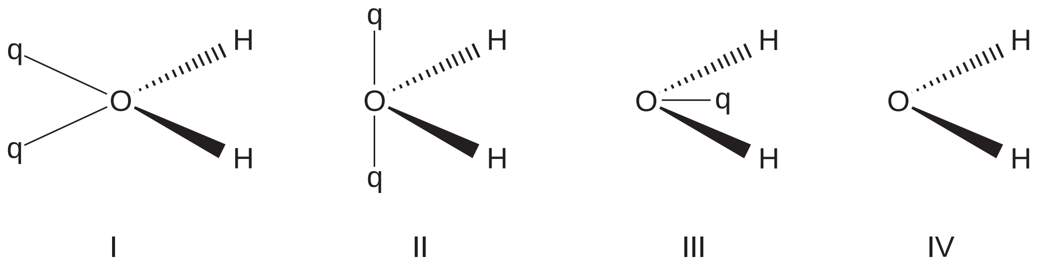

Figure 4.1: Geometries of water monomers for different interaction potentials.

Only the CFMS and the NCC potential use extended functions to describe the interaction between the molecules. The interaction energy of the other, simpler models consists of two parts with small modifications between the different potential:

1. Coulomb interaction V_{CC}: The interaction of charges on different sites μ and ν dominate the total interaction energy.

$$V_{CC} = \frac{1}{4\pi\epsilon_0} \sum_{\mu \neq \nu} \frac{q_\mu q_\nu}{r_{\mu\nu}} \tag{4.1}$$

   The BNS (R_L = 2.0379 Å, R_U = 3.1877 Å) and the ST2 (R_L = 2.0160 Å, R_U = 3.1287 Å) models use additional damping functions[1] S(r) for the Coulomb energy.

$$\begin{aligned} S(r_{OO}) &= 0 && (0 \leq r_{OO} \leq R_L) \\ &= \frac{(r_{OO} - R_L)^2 (3R_U - R_L - 2r_{OO})}{(R_U - R_L)^3} && (R_L \leq r_{OO} \leq R_U) \\ &= 1 && (R_U \leq r_{OO}) \end{aligned} \tag{4.2}$$

2. The interaction between the oxygen atoms is described by a Lennard-Jones (12-6) potential V_{VdW}.

$$V_{\mathrm{VdW}} = \frac{A}{r_{OO}^{12}} - \frac{B}{r_{OO}^{6}} \tag{4.3}$$

The extended potentials (CFMS / NCC) does not contain any Lennard Jones terms. The effect of the Lennard Jones interactions is modelled by a set of extended functions, which combine the Coulomb interaction and the van der Waals energy. Those potentials also contain additional polarization terms.

STILLINGER's CFMS model [257] builds water from protons and oxide ions. So the water geometry is flexible. His monomer has a OH bond length r_e of 0.9584 Å, a bond angle ω_e of

---

[1] Such a damping function should not be confused with the spline function used to smooth out the interaction potential at the cut off radius in MD simulations [85].

104.45° and a dipole moment μ_e of 1.855 D. The whole model is parametrised to reproduce those and other experimental values like IR frequencies.

The Coulomb and van der Waals ineraction energie are combined to form extended pair interaction functions ϕ_{OO}, ϕ_{OH}. The first terms[2] of equation 4.4 and 4.5 (energies in kcal/mol and distances in Å) represent the Coulomb interaction. ϕ_{HH} is the pure Coulomb potential (equation 4.1), since both particles do not have any electrons.

$$\phi_{OO}(r) = \frac{1329}{r} + \frac{24}{1+\exp[2.5(r-2.90)]} + \frac{90}{1+\exp[8(r-2.45)]} + \exp[-6(r-2.70)] \tag{4.4}$$

$$\phi_{OH}(r) = \frac{332.2}{r}\left(10\exp[-3.699r]-2\right) + \left(-184.7(r-r_e)+124.0(r-r_e)^2\right) \cdot \exp[-8(r-r_e)^2] \tag{4.5}$$

The fourth term ϕ_P contains the polarisation energy with some interesting variations. Instead of the electrical field $\vec{\mathrm{E}}$ (section 2.8, page 40) a damping function ([1 - K(r)]) is used to calculate its replacement $\vec{\mathrm{G}}$:

$$\vec{G}_i = -\sum_{i\neq j} \frac{(\vec{r}_{ij}q_i)}{r_{ij}^3}[1-K(r_{ij})] - \sum_{l\neq i}\left(1-\frac{3(\vec{r}_{il}\vec{r}_{il})}{r_{il}^2}\right)\frac{\vec{\mu}[1-K(r_{il})]}{r_{il}^3} \tag{4.6}$$

This damping function leads to a slightly different expression for the induced dipole moment $\vec{\mathrm{p}}_1$ in the dimer compared with equation 2.102 (page 43):

$$\begin{aligned} \vec{p}_1 &= \frac{\alpha}{A_1}\left[-\vec{S}_1 - \frac{D\alpha}{r^3}\left(-\vec{S}_2 + \frac{3D}{r^5}(\vec{S}_1\vec{r})\vec{r} + \frac{3A_2}{A_4 r^2}(\vec{S}_2\vec{r})\vec{r}\right)\right] \\ D &\equiv 1-K(r) \qquad A_n = 1-\frac{n\alpha^2}{r^6} \qquad \vec{S}_i = \sum_{i\neq j}\frac{\vec{r}_{ij}q_j}{r_{ij}^3} \end{aligned} \tag{4.7}$$

To check the results the modified system of equations (2.102) was solved by replacing the vectors by their components and solving the new 6*6 system of equations. This method has the advantage that it is simpler to scale the system up to handle more molecules than with the analytic approach.

A second damping function [1 - L(r)] is used during the calculation of the polarisation energy ϕ_P

$$\phi_P = \frac{1}{2}\sum_{\substack{i,j\\ i\neq j}}\frac{(\vec{\mu}_j\vec{r}_{ij})q_i}{r_{ij}^3}[1-L(r_{ij})] \tag{4.8}$$

Equation 4.8 (distances in Å) does not take the interaction between the induced dipole moments into account.

$$\begin{aligned} 1-K(r) &= \frac{r^3}{r^3 - 1.856(r-r_e)^2\exp[-8(r-r_e)] + 16.95\exp[-2.703r]} \\ L(r) &= \left(1+3.170r+5.024r^2-18.00r^3+23.92r^4\right)\exp[-3.170r] \end{aligned} \tag{4.9}$$

Without those additional damping functions the polarisation would dominate all the other interactions. The model would predict unphysical values. A strong electric field from a close neighbour

---

[2] All figures rounded to 4 significant digits [257].

could reverse the direction of the monomer's dipole moment for example.

$$\mu_{H_2O} = 2\, e\, r_e \cos(0.5\, \omega_e) \left\{ 1 - \frac{\alpha}{r_e^3} \left[1 - K(r_e) \right] \right\} \tag{4.10}$$

For $\mathrm{r_e^3} = \alpha$ ($\mathrm{r_e}$ = 1.1305 Å) the dipole moment would vanish without any damping. This damping yields good results, but is difficult to justify.

Table 4.1 summarizes the parameters of the different potentials and the equilibrium structure of the water dimer we calculated with those potentials with the exception of the NCC potential. All bonds of the simple models are too short and the dimerisation energies too high. The pair interaction of two water molecules therefore is over emphasized. All those potentials were optimized to describe liquid water. None of those effective potentials contains any non additive terms like the polarisation energy. To compensate for this extra energy, the pair interaction has to be increased during the generation of the potential parameters. Although the ST2 potential has the longest oxygen oxygen distance (2.85 Å) the interaction energy is too high (6.84 kcal/mol). The best interaction energy is found with ROWLINSON's potential, while the oxygen oxygen distance (2.69 Å) is poor. The extended potentials, which contain polarisation terms, yield better energies and distances (CFMS: 2.95 Å, 5.402 kcal/mol, with fixed, optimized water geometry). Results obtained with the experimental water geometry (0.9572 Å, 104.52°) do not differ significantly from those with the optimized water geometry (section 11.8, page 329). The CFMS model allows the water molecule to relax (2.896 Å, 6.95 kcal/mol). The relaxation energy (1.95 kcal/mol) is too large in comparison with the quantum chemical (DZP/MP3, BSSE corrected) value of 0.07 kcal/mol. The best values for the angle β (about 47°) yield potentials with a type III geometry for the dimer. All of them are close to the experimental value. The best value (2.9°) for α is found by the ST2 model.

4.2 Comparison with the Quantum Mechanical Potential Curves

A display of the quantum chemical and the classical curves can be found in the appendix (section 11.8, page 329). In this section only graphs are displayed, which are necessary to understand the argument. For the less important graphs references to the appendix are given.

The BNS- and the ST2 models show local minima in the repulsive curves (both $\mathrm{a_{HH}}$ and $\mathrm{a_{OO}}$) like the BSSE uncorrected repulsion curves $\mathrm{a_{HH}}$ (figures 3.29, 3.32, 11.3c, 11.4c). Figures 4.2 to 4.5 display details of the local minimum of the BNS $\mathrm{a_{OO}}$ curve.

The fraction of the Coulomb energy in the total energy approaches zero as the oxygen-oxygen distance gets shorter. The Lennard Jones interaction in this region is only very small. The addition of both energies creates the local minimum. The Coulomb energy is pulled down to zero by a damping function as displayed in figure 4.3. Figure 4.4 shows the change of the Coulomb energy. The damping is necessary to avoid a negative Coulomb energy for small distances. Figure 4.5 shows how the attractive OH interactions overpower the repulsive forces of the OO and HH interactions. The minimum is caused by too strong attractive forces at small distances.

The correction of the BSSE weakens the attractive forces between the two water molecules as shown in chapter 3. The counterpoise correction of the BSSE keeps the molecules apart, because it is no longer possible to improve the wavefunction of one monomer with the other monomer's

	d_{OO} [Å]	α [deg]	β [deg]	$-\Delta$E [kc]	Geo	q_O [e]	q_Q [e]	r_{OQ} [Å]	r_{OH} [Å]	θ [deg]	A [kcÅ^{12}]	B [kcÅ^6]	r_0^c [Å]	E^d [kc]	Lit[a]
BNS	2.76	0	54.7	6.88	I		−0.19562	1.0	1.0	109.47	77366	153.8	2.8	0.048	[126]
ST2	2.85	2.9	52.0	6.84	I		−0.2357	0.8	1.0	109.47	238661	268.9	3.2	0.329	[126]
SPC	2.75	0	26.0	6.59	IV	−0.82			1.0	109.47	629400	625.5	3.2	1.918	[116]
SPC/E	2.75	0	26.0	7.17	IV	−0.8476			1.0	109.47	629080	625.2	3.2	1.917	[109]
Row	2.691	1.25	51.0	5.404	II		−0.3278	0.2539	0.96	105.0	474108	1158	2.7	0.238	[126]
BF	2.72	0	47.0	6.06	III		−0.98	0.15	0.96	105.7	560400	837.0	3.0	1.350	[116]
TIPS	2.78	0	27.0	5.70	IV	−0.80			0.9572	104.52	695000	600.0	3.2	1.962	[117]
TIPS2	2.79	0	46.0	6.20	III		−1.07	0.15	0.9572	104.52	695000	600.0	3.2	1.852	[116]
TIP3P	2.74	0	27.0	6.50	IV	−0.834			0.9572	104.52	582000	595.0	3.2	1.844	[116]
TIP4P	2.75	0	46.0	6.24	III		−1.04	0.15	0.9572	104.52	600000	610.0	3.2	1.797	[116]
CFMS	2.954	−4.9	19.3	5.402	IV	−2.0			0.9584	104.45	complex functions				[257]
CFMS	2.896	−4.6[e]	20.5	6.95	IV	−2.0			relaxed geometry		complex functions				[257]
NCC[b]	2.97	4.0	35.0	5.18	III		−0.5525	0.4481	0.9572	104.52	complex functions				[259]

kc : kcal/mol [a] selection chosen to cover the most with a minimum of papers [b] copied from the lit. [c] minimum of the Lennard Jones energy
[d] contribution VvdW to the dimer's energy [e] The reported angle of 4.6° yields a too low energy, a change of the sign the correct

Table 4.1: Comparison of various potentials from the literature and the calculated optimized dimer structures.

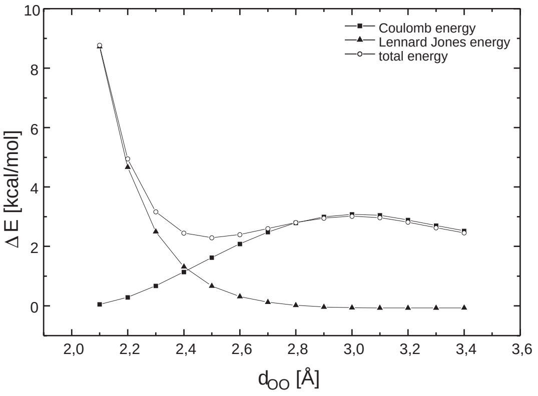

Figure 4.2: Local minimum of the BNS-a_{OO} curve.

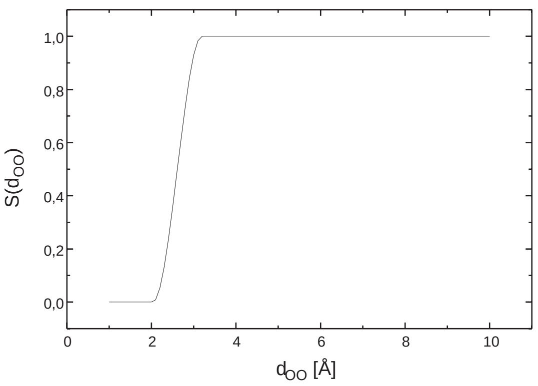

Figure 4.3: Damping function for the Coulomb interaction.

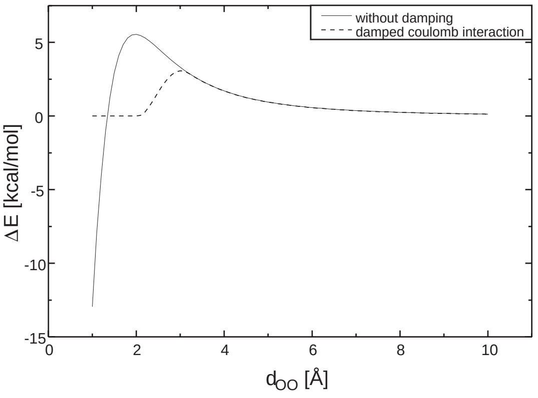

Figure 4.4: Influence of the damping.

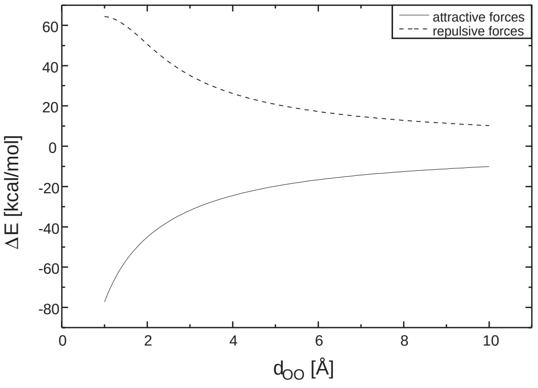

Figure 4.5: Composition of the Coulomb energy.

functions. In the quantum chemical as well as in the classical case the local minimum is caused by too strong attractive interactions at small distances.

All classical dimerisation curves (figures 11.3a - 11.12a, section 11.8) with the exception of the CFMS model (figure 11.13a, 11.13e) have their minimum at too small oxygen-oxygen distances and the interaction between the water molecules is too high (please refer also to table 4.1). The correct description of the minimum of the CFMS curves is not achieved by weaker attractive forces. They are actually stronger. The improvement is achieved by a better description of the repulsive forces. For simple models the repulsive curves are always steep, but they are of short range. This is caused by the r^{-12} term of the Lennard-Jones interaction energy. The minimum of the Lennard Jones curves is between 2.8 Å and 3.2 Å (table 4.1). The equilibrium geometry of the dimers is therefore dominated by attractive Coulomb interaction. The CFMS model by STILLINGER uses exponential terms for the description of the repulsive terms. Those extensive functions produce the right form for the repulsive curves a_{HH} and a_{OO}, but the repulsion starts too early (figures 11.13b, 11.13c, 11.13.f, 11.14a). The correct description of the water dimer with the CFMS model is achieved with strong repulsive terms, which keep the monomers apart.

The a_{OO} curve of the ST2 model (figure 11.4b) has a less distinct local minum and is so better than the BNS curve (figure 11.3b) although both models use nearly the same geometry for the monomers. The coefficient A of the Lennard Jones potential is bigger and the distance r_{OQ} between the charges and the oxygen atom are smaller. This leads to a higher contribution of the Lennard-Jones energy. A damping function is no longer necessary and the local minimum nearly vanishes. The model of ROWLINSON has a even larger value for A. Simultaneously the charges move backwards (geometry II, figure 4.1). This leads to a much steeper curve for a_{HH} and the local minimum vanishes (figure 11.5b), since the negative charges get closer to each other and Coulomb repulsion contributes stronger to the total repulsion energy. The a_{OO} curves for the three and four point models hardly differ, since the short range repulsion is controlled by the Lennard Jones term and not by the Coulomb interaction. The movement of the charge is therefore less important for repulsion energy. An increase in the distance r_{OQ} between the charges is also compensated by greater charges of the four point models, which explains the similarity of the curves.

Another clue to the role of the Lennard-Jones energy for the interaction is given by the a_{HH} curves. Since the distance between the oxygen atoms and the charges is now much bigger (figure 3.29, page 69 for geometries), the hydrogen-hydrogen repulsion gains more importance in comparison with the Lennard Jones interaction energy. Since the electron density at the hydrogens in a water molecule is low, the interaction between two hydrogen atoms has to be dominated by Coulomb repulsion. Because the total repulsion energy is controlled by the hydrogen-hydrogen Coulomb repulsion, the classical a_{HH} curves are generally much closer to quantum mechanical curves than the a_{OO}.

The influence of β (figure 3.2) on the total energy is very strong for the models based on tetrahedra (figures 11.3d, 11.4d). For both models (BNS, ST2) β is very close to the tetrahedral value of 54.7°. This is due to the interaction between the charges q of the free electron pairs and the bonding hydrogen atom. The closer the negative charge is to the monomer's hydrogen atoms, the flatter is the curve (BNS $>$ ST2 $\gg$ ROWLINSON). The flattest curves are produced by 3-point models. Here the oxygen charge does not move and the change of the interaction energy is caused only by the orientation of the hydrogen atoms. The curves of the 4-point models are better than the 3-point models, as they reproduce better the asymmetry of the BSSE corrected curves. They also have the best values for β in the equilibrium structure, because they are closest to the experimental value of $47 \pm 10°$.

The CFMS model's curve $E(\beta)$ is the steepest of all. This overestimate of β on the interaction energy is caused by the Coulomb part of the model. Figure 4.6 displays a comparison of the pure Coulomb interaction energy between an oxide anion O^{2-} and a proton H^+ and the potential energy curve proposed by STILLINGER. STILLINGER's interaction energy is slightly lower than the pure Coulomb potential for large distances r_{OH}. The Coulomb interaction in STILLINGER's model is much stronger compared with the other models. The highest charge on oxygen occurs with the TIPS2 model (1.07 e), which is still much smaller than 2.0 e of STILLINGER's model. The dependence of β on the interaction energy seem to be directly correlated with the Coulomb energy part of the model. The more important the Coulomb part gets the more energy is needed to distort the equilibrium geometry.

Figure 4.6 shows how well the Coulomb and repulsive terms (equation 4.5) work together in STILLINGER's model. At small distances the attractive Coulomb regime is gently changed into a repulsive potential. Any additional repulsive functions are therefore not necessary.

The polarisation energy of the water dimer as a function of α calculated with the CFMS model is shown in figure 4.7. In contradiction to the quantum chemical results (table 11.19) the

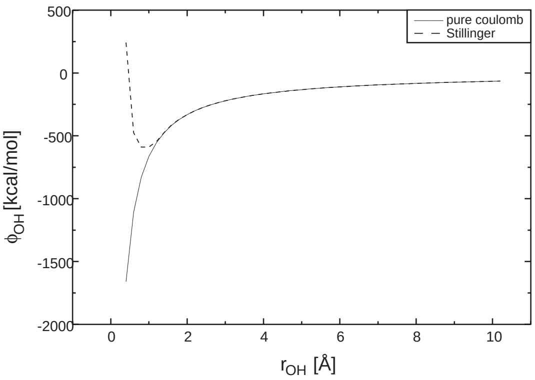

Figure 4.6: OH interaction energies in OH^-.

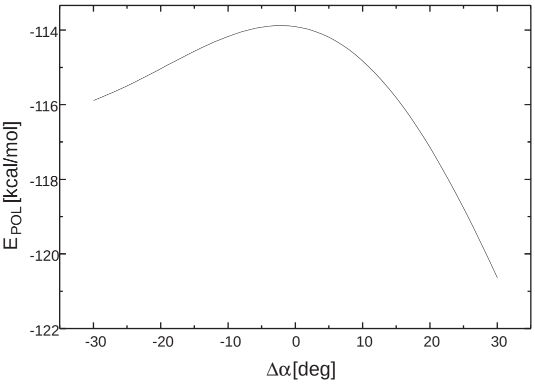

Figure 4.7: Polarisation energy of the CFMS model.

polarisation energy has a maximum rather than a minimum at the equilibrium structure. The polarisation energy in the CFMS model widens the parabola and describes the quantum chemical values better. The energy curve of the CFMS for the variation of W3 (α) (figure 11.14c) is still the steepest curve of all. As before in the case of β the importance of the bond angles is overestimated by the Coulomb energy.

The E(α) curves calculated with the tetrahedral models (BNS, ST2) are steep, but fit much better to the quantum mechanical curve. The best description of the curve is given by ROWLINSON. The curves of models with geometry III (TIPS2, BERNAL and FOWLER, TIP4P) are steeper than the quantum mechanical curves, but fit better to the BSSE uncorrected curve. The three-site models (SPC, SPC/E, TIPS, TIP3P) are also close to the quantum mechanical curve, but exaggerate the curve's anharmonicity. In a three-site model the hydrogen atom H2 is much closer to the centre of negative charge of the other molecule than in a four-site model. The increased Coulomb energy also raises the steepness of the curve.

The comparison of the different potentials with the quantum chemical curves might be summarized as follows:

1. ***No potential describes all curves in a satisfactory manner.***

2. Polarisation seems to be important for the equilibrium structure and adequate fitting to the quantum chemical curves. Both models containing polarisation terms (CFMS and NCC) also contain extended functions. At this stage it is difficult to judge from the classical potential energy calculations whether this good agreement is achieved by the polarisation terms or by the extended interaction functions. The inclusion of polarisation terms is dangerous at low distances and could lead without any damping to poor values for the bond length and the bonding energy of the dimer.

3. The best description of the angles α and β is given by four-site models (geometry III). A value of 0° for α is still in the experimental range and all values for β are close to the experimental one. The TIPS2 potential offers the best description of the quantum chemical results. The oxygen oxygen distance (2.79 Å) is in comparison with the other simple potentials the second longest and the dimerisation energy (6.20 kcal/mol) reasonable. Figures 4.8 - 4.12 compare the TIPS2 curves with the quantum chemical ones.

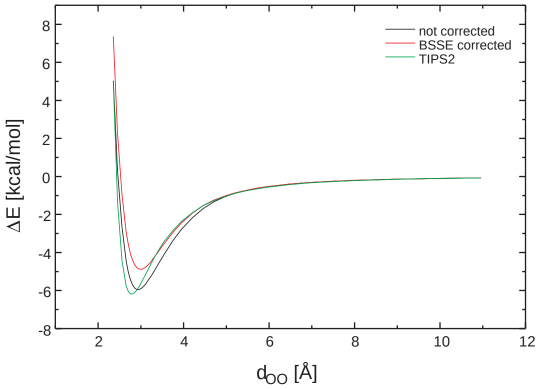

Figure 4.8: Dimerisation curve - TIPS2.

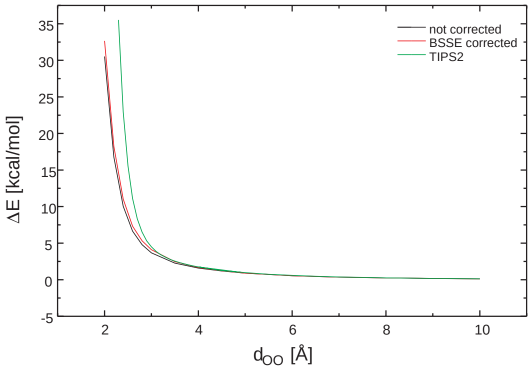

Figure 4.9: OO repulsion - TIPS2.

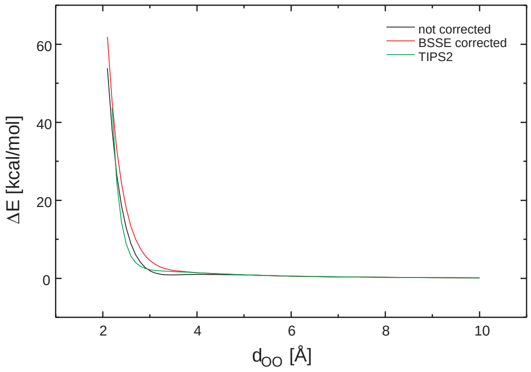

Figure 4.10: HH repulsion - TIPS2.

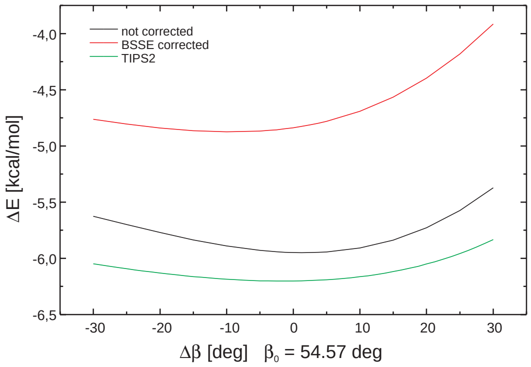

Figure 4.11: Variation of β - TIPS2.

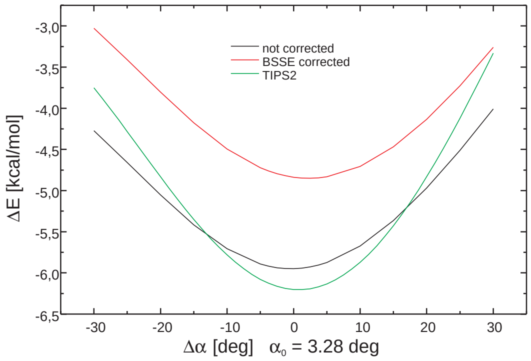

Figure 4.12: Variation of α - TIPS2.

4. The repulsion between the molecules at small distances is controlled by the Lennard-Jones forces and not by the Coulomb energy. To get a good shape of the curve the r^{-12} term should be replaced by an exponential term (CFMS). At the same time the charges should be so small, that they cannot overpower the repulsion term to avoid local minima or damping functions.

4.3 A new model

As shown in section 4.2 no simple water-water interaction pontential describes the water dimer in a satisfactory manner. This section describes the development of a new potential for small water clusters and its application towards the water trimer.

4.3.1 An improved model

The comparison of the quantum chemical results for the water dimer with those from previously published potentials (section 4.2) showed that none of the potentials is actually able to reproduce the *ab initio* results. There are two principal ways to get a better potential:

1. The simplest way is to fit an existing potential to the quantum chemical results and find a new set of parameters.

2. A new potential may be developed by modifying an existing one. The study of the quantum chemical results showed that the water water interaction is dominated by electrostatic and exchange repulsive forces. A first try must therefore be a variation of the noncoulomb oxygen-oxygen interaction term.

Nearly all models contain a parameter which describes the displacement of the centre of charge from the oxygen atom. This movement may be regarded as the polarisation of the oxygen atom by the two hydrogen atoms. Simultaneously this parameter allows us to control the dipole moment of the molecule. There are no ways either experimental or theoretical to get correct values for the partial charges of the atoms in a molecule. The dipole moment is therefore the best property to compare different levels of theory.

A quality function Q is necessary to judge the quality of a fit despite the chosen way. This function was build from different parts:

1. The variances of the quantum mechanical calculated curves (section 3.2.3 - All curves were constructed from the BSSE uncorrected minimum geometry d_{OO} = 2.9354 Å, α = 3.28°, β = 54.57°)

   (a) the dimerisation curve (figure 3.22)
   The dimerisation curve offers the best description of the attractive forces.

   (b) the repulsive curves a_{OO} and a_{HH} (figure 3.30 and 3.31)
   The repulsive curves are necessary for the fine tuning of the repulsive forces in the model. The comparison of the quantum chemical curves with the already published potentials showed that the repulsive forces are important to generate the correct oxygen oxygen equilibrium distance.

   (c) the bending of the three angles (figure 3.3) α, β, W3 (figures 3.27, 3.28, 11.2)
   The inclusion of the those three terms helps us to reproduce the force constants and the shape of the potential energy surface.

2. The variance of the binding energies for the trimers (figures 3.35 - 3.38)
   Cooperative effects are important for the energy and structure of small water clusters. There are two possible methods to incorporate them into a potential:

   (a) Cooperative effects are described by explicit terms in the potential, as the polarisation energy in the CFMS potential.

   (b) The parameters of a pairwise potential are fitted to the values of water trimers so that the new potential enables a reasonable description of small water clusters without explicit use of cooperative effects.

   The later of the two methods was used in this work and cooperative effects are therefore hidden in the parameters of a pairwise interaction potential.

3. The variance of the minimum energy of the d_{OO} curve[3] (table 3.17; d_{OO} = 3.0049 Å, α = 3.31°, β = 54.57°, ΔE = -4.880 kcal/mol) and the energy calculated with the new potential (labelled as minerg)

4. The square sum of the first deviations (mingeo) of the inner coordinates (d, α, β) of the BSSE corrected energy dimer.

$$mingeo = \left(\frac{\partial \Delta E}{\partial d_{OO}}\right)^2_{3.0049\text{Å}} + \left(\frac{\partial \Delta E}{\partial \alpha}\right)^2_{3.31^\circ} + \left(\frac{\partial \Delta E}{\partial \beta}\right)^2_{54.57^\circ} \tag{4.11}$$

   First test showed that the reproduction of the minimum has always been poor although the reproduction of the corresponding energy values has been good. Equation 4.11 has been used to pinpoint the global minimum ($mingeo = 0$). If the new potential has a local minimum at the given geometry, mingeo should vanish.

The dipole moment was not used for the construction of the quality function, because the effective dipole moment of water in water cluster is unknown. It was used as indicator to check, if the fit is physically reasonable. Table 4.2, which summarizes fit results of the fitting, shows that the dipole moment did not change much between the different potentials.

The most severe problems during the fit were caused by the cooperative effects which contribute strongly to the total interaction energy of the water trimers. An ideal pairwise interaction potential should create an error in the trimerisation energy of 3 kcal/mol, since it cannot describe the cooperative effects (section 3.4). A potential which describes the trimers perfectly gives very poor values for all dimers. A compromise had to be found between both forms. Another problem arises from the change of the sign of ΔE_{NPA} (cooperative effects). Interaction potentials which describe the trimers with repulsive cooperative effects well, usually gave extremely poor values for trimers with attractive cooperative effects and vice versa. A suitable potential has to reproduce the correct order of the trimerisation energies in the first place and the absolute values only in the second place.

---

[3] The BSSE correction of the equilibrium geometry was done later in one of the unavoidable slack periods.

All parts of the quality function differ in their size. If the simple sum is optimized, the biggest contribution to the total error controls the development of the optimisation. To avoid this and to minimize all sums equally, the individual terms were weighted. Those weights also allowed a fine tuning of the final results to get a better description of the trimers.

First tests in section 4.2 showed that it is nearly impossible to describe strong repulsive dimers (a_{OO} and a_{HH}) with the chosen set of potentials. The better their description is, the worse are the results for the attractive dimers (dimerisation curve, W1, W2, W3). To ensure a physical reasonable result, the upper limit for repulsive interactions was set at approximately 7 kcal/mol. This energy is about 1.5 times of the optimal interaction energy.

The fit of a new model to the existing quantum mechanical values was done in two steps. The first step of the procedure was done with a Simulated Annealing algorithm [242, 260–268]. This algorithm can free itself out of local minima. Results obtained with such a program were usually close to the global minimum. On the other hand the algorithm does not necessarily reaches the global minimum. The theory only demands that it stops close to it. To ensure that the true global minimum was found, a second calculation was done with a simplex algorithm [242, 269]. The first point of the initial simplex was the result of the 'Simulated Annealing'-step. The other points were constructed from this point by adding 10.0 to each parameter. Both methods were chosen, since they do not require the calculation of any derivatives.

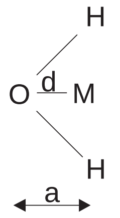

Figure 4.13:

The search for a new model started with a reparametrisation of the TIPS2 potential [116], because it does not contain a damping function and fitted fairly well to the quantum mechanical curves (section 4.2). The monomer's geometry is the experimentally found geometry (r_{OH} = 0.9572 Å, ω = 104.52°). This makes a comparison between the classical potential and the quantum chemical potential easier. The centre of charge M in this model (d = 0.15 Å) is at the same place as the centre of the valence electrons.

$$6d = 2(a-d) \qquad \Rightarrow \qquad d = \frac{1}{4}a = \frac{1}{4}r_{OH}\cos\left(\frac{\omega}{2}\right) = 0.146\ \text{Å} \tag{4.12}$$

The comparison of the quantum chemical values with the results from previously published potentials showed that the oxygen-oxygen repulsion is the most important parameter for improvement. The shallow minima of the Lennard-Jones functions (table 4.1) are already close to the optimized oxygen-oxygen distance. The first set of test potentials had therefore the same structure as the TIPS2 potential but differed in their repulsive terms for the oxygen-oxygen interaction.

A : $a \cdot r^{-12} - b \cdot r^{-6}$ The original TIPS2 form

B : $a \cdot \exp(-r \cdot b) - c \cdot r^{-6}$

C : $a \cdot \exp(-r \cdot b)$

D : $a \cdot r^{-b}$

E : $a \cdot \exp[-(r-c) \cdot b]$

F : like E, but the parameter d for the dislocation of the centre of charge from the oxygen atom was also fitted

All potentials contain another parameter q, which is the negative charge at the centre of charge. Table 4.2 displays the optimized parameters for those potentials. The values for the potentials A

	pot. A	pot. B	pot. C	pot. D	pot. E	pot. F
q [e]	1.0324	1.1153	1.1721	1.0354	1.0730	1.0271
a	593003.7	2072103	130121.9	549239.9	2072110	2072284
b	48.7600	-907.510	3.6205	12.0829	4.7154	5.0074
c		4.9903			-0.0801	0.069752
d	0.15	0.15	0.15	0.15	0.15	0.13173
minerg^{A}	0.0733	0.0302	0.0070	0.0174	0.0449	0.0345
dipole [D]	2.1614	2.3347	2.4537	2.1676	2.2463	2.2402
dimer.^{A}	0.5179	0.5748	0.0105	1.4302	0.5119	0.3873
a_{OO}^{A}	1.6542	5.2712	9.8509	1.1416	2.1744	1.9334
a_{HH}^{A}	2.0625	0.7036	0.0983	2.3267	1.1498	1.0582
W1^{A}	0.0326	0.0462	0.1651	0.0601	0.2231	0.2134
W2^{A}	0.0172	0.0214	0.0085	0.0597	0.2700	0.2349
W3^{A}	0.0083	0.1351	0.2522	0.0723	0.1880	0.1809
trimer I^{A}	5.6736	8.1416	25.300	2.0653	1.8954	1.5931
trimer II^{A}	0.0051	0.0016	0.0006	0.1358	0.9164	0.7308
trimer III^{A}	0.0406	0.0710	0.0186	0.0036	0.4475	0.3655
trimer IV^{A}	1.7053	1.1725	0.5512	1.0704	0.0883	0.1591
total^{C}	12.2352	16.1395	36.2559	8.3657	8.3775	7.2439
trimer I^{B}	-11.4074	-10.9362	-8.7599	-12.3523	-12.4125	-12.5264
trimer II^{B}	-8.3524	-8.3218	-8.3053	-8.6498	-9.2384	-9.1357
trimer III^{B}	-8.0407	-7.9760	-8.1060	-8.3020	-8.9112	-8.8466
trimer IV^{B}	-9.7658	-9.9889	-10.3295	-10.0372	-10.7745	-10.6724

^{A} variance [kcal^{2}/mol^{2}] ^{B} absolute value [kcal/mol] ^{C} dimer counted twice

Table 4.2: Potentials A - F.

	pot. A	pot. B	pot. C	pot. D	pot. E	pot. F
d_{OO} [Å]	2.8298	2.8480	3.0053	2.8058	2.8514	2.8496
α [deg]	0.48	0.33	-0.90	0.68	0.30	-0.57
β [deg]	44.15	43.22	36.54	45.45	43.05	38.37
$-\Delta E$ [kcal/mol]	4.9614	5.0138	4.9076	5.1047	5.4161	5.4224
d_{OO} [Å]	3.0878	3.1583	3.2957	3.0705	3.0865	3.0559
α [deg]	127.74	127.74	127.74	127.74	127.74	127.74
β [deg]	180.0	180.0	180.0	180.0	180.0	180.0
$-\Delta E$ [kcal/mol]	2.8871	2.7788	3.0949	2.9255	3.2360	3.3573

Table 4.3: Optimized geometries of both minima on the dimer's potential energy surface (figure 4.21).

to F are given in such a way, that if r is given in Ångström, the final result will be in kcal/mol. For the calculation of the Coulomb energy the final result has to be multiplied with 332.17752 kcal/mol $\cdot$Å/e^2 to get the energy in kcal/mol if the distance between both charges is given in Ångström and charges as multiple of the elementary unit e.

The best results (quality function, shape of the curves, description of the trimers, opt. dimer geometry) of this first set of test potentials were obtained with potential E. The errors (standard deviation σ) are listed in table 4.4. Figure 4.15 to 4.19 display the quantum mechanical curves and the curves calculated with potential E.

The search began with a fit to values found only for dimers, including all repulsive dimers (ΔE $>$ 7 kcal/mol). The first potential to be tested was the original TIPS2 potential (potential A). The results were disappointing. The next try was the replacement of the repulsive term in the Lennard-Jones term of the potential (potential B). The results were better. All results found in different optimisation approaches (different weights in the total error) gave only small values for the parameter c. This validates the conclusions already drawn from table 4.1 that the attractive the van der Waals potential is of minor importance for the description of the potential energy surface. In the next series of experiments the attractive term was therefore omitted (potential C). This potential gave the best results so far. Potential D was tried to check if the repulsive part of the Lennard-Jones potential can be further improved with a single, optimized repulsive function. Finally potential E was used to test, if a extension (in comparison with potential C) of the oxygen-oxygen interaction potential can describe the quantum mechanical results better. Potential F was tested to see, if any changes in the movement of the centre of charge d leads to a better potential. The small improvement of the variances and the negative value for α in the optimal dimer (table 4.3) were regarded as unimportant for leaving a well-known geometry.

interaction	σ kcal/mol
attractive	0.535
repulsive	1.273
trimer	0.825

Table 4.4: Errors for potential E

The variances of a_{OO} and a_{HH} have been very large at (up to several hundreds kcal^2/mol^2) this state of the search. Those findings lead to the previously mentioned introduction of the weights in the calculation of the error. Those weights helped to realize that a simple potential either describes the repulsive curves well or describes the attractive curves well. The findings obtained with a weighted error function lead to the step wise fixing of an upper limit for allowed points. An upper limit of 7 kcal/mol allowed us to find potentials which describe the attractive and the repulsive curves equally well. At this state of the search the trimers were introduced into the error function. The potential C, which has been the best so far, gave the worst results for trimers. The results of those fits are listed in table 4.2 and table 4.3 displays the associated minima. The analysis of those new potentials showed that the correct sequence of the trimer energies depends mainly on the repulsive oxygen oxygen interaction. The distance where the repulsion comes into play is more important than the shape of the curve. Figure 4.20 displays the repulsive functions of the potentials A, C and E. The shape of all three curves is very similar. The repulsive function of potential C starts to rise first. The longer range of this repulsion prevents the three water monomers from getting closer to each other during the formation of the ring and causes the extremely small trimerisation energy of 8.8 kcal/mol. The binding energies of the other trimers (II, III and IV) with longer oxygen-oxygen distances are well reproduced, but the absolute values are always smaller in comparison with the other potentials. Potential C also has the biggest variance for a_{OO}.

		d_{OO}	α	β	ΔE
		[Å]	[deg]	[deg]	[kcal/mol]
1	min.	2.8514	0.30	43.05	−5.4161
2	min.	2.8514	255.18	316.95	−5.4161
3	min.	2.8514	127.74	180.00	−2.7088
4	tran.	2.8514	307.74	0.00	−2.7088
5	tran.	2.8514	75.48	155.01	−2.4888
6	tran.	2.8514	180.00	204.99	−2.4888

Table 4.5: Stationary points in figure 4.21.

Figures 4.15 to 4.19 show the quantum mechanically calculated curves in comparison with potential E. The curves a_{OO} and a_{HH} (figure 4.16, 4.17) do not show any local minima. The repulsive term is strong enough to overpower the Coulomb forces, when the two monomers get close to each other. No additional damping is necessary. The minimum of the dimerisation curve (figure 4.15) is closer to the origin and the well is deeper than the well of the quantum mechanically calculated curve. The shape of the curves for α and β (figures 4.18, 4.19) is well reproduced by the potential E. Like the dimerisation curve the interaction energy calculated with potential E is bigger than the quantum mechanical calculated energy, but the oxygen-oxygen distance is well reproduced.

Figures 4.21 and 4.22 display the potential energy surface of the water dimer. The oxygen-oxygen distance is set to 2.8514 Å for all configurations. Figure 4.21 shows the bonding region of the surface while figure 4.22 is a contour plot of the antibonding region. In the bonding region three minima and three transition states were found. Table 4.5 and figure 4.14 show the six stationary points in the bonding region. The geometry of the minima 1 and 3 were optimized. The results are displayed in table 4.3.

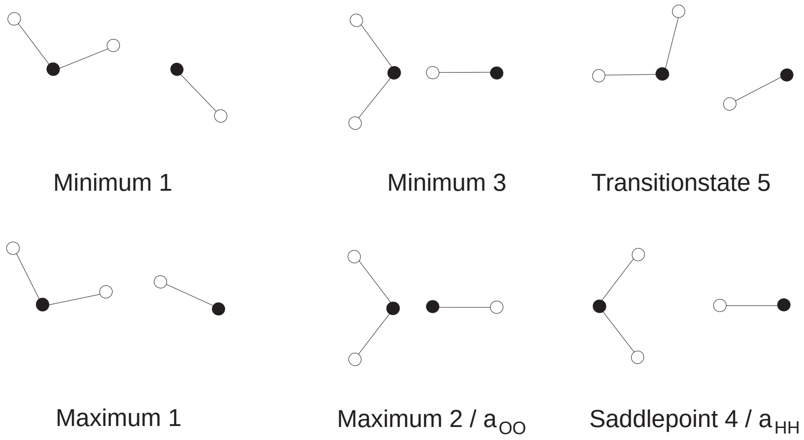
Minimum 1

Minimum 3

Transitionstate 5

Maximum 1

Maximum 2 / a_{OO}

Saddlepoint 4 / a_{HH}

Figure 4.14: Sketches of selected dimer geometries.

Minimum 1 and 2 (figure 4.21) have virtually the same geometry and can be transformed into each other by a reflection. The mirror plane is perpendicular to the plane of symmetry of the dimer and contains both oxygen atoms. Minimum 3 can be transformed into transition state 4 by an improper rotation. The axis of rotation is the dimer's oxygen-oxygen bond and the mirror plane between both oxygen atoms. This shows an interesting feature of the chosen set of coordinates.

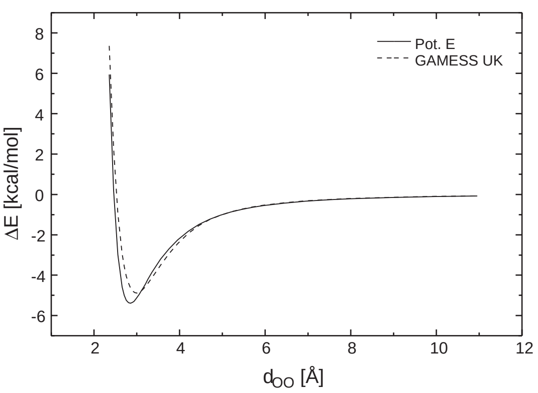

Figure 4.15: Dimerisation curve - Pot. E.

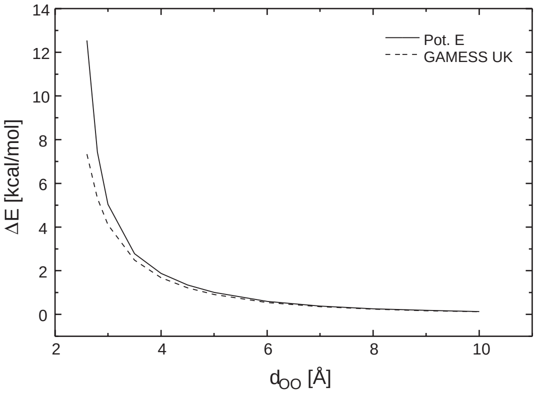

Figure 4.16: OO repulsion - Pot. E.

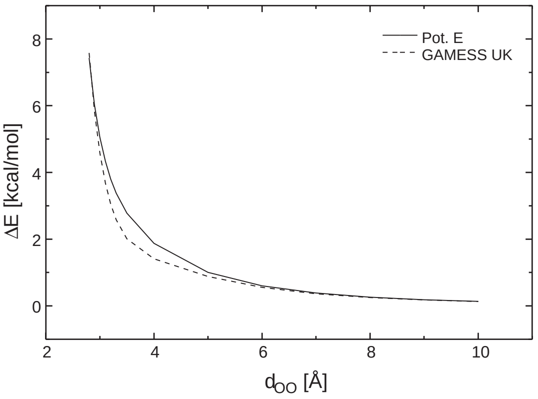

Figure 4.17: HH repulsion - Pot. E.

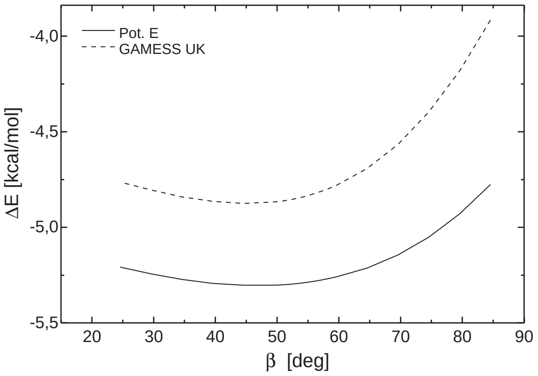

Figure 4.18: Variation of β - Pot. E.

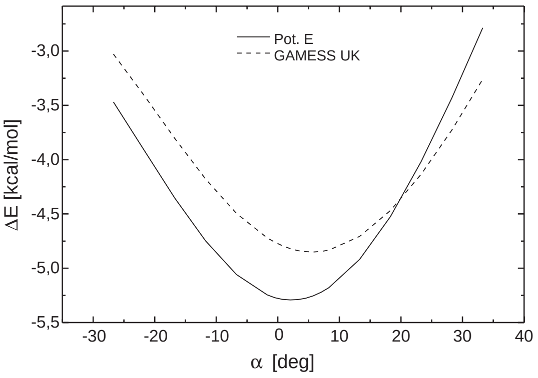

Figure 4.19: Variation of α - Pot E.

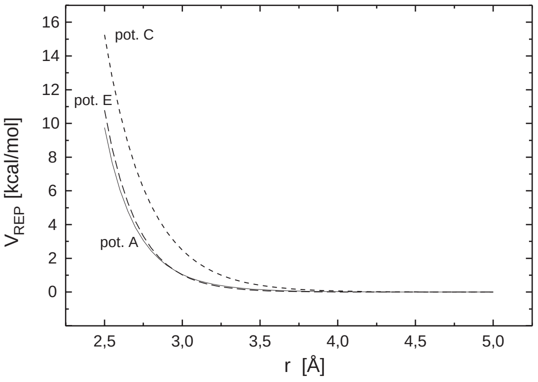

Figure 4.20: Different repulsion functions.

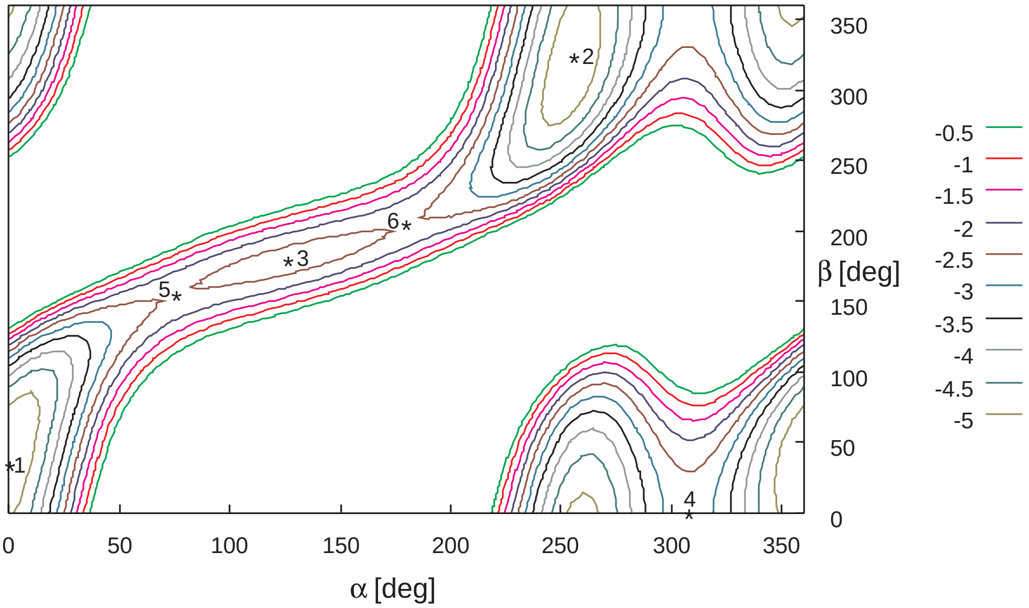

Figure 4.21: Potential energy surface potential E for α and β; d_{OO} = 2.8514 Å / minima.

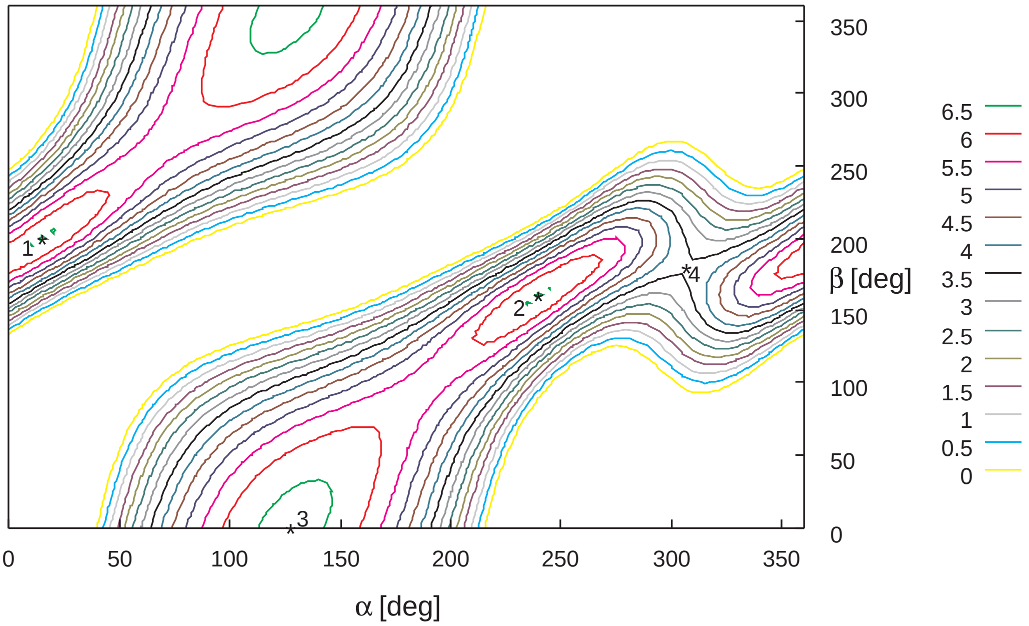

Figure 4.22: Potential energy surface potential E for α and β; d_{OO} = 2.8514 Å / maxima.

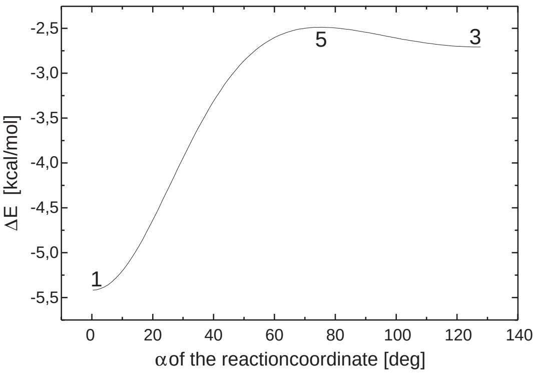

Figure 4.23: Energy profile, path 1-5-3, Pot. E.

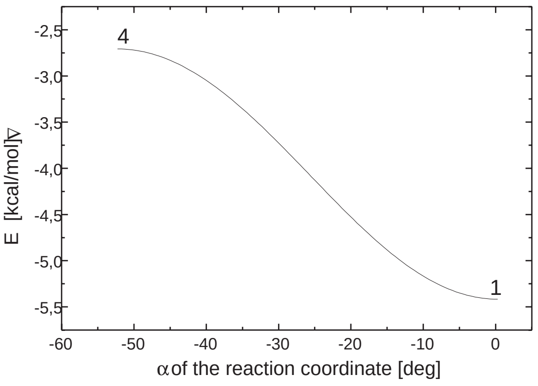

Figure 4.24: Energy profile, path 4-1, Pot. E.

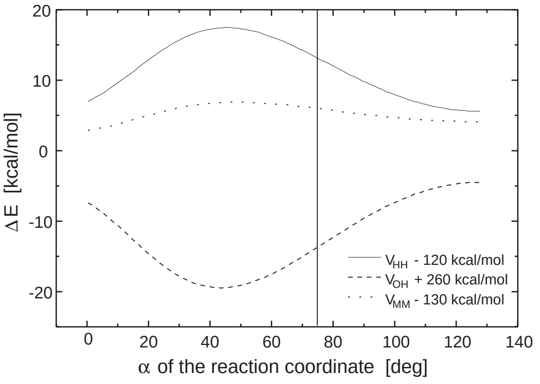

Figure 4.25: Energy composition, path 1-5-3, Pot. E.

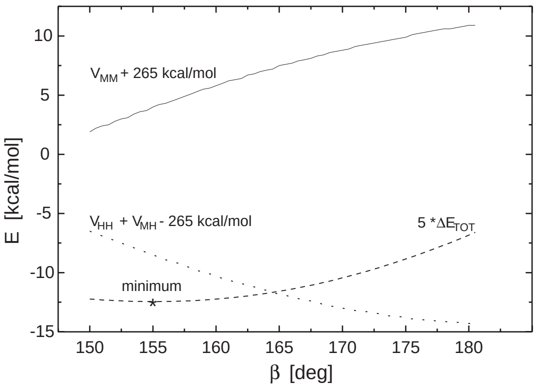

Figure 4.26: Energy composition, point 5, Pot. E.

Although both points have identical geometries geometry 1 marks a minimum and the other point a transition state.

Both points 3 and 4 have the same geometry but they differ in their possibilities to relax (figures 4.23 and 4.24). A movement, which would correspond to the relaxation of transitionstate 4 into geometry 1 or 2, is a movement perpendicular to the potential energy surface at point 3. The chosen set of variables does not allow such a movement at point 3. If the set of inner variables would be totally free of any symmetry restrictions, both points would be equal.

Points 1 and 3 differ through the chosen set of internal coordinates, but this argument does not explain the origin of the transition states 5 and 6 (figure 4.21). Since the oxygen-oxygen distance is fixed at 2.8514 Å for the generation of figure 4.21, the origin of the maximum in figure 4.23 cannot be explained with the repulsive forces between two oxygen atoms. The maximum is caused only by the Coulomb interaction. Figure 4.25 displays the composition of the interaction energy along the path 1-5-3[4]. The vertical line marks the transition state 5. None of the three curves shows any special features at this point. The transition state is not coupled to a minimum or a maximum of a single energy component. Further insight into the problem is offered by a careful analysis of its geometry. A first guess would be at $\alpha = 75.48°$ (one OH bond of the donor lies

---

[4] β was optimized at each point (α, β, ΔE) with $d_{OO} = 2.8514$ Å to find the reaction path.

	1		2		3	4
α [deg]	15.37	0.0	238.77	255.48	127.74	307.74
β [deg]	200.07	180.0	158.47	180.0	0.0	180.0
ΔE [kcal/mol]	6.5331	6.2648	6.5331	6.2648	6.6488	5.5393

Table 4.6: Characteristic points of figure 4.22, d_{OO} = 2.8514 Å.

on the oxygen-oxygen line) and $\beta = 180°$ (figure 4.14), if the interaction between both molecules depends only on Coulomb forces with the charges placed on the individual atoms. Both hydrogen atoms of the second monomer would try to get as close as possible to the oxygen atom to gain as much energy as possible. Figure 4.26 shows how the energy composition changes as β_0 changes from 150° to 180°. The curve for the total energy has a shallow minimum at 155°- the transition state. Moving further towards 180° leads to a rise of the total interaction energy E_{TOT}, while the Coulomb interaction energy containing only the hydrogen atoms V_{HH} + V_{MH} decreases steadily as expected. Simultaneously the Coulomb energy between both centres of charge V_{MM} increases. The rapid increase of the repulsion between the two centres of charge accounts for the geometry of the transition state. This increase is caused by the displacement of the centre of charge from the oxygen in the monomers. During the turn the centres get closer to each other. The geometry of the transition state 5 is therefore a compromise between the attractive forces of the hydrogen-negative charge interaction and the repulsion between both centres of charge.

The same argument holds also for the maxima 1 and 2 in figure 4.22. The distance between both centres of charge has to be as small as possible while distance between the hydrogens and the centres of charge has to be as big as possible. Table 4.6 lists characteristic points of figure 4.22.

Usually it is difficult to find transition states and to optimize their geometry. As shown above potential E and the chosen set of internal coordinates allow us to optimize minimum 3 and to get so the optimized geometry of transition state 4. Table 4.5 displays the optimized geometries of the minima and their energies. During the transition from minimum 1 to minimum 2 increases the oxygen-oxygen distance up to 3.0865 Å. The activation energy of this transition is lowered from 2.71 kcal/mol down to 2.18 kcal/mol. According to potential E should the dimer change its geometry rapidly at room temperature between geometry 1 and geometry 2.

Although potential E reproduces well the shape of the quantum chemical curves are the bonding energies in poor agreement with quantum chemistry. Popkie and Kistenmacher [119, 120] published a simple potential with extended interaction functions without any polarisation terms, which they used for the analysis of larger water cluster. They use a type III monomer geometry with a longer distance d between the centre of charge M and the oxygen atom (0.427 a.u. / 0.226 Å). Their point charge model is build from different parts.

$$\begin{array}{lll} V_{OO} = a_1 e^{-b_1 r} & V_{HM} = \dfrac{-q^2}{2r} & V_{HH} = \dfrac{q^2}{4r} + a_2 e^{-b_2 r} \\ V_{MM} = \dfrac{q^2}{r} & V_{OH} = a_3 e^{-b_3 r} & q = q_O = 2q_H \end{array} \tag{4.13}$$

This is an extension of potential C by adding repulsive terms to the oxygen-hydrogen and to the hydrogen-hydrogen interaction. The authors obtained the parameters for this potential by fitting it to 216 energy values from HF dimer calculations. While potential C gave the best values for the dimers but only poor for the trimer, the potential published by Kistenmacher and Popkie predicts the cyclic water trimer as the most stable trimer with a trimerisation energy of 12.3

		d_{OO} [Å]	α [deg]	β [deg]	ΔE [kcal/mol]
1	min.	2.9834	8.55	56.60	−4.9029
2	min.	2.9834	246.93	303.40	−4.9029
3	min.	2.9834	127.74	180.00	−3.3097
3^*	min.	2.9902	127.74	180.00	−3.3099
4	tran.	2.9834	307.74	0.00	−3.3097
4^*	tran.	2.9902	307.74	0.00	−3.3099
5	tran.	2.9834	90.79	159.42	−3.2548
6	tran.	2.9834	164.89	200.58	−3.2548
1	max.	2.9834	0.76	182.28	13.861
2	max.	2.9834	254.72	177.72	13.861
3	max.	2.9834	127.74	0.00	4.5090
4	sad.	2.9834	307.74	180.00	5.0637

The asterix marks points with an optimized oxygen-oxygen distance.

Table 4.8: Characteristic points of potential N (refer to figure 4.32 and 4.33 for details).

kcal/mol [119], which is close to the quantum chemical value.

First tests to refit this potential with a fixed oxygen charge distance of 0.15 Å gave only poor results. The reparametrisation of the oxygen charge distance d gave very good results. The standard deviations of this new potential N are listed in table 4.7. They are smaller than values given in the literature with an upper interaction limit of 5 kcal/mol.

Figure 4.27 to 4.31 display the quantum mechanical curves and the corresponding curves calculated with potential N.

interaction	σ [kcal/mol]
attractive	0.118
repulsive	0.260
trimer	0.412

Table 4.7: Errors for potential N

The third minimum of N potential is difficult to see. Figure 4.34 display an enlargement of the region, where the minimum should be found. Figure 4.35 shows how the energy changes along the reaction path. The transition state nearly vanishes, although the distance between the charge and oxygen is larger (d = 0.24 Å). Figure 4.36 shows the energy composition[5] along the path. The curves have smaller amplitudes than those in 4.25. The larger oxygen-oxygen distance in potential N reduces the Coulomb interaction. The change of the energy composition during the bending of β is shown in figure 4.37. The reduction of β is again caused by the repulsive interaction between the centres of charge. As both oxygen atoms are at fixed positions during the calculation, the oxygen oxygen repulsion is a constant for all points. The amplitude of change for V_{MM} + V_{OO} is smaller than for potential E, because the distance between the charges is larger. The slope of V_{HH} + V_{HM} is also smaller, since the extra repulsive function in V_{HH} compensates partially for V_{OH}. The extended system of repulsive functions damps the Coulomb interaction and smooths therefore the potential energy surface.

---

[5] The paramter b_1 is so high, that oxygen-oxygen repulsion becomes notable only for very small values of the oxygen-oxgen distance d_{OO}. The good reproduction of the a_{OO} curve (figure 4.28) suggests, that the oxygen-oxygen interaction is dominated by the Coulomb repulsion in equilibrium structures and that well chosen paramters for the hydrogen-oxygen interaction are more important than the oxygen-oxygen repulsion.

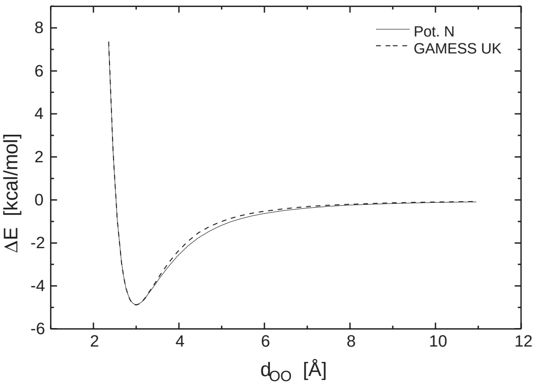

Figure 4.27: Dimerisation curve - Pot. N.

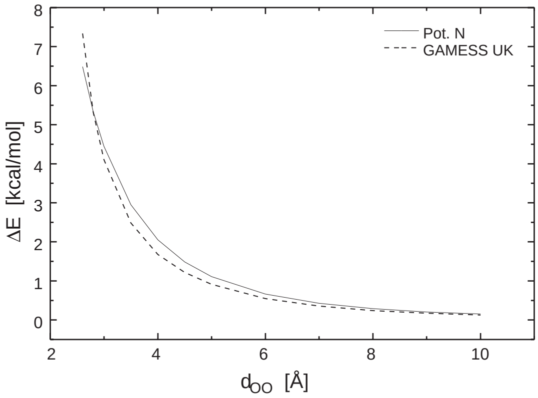

Figure 4.28: OO repulsion - Pot. N.

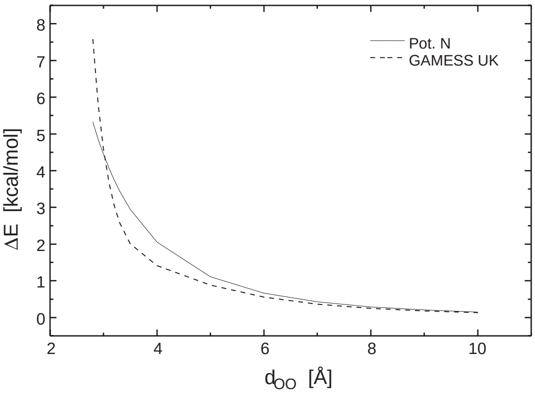

Figure 4.29: HH repulsion - Pot. N.

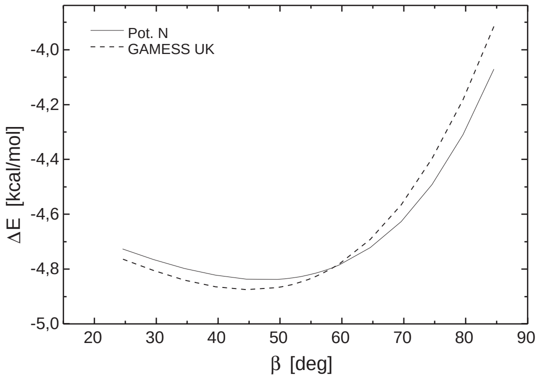

Figure 4.30: Variation of β - Pot. N.

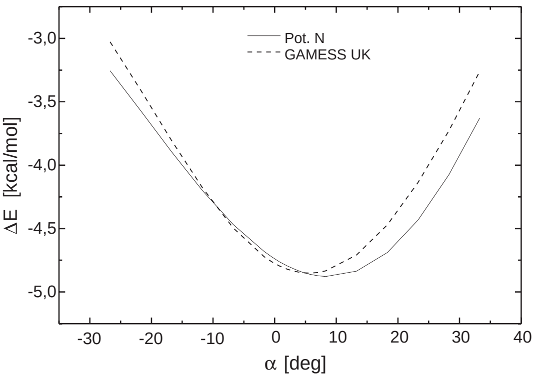

Figure 4.31: Variation of α - Pot N.

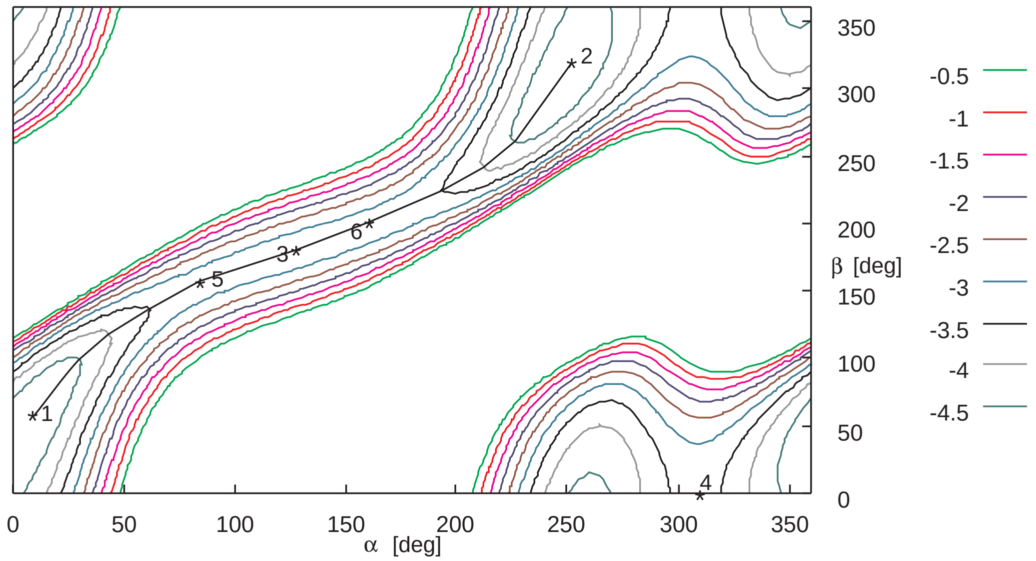

Figure 4.32: Potential energy surface of potential N for α and β; d_{OO} = 2.9834 Å / minima.

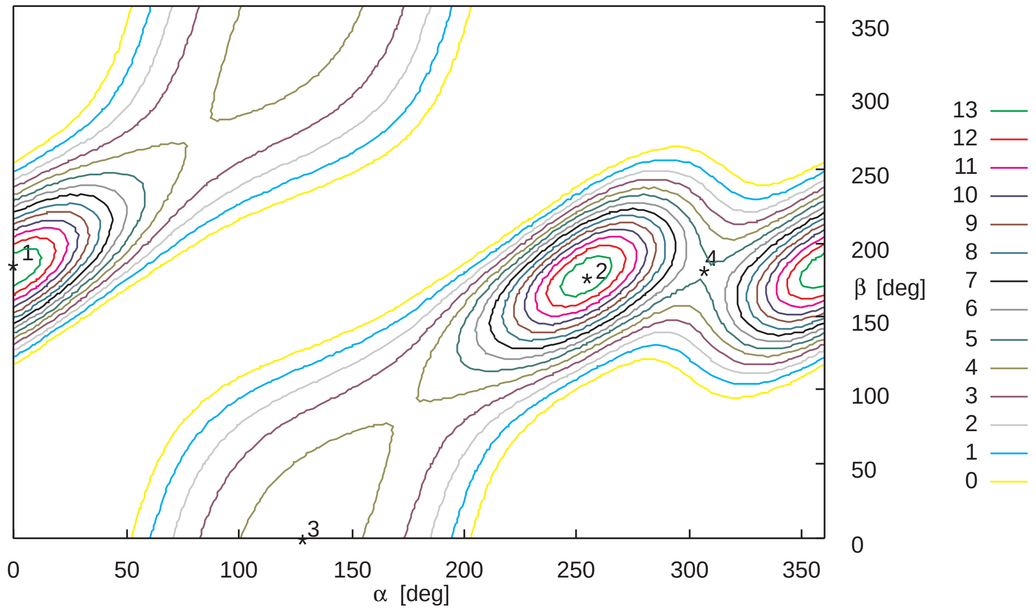

Figure 4.33: Potential energy surface of potential N for α and β; d_{OO} = 2.9834 Å / maxima.

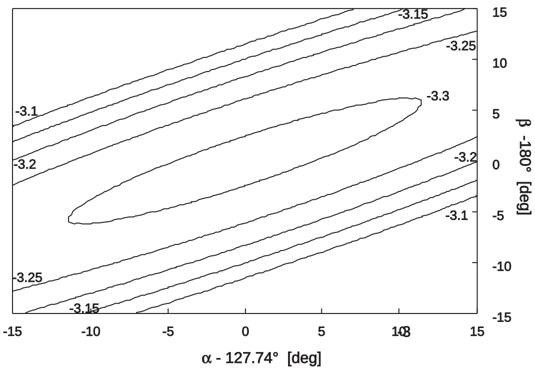

Figure 4.34: Details of minimum 3, Pot. N.

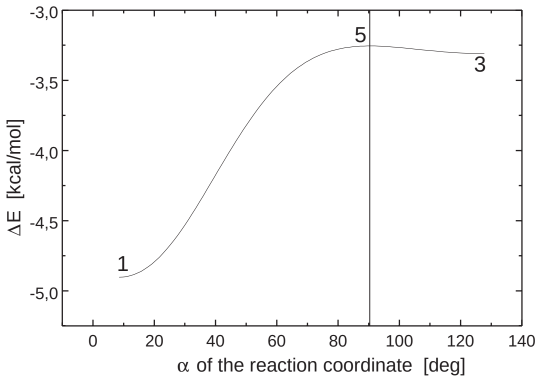

Figure 4.35: Energy profile path 1-5-3, Pot. N.

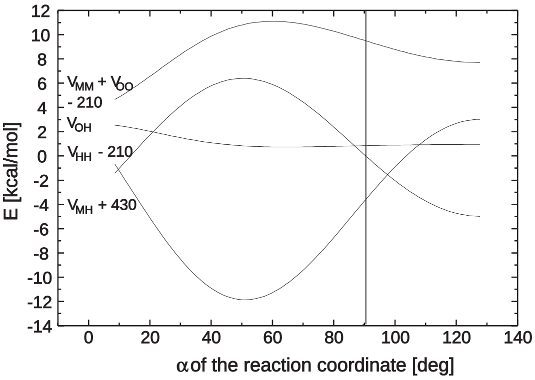

Figure 4.36: Energy composition path 1-5-3, Pot. N.

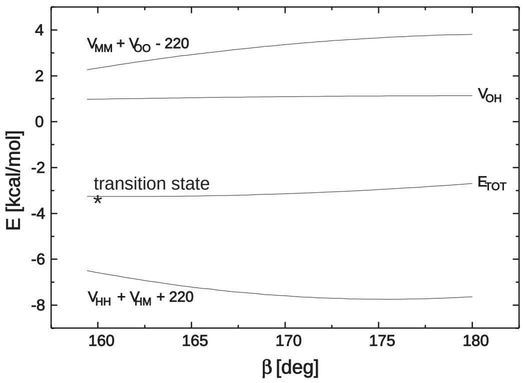

Figure 4.37: Energy composition point 5, Pot. N.

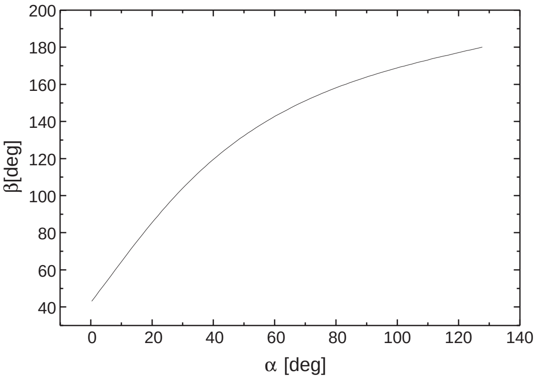

Figure 4.38: Reaction path 1-5-3, Pot. E.

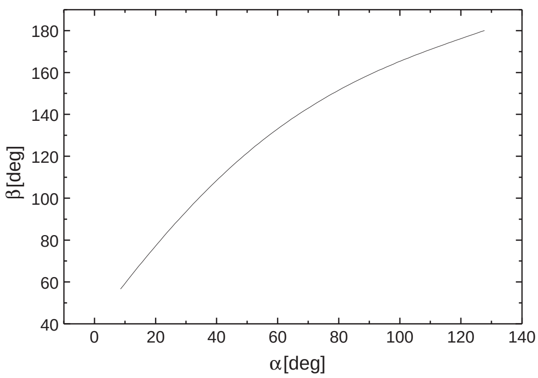

Figure 4.39: Reaction path 1-5-3, Pot. N.

The repulsive oxygen hydrogen interaction also prevents the Coulomb regime at small oxygen-oxygen distances. This behaviour is displayed in the good fits for a_{OO} and a_{HH}. Both curves do not show any local minima.

This extreme flatness of the potential energy surface is also reflected by the reduced activation energy for a change in the dimers geometry along the path 1-4-2 (figure 4.32). The activation energy of 1.57 kcal/mol calculated with potential N is about 0.5 kcal/mol lower than that calculated with potential E. The activation energy is significantly higher than the double of the standard deviation for attractive interactions (0.118 kcal/mol, table 4.7) and should be therefore regarded as a real property of the system, while an energy difference of 0.055 kcal/mol between the points 3 and 5 remains questionable.

The energies of the points 1 and 4^* were calculated quantum mechanically (DZP / MP3). The geometry of point 1 yielded a BSSE corrected interaction energy of 4.857 kcal/mol (BSSE = 0.9949 kcal/mol). This value is in good agreement with that predicted by potential N. The difference between both points is 0.046 kcal/mol (0.94 % of the energy). The geometry of point 3^* (and therefore also point 4^*) gave a BSSE corrected interaction energy of 3.256 kcal/mol (BSSE = 0.899 kcal/mol). The difference between the predicted and calculated values is 0.054 kcal/mol (1.63 % of the energy). The predictions are much closer to the minimum geometry and become poorer as the interaction becomes less favourable. The energy difference between both points is 1.59 kcal/mol and exactly reproduces the 1.57 kcal/mol predicted by potential N. The difference between both values (0.02 kcal/mol) is much smaller as the estimate from the error propagation laws basing on the individual errors E (0.071 kcal/mol, 4.45 % of the activation energy). This result shows how different errors cancel.

$$\Delta E_{TOT} = \sqrt{\sum \Delta E_i^2} = \sqrt{0.046^2 + 0.054^2} kcal/mol = 0.071 kcal/mol \tag{4.14}$$

Figures 4.31 and 4.30 show the potential energy (quantum mechanics and potential N) as a function of the distortion of the dimer angles. Although the positions of the minima differ slightly, potential N reproduces very well the curvature of the quantum mechanical curves. The curvature of the potential energy surface in combination with the cancellation of errors explains the high quality of predictions by potential N.

The study of reaction pathways on the potential energy surface (like the one shown in figure 4.32) is not an easy task, as the oxygen-oxygen distance changes during the turn of the angles. Figure 4.38 and 4.39 show the reaction paths as low energy combinations of α and β for potential E and N. The curve for potential E is more bent than that for potential N, as potential energy surface calculated with potential E has steeper slopes than that of potential N. If the oxygen-oxygen distance is allowed to relax during the calculation, transition states 5 and 6 might vanish. Transition state 5 observed with potential N seems to be an artefact caused by the movement of charge from the oxygen atom. The energy difference of 0.055 kcal/mol between the point 3^* and 5 is already much smaller than the standard deviation of potential N for bonding conformations.

The global minimum of the potential energy surface of potential N has larger angles than the BSSE corrected geometry calculated with GAMESS UK (table 4.12). The increase in α does not matter, since both values are still in the experimental range of 1° ± 10° [118]. The value for β with potential N is more than 12° higher than the quantum chemical, BSSE corrected value of 44.53 but reprodues well the BSSE uncorrected value of 54.57 . A value of 56.6° for β is perfectly reproduces the experimental value of 57° ± 10°. The too large value for the angle β is caused by the high wheight of the dimersiation curve's minimum during the fit (equation

q	a_1	b_1	a_2	b_2	a_3	b_3	r_M
e	kcal/mol	Å^{-1}	kcal/mol	Å^{-1}	kcal/mol	Å^{-1}	Å
1.398323	357205.3	4829.585	653.7789	3.189600	3457.857	3.54541	0.238291

Table 4.9: Parameter for potential N.

term	variance [kcal^2/mol^2]
minerg	0.000007
dimer	0.0103
a_{OO}	0.1050
a_{HH}	0.0355
W1	0.0218
W2	0.0034
w3	0.0265
trimer I	0.2708
trimer II	0.2787
trimer III	0.0000007
trimer IV	0.3638

Table 4.10: Variances of potential N.

term	absolut value	
dipole	2.3343	D
trimer I	−13.269	kcal/mol
trimer II	−8.809	kcal/mol
trimer III	−8.243	kcal/mol
trimer IV	−10.468	kcal/mol

Table 4.11: Absolut values for potential N.

		Gam. UK	Pot. N
d_{OO}	[Å]	2.9926	2.9834
α	[deg]	2.44	8.55
β	[deg]	44.53	56.60
ΔE	[kcal/mol]	−4.914	−4.903

Table 4.12: Global minima for dimers.

4.11). The weights of dimerisation curve, W1 and W3 inhibited also a better reproduction of β, because those curves were created with a BSSE uncorrected value for $\beta = 54.47°$. The energy agreement between both calculations is excellent and at the lower range of the experimental value of 5.44 ± 0.7 kcal/mol. ***Although potential N does not reproduce the quantum chemical values perfectly, potential N offers a rapid way to explore the water dimer's potential energy surface, because all values are within the experimental range. The tiny energy differences between the quantum chemistry and potential N can be neglected safely for further calculations.***

4.3.2 Application of potential N on water trimers

The main problem with potentials based on pair interactions are cooperative effects (See section 3.4, page 74 and subsection 4.3.1). Tables 4.10 and 4.11 show that potential N reproduces the energies as well as the relative energy differences among the four trimers. Since the geometries of the water trimers were fixed during the calculation, it is difficult to tell whether this agreement is fortuitous or a property of potential N. To check this question the geometries of the trimers were optimized with a simplex algorithm [242]. Table 4.13 summarizes the results.

The relative energies do not change. Potential N simulates the cooperative effects well, even when the geometries are allowed to relax. The geometry of trimer I was quantum mechanically optimized. The geometry found with potential N is very close to it. The energy gain during the optimization is caused by an increasement in the oxygen-oxygen distance. Although potential N does not contain any explicit polarisation terms, which enforce a shortening of the oxygen-oxygen

		d_{OO} [Å]	α [deg]	β [deg]	E [kcal/mol]
trimer I	start	2.8014	23.54		−13.268
	end	2.9135	24.18		−13.685
	difference	+0.1121	+0.64		−0.416
trimer II	start	2.9907	9.66	70.74	−8.814
	end	2.9427	18.71	77.55	−9.028
	difference	−0.0480	+9.05	+7.01	−0.219
trimer III	start	3.0049	3.31	54.57	−8.242
	end	2.9437	19.90	83.43	−8.814
	difference	−0.0612	+16.59	+28.86	−0.571
	MP2 geo.	2.9437	8.57	70.51	
trimer IV	start	3.0049	3.31	54.57	−10.468
	end	2.9697	5.79	50.20	−10.547
	difference	−0.0352	+2.48	−4.37	−0.079
	MP2 geo.	2.8440	2.26	54.58	

Table 4.13: Optimisation of trimers I to IV using potential N.

distance, the oxygen-oxygen distance (2.9135 Å) is much smaller than that in the free water dimer (2.9834 Å).

The geometry of trimer II was also quantum mechanically optimized. The oxygen-oxygen distance is larger than the distance in an optimized dimer due to the antibonding cooperative forces (2.98 Å vs 2.93 Å, DZP/MP3 no BSSE correction). The geometry optimisation of trimer II in the new force field reduces the oxygen-oxygen distance until the bond is shorter than in the free dimer. The energy of trimer III was not quantum mechanically optimized. The geometries found for a dimer within the optimized trimers II and III are very close to each other. The increase of β during the optimisation of trimer III reduces the repulsion between the water molecules at the end of the chain. The difference in the total energies of trimer II and III is mainly caused by the interaction between those monomers at the ends of chain. The energy difference between trimer II and III is 0.214 kcal/mol while the difference between the two nonbonding monomers A and C is 0.139 kcal/mol. In both cases this interaction is repulsive (+0.652 kcal/mol for trimer II versus +0.791 kcal/mol for trimer III). The optimisation of the trimers II and III is governed by the reduction of the repulsive forces. The energy gain caused by the rearrangement of the bonding dimers (E_{DIMER}) in trimer II is neglible. In trimer III the reduction of the repulsive forces leads also to slightly weaker dimer bonds ($\Delta E_{DIMER} = +0.061$ kcal/mol/bond) (table 4.14).

Trimer IV is built of two nearly ideal hydrogen bonds. Extra energy is gained from the interaction of the monomers A and C (-0.764 kcal/mol). The same interaction compensates in trimer I the energy loss by the stressed dimer bonds. The small energy gain during the geometry optimisation is caused by the rearangement of the dimer bonds (table 4.14). Similar to the quantum chemical results (sections 3.4) potential N describes trimer IV as possible intermediate during the formation of a cyclic water trimer. Any distortion, which brings the monomers A and C closer together will enhance the formation of trimer I and its distorted conformations.

The angle in the hydrogen bond α of the trimers II and III increases about 10° during the optimisation. The geometries of the trimers III and IV were optimized quantum chemically (DZP/MP2)

		$\mathrm{E}_{\mathrm{DIMER}}$ [kcal/mol]	$\mathrm{E}_{\mathrm{AB}} + \mathrm{E}_{\mathrm{BC}}$ [kcal/mol]	E_{AC} [kcal/mol]	$\mathrm{E}_{\mathrm{TOT}}$ [kcal/mol]	$\Delta\mathrm{E}_{\mathrm{TOT}}$ [kcal/mol]	$\Delta\mathrm{E}_{\mathrm{AC}}$ [kcal/mol]
trimer II	S	−4.835	−9.670	+0.856	−8.814		
	F	−4.840	−9.680	+0.652	−9.028	−0.219	−0.204
trimer III	S	−4.864	−9.727	+1.485	−8.242		
	F	−4.802	−9.605	+0.791	−8.814	−0.571	−0.694
trimer IV	S	−4.864	−9.729	−0.739	−10.468		
	F	−4.891	−9.783	−0.764	−10.547	−0.079	−0.025

S: start, F: finish

Table 4.14: Compostion of the trimerisation energy composition during the optimisation.

to check the importance of the angle for the trimer structure. The results of those calculations are also listed in table 4.13. In trimer III has α a value of 8.57°. The results from quantum chemistry and potential N agree well in trimers with bonding cooperative forces (trimer I and IV), but differ strongly in trimers with repulse cooperative forces. Since the oxygen-oxygen distance is always shortened, α has to be increased in calculations with potential N to compensate for the energy in case of repulsive cooperative forces. In trimer IV central dimer bonds are stronger than those in the trimers II and III (table 4.14) despite of the longer oxygen-oxygen distance. The angle of the hydrogen bond in trimer IV is smaller and closer to the optimum (8.5° in the free dimer). Potential N averages the cooperative forces for all trimers (d_{OO}), but the bonding forces dominate in potential N.

Potential N was used for the exploration of the potential energy surface of the cyclic water trimer. Figure 4.40 displays the general geometry of all trimers. Table 4.15 shows results of geometry optimisations under various constraints. All distances are labelled d, all angles α and all dihedral angles β with one exception. ϵ is the dihedral angle between the two hydrogens pointing upwards.

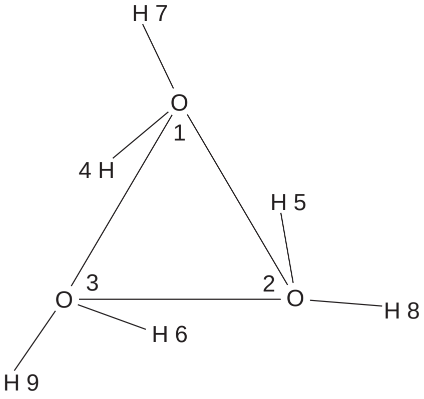

Figure 4.40: Geometry of the cyclic trimers.

Trimer I is the planar trimer with $\mathrm{C}_{3\mathrm{h}}$ symmetry. For the construction[6] of trimer A was H4 kept in the oxygen plane and H was turned upwards. The other hydrogens were generated from this orientation by a C_3 rotation. Finally the sign of H's z-component was changed, so that H9 points downwards. In the next step the out of plane hydrogen were allowed to relax (trimer B). The relaxation increases ϵ. This is the most important relaxation pathway combined with the largest energy gain (0.914 kcal/mol). Then the bonding hydrogens were twisted out of the oxygen plane symmetrically (trimer C) and finally allowed to relax without any constraints (trimer D). The relaxation of the bonding hydrogen atoms gained 0.068 kcal/mol in total. In the last step the trimer was allowed to relax without any constraints at all. The distortion of the oxygen triangle is very small and the energy gain of 0.001 kcal/mol

---

[6] See section 11.9.2 for the conversion of pure rotational coordinates into cartesian.

	trimer I	A	B	C	D	E	QM / MP2
d_{12}	2.9135	2.9205	2.9080	2.9090	2.9077	2.9077	2.7925
d_{23}	2.9135	2.9205	2.9080	2.9090	2.9077	2.9004	2.8092
α_{123}	60.0	60.0	60.0	60.0	60.0	60.2	60.0
α_{413}	24.2	22.8	23.1	23.1	24.4	24.3	19.1
α_{521}	24.2	22.8	23.1	23.1	22.5	22.6	20.6
α_{632}	24.2	22.8	23.1	23.1	22.6	22.6	18.9
β_{4132}	180.0	180.0	180.0	175.0	−172.2	−172.0	−174.3
β_{5213}	180.0	180.0	180.0	175.0	174.4	174.4	−177.2
β_{6321}	180.0	180.0	180.0	−175.0	175.6	175.3	173.1
α_{713}	128.7	111.1	120.5	119.0	119.1	118.9	112.6
α_{821}	128.7	111.1	120.5	119.0	114.5	114.6	116.9
α_{932}	128.7	111.1	120.5	119.0	123.6	123.6	114.0
β_{7132}	180.0	102.8	129.6	−129.6	130.2	129.6	117.3
β_{8213}	180.0	−102.8	−129.6	−129.6	−118.1	−118.1	−120.5
β_{9321}	180.0	102.8	129.6	129.6	140.0	140.5	−123.7
ϵ	0.0	0.0	25.7	27.8	23.5	22.7	23.4
$-\Delta$E	13.685	13.052	13.966	13.986	14.034	14.035	

d in Å; α, β and ϵ in degrees; ΔE in kcal/mol

Table 4.15: Z-matrices for cyclic water trimers.

negligible. The distortion of the global minimum is therefore dominated by the reduction of the repulsive interaction of the elicptic nonbonding hydrogen atoms.

A comparison with a quantum chemically optimized trimer (DZP/MP2) shows the excellent agreement for ϵ and good agreement of the other parameter. Potential N allows therefore a reliable description of cyclic water trimers. The distortion of the cyclic water trimer minimizes the repulsion between the non bonding hydrogens. In trimer I ist the distance between the nonbonding hydrogen atoms larger and the total energy therefore lower. Trimer I is shallow local minimum on the potential energy surface of the cyclic water trimer. Only a very small activation is necessary to initialize the transformation into the global minimum.

Figure 4.42 shows the formation of the cyclic water trimer (global minimum) from the linear trimer IV. The geometry of the trimer was allowed to relax at every step of the ring closure. The reaction pathway is smooth and without activation. Figure 4.41 shows the formation of cyclic trimer starting with free water molecules. The water dimer is readily formed. In the next step adds another water molecule to one end of the dimer and a chain is built. Next the linear trimer relaxes and form the cyclic one without any further activation. The formation of a cyclic water trimer from free monomers or from the dimer in a single step seems to entropically disfavoured.

Figure 4.43 shows the global minimum. Experiments suggest that the water trimer rapidly changes its conformation by tunneling. A possible reaction coordinate is the simultanous movement of two hydrogen atoms. The transition state is reached when the hygrogen atoms are in the plane of the three oxygen atoms. This conformation is shown in figure 4.45. The energy of this possible transition state is 0.256 kcal/mol above the global minimum. Tunneling between the different conformations seems to be likely, considering a total zero point vibrational energy of 13.8 kcal/mol for the free water molecule (section 3.1, page 45).

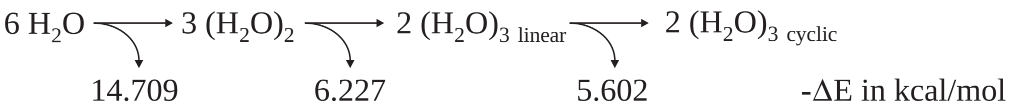

Figure 4.41: Formation of a cyclic trimer.

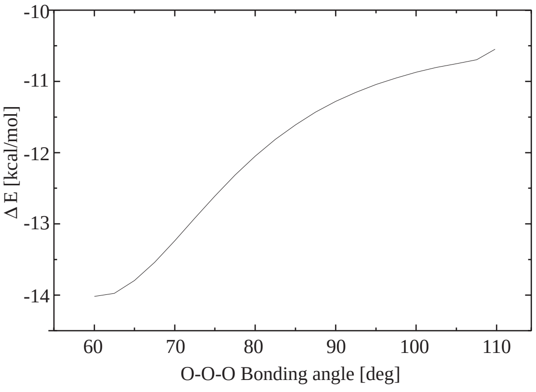

Figure 4.42: Ringclosure of $(H_2O)_3$.

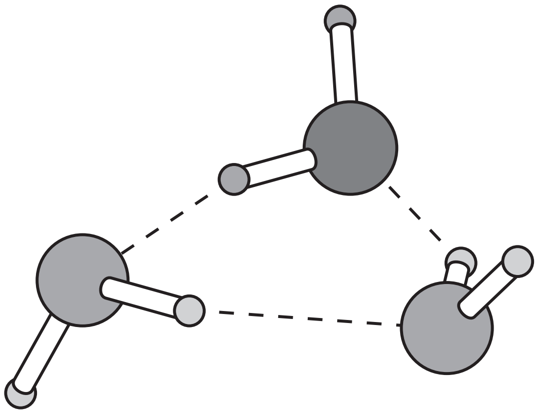

Figure 4.43: Global minimum of $(H_2O)_3$.

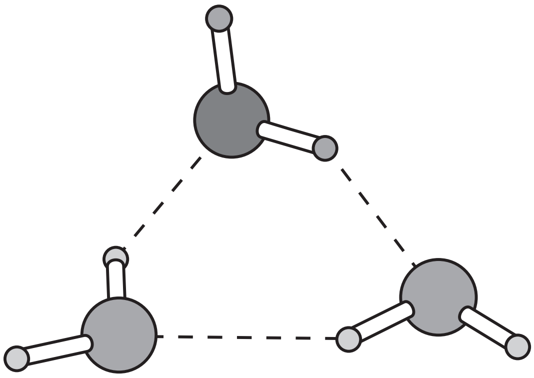

Figure 4.44: Transition state.

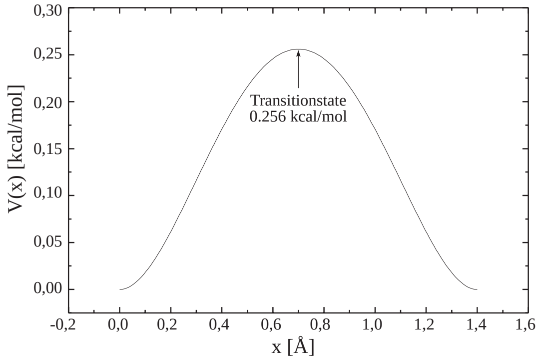

Figure 4.45: Potential energy function.

The nonbonding hydrogen atoms are about 0.7 Å away from the oxygen plane and the tunneling distance is therefore about 1.4 Å long. The potential energy function should have its maximum at the transition state. Figure 4.45 displays a first guess for the function. The fourth order polynomial was chosen to have two minima at the equilibrium geometries at to have its maximum in the oxygen plane (r = 0.7 Å) [270].

$$V(x) = k(x^4 - 4ax^3 + 4a^2x^2) \qquad k = 1.066\frac{kcal}{mol\ \text{Å}^4} \qquad a = 0.7\ \text{Å} \tag{4.15}$$

The probability $P(E)$ that a single hydrogen atom tunnels through the barrier can be calculated according to Schwabl [194d]:

$$P(E) = \exp\left\{-2\int_0^{2a} \frac{1}{\hbar}\sqrt{2m_H(V(x) - E)}dx\right\} \tag{4.16}$$

The lowest boundary value (E → 0) for the tunneling probability can be calculated analytically.

$$\frac{1}{\hbar}\sqrt{2m_H}\int_0^{2a} \sqrt{V(x)} = \frac{4}{3\hbar}\sqrt{2km_H}a^3 = 2.15 \tag{4.17}$$

If all hydrogen atoms move independently in the water trimer, the total probality $P_{TOT}(E)$ of the tunneling between two conformation can be calculated as follows:

$$P_{TOT}(E) = P_1(E) \cdot P_2(E) = P^2 \qquad P_{TOT}(E \to 0) = e^{-2\cdot 2\cdot 2.15} = 0.0002 \tag{4.18}$$

A barrier of 0.256 kcal/mol is therefore small enough to be passed by tunneling. The tunneling probability will increase with the thermal excitation of the proton.

4.4 Summary of the Calculation with a Classical Potential

1. None of the previously used potentials describes the quantum chemical values well. The quantum mechanical results on the other hand agree very well with the published experimental values.

2. The BNS and ST2 potentials have local minima in the a_{OO} and a_{HH} curves. Those minima can be explained by the fact, that the attractive Coulomb forces overpower the repulsive forces. This behaviour might be overcome by a damping function. Such a function is useful to obtain good values, but is difficult to justify.

3. The TIPS 2 model was chosen as start point for the search of a new potential, because the TIPS 2 model yielded the best values.

4. The comparison of simple interaction potentials showed that the place where the oxygen-oxygen repulsion starts to act is more important than the gradient of the curve or its precise algebraic form.

5. The reparametrisation of an existing point charge model by Kistenmacher and Popkie gave a useful potential. This new potential (potential N) describes dimers and trimers well. The standard deviations of the quantum mechanically calculated curves are better than that published with the potential. It also simulates cooperative effects well. This potential will be used in further calculations.

6. All potentials showed a third minimum caused by the displacement of the centre of charge from the oxygen atom. Potential N's potential energy surface is so flat which makes it nearly impossible to find this minimum. This behaviour of potential N seems to be more realistic than the distinct third minimum observed with potential E.
7. The dislocation of the centre of charge from the oxygen atom causes a shift in the maximum of the potential energy surfaces.
8. The cyclic trimer is built from the linear trimer without any further activation. This suggests that the formation of a water trimer starts with the dimer. Next, another water molecule is added to the one of the dimer's ends and the linear trimer is formed. Later this linear trimer relaxes to the cyclic one.
9. The different cyclic conformers might interchange rapidly by tunneling. Calculation with potential N gave an rougth estimate for the activation energy (0.256 kcal/mol) and a zero point tunneling probability of 0.02%.
10. The distortion of the cyclic trimer is mainly caused through reduction of the repulsive forces between the non bonding hydrogen atoms on the same side of the trimer.

Chapter 5

Hückel calculations for the Analysis of $\mathrm{Pt_n}$

The Hückel calculations are tightly connected to the quantum chemical calculations in chapter 6 (page 145) and 7 (page 203) and have been used for both the analysis of the quantum chemical results and as starting point for new calculations. All quantum chemical calculations in chapters 6 and 7 showed, that the stability of the cluster is controlled by the population of the platinum 6s orbitals. A large 6s population on the other hand repells the water molecule. The 6s population in a successfull surface model is high enough to stabilize the platinum cluster and meanwhile small enough to create a strong metal-water bond. As the 6s population is crucial for the quality of a surface model, a method to detect suitable electronic states with the correct 6s population is helpful for the quantum chemical calculations in chapter 6. The Hückel calculations in this chapter are used to identify useful candidates as surface models. The interaction between 5d and 6s electrons in this model is regarded only as a distortion of the 6s band. Such a gross simplification cannot describe all details, but can help us to identify the relevant orbitals for this mechanism.

Extended Hückel calculations [191, 236, 271–281] have been applied previously to metal surfaces [64, 282–287]. The success of this the method and the simplicity of the original Hückel theory tempted us to try Hückel theory on the platinum 6s orbitals.

Hückel calculations have been used in this chapter to analyze the electronic structure of the metal clusters. Section 5.1 demonstrates the application of this method, which is is well established for the analysis of organic, aromatic molecules, to the analysis of platinum 6s orbitals. The remainder of this section concentrates on the application of the new Hückel theory and its quantification to relate the Hückel results with the HF/MP2 results of chapter 6.

It is shown, that very simple calculations at the lowest level of theory can help us to understand the results from modern, sophisticated methods. These calculations, which can be done literally on the back of an envelope, hold the key to the understanding of the 18 valence electron calculations.

5.1 Theory of the Hückel-approximation for the platinum 6s electrons

The Hamiltonian (equation 5.1) of a platinum cluster built from M atoms (atomic number Z = 78 for platinum) describes energy and motion of N = M · Z electrons in the Born-Oppenheimer approximation.

$$\hat{H} = \sum_{i}^{N} -\nabla_i^2 - \sum_{\mu}^{M}\sum_{i}^{N} \frac{Z}{r_{\mu i}} + \sum_{i=1}^{N-1}\sum_{j=i+1}^{N} \frac{1}{r_{ij}} \tag{5.1}$$

$$= \sum_{i}^{M} -\nabla_i^2 + \sum_{i}^{M}\sum_{\mu}^{M} V_{\mu}^{\mathrm{ECP}}(r) + \frac{1}{2}\sum_{i,i\neq j}^{M} \frac{1}{r_{ij}} \tag{5.1 a}$$

In the ground state of the platinum atom (^{3}D, [Xe] 4f^{14} 5d^9 6s^1) the 6s electron moves in the core potential $\mathrm{V}_{\mu}^{\mathrm{ECP}}$ of the inner Z−1 electrons. The assumption of a perfect, spherically symmetric core potential allows us to simplify equation 5.1 and the Hamiltonian contains now the sum of all core potentials and the pair interactions between the M 6s electrons (equation 5.1a). If one assumes further that M−1 electrons form a potential G(r) in which the M$^{\mathrm{th}}$ electron moves, it is possible to separate equation 5.1a into M one-electron equations.

$$\hat{H} = \sum_{i}^{M} -\nabla_i^2 + \sum_{i}^{M} V^{\mathrm{ECP}}(r) + \sum_{i}^{M} G_i(r) = \sum_{i}^{M} \hat{h}_i \qquad \text{with} \qquad G_i(r) = \sum_{j\neq i}^{M-1} \frac{1}{r_{ij}} \tag{5.2}$$

$\hat{\mathrm{h}}_{\mathrm{i}}$ is the effective one-electron operator and is specified in the Hückel approximation via assumptions for the one-electron integrals. The Hückel operator may be regarded as a not fully specified one electron operator, which is constructed from the separation of core and valence electrons.

Hückel molecular orbitals (HMO) for the platinum cluster are linear combinations of orthogonal atomic 6s functions χ_{i} (LCAO method).

$$\Psi \equiv \Psi^{\mathrm{HMO}} = \sum_{i}^{M} c_i\, \chi_i \qquad\qquad \langle \chi_i | \chi_j \rangle = \delta_{ij} \tag{5.3}$$

The coefficients c_{i} of the HMO are specified in a variational calculation. The central element of this calculation is the secular equation.

$$(\mathbf{h} - \boldsymbol{\epsilon}\,\mathbf{S})\,\mathbf{c} = \mathbf{D}\,\mathbf{c} = 0 \tag{5.4}$$

h contains the matrix elements with the hamiltonian $\hat{\mathrm{h}}_{\mathrm{i}}$, $\boldsymbol{\epsilon}$ is the eigen vector and **S** the overlap matrix. Consistent solutions for equation 5.4 arise, when the determinant of the secular matrix D vanishes.

$$|D| = \begin{vmatrix} H_{11} - \epsilon S_{11} & H_{12} - \epsilon S_{12} & \cdots & H_{1M} - \epsilon S_{1M} \\ H_{21} - \epsilon S_{21} & H_{22} - \epsilon S_{22} & \cdots & H_{2M} - \epsilon S_{2M} \\ \vdots & \vdots & \ddots & \vdots \\ H_{M1} - \epsilon S_{M1} & H_{M2} - \epsilon S_{M2} & \cdots & H_{MM} - \epsilon S_{MM} \end{vmatrix} = 0 \qquad \text{with}$$

$$S_{ij} = \delta_{ij} \qquad \text{and} \qquad H_{ij} = \begin{cases} \alpha & \text{for } i = j \\ \beta & \text{if } i \text{ and } j \text{ are neighbours} \\ 0 & \text{for every other case} \end{cases} \tag{5.5}$$

α is the valence ionisation potential, describing the influence of the molecular environment on the atomic ionisation energy. The precise value of α depends strongly on the charge of the molecule and its shape. The second integral β is the resonance integral. Its value is proportional to the orbital overlap and describes the strength of the bond between two neighbouring atoms. Both integrals α

and β have negative values. Since $\mathrm{H_{ij}}$ is only defined for neighbouring atoms, the secular matrix D is a representation of the molecule's connectivity.

The total electronic energy $\mathrm{E^{elec}}$ of the cluster is the sum of the orbital eigenvalues ϵ_i multiplied with the occupation number $\mathrm{b_i}$ (0, 1 or 2):

$$E^{elec} = \sum_{i}^{M} b_i \, \epsilon_i \tag{5.6}$$

$\Psi^* \; \Psi$ is proportional to the electron density and by appliying the orthogonality approximation ($\mathrm{S_{ij}} = \delta_\mathrm{ij}$) to $\langle \Psi^\mathrm{HMO} | \Psi^\mathrm{HMO} \rangle$ the charges on the individual atoms can be connected to the orbital coefficients $\mathrm{c}_{\mu\mathrm{i}}$.

$$1 = \langle \Psi_i^\mathrm{HMO} | \Psi_i^\mathrm{HMO} \rangle \; = \sum_{\mu}^{M} c_{\mu i}^2 \tag{5.7}$$

Since the orbitals do not overlap the charge of the μ^th atom in the $\mathrm{i^{th}}$ orbital proportional to the orbital coefficients $\mathrm{c}_{\mu\mathrm{i}}^2$. The total charge on the μ^th atom is therefore

$$q_\mu = \sum_{i}^{M} b_i \, c_{\mu i}^2 \qquad\qquad \sum_{\mu}^{M} q_\mu = \sum_{\mu}^{M} \sum_{i}^{M} b_i \, c_{\mu i}^2 = M \tag{5.8}$$

The atomic charge[1] of the μ^th atom is $Q_\mu = Z_\mu - q_\mu$ in units of the elemantary charge and can be calculated with equation 5.8.

From $S_{ij} = \delta_{ij}$ follows a zero electron density at the centre of the bond and charges calculated with equation 5.8 should be too high. The absence of any electrons in the centre of the bond causes also the wrong spatial distribution of the orbitals, but the symmetry of the orbitals is correct and agrees with other methods [273].

Equation 5.8 allows us to rewrite equation 5.6 for the total electronic energy.

$$\begin{aligned} E^{elec} &= \sum_{i}^{M} b_i \, \epsilon_i = \sum_{\mu}^{M} q_\mu \, \alpha_\mu + 2 \sum_{\mu,\mu<\nu}^{\mu} p_{\mu\nu} \, \beta_{\mu\nu} \qquad\qquad p_{\mu\nu} = \sum_{i}^{M} b_i \, c_{\mu i} \, c_{\nu i} \\ &= M\alpha + 2\,\beta \sum_{\mu<\nu} p_{\mu\nu} \end{aligned} \tag{5.9}$$

The elements of the bond order matrix $\mathrm{p}_{\mu\nu}$ give a measure how strong the interaction between two atoms μ and ν contributes to the total energy and offers so a measure for the individual bond strength.

5.2 Hückel calculations for $\mathrm{Pt_3}$

The smallest cluster we analysed with the Hückel metod was the $\mathrm{Pt_3}$ triangle. Figure 5.1 shows the two platinum trimers. The cluster is so small, that the Hückel calculation is straight forward. First, we discuss the equilateral triangle ($\sphericalangle_{123} = 60°$):

---

[1] References [288–291] focus on the calcualtion of atomic charges and the spatial distribution of electrons within the molecule.

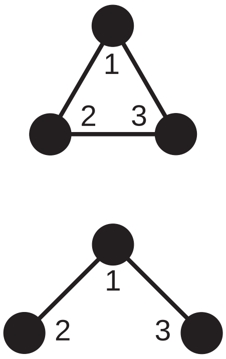

Figure 5.1 Pt_3 cluster.

ϵ_i	$\alpha + 2\,\beta$	$\alpha - \beta$	$\alpha - \beta$
c_1	0.5773	0.8165	0.0
c_2	0.5773	−0.4082	0.7071
c_3	0.5773	−0.4082	−0.7071

Table 5.1 HMOs for the equilateral triangle.

$$\begin{vmatrix} \alpha-\epsilon & \beta & \beta \\ \beta & \alpha-\epsilon & \beta \\ \beta & \beta & \alpha-\epsilon \end{vmatrix} = (\alpha-\epsilon)^3 - 3\,\beta^2\,(\alpha-\epsilon) + 2\,\beta^3 = 0 \qquad \begin{aligned} \epsilon_1 &= \alpha + 2\,\beta \\ \epsilon_2 &= \alpha - \beta \\ \epsilon_3 &= \alpha - \beta \end{aligned} \tag{5.10}$$

Table 5.1 summarizes the Hückel molecular orbitals for the equilateral platinum triangle. The degenerate orbitals are antibonding (α - β). To avoid an asymmetric population of the degenerate orbitals, every orbital should be singly occupied (cluster built from three ^{3}D platinum atoms) in the ground state, resulting in a quartet wave function. The average 6s population is close to one in such a cluster and therefore too high for a strong metal-water bond, since EHT calcualtions by Bigot and Minot [285] showed, that the 6s population of an surface atom is smaller than one ($\approx$ 0.8).

The combination of a ^{1}S with two ^{3}D platinum atoms [292] results in an average 6s population of $\frac{2}{3}$, which suggest a strong metal-water bond. The resulting 6s wavefunction has the same properties as the Hückel MOs for Pt_3^+: $a_1^2\ e^0\ e^0$, singlet. The easiest way to construct such a wavefunction is to start with three ^{1}S atoms. In the next step two electrons from the most antibonding totally symmetric 5d orbital are moved into the totally symmetric 6s orbital. Choosing this way conserves the symmetry of the electronic wavefunction and creates at the same time a 6s population of two.

The transformation of the equilateral triangle into an right-angled triangle (Pt(100) surface model) reduces the symmetry from D_{3h} to C_{2v}. During this transformation the distance between the platinums 2 and 3 is enlarged by a factor of $\sqrt{2}$. The atoms are not directly connected to each other and the overlap integral β becomes zero according to the pure Hückel theory. Equation 6.3 shows the secular determinat and the eigenvalues.

$$\begin{vmatrix} \alpha-\epsilon & \beta & \beta \\ \beta & \alpha-\epsilon & 0 \\ \beta & 0 & \alpha-\epsilon \end{vmatrix} = (\alpha-\epsilon)\,[(\alpha-\epsilon)^2 - 2\,\beta] = 0 \qquad \begin{aligned} \epsilon_1 &= \alpha \\ \epsilon_2 &= \alpha - \sqrt{2}\beta \\ \epsilon_3 &= \alpha + \sqrt{2}\beta \end{aligned} \tag{5.11}$$

Table 5.2 shows the coefficients of the HMO of the right-angled triangle. Changing the symmetry from D_{3h} to C_{2v} lifts the degeneracy of the top orbitals (e e → a_1 b_1). The energy of a_1 orbitals increases, while the energy of the b_1 orbital decreases. The electronic state with a maximum 6s population (three ^{3}D platinum atoms) would be a doublet function: $a_1^2\ b_1^1\ a_1^0$, but again is the 6s population too high. An electronic state function with a with a suitable 6s population (two 6s electrons) be a singlet function ($a_1^2\ b_1^0\ a_1^0$).

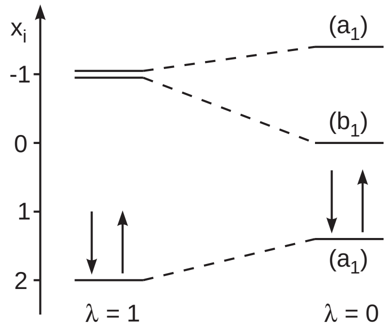

Figure 5.2 Pt_3 Hückel orbital energies.

ϵ_i	$\alpha + \sqrt{2}\,\beta$	α	$\alpha - \sqrt{2}\,\beta$
c_1	0.7071	0.0	0.7071
c_2	0.5	0.7071	−0.5
c_3	0.5	−0.7071	−0.5

Table 5.2 HMOs for the right-angled triangle.

Hückel theory demands β_{23} to be zero, since both atoms are no longer direct neighbours. The 6s orbitals are wide spreading and it's therefore unrealistic to assume, that an increase of the bond length about 40% removes all interactions between those two atoms. To account for this interaction we introduced the scaling factor λ for the overlap integral $\beta_{23} = \beta_{32} = \lambda \cdot \beta$. $\lambda = 1$ accounts for the full interaction between both atoms, while $\lambda = 0$ describes the case with no interaction between both atoms. Equation 5.12 shows the secular determinant of this problem and the corresponding eigenvalues.

$$\begin{vmatrix} \alpha - \epsilon & \beta & \beta \\ \beta & \alpha - \epsilon & \lambda \cdot \beta \\ \beta & \lambda \cdot \beta & \alpha - \epsilon \end{vmatrix} = 0 \qquad \begin{aligned} \epsilon_1 &= \alpha - \lambda \cdot \beta \\ \epsilon_2 &= \alpha + \left(\frac{1}{2}\,\lambda + \sqrt{2 + \frac{1}{4}\,\lambda^2} \right) \beta \\ \epsilon_3 &= \alpha + \left(\frac{1}{2}\,\lambda - \sqrt{2 + \frac{1}{4}\,\lambda^2} \right) \beta \end{aligned} \tag{5.12}$$

Figure 5.2 summarizes the transformation (equation 5.12) of the platinum triangle. $\epsilon_2(\lambda)$ and $\epsilon_2(\lambda)$ are approximately linear functions for $0 \leq \lambda \leq 1$. The energy of the bonding a_1 orbital increases steadily while the energy of the b_1 orbital decreases. For any point $\lambda > 0$ the b_1 orbital is anti-bonding.

The Hückel calculations for Pt_3 suggest, that a suitable Pt_3 surface model should be built from two ^3D and one ^1S platinum. The average 6s population ($\frac{2}{3}$) should create both a strong metal-water bond and strong intermetallic bonds within the platinum cluster. Both triangles should threrefore be described with singlet wave function, in which the totally symmetric 6s orbital is doubly occupied.

5.3 Analysis of the Pt_5 pyramid

The platinum pyramid is the central cluster for the 1-electron theory. Pt_5-H_2O nearly reached the limits of the HF/MP2 method (18 valence electrons, section 6.4) and the Hückel calculations allow us to understand the electronic structure of the platinum cluster. Pt_5 is also the best point to start with 1-electron ECPs on the bulk atoms, because it is the first cluster, which allows a systematic separation of bulk- (white), passive (grey) and active surface atoms (black). Bulk and passive surface atoms do not interact directly with the water molecule and a 1-electron ECP should be sufficient, since the metal-metal bond is dominated by the 6s orbitals. Active surface atoms need ECPs and basis sets, which contain 5d electrons to form the bond between platinum and water. This interface between different ECPs is of central importance for the theory. After the calculation of the 6s HMO (subsection 5.3.1) we focus on this interface and examine the influence of different Hückel parameters for the two groups of platinum atoms (subsection 5.3.2). The third subsection (5.3.3) contains the analysis of the 6s-5d interaction in the metal cluster, while the last one (5.3.4) concentrates on the rotational barrier.

5.3.1 Hückel calcualtions fot Pt5

The calculation of the eigenvalues for Pt_3 was straight forward, because the simple third order characteristic polynomials were easy to solve. Five 6s functions demand a 5 × 5 secular determinant and a fifth order characteristic polynomial, which cannot easily be solved directly. Symmetry can be used to simplify the problem.

Figure 5.3 shows the top view of the Pt_5 pyramid with the mirror planes. The secular determinant of the problem is simplified in two steps:

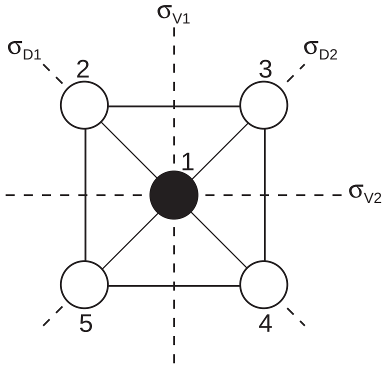

Figure 5.3: Pt_5 pyramid, top view.

1. The secular determinant is divided by β first and then the following replacement is used, which yields the Hückel matrix.

$$-x = \frac{\alpha - \epsilon}{\beta} \quad \rightarrow \quad \epsilon = \alpha + x\,\beta \tag{5.13}$$

2. The secular determinant is then block factorized using the σ_{V2} symmetry plane according to the procedure published by Heilbronner and Bock [273, 274]. This would be the same as using SALC AOs (**s**ymmetry **a**dapted **l**inear **c**ombination of atomic orbitals) according to Cotton [293b].

Equation 5.14 summarizes the simplification of the secular problem.

$$\begin{vmatrix} \alpha-\epsilon & \beta & \beta & \beta & \beta \\ \beta & \alpha-\epsilon & \beta & 0 & \beta \\ \beta & \beta & \alpha-\epsilon & \beta & 0 \\ \beta & 0 & \beta & \alpha-\epsilon & \beta \\ \beta & \beta & 0 & \beta & \alpha-\epsilon \end{vmatrix} = \begin{vmatrix} 1-x & 1 & \sqrt{2} & 0 & 0 \\ 1 & 1-x & \sqrt{2} & 0 & 0 \\ \sqrt{2} & \sqrt{2} & -x & 0 & 0 \\ 0 & 0 & 0 & -1-x & 1 \\ 0 & 0 & 0 & 1 & -1-x \end{vmatrix} = 0 \tag{5.14}$$

The blocks can be handled separately:

$$\begin{aligned} \begin{vmatrix} -1-x & 1 \\ 1 & -1-x \end{vmatrix} &= x\,(x+2) = 0 & \Rightarrow \quad & x_1 = 0 \\ & & & x_2 = -2 \\ \begin{vmatrix} 1-x & 1 & \sqrt{2} \\ 1 & 1-x & \sqrt{2} \\ \sqrt{2} & \sqrt{2} & -x \end{vmatrix} &= -x\,(x^2 - 2x - 4) = 0 & \Rightarrow \quad & x_3 = 0 \\ & & & x_4 = 1+\sqrt{5} \\ & & & x_5 = 1-\sqrt{5} \end{aligned} \tag{5.15}$$

A knowledge of the eigenvalues allows us to calculate the HMO coefficients. Table 5.3 displays the coefficients of the normalized orbitals. Due to the degeneracy of the orbitals only the clusters Pt_5^+ and Pt_5^- should have a pyramidal structure. The geometry of a neutral cluster should relax and lift the degeneration of the e-orbitals, since the wavefunction with one hole in the degenerate

nr	ϵ_i	c_1	c_2	c_3	c_4	c_5	sym
5	$\alpha - 2\,\beta$	0.0	−0.5	0.5	−0.5	0.5	b_2
4	$\alpha + (1 - \sqrt{5})\,\beta$	−0.85065	0.26287	0.26287	0.26287	0.26287	a_1
3	α	0.0	0.70711	0.0	−0.70711	0.0	e
2	α	0.0	0.0	0.70711	0.0	−0.70711	e
1	$\alpha + (1 + \sqrt{5})\,\beta$	0.52573	0.42532	0.42532	0.42532	0.42532	a_1

Table 5.3: Hückel orbitals for Pt5.

orbitals breaks the symmetry of the molecule (Jahn Teller distortion [294–296]). The following analysis therefore concentrates on Pt_5^+ (a_1^2 e e).

Table 5.4 summarizes the population analysis (orthogonal atomic orbitals, equation 5.3) of the Hückel calculation for Pt_5^+. The negative charge accumulates at the bottom of the cluster, which creates a positive charge at the top. Table 5.3 shows that any extra charge in the cluster will assemble in the cluster's basal plane, since orbitals 2, 3 and 4, which do not contain the atomic orbital of the central platinum atom, will be occupied first. Thus a pyramidal geometry creates an 6s electron sink in the basal plane.

	q_i	Q_i
1	0.55279	0.44721
2	0.86181	0.13819
3	0.86181	0.13819
4	0.86181	0.13819
5	0.86181	0.13819
$\sum$	4.00003	0.99997

Table 5.4: Population analysis PT_5^+.

Water interacts with platinum through the platinum's d-orbitals. The atom at the top of the pyramid has therefore to be replaced by an 18 or 10 valence electron platinum atom. Those 5d electrons can interact with the 6s electrons provided they have the correct symmetry. To a first approximation this interaction is neglected. The different electronic states of the central platinum atom only change the number of 6s electrons contributed by the central atom. The ^1S state ($5d^{10}$) does not contribute any electrons while the ^3D state ($5d^9$ $6s^1$) contributes one electron. A combination of a ^1S platinum atom (18 valence electrons, at the top) with four ^3D atoms (1 valence electron, in the basal plane) yields four 6s electrons, which fill the molecular 6s orbitals without breaking the molecular symmetry. The average 6s occupancy is then 0.8 and close to value proposed by BIGOT and MINOT [285]. The charge on the top of the cluster would be −0.55 e and the charge on a base atom would be +0.14 e. The dipole moment of this cluster could be used to simulate the surface electron spill, which creates a negative charge in front of the metal surface and repels the water molecule.

5.3.2 The interface between different ECPs

The interface between different ECPs (top atom with d-orbitals vs. 1 electron basal atoms) has a strong influence on the cluster's electronic structure. Two calculations were done to quantify this influence. First, we assumed that two values (β and γ) for the binding energy integrals $H_{\mu\nu}$ exists. The connections between the basal atoms are described by γ while bonds between the basal plane and the top retain the value of β. Equation 5.16 shows the new secular determinant and the corresponding eigenvalues.

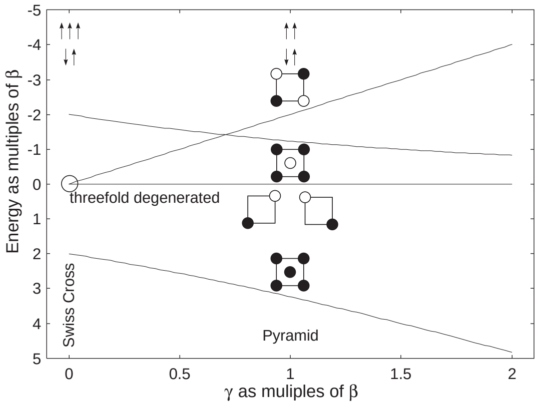

Figure 5.4: Variation of the bond integral $H_{\mu\nu} \equiv \beta$.

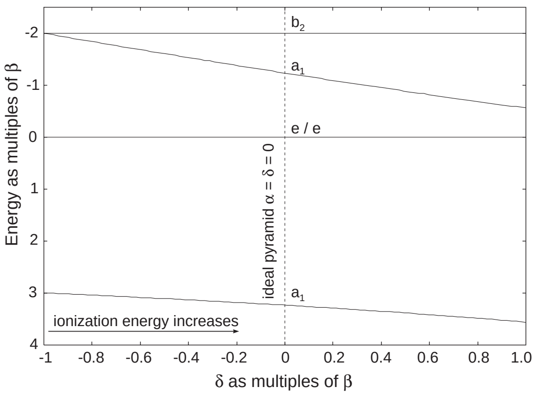

Figure 5.5: Variation of α of the top atom.

$$\begin{vmatrix} \alpha-\epsilon & \beta & \beta & \beta & \beta \\ \beta & \alpha-\epsilon & \gamma & 0 & \gamma \\ \beta & \gamma & \alpha-\epsilon & \gamma & 0 \\ \beta & 0 & \gamma & \alpha-\epsilon & \gamma \\ \beta & \gamma & 0 & \gamma & \alpha-\epsilon \end{vmatrix} = 0 \qquad \begin{aligned} \epsilon_5 &= \alpha - 2\,\gamma \\ \epsilon_4 &= \alpha + \gamma - \sqrt{4\beta^2+\gamma^2} \\ \epsilon_3 &= \alpha \\ \epsilon_2 &= \alpha \\ \epsilon_1 &= \alpha + \gamma + \sqrt{4\beta^2+\gamma^2} \end{aligned} \tag{5.16}$$

For $\gamma = \beta$ equation 5.16 reproduces the results for an ideal pyramid from equation 5.14. The other extreme ($\gamma = 0$) is the result of a Hückel calculation for a cross. Equation 5.16 describes also the transformation of the platinum pyramid into a swiss cross, since the reduction of the bond energy integral γ has the same effect as the elongation of the platinum-platinum bond in the basal plane. In an ideal cross the three orbitals 2, 3 and 5 have the same energy ($\epsilon_{2,3,5} = \alpha$). The energy of the b_2 orbital (α - 2 γ) now changes its relative position with the second a_1 orbital. Meanwhile, the bonding energy of the totally symmetric bonding orbital decreases from $\alpha + 3.2\,\beta$ to $\alpha + 2\,\beta$. In an ideal cross the molecular orbitals are constructed only from the atoms in basal plane (threefold degenerate). It is therefore likely, that the neutral Pt_5 cluster has the shape of a swiss cross (second order Jahn Teller effect [218]). Figure 5.4 summarizes this calculation.

Mixing different ECPs for the platinum atoms also means mixing orbitals with different ionisation energies which cause different values for the valence ionisation energy $H_{\mu\mu}$. δ is the ionisation energy of the top platinum atom and equation 5.17 summarizes the calculation of the energy eigenvalues.

$$\begin{vmatrix} \delta-\epsilon & \beta & \beta & \beta & \beta \\ \beta & \alpha-\epsilon & \beta & 0 & \beta \\ \beta & \beta & \alpha-\epsilon & \beta & 0 \\ \beta & 0 & \beta & \alpha-\epsilon & \beta \\ \beta & \beta & 0 & \beta & \alpha-\epsilon \end{vmatrix} = 0 \tag{5.17}$$

$$\begin{aligned}
\epsilon_5 &= \alpha - 2\,\beta \\
\epsilon_4 &= \frac{1}{2}\,\left(\alpha + 2\,\beta + \delta - \sqrt{\alpha^2 + 4\,\alpha\,\beta + 20\,\beta^2 - 2\,\alpha\,\delta - 4\,\beta\,\delta + \delta^2}\right) \\
\epsilon_3 &= \alpha \\
\epsilon_2 &= \alpha \\
\epsilon_1 &= \frac{1}{2}\,\left(\alpha + 2\,\beta + \delta + \sqrt{\alpha^2 + 4\,\alpha\,\beta + 20\,\beta^2 - 2\,\alpha\,\delta - 4\,\beta\,\delta + \delta^2}\right)
\end{aligned} \tag{5.17 a}$$

For $\delta = \alpha$ equation 5.17 reproduces the results of equation 5.14. Only orbitals 1 and 4 change with the ionisation energy of the top atom. With an increase in ionisation energy, the orbital energy of the bonding a_1-orbital decreases. A small increase in the ionisationation energy of the top platinum stabilises the cluster (Pt_5^+). Figure 5.5 shows the movement of the orbitals as δ changes from $-\beta$ to β at a fixed value for α ($\alpha = 0$).

There are two ways to lower the energy of the bonding a_1 orbital: First, by increasing the interaction between the basal atoms compared with the interaction between the basal plane and the top atom, and second, to increase the ionisation energy of the top atom. Although both methods lower the energy of the $1a_1$ orbital, they act differently on the charge distribution in the cluster. This can be seen by a comparison of the coefficient of the top atom's 6s orbital in the $1a_1$ orbital.

$$c_1 = 1.0 \qquad\qquad c_2 = c_3 = c_4 = c_5 = \frac{1}{4\,\beta}\left(\gamma + \sqrt{4\,\beta^2 + \gamma^2}\right) \tag{5.18}$$

Equation 5.18 shows the coefficients of the $1a_1$ orbital as a function of γ for the first method. With increasing values for the coefficients of the basal atoms become more important relative to those for the top atom (c_1). Therefore, electron density moves from the top to the base of the pyramid. A different electron flow is observed in the second case (equation 5.19).

$$\begin{aligned}
c_1 &= 1.0 \\
c_2 = c_3 = c_4 = c_5 &= \frac{1}{8\,\beta}\left(2\,\beta + \alpha - \delta + \sqrt{\alpha^2 + 4\,\alpha\,\beta + 20\,\beta^2 - 2\,\alpha\,\delta - 4\,\beta\,\delta + \delta^2}\right)
\end{aligned} \tag{5.19}$$

With increasing values of δ the basal atoms become less dominant. The electron flow is reversed and charge accumulates at the top of the pyramid.

The calculations show, that the combination of different ECPs causes problems at the interface. In the Pt_5 pyramid the influence of the top atom on the electronic structure is small. The ionisation energy and the binding energy may vary without changing the ground state of the cluster.

5.3.3 5d-6s interaction in Pt_5

Charge transfer in the cluster is very important for the utility of a platinum cluster as surface model. Figure 5.6 illustrates the connection between Hückel calculations and those of the Hartree-Fock cluster.

Sketch A shows the HMO charge distribution in the Pt_5^+ cluster. The average 6s population per platinum is 0.8, which creates an average charge of +0.2 e per platinum. HMO calculations predict a charge of +0.447 e at the top. 6s electron density has to flow from the top to the bottom of the pyramid to create such a charge distribution (black arrows).

In sketch B the top platinum is replaced by an 18 electron platinum in the ^1S state. This replacement keeps the total 6s population at 4.0, but sets the formal charge of the platinum nucleus at the top equal to zero, because the tenth 5d electron compensates the positive charge at the nucleus. 6s electron density now flows to the top of cluster and creates a negative charge (−0.553 e). The top platinum acts now as a 6s electron sink and the resulting dipole moment can be used to simulate the electron spill.

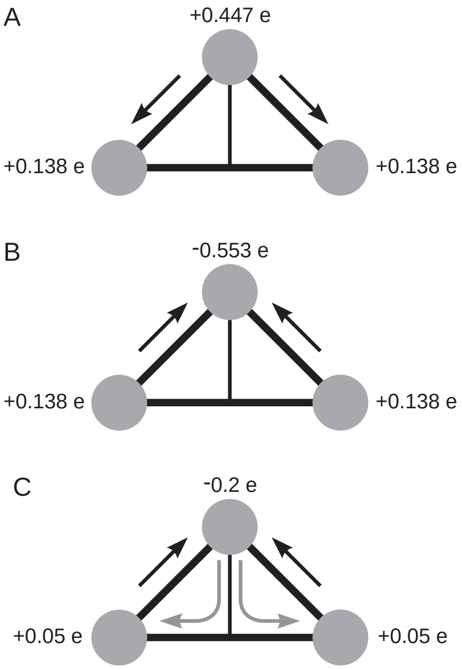

Figure 5.6: 5d-6s interaction in Pt_5

The last sketch, C, shows the result of a real HF calculation. The platinum at the top is described by the 18 valence electrons ECP of Hay and Wadt and the four bulk atoms by an experimental 1-electron ECP (subsection 7.3.1, page 230). This calculation produced a reduced charge at the top (−0.2 e), which cannot be explained with solely by the 6s orbitals. This charge distribution may be explained by a strong interaction between the 5d-orbitals at the top with 6sp orbitals at the base of the cluster. Two principal interaction pathways exist: The first pathway has been observed primarily for orbitals with a strong 6p contribution, while second is preferred by orbitals with a strong 6s contribution.

The first one is very direct with a small 5d-6sp overlap. The 6sp molecular orbitals have such a low energy, that they lie in or below the 5d band. These orbitals are filled with electrons instead of the 5d orbitals, which results in a net charge transfer from the top to the base. This electron flow is usually accompanied by a change of electronic state and may cause severe problems during the scanning of the potential energy surface. The second pathway is based on a strong 5d-6s overlap. If the energy of those 6s molecular orbitals is lower or equal to the 5d orbitals from the top atom, both systems mix provided symmetry permits. This mixing induces a strong electron flow from the top to the bottom. In ill suited cases this flow is so strong that the top platinum becomes positively charged. The bond between water and the cluster is now controlled by strong Coulomb interactions and no longer by orbital interaction. In these cases the binding energy is far too strong and the potential energy curve of the complex has the wrong shape.

The strength of the 5d-6s interaction depends on the symmetry and energy of the 6sp orbitals. In a system with only one type of platinum atom the strength of this interaction depends only on the quality of the basis set and/or the ECP. Problems arise if different types of platinum are used. In such clusters the strength of the 5d-6s interaction is controlled by the interface between the platinums (subsection 5.3.2). The valence ionisation energy α determines the centre of the 6s band, while the bond energy integral β is controlled by the shape of the atomic orbitals (section 5.7). A difference in these Hückel parameters does not change the electronic state of the cluster (subsection 5.3.2), but can distort the electron distribution in the cluster severely via the 5d-6s inteaction.

5.3.4 The rotational barrier in Pt_5-H_2O

Figure 5.7 shows the interaction between the water $1b_1$ orbital and one of the nonbonding (e) platinum orbitals of the platinum pyramid. The grey lines mark the water molecule's mirror

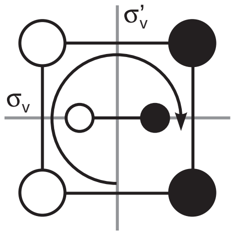

Figure 5.7: Mirror planes.

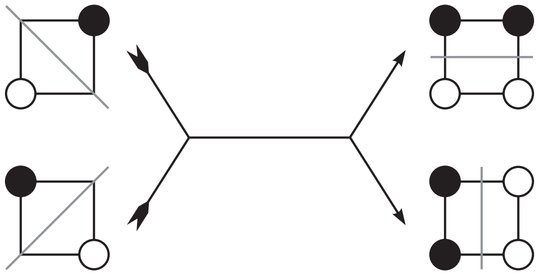

Figure 5.8: Mixing of the nonbonding 6s orbitals.

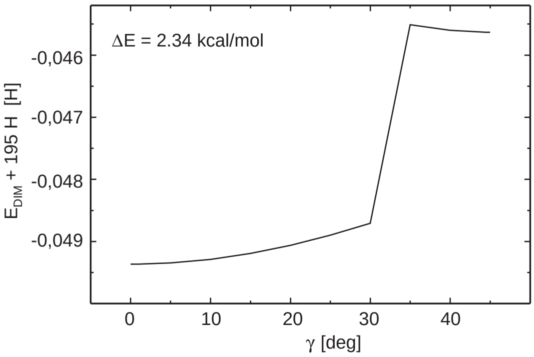

Figure 5.9: Rotation in Pt_5-H_2O / singlet state.

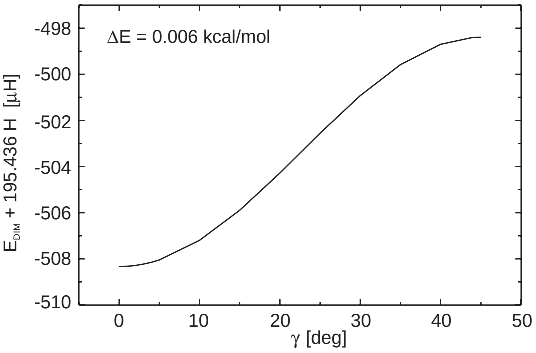

Figure 5.10: Rotation in Pt_5-H_2O / triplet state.

planes. This interaction between the two functions lifts the degeneracy of the nonbonding 6s orbitals (singlet splitting) and a singlet becomes possible.

Figures 5.9 and 5.10 show the total energy of Pt_5-H_2O during the rotation. The four bulk platinums were described with an experimental 1-electron ECP (section 7.2) and the top platinum with the 18 electrons potential by HAY and WADT. The singlet state (figure 5.9) is less favourable than the triplet state and the total energy makes a sudden jump ($\Delta E = 2.34$ kcal/mol) at ϵ[2] $= 30°$. The rotation of the water molecule on the platinum pyramid in the triplet state (figure 5.10) is smooth and without any energy jumps. The explanation for the energy jump is the interaction between the water molecule and the nonbonding 6s orbitals (figure 5.7). The σ'_v mirror plane of the water molecule turns with the nodal plane of the nonbonding 6s orbitals. This is not possible in the singlet state, because the two nonbonding 6s orbitals cannot mix. In the triplet state this mixing is possible and the water molecule can turn easily. The activation energy for the rotation vanishes ($\Delta E = 0.006$ kcal/mol).

Figure 5.8 shows the mixing of the 6s orbitals as the mirror plane rotates. The energy jump in the singlet state in figure 5.9 can be avoided by CASSCF(2,2) (**C**omplete **A**ctive **S**pace SCF, section 2.3, page 22) calculations, in which the active space contains both nonbonding 6s orbitals. Following the rotation the population of each active orbital is equal to one as observed in the triplet

---

[2] ϵ describes the rotation of the water molecule around the platinum-oxygen bond. Figure 6.60 on page 186 shows the geometry of the Pt_5-H_2O cluster.

state. A smooth rotation is not possible without mixing those orbitals.

The strength of the singlet splitting depends on the strength of the interaction between the nonbonding 6s orbitals and the water molecule. The interaction of the water molecule with the top platinum is governed by the 5d orbitals. A large singlet splitting demands a low energy for the nonbonding 6s orbitals. A low energy eigenvalue for these two orbitals may be created in 2 ways, either a strong 5d-6s interaction or a high valence ionisation energy α on the basal platinums. The ability of the water molecule to rotate depends again on the interface between the different ECPs.

5.3.5 Summary on Pt_5

The Hückel calculations on the Pt_5 pyramid showed that even the simplest calculations can help us to understand the results of more elaborate methods. They predict correctly the multiplicity of the ground state and allow us to determine the optimal number of 6s electrons in a cluster. The knowledge of the multiplicity and the degeneracy of the HOMO is helpful for the construction of working surface models (sections 6.4 (page 186) and 7.3.7 (page 244)) and can help us to understand energy jumps from one potential surface to another of the potential energy surface.

They also predict correctly charges and electron distributions, even for clusters with different ECPs. This interface between the ECPs is very important for the simulation of the water-platinum interface with larger model clusters. The difference between the ECPs can be described by two sets of Hückel parameters. Hückel calculations are so simple, that all properties of the ECP-interface can be expressed by analytical formulae. Different ECPs at the top and at the basal plane do not change the electronic state of the cluster and have only a small direct influence on the charge distribution. But this difference in the ECPs has a strong influence on the 5d-6s interaction. Via this pathway usage of different ECPs can distort the electronic structure significantly (subsection 7.3.5 page 240).

5.4 Hückel Calculations for Pt_9 Cluster

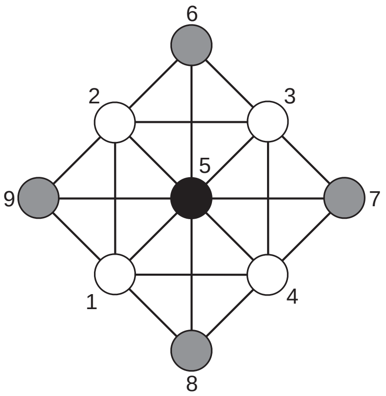

Figure 5.11: Pt_9 cluster, top view.

The next suitable cluster as surface model is the Pt_9 cluster, which is also the largest cluster managable with a 18 electrons ECP at all platinums. Figure 5.11 shows a top view of the cluster. The grey (passive) and black (active) circles mark surface atoms while the white ones represent atoms in the second layer.

The secular determinant for this cluster is big (9 × 9) and therefore difficult to handle. The mathematical problem can be reduced by using SALC's as basis set for the calculation. This was done in three steps. In the first step the atoms of the cluster were divided into three groups. Each group contains all symmetric unique atoms, which interchange their places during the application of any symmetry operator. The first group contains just one atom; atom number 5 in the centre. The second group contains the surrounding atoms 6, 7, 8 and 9. The third finally contains the atoms at the bottom (1,2,3 and 4). In the next step SALCs were constructed from the orbitals in each group. In the last step were the orbitals regrouped according to their symmetry. Section 11.11 (page 354) describes

	Ψ_1	Ψ_2	Ψ_3	Ψ_4	Ψ_5	Ψ_6	Ψ_7	Ψ_8	Ψ_9
sym	a_1	e	e	b_2	a_1	e	e	a_1	b_2
x	$2+\sqrt{8}$	$\sqrt{2}$	$\sqrt{2}$	0	$2-\sqrt{8}$	$-\sqrt{2}$	$-\sqrt{2}$	-2	-2
c_1	.35355	.5	0	0	−.35355	.5	0	0	.5
c_2	.35355	0	.5	0	−.35355	0	.5	0	−.5
c_3	.35355	−.5	0	0	−.35355	−.5	0	0	.5
c_4	.35355	0	−.5	0	−.35355	0	−.5	0	−.5
c_5	.5	0	0	0	.5	0	0	.70711	0
c_6	.25	.35355	.35355	.5	.25	−.35355	−.35355	−.35355	0
c_7	.25	.35355	−.35355	−.5	.25	−.35355	.35355	−.35355	0
c_8	.25	−.35355	−.35355	.5	.25	.35355	.35355	−.35355	0
c_9	.25	−.35355	.35355	−.5	.25	.35355	−.35355	−.35355	0
n_j^{occ}	2	2	2	2	0	0	0	0	0

Table 5.5: Coefficients of the molecular orbitals in Pt_9.

group	1	2	3
$5d^{10}$	−0.5	−0.125	0.25
$5d^9\ 6s^1$	0.25	−0.187	0.125
$5d^8\ 6s^2$	1.0	−0.25	0

Table 5.6: Charges on the Pt_9 cluster.

num e^-	grp. 1	grp. 2	grp. 3
2	0.5	0.125	0.25
4[a]	0.5	0.375	0.5
6	0.5	0.625	0.75
8	0.5	1.125	0.75
8[b]	1	0.75	1

[a] high spin [b] Ψ_4 and Ψ_5 swaped

Table 5.7: 6s population in the Pt_9 cluster.

the details of the calculation.

Table 5.5 lists the results of the Hückel calculations after renumbering according to their energy. The combination of a single ^1S platinum atom (18 valence electrons) in the centre of the cluster with 8 ^3D atoms (1-valence electron) yields a stable cluster. The occupation of the orbitals is also shown in table 5.5. Charge calculations showed that the clusters surface (groups 1 + 2) is negatively charged (table 5.6). The combination of a ^1G platinum ($5d^8\ 6s^2$) with 8 one electron platinum atoms reverses the charge on the central platinum atom. The extra charge flows from the surface to the bottom of the cluster and alters so to the bonding possibilities for a water molecule. The same electron flow is observed, if the cluster is constructed solely from ^3D platinum atoms, despite different multiplicities. Only the combination of a ^1S with eight ^3D platinums guarantees a suitable 6s population and a negative charge of the active platinum[3].

Intra molecular charge transfer is important for real clusters with 6p orbitals. The 6p orbitals mix with the 6s band and this mechanism lowers the energy of the orbitals. These new hybrid orbitals combine with 5d orbitals from the central platinum correct symmetry provided (subsection 5.3.3). Electron flow is one of the major problems with the development of a single electron ECP and is very difficult to handle, as each cluster has its own electron structure. Hückel calcualtions

---

[3] A negative charge at the metal surface enhances the bond between platinum and hydrogen atoms and can create unphysical orientations of the water molecule.

help us to detect the important orbitals and to understand the individual mechanisms.

The Pt_9 cluster is beyond the capacity of the MP2 method and even the HF results are difficult to read. A comparison of the Hückel results and the HF results (section 6.5, page 192) can be used to understand the properties of the 18 valence electrons calculations.

HF calculations with a simple 1 electron ECP showed, that the molecular orbitals Ψ_4 and Ψ_5 change their position on the energy scale and Ψ_5 becomes populated instead of orbital Ψ_4. These changes indicate a principle limitation of the Hückel method for the platinum 6s orbitals and will be discussed in subsection 5.7.

Table 5.7 lists the 6s population of the platinums. The inversion of the orbitals Ψ_4 and Ψ_5 has a strong influence on the charge distribution in the cluster. The active surface platinum becomes more negatively charged (assuming a ^{1}S or ^{3}D platinum in the centre), while the remaining surface atoms (group 2) are positively charged (+0.25, assuming a ^{3}D platinum). The four platinums at the bottom of the cluster do not carry any charge. This charge distribution is closer to the one observed in Pt_9-H_2O, but the total 6s population is lower in the 18 electron ECP calculation (HF: 3.37, MP2: 7.57, table 6.23 $d_{PtO} = 12.2$ Å). The 6s population at the central platinum is 0.42 and the average 6s population is 0.30 on the passive surface atoms and 0.44 on the bulk atoms on the HF level. This charge distribution agrees well with the Hückel results (table 5.7) for a total 6s population of 4. Hückel calculations demand a multiplicity of 3 to create such a charge distribution, but the HF results were extracted from a singulet wavefunction. The degenerate orbitals Ψ_2 and Ψ_3 are populated via a strong 5d-6s interaction. The agreement in the charge distribution between both methods is smaller on the MP2 level. The passive surface atoms are stronger populated than the active (active 0.55, passive 1.18, bulk 0.71). This charge distribution is closer to the results of the Hückel calculation than to the results of the simplified HF calculation (Ψ_4 and Ψ_5 changed their position).

The charge distribution is vice versa. On MP2 level is the active surface atom negatively charged (-1.38 e) and the passive surface atoms carry a positive charge (+0.23 e). This charge distribution is closer to the simplified HF result (active -1 e, passive +0.25 e) than to the pure Hückel results (active -0.5 e, passive -0.12 e). The HF results for Pt_9 (active -0.58 e, passive +0.09 e table 6.23) show the same principle structure than the Hückel results, but differ in the absolute values (active -0.5 e, passive +0.62 e).

The difference between the Hückel results and the MP2 values regarding 6s population and charge distribution questions the validity of the MP2 approach towards Pt_9-H_2O, while the HF results in section 6.5 agree qualitatively and seem so to be more reliable. The principle problem with large clusters is the 5d-6s interaction, which becomes more important as the cluster grows. The interaction with the water molecule on the other hand is controlled by the 6s population and all calculations of this sections show, that the influence of the 5d-6s interaction on the 6s population can be strong (a 6s population of 3.4 with a singlet function). But, the electron distribution of a given 6s population can be described well with Hückel calculations.

5.5 Two Slabs Pt_{17} Cluster

Figure 5.12 displays a top view of the Pt_{17} cluster. It is the extension of the Pt_9 cluster shown in figure 5.11 and the first without an MP2 counter part. The top layer atoms at the cluster's edge rest now on four second layer atoms. Every surface atom has so a complete basis to rest on. A systematic enlargement of the surface model allows us to analyse the role of the central platinum.

	Ψ_0	Ψ_1	Ψ_2	Ψ_3	Ψ_4	Ψ_5	Ψ_6	Ψ_7	$2\Sigma c_i^2$
sym	a_1	e	e	b_1	a_1	b_2	e	e	
x	5.4982	3.	3.	2.	.7153	0.	0.	0.	
χ_0	.3347	.2582	.2582	.0	.0687	−.2887	.2887	.2887	1.0000
χ_1	.3347	.2582	−.2582	.0	.0687	.2887	.2887	−.2887	1.0000
χ_2	.3347	−.2582	−.2582	.0	.0687	−.2887	−.2887	−.2887	1.0000
χ_3	.3347	−.2582	.2582	.0	.0687	.2887	−.2887	.2887	1.0000
χ_4	.1289	.3227	.0645	.2887	−.3050	−.2887	−.2887	.2887	1.1022
χ_5	.1289	.3227	−.0645	.2887	−.3050	.2887	−.2887	−.2887	1.1022
χ_6	.1289	.0645	−.3227	−.2887	−.3050	.2887	.2887	.2887	1.1022
χ_7	.1289	−.0645	−.3227	−.2887	−.3050	−.2887	−.2887	.2887	1.1022
χ_8	.1289	−.3227	−.0645	.2887	−.3050	−.2887	.2887	−.2887	1.1022
χ_9	.1289	−.3227	.0645	.2887	−.3050	.2887	.2887	.2887	1.1022
χ_{10}	.1289	−.0645	.3227	−.2887	−.3050	.2887	−.2887	−.2887	1.1022
χ_{11}	.1289	.0645	.3227	−.2887	−.3050	−.2887	.2887	−.2887	1.1022
χ_{12}	.2454	.3873	.0	.2887	.0181	.0	.0	.0	0.5876
χ_{13}	.2454	.0	−.3873	−.2887	.0181	.0	.0	.0	0.5876
χ_{14}	.2454	−.3873	.0	.2887	.0181	.0	.0	.0	0.5876
χ_{15}	.2454	.0	.3873	−.2887	.0181	.0	.0	.0	0.5876
χ_{16}	.4220	.0	.0	.0	.4855	.0	.0	.0	0.8274

Table 5.8: Occupied orbitals of the Pt17 cluster and population analysis.

As before for the Pt_9 cluster SALCs (The groups of symmetrically equivalent orbitlas are: I: χ_0 to χ_3; II: χ_4 to χ_{11}; III: χ_{12} to χ_{15}; IV: χ_{16}) were used for the Hückel calculations and section 11.12 (page 355) describes the procedure while table 5.8 summarizes the results. The symmetry of the Hückel orbitals can be easiyly specified by the number of nodal planes: The totally symmetric functions (a_1) have no nodal plane while orbitals with a_2 symmetry have up to four nodel planes.

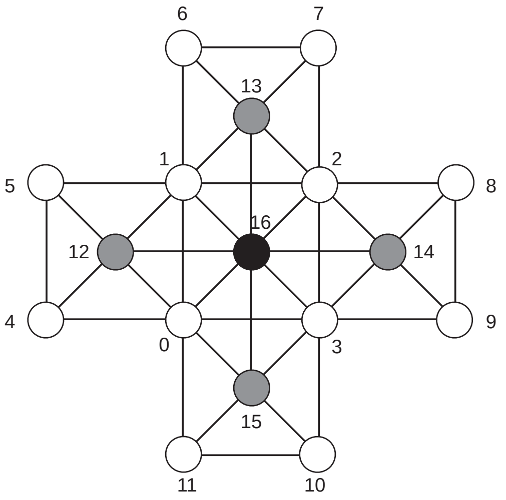

Figure 5.12: Pt_{17} cluster, top view.

Table 5.9 shows the charge distribution calculated for the Pt_{17} cluster constructed with a $5d^{10}$ platinum atom in the centre. The negative charges concentrate at bottom at the cluster, while the surface atoms are positively charged excepting the central atom, which carries a negative charge similar to the charge distribution in Pt_9 with a low 6s population.

Table 5.10 shows the charge of the central $5d^{10}$ platinum atom from pure 6s Hückel calcualtions in differents model clusters. A negative charge is reasonable, since the empty 6s orbital is filled with electrons from the neighbours. It is interesting to note, that the negative charge increases slower than the average 6s population (Pt_5: 0.800, Pt_9: 0.889, Pt_{17}: 0.941). Despite the increase of the average 6s population the charge on the central platinum atom decreases changing from Pt_5 to Pt_9. The amount of negative charge on the central

group	Q [e]
I	0.00
II	-0.10
III	0.41
IV	-0.83

Table 5.9: Charges on the Pt_{17} cluster.

cluster	Q_{cent} [e]	6s pop
Pt_5	-0.553	0.800
Pt_9	-0.500	0.889
Pt_{17}	-0.827	0.941

Table 5.10: Q_{cent} on differnt metal cluster.

atom is proportional to the number of occupied orbitals, which are built with the 6s orbital of this atom. As the number of atoms increases, the number of totally symmetric SALCS becomes slowly bigger. Meanwhile increases the number of the other orbitals dramatically and the probability of the occupation of a totally symmetric orbital does not increase significantly. We assume therefore that the negative charge on the central atom decreases not much lower then -0.85 e while the average 6s population approaches 1.0. The reminding 6s orbitals act as an electron sink, even if the totally symmetric LUMO is occupied in Pt_{17} ($5d^9$ $6s^1$: $q_{cent} = +0.02$ e)[4] . A similar charge transfer has been observed in the Pt_9 cluster build only from ^3D platinums ($q_{cent} = +0.25$ e). A negative charge on the central platinum is only possible, if the central platinum has $5d^{10}$ electron structure and the empty orbital becomes populated by the neighbours. Any other structure causes a positive charge and so a too strong $Pt-H_2O$ interaction.

As the number of 6s orbitals increases an interaction between the 6s orbitals and the 5d orbital becomes more likely, because more symmetrically suitable orbitals are in the energy range of the 5d orbitals. This overlap increases the electron drain from the central orbital and inverses the charge distribution.

The prediction of the ground state's multiplicity and the charge distribution becomes more complicated as the cluster grows. The energy of the nonbonding $3a_1$ orbital (Ψ_8 LUMO) is systematically lower in HF- than in Hückel calculations as simple pure 6s test calculations showed. The HF energy of Ψ_8 is lower than the energies of Ψ_7 and Ψ_6 and the electronic ground state has therefore a multiplicity of 3. With increasing cluster size become the bonding interactions with the second next neighbour within an atomic orbital group more important. Hückel calculations do not take this interaction into account and the calculation of the orbital energies becomes less reliable.

5.6 The Second Next Neighbour

The 6s orbitals are wide spreading and interactions with the second next neighbour are likely. The classic Hückel theory only accounts for the interaction with the next neighbour (β) but not with the second next. To get an estimate of the influence of this neglect several calculations were done, were done with the following assumptions:

$$S_{ij} = \delta_{ij} \qquad \langle\varphi_i|\hat{H}|\varphi_i\rangle = \alpha \qquad \langle\varphi_i|\hat{H}|\varphi_{i+1}\rangle = \beta \qquad \langle\varphi_i|\hat{H}|\varphi_{i+2}\rangle = \gamma\cdot\beta \tag{5.20}$$

---

[4] The coefficient of φ_{16} in the LUMO is 0.39247. Since φ_{16} and χ_{16} are by definition equal, is the coefficient of χ_{16} in the LUMO also 0.39247. In a cluster build from 17 $5d^9$ $6s^1$ platinum atoms (a_1^2 e^2 e^2 b_2^2 a_1^2 b_2^2 e^2 e^2 a_1^1) is therefore the total population of the 6s orbital at the central platinum atom 0.9814 and the charge 0.02 e.

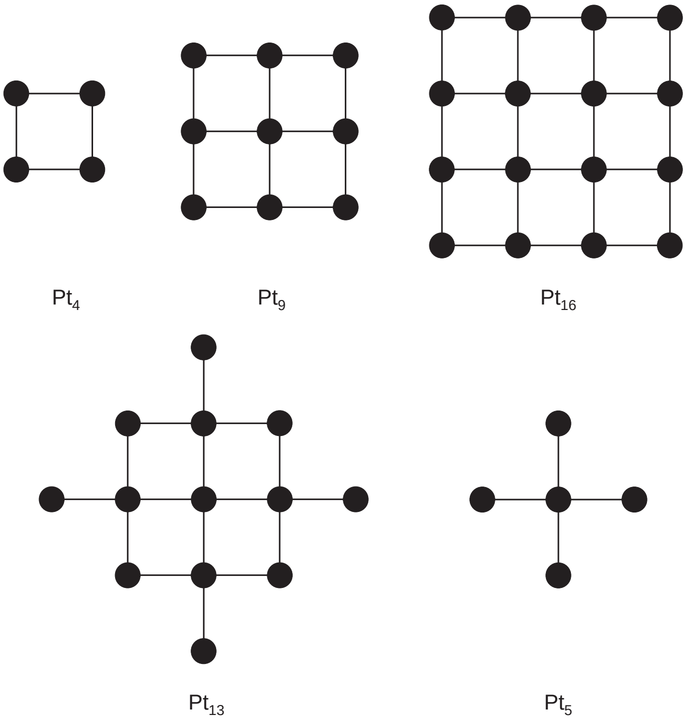

Figure 5.13: Surface model cluster.

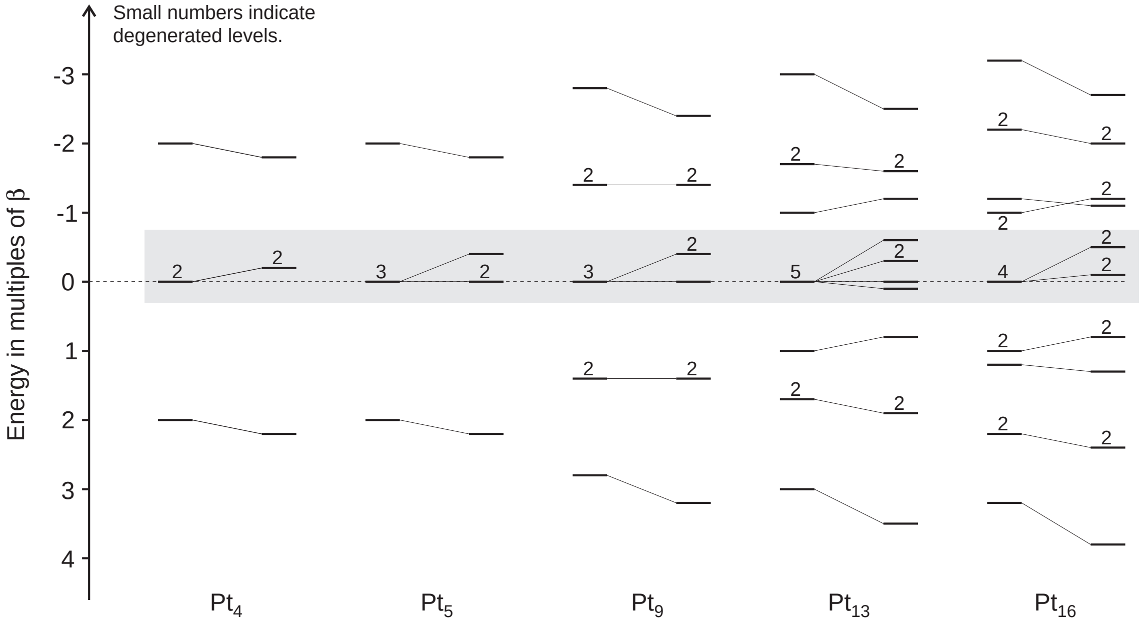

Figure 5.14: Effect of the second next neighbour ($\gamma = 0.2$).

The first set of test clusters were two-dimensional surface models built from 1, 2 and 3 squares (Pt_4, Pt_9, Pt_{16}) and the second set was constructed from crosses (Pt_5, Pt_{13}). Figure 5.13 shows the model cluster.

The second next neighbours are connected by the diagonals of the squares, which facilitates counting. Closed cluster (Pt_4, Pt_9, Pt_{16}) contain more direct bonds between next neighbours then bonds with the second next neighbour (Pt_4 2:1, Pt_9 1.5:1, Pt_{16} 1.3:1). The number of second next neighbours actually decreases with cluster size and should finally reach a ratio of 1:1. Open clusters contain as many direct bonds as bonds with the second next neighbour (Pt_5 4:4, Pt_{13} 16:16) and have so a optimal geometry. Open clusters are therefore good examples for the influence of the second next neighbours.

Figure 5.14 and equation 5.21 show the influence of the interaction with the second next neighbours ($\gamma = 0.2$). The interaction lifts the degeneracy of the HOMO's (marked in grey). The average energy difference between the formerly degenerated orbitals is about 2 γ, which makes in the example 20% of a single Pt-Pt bond ($\Delta E_{Pt2} = 2\,\beta$). An energy difference of this size would certainly lead to a change of the electronic state. Those new states with smaller multiplicity have a lower energy ($\approx 0.5\,\beta$) than before. If the number of unpaired electrons is kept constant and the electrons stay in their original orbitals, the energy gain by the interaction with the second next neighbour is zero for closed structures and negligible small for open structures (Pt_4: 0 β, Pt_9: 0 β, Pt_{16}: 0 β / Pt_5: 0.02 β, Pt_{13}: 0.08 β). The energy gain for open structures (Pt_5: $2 \cdot (4\,\beta^2 + \gamma^2)^{0.5} - 4\,\beta$) is small but increases with cluster size and γ.

$$
\begin{array}{rrr}
Pt_4 & Pt_9 & Pt_{16} \\
x_{01} = -2+\gamma & x_{01} = -\sqrt{8}+2\gamma & x_{01} = \frac{1}{2}[-2+3\gamma+(\gamma-2)\sqrt{5}] \\
x_{02} = x_{03} = -\gamma & x_{02} = x_{03} = -\sqrt{2} & x_{02} = x_{03} = 2\gamma-\sqrt{5} \\
x_{04} = 2+\gamma & x_{04} = x_{05} = -2\gamma & x_{04} = \frac{1}{2}[2+3\gamma-(\gamma+2)\sqrt{5}] \\
 & x_{06} = 0 & x_{05} = x_{06} = -1-\gamma \\
 & x_{07} = x_{08} = \sqrt{2} & x_{07} = x_{08} = \frac{1}{2}(-3\gamma-\sqrt{5}\gamma) \\
 & x_{09} = \sqrt{8}+2\gamma & x_{09} = x_{10} = \frac{1}{2}(-3\gamma+\sqrt{5}\gamma) \\
 & & x_{11} = x_{12} = 1-\gamma \\
 & & x_{13} = \frac{1}{2}[-2+3\gamma-(\gamma-2)\sqrt{5}] \\
 & & x_{14} = x_{15} = \gamma+\sqrt{5} \\
 & & x_{16} = \frac{1}{2}[2+3\gamma+(\gamma+2)\sqrt{5}]
\end{array} \tag{5.21}
$$

The interaction with the second next neighbour stabilizes the LOMOs (lowest occupied orbitals) of the open cluster more then it destabilizes the SOMOs (singly occupied molecular orbital)(figure 5.14, equation 5.16[5]), because the outermost atoms, which are connected to the cluster only by one bond become more involved into the electronic structure of the cluster. This small advantage

---

[5] A Pt_5 pyramid with weak interactions in the basal plane has the same Hückel determinat as a Pt_5 cross with strong interactions between second next neighbours.

results in the energy gain by the introduction of the interaction. Closed structures do not contain any isolated atoms, which benefit more then averagely from the interaction with the second next neighbour. The energy gain of the LOMOs is therefore completely compensated by the splitting of the SOMOs (equation 5.21). This splitting increases with increasing values of γ and may change the relative energetic order of the orbitals. The larger the cluster becomes, the more likely is such a change. Figure 5.14 shows the correlation diagram of Pt_{16}. Even such a small interaction as $\gamma = 0.2$ can change now the relative order of the orbitals.

These simple calculations also show that interactions with the second next neighbour alone cannot explain the movement of the nonbonding a_1-orbitals observed in HF calculations. The energy of the nonbonding orbitals increases and does not drop with the strength of the long range interaction. Other phenomena, which have been neglected so far are the reason for this energy change.

The calculations in this subsection also suggest that the error due to the interaction with the second next neighbour should be small and therefore negligible for small clusters, since the influence of this interaction increases with cluster size. The reliability of those simplified Hückel calculation decreases rapidly, if degenerate HOMOs are unevenly populated. The interaction with the second next neighbour lifts the degeneracy of those orbitals and the Hueckel calculation cannot be used anymore to predict the wavefunctions multiplicity. The calculation also showed, that a closed structure should be preferred rather then an open, since the influence of the second neighbour interactions should not change the total energy of the cluster.

5.7 Quantitative Analysis of the HMO Calculations

Table 5.11 summarizes the results (degeneracy and orbital energies) for all platinum clusters calculated with the Hückel approximation. It was said before, that the splitting of the 6s band is crucial for the quality of the HF calculations. Even approximate values would be helpful to validate the HMO results.

two slabs surface models			closed 2D surface models			open 2D models	
Pt_5	Pt_9	Pt_{17}	Pt_4	Pt_9	Pt_{16}	Pt_5	Pt_{13}
2 × 0.000	1 × 0.000	3 × 0.000	2 × 0.0	3 × 0.000	4 × 0.000	3 × 0.0	5 × 0.000
1 × 3.236	2 × 1.414	1 × 0.715	1 × 2.0	2 × 1.414	2 × 1.000	1 × 2.0	1 × 1.000
	1 × 4.828	2 × 3.000		1 × 2.828	2 × 1.236		2 × 1.732
		1 × 5.498			1 × 3.236		1 × 3.000

Table 5.11: Orbital energies and degeneracies of the HMO calcualtions.

The comparison of the Hückel calculations with Hartree Fock calculations was done in two steps. First, estimates of the Hückel parameter were obtained from Pt_2-calculations. In the second step those parameters were tested on the Pt_5-calculations and refined. Those calculations also allowed us to estimate the influence of the different Hückel approximations on the final result.

5.7.1 Results for the Platinum Dimer

The orbital energies depend on the values of the integrals α and β. It is therefore most important to get reliable numbers. In the first step the numbers were taken from the literature. HOLLOWAY and BENNEMANN [64] optimized the values for α and β to match experimental results and results from other calculations (CNDO). The off diagonal elements (resonance integral β) were calculated with the CUSSACH's formula [271, 272].

$$\beta = H_{12} = \frac{1}{2}\,(2 - |S_{12}|)\;S_{12}\;(H_{11} + H_{22}) = (2 - |S_{12}|)\;S_{12}\;\alpha \tag{5.22}$$

The overlap integrals were calculated from Slater orbitals [191, 297–300]. The Slater exponents ζ were given in their paper.

$$\begin{aligned} \chi_{6s} &= N\,r^{3.2}\,e^{-\zeta r}\,\sqrt{\frac{1}{4\,\pi}} \qquad\qquad \text{and} \\ S_{12} &= N^2 \int (|\vec{r_1}||\vec{r_2} - \vec{R}|)^{3.2}\;\exp(-\zeta\;|\vec{r_1} + \vec{r_2} - \vec{R}|)\;dV \end{aligned} \tag{5.23}$$

The overlap integral was calculated numerically with a Mathematica script [301]. This script was tested before with an 1s orbital and ROOTHAN's formula [300]. This calculation yields $\beta_{6\mathrm{s}} = -6.6$ eV and $\alpha_{6\mathrm{s}} = -9.8$ eV (R = 2.1 Å). The value given in HOLLOWAYS's paper for $\alpha_{5\mathrm{d}}$ is -10.61 eV. Every 6s-HMO with an energy lower than 0.12 β has therefore an energy lower or equal to the 5d electrons. This is actually every bonding orbital[6].

BENNEMAN and HOLLOWAY used in their article parameters, which were optimized to reproduce properties of the platinum dimer in Extended Hückel calculations (EHT). For the development of a new ECP it would be most helpful, if the Hückel calculations not only reproduce the symmetry and the number of nodal planes of the Hartree Fock calculations but also give a rough estimate of the orbital energies.

There are two possible methods for the extraction of useful parameters from Hartree-Fock calculations:

1. The values of α and β are extracted directly from the orbital energies of the platinum dimer.

   $$\text{a)}\quad \alpha = \frac{\epsilon_+ + \epsilon_-}{2} \qquad\qquad \text{b)}\quad \beta = \epsilon_+ - \alpha = \alpha - \epsilon_- \tag{5.24}$$

   ϵ_+ and ϵ_- are the orbital energies of bonding and the antibonding orbital combinations. A comparison of the results for Pt_2 and Pt_2^+ allows us to get an estimate of the electron-electron repulsion energy.

2. The value of β is calculated with one of the many formulae, which extrapolates the value of the resonance integral from the valence ionisation energies. Two expressions are frequently used: a) the formula by WOLFSBERG and HELMHOLTZ [277] (equation 5.25a) and b) the CUSSACH's formula [271, 272] (equation 5.25b).

   $$\text{a)}\quad H_{\mu\nu} = \frac{1}{2}K(H_{\mu\mu} + H_{\nu\nu})S_{\mu\nu} \qquad\qquad \text{a)}\quad H_{\mu\nu} = \frac{1}{2}(2 - |S_{\mu\nu}|)S_{\mu\nu}(H_{\mu\mu} + H_{\nu\nu}) \tag{5.25}$$

   This method requires only the extraction of α from the HF calculation (equation 5.26), because the value of the resonance integral is determined by the chosen basis set. The

---

[6] EHT calculations ($(\alpha - \epsilon)^2 - (\beta - \epsilon \mathrm{S})^2 = 0$) with the same parameters ($\alpha = -0.36014$ H, $\beta = -0.24395$ H, S = 0.432 a.u., R = 2.1 Å = 3.9684 a_0) gave the following orbital energies $\epsilon_+ = -0.426$ H ($+0.27\,\beta$) and $\epsilon_- = -0.202$ H ($-0.65\,\beta$). The EHT uses the following approximation $\mathrm{E}^{\mathrm{tot}} = \mathrm{E}^{\mathrm{elec}}$ and the binding energy ΔE of the platinum dimer (only with 6s orbitals!) is with 82.6 kcal/mol far too high (MP2 benchmark calculation: 60 kcal/mol, table 6.10 page 161).

dicussion in the literature suggests, that it might be necessary to find a empirical correction of the resonance integral to improve the results.

$$\alpha = \epsilon_+ - \beta \tag{5.26}$$

The valence ionisation energy is calculated from the bonding orbital since the antibonding orbital does not contribute to the total energy E, as $\mathrm{b_i}$ equals zero (equation 5.6).

While both methods should result in parameters of similar quality offers the second method a direct link to the extended Hückel theory (EHT). Such an extension allows us the direct comparison with results published previously in the literature.

The key element of the second method is the overlap integral S. The precise values of this integral were extracted from Gaussian 94 calculations. To keep this process as simple as possible, the basis set was restricted to a single zeta 6s function. The spherically symmetric part of the ECP ($\mathrm{U_L^{core}}$, equation 2.65 on page 33) was set equal to zero.

The standard G94 output file does not contain the overlap integrals, but two ways exists to extract the overlap integral from the file.

1. The coefficients of the bonding orbital allow the calculation of the overlap integral S.

$$\Psi = \frac{1}{\sqrt{2+2S}}(\chi_1 + \chi_2) = c_1\chi_1 + c_2\chi_2 \qquad \Rightarrow \qquad S = \frac{1}{2\,c^2} - 1 \tag{5.27}$$

2. The second possibility offers the combination of the Mulliken population matrix B, population number $\mathrm{b_i}$ and the density matrix $\mathrm{c_i}$. This method can be applied to larger molecules.

$$\begin{gathered} \Psi = c_1\chi_1 + c_2\chi_2 \\ b_i = b_i\langle\Psi|\Psi\rangle = b_i(c_1^2 + 2c_1c_2S + c_2^2) = A + 2B + C \qquad \Rightarrow \qquad S = \frac{B}{b_i\;c_1\;c_2} \end{gathered} \tag{5.28}$$

Both methods yielded the same values for S. The results of these calculations are summarized in figure 5.15[7]. A least squares fit of the curve with MicroCal Origin allows us to use the following approximation for further calculations.

$$S_{12} = \langle\chi_1|\chi_2\rangle \approx 1.00256 \exp\left[\frac{-2(R+0.16538)^2}{4.23628^2}\right] + 7.5\cdot 10^{-4} \tag{5.29}$$

The valence ionisation energy α was calculated from the orbital energy ϵ_+ of the bonding orbital and CUSSACH's formula for the resonace integral β (equation 5.25b).

$$\epsilon_+ = \alpha + \beta = \alpha + (2 - |S|)S\alpha \qquad \Rightarrow \qquad \alpha = \frac{\epsilon_+}{1 + S\,(2 - |S|)} \tag{5.30}$$

Table 5.12 summarizes the results for the Hückel parameters obtained with both methods in the chemically important range 2.0 Å $\leq$ R $\leq$ 3.0 Å. While the resonance integral β varies strongly with bond lenghth is the influence of the geometry on the valence ionisation energy small. Even more important than the geometry is the electronic state of the molecule. The valence ionisation energy of the $\mathrm{Pt_2^+}$ is nearly twice as big as for $\mathrm{Pt_2^0}$. The value of the resonance integral shows the

---

[7] Figure 5.15 demonstrates also that any interactions across a distance larger than the distance to the second next neighbour can be neglected in a first approach to platinum clusters.

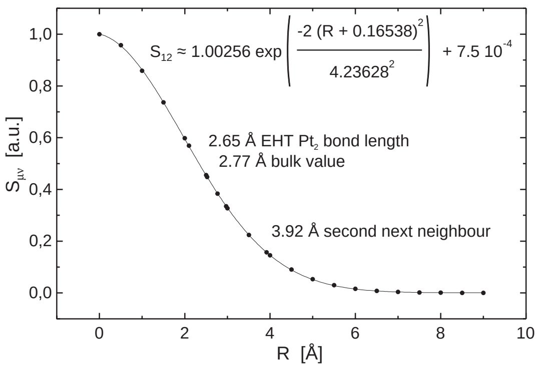

Figure 5.15: $S_{\mu\nu}$ calculated with G94 and the best fit.

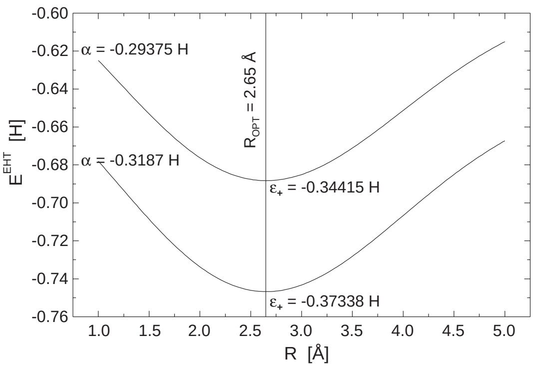

Figure 5.16: EHT results for Pt_2^0.

	equation 5.25b and equation 5.30				equation 5.24a and equation 5.24b			
	Pt_2^+		Pt_2^0		Pt_2^+		Pt_2^0	
r [Å]	$-\alpha$ [H]	$-\beta$ [H]	$-\alpha$ [H]	$-\beta$ [H]	$-\alpha$ [H]	$-\beta$ [H]	$-\alpha$ [H]	$-\beta$ [H]
2.0	0.31510	0.26420	0.16680	0.13986	0.37875	0.20056	0.12177	0.18487
2.5	0.31737	0.22320	0.16559	0.11650	0.38254	0.15804	0.13547	0.14661
3.0	0.32387	0.17735	0.15131	0.10642	0.37521	0.12601	0.13914	0.11858
$\bar{x}$ [H]	0.3187	0.2216	0.1612	0.1209	0.3788	0.1615	0.1321	0.1500
σ_n [H]	0.0037	0.0355	0.0070	0.0140	0.0030	0.0305	0.0075	0.0272

Table 5.12: Hückel parameters from ECP-FH calculations on Pt_2^0 and Pt_2^+.

same behaviour. The value of β for Pt_2^+ is about 10% bigger then for Pt_2^0, if the parameters are calculated with equations 5.24a and 5.24b. This small difference allows us to work with an average value of $\beta = -0.1558$ H ($\sigma_n = 0.0295$ H). It is more difficult to make a reasonable selection of α, because α is nearly three times bigger for Pt_2^+ then for Pt_2^0. It should be noted, that the value of α extracted from the Pt_2^0 calculations is smaller then the ionisation energy of the free atom. The average values is $\bar{\alpha} = -0.25548$ H, but the standard deviation is far too big for $\bar{\alpha}$ to be reasonable for large set of calculations ($\sigma_n = 0.12348$ H). Although difficult to explain by theoretical means it might be useful to work with two sets of parameters depending on the charge of the cluster to account for the reduced electron-electron repulsion.

The lowest 5d ionisation energy is 0.42084 H for a ^{1}S platinum and 0.36552 H for a ^{3}D platinum (HAY & WADT ECP, UHF [189]). The Hückel parameters obtained so far ($\alpha = -0.25548$ H, $\beta = -0.1558$ H) suggest the any 6s MO with an energy lower then 1.1 β (^{1}S) respectively 0.71 β (^{3}D) can interact with an 5d orbital, as ϵ_{5d} depends on the electronic state of the platinum atom.

The second method (equations 5.25b and 5.30) seems not to be appropriate to extract useful Hückel parameters form ECP-HF calculations. The individual values for β vary for defined electronic state as much as values calculated with method 1, but they differ strongly for different states (factor 1.833). For large values of R as β approaches zero α has to compensate for the nuclear repulsion and becomes unreliable. The dependency of α on the electronic state is smaller for method 2 (factor 1.997) then for method 1 (factor 2.867), but still very big. It seems not to be reasonable to extract just one parameter (α) from ECP-HF calculations and to construct the other from this single value.

		Pt_5^{4+}		Pt_5^{3+}		Pt_5^{+}		Pt_5^{0}	
multiplicity		2		1		3		4	
ϵ_{b_2}	[H]	-0.49046		-0.29118		$+0.02166$		$+0.19262$	
ϵ_{a_1}	[H]	-0.76070		-0.53775		-0.18360		-0.19391	$\uparrow$
ϵ_e / ϵ_e	[H]	-0.86772		-0.65065		-0.47368	$\uparrow\uparrow$	-0.29661	$\uparrow\uparrow$
ϵ_{a_1}	[H]	-1.31806	$\uparrow$	-1.06724	$\uparrow\downarrow$	-0.72178	$\uparrow\downarrow$	-0.54233	$\uparrow\downarrow$
E^{TOT}	[H]	$+1.054216$		-0.012697		-1.136859		-1.325930	
Q_{BASIS}	[e]	0.837		0.653		0.161		0.060	
Q_{TOP}	[e]	0.653		0.388		0.355		-0.239	
R_{OPT}	[Å]	dissociation		dissociation		2.7452		2.7714	
E^{TOT}_{OPT}	[H]	—		—		-1.250322		-1.453977	

The small arrows indicate electron occupation.

Table 5.13: Results from ECP-HF calculations.

Figure 5.16 displays the results from EHT calculations (equation 5.31) for the platinum dimer Pt_2. The total energy E^{TOT} was calculated with EHT approximation $E^{TOT} = E^{elec}$. To simplify the computation we used equation 5.29 to estimate the value of the overlap integral S.

$$\begin{vmatrix} \alpha - \epsilon & \beta - S\epsilon \\ \beta - S\epsilon & \alpha - \epsilon \end{vmatrix} = (1 - S^2)\,\epsilon^2 + 2\,(S\,\beta - \alpha)\,\epsilon + (\alpha^2 - \beta^2) = 0 \tag{5.31}$$

The optimized bond length (2.65 Å, bulk Pt: 2.77 Å) does not change much with the value of the valence ionsiation energy α. The variation of α only allows us to fit the EHT bonding energy to ECP-HF results. If an optimized bond length is required, another method for the calculation of β has to be chosen, since the value of the overlap integral is fully determined by the chosen basis set. The EH theory is not able to describe the variation of the bond lenght with the molecule's charge, because the Hückel parameters α and β do not depend on the occupation of the orbitals.

5.7.2 Results for Platinum Pentamer (Pyramid)

Table 5.13 summarizes the ECP-HF (subsection 7.3.1, page 230) results for the Pt_5 pyramide (R = 2.1 Å). Geometry oprimisations were possible only for Pt_5^+ and Pt_5^0. Clusters with higher charges dissociated.

The Hückel calculations (subsection 5.3) predicted correctly the multiplicity of the ground state (quartet). Test calculations for ${}^2Pt_5^0$ did not converge or gave unrealistic charge distributions contradicting symmetry restrictions (The four basis atoms had different charges.).

The orbital energies demand more consideration. While the charge of the cluster decreases, increases the energy of the degenerate orbitals. According to the pure Hückel theory should their energy be equal to the ionisation energy α. Using the Hückel parameters extracted from the ECP-HF calculations of the platinum dimer ($\alpha = -0.24458$ H, $\beta = -0.1558$ H) yielded the following orbital energies:

$\epsilon_{a_1} = -0.760$ H $\qquad \epsilon_e = -0.245$ H $\qquad \epsilon_{a_1} = +0.063$ H $\qquad \epsilon_{b_2} = +0.567$ H

The ϵ_e energy from the simple Hückel calculation agrees fairly well with the result for Pt_5^0, but fails for all other clusters. This movement of orbital energy as a function of the 6s population is important for the prediction of the groundstate's multiplicity. In a large cluster (for example

Pt_{17}) those orbitals may belong to different symmetry species. If the energy of the nonbonding orbitals is small enough, they might interact with the 5d orbitals from the central platinum atom symmetry provided. This interaction lifts the orbitals degeneracy and can change the groundstate's multiplicty.

To understand the physical basis of the movement of the energy of the nonbonding orbitals calculations on different levels of simplification were done. For these calculations α was chosen to be -0.2937 H (ionisation energy of a free ^3D platinum atom) and the off-diagonal elements were calculated with CUSSACH's formula (equation 5.25b). The overlap integral S_{ij} was calculated with equation 5.29. The bond length R_1 of the cluster was set to the experimental bulk value of 2.77 Å. R_2 is the length of the diagonal across the pyramid's base square. Equation 5.32 summarizes the integrals used for the calculations.

$$\begin{array}{lll} \alpha = -029375 \text{ H} & & \\ R_1 = 2.77 \text{ Å} & S_1 = 0.38452 & S_2 = 0.15719 \\ R_2 = 3.91737 \text{ Å} & \beta_1 = -0.18247 \text{ H} & \beta_2 = -0.08509 \text{ H} \end{array} \tag{5.32}$$

The first step of series was the pure Hückel calculation as shown in greater detail in section 5.3.

$$\begin{vmatrix} \alpha-\epsilon & \beta_1 & \beta_1 & \beta_1 & \beta_1 \\ \beta_1 & \alpha-\epsilon & \beta_1 & 0 & \beta_1 \\ \beta_1 & \beta_1 & \alpha-\epsilon & \beta_1 & 0 \\ \beta_1 & 0 & \beta_1 & \alpha-\epsilon & \beta_1 \\ \beta_1 & \beta_1 & 0 & \beta_1 & \alpha-\epsilon \end{vmatrix} = 0 \qquad \begin{array}{l} \epsilon_5 = +0.07120\ H \\ \epsilon_4 = -0.06820\ H \\ \epsilon_3 = -0.29375\ H \\ \epsilon_2 = -0.29375\ H \\ \epsilon_1 = -0.88425\ H \end{array} \tag{5.33}$$

The energy of the $1a_1$ orbital is too low and the nonbonding orbitals have the energy α. Next we take the interaction with the second next neighbour into account (section 5.6). The arrows indicate the change in the orbital energy relative to the pure Hückel calculation (equation 5.33).

$$\begin{vmatrix} \alpha-\epsilon & \beta_1 & \beta_1 & \beta_1 & \beta_1 \\ \beta_1 & \alpha-\epsilon & \beta_1 & \beta_2 & \beta_1 \\ \beta_1 & \beta_1 & \alpha-\epsilon & \beta_1 & \beta_2 \\ \beta_1 & \beta_2 & \beta_1 & \alpha-\epsilon & \beta_1 \\ \beta_1 & \beta_1 & \beta_2 & \beta_1 & \alpha-\epsilon \end{vmatrix} = 0 \qquad \begin{array}{ll} \epsilon_5 = -0.01389\ H & \downarrow \\ \epsilon_4 = -0.09003\ H & \downarrow \\ \epsilon_3 = -0.20866\ H & \uparrow \\ \epsilon_2 = -0.20866\ H & \uparrow \\ \epsilon_1 = -0.94751\ H & \downarrow \end{array} \tag{5.34}$$

All orbital energies are negative, even the antibonding b_2 orbital (-0.014 H). With the exception of the nonbonding orbitals energy increases the ionisation energy of the orbitals. The rise of the nonbonding orbital energies contradicts the results from the ECP-HF calculation.

The overlap integral S_1 (equation 5.32) is large and the movement of the nonbonding orbitals may be explained by the overlap of different 6s orbitals. This assumption was tested next (equation 5.35). Both a_1 and the b_2 orbitals are destabilized, while the nonbonding orbitals are not affected. Meanwhile, decreases the energy of the second a_1 orbital. The orbital energies agree generally much better with ECP-HF results.

$$\begin{vmatrix} \alpha-\epsilon & \beta_1-S_1\epsilon & \beta_1-S_1\epsilon & \beta_1-S_1\epsilon & \beta_1-S_1\epsilon \\ \beta_1-S_1\epsilon & \alpha-\epsilon & \beta_1-S_1\epsilon & 0 & \beta_1-S_1\epsilon \\ \beta_1-S_1\epsilon & \beta_1-S_1\epsilon & \alpha-\epsilon & \beta_1-S_1\epsilon & 0 \\ \beta_1-S_1\epsilon & 0 & \beta_1-S_1\epsilon & \alpha-\epsilon & \beta_1-S_1\epsilon \\ \beta_1-S_1\epsilon & \beta_1-S_1\epsilon & 0 & \beta_1-S_1\epsilon & \alpha-\epsilon \end{vmatrix} = 0 \qquad \begin{array}{ll} \epsilon_5 = +0.30828\ H & \uparrow \\ \epsilon_4 = -0.12998\ H & \downarrow \\ \epsilon_3 = -0.29375\ H & - \\ \epsilon_2 = -0.29375\ H & - \\ \epsilon_1 = -0.39399\ H & \uparrow \end{array} \tag{5.35}$$

Finally, we did a full EHT calculation on the pyramid (equation 5.36).

$$\begin{vmatrix} \alpha-\epsilon & \beta_1-S_1\epsilon & \beta_1-S_1\epsilon & \beta_1-S_1\epsilon & \beta_1-S_1\epsilon \\ \beta_1-S_1\epsilon & \alpha-\epsilon & \beta_1-S_1\epsilon & \beta_2-S_2\epsilon & \beta_1-S_1\epsilon \\ \beta_1-S_1\epsilon & \beta_1-S_1\epsilon & \alpha-\epsilon & \beta_1-S_1\epsilon & \beta_2-S_2\epsilon \\ \beta_1-S_1\epsilon & \beta_2-S_2\epsilon & \beta_1-S_1\epsilon & \alpha-\epsilon & \beta_1-S_1\epsilon \\ \beta_1-S_1\epsilon & \beta_1-S_1\epsilon & \beta_2-S_2\epsilon & \beta_1-S_1\epsilon & \alpha-\epsilon \end{vmatrix} = 0 \qquad \begin{array}{ll} \epsilon_5 = -0.03579\ H & \downarrow \\ \epsilon_4 = -0.15921\ H & \downarrow \\ \epsilon_3 = -0.24758\ H & \uparrow \\ \epsilon_2 = -0.24758\ H & \uparrow \\ \epsilon_1 = -0.40140\ H & \uparrow \end{array} \tag{5.36}$$

The results of the full EHT calculation agree well with ECP-HF calculations despite the model's simplicity. The nonbonding orbitals (-0.248 H) still have a higher energy then α and the energy of the 1a$_1$ orbital agrees well with the ECP-HF result. The rise of the energy of the degenerate orbitals is smaller than expected from equation 5.34. The interaction among the second next neighbours cause a steep in the orbital energies (equation 5.35), while pure orbital overlap has no influence. The inclusion of orbital overlap into the calculation partly compensates for the energy rise caused by the interaction with the second next neighbour. The same argument holds for the energy of the 1a$_1$ orbital. The orbital overlap overpowers the effect of the second next neighbour. The energy of the of the 2a$_1$ orbital (-0.036 H) is lowered by both interactions and is now in good agreement with the ECP-HF results (-0.194 H). Only the inclusion of both interactions, orbital overlap and interaction with the second next neighbour, into the calculations allows us a reliable description of all orbital energies and to explain the movement of the nonbonding a$_1$ orbitals. This model is still not able to explain the energy drop of the nonbonding orbitals observed in the ECP-HF calculations.

The results from equation 5.33 to 5.36 can be summarized as follows:

1. Pure Hückel calculations describe orbital symmetries and their energies relative to each other correctly. They also allow us to predict the groundstate's multiplicity correctly. The absolute energies agree only qualitatively with the ECP-HF results and the prediction of a 5d-6s interaction from these calculations is difficult.

2. The interaction with the second next neighbour stabilizes the cluster and can lift degeneracies. The inclusion of this interaction gives faulty values for the energy shift of the nonbonding orbitals.

3. The inclusion of orbital overlap in the pure Hückel calculation destabilizes most orbitals. The bonding orbital energies are now in the correct energy range. A comparison of the results from equation 5.34 and 5.35 shows, that orbital overlap is more important for the quality then the interaction with the second next neighbour.

4. Only the inclusion of orbital overlap **and** second next neighbour interaction (EHT) gives reliable results for both orbital energy and energy shift of the nonbonding orbitals, because the orbital overlap damps the influence of the second neighbour interaction. Only these calculations allow a trustworthy prediction of the 5d-6s interaction.

5. The orbital energies correlate directly with charge of the cluster and not with the wavefunctions multiplicity. The set of Hückel parameters extracted from Pt_2^0 should therefore be more reliable for calculations on neutral clusters.

5.8 Summary and Conclusions from the 6s Hückel calculations

1. The assumption of a perfect 77-electrons ECP for the platinum 6s electron allows us to investigate the influence of the 6s band on the stability of the metal cluster independently from 5d the other electrons. The Hückel molecular orbitals have the correct symmetry and the Hückel calculation predicts correctly the energetic order of the molecular orbitals in small platinum clusters.

2. The Hückel calculations predict correctly the multiplicity of the electronic groundstate and allow us so to construct a working surface model with a 18 valence electrons ECP at the central platinum atom.

   The 6s population of the surface model is of special interest, as EHT calculations showed that the 6s electron density at the surface of the cluster is lower than in the bulk [285]. A similar electron distribution has been observed in nickel clusters [302], which suggests that the reduction of the s electron density at the surface is a general property of transition metal clusters of this group having a strong influence on the adsorption process.

3. The Hückel calculations for Pt_3 suggest, that a suitable Pt_3 surface model should be built from two ^3D and one ^1S platinum. Both triangles should threrefore be described with singlet wave function, in which the totally symmetric 6s orbital is doubly occupied.

4. (a) The Pt_5 pyramid should be built from a ^1S platinum atom at the top and 4 ^3D atoms at the basis. The electronic groundstate would have a triplet wave function. Such construction creates a negative charge at the top, which simulate the electron spill correctly. The charge distribution and the orbital energies vary only slightly on any differences in the valence ionisation energies or resonance energies caused by the mixture of two different ECPs. The combination of five ^3D atoms would result in a quartet function. In such a cluster would be average 6s population too high and the cluster would not be suitable simulate a surface correctly.

   (b) The triplet 6s wavefunction (4 ^3D and 1 ^1S) allows the rotation of the water molecule, whereas the singlet wave function does not allow the rotation.

   (c) The Hückel calculations give a first estimate on the influence of the mixing of different ECPs in one platinum cluster. Small differences in α and β do not change the electronic structure of the Pt_5 pyramid.

5. The Pt_9 surface model should be build from a ^1S platinum in the centre and 8 ^3D atoms. Such a structure would carry a negative charge at the central platinum atom and would have a singlet wavefunction in the groundstate. Since open shell calculations are handled by UHF calculations should the computational effort for $^3Pt_5$ and $^1Pt_9$ of similar size.

6. A Pt_{17} structure should also have a singlet groundstate with a negative charge in the centre. The average 6s population is 0.914 and the water molecule should bond less tight since the 6s platinum electrons and the oxygen atom from the water molecule repel each other. The nonbonding orbitals of the cluster belong to different symmetry species. The degeneracy of those orbitals may be broken by the interaction with the second next neighbour. This

procedure might lead to a change of the groundstate's multiplicity. A Pt_{17} cluster as surface model is therefore not suitable as a surface model.

7. Two pathways for inner cluster charge transfer have been identified:

   (a) The partly filled 6s molecular orbitals have orbital energies lower or equal to the 5d orbitals energies. The 6s orbitals are filled instead of the 5d functions resulting in a charge transfer from the top to the base.

   (b) 6s molecular orbitals have their energy in the range of the 5d orbitals. The 5d orbitals overlap with those orbitals providing correct symmetry. This overlap leads to an electron flow away from the central atom. The strength of this flow depends on the difference in the orbital energies.

   Both pathways become more important as 6p orbitals are included into the calculation, because they are empty and facilitate so the charge transfer.

8. The calculations on the pyramidal Pt_5 system predicted correctly the charge distribution in the cluster. The interaction between water and the metal structure depends heavily on the charge of the central atom. The Hückel calculations allow us therefore to select a surface model, which simulates the electron spill off the metal surface correctly. The comparison with the ECP-HF calculations for Pt showed, that the orthogonality approximation $\mathrm{S_{ij}} = \delta_{\mathrm{ij}}$ yields too high charges and too large dipole moments.

9. The interaction with the second next neighbour lifts the degeneracy of the nonbonding orbitals in large clusters. Closed structures will not be affected strongly by this interaction, while the total energy of open structures changes strongly with this interaction. The calculation showed also that with increasing cluster size the interaction with the other neighbours becomes more important. A suitable surface model should therefore be small and have closed structure to keep the error caused by the second next neighbour interaction at a minimum. The comparison with the ECP-HF calculations on Pt_5 showed, that the simple Hückel model cannot predict correctly the energy shift of the nonbonding orbitals.

10. Hückel parameters extracted from ECP-HF calculations give reasonable number for the orbitals energies, but the precession is too poor to allow precise predictions on the interaction with other orbitals. They show, that any 6s molecular orbital with an energy less then 0.71 β gets into the energy range of the platinum 5d orbitals.

11. Numerically reliable predictions are possible EHT calculations. The valence ionisation energy is the same as the ionisation energy of the free atom. The off-diagonal element of the Hückel matrix can be calculated with CUSSACH's formula and the value of the overlap integral can be calculated correctly with a simple gaussian function. Those EHT calculations gave reasonable orbitals energies.

Chapter 6

Platinum atom calculations involving 18 Valence Electrons

This section summarizes the results obtained with the 18 valence electrons ECP from HAY and WADT [189, 214, 215] for the interaction of a platinum cluster with a single water molecule. HAY and WADT recommend the usage of this ECP for calculations on molecules with direct metal-metal bonds. Despite their recommendation[1] the 10 valence electron ECP has been used for calculations on platinum clusters [189, 303]. The first section of this chapter includes a comparison of both effective core potentials.

Each part of this section concentrates on a specific platinum cluster. The first subsection analyses the cluster itself while the second focuses on the platinum water interaction. In addition to the bonding energy we analyse the energy required to reorientate the hydrogen atoms of the water molecule. This energy is important for the structure of the water bilayer, which forms the basis of the platinum-water interface. The last section compares of platinum clusters of different sizes.

To understand the importance of the platinum 6s orbital for chemical bonding forward reference to the one electron ECP calculations in chapter 7 may to be necessary. In some sections, especially those on Pt_5 and Pt_9, references on Hückel calculations are made (chapter 5, page 117). A comparison of the results for both clusters Pt_5 (section 6.4) and Pt_9 (section 6.5) shows the mechanism, which controls the orientation of the water molecule's bonding plane.

The final section contains a brief summary of EHT calculations (YaEHMOP [304]). This package contains all parameters necessary for those calculations. During the *ab initio* calculations numerous quantum chemical difficulties occured, which have not been mentioned previously in the literature [64, 65, 303]. Extended Hückel calculations were therefore done to check, whether these difficulties are caused solely by problems with the higher level theory or can be observed even at very low levels of theory.

---

[1] HESS [305] also recomends generally the exclusion of the 5s and 5p subshell from the effective core.

6.1 One platinum atom

The examination of the water platinum interaction begins with the smallest possible platinum cluster - a single platinum atom. Despite its small size, such a system already exhibits most features of the problem.

Two pseudopotentials from Hay and Wadt for platinum (Z=78) are frequently used in the literature [189, 214, 215]. The first, abbreviated as LanL1[2], uses the 5d, 6s, 6p orbitals as valence space while the second, abbreviated as LanL2, uses the 5s, 5p, 5d, 6s, 6p orbitals. The first potential (LanL1) replaces 68 core electrons and the second (LanL2) 60 electrons. Table 6.1 summarizes the ECPs used in this section:

	core elec.	valence elec.	valence space	basis set
LanL1MB	68	10	5d 6s 6p	single zeta
LanL1DZ	68	10	5d 6s 6p	double zeta
LanL2MB	60	18	5s 5p 5d 6s 6p	single zeta
LanL2DZ	60	18	5s 5p 5d 6s 6p	double zeta

Table 6.1: ECPs used in chapter 6

A single platinum atom described with the LanL1 potential contains 10 electrons, as does a single water molecule. A water trimer at the MP3 level of calculation already reaches the limits of the available computing resources as shown in section 3.4 (page 74) Two possibilities exist to reduce the size of a single job:

1. a reduction of the correlation level (MP2) or no correlation at all (HF).
2. the usage of a pseudopontial with the fewer electrons like the LanL1 potential despite the recomendation of Hay and Wadt.

The next two sections concentrate on those questions. All calculations involved a double zeta basis set provided with the quantum chemical program [222] in order to to have basis sets of similar quality both on the platinum cluster and on the water molecules.

6.1.1 The electronic states of platinum

First experiments with different programs on different machines yielded inconsistent results. Table 6.2 lists some results for a single platinum atom with different programs using LanL1 and a double zeta quality basis set.

Obviously GAMESS US is not suitable for the problem as the energies for ^{3}D state differ very much from the value published by Hay and Wadt. More disturbing is the fact, that the energy of the ^{3}D state calculated with GAMESS US is higher than the energy of the ^{1}S state, which contradicts experiment.

The energy eigenvalues for the ^{1}S state are nearly the same for all programs while the values for the ^{3}D state differ considerably. This behaviour suggests that the main problem is not the pseudo potential, but the method used for the calculation of open shell wavefunctions. The energies calculated with Gaussian 94 and a basis set limited to 5 d- and 7 f-type orbitals are close to the

---

[2] To avoid a new abbreviation we use here the keyword used by Gaussian 94 to specify a specific ECP.

	^{1}S (5d^{10} 6s^0)	^{3}D (5d9 6s1)	
	RHF	ROHF	UHF
GAMESS UK	-26.19995	—	-26.23896
GAMESS US	-26.19995	-26.11322	-26.11809
Gaussian 94 / 5d 7f	-26.19995	-26.23815	-26.23821
Gaussian 94 / 6d 10f	-26.19995	-26.23889	-26.21367
Lit [214]	—	-26.23774	

Table 6.2: Energies in Hartree from different quantum chemistry codes for platinum with the LanL1 ECP

value published by Hay and Wadt. The UHF wavefunction calculated with a 6d/10f basis set (cartesian orbitals) again does not match the literature value, while the ROHF value does. The UHF result from GAMESS UK (also cartesian orbitals) again matches the literature value. Sadly GAMESS UK does not allow ROHF calculations for atoms with high multiplicities. This limit prohibited an investigation of the influence of pseudo orbitals on open shell calculations.

According to table 6.2 Gaussian 94 with 5d/7f basis provides the best choice to tackle the problem. The energies of the ^{3}D state lie lower than the literature value, because Hay and Wadt used a single zeta quality basis set and Gaussian 94 a double zeta quality.

Figure 6.1 displays the energies of some electronic states compared with the ground state, calculated with the LanL1 and the LanL2 potential. The triplet states have been calculated independently with the UHF method (solid lines) and the ROHF method (dashed lines). The ^{3}D state was found in both cases to be the ground state. Since the ground state energies do not differ much (table 6.2) only the ^{3}F state (5d^8 6s^2, high spin) moves on the energy scale. The difference in the excitation energies (^{3}D → ^{3}F) between UHF and ROHF calculations is bigger for the LanL2 ECP than for LanL1 one and changes the relative order of the different states.

Figure 6.1 shows two principal features of the ECP's published by Hay and Wadt:

1. The ^{1}S and the ^{3}F states change their relative positions on the energy scale on the introduction of correlation effects (LanL1 ECP). Hay and Wadt [189] pointed out in their original work, that the LanL1 potential is particularly ill-suited for correlation calculations.

2. The ROHF calculations reproduce correctly the relative order of the different states, while the UHF calculation exchanges the ^{1}S and the ^{3}F states.

The experimental (^{3}D → ^{1}S) excitation energy is well reproduced by the LanL2-MP2 calculations. As shown later the strength of the platinum-platinum bond increases with the occupation of the 6s orbital, while simultaneously the water-platinum interaction becomes weaker. The correct reproduction of the ^{3}D → ^{1}S excitation energy is therefore necessary for a reliable prediction of relative water-platinum interaction energies from quantum chemical calculations for different electronic states.

Another series of problems arises from the small ^{3}D → ^{3}F excitation energies (LanL2-MP2). Since both states are energetically close to each other, the HF-calculations can converge to either of these states during a scan of the potential energy surface and so cause unphysical behaviour. This problem becomes more important with the growth of the metal cluster as the number of electronic states increases rapidly and the different electronic states become more densely packed. The ^{1}S →

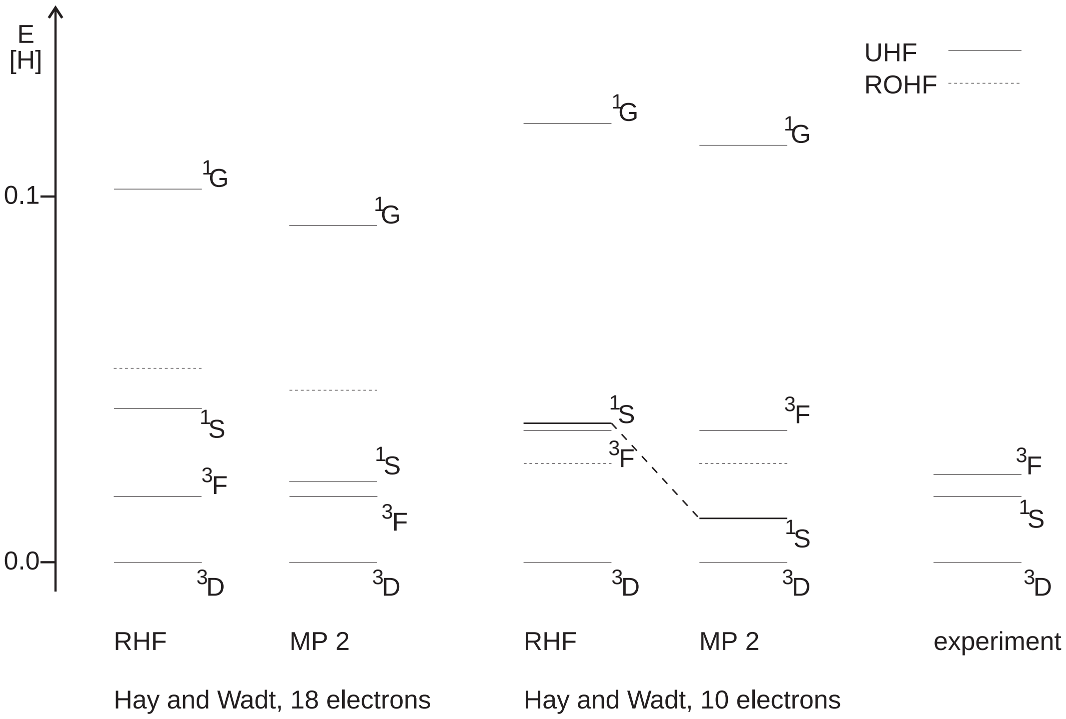

Figure 6.1: Electronic states of a platinum atom exp. values [306a]

^{1}G ($5d^8$ $6s^2$, low spin) activation energy is larger than the triplet activation energy and a scan of the potential energy surface should therefore be easier in the singlet than in the triplet state.

Hay and Wadt reported for the LanL1 potential [214], that the ^{3}F state has a lower excitation energy than the ^{1}S state both for relativistic ECP calculations (RECP) and for relativistic Hartree Fock calculations (RRHF). It is therefore not possible to reproduce the correct order of exciations energies with the HW potentials. Topiol and Basch [307] showed, that the relative order of the energies of electronic states depends strongly of the quality of the ECP's relativistic part and that the important part is the $^3\mathrm{D} \rightarrow {}^1\mathrm{S}$ excitation energy, which is negative for non-relativistic calculations. Other papers [308, 309] also showed that J-averaged calculations at either Hartree-Fock or ECP level reproduce the wrong ordering of electronic states ($^3\mathrm{D} < {}^3\mathrm{F} < {}^1\mathrm{S}$). In regard to this problem LanL2-UMP2 calculations should perform correctly despite the wrong order of states compared with ROMP2 calculations, since the excitation energies are well reproduced.

6.1.2 Platinum and a single water molecule

Table 6.3 summarizes the results of the geometry optimization of a single platinum atom (LanL2DZ) interacting with a rigid water molecule.

The ^{1}A' wavefunction could be regarded as the combination of a ^{1}S platinum atom and a $^1A_1$ water molecule while the ^{3}A' could be obtained by the combination of a ^{3}D platinum atom with a ground state water molecule. Interesting is the comparison of the Hartree Fock calculations of the triplet states. The results of the ROHF and the UHF calculations are nearly equal. The stationary point found by the optimisation algorithm in both cases is a true minimum, as a check of the second derivatives showed. The association curves calculated with a set of single point calculations showed different behaviour. The UHF curve has its minimum at the same position as the optimised result,

		pt_h2o_01	pt_h2o_01t	pt_h2o_01u	pt_h2o_02	pt_h2o_02u
method		RHF	ROHF	UHF	RHF-MP2	UHF-MP2
state		^{1}A'	^{3}A'	^{3}A'	^{1}A'	^{3}A'
r	[Å]	2.1829	2.7140	2.6948	2.0986	2.4952
γ	[deg]	125.66	134.16	133.93	116.43	123.20
q_{Pt}	[e]	−0.097	−0.050	−0.052	−0.162	−0.103
q_O	[e]	−0.675	−0.672	−0.671	−0.602	−0.612
q_H	[e]	+0.386	+0.361	+0.362	+0.382	+0.358
Δq	[e]	−0.097	−0.050	−0.052	−0.162	−0.103
μ	[D]	2.8850	3.6731	3.7302	2.9224	3.8221
ΔE_S	[kcal/mol]	−7.606	−29.022	−29.315	−22.561	−21.312
ΔE_T	[kcal/mol]	+18.702	−2.714	−2.782	−9.136	−7.904
- E	[H]	194.242865	194.276994	194.277461	194.539696	194.537707
spin density$_{Pt}$		0.0	1.9932	1.9913	0.0	1.9726

ΔE_S: $^1Pt + H_2O \rightarrow Pt-H_2O$ ΔE_T: $^3Pt + H_2O \rightarrow Pt-H_2O$ Δq: charge transfer

Table 6.3: platinum water adduct - equilibrium geometries

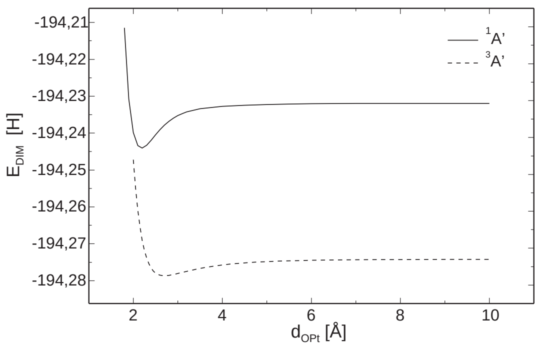

Figure 6.2: HF results for Pt−H$_2$O.

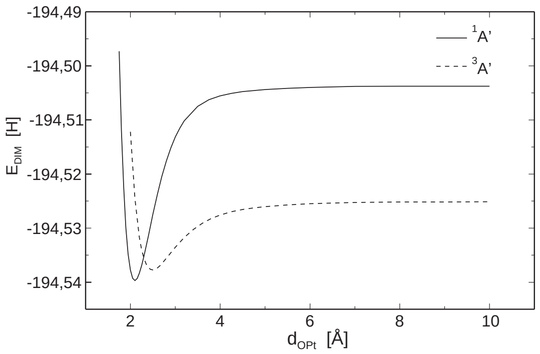

Figure 6.3: HF results for Pt−H$_2$O.

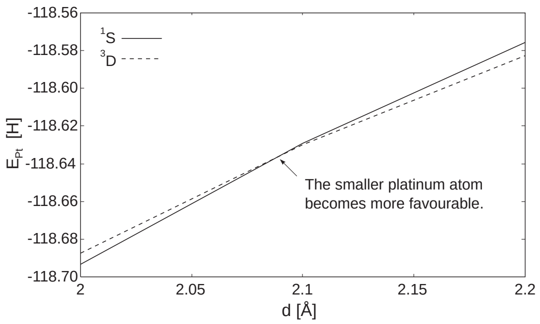

Figure 6.4: Platinum states close to negative charge.

while the ROHF-curve on the other hand does not show a minimum at all. An analysis of the results showed that this and other convergence problems are caused by a problem with ROMP2 calculations within Gaussian 94. Better results were obtained from UHF wavefunctions.

The energy difference between the two curves in figure 6.2 and 6.3 is the same as the difference between the platinum ^{3}D and ^{1}S states. As the MP2 level favours the ^{1}S in comparison with the ^{3}D state (figure 6.3) the curves become closer together as the correlation level increases from HF to MP2. The correlation calculation allows the electrons to avoid each other and the distance between the platinum atom and the water molecule d_{OPt}becomes shorter and so the binding energy increases. The driving force is the platinum atom. Figure 6.4 displays the total energy of the platinum ^{1}S and the ^{3}D state on the approach of of a negative charge of -0.6 e. The value of -0.6 e is roughly the charge on the oxygen atom in a water molecule (table 3.1, page 46). For small values of d the smaller platinum atom becomes more favourable, as the 6s orbitals are more extended than those of the 5d. The crossing point[3] of those two curves (2.0787 Å, -118.641723 H) corresponds closely to that of the two association curves ($r = 2.2954$ Å, $\gamma = 119.811°$, -194.535248 H). The crossing of the curves in figure 6.3 can therefore be explained by a polarisation of the metal atom as the water molecule approaches the platinum atom [12, 310].

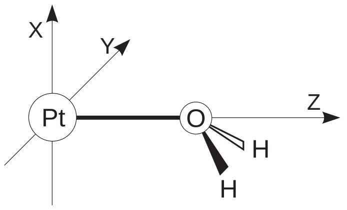

Figure 6.6: Pt$-$H$_2$O geometry.

Figure 6.5 displays the formation of the Pt$-$H$_2$O adduct and figure 6.6 the complex in the chosen system of coordinates. On the left side of figure 6.5 are the orbitals of platinum (^{3}D) and on the right side are the orbitals of a water molecule ($^1A_1$). In the centre of the figure are the orbitals of platinum (^{1}S) with a nearby negative charge, which breaks the sperical symmetry, and the orbitals of the adduct.

With a negative charge at a distance of 6 Å the platinum d-orbitals split according to a first estimate with ligand field theory [293a]. The $d_{x^2-y^2}$ and the d_{xy} orbitals have the lowest energy, the d_{xz} and the d_{yz} orbital are in the middle of the energy scale and the d_{z^2} has the highest energy. As the negative charge gets closer to the atom, a hybrid orbital between the 6s-, 6p_z- and the 5d_{z^2} orbital is formed. This orbital (ψ_1) is still dominated by 5d_{z^2}. The energies of those orbitals are displayed in figure 6.5.

A first molecular orbital attempt to describe the interaction between water and platinum would be the interaction of the 5d_{z^2} orbital with one of the water molecule's free electron pairs. According to the VSEPR model [10–12, 311], the free electron pairs of the water molecule could be obtained by a linear combination of the 1b_1 (ψ_2) and the 3a_1 (ψ_3) orbitals of the water molecule. Such a combination of those two orbitals is possible, because both orbitals transform according to a' in the adduct. The combination $\psi_{EP1} = \psi_2 + \psi_3$ forms an orbital which describes the first free electron pair and points directly to the platinum atom, whereas the second combination $\psi_{EP2} = \psi_2 - \psi_3$ represents the second free electron pair, which points away from the platinum atom.

Such a simple model would result in three molecular orbitals. The first MO $\Psi_1 = \psi_1 + \psi_{EP1} = c_1\,\psi_1 + c_2\,\psi_2 + c_3\,\psi_3$ describes the bonding interaction between water and the metal; the second orbital $\Psi_2 = \psi_1 - \psi_{EP1} = c_1\,\psi_1 - c_2\,\psi_2 - c_3\,\psi_3$ is the antibonding combination and the third

---

[3] The crossing points were found with a small C program using the intersection algorithm [242] and Gaussian 94 as a subroutine called with the `system`-function. The corresponding input files were written by the program before the function call.

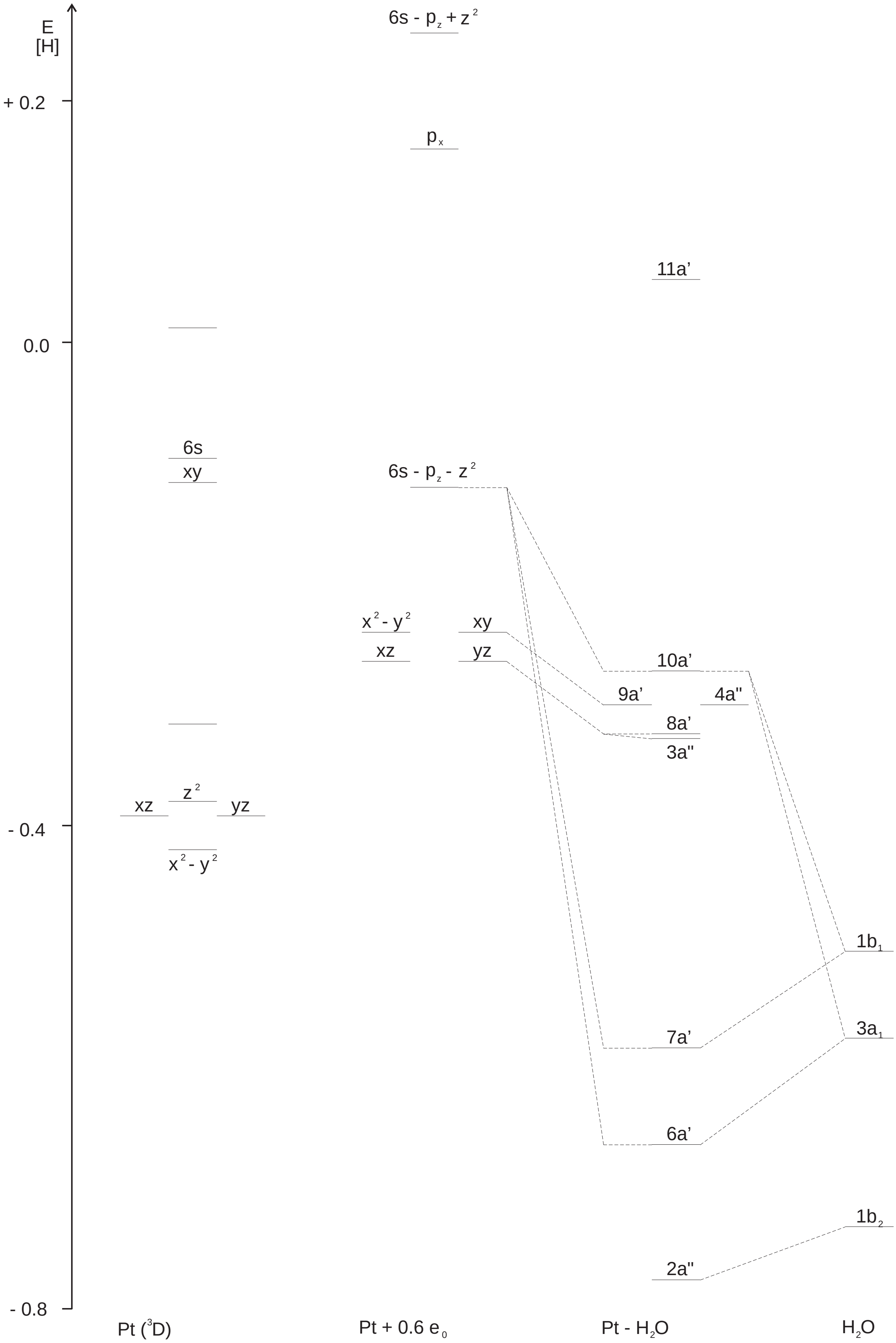

Figure 6.5: Formation of $Pt-H_2O$.

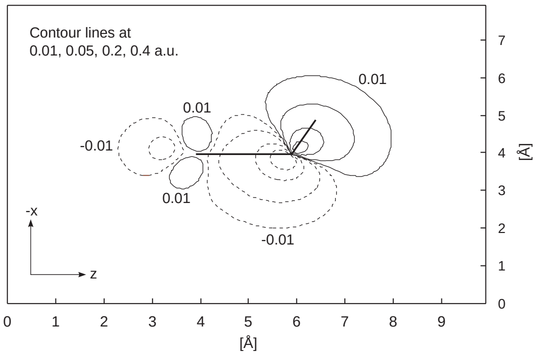

Figure 6.7: 6a' orbital of Pt$-$H$_2$O.

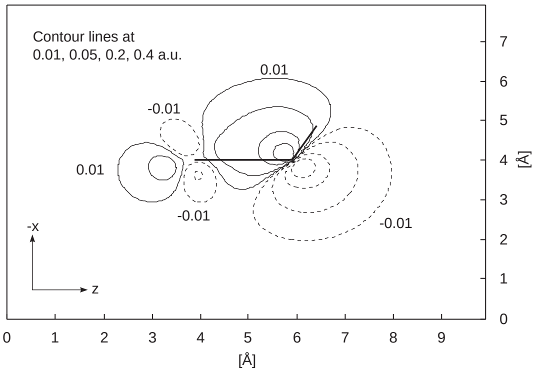

Figure 6.8: 7a' orbital of Pt$-$H$_2$O.

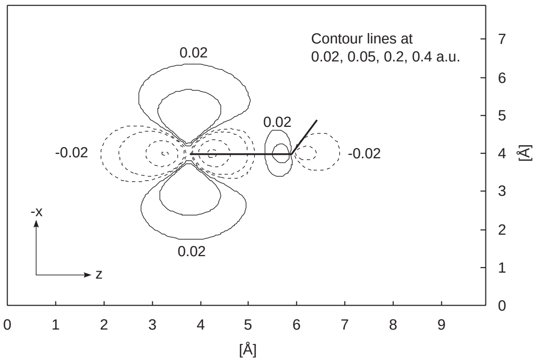

Figure 6.9: 10a' orbital of Pt$-$H$_2$O.

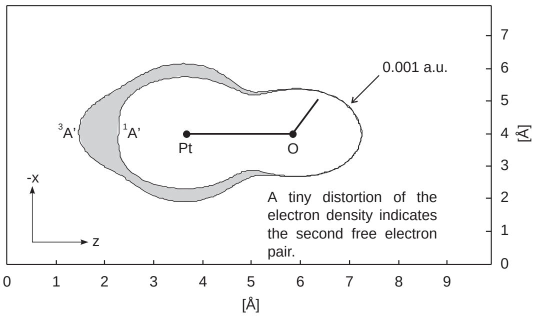

Figure 6.10: Movement of the total electron density.

orbital $\Psi_3 = \psi_{\mathrm{EP2}} = c_2\ \psi_2 - c_3\ \psi_3$ is the nonbonding free electron pair. Figures 6.7 to 6.9 display the three central orbitals of the water-platinum bond. Only the second orbital, the antibonding combination of the platinum $5d_{z^2}$ orbital with free electron pair, can be found in figure 6.9. The remaining two orbitals Ψ_1 and Ψ_3 cannot be found among the Hartree-Fock orbitals.

Orbital 6a' shown in figure 6.7 is the bonding combination of ψ_1 and ψ_3 whereas orbital 7a' (figure 6.8) is the combination of ψ_1 and ψ_2. The orbitals ψ_2 and ψ_3 of the water molecule do not mix. Hence, a bonding interaction between the platinum $5d_{z^2}$ orbital and a free electron pair from the water molecule cannot be found among the Hartree-Fock orbitals. Instead the $3a_1$ and $1b_1$ orbitals on water interact directly with the metal.

Figures 6.7 and 6.8 show, that ψ_1 is slightly tilted from the z-axis to enhance the overlap of the water and platinum orbitals. This tilt is caused by a small admixture of the $5d_{xz}$ orbital to ψ_1. The small contribution turns the $6sp-5d_{z^2}$ hybrid orbital into the right direction for a maximum overlap. The contribution of the $5d_{xz}$ controls the bonding angle γ between the PtO bond and the plane of the water molecule. The remains of the $5d_{xz}$ orbitals form the 8a' orbital of the adduct. This mechanism also braks the degeneracy of the d_{xz} and the d_{yz} orbitals (3a").

The platinum 6s orbital has the same symmetry as Ψ_2. Both transform according to a' in the adduct and interaction is likely. A similar interaction has already been observed for the free platinum atom and the platinum atom near a negative charge. The orbitals 10a' and 11a' are created in this way. They differ mainly through the 6s contribution to Ψ_1. Orbital 10a' resembles a $5d_{z^2}$ orbital while 11a' resembles the 6s orbital. While the orbitals 6a' and 7a' are located at the water molecule the orbitals 10a' and 11a' are located at the platinum atom. An analysis of the spin density of the $^3A'$ state, in which the orbitals 10a' and 11a' are singly occupied, indicates, that both electrons are located at the platinum atom.

The bond between platinum and water formed via the interaction of two doubly occupied orbitals is similar to the hydrogen bond in the water dimer, but the charge transfer is up to 10 times stronger in $Pt-H_2O$ (table 3.8 (page 53) for properties of the water dimer). The charge transfer is supported by the partial occupation of the formerly unoccupied 6s orbital with the extra charge from the water molecule. This movement of electrons from an occupied orbital into an empty one is an example of polarisation (subsection 2.5, figure 2.3, page 28). The strength of the bond between platinum and water is therefore controlled by the polarisation of the platinum atom by the water molecule.

A suitable description for the $Pt-H_2O$ complex would therefore be an inner orbital complex [1a, 28a]. The interaction with the water molecule causes the promotion of an inner 5d electron into an outer 6s orbital. The free 5d orbital is then used for the construction of the bond between the platinum atom and the free electron pair from the water molecule. In VB terms this interaction has to be described more as a covalent bond than an ionic one.

At the first view the $^3A'$ state should be more stable than the $^1A'$ state, since it is built from ground state components and the platinum atom already has a 5d vacancy. But the 11a' orbital is strongly antibonding and the occupation of this orbital weakens the platinum-water bond. Figure 6.10 shows the electron densities of the $^1A'$ and the $^3A'$ state at the crossing point of the association curves. Solid lines mark the total electron density of 0.001 a.u., while the grey shaded area highlights the difference between both states. The antibonding character of the 11a' orbitals can be deduced from the shape of these curves. Electron density is moved away from the centre of the platinum atom to the outer regions of the atom. This electron shift increases as the electrostatic repulsion between the platinum and the negatively charged oxygen atom. At the crossing point electron movement costs no energy and so facilitates a change of electronic state.

The antibonding character of orbital 11a' can also be deduced from the Mulliken population analysis [288–291]. In the $^1A'$ state, with an optimized geometry, the overlap population (MOP) between platinum and oxygen has a value of 0.036 while the MOP between platinum and hydrogen is -0.013. The interaction between platinum and hydrogen is antibonding despite the opposite charges. The excitation (UHF calculation) of a single electron at this geometry reduces both the interactions between platinum and oxygen ($MOP_{PtO} = -0.033$) and platinum and hydrogen ($MOP_{PtH} = -0.010$). After relaxation (elongation of the platinum-oxygen bond, widening of the bond angle γ, table 6.4) the interaction between oxygen and platinum is weakly bonding ($MOP_{PtO} = 0.005$), whereas the interaction between hydrogen and platinum ($MOP_{PtH} = -0.003$) is weakly antibonding. The elongation of the platinum-oxygen bond reduces the repulsion between the platinum 6s electrons and the valence electrons of oxygen. Simultaneously the bond angle γ increases and so enhances the overlap of the $5d_{z^2}$ orbital and the $3a_1$ orbital.

The character of the 6s orbital can be described as double-edged. It is necessary to accept the extra charge from the water molecule during the formation of the bond, so acting as a polarisation function. If the 6s orbital is too strongly occupied, the extension of the electron space (figure 6.10) repels the water molecule and the bond becomes weaker. A similar correlation between the occupation of the 6s orbital and the binding energy has been observed in $Pt-CO$ [312].

The water molecule has the possibility to waggle. Table 6.4 compiles the geometries and energies

	w1t_0	w1t_0d	w1s_0	w1t_180	w1s_180
method	UHF-MP2	UHF-MP2	RHF-MP2	UHF-MP2	RHF-MP2
state	$^3B_1$	$^3A_1$	$^1A_1$	$^3A_1$	$^1A_1$
r [Å]	3.6093	3.5934	3.1523	2.4952	2.0954
γ [deg]	0.0	0.0	0.0	180.0	180.0
q_{Pt} [e]	−0.023	−0.020	−0.046	−0.075	−0.111
q_O [e]	−0.653	−0.656	−0.636	−0.639	−0.652
q_H [e]	+0.338	+0.338	+0.341	+0.357	+0.382
Δq [e]	−0.023	−0.020	−0.046	−0.075	−0.111
μ [D]	2.3463	2.3911	2.0889	4.4830	3.6750
ΔE_T [kcal/mol]	−1.060	−1.613	+11.082	−6.871	−5.519
−E [H]	194.526799	194.527682	194.507450	194.536060	194.533906
spin density$_{Pt}$	2.0000	1.9986	0.0	1.9803	0.0

Table 6.4: Platinum water adduct - extrema of a systematic change of γ.

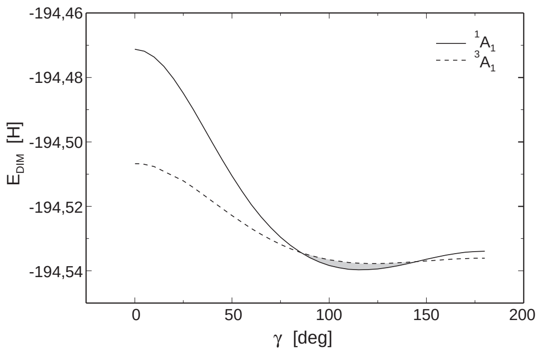

Figure 6.11: Water waggle movement.

of the extrema of such movement and figure 6.11 shows the energy of the complex as a function of γ. The platinum oxygen distances r were kept to their equilibrium values (^3A : 2.6948 Å, ^1A : 2.4952 Å).

The curves have exactly the shape one expects for the interaction of platinum and water via a free electron pair, but both curves intersect. A comparison of table 6.2 and 6.11 shows, that at the turning points (0°, 180°) the triplet states are more favourable than the singlet states. Even with an optimized platinum oxygen distance the difference is very large. For $\gamma = 0°$ the singlet state with an interaction energy of +11.1 kcal/mol is extremely unfavourable, while the triplet state ($^3A_1$) with −1.61 kcal/mol is still bonding. The singlet state is actually favoured only in a small area ($r \leq 2.3$ Å, $80° \leq \gamma \leq 145°$, grey shaded in figure 6.11). It is a typical problem with such a calculation, namely that the relative energies of the electronic states change as the geometry changes. Gavezzotti et al. observed a similar behaviour of Pt_n-CO cluster [303].

6.1.3 The Influence of the Pseudo Potential

Table 6.5 shows the results for $Pt-H_2O$ obtained with different ECPs. The importance of the platinum 5d orbitals for the metal-water bond is obvious from a comparison of the results for a preliminary 1-electron ECP (subsection 7.3.1, page 230) with results obtained with the LanLx-

		LanL1		LanL2		1 e^- ECP$^{(a)}$
		RHF	MP2	RHF	MP2	UHF
r	[Å]	2.4574	2.2686	2.1829	2.0986	3.8498
γ	[deg]	124.43	108.19	125.66	116.43	180.0
q_{Pt}	[e]	−0.069	−0.165	−0.097	−0.162	−0.010
q_O	[e]	−0.660	−0.578	−0.675	−0.602	−0.678
q_H	[e]	+0.365	+0.375	+0.386	+0.382	+0.344
Δq	[e]	0.069	0.165	0.097	0.162	0.010
μ	[D]	2.8150	2.6533	2.8850	2.9224	2.7302
$\Delta E_S^{(b)}$	[kcal/mol]	−4.935	−16.358	−7.606	−22.561	—
$\Delta E_T^{(c)}$	[kcal/mol]	+19.500	−6.494	+18.702	−9.136	−0.395

(a) Please refer to subsection 7.3.1 (page 230) for details.

(b) $^1Pt + H_2O \rightarrow {}^1Pt{-}H_2O$ (c) $^3Pt + H_2O \rightarrow {}^1Pt{-}H_2O$

Table 6.5: Comparison of different ECPs.

potentials. During the optimisation the hydrogen atoms turn away from the platinum atom, so that the interaction between water and platinum occur solely via the $3a_1$-orbital. The equilibrium distance r_{PtO} (3.85 Å) is far too long to speak of a chemical bond and the interaction energy of 0.4 kcal/mol is only a small fraction of the value observed with the other ECPs.

All LanL1 bond lengths are longer than those calculated with the LanL2 potential and the binding energies calculated with LanL1 potential are always smaller than the energies calculated with the LanL2 potential. The same reasoning shows, that the repulsion (ΔE_T) at Hartree-Fock level is larger for the LanL1 potential than for LanL2. ROHLFING et al. [306] observed a similar effect for the interaction between platinum and a hydrogen atom. At Hartree-Fock level the charge transfer calculated with the LanL1 potential (0.069 e) is smaller than that calculated with the LanL2 potential (0.097 e). At MP2 level the charge transfer for both potentials is of similar size (0.16 e). As shown in subsection 6.1.2 correlation calculations are very important for the correct description of the platinum-water interaction. In both cases LanL1 and LanL2 the PtO bond shrinks in calculations at MP2 level. The influence of correlation on the LanL2 bond is smaller (−3.9%) than for the LanL1 bond (−7.7%). This result agrees with the conclusions drawn from the contributions of the correlation energy to the total binding energies at MP2 level (LanL1: 69.7%, LanL2: 66.2%), although the absolute value of the correlation energy for LanL2 calculations (14.9 kcal/mol) is larger than that for LanL1 (11.4 kcal/mol). The MP2 results for the LanL2 potential should be more reliable as the correlation space is larger and the 5s and 5p orbitals include parts of the core-valence correlation. Despite the larger correlation space, the coefficient of the Hartree-Fock function remains 0.9738. This value is close to coefficients found at Hartree-Fock level for the water dimer (section 3.1, table 3.6, page 50). The MP2 method should therefore include most of the correlation effects in the platinum-water bond.

The influence of electron correlation is larger on the ^1S state than on the ^3D state, since the electrons are more closely packed. The total energy of ^1Pt and H_2O moves further on the energy scale than that of ^3Pt and H_2O. This larger movement in energy of ^1Pt and H_2O compensates partly for the correlation energy of the adduct (LanL2: ΔE_S^{corr} = 14.95 kcal/mol < 27.84 kcal/mol = ΔE_T^{corr}). Since correlation calculations behave differently on reactants and products, the introduction of correlation methods has a pronounced effect on the potential energy surface.

		uncorrected	corrected
r	[Å]	2.0986	2.1360
γ	[deg]	116.43	119.90
ΔE_S	[kcal/mol]	22.561	16.855

Table 6.6: BSSE in $^1Pt-H_2O$ at MP2 level.

r_0	2.13597	Å
γ_0	119.902	deg
E_0	−16.8546	kcal/mol
D_2	90.0426	kcal/mol/Å^2
D_3	−158.790	kcal/mol/Å^3
A_2	0.00253	kcal/mol/deg^2
A_3	−0.00002	kcal/mol/deg^3
K_1	0.116338	kcal/mol/Å/deg

Table 6.7: Parameters for V_{BSSE}

6.1.4 Effect of the BSSE on the platinum-water interaction

The same method as for the calculation for the BSSE on the water dimer (subsection 3.2.4, page 70) was used to estimate the effect of BSSE on the water-platinum interaction. The platinum atom was described with the LanL2 ECP and a double zeta basis set (G94 keyword: `LanL2DZ`). The double zeta basis set was chosen to have two basis sets of similar quality, so as to minimize that part of BSSE caused by different sizes of basis.

Table 6.6 summarizes the results from the last step of the BSSE corrected geometry optimisation (60 points, energy maximum −16.0 kcal/mol). Using the BSSE corrected geometry (table 6.6) in a quantum chemical calculation at MP2 level with a FCP BSSE correction according to Boys and Bernardi yielded an interaction energy of −16.855 kcal/mol. The precise difference between force field prediction and quantum chemical calculation is about 0.0001 kcal/mol.

During the geometry optimisation the BSSE decreased from an initial value of 5.877 kcal/mol down to 5.522 kcal/mol (25% of the interaction energy). The BSSE is therefore in the range of the binding energy in a water dimer and about five times larger than that observed in the water dimer.

$$V_{\mathrm{BSSE}}(r,\gamma) = E_0 + D_2\,(r-r_0)^2 + A_2\,(\gamma-\gamma_0)^2 + K_1\,(r-r_0)\,(\gamma-\gamma_0) + D_3\,(r-r_0)^3 + A_3\,(\gamma-\gamma_0)^3 \quad (6.1)$$

Table 6.7 displays the parameters of the potential $V_{BSSE}(r,\gamma)$. These are only valid in a small range 2.10 Å $\leq$r $\leq$ 2.24 Å and 106.43° $\leq \gamma \leq$ 126.43°. Due to this small area of definition the anharmonic part of the bond length force field is always smaller than the harmonic part. The figures show that ***the bond length is much more important for the energy than the bond angle, which has only a small influence on the bond energy.***

Since the coupling constant K_1 has a positive value (0.11 kcal/mol/Å/deg), an extension of the bond length produces a reduction in bond angle to keep the binding energy as low as possible. This rotation can be explained by the molecular orbital mechanism outlined in subsection 6.1.2. As the bond length increases the water $3a_1$ orbital turns towards the platinum atom. The nonbonding lobe of the $3a_1$ orbital stretches slightly further than the lobes of the nonbonding oxygen p-orbital. This movement stabilizes the 6a' orbital of the adduct. In the other case, the reduction in bond length, the 7a' orbital becomes more stable and compensates for the compression of the molecule.

A similar BSSE effect was observed in quantum chemical calculations on the ^{3}A' state of the adduct. The effect of BSSE on the uncorrected geometry is 3.861 kcal/mol, which yields 49% of the binding energy. Regardless of the electronic state the BSSE is always large and complicates

		LanL2DZ		LanL1MB		1 e^- ECP[(a)]	
		PtH	PtH^+	PtH	PtH^+	PtH	PtH^+
r	[Å]	1.5483	1.4753	1.6284	1.5178	1.4822	1.9252
q_{Pt}	[e]	0.085	0.063	−0.091	0.690	−0.063	0.163
q_H	[e]	−0.085	0.037	0.091	0.309	0.063	0.837
dipole	[D]	2.4459	0.9093	2.3983	0.1316	3.0307	−0.0627
Pop 5d		9.096	8.839	9.130	9.055	0.0	0.0
ΔPop5d		0.257		0.075		0.0	
ΔE_{ION}	[H]	0.3092		0.3086		0.3419	
ΔE_{BOND}	[H]	0.0685	0.2575	0.0454	0.2350	0.0560	0.2123

(a) Please refer to section 7.3.1, page 230 for details.

Table 6.8: Properties of $^2\Sigma^+$ PtH for different ECPs

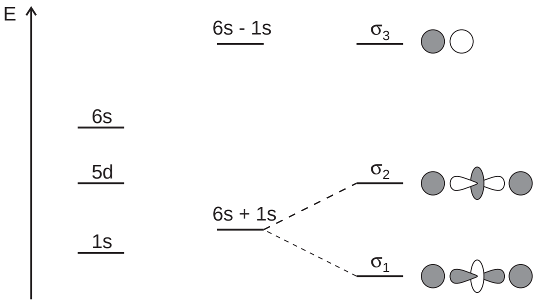

Figure 6.12 σ-MOs of PtH.

orbital	PtH	PtH^+
5d	9.096	8.839
6s	0.771	0.182
1s	1.069	0.938

Table 6.9 Mulliken Population from LanL2DZ calculations.

any scanning of the potential energy surface.

6.1.5 The Platinum-Hydrogen interaction

PtH was one of the first molecules for relativistic quantum chemical calculations on platinum [12, 306, 308, 309, 313–320]. Table 6.8 compiles some results for PtH for the $^2\Sigma^+$ state (4 δ, 4 π and 3 σ electrons).

The preliminary results obtained with the 1-electron ECP (subsection 7.3.1, page 230 for details) indicate that the 5d orbitals are less dominant in bonding and the bond between platinum and hydrogen is controlled by the interaction of the s-orbitals.

Figure 6.12 shows a simplified sketch of the σ-MOs in PtH. The electronic structure can be rationalized by the combination of a ^3D platinum atom with a ^2S hydrogen atom. Despite the conclusions drawn from table 6.8 the $5d_{z^2}$-orbital contributes significantly to the σ_1 and σ_2 orbitals. The construction of the orbitals can be explained in two steps. First, the platinum 6s and the hydrogen 1s orbital form two pairs of orbitals. The contribution of the platinum 6p orbitals to the bond is negligible. This movement of the electrons facilitates the interaction of the bonding s orbital with the $5d_{z^2}$-orbital. This procedure creates two new orbitals σ_1 and σ_2, which form the central part of the chemical bond. The remaining platinum 5d electrons do not contribute to the bond and form two π and two δ orbitals.

The 5d-orbitals cause the shrinking of the platinum hydrogen bond during the ionisation of the molecule. The Mulliken population analysis (table 6.9) shows, that the charge comes mostly from the platinum 6s-orbital. A more detailed analysis shows further, that the largest change in the population is observed in the outer regions of the platinum 5d-orbitals. This movement reduces the electron-electron repulsion between the cores and simultaneously stabilizes the σ_1 orbital. This purely relativistic effect has been observed previously by others [306, 309, 315] and cannot be reproduced by a simple 1-electron potential. The removal of an electron from the σ-MO weakens the bond and extends the seperation between the atoms. This problem will be discussed in greater detail in subsection 7.3.4 (page 239).

As observed previously in the interaction between platinum and water bonds calculated with the LanL1 potential are longer and weaker, and this seems to be a principal feature of ECPs. The LanL2 HF calculations reproduce more accurately the experimental bond length of 1.54 Å [321]. The inclusion of correlation has a significant influence on the bond length and tightens the bond. The effect is more pronounced on the charge distribution in the molecule. LanL2 calculations on the $^2\Sigma^+$ state give always a Pt^+H^- for MB od DZ bases, whereas LanL1 calculations produce Pt^-H^+. The charge distribution calculated with the LanL2 potential agrees well with experimental change in the workfunction [322, 323] for low coverages as well as the gasphase dipole moment [321].

As for water platinum interactions correlation effects are important for the platinum hydrogen bond. MP2 calculations with the LanL2DZ potential yielded a bond length of 1.494 Å while MP2 calculations with LanL1MB ECP resulted in a bond length of 1.565 Å. Both results fail to reproduce the experimental value to roughly the same extent. On the next level (MP3) the LanL2DZ bond length becomes longer (1.4993 Å) while the LanL1MB bond length does not change. At this level, the 1 electron calculation, a bond length of 1.485 Å reproduces perfectly well the LanL2 result.

The calculations on PtH show, that even the simplest molecules are better described with the LanL2 potential than with LanL1 ECP one. As long as the computing facilities are available is the 18 valence electron ECP is the one of choice.

6.1.6 Summary of the results for single platinum atom

Although a single platinum atom is the smallest platinum cluster possible, it demonstrates most of the main features in the adsorbate-platinum interaction and allows a detailed analysis of the binding mechanism. Due to the large number of electrons in a platinum atom, ECPs are commonly used for the description of the atom. The potentials of HAY and WADT are provided with the software and so offer a good starting point for further investigations. The potentials by HAY and WADT differ in the number of electrons used in the calculations. The LanL2 potential includes the 5s and 5p electrons and so allows a better description of correlation effects. The LanL1 potential, which does not include these electrons, allows us a good, low cost description of the adsorbate-platinum interaction. Bonds calculated with the LanL1 potential tend to be longer and weaker than LanL2 bonds, but show the same characteristics. Whenever possible the LanL2 potential should therefore be the ECP of choice.

The bond between water and platinum is formed by the interaction of $3a_1$ and the $1b_1$ orbitals of water molecule with platinum 5d orbitals. The platinum 6s orbital has a double function. First it facilitates the interaction by accepting electron density, which was formerly in the 5d region. This electron movement allows the formation of an inner orbital complex. Since the 6s orbital is more widely spreading than 5d orbitals, the electron density is moved from the platinum core to its outer regions and therefore closer to the oxygen atom. The Coulomb repulsion between the platinum 6s-electron density and the oxygen atom weakens the bond between them. This can be observed from the different binding energies for water for to ^{1}S and ^{3}D platinum. The bond between the ^{3}D platinum atom (with the occupied 6s orbital) and water is weaker than the bond between ^{1}S platinum (empty 6s orbital) and water. The excitation of a single electron by the electronic field of the bond partner is called polarisation and depends strongly on the orientation of both partners relative to each other. The $Pt-H_2O$ cluster with a ^{1}S platinum is actually only stable in a small region around the optimized geometry. A reliable scan of the potential energy surface should therefore consider various electronic states.

Calculations on PtH show the strong influence of the 5d electrons on the bonds formed purely by interaction of s-orbitals. This strong influence has a relativistic origin. Relativistic effects expand the 5d-orbitals and contract simultaneously the 6s-orbital. The electrons get closer to each other and interaction between both groups becomes more likely. This result emphazises the use of relativistic potentials, as already demonstrated for the free atom.

Counterpoise calculations on $Pt-H_2O$ (^{1}A' state) showed the strong BSSE effect on the platinum-water interaction due to the combination of basis sets of different quality. The effect of BSSE on the bond length is about 2% while that on the bond energy is up to 25%. Those simple calculations should therefore provide good geometries but poor energies.

6.2 Platinum Dimer

The investigation of the interaction between the platinum dimer and a water molecule provides the next stage in generating a working surface model. The calculations offer answers to the following questions:

- How do platinum atoms interact with each other?
- How does this interaction control the interaction between water and the platinum cluster?
- A dimer allows the simulation of different adsorption sites. Which mechanism controls the adsorption site?

The questions cannot be answered ia a straightforward manner. The different sites have different symmetries and a smooth change from one to the other is not always possible. The first part of this section concentrates on the direct interaction between the platinum atoms to provide a model of the cluster itself, while the second part focuses on the interaction of the cluster with a water molecule.

6.2.1 The electronic structure of the platinum dimer

The stability of the platinum dimer depends strongly on its electronic structure. Table 6.10 lists the results for different platinum dimers. The different electronic states can be associated with the electronic states of the free platinum atoms from which the dimer was built. The platinum dimers in table 6.10 are therefore classified according to the electronic states of the atoms, from which the dimer was built.

The first block of table 6.10 contains the results for the platinum dimer with a bulk bond length [36] of 2.77 Å (MP2 calculations). With increasing population of the 6s-orbitals (pop 6s) the platinum dimer becomes more stable. The 6s band in the metal clusters forms the metallic bond between the atoms and not the 5s-orbitals.

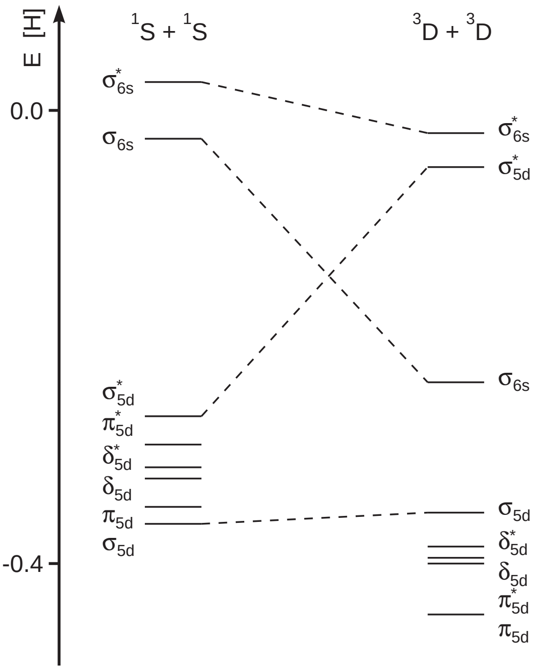

Figure 6.13: Orbitals of Pt_2.

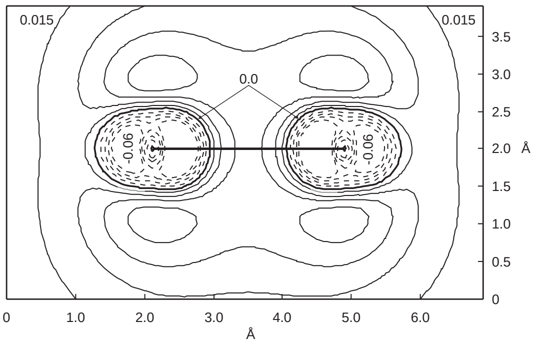

Figure 6.14: σ_{6s} orbital (LUMO) in the $^1S-^1S$ dimer.

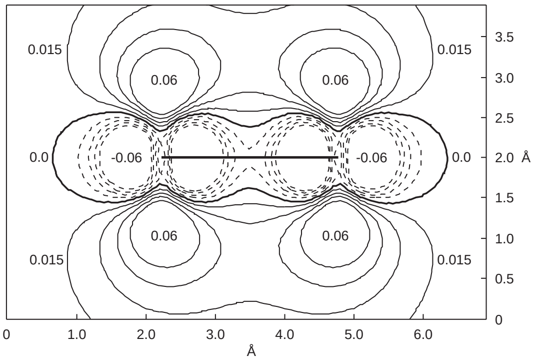

Figure 6.15: σ_{6s} orbital (HOMO) in the $^3D-^3D$ dimer.

Figure 6.13 shows a simplified diagram of the valence orbitals in the platinum dimer. In a platinum dimer built from two ^{1}S platinum atoms no electron should populate the σ_{6s} orbital, but the opposite was found (pop 6s = 0.279). As in the $Pt-H_2O$ bond, the $5d_{z^2}$ and the 6s orbital mix to form the bond and the σ_{6s}-orbital becomes populated. The $^3D-^3D$ dimer was constructed from the $^1S-^1S$ dimer by exciting both electrons from the σ^*_{5d} orbital into the σ_{6s} orbital. The σ_{5d} and the σ_{6s} orbitals get closer to each other in energy and can interact. In the $^1S-^1S$ dimer the σ_{6s} orbital is built purely from 6s orbitals (94%) whereas the 6s contribution to the σ_{6s} orbital in the $^3D-^3D$ dimer is reduced to 70%. The $5d_{z^2}$-orbitals contribute significantly to the shape of the molecular orbitals but little to the metal-metal binding energy. Figures 6.14 and 6.15 illustrate this effect (contour lines at 0.0, 0.015, 0.03, 0.045, 0.06). Figure 6.14 displays the σ_{6s}-orbital in the $^1S-^1S$ dimer. The molecular orbital has the dominant shape of a σ-orbital formed from s-functions, whereas the the σ_{6s} orbital in the $^3D-^3D$ orbital (figure 6.15) shows features of a σ-bond formed from d-functions.

With increasing values of the 6s-population, the platinum dimer becomes more stable. These results agree well with the literature [285, 314, 318, 324–326]. The dominance of the 6s orbitals for metallic binding in platinum allows us to use effective one-electron pseudopotentials for the metal cluster [318, 327–331], as will be discussed in chapter 7 (page 203).

The first part of table 6.10 shows the importance of electron correlation on the dissociation energy. The dissociation energy of the dimer (ΔE(DISS)) increases about 13.2 kcal/mol ($^1S-^1S$) / 17.7 kcal/mol ($^1S-^3D$) between HF and MP2. Inclusion of electron correlation also changes the

construction		^{1}S + ^{1}S	^{1}S + ^{3}D	^{3}D + ^{3}D
symmetry		$^1\Sigma_{gg}$	$^3\Sigma_{gu}$	$^1\Sigma_{gg}$
method		HF/MP2 single point, d_{PtPt} = 2.77 Å		
pop 6s		0.27858	1.60974	1.96434
pop 5d		19.5789	18.2424	17.9599
Δ_{POP}		0.14252	0.14786	0.0758
E(HF)	[H]	−236.369911	−236.463285	−236.339891
E(MP2)	[H]	−236.550939	−236.623935	−236.658279
$\Delta E(^3D)$	[kcal/mol]	+10.851	−34.954	−56.506
ΔE(Diss)	[kcal/mol]	−15.964	−48.362	−56.506
method		HF/MP2 geometry optimized		
r_{OPT}(MP2)	[Å]	2.7592	2.5939	2.3579
E(MP2)	[H]	−236.550950	−236.628461	−236.663187
$\Delta E_{OPT}(^3D)$	[kcal/mol]	+10.844	−37.795	−59.585
ΔE_{OPT}(Diss)	[kcal/mol]	−15.971	−51.102	−59.585
pop 6s		0.282288	1.50612	1.94306
pop 5d		19.57304	18.32954	17.91898
Δ_{POP}		0.14408	0.1643	0.13796
method		HF geometry optimized		
r_{OPT}(HF)	[Å]	3.0807	2.6638	2.5379
E(HF)	[H]	−236.373307	−236.464682	−236.380714
$\Delta E(^3D)$	[kcal/mol]	+50.383	−6.956	−45.734
ΔE(Diss)	[kcal/mol]	−2.683	−33.489	−45.734
pop 6s		0.0326	1.64226	1.92472
pop 5d		19.91274	18.21044	17.92516
Δ_{POP}		0.05466	0.1473	0.15012

experiment [332, 333] : r = 2.34 Å, ΔE = 85 kcal/mol, $^1\Sigma$ ground state

$\Delta E(^3D)$ Dissociation energy relative to two ^{3}D platinums

ΔE_{OPT}(Diss) Dissociation energy to the named electronic states (see **construction**)

Δ_{POP} = 20 − pop 6s − pop 5d

Table 6.10: Properties of the platinum dimer.

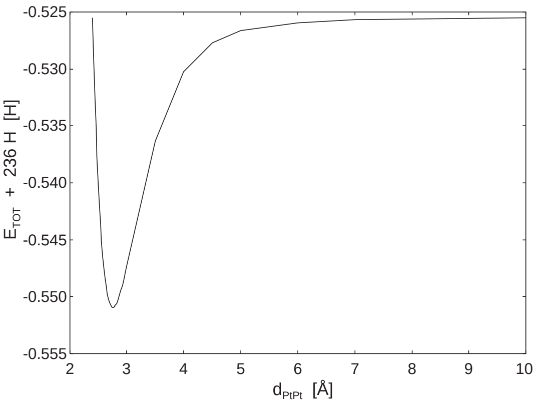

Figure 6.16: Dissociation of the $^1S-^1S$ dimer.

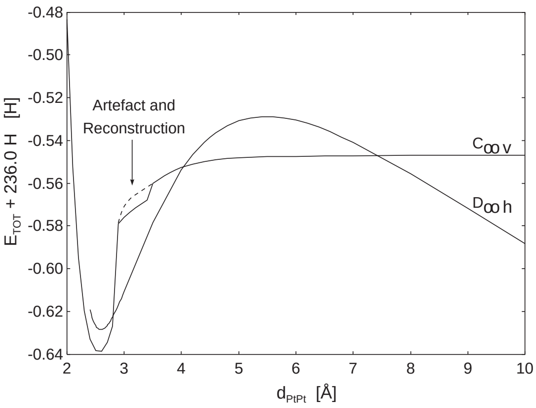

Figure 6.17: Dissociation of the $^1S-^3D$ dimer.

relative order of the total dimer energies. At HF level the $^1S-^3D$ dimer is more stable than the $^3D-^3D$ dimer while at the MP2 level the $^3D-^3D$ dimer is the most stable one. The importance of electron correlation is also reflected in the optimized bond length, when the equilibrium distance is reduced by roughly 10% in the case of the $^1S-^1S$ dimer.

Effects of electron correlation are most powerful in the $^1S-^1S$ dimer. MP2 calculations yielded an increase in the 6s population from 0.065 at HF level to 0.279 at MP2 level ($r_{PtPt} = 2.77$ Å). This additional population increases the bond strength and shortens therefore the bond length during geometry optimisation. The mixing of the σ_{5d} and the σ_{6s} orbitals moves electron density from a bonding 5d orbital into another bonding orbital, which leaves the 5d band slightly anti-bonding since no electron density is removed from the σ^*_{5d} orbital. During electron correlation calculations electron density is moved from the anti-bonding 5d orbitals into the σ_{6s} orbital, which increases the binding energy dramatically. The coefficient of the root configuratuin ($c_0 = 0.95$) in the Møller-Plesset perturbation calculation is smaller than that for the water molecule ($c_0 = 0.97$). A high value of c_0 is an indicator of the validity of the perturbational approach. The influence of electron correlation is not small compared with the HF-function regarding the platinum dimer and the perturbational approach becomes less valid. More advanced methods like CI should be chosen, but are very costly for the large clusters necessary to describe the platinum surface.

At this level a difference between Extended Hückel and Hartree-Fock calculations becomes apparent. Bigot and Minot [285] describe this electron movement as excitation. According to the HF/MP2 calculation a doubly occupied σ_{6s} orbital forms the basis of the metal-metal bond in platinum. UPS spectra also provide evidence of a strong occupation of the 6s orbitals (0.42 s-electrons/per atom) [334a, 335]. SO ETH calculations a priori seem to be unable to describe the relativistic interaction between the 5d and the 6s band completely.

Table 6.10 provides evidence of the small contribution of the 6p orbitals to the metallic bond. The valence electron population not used in the 5d and 6s orbitals (Δ_{POP}) has an average value of 0.15. This value hardly changes with the level of the computational procedure or the population of the 6s orbitals. The bond between the platinum atoms is built exclusively from 5d and 6s orbitals, while the 6p orbitals are less important.

The dissociation energies shown in table 6.10 were calculated from single point calculations and not from complete dissociation curves, because the wavefunctions change their multiplicity and/or symmetry during the dissociation. The $^1S-^1S$ dimer was simple to calculate (figure 6.16), since

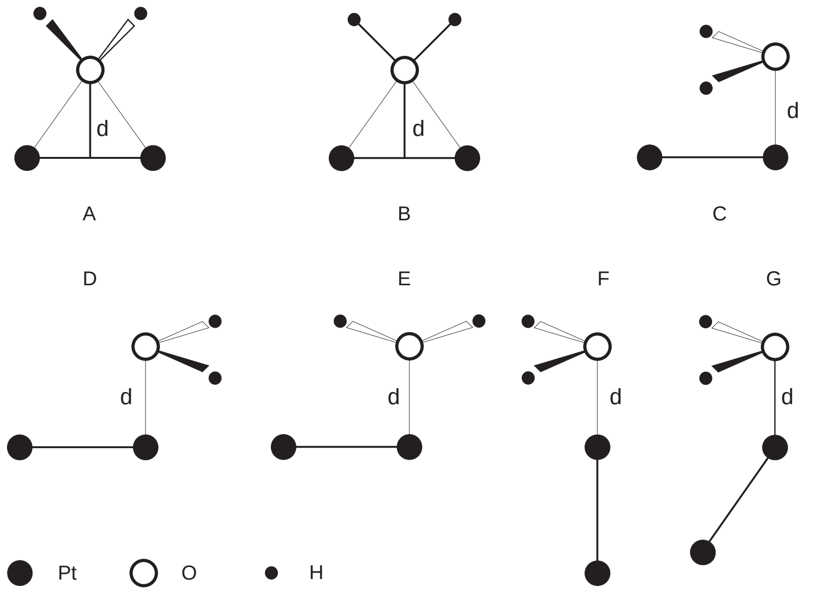

Figure 6.18: Different geometries for Pt_2-H_2O.

both symmetry and multiplicity were conserved during the dissociation.

The $^1S-^3D$ dimer was more difficult to compute because the symmetry changes from $D_{\infty h}$ to $C_{\infty v}$. At large distances both platinum atoms have different electronic structures while the electronic structures are equivalent at equilibrium distance. To calculate the dissociation curve the symmetry of the initial dimer was reduced artificially[4] to $C_{\infty v}$ but this method lowered the total energy of the dimer (figure 6.17).

The dissociation of the $^3D-^3D$ was impossible to calculate, because the multiplicity of the wavefunctions changes from 1 to 5 during the dissociation. This is a standard problem in platinum clusters and becomes more pronounced as the number of platinum atoms increases. During the final simulation of the metal surface the cluster's geometry does not change and the electronic state of the cluster as a function of the metal bond distance becomes unimportant. The work on this problem therefore ends here.

6.2.2 Platinum Dimer and Water

Figure 6.18 compiles the different geometries for the Pt_2-H_2O system, which were examined in this work. The first geometries A and B simulated bridging sites, whereas the geometries C to E describe on-top sites. Finally, geometry G describes the edge of a Pt_5 pyramid and geometry F is the extreme form of an on-top coordination without any physical background.

6.2.2.1 Influence of the geometry

Table 6.11 lists the results for the interaction of the $^1S-^1S$ dimer with water. The column d_{OPT} contains the optimized distance between the water molecule and the metal surface (6.18 displays

---

[4] The manipulation of the symmetry started with the PtAu molecule. In the next step the charge of the gold atom was reduced by one (Gaussian 94 key word `massage`) and finally the platinum ECP and the basis set were defined manually in the input file for the gold atom.

geo	d_{OPT} [Å]	Δq [e]	(E_{TOT} + 312) [H]
B	1.9072	0.132	-0.813502
A	1.7055	0.174	-0.832082
D	2.0574	0.189	-0.849604
E	2.0541	0.190	-0.857023
F	2.1120	0.155	-0.859522
C	2.0483	0.213	-0.862900
G	2.1142	0.175	-0.865975

Table 6.11: $^1S-{}^1S$ dimer and water.

geo	d_{OPT} [Å]	Δq [e]	(E_{TOT} + 312) [H]
B	2.7190	0.054	-0.836039
A	2.5190	0.084	-0.883404
C	no minimum → converts into C		
E	SCF does not converge		
C	2.4191	0.143	-0.898288
F	2.2613	0.135	-0.902415
G	2.2734	0.138	-0.903141

Table 6.12: $^3D-{}^1S$ dimer and water.

the definition of d for each geometry). At the first glance the water molecule seems to be strongly bound in the geometries A and B, because the water molecules are close to surface. These water molecules penetrate the space between platinum atoms. The actual bond length between the platinum atoms and the oxygen atom is much longer than in the other geometries (B: 2.375 Å, A: 2.197 Å).

The lower total energy of geometry A versus geometry B demonstrates the dominance of the water molecule's free electron pairs for the chemical bond between water and the metal. The importance of the second neighbour on the surface for the chemical bond is reflected in the sequence of energies for the geometries C → E → D. The interaction between the neighbour platinum atom and the water molecule is interpreted by the Mulliken overlap population (MOP). The overlap population increases with total energy (C: 0.025 E: 0.016, D: −0.002).

Table 6.12 shows the results for the low energy Pt_2 triplet state interacting with water. The SCF calculation did not converge on geometry E and the minimum in the energy curve for geometry D vanished. During the optimisation of geometry D the water molecule flipped and geometry D turned into geometry C. The only molecule from the on-top series remaining is therefore molecule C and so is the most stable.

The geometries C and F exchange their relative energy positions and the two end-on geometries (F and G) become the energetically most stable. Despite their relative stability the charge transfer is the smallest for end-on geometries and it is therefore impossible to use charge transfer as a global measure of stability over the whole conformational space, because both bond length and charge transfer do not change systematically with total energy. On the other hand, charge transfer and bond energy correlate well with the total energy for a fixed Pt-Pt-O angle (geometries A and B, geometries C, D and E). The exception from this rule (geometries F and G) may indicate a change in the mode of bonding (details in subsection 6.2.2.4).

6.2.2.2 The water metal interaction in Pt_2-H_2O

The results obtained for different geometries can be explained by differernt bonding mechanisms and this section focuses on the molecular orbital mechanism of the metal-water bond in the geometries A, C and G.

As for the water dimer or $Pt-H_2O$, the chemical bond between water and the platinum dimer is not formed from free electron pairs but from individual interactions of the $3a_1$ and the $1b_1$ orbitals with platinum d-orbitals. The C_{2v} symmetry of geometry A conserves the symmetry species of

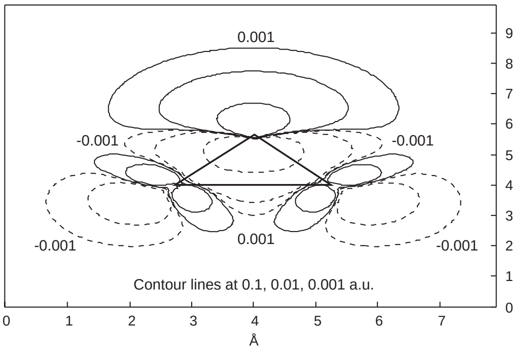

Figure 6.19: Geometry A: Bonding orbital a_1 symmetry.

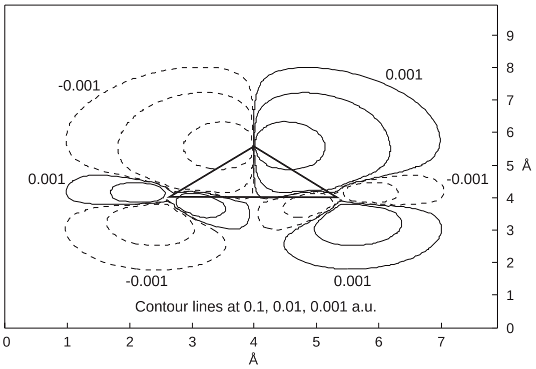

Figure 6.20: Geometry A: Bonding orbital b_2 symmetry.

these orbitals during bonding. Appropriate partners for the $3a_1$ orbital are therefore the σ_{5d}, π_{5d} and the δ_{5d} orbitals. The $1b_1$ orbital changes its symmetry character and transforms in Pt_2-H_2O according to b_2. This change is caused by the inversion of the order of the mirror planes by the heavy atoms. The water molecule can interact with the PtPt antibonding orbitals such as σ^*_{5d}, π^*_{5d} and the δ^*_{5d}, which also transform according to b_2 in geometry A. Figures 6.19 and 6.20 show these orbitals, which are dominated by the original water molecular orbitals.

The metal part of the bonding molecular orbitals in geometry A is clearly dominated by the platinum π-orbitals. The analysis of the eigenvectors showed that the contribution of the σ_{6s} orbitals is considerable. The σ_{6s} orbital transforms according to a_1 and can mix with σ_{5d}, π_{5d} and δ_{5d} orbitals. This mixing results in a 6s population of 1.02, which is much higher than for the free dimer (0.28, table 5.9). The 6s population suggests a $^3D-^1S$ dimer, which is inconsistent with the multiplicity of the molecule. A direct correlation between the 6s population and the electronic states of the individual platinum atoms in the dimer is no longer possible. As shown in section 6.1.2 the bonding of an individual water molecule to the platinum atom is always associated with a small electron transfer from 5d into 6s to enhance bonding (6s population in $^1Pt-H_2O$: $d_{PtO} = 2.11\text{Å} \rightarrow 0.679$, $d_{PtO} = 10\ \text{Å} \rightarrow 0.003$). This effect is much stronger in the platinum dimer. The adsorption of water not only reduces the symmetry of the molecule from $D_{\infty h}$ to C_{2v}, but further 5d orbitals of an allowed symmetry species are in a suitable energy range for 5d 6s overlap.

Figures 6.22 and 6.23 show the bonding orbitals in geometry C. The structure of the molecular orbitals is more complex than before. It is impossible to construct a σ-PtO bond from a π_{5d} or π^*_{5d} as for geometry A, because the symmetry of the 5d-orbital causes a zero overlap (figure 6.21). The σ and δ orbitals possess suitable symmetry for bonding. Figures 6.22 and 6.23 show that the chemical bond is constructed from the σ_{5d} orbital. The orientation of the metal orbital is controlled by a small contribution from the π_{5d} orbitals. The linear combination of π_{5d} and π^*_{5d} ($\varphi_1 = 0.707{\cdot}[\pi_{5d} + \pi^*_{5d}]$) results in a single platinum 5d orbital, which is used to orientate the metal orbitals. The other metal orbitals are similar linear combinations, and the metal part of the bonding orbital accumulates at the bonding platinum atom (left-right asymmetry in the PtPt bond). The 6s contribution to the metal-metal bond is much higher than in geometry

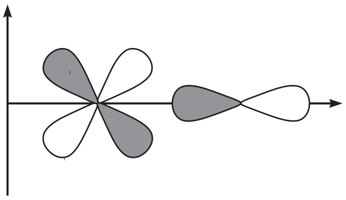

Figure 6.21: Zero π_{5d}-$3a_1$ overlap.

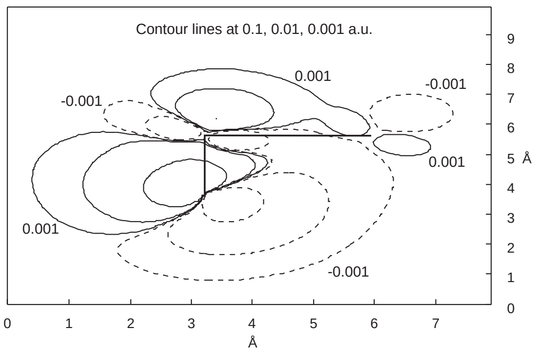

Figure 6.22: Geometry C: Bonding orbital (water $3a_1$).

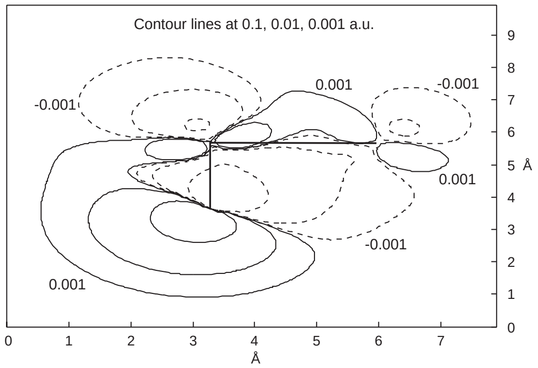

Figure 6.23: Geometry C: Bonding orbital (water $1b_1$).

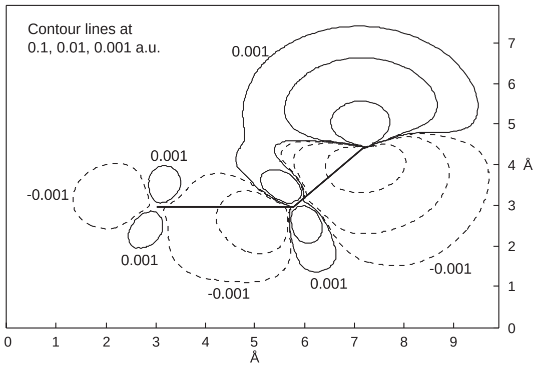

Figure 6.24: Geometry G: Bonding orbital (water $3a_1$).

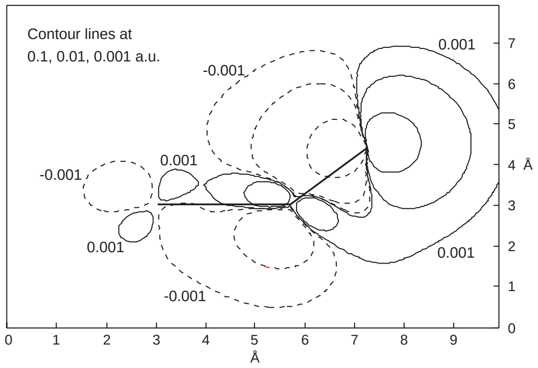

Figure 6.25: Geometry G: Bonding orbital (water $1b_1$).

A (6s population A: 1.02, C: 1.39) and the total energy is therefore lower.

In C_s symmetry, which is lower than the C_{2v} symmetry of geometry A, more orbitals transform according to a' so both σ_{61} orbitals have more opportunity to interact with the 5d orbitals, thereby accounting for the high 6s population and the low total energy.

Geometry G has also C_s symmetry. The 6s population is even higher (1.80) than for geometry C but the water-dimer bond is slightly stronger (37.7 kcal/mol vs. 36.0 kcal/mol). This contradiction can be explained by a gain in energy due to stronger metal-metal bond (details subsection 6.2.2.4) on the expense of the platinum-water bond. This bond in geometry G (2.11 Å) is 3% longer than that in geometry C (2.05 Å). Figures 6.24 and 6.25 show the bonding orbitals in geometry G. The π_{5d} orbital contributes more strongly to the platinum-water bond as one lobe of π_{5d} points directly towards the water molecule. The enhanced orbital overlap partially compensates for the longer bond. ***The symmetry and the shape of the available metal orbitals thus control the site of adsorption.***

During the interaction between the water molecule and the platinum dimer the 6s orbitals become more populated. This extra population has two origins. Firstly, the newly formed complex has lower symmetry than the free dimer. This reduced symmetry allows the 6s orbitals to mix with additional 5d orbitals, which now have the correct symmetry. Secondly, the occupation of the 6s orbitals creates a hole in the 5d band, which forms the basis for the chemical bond to the water molecule. Meanwhile, the 6s electrons have more space to fill because Pt_2 is much larger

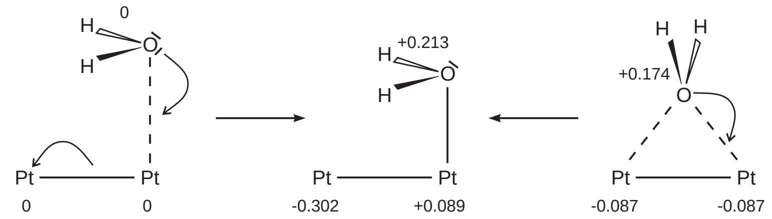

Figure 6.26: Electron movement in Pt_2-H_2O.

than a single atom. This extra space is used to reduce the repulsion between the 6s electrons and oxygen electrons and so facilitates the formation of a strong water metal bond ($Pt-H_2O$: −22.6 kcal/mol, Pt_2-H_2O : −37.7 kcal/mol (geometry C)).

The mechanism is illustrated in figure 6.26. As the water molecule approaches the platinum cluster electron density flows from the water molecule to platinum dimer. At the target platinum negative charge is unstable due to the electrostatic repulsion between the 6s electrons and the oxygen. This charge therefore flows directly to the end platinum atom. Such an extended charge flow is characteristic of cooperative intramolecular forces. The second platinum, which acts as a charge acceptor, indirectly strengthens the bond between water and the model cluster.

Table 6.13 summarizes the charges on the platinum atoms and the total charge flow. The water molecule bonds directly to Pt2. The negative charge accumulates at the free end of the cluster, while the bonding platinum atom carries only a small charge. A natural orbital analysis of geometry C gave the same picture. The platinum-platinum bond becomes weaker in favour of the water-platinum bond, as the strong polarisation of the cluster reduces the covalent/metallic bond strength.

geo	q_{Pt1} [e]	q_{Pt2} [e]	Δq [e]
A	-0.087	-0.087	0.174
B	-0.066	-0.066	0.132
C	-0.302	0.089	0.213
D	-0.248	0.059	0.184
E	-0.283	0.093	0.190
F	-0.160	0.005	0.155
G	-0.111	0.064	0.175

Table 6.13: Charges and charge transfer in Pt_2-H_2O.

No single orbital is predestined to form the basis of the metal-water bond. For each geometry other orbitals are involved in the chemical bond. The possibility for the water molecule to adsorb to the dimer depends on the existence of an orbital with correct symmetry in a certain energy range. The bond strength correlates to the 6s population necessary to form those orbitals.

6.2.2.3 Influence of the electronic state of the platinum dimer

To determine accurate values for the platinum-water interaction, complete dissociation curves were calculated at selected geometries. These calculations proved to be demanding and not all possible states and geometries have examined. Figures 6.27 to 6.29 show the curves and table 6.14 compiles the results. Both open and closed shell wavefunctions were used for the comparison.

Table 6.14 shows clearly that with increasing 6s population the cluster becomes more stable (E_{TOT}). This result agrees with those obtained in section 6.2.1. Simultaneously the platinum-water bond becomes weaker (ΔE and d_{OPT}). The binding energy of a water molecule in the on-top position (geometry C) in the triplet state is close to the experimental value of 12 to 15 kcal/mol [38], while the interaction with the singulet dimer is too strong. This result is in good agreement with those for the $Pt-H_2O$ system. A high occupation of the 6s orbitals increases the

geo[a]	case	2S + 1	6s Pop in Pt_2	d^a_{OPT} [Å]	(E_{TOT} + 312) [H]	ΔE [kcal/mol]
A	I	1	1.02112	1.7055	−0.832082	−25.195
A	II	1	1.98086	3.0866	−0.900399	−0.736
A	III[b]	1	2.43924	2.56[c]	−0.810391	−3.071
A	IV	3	2.08094	2.5196	−0.883404	−2.371
A	V[b]	3	1.87622	2.199	−0.816101	—
G	I	1	1.79583	2.1142	−0.865975	−37.719
G	II	3	2.12678	2.2734	−0.903142	−14.680
C	I	1	1.39309	2.0483	−0.862900	−36.048
C	II	3	2.06033	2.4191	−0.898287	−11.672

[a] figure 6.19 [b] no complete curve

[c] not optimized, value extracted from the curve fragment

Table 6.14: The platinum-water bond as a function of the 6s population

cluster's stability but weakens the water metal bond due to repulsion between the extended 6s electrons and the oxygen atom. This can be observed for the singlet wave functions (geometry A, cases I and II) as well for triplet wave functions (geometry A, case IV and V). Geometry A (case III) should not be used for direct comparison because the density matrix breaks the molecule's symmetry whereas the electron density of the other molecules with geometry A show the correct symmetry.

The weakening of the metal-water bond is not dominated by the multiplicity of wave functions multiplicity as shown by direct comparison of the results for geometry A. As soon as the 6s population approaches 2.0, the cluster becomes more stable and the water-metal bond becomes weaker regardless of multiplicity. This effect is less pronounced for the triplet case.

It was not possible to construct singlet wave functions with higher 6s populations for geometries G and C than those listed in table 6.14. The σ_{6s} orbital (a' symmetry) can overlap with many other orbitals, so that the SCF calculation converged to the ground state every time we tried to construct a wavefunction with a different 6s population. Only geometry A allowed the construction of a singlet wave function with a high 6s population. The binding energy of the water molecule is exceptional small. This result again rules a pure spin-effect in water bonding out and the bonding energy of the water molecule is even smaller than in the triplet state. The existence of the second singlet species is again caused by symmetry mixing and orbital density. Few orbitals can overlap with σ_{6s} and a mixture of those energetically well separated orbitals during the SCF calculation is unlikely. The HOMO of this new cluster is very similar to that of the $^3D-^3D$ dimer, whereas the other two clusters (geometry G and C) have highly deformed σ-bonds.

In all three cases the LUMO is built from the remaining parts of the σ_{6s} orbital. In a triplet wavefunction the 6s orbitals are fully occupied; however the σ_{6s} orbital is distributed between two other molecular orbitals. The singlet and the first triplet states are well separated. No curve crossing has been observed as for $Pt-H_2O$. On the other hand, more electronic states exist with the same multiplicity and similar total energies. The computation of the complete potential energy surface is therefore more complicated than for $Pt-H_2O$.

The occupation of the 6s orbitals and hence the electronic state of the cluster can be manipulated via the oxygen-platinum distance. Figure 6.30 displays the strongest bonding singlet states

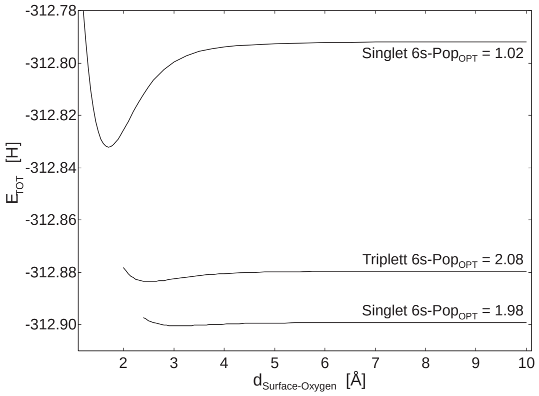

Figure 6.27: Dissociation of geometry A.

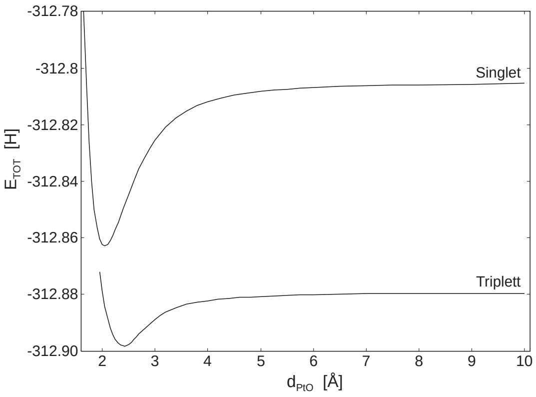

Figure 6.28: Dissociation of geometry C.

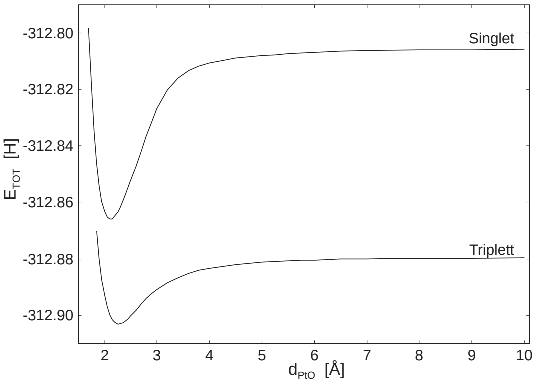

Figure 6.29: Dissociation of geometry G.

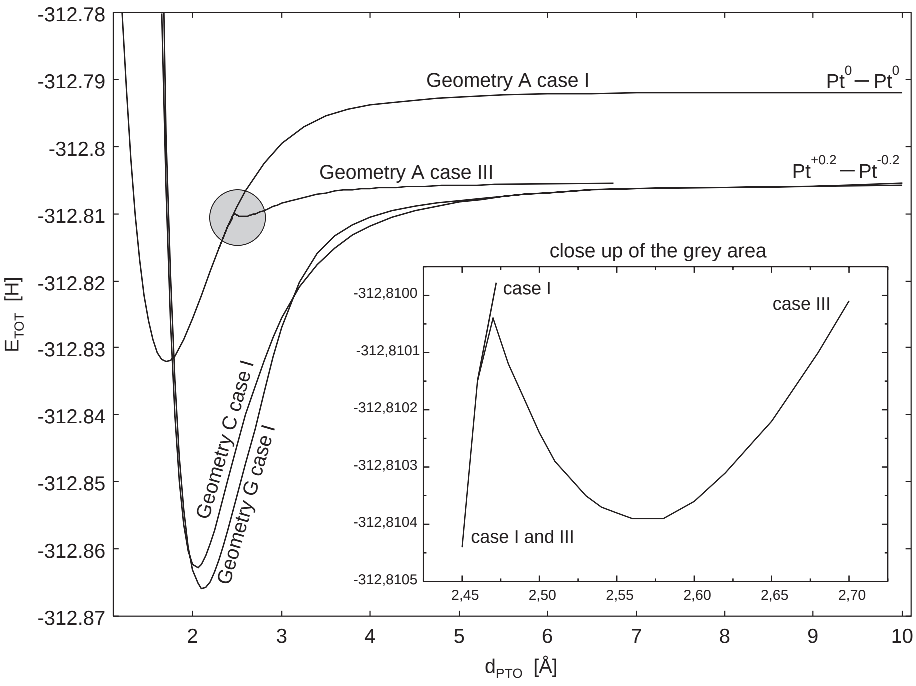

Figure 6.30: Different dissociation curves.

(geometries A, C, G case I) and a portion of the curve for geometry A case III. The starting points for geometry A (curves I, II, and III) were generated from single point calculations with different platinum-oxygen separations. The different electronic states generated in this way were stabilized by shifting the virtual orbitals. This method worked only partially in case III. At short separations the repulsion of the 6s electrons by the oxygen atoms becomes smaller and therefore they spread more widely. The system has two possibile ways to relax: It either flips the electronic state of platinum dimer, turning case AIII turns into case AI, or can follow the potential curve. This flipping is shown in the inset in figure 6.30. All three curves converge to the same dissociation-point, where the 6s population in the platinum dimer is 1.430. Comparing those cases a bridging position for the water molecule is less likely than case AI suggests.

The Pt_2-H_2O cluster at $d_{PtO} = 10$ Å differs not only in the 6s population but also within the charge distribution in the cluster. Geometry A case I dissociates correctly into a water molecule and a platinum dimer with uncharged atoms, while the in other cases (CI, GI, AIII) it dissociates into a dimer with charged platinum atoms ($|q_{Pt}| = 0.2$ e)[5].

At a distance of 8 Å from the surface the orientation of the water molecule relative to the dimer should be negligible. A small distortion of the plane of the water molecule by 1 degree reduces the symmetry from C_{2v} to C_s. In case AI the total energy drops dramatically and case AI converts into case AIII. Meanwhile, the charges on the platinum atoms increase to |0.2 e|. Such a large increase cannot be explained physically with such a small distortion of the molecular geometry. On the other hand, the conversion of geometry C (case CI) into geometry A (case III) hardly changes the charge distribution and the total energy and no jump can be observed despite the break of symmetry. The jump from case AI to case AIII / case CI can be explained by the mixing of the 25th (a_1 symmetry, platinum π_{5d} + water $3a_1$) and 23rd orbital (b_2 symmetry, HOMO, σ^*_{5d}) molecular orbitals. The reverse step, the disentangling of the orbitals while changing from C_s to C_{2v} symmetry is not possible. The mixed orbitals do not a provide suitable description of the Pt_2-H_2O system due to the physically incorrect charges on the platinum atoms and the jump between geometries A and C/G (case I) is not physically reasonable either. The explanation of this behaviour is the mixing of two different electronic states with similar energies (near-degeneracy effects [336a]). A more appropriate theoretical approach is a multirefence calculation. First test CAS SCF(2,2)-calculations (**c**omplete **a**ctive **s**pace SCF (section 2.3, page 22)) containing the HOMO and second next orbital to the LUMO of the Hartree-Fock calculation yielded good results. No energy shift can be observed between the geometries A and C and the charge on the platinum atoms in geometry C become reasonable small ($|q_{Pt}| = 0.000041$ e). The 6s population is close to its maximum value (1.828), which reduces the binding of the water molecule. The inclusion of further orbitals into the correlation space allows a reasonable description of the chemical bond. First test calculations showed[6] that the next important excitation contains occupied molecular orbitals containing the water $3a_1$ orbital and virtual orbitals built from the water $1b_2$ orbital. Such an electronic excitation reduces the electron density in the congested centre of the molecule. A complete multireference analysis of the Pt_2-H_2O system is beyond the scope of this work.

---

[5] Charged platinum atoms are impossible for geometry A (C_{2v} symmetry). Gaussian 94 complains about an unsymmetric density matrix, but all calculations converge quickly.

[6] The important orbitals for the active space were found with a small program, which tested all double exciations individually. Only the energetically most significant were chosen for the active space.

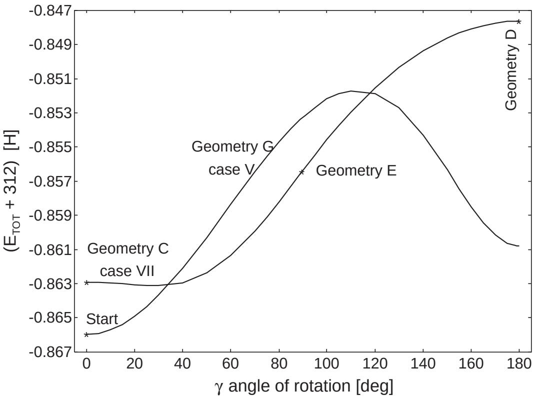

Figure 6.31: Rotation around the PtO bond.

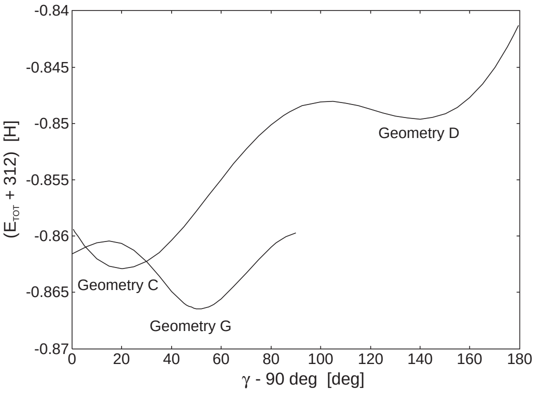

Figure 6.32: Wagging of the water molecule.

6.2.2.4 Movement of water on the surface

As shown in the previous section the electronic state of the platinum dimer depends on the oxygen-platinum distance. This section considers of the connection between different geometries corresponding to the same (or similar) oxygen-platinum distances.

Figures 6.31 and 6.32 show that all clusters with C_s symmetry can be easily interconverted. Figure 6.31 shows the total energy as function of the rotation around the PtO bond. The geometries C, E and D are joined by a straight line. The second curve shows the same plot for geometry G. Geometry G is only energetically more stable than the other clusters in a small conformational region. Figure 6.32 shows the total energy as a function of the angle of the water molecular plane and the PtO bond. The curve starting from geometry G represents the global minimum in only a small section of the conformational space. The geometries C and D are separated by a small maximum. With increasing 6s population (changing from singlet state to the triplet) the water-platinum bond becomes weaker. The relative height of the maximum is reduced and the interconversion of geometries C and D becomes more likely. This explains the conversion of geometry D into geometry C during the optimisation of the triplet state of geometry D (subsection 6.2.2.1).

Figures 6.34 and 6.35 show the conversion of geometry A (case I) into geometry D, starting from geometry A. The distance from the surface (PtPt bond) seems to be shorter in geometry A despite the smaller binding energy. Figure 6.34 shows that the effective PtO distance is longer due to the molecule's geometry. The effective PtO distance and the binding energy agree well with those values obtained in the previous sections. Figure 6.35 shows the total energy of the cluster as the water molecule moves from geometry A into geometry D. Figure 6.36 shows the variation of the angle between the surface-oxygen bond d (see figure 6.19 for the definition of d) and the water molecular plane γ as a function of the distance from the centre. The water molecule moves smoothly into its final position as the water molecule approaches its destination.

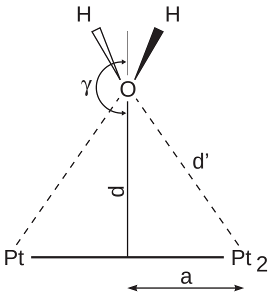

Figure 6.33: Pt_2-Geometry A to D.

Figures 6.37 and 6.38 show the results of the same calculation starting from geometry C. The distance from the surface first shrinks and then increases, while the PtO bond increases continuously

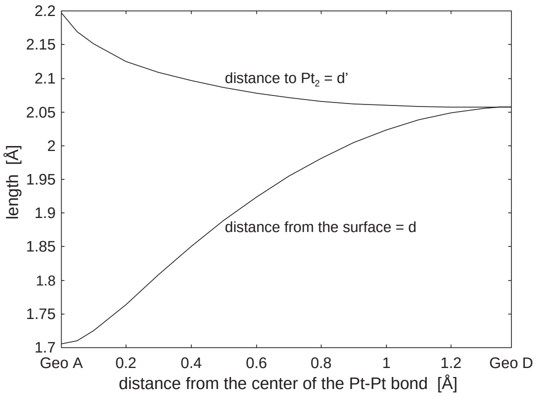

Figure 6.34: Shift along the PtPt bond, start geometry A, distance.

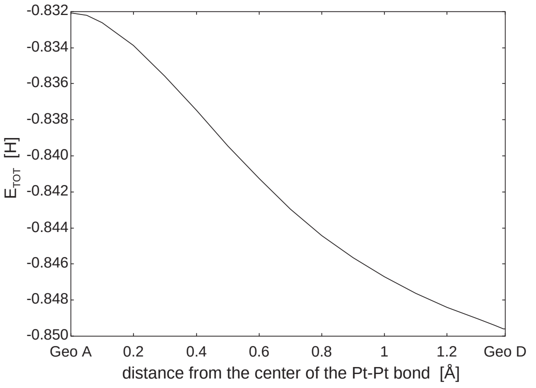

Figure 6.35: Shift along the PtPt bond, start geometry A, energy.

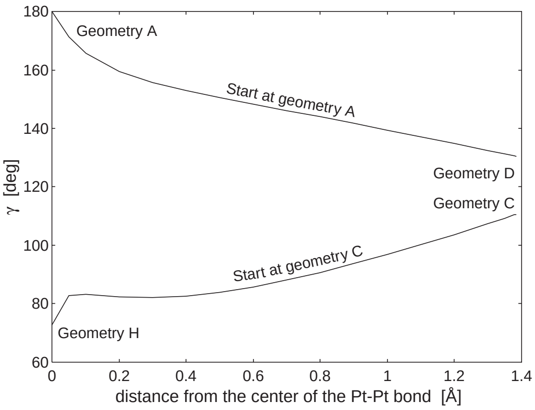

Figure 6.36: Shift along the PtPt bond, start geometry A, wagging.

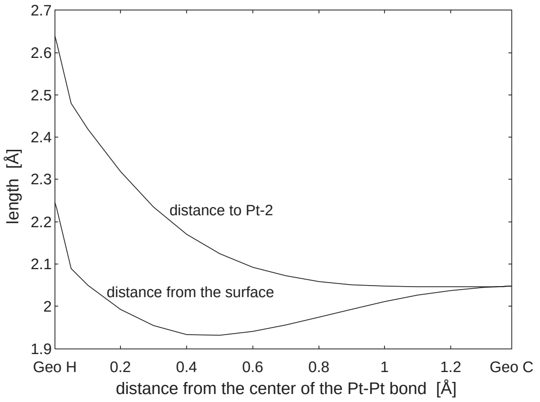

Figure 6.37: Shift along the PtPt bond, start geometry C, length.

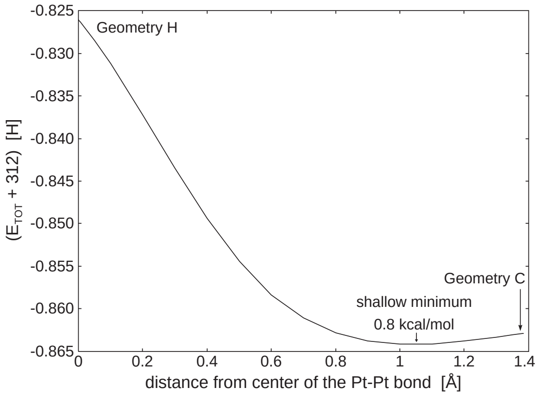

Figure 6.38: Shift along the PtPt bond, start geometry C, energy.

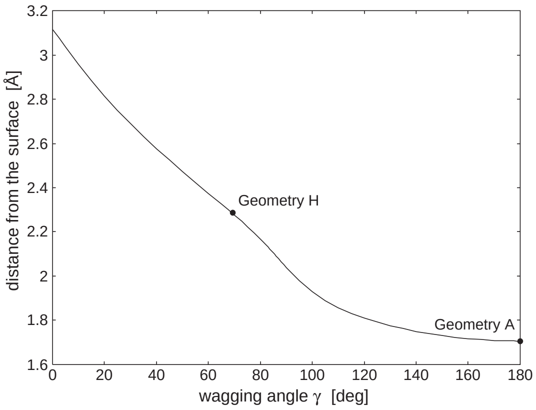

Figure 6.39: Wagging of the H_2O in geometry A, bond length.

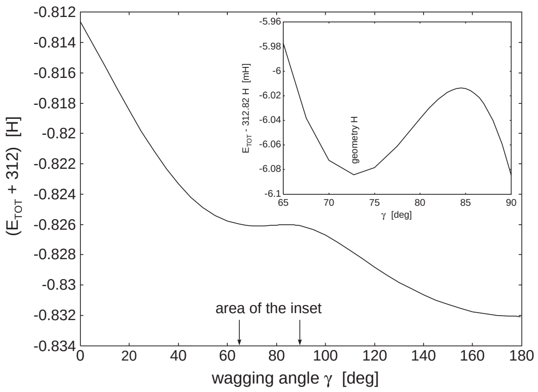

Figure 6.40: Wagging of the H_2O in geometry A, total energy.

(figure 6.37). Unlike the previous cases geometry C does not change into geometry A, but into geometry H, where the oxygen atom rests directly above the centre of the PtPt bond while the hydrogen atoms are tilted downwards and point towards the neighbouring platinum atom. The second plot in figure 6.36 displays the tilt angle of the water molecular plane during this movement. The geometry still has C_s symmetry and the platinums carry opposite charge. The electronic structure and the symmetry of geometry C have been conserved during the calculation. During this movement the water molecule passes through a shallow minimum (0.8 kcal/mol relative to geometry C, figure 6.38).

The next series of calculations describes the movement of the water molecule in geometries A and H. During these calculations we changed the angle between the bond between the surface and the water molecular plane γ, while the bond length d was allowed to relax at a constant $a = 0$ (figure 6.33). The results of these calculations are summarized in figures 6.39 and 6.40. Figure 6.39 shows the optimized distance to the surface during the rotation. The bond distance changes smoothly the rotational angle. Only the slope of the curve at small values of rotational angle is suspicious. Symmetry demands that the bond length should change smoothly over the 0 degree point and the curve should not have a cusp. The same is observed for the energy (figure 6.40). At zero degrees the cluster has again C_{2v} symmetry, but the platinum atoms are charged differently ($|\bar{q}_{Pt}| = 0.172$ e). The inset in figure 6.40 shows the local energy maximum, which makes a direct transformation from geometry A into geometry C impossible, because a small activation energy has to be overcome and the software follows the path of lowest energy.

Finally, the transformation from geometry C into geometry F via geometry G was analyzed. Figures 6.42 shows the length of the platinum-oxygen bond and the population of the 6s orbitals. The shortest equilibrium length was observed for geometry C (90°). At this point the total 6s population has its highest value. As geometry C changes into geometry G this bond becomes longer and simultaneously increases the total 6s population. The enlarged distance to the oxygen atom reduces the repulsion between the 6s electrons and the oxygen and results a higher population of the 6s band. At the bottom of figure 6.41 the 6s populations of the individual platinum atoms are displayed. For Pt-Pt-O angles above 140° the total 6s population remains constant, while the 6s population of the individual platinum atoms changes continuously. This movement of the 6s electron density demonstrates the possibility of intermetallic charge transfer in cooperative forces.

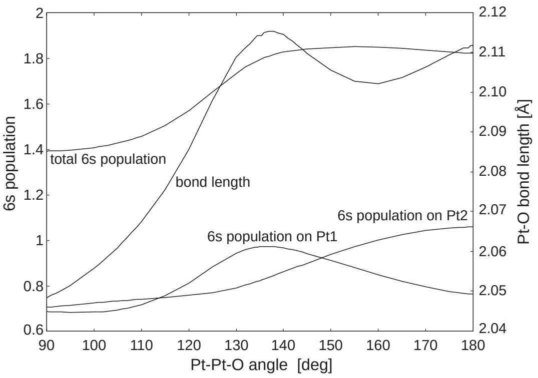

Figure 6.41: Geometry C to F, 6s population.

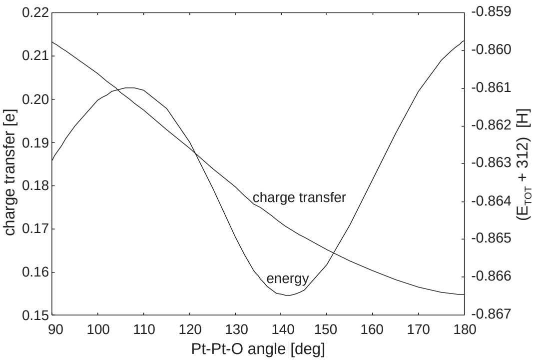

Figure 6.42: Geometry C to F, total energy.

The total energy (figure 6.42) of the cluster does not follow the 6s population, but has a distinct minimum close to geometry G (135°). Figure 6.42 also displays the charge transfer from the water molecule to the platinum dimer. The charge transfer decreases steadily during the motion and exhibits no other features. The global minimum of the total energy at 140° is close to geometry G. At this peak the total 6s population reached its maximum while the charge transfer is still high.

γ	geo	MOP PtPt	MOP PtO
90°	C	0.120739	0.072887
135°	G	0.303253	0.059046
140°	—	0.311012	0.054689
180°	F	0.256784	0.040784

Table 6.15: Mulliken overlap population in Pt_2-H_2O.

Table 6.15 shows the Mulliken overlap population of selected bonds in the Pt_2-H_2O system during the transformation of geometry C into geometry F. The platinum-platinum bond becomes stronger, while the platinum-oxygen bond simultaneously becomes weaker.

This interplay of 6s-electron density and charge transfer within the platinum-water bond explains why the water molecule bonds strongly to the platinum dimer with small charge transfer in geometry G. It is not a change in binding mechanism, but a change in the 6s-population, which compensates for the weak bond (see subsection 6.2.2.1). The 6s population changes again as the bond between the water molecule and the dimer breaks. In geometry C the 6s population increases by 0.037. This increase reflects the reduced repulsion between the 6s electrons and oxygen. This small difference indicates that most of the extra charge from the water molecule has to be stored in the 5d-band. Geometry G is more complicated: the 6s population decreases by 0.365 during the dissociation. This extra 6s population in the Pt_2-H_2O comples can be explained by the higher contribution of the 6s orbitals to the bonds between the water molecule and the platinum to compensate for the longer bond, as the 6s orbitals are more widely spreading than the 5d.

Figure 6.43 shows the connections between different geometries and electronic states. Double headed arrows indicate two way connections, while single headed arrows indicate one way connections. It is possible to go from a totally covalent platinum dimer without water (end of the dissociation curve for geometry A, case I, figure 5.30) to a partially ionic bonded dimer (end of the dissociation curves for the geometries G and C, figure 5.30), but **not** the other way round. For a given geometry (e.g. geometry A) two dissociation pathways exist to different end points, which cannot be transformed into each other. More advanced calculations like CAS-SCF would be required for a more physical description of the water platinum interaction.

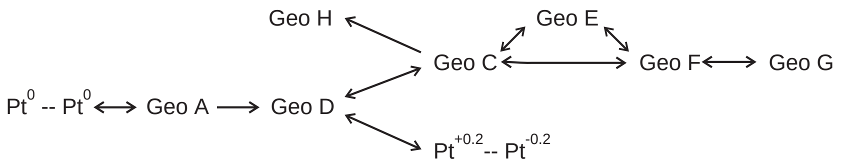

Figure 6.43: Connection between different geometries and states.

6.2.3 Summary of the results for the platinum dimer

The platinum-platinum bond is dominated by the 6s orbitals. The strength of the metallic bond and therefore the total energy of the cluster increases with the occupation of the 6s orbitals (table 6.10). Electron correlation is essential for the correct description of this bond. The coefficient of the ground state (c_0) in the Møller-Plesset calculation is 0.95 and smaller then the value for water (0.97). At first sight, the influence of electron correlation seems to be small enough to proceed with this method. The existence of energetically close electronic states makes the application of more advanced methods necessary. First CASSCF calculations yielded a wave function with a very small contributions from the ground state ($c_0 = 0.8$). This result indicates that the influence is not small and the Møller-Plesset approach to electron correlation is inappropriate. MC-SCF calculations, on the other hand, are costly and not simple (Root flipping has been observed with Pt_2 [336b]). In this work we therefore continue to use Møller-Plesset calculations despite the known problems, to get an initial idea of the role of correlation effects.

The following conclusions could be drawn from the Pt_2-H_2O calculations neglecting the advanced correlation problem:

1. As shown previously for Pt_1-H_2O the interaction between water and the metal decreases with increasing 6s population (table 6.14). The principal problem, strong metallic bonds versus strong water metal interactions, remains unsolved. Since the intermetallic bonds contribute more strongly to the total energy than the water-metal bond, excited metal states are necessary for the correct description of the bond.

2. The interaction of the water molecule with the platinum dimer reduces the overall symmetry of the problem. Metal orbitals, which were previously well separated by symmetry, can now interact. This additional overlap results in an increase of the 6s population, which weakens the water-metal bond. Even very small distortions of the initial geometry (e.g. 0.01° in bond angles) can break the symmetry[7]. This break causes an increase in the 6s population, which results in unphysical jumps between potential energy surfaces. Those jumps can be avoided with costly MC-SCF calculations.

3. A smooth transition between electronic states generated with the method described above are possible (Figures 6.43), but not always in both directions. It is difficult to construct a smooth potential energy surface covering the whole of conformation space.

4. The valence orbitals of the water molecule bond to any orbital with correct symmetry and energy. During the formation of the bond the molecular orbitals of the free dimer mix to form

---

[7] Even at a distance of 100 Å the water molecule is symmetrically present. A simple HF calculation does not converge to the $^1S-^1S$ dimer as observed for the free dimer, but not to the $^3D-^3D$ dimer.

the basis of the water-metal interaction. This mixing is caused by two independent factors:

   (a) The presence of the water molecule reduces the symmetry (see above).
   (b) The water molecule polarizes the platinum cluster and creates a hole in the 5d band for the formation of the bond. The occupation of the formerly empty platinum orbitals with electrons is the quantum chemical equivalent of polarisation (figure 2.3, page 28).

   The interplay of polarisation and 6s population is illustrated for geometry A: The 6s population of the free dimer should be as low as possible for a strong bond to form between the dimer and water. The higher the 6s population, the weaker the adsorption becomes (table 6.14) due to strong repulsion between the 6s electrons and the oxygen. The free dimer created by the dissociation of case AI (figure 6.30) has a total 6s population of 0.279. During the formation of the bond between the dimer and the water molecule electron density (0.174 e) moves from the water molecule into the 5d-band of the dimer. Electron density must therefore move into the 6s orbitals. The observed 6s population (1.021) is twice as large, as this estimate predicts ($0.279 + 0.174 = 0.453$). The extra 0.568 electrons stabilize the cluster by symmetry-allowed orbital mixing in both the metal-metal and metal-oxygen bond. A higher occupation of the 6s orbitals is not possible, since symmetry forbids the corresponding orbital interactions. The exact position of the water molecule mirrors the delicate balance between electrostatic repulsion, 6s population in terms of metal cluster stability and polarisation.

5. The electrons in the 6s orbitals are very mobile and can move freely in the cluster (figures 6.26 and 6.41). This flexibility offers the possibility of far reaching charge transfer and so for cooperative forces in the water-platinum interaction.

6. A comparison of the different geometries shows, that

   (a) the bridging positions for the water molecule are energetically unfavourable.
   (b) the interaction of the hydrogen atoms with the surface platinum atoms contributes significantly to the total interaction energy.
   (c) the symmetry and shape of the available metal orbitals control the site of adsorbtion.
   (d) the second layer (geometries F and G) is also important for the binding of the water molecule.

   An ideal surface model should therefore be build from at least two slabs of platinum and at the surface there should be a sufficient numner of platinum atoms to interact with the hydrogens (section 6.5 (page 192) on Pt_9).

6.3 The platinum trimer

The smallest physically realistic Pt_3-cluster is the equilateral triangle. This cluster represents a small section of the Pt(111) surface and so can opperate as a surface model. A second cluster, a triangle with a 90° angle, poorly describes the Pt(100) surface, and so this section focuses on the equilateral triangle.

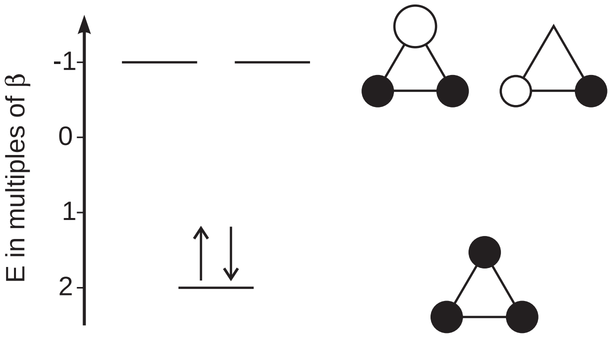

Figure 6.44: Hückel results for equilateral Pt_3.

6.3.1 Electronic structure of the equilateral Pt_3-cluster

Hückel calculations can be used to predict correctly the multiplicity of the ground state (section 5.2, page 119). This method was developed originally for clusters using a single valence electron ECP for the bulk atoms. Despite this restrictions this approach can be apllied to clusters in this section under certain conditions.

First we assume that all 10 valence electrons (5d/6s) populate the 5d band completely. Electrons are then moved from the highest antibonding 5d-orbitals into the 6s band, as many electrons being moved as necessary to fill all bonding 6s orbitals. Problems occur if the electrons are removed from degenerate 5d-orbitals. When the 5d electrons have to be rearranged to avoid asymmetric electron densities in the metal cluster. This problem is less significant, as long as the number of electrons moved is small. Usually one or two electrons may be moved, because the highest 5d orbital is nondegenerate.

Figure 6.44 shows the results of the 6s-Hückel calculations for the case of the equilateral triangle. Hückel calculations in section 5.2 (page 119) predict for the most stable equilateral platinum triangle the 6s band occupied with two electrons and the wavefunction has a multiplicity of 1. Such a trimer can be build from two ^3D and one ^1S platinum atoms [337]. This electron configuration produces an average 6s population of 0.66 per platinum.

Three electron configurations were studied in greater detail:

A No extra electrons remain in the 6s band. This calculation should be close the combination of three ^1S platinums.

B A UMP2-calculation in which one 5d electron remains in the 6s band. Such a calculation tries to model the combination of two ^1S and one ^3D platinum atoms.

C The starting function involves the promotion two electrons into the 6s band, to simulate the combination of two ^3D and one ^1S platinum atoms as predicted by the Hückel calculations.

As predicted by the Hückel calculations case C represents the most stable electron configuration at the Hartree-Fock as well as at the electron correlation level (table 6.16). The introduction of electron correlation does not change the relative order of the electronic states as observed previously for Pt_2. It was not possible to compute successfully any other electronic state with a higher 6s population.

Table 6.17 shows the MP2 6s population in all three cases. The total populations of the 6s orbitals in cases A and B are much higher then expected (predicted as 0 for case and 1 for case

case		$(-E_{TOT} - 354)$ H
A	HF	0.552021
B	HF	0.624394
C	HF	0.625982
A	MP2	0.860970
B	MP2	0.979235
C	MP2	1.053677

Table 6.16: HF and MP2 energies for Pt_3.

case	6s pop
A	0.79350
B	1.98513
C	2.31798

Table 6.17: MP2 6s population in Pt_3.

orbitals	A	C
2 - 35	0.00185	0.00048
2 - 39	0.00226	0.00148
3 - 35	0.00284	0.00023
3 - 39	0.00351	0.00246
sum	0.01046	0.00465

6s orbitals: 2, 3
5d orbitals: 35, 39

Table 6.18: Overlap population in Pt_3.

B), while the 6s population in case C is close to the expected value of 2.0. The introduction of electron correlation enables the occupation of the 6s orbitals to stabilize the cluster (core-valence correlation). The MP2 calculation compensates partially for the static electron correlation caused by the nearly degenerate electronic states. As the occupation of the 6s orbitals increases, this relaxation pathway becomes less important and the additional 6s population decreases (case A: 0.79, case C: 0.32). Table 6.18 accounts for this mechanism in cases A and C. These states have been chosen because both wave functions have the same multiplicity. The atomic orbitals 2 and 3 form the 6s orbital on the first platinum and the atomic orbitals 35 and 39 represent the $5d_{z^2}$-orbital on the neighbouring platinum atoms (double zeta basis set). As the 6s population increases from case A to case C the Mulliken overlap population between the individual atomic functions decreases as well as the total overlap population between both orbitals, indicating the reduced importance of this relaxation pathway.

The mixing of the 5d and 6s orbitals is the first of the two major relaxation pathways for platinum clusters (subsection 5.3.3, page 125). With the second pathway 6s- or 6p orbitals are populated instead of 5d orbitals (section 6.3.2.3).

6.3.2 The interaction of water with Pt3-cluster

The equilateral triangle offers two different adsorption sites: the hollow site coordination over the centre of the triangle and the on-top position above a platinum atom. The first part of this section focuses on the hollow site, the second on the on-top coordination with all possible geometries, and the third is a brief summary of the results for the case of the right-angled triangle.

6.3.2.1 Water bound to the hollow site on the cluster

Figure 6.45 displays the model for the hollow-site adsorption of water on platinum(111) (geometry I). The molecular plane of the water molecule is also the σ_v mirror plane of the platinum cluster and the two oxygen-hydrogen bonds point upwards, yielding C_s symmetry for the cluster. In the first set of calculations, the rotational angle ω was kept constant at 30°, while α was allowed to vary. Optimisation (table 6.19) of the distance between the metal surface and oxygen on the water molecule yielded a bond length of 1.8827 Å at RMP2 level, whith the hydrogens pointing straight ($\alpha = 180°$).

The HF and MP2 energies differ markedly as shown in figure 6.46. The HF potential energy curve has no minimum, but displays a sharp edge close to 2.5 Å. On the other hand the MP2 potential energy curve has a shallow local minimum of −2.4 kcal/mol compared with the maximum at 1.88 Å. After passing through the maximum the energy of the cluster drops dramatically by about 15.6 kcal/mol and equilibrates at a surface-oxygen distance around 5 Å.

To understand the difference between the curves, the 6s populations at HF and MP2 level were analyzed. Figure 6.47 displays the energy and the 6s population calculated from the HF wavefunction. Starting at the expected minimum at 2.0 Å (The HF minimum is always slightly further from the metal surface than the MP2 minimum.) the 6s population increases steadily as repulsion of the oxygen atom diminishes. At about 2.5 Å the 6s population increases rapidly and the jump occurs in the energy curve, where the electron configuration of the metal cluster changes. At short distances the cluster with the lowest 6s population is more stable then that with two 6s electrons, since the repulsion between electrons and the oxygen is minimized. When the oxygen is further from the surface, the 6s electrons move from the 5d band into the 6s band and so stabilize the metal cluster. At this points the slope of the energy curve changes, since another electronic state on the metal interacts with the water molecule. Figure 6.47 shows the transformation of the $^1S^1S^1S$ platinum cluster (The initial 6s population 1.105 is caused by the water metal interaction.) into the $^3D^3D^1S$ cluster through changing the distance between the water molecule and the cluster and provides an excellent example for the polarisation of the metal cluster by the water molecule. Similar effects have been observed by DAI et al. for Pt_3-H and Pt_3-H_2 [338, 339].

Figure 6.48 shows the same transition at MP2 level. The 6s population increases dramatically (A value of 8.45 is still possible for the 6s population as a double zeta basis set was used on platinum. Two orbitals per platinum allow a maximum 6s population of 12, which is not physically reasonable.) during the fall in total energy. At longer distances the 6s population stabilizes at a value of 1.84, which is close to the 6s population of 2 expected for the $^3D^3D^1S$ platinum trimer. This unphysically high value for the 6s population is caused by the incorrect mixing of the two platinum states during the MP2 calculation. Figure 6.49 shows the MP2 energy and the coefficient c_0 of the ground state in the development of the wavefunction. As the distance between the platinum trimer and the water molecule increases c_0 also increases. This increase in the ground state wave function is possibly due to a reduction in importance of the dynamic correlation coupling the bonding and antibonding water-metal orbitals (section 6.2.2.3). At even longer distances the static electron correlation in the metal cluster becomes more important and c_0 drops dramatically to an extremely small value of 0.88, which is far beyond the definition of a small perturbation in the MP2 method. Figures 6.48 and 6.49 demonstrate the breakdown of the Møller-Plesset perturbational approach to the water-platinum cluster interaction.

Figure 6.50 shows the rotation of the water molecule lying above the hollow site around the PtO bond (RMP2 level), which reduces the symmetry from C_S to C_1. The curve is smooth indicating no changes in the electronic state, but the total energy of the cluster is much lower than observed for the Pt_3-H_2O cluster with C_s symmetry ($\Delta_{C_1}^{C_S}E$ = 57 mH = 35.8 kcal/mol). The mechanism of this jump ($\Delta_{C_1}^{C_S}E$) is the same as observed before for Pt_2-H_2O: The rotation decreases the total symmetry of the cluster facilitating the population of the 6s orbitals and stabilizing the metal cluster (symmetric 6s population: 1.1646, asymmetric 6s population: 1.5172). The orientation of the water molecule itself has little effect on total energy (43.7 μH, 0.027 kcal/mol). The broken symmetry also produces a shift of the extrema in figure 6.50 of about 3 degrees, as showed by the marker. At the expected extrema (0°, 30°, 60°, 90°) Gaussian 94 identifies the broken symmetry of the density matrix. Calculations with the correct symmetry yielded higher total energies for the cluster.

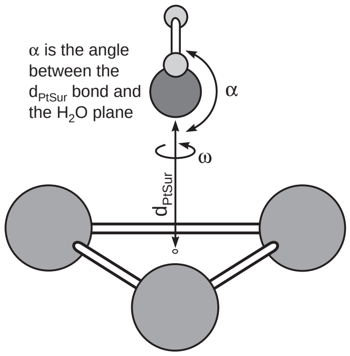

Figure 6.45: The hollow site of Pt(111).

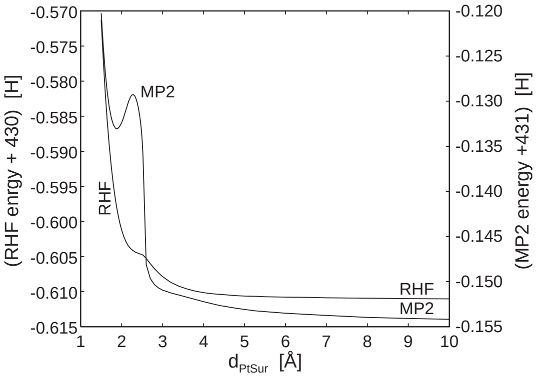

Figure 6.46: Dissociation energies HF/MP2.

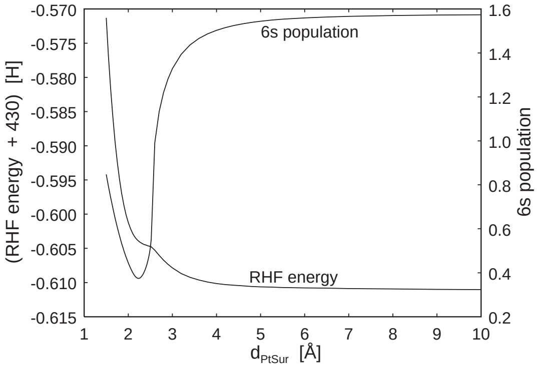

Figure 6.47: RHF energy and HF 6s population.

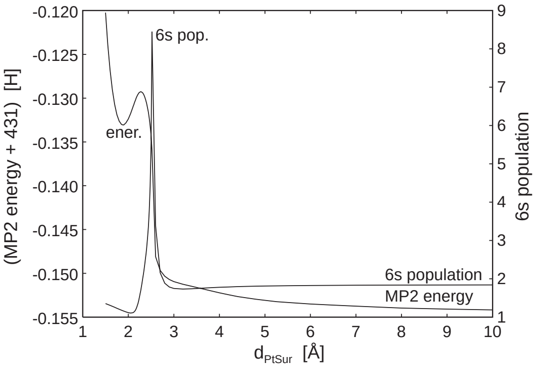

Figure 6.48: MP2 energy and MP2 6s population.

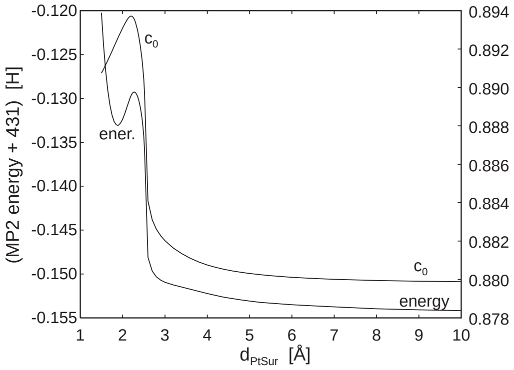

Figure 6.49: MP2 energy and ground state coefficient.

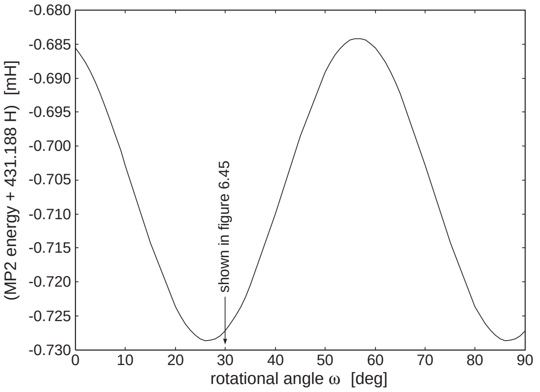

Figure 6.50: Rotation of the hollow site water.

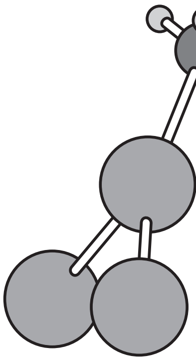

Figure 6.51: Geometry IV.

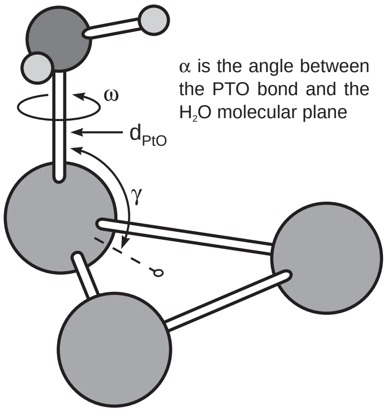

Figure 6.52: Geometry II.

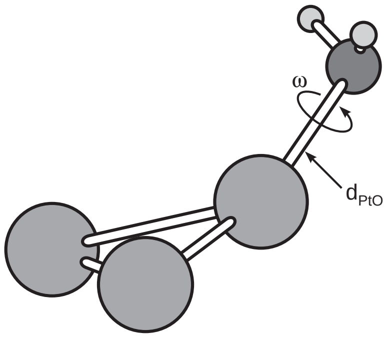

Figure 6.53: Geometry III.

6.3.2.2 Water bound on top

All variables of the cluster shown in figure 6.45 were optimized simultaneously. The result of this optimisation (geometry IV) is shown in figure 6.51. In the course of the optimisation the Pt-Pt-Pt angle increasesfrom 60° to 72° and the water molecule (r_{OH} = 0.9881 Å, $\sphericalangle_{HOH}$ = 105.36°) moves from the hollow position to an unphysical on-top position. This result leads us to the closer examination of the two clusters shown in the figures 6.52 and 6.53. Geometry II is a fragment of an on-top water molecule bound to the Pt(111) surface. Three parameters have been examined in detail: Stretching and dissociation of the PtO bond (d_{PtO}), rotation of the water molecule around the PtO bond (ω), and the waggling of the water molecule (γ). γ is the angle between the PtO bond and the centre of the platinum trimer (figure 6.52). The examination of the $E(\gamma)$ curve demonstrated the existence of a second local minimum (geometry III) shown in figure 6.53. This structure can be seen as a face of a platinum tetrahedron with a water molecule in on-top position.

Figure 6.54 displays the dissociation of the PtO bond. The potential energy curve is smooth, but the binding energy of the water molecule is too high (ΔE_{DISS} = 42.644 kcal/mol), indicating low 6s occupancy for an on-top coordination (table 6.19). Figure 6.55 shows the total energy of the cluster as a function of rotational angle ω. The energy minimum at 0°, coinciding with geometry II, is another example for the importance of hydrogen-platinum interactions in the water metal system (ΔE_{ROT} = 17.882 kcal/mol). This interaction is also apparent from the strong Mulliken overlap population (bonding Pt: −0.036, next neighbour: 0.028, second next neighbour: 0.006) between the hydrogens and the surface atoms, at which they are pointing.

Figure 6.56 shows the cluster energy and PtO bond length (d_{PtO}) as the angle between the PtO bond and the metal surface (γ) increases (α, tha angle between H_2O plane and the PtO bond, fixed at 106.36°). As the water molecule is moved around the cluster the bond length increases and reaches a plateau at 2.21 Å. The local minimum at 150° proofs the existence of a second stable Pt_3-H_2O structure (geometry III). A single point calculation with a slightly distorted geometry gave a cluster (geometry IIIa) with a lower energy then expected (table 6.19) from figure 6.56. A similar effect has been observed previously for Pt_2-H_2O.

The movement of the water molecule allows a higher 6s population (geometry II: 2.03, geometry III: 2.28) and stabilizes the cluster ($\Delta_{II}^{III}E(MP2) = 0.35$ kcal/mol (table 6.19)). At this point the C_S symmetry stabilizes the 5d-6s separation and inhibits further 6s population. As for the Pt_2-H_2O

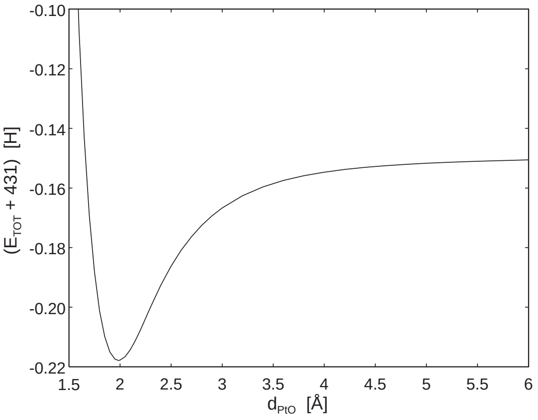

Figure 6.54: Dissociation of geometry II.

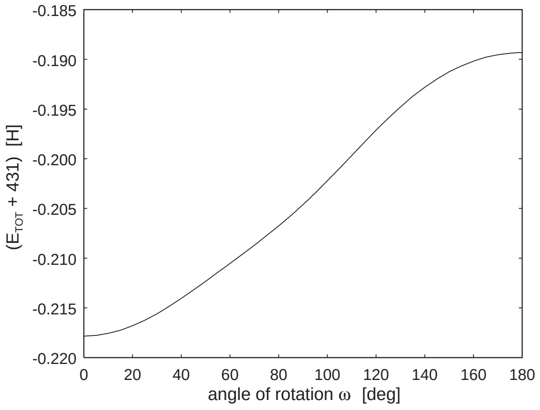

Figure 6.55: Rotation of H_2O in geometry II.

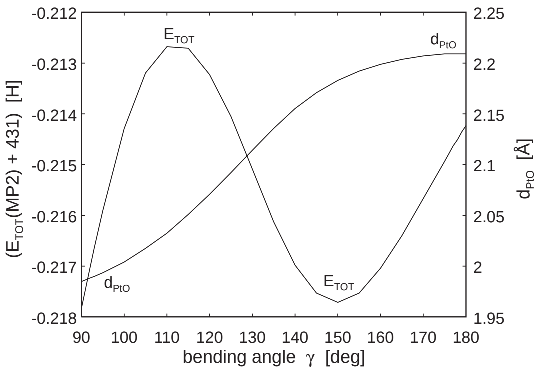

Figure 6.56: Movement of the water molecule.

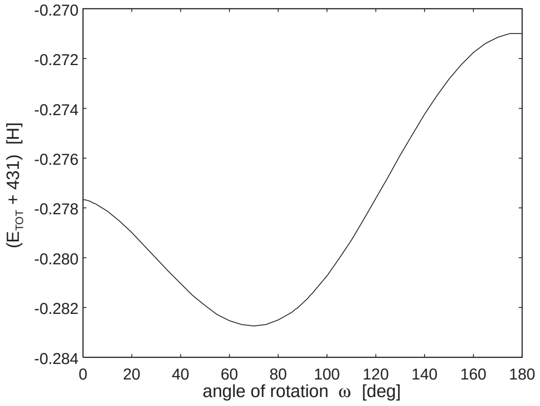

Figure 6.57: Rotation of H_2O in geometry III.

		geometry I	geometry II	geometry III	geometry IIIa	geometry IV
site		hollow	on-top	on-top	on-top	on-top
β	[deg]	60.00	60.00	60.00	60.00	72.63
d_{PtO}	[Å]	2.4702	1.9848	2.1430	2.1430	2.2314
ω	[deg]	90.0	0.0	0.0	0.001	0.0
γ	[deg]	90.0	90.0	144.74	144.74	177.67
α	[deg]	180.0	106.38	119.68	119.68	118.51
$(E_{RHF} + 430)$	[H]	-0.598111	-0.659990	-0.647864	-0.667820	-0.653290
$(E_{MP2} + 430)$	[H]	-0.133059	-0.217826	-0.218377	-0.277631	-0.262339
6s population		1.1646	2.0303	2.2853	3.0541	2.2498

α: angle between the H_2O plane and the PTO bond

β: Pt-Pt-Pt angle at the H_2O bonding platinum

Table 6.19: Optimized structures for Pt_3-H_2O.

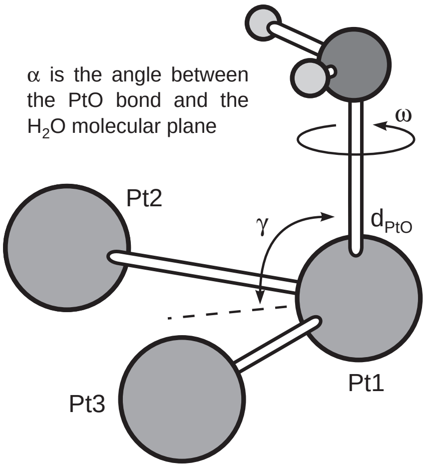

Figure 6.58: Pt_3-H_2O geometry V.

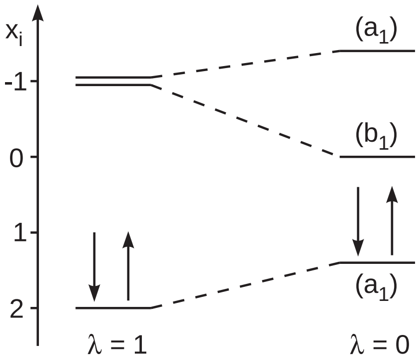

Figure 6.59: Hückel orbital energies.

system (section 6.2.2.2, page 164) electron density flows into the 6s band, away from the PtO bond and towards the ends of the metal cluster while the total 6s population increases. This movement reduces the repulsion between the 6s electrons and the oxygen and stabilizes the bond between platinum and water.

A single point calculation with C_1 symmetry ($\omega = 0.001°$) gives a lower total energy, because the reduced symmetry allows further population of the 6s orbitals (geometry III: 2.28, geometry IIIa: 3.05). Figure 6.57 shows the rotation of the water molecule. The curve for geometry III has a local minimum at 70° in contrast to the rotation of the water molecule in geometry II (figure 6.55). This minimum is caused by an extended charge transfer (minimum: 0.134 e, geometry IIIa: 0.123 e), which counteracts the small decrease of the 6s population (minimum: 3.046, geometry IIIa: 3.054). The decrease of the 6s population destabilizes the cluster, whereas charge transfer form the water molecule to the Pt_3 part stabilizes the cluster. Similar behaviour has been observed in Pt_2-H_2O (section 6.2.2.4, page 171). The local minimum in figure 6.57 is another example of the competition between charge transfer and 6s population for the strength of the platinum water bond. During the rotation the total charge on the platinum atom increases and simultaneously the charge distribution becomes more homogeneous. At the local minimum one hydrogen points directly at the platinum below indicating a strong Coulomb interaction between surface platinum atoms and the hydrogens in the water molecule.

6.3.2.3 Pt3 surface model for the Pt(100) surface

A platinum triangle with a right angle is a poorer model for the Pt(100) surface than the equilateral triangle for the Pt(111) surface. Since quantum chemical results do not differ much between those two cluster geometries, this section presents a brief summary of the results.

As the distance between platinums Pt2 and Pt3 (figure 6.58) increases the interaction between the atoms decreases. Hückel calculations (section 5.2, page 119) predict, that the degeneracy of the antibonding orbitals is lifted. While one orbital transforms into a nonbonding orbital the second becomes more antibonding. Meanwhile, the bonding orbital becomes less strongly bonding, as the interaction between both platinums declines (figure 6.59). Equation 6.2 describes the Hückel orbital energies (ϵ) as a function of the scaling factor λ ($0 \leq \lambda \leq 1$; $\lambda = 0 \rightarrow$ no interaction, $\lambda =$

1 → full interaction) for the resonance integral involving platinums Pt2 and Pt3.

$$\epsilon_i = \alpha + x_i\, \beta$$
$$x_1 = -\lambda \qquad x_2 = \frac{1}{2}\,\lambda + \sqrt{2 + \frac{1}{4}\,\lambda^2} \qquad x_3 = \frac{1}{2}\,\lambda - \sqrt{2 + \frac{1}{4}\,\lambda^2} \tag{6.2}$$

Figure 6.59 shows a plot of the corresponding orbital energies. The left side of the plot displays the equilateral configuration ($\lambda = 1$), the right side the Hückel equivalent of a linear molecule or a right-angled triangle ($\lambda = 0$). The true right-angled triangle lies somewhere between these limits. Since Hückel calculations predict a singlet ground state for the surface model, the calculations concentrated on the singlet wave functions. The optimisation (geometry V) of the cluster shown in figure 6.58 yielded a total MP2 energy of −431.181 H (table 6.20). The dissociation curve of the water molecule is smooth, yielding a water-metal binding energy of 34.51 kcal/mol. This high value for the binding energy is consistent with the low 6s occupancy of 1.75. The right angle in the platinum cluster enables a stronger interaction of the surface platinums with hydrogens (MOP 0.032), but the rotational energy E_{ROT} (14.1 kcal/mol) is about 4 kcal/mol lower than in geometry II. This difference can be explained by shorter PtH distances in geometry V (3.5333 Å) with a correspondigly stronger interaction (MOP 0.004) compared with a distance of 3.7127 Å and an overlap population of 0.003 in geometry II.

As in calculations on the equilateral structure γ was varied systematically between 90° and 180° with a fixed value of 1.9896 Å for the PtO bond. The resultant curve is similar to that for geometry II (not shown in section 6.3.2.2), although the energy difference between 90° and 180° is much smaller for geometry V (7.9 mH compared with 13.3 mH). Both curves have a shallow local minimum (geometry II: 135°, geometry V: 145°), which suggest the existence of a second stable geometry for cluster V similar to geometry III, but with a higher value for γ.

The optimisation of geometry V was repeated for the triplet state (geometry Va). The total MP2 energy (-431.760 H) of the cluster Va is lower then for geometry V, which is consistent with the increased 6s population of 3.03. No changes of electronic state were observed in the dissociation of the water molecule. The low value of water-metal interaction energy (14.038 kcal/mol), which agrees well with the experimental bonding energy, is a consequence of the high 6s population and consistent with the long PtO bond length of 2.409 Å.

The 6s populations of the clusters V and Va suggest a second pathway for the 5d-6s interaction, to be discussed in greater detail in the subsections 6.4.2.1 and 5.3.3 (page 125). The totally symmetric 6s orbital (a_1) has such a low energy, that a population of this orbital is energetically more favourable than the occupation of an antibonding 5d orbital. Without any artificial electron redistribution, as was necessary in $Pt-H_2O$ and Pt_2-H_2O, the HF-calculation converges to the optimal 6s population. In the triplet case the a_1 orbital is still doubly occupied and the b_1 orbital is singly occupied. The other singly occupied orbital is an antibonding 5d orbital. In the course of the HF calculation b_1 mixes with 5d and it is not possible to identify the b_1 orbital as a separate orbital. This mixing lowers the energy of the b_1 orbital and it becomes more bonding. In contrast to figure 6.59 a 6s population is possible, which remains bonding. The energy of nonbonding 6s orbitals is only poorly described by Hückel calculations. Orbitals found slightly antibonding in Hückel calculations were found to be slightly bonding in Hartree-Fock. The b_1 orbital may lie closer to the 5d band, as the Hückel calculations suggest. Section 5.3.3 (page 125) discussed this problem in greater detail.

The Hückel calculations predict, that the equilateral geometry should be more stable then the

	geometry V	geometry Va
d_{PtO} [Å]	1.9896	2.4087
α [deg]	107.94	102.47
6s pop.	1.75363	3.03265
(E_{MP2} + 431) [H]	−0.180674928	−0.218744777
(E_{HF} + 431) [H]	−0.651190500	−0.759573398

$\omega = 0°$, $\gamma = \beta = 90°$

Table 6.20: Geometries for the right-angled Pt_3-triangle.

right-angled geometry for similar 6s populations, because the 6s electrons dominate the stability of the metal cluster. This prediction was verified by MP2 calculations. Geometry V ($E_{MP2} = -431.181$ H) has a 6s population of 1.753 while the 6s population in geometry II ($E_{MP2} = -431.218$ H) is only slightly higher 2.03. An increase in 6s population (without change in electronic state) of about 0.3 should give an extra energy of 0.5 mH (energy difference between geometry II and III) and not 36 mH as observed between geometry II and V. Geometries Va and IIIa have similar 6s populations (Va: 3.033, IIIa: 3.054) but the energy between the clusters differs about 58 mH. The right-angled geometry is always energetically higher then the equilateral triangle.

6.3.3 Summary of the results for Pt_3

1. The Hückel (chapter 5, page 117) scheme can be used with some restrictions for 18 electrons ECP calculations. Problems occur only with the nonbonding orbitals.

2. Two relaxation pathways for the 5d-6s interaction have been identified:

   (a) 5d and 6s orbitals mix to form hybrid orbitals, provided they have correct symmetry.

   (b) If the 6s orbital energies are low enough, these 6s orbitals are populated in preference to the 5d orbitals.

   Both pathways increase the 6s population and can obscure the Hückel predictions. The exact mechanism and the correlation between Hückel and HF calculations was discussed in subsection 5.3.3, page 125.

3. The equilateral triangle with water in the hollow position demonstrates the correlation of the platinum-oxygen distance and the 6s population. As the water molecule moves away from the surface electron density flows from the 5d band into the 6s orbitals. This electron flow is so large, that the movement of the water molecule causes a change in the electronic state of the metal cluster.

4. The equilateral triangle with water in the hollow position provides a good example of the breakdown of the MP2 method in respect of the water-platinum interactions. The dynamical correlation can be included very well, but the static electron correlation is beyond the scope of this method.

   In small clusters the different electronic states are well separated in energy and electron correlation is dominated by dynamical effects. In these cases the MP2 method works reasonably well. The energy difference between the electronic states becomes smaller, as the cluster size increases. This picture is controlled by static electron correlation and the MP2 approach breaks down.

5. The results obtained for $Pt-H_2O$ and Pt_2-H_2O have been confirmed in those for Pt_3-H_2O:
    (a) The 6s population stabilises the cluster, but weakens the water-metal interaction. The higher the 6s population, the lower the total energy of the cluster, and the water-platinum bond becomes weaker.
    (b) Electron density flows into the 6s-band away from the water-platinum bond to the edges of the cluster. This electron flow forms the basis of cooperative forces in the water-metal interaction.
    (c) The reduction of the cluster's symmetry facilitates the occupation of the 6s orbitals. Some movement of the water molecule break the original symmetry and can cause unphysical jumps between potential energy surfaces. CAS-SCF calculations can help to minimize the size of the jumps, but the important orbitals are more difficult to find than in Pt_2-H_2O. The energy jump becomes smaller as the active space increases, but the computational costs rise. A detailed analysis of this problem is beyond the limits of the thesis and will be subject of further research.
    (d) The interaction between the hydrogen atoms on the water molecule and the platinums below is weak, but has a significant influence on the orientation of the water molecule.

This agreement with the results found so far shows, that these phenomena are not dependent on cluster size but underlie the water-metal interaction.

6.4 The Pt_5-pyramid

Several geometries are possible for a Pt_5 cluster. This section focuses only on the tetragonal pyramid (figure 6.60) with a platinum-platinum distance of 2.77 Å. The pyramid was chosen for several reasons:

1. The first successful quantum chemical calculations on platinum-water interactions were performed with such a cluster [64].
2. The calculations on Pt_2-H_2O (section 6.2.2) and Pt_3-H_2O (section 6.3.2) showed that the most stable clusters are either the vertices or faces of a pyramid.
3. Three-dimensional surface models are closer to reality than two-dimensional models (section 6.6), because the width of the 5d band lies closer to the experimental value.

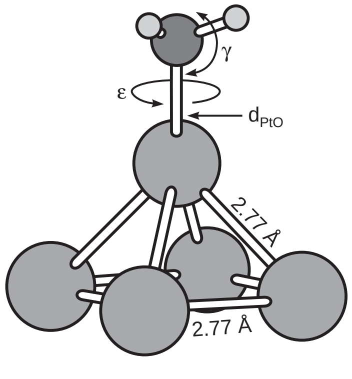

Figure 6.60: Geometry of the Pt_5-H_2O cluster.

With increasing cluster size, the problems with different electronic states are magnified. Even the smallest change in γ (the angle between the platinum-oxygen bond and the molecular plane of the water molecule) and ϵ (the rotational angle around the platinum-water bond) induced large changes in total energy. A total of 46 calculations was done to analyse these energy jumps: A smooth description of the potential energy surface was only possible when the symmetry instruction in Gaussian 94 was turned off (keyword: `NoSYMM`) with an initial-guess function chosen from a totally asymmetric cluster. CISD (**c**onfiguration **i**nteraction **s**ingle and **d**ouble excitations) calculations showed, that the symmetry module of G94 generated wavefunctions which did not describe the ground state, but always another state. A set of CAS-SCF calculations including orbitals close to the HOMO-LUMO gap showed that no simple solution to this problem was available.

6.4.1 Electronic structure of the Pt_5-pyramid

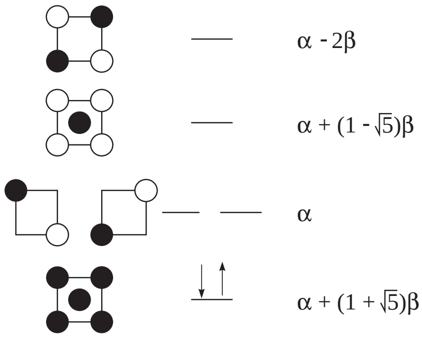

Figure 6.61: Hückel results for Pt_5.

Figure 6.61 shows the results of the Hückel calculations (section 5.3.1, page 122). Either two or four 6s electrons could form stable metal clusters. Previous results suggest that the highest 6s population should create the most stable metal cluster. The troublesome Pt_5 cluster mentioned above have a 6s population higher then 2, but the clusters were unsuitable as models for thesurface, since a distortion of ϵ about 20° (rotation around the platinum-oxygen bond) caused a second unphysical energy jump. This problem is caused by the degenerate nonbonding 6s molecular orbitals. The binding of the water molecule to the metal cluster lifts this degeneracy and the singlet wave function becomes more favourable than the triplet function. For a smooth rotation around the platinum-water bond the orbitals mix, as their nodal planes rotate with the water molecule to ensure a smooth transition (subsection 5.3.4, page 126 for details). A 6s population of 2 instead of 4 eliminates this problem and simplifies the description of the energy surface.

This simplification should have only a small influence on the strength of the platinum-water bond. The cluster can be separated into two layers: the platinum atom in the top layer, which contributes directly to the water-metal bond and the four atoms at the second layer, which do not contribute significantly to the bond. The strongest influence on the platinum-water bond strength has the 6s population at the top of the pyramid. The 6s orbital of the top platinum does not participate in the nonbonding orbitals, as shown in figure 6.61. Electrons in the nonbonding orbitals should therefore stabilize the cluster but should have little influence on the metal-water bond. Hückel calculations predict a 6s population of 0.553 at the top of the pyramid in both cases and the repulsion between the platinum at the top and the oxygen should therefore be the same.

A platinum cluster with a total 6s population of 2 should therefore serve as an ideal model, since the total energy of the metal cluster is not important for the interface model.

6.4.2 The interaction of the Pt_5-pyramid with water

All systematic attempts to create a cluster similar to that predicted by the Hückel results failed. The quantum chemical calculations started with the hydrogens pointing straight upwards ($\gamma = 180°$), because the high symmetry of the cluster (C_{2v}) reduced the runtime of the Gaussian 94 jobs. Any small distortion of the angles γ and ϵ ($\Delta\gamma = \Delta\epsilon = 0.001°$) caused unphysical energy jumps as observed previously for Pt_3-H_2O and Pt_2-H_2O. These jumps are caused by an abrupt change in the symmetry of the cluster. A small distortion in γ reduces the symmetry to C_S and a distortion in ϵ reduces the symmetry to C_1. The distortion of ϵ is more critical than that of γ. The reverse approach, starting from an asymmetric cluster, produced an asymmetric wavefunction on the symmetric cluster after the removal of the distortion.

The occupation of the 6s orbitals and hence the electronic state of the cluster depends critically on the distance between the platinum cluster and the water molecule. All test calculations (including all distortions) were repeated for different platinum-oxygen bond lengths. Finally a cluster was found that could be distorted ($\Delta\gamma$, $\Delta\epsilon$) without any energy jumps, but retains a symmetric wavefunction.

d_{PtO}	[Å]	2.2973
γ	[deg]	141.77
ϵ	[deg]	45.0
6s pop	total	2.976
6s pop	top	0.734
q_{TOP}	[e]	−0.2035
Δq	[e]	0.1261
E_{TOT}	[H]	−668.101599
ΔE_{DISS}	[kcal/mol]	17.229

Table 6.21: Optimized Pt_5-H_2O cluster.

Table 6.21 summarizes the results for the optimized Pt_5-H_2O cluster. The dissociation energy of 17.229 kcal/mol is close to the experimental value, which agrees well with a 6s population of 0.734 at the top of the pyramid. This value is close to the value of 0.7 to 0.8 suggested in the literature for surface platinum atoms [285]. The platinum atom at the top carries a negative charge of −0.203 e. This negative charge is caused by the 6s population within the cluster (subsection 5.3.1, page 122), but serves as a model for the electron spill at the surface, which weakens the water-metal bond.

In the free platinum cluster ($d_{PtO} = 12.2973$ Å, section 6.4.2 for details) the total 6s population has a value of 2.958 and the 6s population on the top platinum is 0.714. During formation of the water-platinum bond the total 6s population increases by about 0.018. The change of the 6s population on the top platinum is +0.020. The formation of the bond leads to a smallincrease in 6s population at the top, while the bulk atoms at the foot of the pyramid do not change significantly. The charge transfer from the water molecule to the metal cluster is 0.1261 e. This charge accumulates at the top of the platinum pyramid ($q_{TOP} = -0.2035$ e in Pt_5-H_2O, $q_{TOP} = -0.0874$ e in the free pyramid, $\Delta q_{TOP} = -0.1161$ e). Only 7.9% of the total charge transfer flows into the base of the pyramid. The charge on the top platinum increases about 0.1161 e, but the 6s population increases only by about 0.02 e. Hence most of the charge flows into the 5d orbitals of the top platinum. The binding mechanism is the same as observed before: The water molecule binds locally to a platinum. With this bond formation electron density flows into the bonding platinum's 5d orbitals. This flow is again connected to a small increase in the 6s population. The 6s electron density stays on the top platinum, because intramolecular charge transfer is not supported by the water hydrogens. In the Pt_2-H_2O and Pt_3-H_2O clusters with large intramolecular charge transfer the negative charge on the surface platinums is stabilised by Coulomb interactions with the positive hydrogens above the surface. In the Pt_5-H_2O cluster the distance between the bulk platinums at the bottom and the hydrogens at the top is too long to support this mechanism. The hydrogens point upwards and the cluster's geometry is close to the bilayer structure suggested by the ice rules for water bilayers ($\gamma \approx 125°$, sections 1.1.3 (page 4) and 8.2 (page 265)).

Figures 6.62 (including the water $3a_1$ orbital) and 6.63 (including the water $1b_1$ orbital) show the bonding orbitals of the platinum-oxygen bond. This bond is localised between the top platinum and the oxygen, because the coefficients of the other atomic orbitals contributing to this molecular orbital are smaller than a tenth of the values for the bonding platinum. The platinum atoms on the base of the pyramids are 1.4 Å below and above from the cluster's mirror plane shown in the figures. The observed contribution of the basal atoms to the electron density in the mirror plane is therefore naturally low.

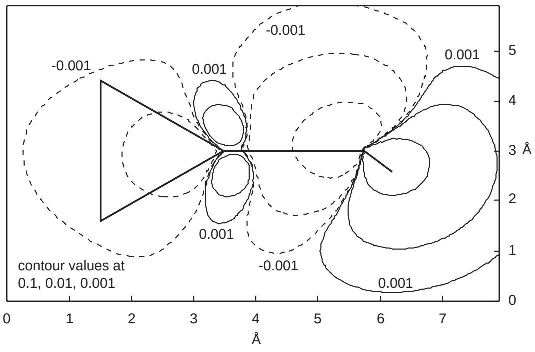

Figure 6.62: Bonding orbital in Pt_5-H_2O (H_2O $3a_1$).

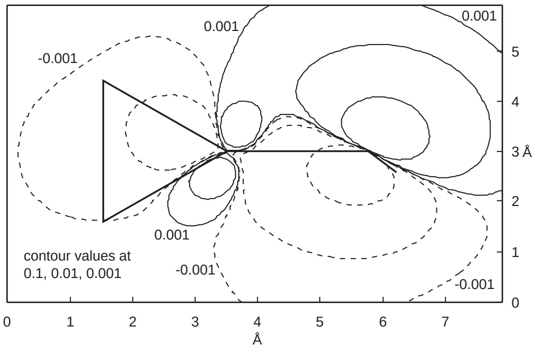

Figure 6.63: Bonding orbital in Pt_5-H_2O (H_2O $1b_1$).

6.4.2.1 Dissociation

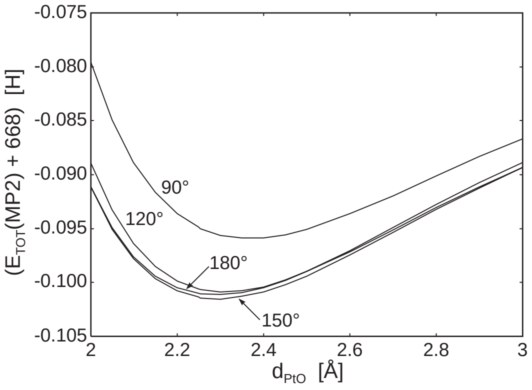

Figure 6.64: Dissociation Pt_5-H_2O.

Figure 6.64 shows the total energy of the Pt_5–H_2O pyramid as a function of the platinum-oxygen distance d_{PtO} for various values of γ. The curve for the optimised geometry ($\gamma = 141.8°$) is is very similar to that for $\gamma = 150°$.

The range for d_{PtO} (2 Å $\leq d_{PtO} \leq 3$ Å) is much smaller than before, since all quantum chemical calculations on Pt_5 clusters showed that distance-related energy jumps are seen first in this interval. Table 6.22 lists the important parameters for the minima of the dissociation curves. The total 6s population varies only little lying between 2.96 and 2.98 for all points. The same is observed for the 6s population of the top platinum atom: All values lie in a small interval between 0.72 and 0.74. These values for the 6s population agree well with those found for the free platinum pentamer. In the free platinum cluster ($d_{PtO} = 12.2973$ Å) the total 6s population has a value of 2.958 and the 6s population on the top platinum is 0.714. Since energy discontinuities are generally assiciated with large chanhes in 6s population, a relatively constant 6s population suggests such discontinuities are unlikely.

With increasing values of γ the charge on the top platinum becomes smaller. The charge decrease is proportional to the charge transfer between the platinum cluster and the water molecule. This change is caused by the relative importance of the water $3a_1$ and $1b_1$ orbitals for the platinum-water bond. For large values of γ the bond is dominated by the $3a_1$ orbital. The widely spreading $3a_1$ orbital is partially bonding and charge transfer along this orbital is unfavourable. For small values of γ (around 90°) the platinum-water bond is dominated by the $1b_1$ orbital, which is strictly non-bonding and tighter. Charge transfer is therefore easier from the non-bonding $1b_1$ orbital (Compare with subsection 6.1.4, where the platinum-water bond is not obscured by additinal platinum-hydrogen interactions).

The 6s population increases slightly with increasing values of γ and so shows an opposite effect to the charge transfer. This increase of the 6s population can be explained via the different water orbitals. The platinum-water orbital containing the $3a_1$ water orbital has a higher 6s contribution

γ [deg]	d^{*}_{PtO} [Å]	(E_{TOT} + 668 H) [H]	ΔE_{ADS} [kcal/mol]	6s pop total	6s pop top	q_{TOP} [e]	Δq [e]
90	2.35	−0.095912	13.661	2.964	0.720	−0.303	0.1814
120	2.30	−0.100896	16.788	2.974	0.729	−0.239	0.1515
142^{**}	2.30^{**}	−0.101599	17.229	2.976	0.734	−0.203	0.1261
150	2.30	−0.101526	17.183	2.977	0.735	−0.193	0.1180
180	2.30	−0.101146	16.945	2.978	0.738	−0.178	0.1041

* not optimized ** optimised cluster

Table 6.22: Local minima in the Pt5 H2O dissociation.

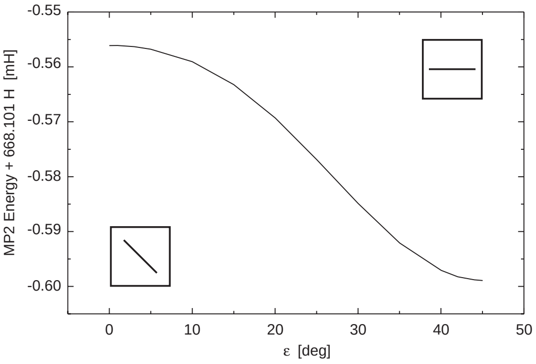

Figure 6.65: Rotation of H_2O around the PtO bond in Pt_5-H_2O.

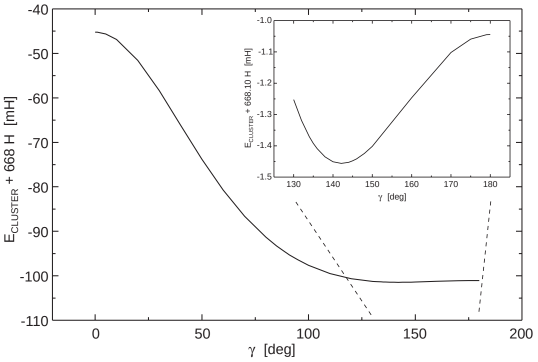

Figure 6.66: Wagging of H_2O in Pt_5-H_2O.

than the $1b_1$ orbital. With the increasing dominance of the $3a_1$ orbital the 6s population increases despite charge transfer and orientation of the water molecule.

6.4.2.2 Rotation

Figure 6.65 shows the total energy of the Pt_5-H_2O as a function of the rotational angle ϵ. The optimized structure ($\gamma = 142°$, $\epsilon = 45°$) is at the minimum of the smooth curve. No energy jumps are observed during the rotation, reducing the cluster symmetry from C_S to C_1.

Bonding to the water molecule lifts the degeneracy of the non-bonding 6s orbitals. In the singlet state of the $^1S + 4 \times {}^3D$ platinum pentamer one of these orbitals is double occupied, while the other remains empty. During the rotation of the water molecule the nodal planes of the non-bonding platinum 6s orbitals move with the water molecule (sections 5.3.4, page 126 for details). This is not possible with unsymmetrical occupied 6s orbitals. Figure 6.65 shows a graph with no jump about 20°, which indicates the absence of this problem of the unsymmetrical 6s population. Figure 6.65 proofs so, that the platinum cluster used for this set of calculations is build from 3 ^1S platinums and 2 ^3D atoms despite the high 6s population of 2.96. This high 6s population is caused by relaxation pathways, which were be discussed in section 5.3.3 (page 125) in greater detail.

The rotational barrier is negligible small (0.03 kcal/mol) and the water molecule can rotate freely around the platinum-water bond. This rotation is so easy, because the bulk platinums at the bottom do not interact with the hydrogens (overlap population 0.0002). The rotational barriers observed in Pt_2 and Pt_3 are mainly caused by the platinum hydrogen interaction.

6.4.2.3 Wagging

Figure 6.66 shows the total energy of the Pt_5-H_2O cluster as a function of the angle γ between the plane of the water molecule and the PtO bond. The bond length in all calculations was kept at 2.25 Å, the optimized bond length for $\gamma = 180°$.

The energy required to move the hydrogens upwards ($\gamma > 141.77°$) is very small (0.26 kcal/mol, detail plot in figure 6.66), while the energy for the reverse movement ($\gamma < 141.77$) is difficult (35.29 kcal/mol). This exceeds the strongest binding energy found in this system (-17.3 kcal/mol). The bond between platinum and hydrogen is much weaker than that between platinum and oxygen. The platinum-oxygen bond should therefore be much longer than 2.254 Å as used in the calculation. The relaxation of the bond length during the rotation lowers the barrier, but was too costly to compute.

The low orientational energy of the hydrogens is important for the structure of the water bilayer on the platinum(111) surface. The influence of the metal surface on the orientation of the water molecules is very small and the hydrogens will be orientated according to the growing ice lattice.

6.4.3 Summary of the results for the platinum pyramid

1. Without the Hückel calculations it would have been impossible to find a suitable Pt_5-H_2O cluster as a working surface model. The chosen 6s population allowed us to construct a potential energy surface without any energy discontinuities due to changes in the symmetry of the cluster.

2. The 6s population on the top platinum atom (0.714) agrees with the values predicted by Bigot and Minot (0.7 - 0.8) [285] for surface atoms, but is about 34% higher than the Hückel value (0.533). This error is acceptable in view of the simplicity of the Hückel model (section 5.3, page 121).

3. The platinum pyramid has a small dipole moment, which can be used as a model for the electron spill at the surface. This dipole moment points into the wrong direction, if the cluster is used to model another adsorption site as done in the literature [64]. The platinum pyramid is only suitable as a model for the on-top position of the water molecule.

4. The negative charge of the top platinum and the high 6s population of 0.7 on this atom guarantee the correct binding energy (17.23 kcal/mol), since as both properties, 6s population and charge on the top platinum, dominate the Coulomb repulsion between oxygen and the metal.

5. The binding mechanism between platinum and water is the same as that before for the other Pt_n-H_2O clusters. The $3a_1$ and $1b_1$ orbitals of the water interact with platinum 5d orbitals. This interaction leads to a small increase in 6s population, but here the intramolecular charge transfer of the 6s electrons is not possible. The bulk platinum atoms in the bottom layer, the possible destination of 6s electron flow, are too far from the hydrogens of the water molecule to stabilize the additional 6s electron density through Coulomb interaction.

6. All calculated dissociation curves were smooth and without any discontinuities involving different electronic states. The 6s population did not change during the dissociation, which indicates the energy differences to the other states is larger than the polarisation energy of the metal cluster by the water molecule.

7. The rotational energy of the water molecule is negligibly small (0.03 kcal/mol) and the total energy curve of the cluster does not show any discontinuities at 20°. This suggests, that the metal cluster can be described as the result of the combination of 3 ^{1}S and 2 ^{3}D platinums despite the high 6s population of 2.9. The high 6s population can be explained by two relaxation pathways, which were discussed in section 5.3.3.

8. The orientation of the hydrogens (γ) can be changed easily (0.26 kcal/mol) as long as the hydrogens point away from the surface. Both the small orientational energy and the rotational energy suggest that the precise structure of the water bilayer is controlled by the ice structure and not by the platinum. The platinum-water interactions do not allow the hydrogens to point directly to the metal surface ($\gamma \leq 90°$).

9. The chosen Pt_5-H_2O pyramid is a suitable model for a revised classical water-platinum interaction potential, but the lack of further surface atoms in the top layer results in too small energy barriers for the orientation of the individual water molecules. Attempts to compute extended surface models with such a model would therefore give poor results, as the interface structure would be dominated by the water-water interaction potential.

6.5 The Pt_9-cluster

The Pt_9-H_2O cluster is the largest of the series of calculations. Due to its size and the long runtimes of the computer jobs (optimisation: 9d 17h), calculations were restricted to single point calculations (approx. 24h runtime). Figure 6.67 shows the optimized structure. The dissociation energy was computed by setting d_{PtO} to 12.1662 Å and using the wavefunction of the optimised cluster as guess function. This procedure works well at Hartree-Fock level as the total 6s population does not change much (Pt_9-H_2O: 3.666, free Pt_9: 3.374), but fails at MP2 level (Pt_9-H_2O: 6.187, free Pt_9: 7.571). The breakdown of the MP2 approximation is already evident from the optimized cluster, as the coefficient of the groundstate wave function c_0 is as low as 0.67.

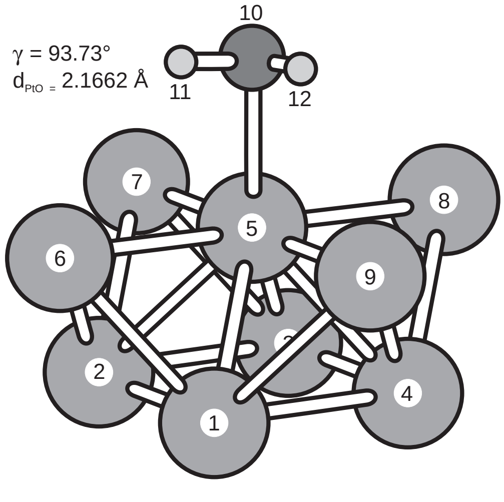

Figure 6.67: Optimized Pt_9-H_2O.

Even at Hartree Fock level the bonding mechanism is not easy to extract from the two points. The binding energy is low ($\Delta E = 2.724$ kcal/mol) despite a low 6s population on platinum 5 (0.446). Strong Coulomb interactions ($q_{Pt-5} = -0.956$ e, $q_{Pt-6} = +0.066$ e) weaken the platinum-oxygen bond. The charge distribution at the platinum surface (atoms 6, 7, 8, 9) reflects the mirror image charges caused by the water molecule at the platinum surface, but here the charge is not associated with 6s electron density as observed previously. Platinums 6 and 9 are more negative than platinums 7 and 8 (mirror charges, positive hydrogens lie above them), but the 6s populations at these atoms are lower (Pt-6: 0.295, Pt-7: 0.458). At platinum atoms 6 and 9, which Coulomb interact with the hydrogen atom of the water molecule, the 5d electron population is high, suggesting that the platinums were originally ^{1}S states, whereas platinums 7 and 8 were

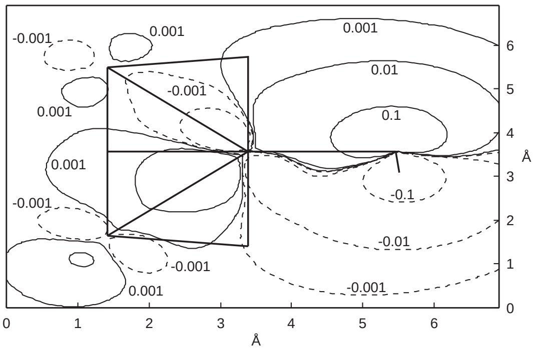

Figure 6.68: Bonding orbital in Pt_9-H_2O (H_2O $3a_1$).

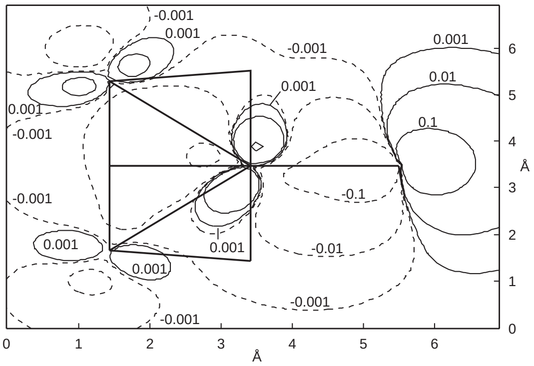

Figure 6.69: Bonding orbital in Pt_9-H_2O (H_2O $1b_1$).

in ^3D state. The polarisation of the surface can be inferred from the charge difference between platinum atoms 6 and 7. The binding of the water molecule increases the difference by about 0.06 e. Meanwhile the difference in 6s populations changes by 0.2214. A large change the 6s population causes a small change in the charge distribution. This suggests, that the 6s electron flow is directly associated with a change in 5d electron density, suggesting a circular electron current. A detailed analysis of this mechanism in Pt_9-H_2O incorporating all valence electrons is beyond the scope of this work, and is subject of further research.

Charge transfer from the water molecule to the platinum cluster is 0.208 and during the formation of the platinum-water bond the charge on platinum 5 increases by 0.375 e, nearly twice as much as the charge transfer. Meanwhile, the 6s population on platinum 5 increases by only 0.022, inferring that the addititional charge has to be in the 5d band. This part of the interaction is the same as observed previously for the smaller clusters: The free electron pair of the water molecule overlaps with a platinum 5d orbital (figures 6.68 and 6.69), which leads to a small rise of the 6s population. This new bond is again localised between the atoms, but the circular 5d-6s electron flow obscures the mechanism.

With increasing size of the platinum cluster the MP2 method becomes less valid for the calculations of the platinum-water interface. This trend is visible in the coefficient of the ground state c_0 in the MP2-wavefunction:

Pt_n	1	2	3	5	9
c_0	0.97	0.95	0.88	0.78	0.68

Table 6.24: Ground state coefficient c_0 versus cluster size.

With increasing cluster size the different electronic states become energetically less distinguishable and static electron correlation becomes more important. The Pt_9-H_2O is certainly beyond the limitations of the method.

The MP2 binding energy of the water molecule is much higher than that of the HF calcualtion. This increase is not caused by a stronger platinum-oxygen bond as the Mulliken overlap population is nearly the same at HF and MP2 levels (MP2: 0.101, HF: 0.106), but by an increase in the platinum-hydrogen interaction (MP2: 0.017, HF: 0.008). At MP2 level the 6s population at platinum 5 is lower than at HF level (MP2: 0.261, HF: 0.446) and the Coulomb repulsion between

	Pt_9-H_2O / $d_{PtO} = 2.1662$ Å		Pt_9-H_2O / $d_{PtO} = 12.1662$ Å	
	RHF	MP2	RHF	MP2
6s pop Pt5	0.4465	0.2615	0.4240	0.3257
6s pop Pt6	0.2951	0.8322	0.3207	1.2316
6s pop Pt7	0.4581	1.1746	0.2789	1.1322
6s pop Pt8	0.4581	1.1746	0.2789	1.1322
6s pop Pt9	0.2951	0.8322	0.3207	1.2316
q_{Pt5} [e]	−0.9564	−0.6733	−0.5810	−1.3843
q_{Pt6} [e]	0.0664	0.1055	0.1040	0.2340
q_{Pt7} [e]	0.1590	0.1568	0.0717	0.2308
q_{Pt8} [e]	0.1590	0.1568	0.0717	0.2308
q_{Pt9} [e]	0.0664	0.1055	0.1040	0.2340
6s pop total	3.6661	6.1869	3.3737	7.5715
6s pop surface	1.9530	4.2750	1.6232	5.0534
$q_{surface}$ [e]	−0.5057	−0.1486	−0.2297	−0.4547
MOP PtO	0.1061	0.1006	0.0	0.0
MOP PtH	0.0085	0.0166	0.0	0.0
Δq_{CT} [e]	0.2078	0.2733	0.0	0.0
ΔE [kcal/mol]	2.724	53.47	—	—

Table 6.23: Electronic properties of the Pt_9-H_2O cluster.

oxygen and platinum is much smaller. However, the calculation of the true binding energy is more difficult. At HF level the total 6s population does not change much during the dissociation process (opt: 3.666, free: 3.374), whereas the total 6s population changes dramatically at MP2 level (opt: 6.187, free: 7.571), suggesting a different binding mechanism: The interaction with the water molecule forces the 6s electrons into the metal core in a similar way similar to that observed for Pt_3-H_2O with the water molecule at the hollow site. But the interaction of water at the hollow site with the platinum triangle provided the first evidence for the breakdown of the Møller-Plesset approximation for the platinum-water interface. The charge distribution and the individual 6s populations of the surface atoms on the other hand show the same pattern as the HF values indicating the same or a similar mechanism. The derived binding energy of 53.47 kcal/mol therefore has to be treated with caution.

The structure of the water bilayer on the platinum surface can be inferred by the BFP rules (subsection 1.1.3, page 4) and the orientational energy of the hydrogen atoms is important for the realisation of this structure. To compute the rotational energy γ equal to 179.9° and not to 180° and d_{PtO} kept constant. This method avoids complications with symmetry, because $\gamma = 180°$ increases the symmetry to C_{2v}. The orientational energy is high at MP2 level (12.473 kcal/mol) reflecting a strong platinum-hydrogen interaction, but small at HF level (0.499 kcal/mol). This is larger than the values for Pt_2-H_2O clusters (geometries C and D, $\Delta E = 8.343$ kcal/mol) with singlet wavefunctions. For the triplet states of the Pt_2-H_2O cluster, the energy barrier is reduced and the second minimum vanishes (figure 6.32, page 171 and table 6.12, page 164). The high orientational energy for Pt_9-H_2O is suspect, as the validity of the electronic state of the platinum cluster was not checked and the MP2 calculations were used beyond their allowed range. The true value is likely to be smaller close to that of Pt_5-H_2O considering the HF results for Pt_9-H_2O.

cluster	geometry	sym	r_{PT} [Å]	energy gap** [H]	5d band** [H]	μ^{**} [D]	$-E_{TOT}$/atom [H]
Pt ^{3}D	single atom			0.3312	0.06183		118.284142
Pt ^{1}S	single atom			0.3333	0.0		118.262749
I	linear	$D_{\infty h}$	2.7592	0.2479	0.10029	0.0	118.275475
II	equilat. triangle	D_{3h}	2.7722	0.1997	0.14967	0.0	118.286990
III	rhombus	D_{2h}	2.5875	0.2132	0.24687	0.0	118.330218
IV	tetrahedron	T_D	2.8383	0.1818	0.16066	0.0	118.293919
V	trapezium	C_{2v}	2.6145	0.2553	0.23439	0.1245	118.358075
VI	tetrah. + rhomb.	C_S	2.6438	0.2232	0.27539	3.2038	118.364361
VII	pyramid	C_{4v}	2.6449	0.1800	0.18268	1.9581	118.339041
VIII	square	D_{4h}	2.6753	0.1551	0.17764	0.0	118.294075
IX	double cone	D_{2h}	2.6069	0.1816	0.28528	0.0	118.319533
X	swiss cross	D_{4h}	2.5187	0.2021	0.25700	0.0	118.309895

* MP2 value ** HF value

Table 6.25: Small Pt_n Cluster, singulet wavefunction, MP2 optimized structure.

6.6 The electronic structure of the metal cluster as a function of its size

Table 6.25 and figure 6.70 summarize the results for a selection of optimized platinum clusters. The optimisation was done at MP2 level, while the electronic properties refer to HF values. These calculations were performed to determine the optimal cluster to be used as surface model (Gaussian 94 default settings).

A suitable surface model has to fulfill certain conditions:

1. $d_{PtPt} = 2.77$ Å [28, 36, 37, 65]
2. 5d band width ≈ 6.5 eV $= 0.24$ H [48, 49, 334b]
3. a small or vanishing energy gap between HOMO and LUMO to simulate the metal character
4. $-\epsilon$(HOMO) ≈ 5.65 eV - 5.7 eV to simulate the work function correctly [15]

The total energy per platinum of the clusters increases gradually with the cluster size: $Pt_1 \rightarrow -118.2735$ H, $Pt_2 \rightarrow -118.2755$ H, $Pt_3 \rightarrow -118.2870$ H, $Pt_4 \rightarrow -118.3061$ H, $Pt_5 \rightarrow -118.3382$ H (average values). But, the total energy of the cluster does not provide a good criterion for the validity of the cluster as surface model, because the total energy depends strongly on the electronic state (6s population) and the geometry of the cluster (Pt_4: rhombus $\rightarrow -118.330$ H, tetrahedron $\rightarrow -118.294$ H).

The third criterion is impossible to fulfill for these clusters due to the limited size. The clusters are therefore models for semiconductors in the best case. The smallest energy gap was found for the platinum square, but the 5d band width is too small for a suitable surface model. According to the 5d band width, suitable models are the clusters III, VI, VII, IX and X.

From these clusters the platinum pyramid has the smallest band gap of 0.18 H. The optimised platinum-platinum distance (2.64 Å) of the pyramid is closest to the required 2.77 Å. The pyramid

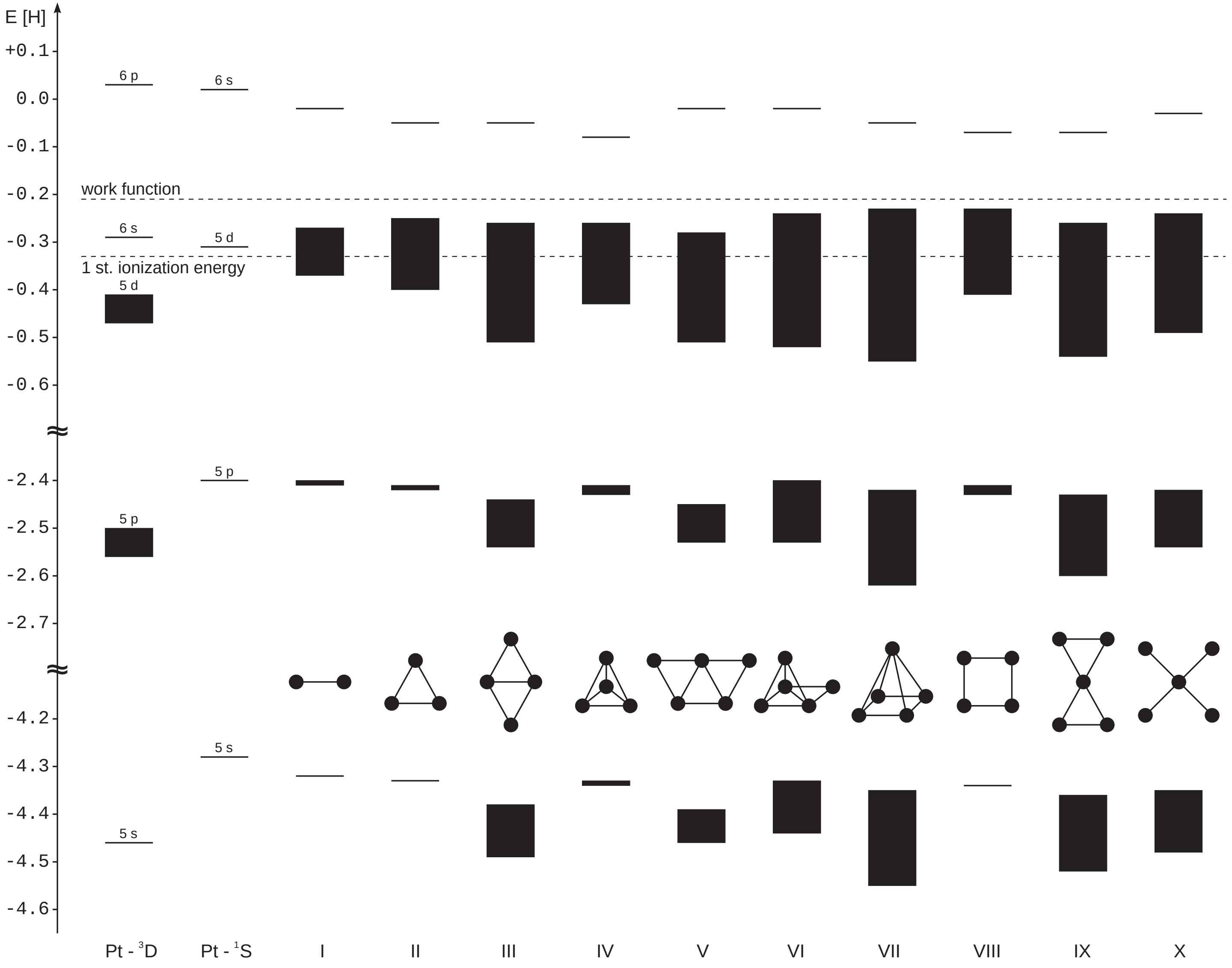

Figure 6.70: Band structure of small platinum cluster.

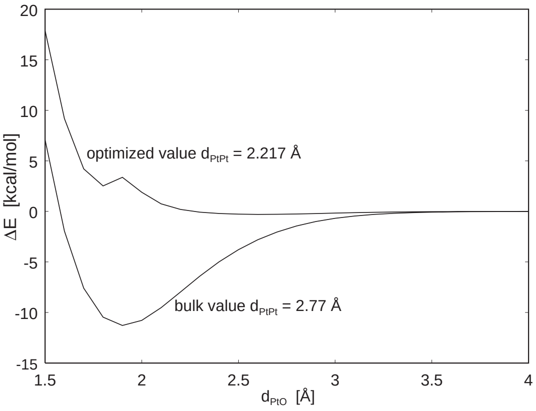

Figure 6.71: Pt_5-H_2O binding energy (EHT).

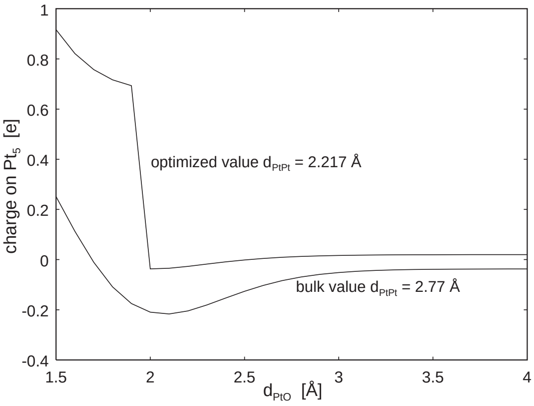

Figure 6.72: Charge on Pt5 in Pt_5-H_2O for different values of d_{PtPt} (EHT).

therefore provides the most suitable surface model. The symmetry of the pyramid creates two subsets of atoms in the cluster: the platinum at the top and the four basal platinums. These two groups of atoms carry different charges. The negative end of the corresponding dipole (1.96 D[8]) is located at the top (q_{TOP} = -0.0299 e). This dipole moment (similar to the experimental dipole moment of the water molecule 1.85 D) can be used to simulate the electron spill at the metal surface. The simulation works only for one side of the cluster: The base of the pyramid is a poor model for the surface, since the dipole moment points into the wrong direction.

The calculations on Pt_2-H_2O and Pt_3-H_2O already suggest the use of a three dimensional surface model. The calculations on small platinums clusters reinforce this assumption: The best model appears to be the platinum pyramid.

6.7 EHT calculations on the Pt_n-H_2O system

The platinum-water interface has been analysed using Extended Hückel (EHT) calculations [64, 101]. None of the problems mentioned previously, like polarisation or the different electronic states, were not identified by these authors.

The EHT package YaEHMOP [304, 311] contains all parameters for the simulation of the water-platinum interface. The main difference from the calculations of HOLLOWAY et al. [64] is the platinum basis set. YaEHMOP uses two Slater functions for the platinum 5d orbital, while HOLLOWAY et al. used only one.

Figures 6.72 and 6.73 summarize the results for two Pt_5-H_2O clusters (γ = 135°). Both clusters differ in the platinum-platinum distance in the pyramid. The first uses the bulk value of 2.77 Å and the second the optimised[9] platinum-platinum bond length of 2.217 Å. The curve (figure

---

[8] The experimental dipole moment of water in 1.85 D. According to equaition 2.99 (page 42) the maximum Pt_5-H_2O interaction energy is 6.68 to 3.85 kcal/mol, if both dipole moments are assumed to lie at the centres of the molecules (d = 2.5 to 3 Å, 1 eÅ = 4.8 D, 1 e^2/Å = 332.17752 kcal/mol). Dipole-dipole interactions account for roughly one third of the total interaction energy.

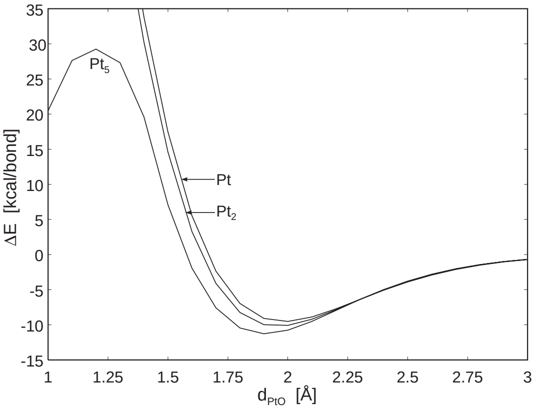

Figure 6.74: EHT results fot $\mathrm{Pt_n-H_2O}$ (n = 1,2,5).

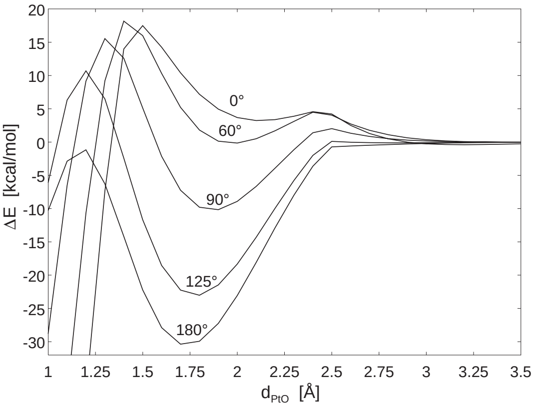

Figure 6.75: EHT results for $\mathrm{Pt_9-H_2O}$.

6.71) calculated with the bulk value is smooth and has no kinks in the analysed area ($1.0 \leq d_{\mathrm{PtO}} \leq 10.0$ Å). The maximum binding energy of 11.281 kcal/mol at $d_{\mathrm{PtO}} = 1.9$ Å agrees well with experiment. The same set of calculations for the optimized platinum-platinum distance produced a totally different shape of curve. The water molecule is repelled by the surface and the interaction energy changes suddenly.

Figure 6.72 shows the charge on the top platinum during the formation of the bond. The curve for the bulk value is again smooth over the range considered while the curve for the optimized platinum cluster produces a sudden jump, indicating a change in the electronic structure of the cluster induced by the water molecule.

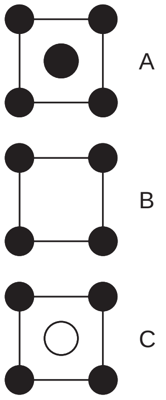

Figure 6.73:

The 6s orbitals interact with the 5d band of the core, creating three rather than two totally symmetric 6s orbitals with various contributions of 5d orbitals (figure 6.73): The first totally symmetric orbital (A) lies deep in the 5d band and does not change its position during the formation of the bond. The second orbital (B) is the LUMO of the cluster. As the water molecule approaches the pyramid the energy of the LUMO lowers until finally the LUMO and the HOMO change their relative positions and hence the population. This change in population causes the sudden jump in the energy and the charge on the top platinum. The final totally symmetric orbital (C) has such a high energy that its relative position has no influence on the charge distribution.

Figure 6.74 shows the binding energy of the water to various platinum clusters. The curves have same shape and the position of the minima does vary much for different clusters. Figure 6.75 displays the same set of calculations for $\mathrm{Pt_9-H_2O}$ with different values for γ, the angle between the water molecular plane and the platinum-oxygen bond. As the hydrogens get closer to the surface the activation energy of the adsorption process increases. An energy jump is difficult to identify in the plot, but between 2.5 Å and 2.4 Å the charge on platinum 5 in the centre of the surface changes abruptly from -0.3 e to $+0.5$ e. This abrupt jump reflects a change in the electronic structure of the cluster.

The EHT calculations show clearly that polarisation effects and the presence of nearby electronic states still cause problems at low level theory. Even at this low level it is impossible to construct a working surface model with medium sized platinum clusters (eg $\mathrm{Pt_9}$). It might be worth testing

---

[9] The optimisation was done with the program's `walsh`-option and a very fine grid.

this method with very large clusters, where the different electronic states lie so close to each other that smooth transitions are possible.

6.8 Summary of the calculations with a 18 valence electrons platinum atom

Two ECPs are commonly used for the simulation of the platinum surface: LanL1 and LanL2. Despite the recommendation of Hay and Wadt [189] the LanL1 ECP has been used in clusters with strong metal-metal interactions.

Our calculations showed, that the platinum-water bond is affected only slightly using these two potentials. Bonds computed with the LanL1 potential tend to be longer and weaker, but show the same characteristics than those predicted by the LanL2 ECP. The LanL1 potential appears to be a good low cost-alternative to the more expensive LanL2 ECP. Calculations with larger clusters showed, that with increasing cluster size intermetallic charge transfer in the platinum cluster becomes more important. For medium sized clusters the LanL2 ECP provides a more accurate description of the intermetallic charge transfer than the LanL1 potential.

The intermetallic bond is dominated by the 6s orbitals. The total energy of the metal cluster decreases with the population of the 6s potential. With increasing cluster size the 5d and the 6s bands become larger while the 5d-6s interaction becomes stronger. This interaction results in a multitude of electronic states which have similar energies. The small energy differences make static electron correlation more important and near degeneracy effects complicate the quantum chemical calculations. A simple approach to electron correlation such as MP2 becomes less appropriate and more elaborate methods are necessary. The computational costs rise dramatically with the number of electrons and it is therefore impossible to increase the level of theory with increasing cluster size.

The bond between platinum and water is formed via platinum 5d orbitals in all $Pt_n - H_2O$ clusters and the plots of the bonding orbitals are in good agreement. A very model for this interaction would be an inner orbital complex: 5d electrons are promoted into the 6s band and the resulting hole in the 5d band is filled with electrons from the lone electron pair on the water molecule. The results from the quantum chemical calculations are more detailed and complex, but do not contradict this simple model. The $3a_1$ and $1b_1$ orbitals of the water molecule interact separately with the occupied 5d orbitals in the metal cluster. For the formation of the bond between platinum and water the symmetry of the available orbitals is important and controls the adsorption site: Both water orbitals have to find suitable partners to reproduce a strong bond. All quantum chemical calculations so far predict an on-top coordination of the water molecule in agreement with experimental data in the literature.

The interaction between platinum and water is similar to the hydrogen bond observed in the water dimer and the adsorption of water on platinum base on the interaction of fully occupied orbitals. During the formation of this bond the 5d-6s interaction in the cluster changes leading to a small increase of 6s population, which is much smaller than two as predicted by the simple model. The increase in 6s population is the origin of the second problem in the description of the platinum-water interface: The 6s orbitals are more widely spreading than the 5d orbitals and electron transfer from a 5d orbital into the 6s band provides a transfer of electron density from the platinum core to the edges of the cluster. Such an electron transfer increases the Coulomb repulsion between the platinum atom and the oxygen valence electrons and weakens the platinum-water bond. This Coulomb repulsion can be used to understand the prefered on-top adsorption of water on Pt(111). At those sites is the electron density lower than at bridging or hollow sites and so Coulomb repulsion between the metal and oxygen minimal.

The dilemma of the quantum chemical description of the platinum-water interface can be summarized as follows: ***Depending on the 6s population either the platinum cluster or the platinum-water bond is energetically favoured. A stable metal cluster with a strong platinum-water bond is unlikely.***

The proximity of the water molecule has two effects on the platinum cluster: polarisation of the metal cluster and a symmetry effect. The dipole moment of the water molecule interacts mainly with 6s electrons of the platinum cluster. Coulomb repulsion forces the 6s electrons into the 5d band of the metal cluster as the water molecule approaches the surface. This electron rearrangement is sufficiently strong, that the electronic state of the metal cluster can change. Such a change is not smooth, but can cause sudden jumps in the interaction energy surface. A scan of the potential energy surface demands therefore sophisticated techniques to force convergency to selected electronic states. On the other hand, it is possible to control the electron distribution in the cluster by the platinum-oxygen distance.

The presence of the water molecule reduces the overall symmetry of the problem and facilitates the 5d-6s interaction despite the length of the platinum-oxygen bond. A small change in bond angle ω ($\Delta\omega = 0.001°$) reduces the point group to C_1, which enables a complete mixing of the 5d and 6s orbitals and thus increases the 6s population. This small change in bond angle causes a drop in total energy and makes a complete scan of the potential energy surface even more complicated than before. A sudden jump in interaction energy does not always indicate such a symmetry effect. It is also possible that this transition happens without any obvious signs. Such hidden transitions can be found by a careful analysis of the eigenvectors or by a reverse scan of this portion of the potential energy surface, because those symmetry induced changes of the electronic state work only in one direction from a symmetric wavefunction to an unsymmetric (figure 6.43, page 175).

The symmetry problem can be avoided by switching off the symmetry module in Gaussian 94. Results from those calculations have three disadvantages:

1. The lack of any symmetry during the calculation creates a huge 6s population and a stable metal cluster, but the platinum-oxygen bond is very weak.

2. The interpretation of charge transfer and the eigenvectors is difficult, because the alignment between the geometry of the cluster and the symmetry of the electronic structure is broken. Unphysical charge distributions in the metal cluster have been observed.

3. The runtime of the Gaussian 94 jobs becomes much longer, if symmetry is not used to reduce the number of integrals during the calculation.

The bond between water and platinum is dominated by a strong platinum-oxygen interaction, but the other surface atoms contribute weakly to the adsorption energy. The hydrogens interact weakly with the platinums below and contribute significantly to the geometry of the $\mathrm{Pt_n-H_2O}$ cluster. Simple calculations on PtH showed that the platinum-hydrogen bond is formed primarily by s-orbitals. Relativistic effects initiate the mixing of the σ-orbitals with the 5d electrons, but geometry and energy of the platinum-hydrogen interaction can be well simulated by a relativistic one-electron ECP. Therefore, the strength of the platinum-hydrogen interaction depends on the 6s population, which is itself influenced by the water molecule on the surface. As the water molecule bonds to the surface the 6s population simultaneously increases. 6s electron density can flow to another surface atom and interact with the hydrogen above. Strong cooperative forces have a significant effect on the geometry and energy of water adsorption.

The identification of the electronic ground state and the analysis of the wavefunction become more complicated as the cluster size increases. Hückel calculations on the 6s orbitals (chapter 5, page 117) can help to identify the groundstate, to understand the electronic structure and to analyse features of the potential energy surface. The combination of Hückel and HF calculations allowed us to construct a working Pt_5-H_2O surface model. A pyramid was chosen for the metal cluster for two reasons: Firstly, the results for Pt_2-H_2O and Pt_3-H_2O showed that a suitable surface model should contain at least two layers of platinum atoms. Secondly, MP2 calculations on a variety of small platinum clusters showed that two-layer clusters are preferable for surface models, because their properties resemble experimental bulk values.

The average 6s population (0.714) in Pt_5-H_2O is close to that predicted BIGOT and MINOT (0.7 - 0.8) [285] for surface atoms and the Pt_5-H_2O cluster should give optimal results (ΔE_{BOND} = 17.23 kcal/mol), but the absence of platinum atoms below the hydrogens suggest the orientational energy (ΔE_{ROT} = 0.03 kcal/mol, ΔE_{WAG} = 0.26 kcal/mol) is too small. Pt_5 gives also first evidence of the advanced interaction between 5d and 6s electrons. The 6s orbitals can interact with 5d orbitals provided they have correct symmetry. This interaction causes an increase in the 6s population and can change the charge distribution in the cluster. This mechanism was discussed in great detail in subsection 5.3.3, page 125.

Pt_9-H_2O shows another type of 5d-6s interaction. The 6s electron flow connected with the interaction with the water molecule and the platinum cluster is coupled with the rearrangement of the 5d electrons. The charge distribution on the surface atoms resembles the inverse mirror image of the charge distribution in the water molecule, in agreement with the simple theory of surface interactions. This charge distribution cannot be explained by the movement of the 6s electrons alone. The 5d electrons also move during the bond formation and the correlation between such electron rearrangements suggest a circular mechanism. This electron circulation occurs simultaneously with the change of the 6s population caused by the formation of the bond between platinum and oxygen. The superposition of both electron rearrangements makes it difficult to understand the electronic structure of the Pt_9-H_2O cluster.

The Pt_9-H_2O cluster is the first cluster certainly beyond the limits of the MP2 method. The binding energy of the water molecule is too high (SCF: 2.724 kcal/mol, MP2: 53.47 kcal/mol), but such a difference can be caused by a change of the 6s population during the dissociation. The same is also observed for the orientational energy of the hydrogens (SCF: 0.499 kcal/mol, MP2: 12.473 kcal/mol). The interaction between the nonbonding surface atoms and the hydrogens seems to be artificially enhanced in the MP2 method and it is likely, that the reorientation of the water molecule is facile despite the presence of the surface atoms. These results for Pt_5-H_2O and Pt_9-H_2O suggest that the structure of the bilayer is primarily controlled by the water-water interactions in the ice phase.

EHT calculations on Pt_9-H_2O and Pt_5-H_2O showed that the problems caused by the 5d-6s interaction and near degeneracy effects exist also at low levels of theory and the results from those calculations have to be treated with caution.

Chapter 7

Calculations with 1-Valence Electron per Platinum

The previous chapter focused on quantum chemical calculations with 18 valence electrons. The limitation of the chosen computational method (LanL2DZ, MP2) are reached at the Pt_9-H_2O cluster and it was not possible to develop a good model for the water-platinum interactions within this cluster. Medium sized clusters similar to Pt_9-H_2O are necessary for the analysis of the water-platinum interface, because these clusters can be used to examine the interaction between water and passive surface atoms. Three methods exist to calculate large clusters:

1. DFT calculations are computationaly less demanding and may allow us the calculation of large clusters.

2. As the number of electrons decreases the computational costs decrease also. The concurrent results for Hückel (chapter 5) and LanL2DZ (chapter 6) calculations suggests, that the it might be possible to describe the bulk and passive surface atoms with 1-valence electron ECP [340, 341].

3. Low level calculations are computationally less demanding than those at MP2 level, but extended Hückel calculation in section 6.7 (page 197) showed that energy discontinuities persist even at low levels of theory.

The quantum chemical calculations in chapter 6 (page 145) showed, that the stability of the cluster is controlled by the population of 6s orbitals and so it should be possible to use the second method, which has two further advantages:

1. As the number of electrons decreases the number of electronic states decreases also. Such a reduction in the density of electronic states reduces the importance of static correlation and it might be possible to cover most of the correlation effects by MP2 calculations.

2. The number of electrons is so small, that the coputational cost will be minimal.

The second method was chosen to proceed despite one major problem: The interaction between 5d and 6s electrons in this model is regarded only as a distortion of the 6s band. The chosen simplification cannot describe the circular 5d-6s electron rearrangements observed in Pt_9-H_2O

(section 6.5, page 192) in great detail, but still can help to identify the relevant orbitals for this mechanism.

The 6s Hückel approach towards platinum clusters assumes a perfect 1-valence electron ECP (page 5.1, page 117). In section 7.1 we extract from the 18 valence electrons HAY and WADT ECP [189] the properties of the 6s electron on the Hartree-Fock level. The 18 electrons ECP has been chosen instead of the nodeless 10 electrons ECP to compare the results directly with chapter 6. This procedure allows us to take relativistic effects partially into account. A relativistic all electron calculation would have been the better basis, but is beyond the scope of this work. Completening the construction of nodeless wavefunctions we give a table with other electronic properties of the platinum atom and the platinum dimer as basis for the development of a working 1-electron ECP for the bulk atoms.

The last two sections describe the analysis and the development of a new 1-valence electron ECP. The 6d orbitals and the underlying potential function are in the focus of interest. A set of analytical equations was found, which showed that a new 1-valence electron ECP cannot be developed from the LanL2 ECP alone (section 7.2). The combination of the 6s Hückel theory with the new 1-electron ECP was then applied to the Pt_5-H_2O problem (section 7.3).

7.1 Numerical properties for the new 1-electron ECP

The good correlation of Hückel and Hartree-Fock results suggests the development of an individual 1-electron ECP for the simulation of the platinum-water interface. ZURITA et al. used previously such a potential for the calculation of PtH [318] and other problems [327, 328]. The main problem in comparison to copper [329–331, 342–346] or nickel [347–349] is the open 5d shell for the simulation of the ^{3}D groundstate [305]. The hole in the 5d shell can interact with its enviroment and several extra forces have to be considered [329, 350]:

1. **core-core repulsion:** The point charge at the platinum core of the 1 electron ECP does not stretch far enough to represent the core-core repulsion correctly. ZURITA et al. [318] used an exponential function to simulate the repulsion.

$$\Delta E_{\text{core-core}} = A\, e^{-\alpha\, r} \qquad \begin{array}{l} A = 22.8279 \text{ a.u.} \\ \alpha = 4.6803 \text{ (a.u.)}^{-1} \quad \rightarrow \quad \tau_{0.5} = 0.148 \text{ a.u.} \end{array} \tag{7.1}$$

   HAY and WADT [189] observed the break down of the core-core repulsion only for ionic compounds as CaO or KF. Since the bonds in the metal cluster and between platinum and water are covalent, this error should be small. For the simulation of the platinum-water interface we also neglect any rearrangements of the metal surface caused by the water molecule, because a reconstruction of the surface has only been observed for high potentials in electrochemical experiments [7, 351]. The core-core repulsion contributes so a small, constant term to all energies in the platinum cluster, which cancels out during the calculation of energy differences. The oxygen-platinum repulsion is dominated by the interaction between the LanL2 ECP in the centre of the cluster and the oxygen atom. The other surface platinums account only little to this energy due to the longer distance to the second next surface atom and the exponential decay of $\Delta E_{\text{core}-\text{core}}$. The 18 valence electron ECP calculations showed that the hydrogen atoms in the water molecule can get close to the surface (aprox. 2.2 Å, subsection 6.5 page 192), but the electron density of the highly charged hydrogen does not stretch far and the interaction between both cores is likely to be small.

2. **core-valence correlation:** Figure 6.1 (page 148) in subsection 6.1.1 shows the important contribution of electron correlation to the correct description of the platinum atom. The strong correlation interaction between the 5d and 6s orbitals cannot to be accounted for with an 1-valence electron ECP.

   The core-valence correlation problem has been observed by HAY and WADT too [189]. They published that with decreasing size of the valence space becomes the correlation energy unrealistic large and that as many valence electrons as possible should be used for reliable calculations of the correlation energy.

3. **core polarisation:** In a free platinum stom the 5d hole can be assumed to be distributed evenly around the 5d core, but this hole concentrates in a chemical environment at one place. The hole in the 5d orbitals is extremely mobile and can be influenced easily by the environment of the platinum atom. ZURITA et al. describe the core polarisation and the core-valence correlation through an effective core-polarisation potential (CPP) proposed by MÜLLER [318, 350], which includes core-valence correlation.

   The polarisability α_λ of the 5d subshell in equation 7.2 ZURITA assumed to be 11.37 a_0^3. $\mathbf{f}_\lambda$ is the electric field at the core λ produced by all electrons and the other cores.

$$\hat{V}_{\mathrm{CPP}} = \frac{-1}{2} \sum_\lambda \boldsymbol{\alpha}_\lambda \, \mathbf{f}_\lambda \, \mathbf{f}_\lambda \tag{7.2}$$

The core-core repulsion cancels largely in the simulation of the platinum-water interface and can be therefore neglected in a first approach. More difficult are the core-valence correlation and the core polarisation. The 18 electrons ECP calculation showed, that the 5d-6s interaction becomes more important as the cluster grows. For medium sized clusters such as Pt_9 or Pt_{17} it might be possible to describe the surface reasonably well focussing only on the 6s electrons. The core-valence correlation is nearly impossible to simulate with a simple 1-electron ECP, but the effect should be small for platinum clusters with filled 6s orbitals (subsection 6.3.1, page 177). Electron correlation effects are caused by electron pair interactions and the correlation energy is approximately constant as long no bond breaks [352]. The water molecule interacts with active surface atom, which has a large valence space and the metal cluster is rigid for all calculations.

7.1.1 Numerical Results for the 6s orbital

The 6s orbital was the first orbital, which was transformed into a nodeless form. Subsection 7.1.1 was divided into separate parts to describe every step of the transformation, while 7.1.2 and 7.1.3 are only compilations of the results for the remaining orbitals.

7.1.1.1 The 6s Wavefunction

Gaussian 94 uses a sum of gaussian functions for the description of the radial function and spherical harmonic functions for the angular part. The radial part is fully characterized by a list of coefficients k_i and exponents α_i.

$$\begin{aligned} &R(r) \propto \sum_{i=1}^{M} k_i \, e^{-\alpha_i r^2} \\ &\Psi(r,\theta,\varphi) = Y(\theta,\varphi) \sum_i \frac{k_i}{N_i} \, e^{-\alpha_i r^2} = Y(\theta,\varphi) \sum_i d_i \, e^{-\alpha_i r^2} \qquad d_i = \frac{k_i}{n_i} \end{aligned} \tag{7.3}$$

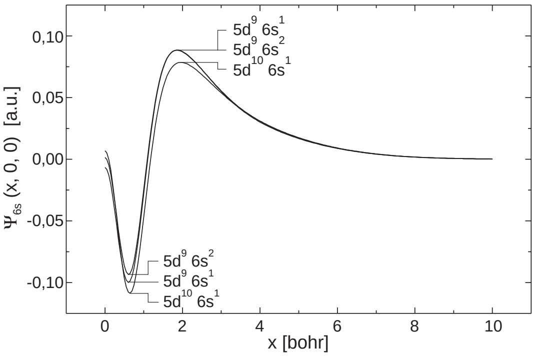

Figure 7.1: 6s orbital, LanL2 ECP, cut along the x axis.

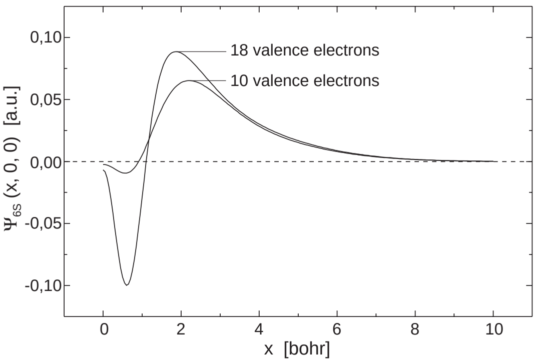

Figure 7.2: 6s orbital, $5d^9 6s^1$, different ECPs, cut along the x axis.

N_i is the normalisation constant of the individual gaussian function and N_T the normalisation constant of the orbital. The individual normalisation constants N_i include the angular part.
s-orbital:

$$N_i^2 = \int_0^{\infty} \int_0^{\pi} \int_0^{2\pi} \left(e^{-\alpha_i\, r^2}\right)^2 \; r^2 \; \sin\theta \, dr \, d\theta \, d\varphi = \left(\frac{\pi}{2\,\alpha_i}\right)^{\frac{3}{2}} \tag{7.4}$$

d_{z^2}-orbital:

$$N_i^2 = \int_0^{\infty} \int_0^{\pi} \int_0^{2\pi} \left((3\cos^2\theta - 1)\, r^2 \; e^{-\alpha_i\, r^2}\right)^2 \; r^2 \; \sin\theta \, dr \, d\theta \, d\varphi = \frac{16}{15} \sqrt{\frac{\pi^3}{(2\,\alpha_i)^7}} \tag{7.5}$$

Equations 7.4 and 7.5 work well for non contracted wavefunctions (M = 1). For contracted wavefunctions ($M \geq 2$) the overlap between gaussians with different α_i contributes also to the norm. The total norm N_T for contracted wavefunctions was calculated according to equation 7.6.

$$N_{ST}^2 = \sum_{i,j} d_i \; d_j \; \left(\frac{\pi}{\alpha_i + \alpha_j}\right)^{\frac{3}{2}} \qquad\qquad N_{DT}^2 = 3 \sum_{i,j} d_i \; d_j \sqrt{\frac{\pi^3}{(\alpha_i + \alpha_j)^7}} \tag{7.6}$$

N_T was equal to 1.0 for all orbitals. The constants k_i for contracted wavefunctions are given in such a way, that they already include the normalisation of the off-diaogonal elements ($i \neq j$).

The calculations were checked by a direct comparison of equation 7.3 and a Gaussian 94 cube calculation[1]. Equation 7.3 reproduces exactly the G94 values in the cube file for a cut along the x-direction (LanL2DZ ECP by Hay and Wadt) and forms so a valid basis for the following calcualtions.

Figure 7.1 displays the platinum 6s orbital for different states calculated with LanL2DZ ECP by Hay and Wadt. The curves for an open d-shell ($5d^9$) are very similar and different form the one for the closed shell ($5d^{10}$). Only the closed shell wavefunction is spherically symmetric. The oval shape of the open shell functions is caused by an exchange interaction of the singly occupied $5d_{z^2}$ and 6s orbital[2]. This behaviour is shown by the intersection points of the nodal plane and the xz axis. For the spherical symmetric closed shell function is this point $x_0 = z_0 = 1.75$ a.u.. For the elipsoid open shell function is this point at $x_0 = 1.35$ a.u. and $z_0 = 1.1$ a.u..

---

[1] All functions have been tested this way.

[2] Free atoms are always spherically symmetryic and deviations from this ideal form are artefacts caused by the method of computation [353, 354].

In figure 7.2 we compare the 6s orbitals for different ECPs. The LanL2 and the LanL1 potential have their maximum roughly at the same place, but differ close to the nucleus. The valence space of the LanL1 ECP contains only the 5d- and 6sp electrons and the 6s wavefunction should therefore be nodeless. This extra node at approximately 0.9 bohr is caused by the 5d-6s interaction and cannot be observed in a cut along the z-axis. Only 1-valence electron ECP calculations produced sperically symmetric 6s orbitals for the ^{3}D state.

7.1.1.2 Radial 6s Density

The platinum 6s-orbital contains an additional $5\mathrm{d}_{\mathrm{z}^2}$ contribution, which reduces its symmetry. Using equations 7.3 to 7.5 $\Psi(\mathrm{r},\theta,\varphi)$ can be written in the following way:

$$\Psi(r,\theta,\varphi) = \sum_{i=1}^{7} a_i\, e^{-\alpha_i r^2} + r^2\, (3\cos^2\theta - 1) \sum_{i=8}^{11} a_i\, e^{-\alpha_i r^2} \qquad a_i = c_\mu\, d_i \tag{7.7}$$

c_μ is the expansion coefficient of a basis function χ_μ in an orbital $\Psi = \sum \mathrm{c}_\mu\, \chi_\mu$. The radial electron density is calculated as follows:

$$\begin{aligned} \rho(r) &= \int_0^{\pi} \int_0^{2\pi} \Psi^2(r,\theta,\varphi)\, r^2\, \sin\theta\, dr\, d\theta\, d\varphi \\ &= 4\,\pi\, r^2 \left(\sum_{i=0}^{7} a_i\, e^{-\alpha_i r^2} \right)^2 + \frac{16}{5}\,\pi\, r^6 \left(\sum_{i=8}^{11} a_i\, e^{-\alpha_i r^2} \right)^2 \end{aligned} \tag{7.8}$$

The s and the d part of the wave function do not mix, since the angular parts of the wavefunctions are orthogonal. While the influence of the d-orbitals onto the shape of the 6s orbital is big, the radial electron density is dominated by the s orbitals (99.48%).

Figure 7.1.1.2 shows a comparison of the 6s radial density for different ECPs. The maximum of the 1-electron potential (subsection 7.3.1) lies further out, but is slightly smaller and broader. The 6s electron is so much more loosely bound. This result is also reflected in the smaller ionization energy (18 electrons : 0.296 H, 1 electron : 0.283 H.)

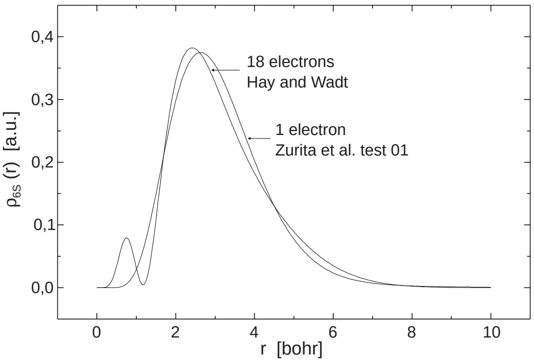

Figure 7.3: Radial 6s electron density for different ECP.

Physics is not described by a wavefunction but by the radial electron density. This approach towards a new 1-valence electron potential therefore starts with radial electron density function and not with the wavefunction itself. For the analysis of the radial electron density the first two derivatives have been calculated numerically[3].

$$f'(x) = \frac{f(x+h) - f(x-h)}{2\,h} \qquad f''(x) = \frac{f(x+2h) + f(x-2h) - 2f(x)}{4\,h^2} \qquad h \ll 1 \tag{7.9}$$

---

[3] The derivatives and the roots have been calculated numerically. The point of inflexion has been found with the intersection algorithm. The integrals have been calculated numerically with the trapezium method (Infinity was reached at 500 a.u..), which proofed to be sufficient.

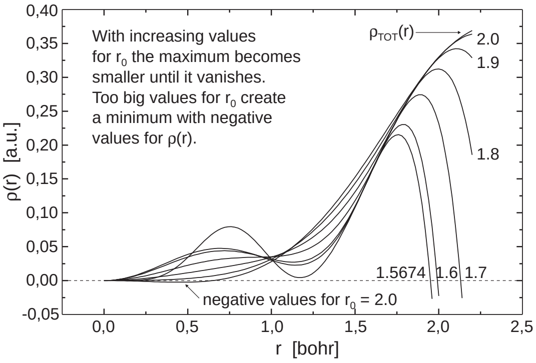

Figure 7.4: Replacement polynominals for different transition points (r_0).

7.1.1.3 Simplification of the Radial 6s Electron Density Function

The radial electron density of the 6s orbital is unsuitable as a model function due to the small first peak. A suitable density function (ρ_{simp}(r)) for a 1-valence electron potential should have only one maximum and decrease steadily towards zero for r = 0. To achieve this the first part of the density function is replaced by a 8th order polynomial (p(r)).

The polynomial replacement p(r) of the radial electron density function ρ(r) at the first peak has to fulfill several conditions. Tests with a lower number of restrictions failed.

1	$\mathrm{p(r_0)} = \rho(\mathrm{r_0}) = \mathrm{f}$	For a smooth transition between p(r) and ρ(r)
2	$\mathrm{p'(r_0)} = \rho'(\mathrm{r_0}) = \mathrm{g}$	For a smooth transition between p(r) and ρ(r)
3	$\mathrm{p''(r_0)} = \rho''(\mathrm{r_0}) = \mathrm{gg}$	For a smooth transition between p(r) and ρ(r)
4	$\mathrm{p(r = 0) = 0}$	Correct behaviour at r=0
5	$\mathrm{p'(r = 0) = 0}$	Correct behaviour at r=0
6	$\int \mathrm{p(r)\,dr} = \int \rho(\mathrm{r})\,\mathrm{dr} = \mathrm{A}$	To keep the number of electrons constant
7	$\mathrm{p(r) = p(-r)}$	Found emperically as $\rho(\mathrm{r}) \propto \mathrm{r}^2 \cdot \mathrm{f}^2(\mathrm{r})$
8	No maximum between 0 and $\mathrm{r_0}$	Simplification of ρ(r)

Several functions have been tested. The most successful function was an eighth order polynomial.

$$p(r) = c_1\,r^8 + c_2\,r^6 + c_3\,r^4 + c_4\,r^2 \tag{7.10}$$

The other important parameter of the calculation is the point $\mathrm{r_0}$ where the polynomial $\mathrm{p(r_0)}$ changes into the density function $\rho(\mathrm{r_0})$ (figure 7.4). The coefficients $\mathrm{c_1}$ to $\mathrm{c_4}$ can be calculated with the following equation.

$$\begin{pmatrix} r_0^8 & r_0^6 & r_0^4 & r_0^2 \\ \frac{1}{9}\,r_0^9 & \frac{1}{7}\,r_0^7 & \frac{1}{5}\,r_0^5 & \frac{1}{3}\,r_0^3 \\ 8\,r_0^7 & 6\,r_0^5 & 4\,r_0^3 & 2\,r_0 \\ 56\,r_0^6 & 30\,r_0^4 & 12\,r_0^2 & 2 \end{pmatrix} \cdot \begin{pmatrix} c_1 \\ c_2 \\ c_3 \\ c_4 \end{pmatrix} = \begin{pmatrix} f \\ A \\ g \\ gg \end{pmatrix} = \begin{pmatrix} +0.30424713 \\ +0.13915523 \\ +0.33762438 \\ -0.80386548 \end{pmatrix} \qquad r_0 = 1.916 \tag{7.11}$$

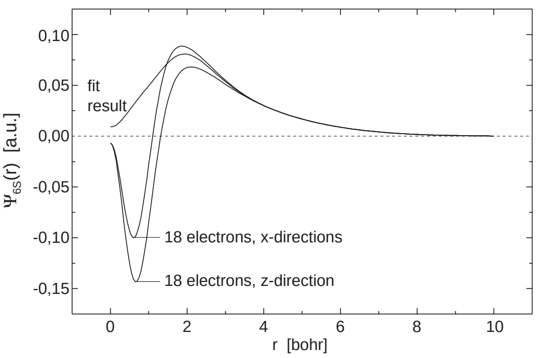

Figure 7.5: New 6s wavefunction, final version.

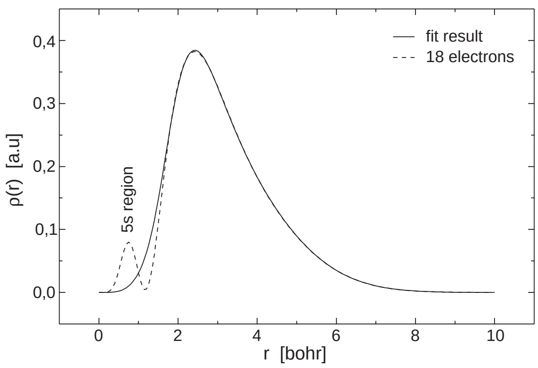

Figure 7.6: New 6s radial electron density, final version.

$$
\begin{aligned}
c_1 &= \frac{1}{16\,r_0^6}\left(\frac{-315\,A}{r_0^3} + \frac{171\,f}{r_0^2} - \frac{36\,g}{r_0} + 3\,gg\right) = -0.00102984\\
c_2 &= \frac{1}{16\,r_0^4}\left(\frac{945\,A}{r_0^3} - \frac{497\,f}{r_0^2} + \frac{98\,g}{r_0} - 7gg\right) = +0.00186327\\
c_3 &= \frac{1}{16\,r_0^2}\left(\frac{-345\,A}{r_0^3} + \frac{465\,f}{r_0^2} - \frac{80\,g}{r_0} + 5\,gg\right) = +0.02938057\\
c_4 &= \frac{1}{16}\left(\frac{315\,A}{r_0^3} - \frac{123\,f}{r_0^2} + \frac{18\,g}{r_0} - gg\right) = +0.00085881
\end{aligned}
\tag{7.12}
$$

The solutions for the coefficients $\mathrm{c_i}$ were calculated analytically to keep the program simple. As $\mathrm{r_0}$ increases, the first maximum becomes smaller and finally vanishes. For $\mathrm{r_0} = 2.0$ a.u. p(r) becomes negative and therefore unsuitable. The search started at $\mathrm{r_0} = 1.5674$ a.u., the point of inflexion of the density function, which proved far too small. The development of p(r) is shown in figure 7.4. The final value $\mathrm{r_0} = 1.916$ a.u. was found during an optimization under the additional constrain, that the final wave function should have an absolute value close to $6.6{\cdot}10^{-3}$ a.u. at the origin like the original 6s function.

7.1.1.4 The quest for the new 6s Wavefunction

In first tests we extracted the new wavefunction directly from the simplified radial electron density ρ_{simp}(r) (equation 7.13a). For these calculations an array of 201 points between 0 and 10.0 a.u. was used.

$$
\text{a)}\;\; \rho_{\mathrm{simp}}(r) = \begin{cases} p(r) & r < r_0 \\ \rho(r) & r \geq r_0 \end{cases} \qquad \text{b)}\;\; \rho_{\mathrm{FIT}}(r) = 4\,\pi\,r^2\,\left(\sum_{i=1}^{8} a_i\; e^{-\alpha_i r^2}\right)^2 = 4\,\pi\,r^2\;\Psi_{\mathrm{FIT}}(r) \tag{7.13}
$$

The Levenberg-Marquardt-Algorithm [242] has been used to fit a new, pure s, radial density function ρ_{FIT}(r) to ρ_{simp}(r) (equation 7.3b). The search for a new wavefunction started from the original wavefunction by Hay and Wadt (8 gaussians). Although good results have been obtained for the density function, only poor results have been found for the corresponding wavefunction Ψ_{FIT}. This bad behaviour is caused by the r^2 term. As r becomes smaller, the exact value for Ψ_{FIT} becomes unimportant, because r^2 becomes very small and Ψ_{FIT} hardly contributes to the error function $\chi^2 = \sum(\rho_{\mathrm{simp}}(\mathrm{r_i}) - \rho(\mathrm{r_i}))^2$.

The next series of experiments used a simplified target wavefunction Ψ_{simp} constructed from ρ_{simp} (equation 7.13a) for the fit procedure.

$$\Psi_{\text{simp}}(r) = \begin{cases} \dfrac{1}{2\,r}\sqrt{\dfrac{\rho_{\text{simp}}(r)}{\pi}} & r > 0 \\ 8.6 \cdot 10^{-3} & r = 0 \end{cases} \tag{7.14}$$

The value for r = 0 was extrapolated from the values at 0.05 and 0.10 a.u.. This manipulation provided excellent results both for Ψ(r) and ρ(r). In the next step the number of functions was reduced stepwise from eight to five. Such a simplified function will increase later the speed of the quantum chemical calculations. All fits gave the same small value for $\chi^2 = 0.0000053$. The best value for four gaussians was about a thousand-times worse than the value for five functions. The lowest number of functions to describe Ψ_{simp} is therefore five. After the fitting Ψ_{simp} had to be normalized, since the norm (1.0004) was slightly bigger than 1.

Figures 7.5 and 7.6 show the wavefunction and the radial electron density in comparison with the 18 electron function by HAY and WADT. Table 7.1 displays the data for Ψ_{simp} in a suitable Gaussian 94 input format.

The fifth function is the same as in the original function by HAY and WADT and was not allowed to change during the fit, because a previous analysis showed, that this function dominates the 6s orbital and has no influence on the function at small distances r.

i	α_{i} [a.u.]	k_{i} [a.u.]
1	1.4832274932	0.7830538861
2	1.7464593543	−0.4961301298
3	0.7565909320	−0.6700116072
4	0.2490175212	0.4479071977
5	0.058	0.84346

Table 7.1: Ψ_{simp} in Gaussian 94 input format.

The new function Ψ_{FIT} has no nodal plane and resembles, despite its spherical symmetry, the 10 electron function (not shown in figure 7.5). The new wavefunction was fed into Gaussian 94 and the cube file confirmed the data given in table 7.1. The Gaussian 94 wavefunction has the same values as prediction by the fit program at every point of the cube file.

7.1.2 Numerical Results for the Pt 6p Orbital

The 6p$_{\text{z}}$ orbital was used to development the new radial wavefunction for the p-orbitals.

$$P_{Pz} = r\,\cos\theta\; e^{-\alpha r^2} \qquad N_P^2 = \frac{1}{2}\sqrt{\frac{\pi^3}{(2\alpha)^5}} \tag{7.15}$$

$$R(r) = \sum_i k_i\, e^{-\alpha_i r^2} \qquad d_i = \frac{k_i}{N_i} \tag{7.15\,a}$$

$$P_{Cz} = r\,\cos\theta \sum_i d_i\, e^{-\alpha_i r^2} \qquad N_C^2 = \frac{1}{2}\sum_{ij} d_i\, d_j \sqrt{\frac{\pi^3}{(\alpha_i + \alpha_j)^5}} \tag{7.15\,b}$$

Equation 7.15 shows the wavefunction of a primitive p$_{\text{z}}$ orbital with only one gaussian, equation 7.15a the expansion for a more complex radial wavefunction and equation 7.15b finally the used wavefunction and its norm. As observed previously for the 6s orbital N_{C} equals 1.0 for the LanL2DZ potential, if the primitive functions have been normalized (equation 7.15) prior to the synthesis of the complex function.

n	α_i	a_i	k_i
1	0.87944	−0.16288	−0.13413
2	0.72491	0.40691	0.42664
3	0.58257	−0.27824	−0.38340
4	0.10622	0.04229	0.48912
5	0.03014	0.01169	0.65264

a_i are the coefficients used for the calculation (equation 7.16)
and k_i are the final coeeficients used as Gaussian 94 input.

Table 7.2: Results for the new 6p wavefunction.

Equation 7.15b was checked with Gaussian 94 as before the 6s orbital. Equation 7.15b reproduces the results from Gaussian 94 cube file to the last digit.

The radial electron density ρ(r) has been calculated as follows:

$$\rho(r) = \int_0^{\pi} \int_0^{2\pi} \Psi^2(r)\, r^2 \, \sin\theta \, d\theta \, d\varphi = \frac{3}{4}\,\pi\, r^4 \left(\sum_i \alpha_i \, e^{-\alpha_i \, r^2} \right)^2 \tag{7.16}$$

Figure 7.7 displays the radial electron density and the corresponding 6p orbital calculated with 18 electrons ECP. In the next step a polynomial has been used to replace the density function for small r and to eliminate the first peak (subsection 7.1.1.3 for details.). From the target density function ρ_T was the target radial function $\mathrm{R_T}$ extracted.

$$R_T(r) = \begin{cases} \dfrac{1}{2\,r^2}\sqrt{\dfrac{3\,\rho_T(r)}{\pi}} & r > 0 \\ 0.020 & r = 0 \end{cases} \tag{7.17}$$

The target radial function $\mathrm{R_T}$(r) has been used to find a new radial function. Figure 7.8 shows the $\mathrm{R_T}$(r) and the best fist finally used. Both curves match perfectly and figure 7.9 demonstrates the good agreement of the radial densities. The most cost effective results has been found with 5 gaussian functions (table 7.2). Figure 7.10 finally displays the new wavefunction Ψ_FIT and the original Hay and Wadt function.

7.1.3 Numerical Results for the Pt 6d orbital

The new ECP represents the $5d^9$ core of the platinum atom. The ^{3}D state calculated with Gaussian 94 and the 18 valence electron potential from Hay and Wadt creates the hole in the $5d_{z^2}$ orbital. It was not possible to promote the 6s electron into the $6d_{z^2}$ orbital, because all calcualtions converged into the ^{3}D ground state. Convergency was achieved by promoting the 6s electron into the $6d_{xz}$ orbital. The $6d_{xz}$ orbital was therefore used for the following calculations.

$$D_{Pxz} = r^2 \, \sin\theta \, \cos\theta \, \cos\varphi \, e^{-\alpha r^2} \qquad N_P^2 = \frac{1}{4}\sqrt{\frac{\pi^3}{(2\alpha)^7}} \tag{7.18}$$

$$R(r) = \sum_i k_i \, e^{-\alpha_i r^2} \qquad d_i = \frac{k_i}{N_i} \tag{7.18 a}$$

$$D_{Cxz} = r^2 \, \sin\theta \, \cos\theta \, \cos\varphi \sum_i d_i \, e^{-\alpha_i r^2} \qquad N_C^2 = \frac{1}{4}\sum_{ij} d_i \, d_j \sqrt{\frac{\pi^3}{(\alpha_i+\alpha_j)^7}} \tag{7.18 b}$$

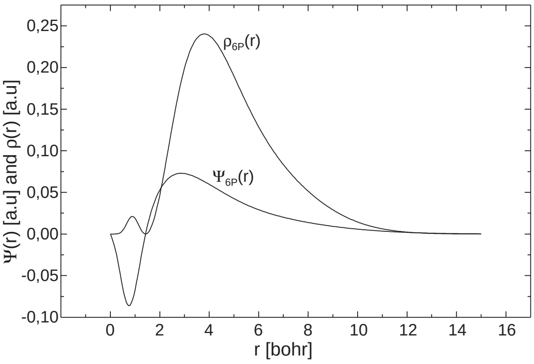

Figure 7.7: 6p radial density function (LanL2).

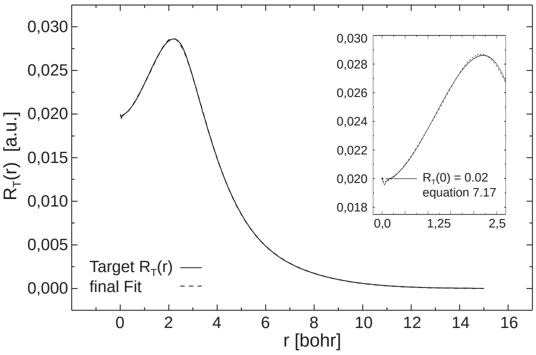

Figure 7.8: 6p target radial function and best fit.

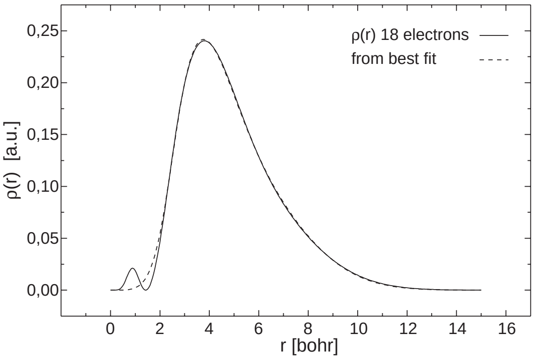

Figure 7.9: Original LanL2 6p radial density and the new one.

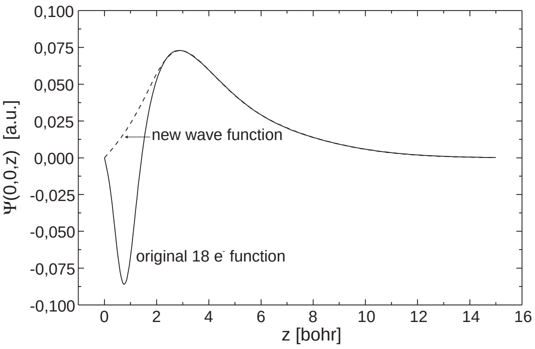

Figure 7.10: New and original radial 6p wavefunction.

Equation 7.18 shows the wavefunction of a primitive d_{xy} orbital with only one gaussian, equation (7.18a) the expansion for a more complex radial wavefunction and equation 7.18b finally the used wavefunction and its norm. As observed before for the 6s orbital, N_C is equal to one, if the primitive functions have been normalized prior to the synthesis of the complex function.

The Gaussian 94 cube calculation was done along the XZ axis ($\frac{1}{2}\sqrt{2}$ / 0 / $\frac{1}{2}\sqrt{2}$). The agreement between the G94 results and the equation 7.18b is slightly worse than before, but still very good. This small error is caused by a misalignment of the unitvector due to the truncation of the numbers to 6 digits, but does not increase infinitely with r. The agreement at r = 10 a.u. is perfect.

The radial electron density $\rho(\mathrm{r})$ has been calculated as follows:

$$\rho(r) = \int_0^{\pi} \int_0^{2\pi} \Psi(r)^2\, r^2\, \sin\theta\, d\theta\, d\varphi = \frac{4\,\pi}{15}\, r^6\, \left(a_i\; e^{-\alpha_i r^2}\right)^2 \tag{7.19}$$

Figure 7.11 displays the radial electron density and the corresponding 6d orbital calculated with 18 electrons ECP. In the next step a polynomial replaced the density function for small r to eliminate the first peak (subsection 7.1.1.3 for details). From the target density function ρ_T (equation 7.19) was the target radial function R_T extracted.

$$R_T(r) = \begin{cases} \frac{1}{2\,r^3}\sqrt{\frac{15\,\rho_T(r)}{\pi}} & r \geq 0.10 \\ 1.1\,R_T(0.10) & r = 0.05 \\ 1.03\,R_T(0.05) & r = 0 \end{cases} \tag{7.20}$$

The values for r = 0.05 and r = 0.0 have been chosen to achieve better convergence. The influence of this change onto the radial electron density is neglible, but the numerical benefits are great. Figure 7.12 shows the pure radial functions from different origins: $R_T(r)$, from a single gaussian and the original function from the quantum chemical calculation.

$$\alpha = \frac{3}{2}\,\frac{1}{r_{max}^2} = 0.119596 \tag{7.21}$$

The exponent α of the gaussian in figure 7.14 has been chosen, that the new wavefunction and the old have their maxima at the same radial position r_{max}.

In contrast to the calculatins for the 6s and 6p orbital it was not possible to find a new radial function with the same number of gaussians or less. The first usable results were obtained with 4 gaussians (one more than HAY and WADT). Figure 7.13 shows the results of this attempt. The radial electron density functions agree well for small values of r but diverge for larger values. $R_T(r)$ has its maximum values close to r = 0. Any differences between R_T and the new function R_{FIT} for small r therefore dominate the error function. The LEVENBERG-MARQUARDT algorithm tries to minimize this contribution. On the other hand, huge differences in the radial electron density function are caused by the small differences between R_T and R_{FIT} for large values of r muliplied by r^6, since $\rho(r)$ sclaes with r^6 (equation 7.19).

Further achievment may be obtained be increasing the number of gaussians. Regarding the nearly vanishing importance of the 6d orbital for the platinum platinum interaction in bulk metal (dominated by $6sp^n$ hybrid orbitals) it seems not be worthwhile to follow this line.

Nearly the same quality was achievde by using a single gaussian. The exponent was chosen in such a way, that the target radial density function and the new one have the maxima at the same place (equation 7.21). The wave function and the resulting electron density function are shown in the figures 7.14 and 7.15.

The LanL2DZ 6d orbital is dominated by the gaussian with the smallest exponent ($\alpha = 0.1370$). This gaussian forms a basis function on its own in the LanL2DZ basis and represents a 5d orbital. This basis set was formed originally from the original HAY and WADT basis by splitting the 5d function into two parts. The function is therefore more suitable to describe the long range part of a 5d function than to describe a 6d orbital. This limitation of the basis set explains also the large first large peak in the radial electron density, which complicates the construction of the new wavefunction. It seems to be more favourable to determine the 6d orbital by molecular properties of platinum compounds during the development of the new ECP.

7.1.4 Summary and compilation of all 1 electron properties

In subsection 7.1 we analysed the properties of the platinum valence electron (n=6). The calculations resulted in a set of new expressions for the radial part of the orbitals (tables 7.1, 7.2 and equation 7.21). The new functions are nodeless and agree very well with the original functions in the valence region. The 6d orbital has a strong 5d contribution and a positive eigenvalue, which

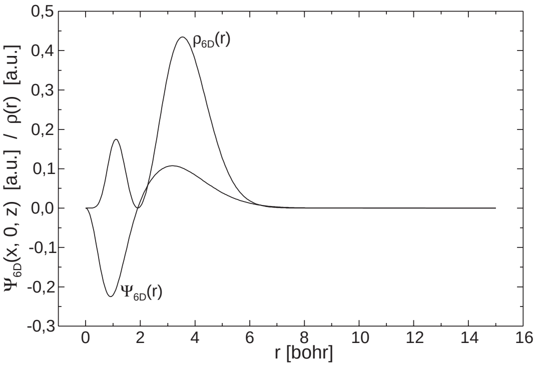

Figure 7.11: $6d_{xz}$ radial electron density.

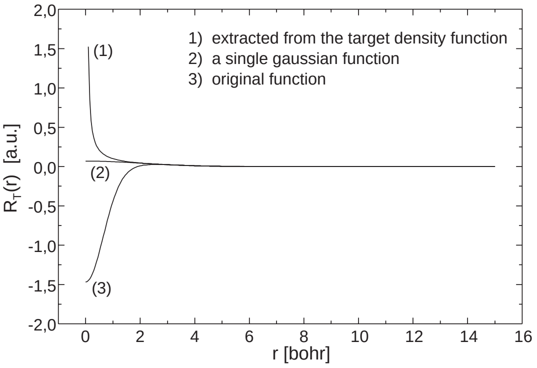

Figure 7.12: Different $6d_{xz}$ radial functions.

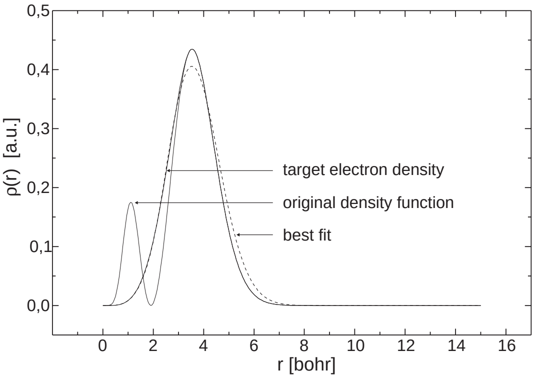

Figure 7.13: Radial $6d_{xz}$ electron density (4 gaussians).

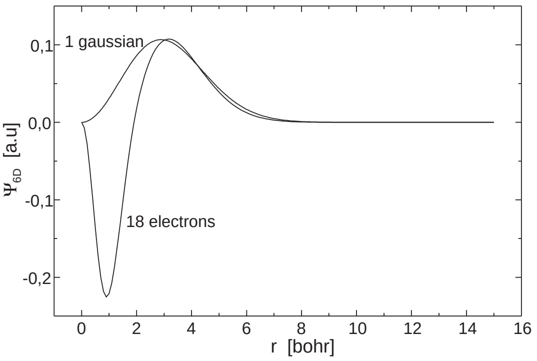

Figure 7.14: $6d_{xz}$ wavefunction cut along the XZ axis.

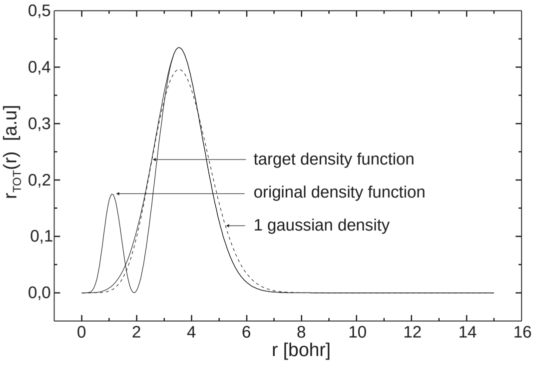

Figure 7.15: $6d_{xz}$ density functions.

questions the quality of 6d orbital. These nodeless orbitals can form the basis of a new 1-valence electron ECP to represent the bulk atoms in the metal cluster, while the orbital energies can be taken directly form calculations with the HAY and WADT ECP (LanL2DZ 6s: −0.29574 H, 6p: −0.13581 H, 6d: +0.2384 H) to achieve a seamless transition between active and passive surface and bulk atoms.

These values alone proofed not to be sufficient for the development of an experimental 1-valence electron ECP. Additionally we calculated the electron affinity from the HAY and WADT LanL2 ECP (+0.051 H). The new 1-electron ECP has also to reproduce the properties of the $^3D-^3D$ platinum dimer (subsection 6.2.1, page 159). The bond length has to be approximately 2.3579 Å and the bonding energy close to 0.08 H.

Here is a list of desired properties for a new 1-valence electron ECP:

1. The energy of the 6s orbital should be −0.2957 H and its shape should be similar to the plot shown in figure 7.5, if the orbital is allowed to change during the creation of the new ECP.
2. The energy of the 6p orbital should be −0.1358 H and its shape should be similar to the plot shown in figure 7.10.
3. The 6d orbital can be described with a single gaussian ($\alpha = 0.1196$ a.u., figure 7.14). The energy of this orbital should be close to +0.2384 H.
4. The bonding energy of the optimized platinum dimer should be 0.08 H.
5. The bond length in the optimized platinum dimer should 2.3579 Å.
6. The electron affinity of platinum atom should be 0.0512 H.
7. The ECP has to vanish for large distances r from the nucleus: $U_{ECP}(r \to \infty) = 0$

The last point describes a property of the ECP and not of an electron. It was included into the list for completeness sake. The list contains now all parameters used for the development of the new ECP.

7.2 Principle questions about a 1 electron ECP

In section 7.1 we developed a set of suitable properties for a 1-valence electron ECP. The first approach to a new ECP was very naive. We used Gaussian 94 as black box and used the 'Simulated Annealing' algorithm to find a new set of ECP parameters. All these experiments were very successful in their own way. The new ECP was able always to reproduce all target properties despite one. To make things really unpleasant, it was always another property than in the previous experiment.

During these calculations we developed a Pt_9-H_2O surface model (same geometry as in figure 6.67, page 192), which gave very useful results: The optimised bond length was 2.3383 Å and the water molecule was nearly parallel to the metal surface $\gamma = 107.6°$. The bonding energy (15.14 kcal/mol) was very close to the experimental value and the energies to reorientate the water molecule agreed well with values obtained in chapter V. 3.3 kcal/mol were necessary to move the hydrogens upwards ($\gamma = 107.6° \to \gamma = 180°$) is reasonable small and the rotational energy barrier of 0.028 kcal/mol negligible. The chosen ECP gave very good values for Pt_9-H_2O but only poor for Pt_5-H_2O. Polarisation effects caused a sharp bent of the dissociation curve at a platinum-oxygen distance of 2.5 to 3.2 Å. The polarisation effects were caused by badly chosen parameter in U_P^{core} (equation 2.65), which moved the 6p electron density too close to the nucleus. For small values of d_{PtO} the platinum cluster is polarized by the water molecule and 6p orbitals become populated instead of 6s orbitals (subsection 5.3.3, page 125).

The strong influence of the ECP parameter nourished the suspicion, that anything is possible regardless of physical reality with a suitable set of ECP parameters. We decided therefore to commence with a principal analysis of the ECP to understand all parameters of the calculation in detail.

7.2.1 Is it possible to use the method from Hay and Wadt?

The central formula (equation 2.59a, page 32) for the development of a new 1-electron ECP is:

$$U_l^{core}(r) = E_{nl} - \frac{\hat{h}\,\chi_{nl}}{\chi_{nl}} = E_{nl} - \frac{l\,(l+1)}{2\,r^2} + \frac{Z}{r} + \frac{\chi''_{nl}}{2\,\chi_{nl}} \tag{7.22}$$

If r approaches infinity should U_l^{core} vanish for physical reasons. This leads to the following equation for the ECP:

$$\lim_{r\to\infty} \frac{l\,(l+1)}{2\,r^2} = 0 \qquad\qquad \lim_{r\to\infty} \frac{Z}{r} = 0$$

$$U_l^{core}(r\to\infty) = E_{nl} \;+\; \frac{\chi''_{nl}}{2\,\chi_{nl}} \;=\; E_{nl} \;+\; \frac{1}{2\,\chi_{nl}}\,\frac{\partial^2}{\partial r^2}\,\chi_{nl} \tag{7.23}$$

For large values of r the gaussian with the smallest exponent will dominate equation 7.23.

$$\chi_{nl} = e^{-\alpha r^2} \qquad\qquad \chi''_{nl} = (4\,\alpha^2\,r^2 \;-\; 2\,\alpha)\;e^{-\alpha r^2}$$

$$U_l^{core}(r\to\infty) = E_{nl} + (2\,\alpha^2\,r^2 \;-\; \alpha) \tag{7.24}$$

It is therefore impossible to create a new potential with the method described by Hay and Wadt from a gaussian type wave function, because U_l^{core} approaches infinity for large values of r. A gaussian type function shows the wrong behaviour for large r. A Slater type function ($e^{-\alpha r}$) is closer to the true radial function and the kinetic energy term approaches α^2 as r gets infinite.

7.2.2 Which conditions has a gaussian type wavefunction to fulfill?

orb.	ϵ_i [H]
6s	-0.29574
6p	-0.13581
6d	**+0.23842**

Table 7.3: LanL2 eigenvalues.

Table 7.3 shows the eigenvalues for the 6s, 6p and 6d orbital calculated with the 18 valence electron ECP from Hay and Wadt. The development of a new 1-valence electron ECP from this potential started with the analysis of the d orbitals, since the original potential is not provided with a basis set for f orbitals. The pure theory of core potentials demands, that the development of a new potential should at least start with L=3 and not with the d-orbital (L=2) [189]. Those simplifications can be justified with two arguments: First, quantum chemical calculations on small platinum clusters showed, that the intermetallic bond is formed purely from 6sp orbitals and 6d orbitals are not involved. A restriction of L=2 is therefore a restriction of the ECP to the active orbitals in intermetallic bonds. Second, a similar simplification has been used successfully before on uranium [221], where Kahn et al. selected L=3 and not L=4 as requested by theory. Setting L=2 restricts therefore the general usage of the new potential to a small class of problems, but should be possible in principle.

Which conditions next to the reproduction of the correct eigenvalues should the ECP fulfill ?

1. The wavefunctions χ should fulfill the energy minimization criterion

$$\frac{<\chi\,|\,\hat{H}\,|\,\chi>}{<\chi\,|\,\chi>} = \text{minimal} \tag{7.25}$$

2. The ECP should create the correct shape of the original function χ and the energy eigenvalue, if χ is split into the generating gaussians.

3. The ECP should vanish for large values of r and not reach too far.

4. If the ECP is used for the calculation of Pt_2 ($6s^2$) the binding energy and the interatomic distance should be reproduced correctly from the Hay and Wadt calculation ($5d^{18}6s^2$, subsection 6.2.1, page 159).

7.2.3 Is a positive eigenvalue for the 6d orbital physically reasonable?

A positive energy eigenvalue implies, that the nucleus repels the electron. This is physically unreasonable. The 6d electron should be bonded weakly at a long distance from the nucleus, but should be bonded. It is therefore reasonable to assume that the 6d eigenvalue should be small and negative.

To check this assumption a fourth gaussian was added to the Hay and Wadt basis set. Now the calculation of the 6d orbital was repeated with the augmented basis set and the exponent of the new gaussian steadily decreased (table 7.4). As the exponent becomes smaller the new gaussian becomes more important for the wavefunction. At the optimum ($\alpha_{\text{NEW}} = 0.0139$, $\epsilon_{6d} = 0.05187$ H) are the other coefficients negligible ($c_1 = 0.05$, $c_2 = 0.06$). Passing this minimum the coefficients for the original functions approach zero and the coefficient of the new gaussian one, but the energy increases again. As the electron density moves away from the nucleus the binding energy becomes zero. Finally, the exponent is too small and the function vanishes from the 6d orbital.

α_{NEW}	c_{NEW}	ϵ_{6d} [H]
n.n.	n.n	0.23842
0.13	11.4531	0.10444
0.10	2.23576	0.06945
0.05	1.09476	-0.00817
0.02	0.99382	-0.04957
0.01	**0.99714**	**-0.05034**
0.009	0.99773	-0.04946
0.008	0.99828	-0.04831
0.001	1.0	-0.02342
0.0001	1.0	-0.00816
0.00001	0.0	0.23842

Table 7.4: 6d orbital with a augmented basis set.

The optimum is close to the values expected for a hypothetical 1d electron at the hydrogen nucleus (subsection 7.2.4). This result suggests, that the ECP from Hay and Wadt in its given form is unable to describe the 6d electrons correctly. The short range of the ECP prevents a correct modulation of the wavefunction far away from the nucleus and the Coulomb regime takes over.

This result for the 6d electrons allows us to choose between two forms for the new ECP:

1. The ECP tries to reproduce the positive eigenvalue for the 6d electrons to be consistent within the potentials regardless of physics.

2. The ECP tries to reproduce some new, physical reasonable properties of the 6d electrons. This method raises the question of the origin of those new properties.

First, we tried to find a new 1-valence electron ECP, which guarantees a smooth transition between two symmetrically different platinum atoms.

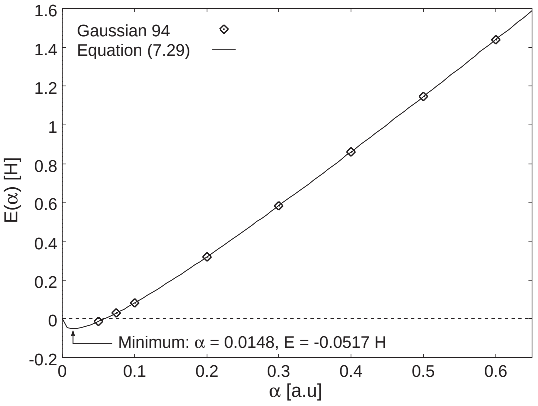

Figure 7.16: Test of equation 7.29 with Gaussian 94.

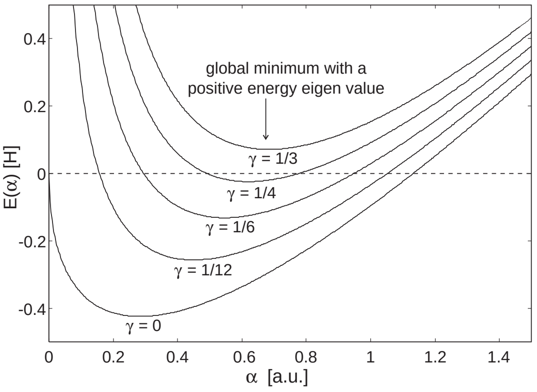

Figure 7.17: Global minimum with a positive energy eigenvalue.

7.2.4 How does Gaussian 94 calculate the energy of the orbitals?

Previous work showed (subsection 7.1.3) that the 6d orbital can be represented with a single gaussian. The first task was therefore to find an analytic expression for the orbital energy as a function of the orbital exponent α. To simplify this first attempt, the ECP was set equal to zero. This simplification reduces the task to a hydrogen like problem. The very first job was therefore to find an analytic expression for a single gaussian s, p and d function at a hydrogen nucleus.

At the beginning the hamiltonian was split into the kinetic and the coulomb energy and expectation values for both fragments were calculated separately.

$$\hat{H} = -\frac{1}{2}\nabla^2 - \frac{1}{r} = \hat{T} + \hat{C}$$

$$E = \frac{<\chi\,|\,\hat{H}\,|\,\chi>}{<\chi\,|\,\chi>} = \frac{<\chi\,|\,\hat{T}\,|\,\chi>}{N^2} + \frac{<\chi\,|\,\hat{C}\,|\,\chi>}{N^2} = T + C \qquad N^2 = <\chi\,|\,\chi> \tag{7.26}$$

The calculations for the individual orbitals may be summarized as follows:

s

$$\chi = e^{-\alpha r^2} \qquad N^2 = \frac{1}{2}\sqrt{\frac{\pi^3}{2\alpha^3}} \qquad E = T + C = \frac{3}{2}\alpha - 2\sqrt{\frac{2\,\alpha}{\pi}} \tag{7.27}$$

p_z

$$\chi = r\,\cos\theta\, e^{-\alpha r^2} \qquad N^2 = \frac{1}{2}\sqrt{\frac{\pi^3}{(2\alpha)^5}} \qquad E = T + C = \frac{5}{2}\alpha - \frac{4}{3}\sqrt{\frac{2\,\alpha}{\pi}} \tag{7.28}$$

d_{z^2}

$$\chi = r^2\,(3\cos^2\theta - 1)\,e^{-\alpha r^2} \qquad N^2 = \frac{3}{8}\sqrt{\frac{\pi^3}{2\alpha^7}} \qquad E = T + C = \frac{7}{2}\alpha - \frac{16}{15}\sqrt{\frac{2\,\alpha}{\pi}} \tag{7.29}$$

The validity of the equations 7.27 to 7.29 was checked by a direct comparison with results from Gaussian 94. The equations reproduced the energy eigenvalues for single gaussian wave functions to the last digit. Figure 7.16 shows the results of this test for a d-type function.

In the next step the functions were tested in ECP calculations with all factors d_i set to zero. The same results were obtained as before for the hydrogen atom. The equation 7.27 to 7.29 represent correctly the energy of a single electron in an infinite weak core potential. All energy functions

E(α) have a minimum, which marks the best single gaussian wavefunction for an orbital. This minimum of equation 7.29 was found analytically:

$$\frac{dE}{d\alpha} = \frac{7}{2} - \frac{16}{15\,\pi}\sqrt{\frac{2}{\pi\,\alpha}} = 0 \qquad \alpha_{\min} = \frac{1024}{2 \cdot 11025\,\pi} = 0.0148 \tag{7.30}$$

7.2.5 Under which conditions is global minimum with a positive eigenvalue possible?

The kinetic energy term $\frac{7}{2}\,\alpha$ vanishes as the electron density moves away from the nucleus ($\alpha \to 0$). The same argument holds for the Coulomb energy as it scales with $\sqrt{\alpha}$. To make the minimum global the ECP has to generate a positive energy eigenvalue as α approaches nought. In the best case (E(α) $\leq$ E($\alpha - \delta$), $\delta > 0$) this condition implies that the potential V(r) converges to a positive nonzero value as r becomes infinite. In the other case (E(α) $<$ E($\alpha - \delta$), $\delta > 0$) V(r) itself becomes infinite as r becomes infinite. This condition leads to constant growth of E(α) as α approaches nought. The second condition was tested with a simple parabola V(r) = $\gamma \cdot \mathrm{r}^2$ and an s-orbital.

$$V(r) = \gamma\,r^2 \qquad \frac{<\chi_S\,|\,V(r)\,|\,\chi_S>}{<\chi_S\,|\,\chi_S>} = \frac{3\,\gamma}{4\,\alpha} \qquad E_S^{\mathrm{tot}}(\alpha) = \frac{3}{2}\,\alpha - 2\sqrt{\frac{2\,\alpha}{\pi}} + \frac{3\,\gamma}{4\,\alpha} \tag{7.31}$$

Equation 7.32 allows us to choose a suitable γ to place the minimum at each $\alpha > \frac{8}{9\,\pi}$. For $\alpha < \frac{8}{9\,\pi}$ turns the minimum into a maximum.

$$\frac{dE_S^{\mathrm{tot}}}{d\alpha} = \frac{3}{2} - \sqrt{\frac{2}{\pi\,\alpha}} - \gamma\,\frac{3}{4\,\alpha^2} = 0 \qquad \gamma = \frac{4\,\alpha^2}{3}\left(\frac{3}{2} - \sqrt{\frac{2}{\pi\,\alpha}}\right) \tag{7.32}$$

These results suggest (figure 7.17) that it is possible to find a potential, which creates a positive energy eigenvalue and this value is the same time the global minimum. It is only possible to bind an electron with a positive energy eigenvalue, if the V(r) has a positive, non vanishing value as r approaches infinity, other wise would the global minimum be at $\alpha = 0$ (equation 7.27). Such a potential is physically unreasonable and the search in this direction stopped right here.

7.2.6 How does Gaussian calculate the ECP?

The ECP input for G94 has the same form as published by Hay and Wadt [222].

$$r^2\,[U_l^{\mathrm{core}}(r) - U_L^{\mathrm{core}}(r)] = \sum_k d_k\,r^{n_k}\,\exp(-\zeta_k\,r^2) \qquad l = 0, 1, \ldots, L-1 \tag{2.65}$$

$$r^2\left[U_L^{\mathrm{core}}(r) - \frac{N_C}{r}\right] = \sum_k d_k\,r^{n_k}\,\exp(-\zeta_k\,r^2) \qquad l = L \tag{2.65 a}$$

L is the maximum angular quantum number. Equation 2.65a leads to the following expression for $\mathrm{U}_{\mathrm{L}}^{\mathrm{core}}$:

$$\begin{aligned} U_L^{\mathrm{core}}(r) &= \frac{N_C}{r} + \sum_k d_k\,r^{n_k-2}\,\exp(-\zeta_k\,r^2) \\ &= \frac{N_C}{r} + V(r) \qquad V(r) = \sum_k d_k\,r^{n_k-2}\,\exp(-\zeta_k\,r^2) \end{aligned} \tag{7.33}$$

The introduction of equation 7.33 into the system's hamiltonian leads to the following equation for the hamiltonian of a 1-electron platinum atom ($\mathrm{N_C} = 77$):

$$\begin{aligned} \hat{H}_{\mathrm{ECP}} &= -\frac{1}{2}\nabla^2 - \frac{78}{r} + U_L^{\mathrm{core}}(r) = -\frac{1}{2}\nabla^2 - \frac{1}{r} + V(r) = \hat{H}_H + V(r) \\ E_{\mathrm{ECP}} &= \frac{<\chi\,|\,\hat{H}_{\mathrm{ECP}}\,|\,\chi}{<\chi\,|\,\chi>} = E_H + \frac{<\chi\,|\,V(r)\,|\,\chi}{<\chi\,|\,\chi>} = E_H + \bar{V} \end{aligned} \tag{7.34}$$

The total energy of the system is therefore the hydrogen energy (equations 7.27 to 7.29) plus the expectation value $\bar{\mathrm{V}}$ of V(r). Equation 7.35 compiles all formula used for d-type gaussians, which form the basis of all following calculations. Equation 7.34 and equation 7.35 (for n=0 to n=4) have been tested with G94 for a d-type gaussian.

$$\begin{array}{llll} \text{input} & V_D(r) & \bar{V}_D & \\ 0 & \dfrac{1}{r^2}\,e^{-\beta r^2} & \dfrac{16}{5}\sqrt{\dfrac{2\,\alpha^7}{(2\alpha+\beta)^5}} & \\ 1 & \dfrac{1}{r}\,e^{-\beta r^2} & \dfrac{128}{15}\sqrt{\dfrac{2\,\alpha^7}{\pi\,(2\alpha+\beta)^6}} & \\ 2 & e^{-\beta r^2} & 8\sqrt{\dfrac{2\,\alpha^7}{(2\alpha+\beta)^7}} & \\ 3 & r\,e^{-\beta r^2} & \dfrac{384}{15}\sqrt{\dfrac{2\,\alpha^7}{\pi\,(2\alpha+\beta)^8}} & \\ 4 & r^2\,e^{-\beta r^2} & 28\sqrt{\dfrac{2\,\alpha^7}{(2\alpha+\beta)^9}} & \\ n \text{ odd} & r^{n-2}\,e^{-\beta r^2} & \dfrac{64\,k!}{15}\sqrt{\dfrac{2\,\alpha^7}{\pi\,(2\alpha+\beta)^{2(k+1)}}} & k = \dfrac{n+3}{2} \\ n \text{ even} & r^{n-2}\,e^{-\beta r^2} & \dfrac{64}{15}\,\dfrac{K}{2^k}\sqrt{\dfrac{2\,\alpha^7}{(2\alpha+\beta)^{2k+1}}} & k = \dfrac{n+4}{2} \\ & & & K = 1\cdot 3\cdot\dots\cdot(2\,k-1) \end{array} \tag{7.35}$$

The ECP calculations for the d-orbital are straight forward as L was chosen to be 2. Calculations for the 6s and 6p orbital are slightly more complicated due to the definition of $\mathrm{U_l^{core}}$ (equation 2.65).

$$\begin{aligned} \hat{H}^S_{\mathrm{ECP}} &= -\frac{1}{2}\nabla^2 - \frac{1}{r} + V_D(r) + \sum_k d_k\, r^{n_k-2}\,\exp(-\zeta_k\, r^2) = \hat{H} + V_S(r) \\ V_S(r) &= V_D(r) + \sum_k d_k\, r^{n_k-2}\,\exp(-\zeta_k\, r^2) = V_D(r) + V_S^{\mathrm{INP}} \end{aligned} \tag{7.36}$$

There are two possibilities to circumvent this complication for atomic test calculations:

1. All coefficients in the s-p input section are set equal to zero and the $\mathrm{U_l^{core}}$ is solely defined by the d-part of the input.
2. The d-coefficients are set zero and the $\mathrm{V_S(r)}$ is solely defined by the input in the s-section.

The later of the two possibilities was chosen for the test calculations. As before for the d-orbitals the results calculated with equation 7.37 for an s-orbital agree to the last digit with results found with Gaussian 94.

$$V_S(r) = e^{-\beta r^2} \qquad\qquad \bar{V}_S = 3\sqrt{\frac{2\,\alpha^3}{(2\,\alpha+\beta)^5}} \tag{7.37}$$

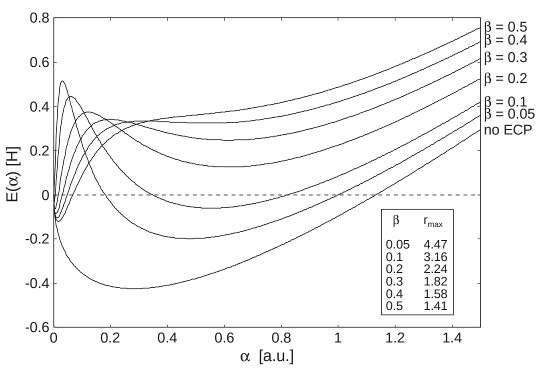

Figure 7.18: Plot of equation 7.39, $V_{\max} = 1.0$.

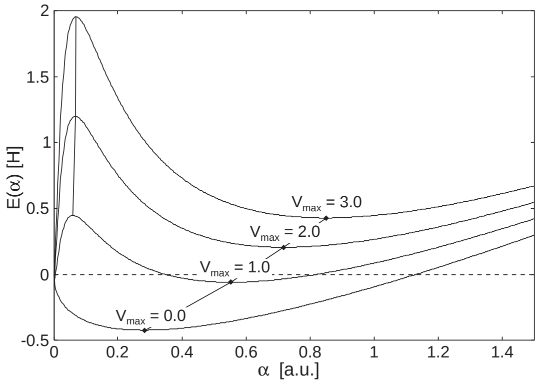

Figure 7.19: Plot of equation 7.39, $\beta = 0.1$.

7.2.7 What happens if the ECP vanishes as r becomes infinite?

By the multiplication of the polynomial (equation 7.31) with a gaussian $V_S(r)$ vanishes as r becomes infinite. V(r) has therefore a maximum.

$$V(r) = r^n \, e^{-\beta r^2}$$

$$\left(\frac{dV}{dr}\right)_{r=r_{max}} = 0 \qquad r_{max} = \sqrt{\frac{n}{2\beta}} \qquad V(r_{max}) = \left(\frac{n}{2\beta}\right)^{\frac{n}{2}} e^{-n/2} \tag{7.38}$$

$$n = 2 \qquad \longrightarrow \qquad r_{max} = \frac{1}{\sqrt{\beta}} \qquad V(r_{max}) = \frac{1}{e\,\beta}$$

Equation 7.38 enables us to transform V(r) into $V_T(r)$, which allows us to compare different ECPs more easily.

$$V_T(r,\, V_{max},\, \beta) = \frac{V_{max}}{V(r_{max})}\, r^2\, e^{-\beta r^2} = V_{max}\, \beta\, e\, r^2\, e^{-\beta r^2} \tag{7.39}$$

Equation 7.39 allows us to preset the maximum value of the ECP. The energy of a s-electron moving in an ECP described by equation 7.39 is given below.

$$E(\alpha) = \frac{3}{2}\alpha - 2\sqrt{\frac{2\,\alpha}{\pi}} + 3\, V_{max}\, \beta\, e\, \sqrt{\frac{2\,\alpha^3}{(2\,\alpha + \beta)^5}} \tag{7.40}$$

Figure 7.20 shows the composition of the total energy (equation 7.40). $\bar{V}_S$ vanishes with increasing values of α as $\bar{V}_S$ scales with α^{-1} for large values of α. Since the slope of the Coulomb energy is smaller than the slope of the kinetic energy term for large α is the right side of figure 7.20 dominated by the kinetic energy term. Both the kinetic energy term and the Coulomb energy vanish as α becomes zero. The left-hand side of figure 7.20 is therefore dominated by $\bar{V}_S$. The balance between $\bar{V}_S$ and the kinetic energy creates the environment for a local minimum. As the maximum of $\bar{V}_S$ moves to the right side (increasing values of β) into the reign of the kinetic energy the local minimum should vanish. Figure 7.18 shows the total energy for different values of β. As the maximum of V_S gets closer to the nucleus the local minimum becomes shallower until it vanishes finally. At the same time $\bar{V}_S$ at the left side becomes less dominant, the Coulomb regime controls the shape of the curve and the global minimum becomes deeper. In contrast to figure 7.18 shows figure 7.19 the influence of V_{MAX} on the total energy. The position of the maximum hardly moves whereas the position of the minimum moves nearly linearly with increasing values of V_{MAX}.

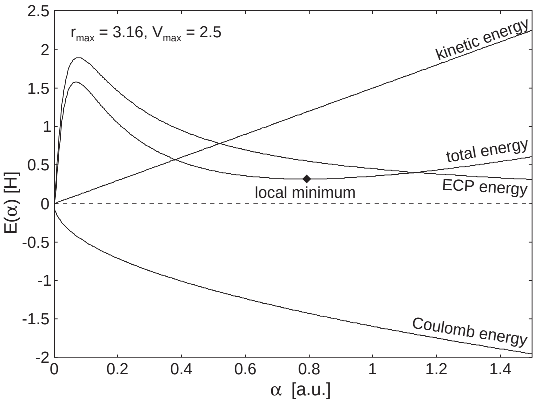

Figure 7.20: Individual energy contributions; equation 7.39, $\beta = 0.1$, $\mathrm{V_{max}} = 2.5$.

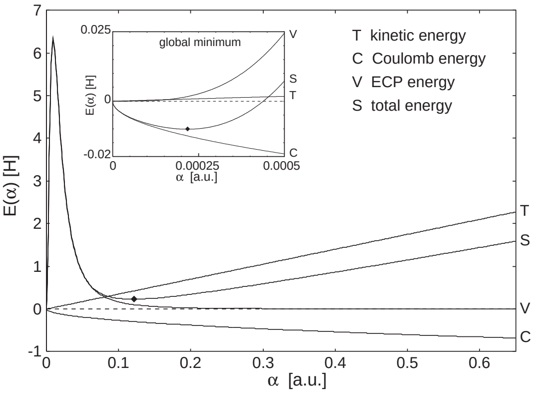

Figure 7.21: ECP with local minimum; $\mathrm{E_T} = 0.23$, $\alpha = 0.12$, $\beta = 0.016$, $\mathrm{d} = 2.53 \cdot 10^{-5}$.

Unlike figure 7.18 the local minimum won't vanish, because there will be always a point at large values of α where the kinetic energy becomes stronger than $\bar{\mathrm{V}}_\mathrm{S}$.

7.2.8 Which form has an ECP with a local minimum and a positive eigenvalue for d-electrons?

To construct an ECP which fulfills all conditions a function of the type $\mathrm{r^n} \cdot \exp[-\beta \mathrm{r}^2]$ was added to the hydrogen Hamiltonian. Following the discussion of $\mathrm{n} = 6$, a general description is given.

$$V_D(r) = d\, r^6\, e^{-\beta r^2} \qquad\qquad \bar{V}_D = 693\, d \sqrt{\frac{2\,\alpha^7}{(2\,\alpha+\beta)^{13}}} \tag{7.41}$$

The ECP function $\mathrm{r^n} \cdot \exp[-\beta \mathrm{r}^2]$ was multiplied by a factor d and $\bar{\mathrm{V}}_\mathrm{D}$ added to the hydrogen energy $\mathrm{E_H}$ in order reproduce the given energy eigenvalue $\mathrm{E_T}$ of 0.23 H for the 6d orbital.

$$\Delta E = E_T - E_H = E_T - \frac{7}{2}\,\alpha + \frac{16}{15}\sqrt{\frac{2\,\alpha}{\pi}} \tag{7.42}$$

$$= d\,\bar{V}_D = 693\, d \sqrt{\frac{2\,\alpha^7}{(2\,\alpha+\beta)^{13}}} \qquad \rightarrow \qquad d = \frac{\Delta E}{693}\sqrt{\frac{(2\,\alpha+\beta)^{13}}{2\,\alpha^7}} \tag{7.42\,a}$$

The condition for a minimum is the vanishing first derivative of the total energy.

$$\frac{dE}{d\alpha} = \frac{7}{2} - \frac{8}{15}\sqrt{\frac{2}{\pi\,\alpha}} + 693\, d \sqrt{\frac{2\,\alpha^5}{(2\,\alpha+\beta)^{13}}}\left(\frac{7}{2} - 13\,\frac{\alpha}{2\,\alpha+\beta}\right) = 0 \tag{7.43}$$

The introduction of the second half of equation 7.42a into equation 7.43 gave the following equation, which can be solved analytically.

$$\frac{dE}{d\alpha} = \frac{7}{2} - \frac{8}{15}\sqrt{\frac{2}{\pi\,\alpha}} + \frac{\Delta E}{\alpha}\left(\frac{7}{2} - 13\,\frac{\alpha}{2\,\alpha+\beta}\right) = 0 \tag{7.44}$$

$$\beta = \alpha\left(\frac{7}{26} - \frac{\alpha}{13\,\Delta E}\left(\frac{8}{15}\sqrt{\frac{2}{\pi\,\alpha}} - \frac{7}{2}\right)\right)^{-1} - 2\,\alpha \tag{7.44\,a}$$

A stationary point (α, $\mathrm{E_T}$) in the $\mathrm{E}(\alpha)$ curve can be created with an ECP $\mathrm{V_D}(\mathrm{d},\beta)$ (equation 7.41). The central parameter is $\Delta\mathrm{E}$, which controlls both parameters d and β of the ECP. Figure

7.21 shows the total energy as a function of α calculated with the solutions of the equations 7.44a and 7.42a. At $\alpha = 0.12$ is a local minimum with an energy eigenvalue of 0.23 H. The close up in the upper left corner shows the global minimum at $\alpha \approx 2.5 \cdot 10^{-4}$. $\mathrm{V_D}(\mathrm{r})$ has its maximum at 13.8 bohr. $\mathrm{V_D}(\mathrm{r})$ spreads widely, but still vanishes as r becomes infinite. Regarding an interatomic distance of 5.23 bohr (2.77 Å) in bulk platinum this ECP would reach its maximum at the second next neighbour, which is physically unreasonable.

The maximum of the standard ECP function depends on the exponent n and β in the gaussian function (equation 7.38). The only free variable to move this maximum is n, because β is determined by the conditions $\mathrm{E_T}$ and α_{MIN}. The next step was therefore the development of set equations, which allow the calculation of β and d for any given exponent n.

For odd exponents n:

$$\bar{V}_D(\alpha) = \frac{64\,k!}{15}\sqrt{\frac{2\,\alpha^7}{\pi\,(2\alpha+\beta)^{2(k+1)}}} \qquad k = \frac{n+3}{2} \tag{7.45}$$

$$E_T(\alpha) = E_H(\alpha) + d\,\bar{V}_D(\alpha) \tag{7.45\,a}$$

$$d = \frac{E_T(\alpha) - E_H(\alpha)}{\bar{V}_D} = \frac{\Delta E}{\bar{V}_D} = \frac{15\,\Delta E}{64\,k!}\sqrt{\frac{\pi\,(2\alpha+\beta)^{2(k+1)}}{2\,\alpha^7}} \tag{7.45\,b}$$

$$\frac{d\bar{V}_D}{d\alpha} = \frac{\bar{V}_D}{\alpha}\left(\frac{7}{2} - 2\,(k+1)\,\frac{\alpha}{2\alpha+\beta}\right) \tag{7.45\,c}$$

$$\frac{dE_T}{d\alpha} = \frac{7}{2} - \frac{8}{15}\sqrt{\frac{2}{\pi\alpha}} + d\,\frac{\bar{V}_D}{\alpha}\left(\frac{7}{2} - 2\,(k+1)\frac{\alpha}{2\alpha+\beta}\right) \tag{7.45\,d}$$

$$= \frac{7}{2} - \frac{8}{15}\sqrt{\frac{2}{\pi\alpha}} + \frac{\Delta E}{\alpha}\left(\frac{7}{2} - 2\,(k+1)\frac{\alpha}{2\alpha+\beta}\right) = 0 \tag{7.45\,e}$$

$$\beta = 2\,\alpha\,(k+1)\left(\frac{7}{2} - \frac{\alpha}{\Delta E}\left(\frac{8}{15}\sqrt{\frac{2}{\pi\,\alpha}} - \frac{7}{2}\right)\right)^{-1} - \;2\,\alpha \tag{7.45\,f}$$

For even exponents n:

$$\bar{V}_D(\alpha) = \frac{64}{15}\,\frac{K}{2^k}\sqrt{\frac{2\,\alpha^7}{(2\alpha+\beta)^{2k+1}}} \qquad k = \frac{n+4}{2}, \quad K = 1\cdot 3\cdot 5\cdot\dots\cdot(2k-1) \tag{7.46}$$

$$E_T(\alpha) = E_H(\alpha) + d\,\bar{V}_D(\alpha) \tag{7.46\,a}$$

$$d = \frac{E_T(\alpha) - E_H(\alpha)}{\bar{V}_D} = \frac{\Delta E}{\bar{V}_D} = \frac{15\,2^k\,\Delta E}{64\,K}\sqrt{\frac{(2\alpha+\beta)^{2k+1}}{2\,\alpha^7}} \tag{7.46\,b}$$

$$\frac{d\bar{V}_D}{d\alpha} = \frac{\bar{V}_D}{\alpha}\left(\frac{7}{2} - (2\,k+1)\,\frac{\alpha}{2\alpha+\beta}\right) \tag{7.46\,c}$$

$$\frac{dE_T}{d\alpha} = \frac{7}{2} - \frac{8}{15}\sqrt{\frac{2}{\pi\alpha}} + d\,\frac{\bar{V}_D}{\alpha}\left(\frac{7}{2} - (2\,k+1)\frac{\alpha}{2\alpha+\beta}\right) \tag{7.46\,d}$$

$$= \frac{7}{2} - \frac{8}{15}\sqrt{\frac{2}{\pi\alpha}} + \frac{\Delta E}{\alpha}\left(\frac{7}{2} - (2\,k+1)\frac{\alpha}{2\alpha+\beta}\right) = 0 \tag{7.46\,e}$$

$$\beta = \alpha\,(2\,k+1)\left(\frac{7}{2} - \frac{\alpha}{\Delta E}\left(\frac{8}{15}\sqrt{\frac{2}{\pi\,\alpha}} - \frac{7}{2}\right)\right)^{-1} - \;2\,\alpha \tag{7.46\,f}$$

By the introduction of definition of k into equations 7.45f and 7.46f both equations become equal. This equation (7.47) together with the equations 7.45b and 7.46b allow us to create a local

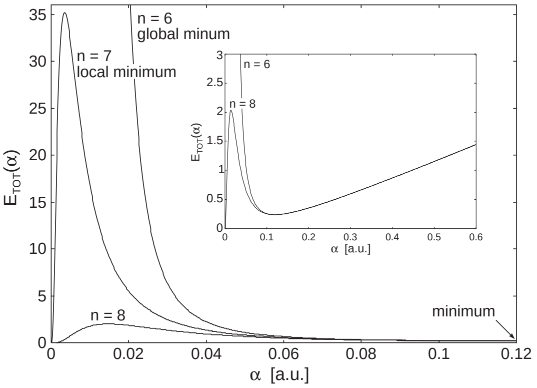

Figure 7.22: Local minimum for n = 6, 7 and 8.

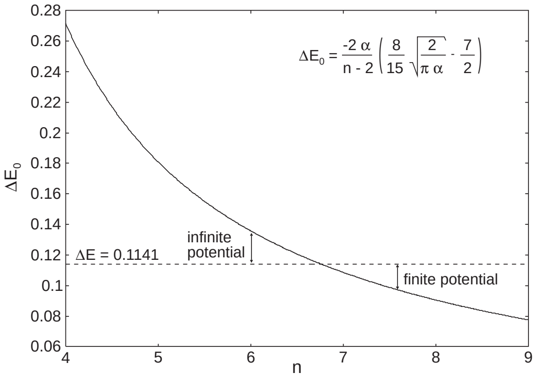

Figure 7.23: Minimum energy difference for a finite potential.

minimum (α, $\mathrm{E_T}$) for any given exponent n.

$$\text{odd:}\quad 2\left(\frac{n+3}{2}+1\right)=n+5 \qquad\qquad \text{even:}\quad 2\,\frac{n+4}{2}+1=n+5$$

$$\beta=\alpha\,(n+5)\,\left(\frac{7}{2}-\frac{\alpha}{\Delta E}\left(\frac{8}{15}\sqrt{\frac{2}{\pi\,\alpha}}-\frac{7}{2}\right)\right)^{-1}\;-\;2\,\alpha \tag{7.47}$$

$$=-0.13746\;+\;n\,0.02035 \qquad\qquad (\alpha=0.1196,\;E_T=0.23842\text{ (equation 7.21))}$$

The results of these calculations are listed in table 7.5 for $\alpha = 0.1196$ and $\mathrm{E_T} = 0.23842$. n is the exponent in the Gaussian input section, where as V(r = 10.0), $\mathrm{r_{MAX}}$ and V($\mathrm{r_{MAX}}$) are properties of the effective potential according to the equations 7.33 and 7.38. As n increases from 6 to 7 changes β its sign and the global minimum becomes local. This is shown in figure 7.22. The plot shows $\mathrm{E_T}(\alpha)$ for n = 6, 7 and 8. With increasing values for n moves the maximum of the energy curve closer to the nucleus and bevomes smaller. The linear dependency of β_{OPT} on n facilitates the calculation of the limes of $\mathrm{r_{MAX}}$.

The combination of equation 7.47 with equation 7.38 leads to an equation, which allows us to describe the development of the maximum of the effective potential with a simple formula and to get a good estimate of the limes.

$$r_{max}(n)=\sqrt{\frac{n-2}{-0.27492+n\,0.0407}} \qquad\qquad \lim_{n\to\infty} r_{max}=4.95682 \tag{7.48}$$

This result agrees well with 4.98 bohr calculated with equation 7.46f for n = 550. With increasing values for n the maximum of the effective function $\mathrm{V_D}$(r) moves closer to the maximum of the radial electron density, while the preexponetial factor $\mathrm{d_{OPT}}$ decreases exponentially. With increasing values of n becomes $\mathrm{d_{OPT}}$ exponentially smaller. This devellopment can be described with the following expression: $\ln(\mathrm{d_{OPT}}) \approx -1.60669 - \mathrm{n}\cdot 1.08572$. Each time n is increased by 1 $\mathrm{d_{OPT}}$ decreases approximately by a factor of 3.

The value of β depends on the energy difference ΔE between the hydrogen energy and the target energy (equations 7.42 and 7.47). For $\Delta\mathrm{E_0}$ β equals nought. If ΔE is larger than $\Delta\mathrm{E_0}$ β becomes positive and the ECP vanishes as r becomes infinite. Figure 7.23 shows $\Delta\mathrm{E_0}$ as a function of n. The equation used for the plot follows directly from equation 7.47.

$$\beta=0 \qquad\qquad \Rightarrow \qquad\qquad \Delta E_0=\frac{2\,\alpha}{n-2}\left(\frac{7}{2}-\frac{8}{15}\sqrt{\frac{2}{\pi\,\alpha}}\right) \tag{7.49}$$

n	β_{OPT}	$\mathrm{d}_{\mathrm{OPT}}$	V(r=10.0)	$\mathrm{r}_{\mathrm{MAX}}$	V($\mathrm{r}_{\mathrm{MAX}}$)
0	−0.137463	1.4075E−01	1.3133E+03	—	—
1	−0.117115	5.1563E−02	6.2891E+02	—	—
2	−0.096768	1.8597E−02	2.9649E+02	—	—
3	−0.07642	6.6319E−03	1.3821E+02	—	—
4	−0.056073	2.3449E−03	6.3877E+01	—	—
5	−0.035725	8.2362E−04	2.9326E+01	—	—
6	−0.015378	2.8774E−04	1.3392E+01	—	—
7	0.00497	1.0008E−04	6.0888E+00	22.429	46.631
8	0.025317	3.4683E−05	2.7581E+00	10.886	2.8732
9	0.045664	1.1982E−05	1.2455E+00	8.7548	1.4263
10	0.066012	4.1282E−06	5.6092E−01	7.7843	1.0194
11	0.086359	1.4190E−06	2.5203E−01	7.2186	0.83895
12	0.106707	4.8680E−07	1.1301E−01	6.8452	0.7409
13	0.127054	1.6669E−07	5.0584E−02	6.5794	0.68131
14	0.147402	5.6988E−08	2.2605E−02	6.38	0.64255
15	0.167749	1.9455E−08	1.0087E−02	6.2248	0.61625
16	0.188097	6.6330E−09	4.4955E−03	6.1004	0.59795
20	0.269487	8.8673E−11	1.7544E−04	5.779	0.56557
50	0.87991	5.9993E−25	3.6650E−15	5.2226	0.651
100	1.89728	1.0352E−48	4.1403E−33	5.082	0.84277

Table 7.5: Local minum created with various exponets n (calculated with equations 7.45 and 7.46).

With decreasing values of n ΔE_0 becomes larger. Small values for n are therefore only possible for large values of ΔE. Figure 7.24 shows how β changes with increasing values for ΔE for various n. All curves converge to different values for β, but the maximum off the effective function is for all curves at the same place (6.39 bohr).

$$\lim_{\Delta E \to \infty} \beta = \alpha \left(\frac{2}{7}(n+5) - 2 \right) = \beta_{max} \qquad r_{max} = \sqrt{\frac{n-2}{2\,\beta_{max}}} = \sqrt{\frac{7}{4\,\alpha}} \tag{7.50}$$

With increasing values for ΔE it becomes possible to construct a local minimum with a small exponent, but the maximum of the ECP cannot get closer to the nucleus than 3.9 bohr. This maximum is close to the next neighbour in bulk platinum ($\mathrm{d}_{\mathrm{PtPt}}$ = 5.23 bohr).

The possibility to construct a working ECP from equation 7.47 is restricted by two points:

1. The smallest possible value for d in the Gaussian 94 input section.

2. The highest value for n, which is tolerated by the Gaussian 94 ECP module

The smallest possible value for d allowed by Gaussian 94 is $1{\cdot}10^{-8}$, which would allow us to go as high as n = 15 (table 7.5) as exponent in the input section. Tests with n = 6 and n = 5 showed, that ECPs with high exponents are numerically challenging for Gaussian 94 and the calculations do not converge. ***It is therefore impossible to realize an ECP with a local minimum and a positive energy eigenvalue with single ECP function in Gaussian 94.***

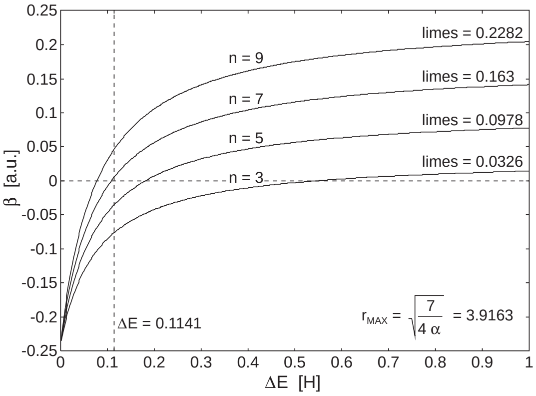

Figure 7.24: β as a function of ΔE for various n (α = 0.1141).

7.2.9 Is it possible to create a local minimum with two or more functions?

Whether a potential vanishes at infinite values for r or becomes infinite itself depends on ΔE (equation 7.47, 7.49 and figure 7.24). With increasing values for ΔE it becomes more likely, that small values for n still form a finite and therefore physical reasonable potential. The idea is therefore to add a second function to the potential to decrease the total energy. Equation 7.35 list the expectation values for different potentials. The expectation value of potentials with n $\geq$ 3 vanishes as α becomes infinite.

$$\lim_{\alpha \to \infty} \bar{V}_D \propto \alpha^{-\frac{n-2}{2}} = 0 \qquad \text{for } n \geq 3 \tag{7.51}$$

The choice of n $\geq$ 3 guarantees that the kinetic energy dominates the total energy for large values of α and that no extra function is necessary to keep the minimum at the correct place. The repulsive function to create the minimum was chosen to have n = 4, as previous calculations showed that Gaussian 94 still calculates correctly this ECP.

$$E_T(\alpha) = \frac{7}{2}\alpha \;-\; \frac{16}{15}\sqrt{\frac{2\,\alpha}{\pi}} \;-\; d_A\,\frac{384}{15}\sqrt{\frac{2\,\alpha^7}{\pi\,(2\alpha+\beta_A)^8}} \;+\; d_R\,28\sqrt{\frac{2\,\alpha^7}{(2\alpha+\beta_R)^9}} \tag{7.52}$$

The index 'A' identifies the parameter of the attractive energy and 'R' the repulsive part. The hydrogen energy E_H in equation 7.42 has to be replaced by a basic energy E_B, which includes the attractive third order energy.

$$\Delta E = E_T \;-\; E_B \;=\; E_T \;-\; E_H \;-\; d_A\,\bar{V}_D^3 \tag{7.53}$$

$$= E_T \;-\; \frac{7}{2}\alpha \;+\; \frac{16}{15}\sqrt{\frac{2\,\alpha}{\pi}} \;+\; d_A\,\frac{384}{15}\sqrt{\frac{2\,\alpha^7}{\pi\,(2\alpha+\beta_A)^8}} \tag{7.53\,a}$$

$$= d_R\,\bar{V}_D^4 = d_R\,28\sqrt{\frac{2\,\alpha^7}{(2\alpha+\beta_R)^9}} \qquad \rightarrow \qquad d_R = \frac{\Delta E}{28}\sqrt{\frac{(2\alpha+\beta_R)^9}{2\,\alpha^7}} \tag{7.53\,b}$$

In the next step equation 7.52 is differentiated, set equal to nought and β_R calculated after d_R has been replaced by equation 7.53b. The only difference to equation 7.47 is the new term in the

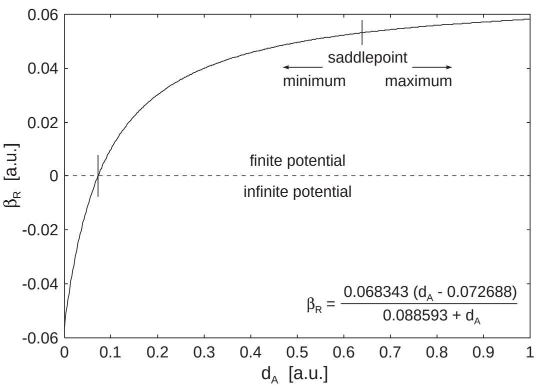

Figure 7.25: β_{R} versus $\mathrm{d_A}$.

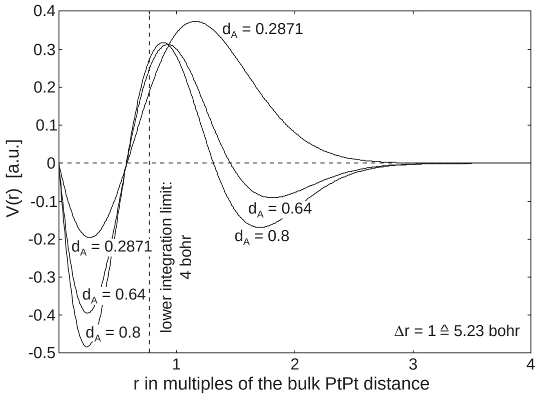

Figure 7.26: The ECP as a function of r.

centre, which contains the first derivative of $\bar{\mathrm{V}}_{\mathrm{D}}^{3}$.

$$\frac{dE}{d\alpha} = \frac{7}{2} - \frac{8}{15}\sqrt{\frac{2}{\pi\,\alpha}} - \frac{d_A\,\bar{V}_D^3}{\alpha}\left(\frac{7}{2} - 8\,\frac{\alpha}{2\alpha+\beta_A}\right) + \frac{\Delta E}{\alpha}\left(\frac{7}{2} - 9\,\frac{\alpha}{2\alpha+\beta_R}\right) = 0 \qquad (7.54)$$

$$\beta_R = \alpha(n+5)\left(\frac{7}{2} - \frac{\alpha}{\Delta E}\left(\frac{d_A\,\bar{V}_D^3}{\alpha}\left(\frac{7}{2} - 8\,\frac{\alpha}{2\alpha+\beta_A}\right) + \frac{8}{15}\sqrt{\frac{2}{\pi\,\alpha}} - \frac{7}{2}\right)\right)^{-1} - 2\alpha \qquad (7.54\,a)$$

β_{R} depends on three parameters. If we assume to facilitate the discussion, that the minimum of $\bar{\mathrm{V}}_{\mathrm{D}}^{3}$ is at the same place ($\alpha = \alpha_{\mathrm{MIN}} = 0.1196$) as the minimum of the total energy, vanishes the first central term from equation 7.54a. In this case equations 7.54 and 7.47 become equal and the value of β_{R} is solely determined by ΔE.

$$\frac{d\bar{V}_D^3}{d\alpha} = \frac{184}{15}\sqrt{\frac{2\,\alpha^5}{\pi\,(2\alpha+\beta_A)^8}}\left(\frac{7}{2} - \frac{8\,\alpha}{2\alpha+\beta_A}\right) = \frac{\bar{V}_D^3}{\alpha}\left(\frac{7}{2} - \frac{8\,\alpha}{2\alpha+\beta_A}\right) = 0 \qquad (7.55)$$

$$\beta_A = \frac{2}{7}\,\alpha = 0.0342 \qquad (7.55\,a)$$

Introducing equation 7.53 into equation 7.54a and setting $\mathrm{E_T} = 0.23842$, $\alpha = 0.1196$ leads to the following equations:

$$\Delta E = 0.11415 + 2.16385\,d_A$$

$$\beta_R = \frac{270\,\alpha\,\Delta E}{105\Delta E - 16\,\alpha\sqrt{\frac{2}{\pi\alpha}} + 105\,d_A} - 2\,\alpha = \frac{0.068343\,(d_A - 0.072688)}{0.088593 + d_A} \qquad (7.56)$$

Figure 7.25 shows the dependency of β_{R} on $\mathrm{d_A}$. β_{R} changes its sign at $\mathrm{d_A} = 0.0727$ and then approaches its possible maximum of 0.0683 (equation 7.50). The maximum of the repulsive function can therfore not get any closer than 3.404 bohr, which is closer than the next neighbour in bulk platinum. The transition from a minimum into a maximum via a saddlepoint has been satisfyingly checked with Gaussian 94 for $\mathrm{d_A} = 0.2871$ (minimum), 0.64 (saddle point) and 0.8 (maximum). This change restricts the $\mathrm{d_A}$ to the following range: $0.073 \leq \mathrm{d_A} \leq 0.64$ and the maximum of the repulsive function varies between infinity and 4.33 bohr. The attractive ECP function moves this maximum to higher values of $\mathrm{d_A}$. The ECP itself is shown in figure 7.26. For comparisson is the radius given in multiples of the bulk platinum-platinum distance. With increasing values of $\mathrm{d_A}$ emerges a second minimum in the region of the second neighbour (8 to 9 bohr). $\mathrm{d_A} = 0.2871$ creates the last potential with a all-positive tail at large values of r.

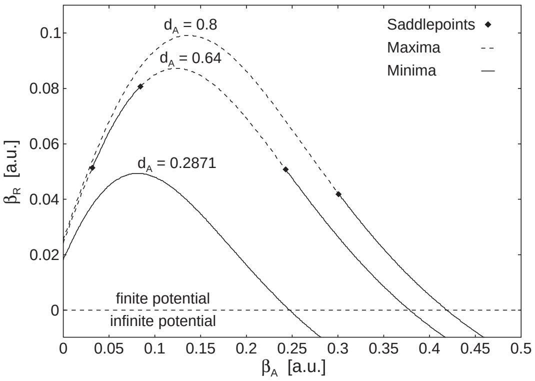

Figure 7.27 Variation of β_A.

$\mathrm{d_A}$	β_R	$\mathrm{r_{MAX}}$
a.u.	a.u.	a.u
0.2871	0.039	5.06
0.64	0.0532	4.33
0.8	0.0559	4.23

Table 7.6 Results for $\mathrm{d_A}$.

$$\text{tail} = \int_4^\infty V(r)^2\, dr = \int_4^\infty \left(-d_A\, r\, e^{-\beta_A r^2} \;+\; d_R\, r^2\, e^{-\beta_R r^2}\right)^2 dr \tag{7.57}$$

As shown in figure 7.26 changes the amplitude of V(r) with $\mathrm{d_A}$. A good measure for this oscilation is the function tail[4] (equation 7.47). The lower limit was chosen to be 4 bohr, as the ECPs published in the literature vanish in this region. 'Tail' has its minimum at $\mathrm{d_A} = 0.64$ and marks so the saddlepoint.

The combination of equation 7.56 with equation 7.53 leads to expression for $\mathrm{d_R}$ as a function of $\mathrm{d_A}$.

$$\begin{aligned} d_R &= 0.21176 \left(\frac{0.052753 + d_A}{0.088593 + d_A}\right)^{\frac{9}{2}} \cdot\, (0.11415 + 2.16385\, d_A) \\ &\approx 0.02417 + 0.45822\, d_A \qquad\qquad \text{for large values of } d_A \end{aligned} \tag{7.58}$$

$\mathrm{d_R}$ grows nearly linearly with increasing values for $\mathrm{d_A}$. The attractive function can increase $\Delta\mathrm{E}$ above $\Delta\mathrm{E_0}$ and therefore enables the usage of smaller exponents; it also increases $\mathrm{d_R}$ and fascilitates so the calculation.

The best function found so far (figure 7.26) has still its maximum at the next neighbour (The repulsive forces have their maximum at 5.06 bohr!). The next step is therfore to analyse, if changes in β_A allow us to bring the maximum closer to the nucleus.

So far only $\mathrm{d_A}$ was varried to analyze the influence of the second function onto the maximum of the repulsive function. Now, β_A is varied for constant values of $\mathrm{d_A}$. The first derivative of $\bar{\mathrm{V}}_\mathrm{D}^3$ does not vanish in equation 7.47 and the simplification shown in equation 7.56 cannot be used any more.

$$\beta_R = \alpha(n+5)\left(\frac{7}{2} - \frac{\alpha}{\Delta E}\left(\frac{d_A\,\bar{V}_D^3}{\alpha}\left(\frac{7}{2} - 8\,\frac{\alpha}{2\alpha + \beta_A}\right) \;+\; \frac{8}{15}\sqrt{\frac{2}{\pi\,\alpha}} \;-\; \frac{7}{2}\right)\right)^{-1} \;-\; 2\alpha \tag{7.54 a}$$

The results of such calcualtions are shown in figure 7.27. For the calculation the values of $\mathrm{d_A}$ have been chosen to be consistent with plot 7.25 (table 7.6). For $\mathrm{d_A} = 0.8$, which has been a maximum so far, exist a small region ($0.30 \leq \beta_\mathrm{A} \leq 0.42$) which allows the construction of a

---

[4] The integral was calculated numerically with the trapezium method. Infinity was reached at a distance of 30 bohr from the nucleus.

minimum at $\alpha = 0.1196$. The transition at the saddlepoint is marked with a bullet point in figure 7.27. At the saddlepoint equals β_{R} 0.04 bohr^{-2} and the repulsive function has therefore its maximum at 4.77 bohr. The ECP has its maximum further away from the nucleus at 4.93 bohr. Although the variation of β_{A} allows us to construct functions with high values of β_{R} the maximum of the ECP does not get any closer to the nucleus. The curve for $\mathrm{d_A} = 0.64$ indicates 3 saddlepoints in the energy curve. The first is at same place as the one shown in figure 7.25 while the second is found for $\beta_{\mathrm{A}} = 0.24$. The third is at $\beta_{\mathrm{A}} = 0.084$ and marks the end of the central minimum region. For all three points is the maximum of the ECP function at 4.8 bohr. Finally, the curve for $\mathrm{d_A} = 0.2871$ allows us to construct a local energy minimum in the pysically reasonable region $(0 < \beta_{\mathrm{A}} \leq 0.25)$.

The set of points $(\beta_{\mathrm{A}}, \mathrm{d_A})$ which allows us the construction of a physically reasonable potential is limitted by two borders:

1. At one border turns β_{R} negative and the ECP becomes therefore infinite.
2. At the second border turns the local minimum into a maximum. The transition is marked by a saddlepoint in the $\mathrm{E}(\alpha)$ curve.

While the first border is simply the root of equation 7.54a, requires the second border more consideration. A saddlepoint exits at points where the first and the second derivative of the energy function vanish. The same simplifications used for the calcualtion of equation 7.47 from the equations 7.45f and 7.46f work also here.

$$\begin{aligned} \frac{d^2 \bar{V}_D^n}{d\alpha^2} &= \frac{d}{d\alpha}\,\bar{V}_D^{n'} = \frac{d}{d\alpha}\left(\frac{\bar{V}_D^n}{\alpha}\left(\frac{7}{2} - (n+5)\,\frac{\alpha}{2\alpha+\beta}\right)\right) \\ &= \frac{\bar{V}_D^n}{\alpha}\left(\frac{4\,n\,(n-2)\,\alpha^2 \;-\; 28\,n\,\alpha\,\beta + 35\beta^2}{4\,(2\alpha+\beta)^2}\right) \end{aligned} \tag{7.59}$$

The second derivative of the total energy is therefore:

$$\begin{aligned} E''(\alpha) \;=\; \frac{4}{15}\sqrt{\frac{2}{\pi\,\alpha^3}} \;-\; d_A\,\frac{\bar{V}_D^3}{\alpha^2}\left(\frac{12\,\alpha^2 \;-\; 84\,\alpha\,\beta_A \;+\; 35\,\beta_A^2}{4\,(2\alpha+\beta_A)^2}\right) \\ +\; d_R\,\frac{\bar{V}_D^4}{\alpha^2}\left(\frac{32\,\alpha^2 \;-\; 112\,\alpha\,\beta_R \;+\; 35\,\beta_R^2}{4\,(2\alpha+\beta_R)^2}\right) \end{aligned} \tag{7.60}$$

The determination of the saddlepoints is possible with equation 7.60. Equations 7.53 and 7.54a link the pairs $(\beta_{\mathrm{A}}, \mathrm{d_A})$ and $(\beta_{\mathrm{R}}, \mathrm{d_R})$ which reduces the number of variables in equation 7.60 and facilitaes the calculation of the roots. The result of this search is shown in figure 7.28[5]. The set of pairs $(\beta_{\mathrm{A}}, \mathrm{d_A})$ which allow us the calculation of physically reasonable ECPs is gray shaded.

The curves shown in figure 7.27 are vertical cuts through the plane shown in figure 7.28. The bulge in the lower part of the right border explains the scattering of the saddlepoints in figure 7.27. The curve for $\mathrm{d_A}$ 0.8 cuts the right border once, the curve for $\mathrm{d_A} = 0.64$ thrice and finally the curve for $\mathrm{d_A} = 0.2871$ never cuts the right border.

Figure 7.28 allows us also to find the ECP function, which has its maximum closest to the nucleus. As shown already in figure 7.27 moves the maximum of the ECP closer to the nucleus with increasing values of β_{R}. In figure 7.28 is this area were the isoexponent curve for $\beta_{\mathrm{R}} = 0.08$ cuts the right border. The centre of this area is roughly at $\mathrm{d_A} = 0.571$ and $\beta_{\mathrm{A}} = 0.093$. The

---

[5] Section 11.13 (page 357) gives detail on the construction of figure 7.28.

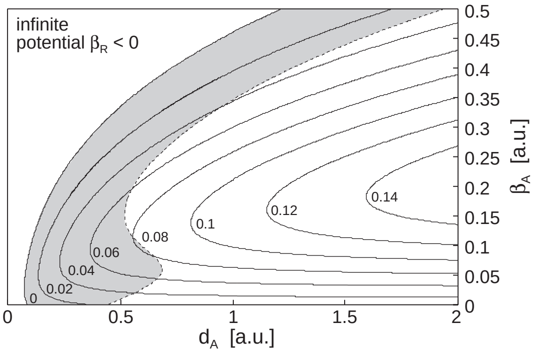

Figure 7.28: β_R as a function of $\mathrm{d_A}$ and β_A.

corresponding values for β_R and $\mathrm{d_R}$ are 0.079 and 0.168. The maximum of the repulsive function is closer to the nucleus than before (3.56 bohr), but the maximum of the composite ECP function is still at 4.84 bohr. It seems to be impossible for the effective ECP to have a maximum closer to the nucleus than 4.8 bohr. If the maximum gets any closer, the local minimum turns into a maximum.

Equation 7.54a shows, how the form of the ECP depends on $\mathrm{d_A}$ and β_A. The form of the ECP is solely determined by the energy difference ΔE and the first derivative of the attractive part of the potential. Since β_A and $\mathrm{d_A}$ are allowed to take any value between zero and infinity is any value possible for ΔE and the first derivative. For this reason is the graph shown in figure 7.28 is representative for all possible attractive functions, since all possible values for ΔE and the first derivative are covered. It is therefore impossible to create an ECP for a local minimum (α = 0.1196, $\mathrm{E_T}$ = 0.23482 H) with a maximum closer to the nucleus than 4.8 bohr. This value is close to the distance to the next neighbour in bulk platinum metal. It is physically unreasonable, that the ECP has its maximum at the next neighbour. ***It is therefore impossible to create a physical reasonable ECP for a local minimum with positive energy eigenvalue with any number of attractive functions.***

7.3 How describe the 6d electron?

It is impossible to create an ECP, which reproduces all results of the Hay and Wadt LanL2DZ potential, as shown in subsection 7.2.9. In this section we analyze the ECP from Zurita et al. [318] to find a suitable expression for $\mathrm{U_L^{core}}$ (equation 2.65, page 33 and subsection 7.2.2), which helps us to analyze the platinum 6s valence space independently of the 5d orbitals.

7.3.1 What problems are connected with the ECP by Zurita et al.?

Two problems are connected with the 1 electron ECP published by Zurita et al. [318]:

1. To get physically reasonable results Zurita et al. extended the Hamiltonian of the system. So they incorporated additional terms for the core polarisation, core-valence correlation and core-core repulsion effects (section 7.1, page 204).

2. The ECP is given in a totally different form than the one used for the Gaussian input section.

$$U^{\mathrm{core}}(r) = \frac{-1}{r} + \sum_i W_l\,\hat{P}_l \qquad W_l = e^{-\alpha_l r^2} \sum_i C_{i,l}\, r^{n_{i,l}} \qquad \hat{P}_l = \sum_{m=-l}^{l} |l\,m><l\,m| \quad (7.61)$$

l	α_i	$C_{i,l}$	$n_{i,l}$
0	0.637336	8.356863	0
		−3.288355	2
1	0.405865	3.399651	0
		−0.781761	2
2	0.263744	0.132669	2
3	0.75	−14.733284	2
		2.944590	4

Table 7.7: Parameters of ZURITAS's ECP.

	test 1	HAY and WADT
6s	−0.28284 H	−0.29574 H
6p	−0.12917 H	−0.13581 H
6d	−0.05401 H	+0.23842 H

Table 7.8: Einergy eigenvalues form test 1.

> Before the ECP can be used with Gaussian 94 any potential given in the form according to equation 7.61 has to be transformed into the form published by HAY and WADT prior to its application in Gaussian 94.

Table 7.7 lists the parameter of ZURITA's ECP. The first test of this potential was done in a straight-forward manner. ZURITA et al. did not use a reference function in their potential like HAY and WADT (equation 2.65). Equation 7.61 contains therefore all information to create the ECP for a given angular quantum number U_l^{core}. The transformation of the potential was done in two steps. First, we sat the coefficients $C_{i,l}$ for $l = 3$ (f-orbital) equal to nought. This change ensured, that Gaussian 94 creates the ECP only from the input given in the section for $l < 3$ in the job-file. This section contains now all parameters for the complete potential. In the second step all exponents $n_{i,l}$ for $l < 3$ were increased by 2 to account for r^{-2} term in equation 2.65.

The results of this first test are shown in table 7.8. The energy eigenvalues for the 6s and 6p orbital agree within 5%, whereas the orbital energies for the 6d orbital are totally different. The ionisation energy found with simplified potential agrees well with energies found with HAY and WADT potential with the augmented basis set (table 7.4, $\epsilon_{6d} = -0.0503$ H) and with the pure Coulomb interaction (hydrogen nucleus) according to equation 7.30 (figure 7.16, $\epsilon_{6d} = -0.0517$ H). According to this calculation the 6d electron moves in a weak Coulomb field far away from the nucleus. The geometry optimisation of the platinum dimer did not work due to a malfunction in the calculation of the energy derivatives. The optimisation was done stepwise (figure 7.33). The platinum-platinum distance was found to be 2.1 Å (89% of the LanL2DZ value) and the dimerisation energy was 37.56 kcal/mol (63 % of the LanL2DZ value[6]). To check whether this faulty bond lenght is caused by the gross simplification in the first test, the another test calculation included the f-term. Increasing the coefficient $n_{2,3}$ from 4 to 6 for the input yields an exponent Gaussian cannot handle anymore. The first task was therefore to fit the given potential with new set function with exponents smaller or equal to 3. This function was subtracted from the functions given for $l < 3$ and the results were fitted again with new set of gaussian functions. The results of this transformation are shown below (test 2).

---

[6] The dissociation energy of the $^3D-^3D$ dimer is 59.58 kcal/mol and those of the $^1S-^1S$ dimer 15.97 kcal/mol (table 6.10, page 161). An increase of the binding energy by 43.61 kcal/mol can be attributed to the occupation of the σ_{6s} orbital. If we take this energy increase as the bining energy of two 6s orbitals, calculation 1 covers 86% of the binding energy.

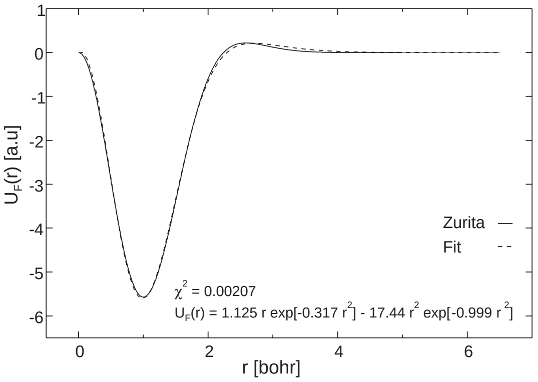

Figure 7.29: Fit for the new f term (test 2).

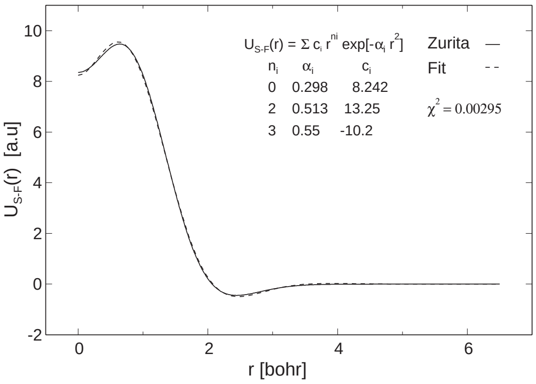

Figure 7.30: Fit for the new s-f term (test 2).

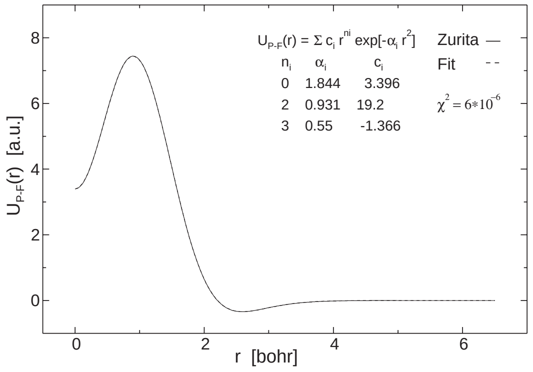

Figure 7.31: Fit for the new p-f term (test 2).

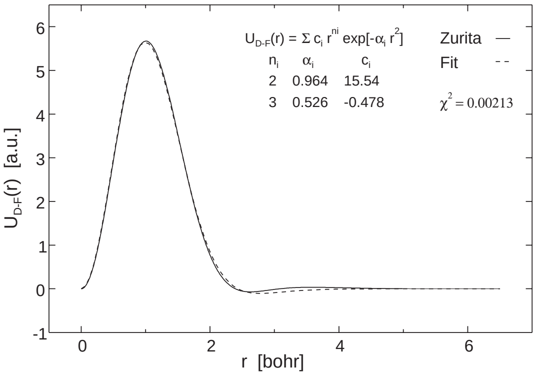

Figure 7.32: Fit for the new d-f term (test 2).

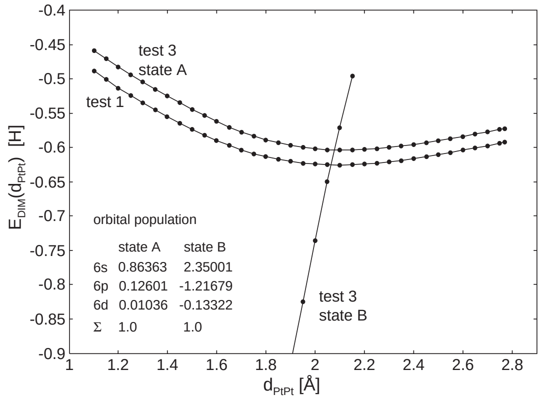

Figure 7.33: Dimerisation energy from test 1 and test 3.

orbital	energy
6s	-0.27021 H
6p	-0.11895 H
6d	-0.05435 H

Table 7.9: Results from test 2.

orbital	energy
6s	-0.27717 H
6p	-0.12908 H
6d	-0.05401 H

Table 7.10: Results from test 3.

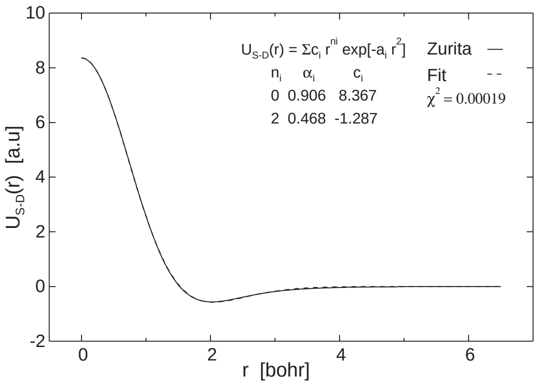

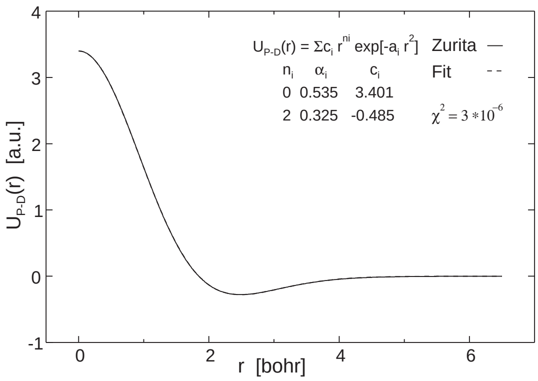

Figure 7.34: Fit for the new s-d term (test 3).

Figure 7.35: Fit for the new p-d term (test 3).

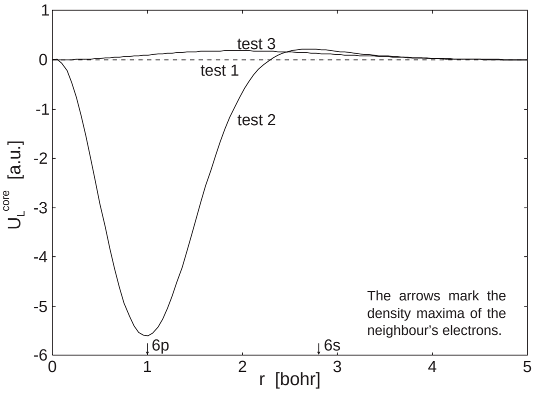

Figure 7.36: $\mathrm{U_L^{core}}$ in the 3 different tests.

Table 7.9 lists the orbital energies from the second test. They agree within 8% with the orbital energies obtained in the first test. The agreement with the energy eigenvalues from the HAY and WADT potential is poorer with 12%, but still reasonable regarding the quality of the fits. The optimisation of the platinum dimer went totally astray. The optimisation algorithm did not work and the dimerisation energy for the first step was 131 H and far too high.

The third test was done with the d-function as the base function $\mathrm{U_L^{core}}$. This time the d-function was subtracted from the functions given in the paper by ZURITA et al. and the reminder was fitted with a new set of gaussian polynomials. The fits and the corresponding functions are shown in figures 7.34 and 7.35. Table 7.10 lists the results for the orbital energies and they agree well with the results from tests 1. The dimerisation energy at a optimised platinum-platinum distance of 2.1 Å is smaller than for test 1 ($\mathrm{E_{DIM}}$ = 31.15 kcal/mol), but much better than fit test 2. Figure 7.33 shows the dimerisation energies as a function of the Pt-Pt distance. The figure shows also the potential energy curve of a second electronic state found in the third test. The dimerisation energy leaves rapidly the physically reasonable region and the geometry optimisation was therefore not completed.

The contradicting results for the platinum dimer from test 1/3 and test 2 can be explained with the different forms of the pseudopotentials (figure 7.36).

$$U^{\mathrm{core}}(r) = U_L^{\mathrm{core}}(r) \ + \sum_{l=0}^{L-1} \sum_{m=-l}^{m=-l} |\, lm> \ [U_l^{\mathrm{core}}(r) - U_L^{\mathrm{core}}(r)] \ <lm\,| \tag{2.64}$$

The pseudopotential in the form defined by HAY and WADT (equation 2.64) contains the spherically symmetric term U_L^{core}, which works on all electrons despite their angular quantum number. The pseudopotential by ZURITA et al. (equation 7.61) does not contain such a term. For a single atom the precise form of this function does not matter, since all functions U_l^{core} have the correct form. The right form of the functions U_l^{core} ensures the correct ionisation energies. In a polyatomic compound the energy is not only determined by the electrostatic field from the mother nucleus but also by the fields of the neighbouring nuclei. The term U_L^{core} on the first nucleus has no restrictions in the angular quantum number and has so a strong influence on all electrons at the second platinum atom. Whereas the bra-vector of equation 2.64 forms with the wavefunction $|\, l'm' >$ on the neighbour atom the overlap integral $S = <lm\,|\,l'm'>$. For any distance $R > 0$ between the two atoms equals $|\, S\,|$ a value smaller than 1. The electron feels therefore the full strength of U_L^{core} but only a fraction of U_l^{core}. In the second test U_l^{core} contains the repulsive part of the ECP and the electrons feel therefore a too strong attraction by the neighbour atom's nucleus. The too strong attraction is visible in the big difference in the electron-nuclei energies ($d_{PtPt} = 2.77$ Å) in the different tests. Test 1 yields an interaction of -1.2888 H while test 2 gave an energy of -132.5 H. The other energies (nucleus-nucleus, kinetic energy of the electrons) are of similar size. U_L^{core} can therefore be used to manipulate the atom-atom interaction and it might be possible to partially simulate the the core-core repulsion by keeping the platinum atoms at the correct distance from eachother.

7.3.2 What's next?

At this point two conclusions can be drawn from the calculations done so far.

1. It is impossible to transform the ECP from ZURITA et al. with a well defined 6d-orbital in a straight forward manner. Problems are caused by the spherically symmetric part of the potential, which is not part of the method used by ZURITA. This part of the potential has to be developed from the scratch for a new ECP.

2. The calculation in section 7.2 showed, that it is impossible to create an ECP, which reproduces the results of the values for the 6d electron obtained with the potential from HAY and WADT. The other orbitals (6s and 6p) are easier to handle. This 6d-problem is caused by the positive eigenvalue of 6d-function, which is most likely an artefact of the LanL2DZ potential.

The next step is the combination of the results for the LanL2 potential (6s and 6p) with the ECP for the 6d function by ZURITA. The combination reduces the number of problems to one - the spherically symmetric part. This allows us also to minimize the number of gaussians for each ECP function.

The first step of this new approach was the development of an ECP for the 6s and 6p electrons, which reproduces the properties of the LanL2DZ calculations with a minimum of functions. Figure 7.37 summarizes the results for the 6s function. The agreement between the ideal function (straight line) and the new function (dotted line) is poor, but only two gaussians were necessary to create the curve. Although the electron density is closer to the nucleus with the new ECP is the energy eigenvalue higher (2 mH). Hückel calculations (section 5.3.2, page 123) on the Pt_5 pyramid showed, that small differences in the valence ionisation energy α have a small influence on the electronic structure of the pyramid (figure 5.5, page 124). If we take beta to be -0.1558 H (subsection 5.7.1, page 135) an energy difference of 2 mH correspondends to $0.012\ \beta$ and is therefore neglible.

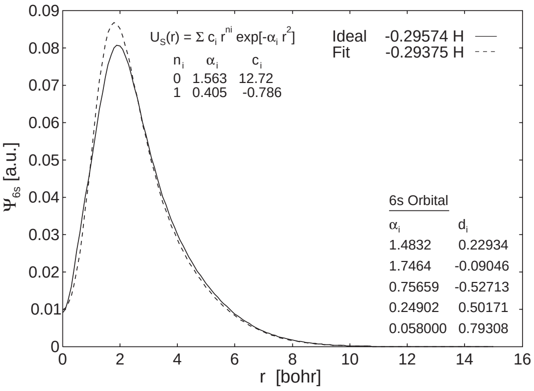

Figure 7.37: 6s orbital.

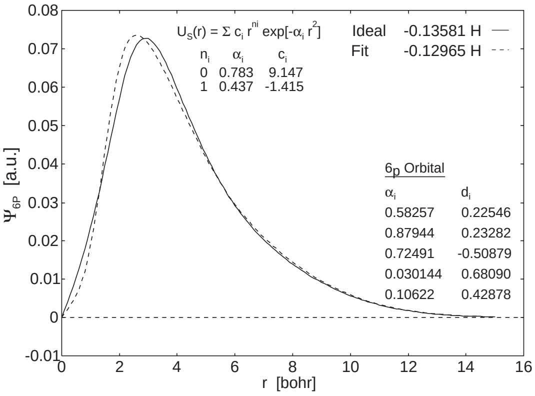

Figure 7.38: 6p orbital.

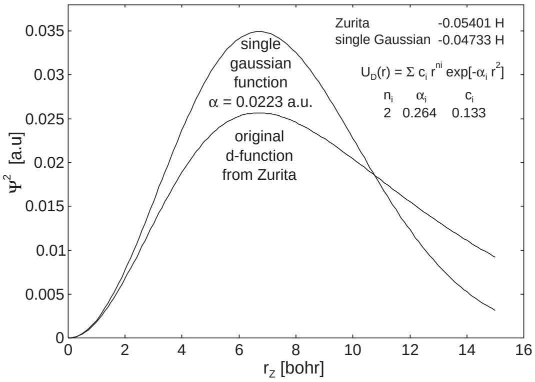

Figure 7.39: 6d orbitals.

The final fitting in a long series of fruitless attempts was done with a program basing on the simulated annealing algorithm and for the quantum mechanical calculations Gaussian 94 was called as a subroutine. To give the Hartree-Fock calculation more freedom we split the contracted 6s orbital from section 7.1.1 into single gaussians. The qualityfunction Q was then created from two parts: first, the square of differences between the calculated wavefunction and the ideal one and second, the squared differences in the energy eigenvalues $\Delta\epsilon^2$, since it proofed to be futile to use the coefficients in the wavefunction to judge the function's quality.

$$Q = 100 \sum_i \left[\Psi_{\mathrm{FIT}}(r_i) \; - \; \Psi_{\mathrm{ORG}}(r_i)\right]^2 \; + \; 10 \cdot \Delta\epsilon^2 \tag{7.62}$$

The data for the comparison of the wavefunctions were created with the Gaussian 94 '`cube command`' with a step size of 0.1 bohr along the z-axis (15 bohr to cover the outer regions).

The same procedure was used for the calculation of the 6p-orbital. Figure 7.38 summarises the results. The quality of the fit is poorer than before, but again only two gaussians were necessary for the ECP. The electron density is closer to the nucleus and the energy eigenvalue is 6 mH higher than the value calculated with ZURITA's potential. It is interesting to note, that the attractive parts for both ECPs (6s and 6p) have similar exponents (6s: 0.40 a.u., 6p: 0.44 a.u.). This result supports the idea of HAY and WADT, that all electrons move in an attractive spherically symmetric field created by the core. The precise ECPs for different values of the angular quantum number are then smaller derivations of this general potential.

Figure 7.39 shows the 6d-orbital. The wavefunction by ZURITA et al. can be replaced by a single gaussian ($\alpha = 0.0223$ a.u.) to keep the calculation as simple as possible. Both functions have their maximum at the same place. For all calculations we used ZURITA's ECP as published before. The energy difference $\Delta\epsilon$ between the original system and the simplified 6d system is 6.7 mH and similar to values found before. As shown in figure 7.39 is the spatial extension of the single gaussian smaller than for the original function. The influence of those new 6d electrons onto the neighbours is therefore smaller.

The new ECP used for the rest of the calculations is a combination of two older ECPs. The calculations on the LanL2DZ potential for the 6s and 6p orbital were combined with a simplified form of ZURITA 6d-orbital and ECP, because it is impossible to create a proper 6d ECP from the LanL2DZ potential as shown before. This new potential contains one unknown variable - the spherically symmetric part. This new potential allows us to work with smaller exponents for the polynomial of the ECP and to develop a potential, which is suitable for the G94 geometry optimiser.

7.3.3 How does $\mathrm{U}_\mathrm{L}^\mathrm{core}$ controll the dimer's properties?

```
Pt 0
Pt-ECP 3 77
f potential
1
${na} ${ba} -${da}
s-f potential
3
2 1.56304868 12.72241997
3 0.40533958 -0.78658492
${na} ${ba} ${da}
p-f potential
3
2 0.78303679 9.1466791
3 0.43658528 -1.4152290
${na} ${ba} ${da}
d-f potential
2
4 0.263744 0.132669
${na} ${ba} ${da}
```

Figure 7.40: G94 input.

A geometry optimisation of the platinum dimer with the new ECP and no sperically symmetric part yielded a bond length of 2.13 Å and a total dimer energy of −0.6247 H. No problems occured during the calculation with Gaussian 94. The dimerisation energy is 23.4 kcal/mol. The bond length has the same value as before for the test 1 and 3, while the interaction energy is only about $\frac{2}{3}$ of the values obtained before and half the HAY and WADT dimerisation energy (subsection 6.2.1, page 159).

The energy and bond length of the platinum dimer are controlled by $\mathrm{U}_\mathrm{L}^\mathrm{core}$ (subsection 7.3.1). If we choose $\mathrm{U}_\mathrm{L}^\mathrm{core}$ to reproduce these two values it might be possible to account for the core-core repulsion (subsection 7.1) with the new 1-valence electron ECP. To test the influence of $\mathrm{U}_\mathrm{L}^\mathrm{core}$ on the dimerisation energy, we substracted $\mathrm{U}_\mathrm{L}^\mathrm{core}$ from $\mathrm{U}_\mathrm{l}^\mathrm{core}$ (figures 7.37 and 7.38) in the input section of the G94 input file (example on the left, na: exponent of the polynomial, ba: exponent of the gaussian, da: coefficient of the gaussian). This procedure guarantees, that $\mathrm{U}_\mathrm{l}^\mathrm{core}$ does not change its form, whatever form $\mathrm{U}_\mathrm{L}^\mathrm{core}$ has (equation 6.85). The properties of the dimer are now solely determined by $\mathrm{U}_\mathrm{L}^\mathrm{core}$.

First optimisation test were done with pure powers of r^n ($\mathrm{n} = 0, -1, -2$). These functions can be created easily by choosing the gaussian exponent (ba in the input file) to be zero. With increasingly smaller values of d increase both the bond length and the interaction energy. A suitable selection of β should allows us to stretch the bond and to increase simultaneously the strength of the bond, which contradicts chemical experience, where a long bond is a sign for a small interaction energy. With decreasing values for n becomes this effect smaller, which agrees well with the increasingly more localized character of the function.

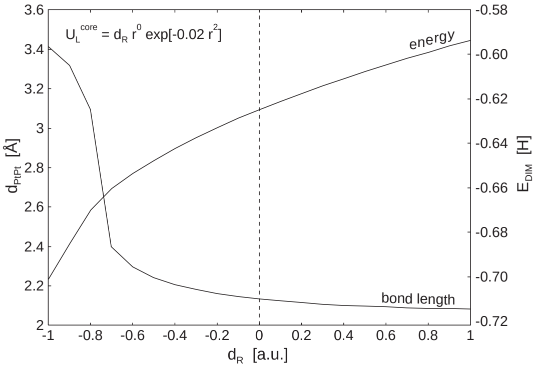

Figure 7.41: 2^{nd} test for U_L^{core} ($\beta = 0.02$).

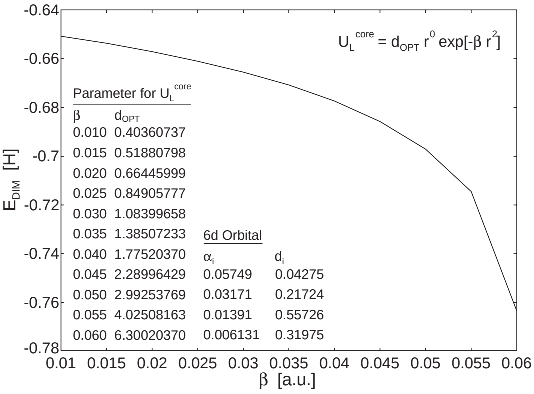

Parameter for U_L^{core}

β	d_{OPT}
0.010	0.40360737
0.015	0.51880798
0.020	0.66445999
0.025	0.84905777
0.030	1.08399658
0.035	1.38507233
0.040	1.77520370
0.045	2.28996429
0.050	2.99253769
0.055	4.02508163
0.060	6.30020370

6d Orbital

α_i	d_i
0.05749	0.04275
0.03171	0.21724
0.01391	0.55726
0.006131	0.31975

Figure 7.42: Order 2: E_{TOT} for an optimized bond length of 2.3578 Å.

With increasing values of β (figure 7.41, higher values for β not shown) the effect becomes smaller until finally the bond length decreases with an increasing interaction energy and the properties of the dimer are normal again. The exploitable region for the manipulation of the dimer is limited by two points:

1. The dimer dissociates, if β is too small and therefore the minimum of U_L^{core} too far away from the nucleus.

2. If β is too big and the minimum of U_L^{core} therefore too close to the nucleus, the U_L^{core} function has no influence on the dimer's properties.

It should be therefore possible to construct an attractive function for a given exponent n, which guarantees the reproduction of the dimer's properties. This idea was tested in the next set of calculations. The single gaussian for the 6d orbital was now replaced by the contracted wave function for the 6d-orbital from the first set of claculations with ZURITA's potential to increase the accuracy of the long range behaviour (table in figure 7.42).

Figure 7.42 shows the results of such claculations. The values for d_{OPT} have been chosen[7] to give an optimized PtPt bond length of 2.3578 Å, which is the value found with the HAY and WADT potential with a 5d186s2 electron configuration (subsection 6.2.1, page 159). The energy of the dimer (E_{DIM}) becomes increasingly more negative as β increases and the minimum of U_L^{core} gets closer to the nucleus. Figure 7.42 suggests, that at least one couple of (β, d_{OPT}) should exist, which allows the reproduction of the correct properties of the platinum dimer.

Figure 7.43 shows, how the bond length changes with increasing values of d_A. The closer the minimum gets to the nucleus the smaller becomes the influence of the attractive function on the dimer's properties. As β becomes larger than 0.06 it becomes impossible to construct an optimized dimer with a bond length of 2.3579 Å, because the attractive function vanishes too fast. Although it is not possible to reproduce the correct bond length, the reproduction of the bonding energy is still possible (figure 7.44). A value of 0.06 a.u. for β_A seems not to be suitable for further calculations, because such a potential spreads very far (half width = 3.4 bohr).

---

[7] A small C++ program was written to find an optimized value d_{OPT} which forces the geometry optimisation module of Gaussian 94 to converge on a platinum-platinum bond length of 2.3578 Å.

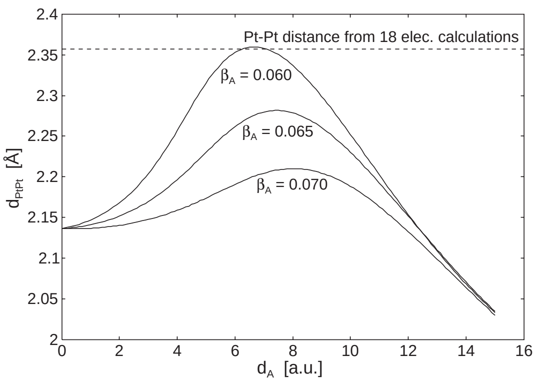

Figure 7.43: Influence of d_A on the bond length for fixed values of β_A.

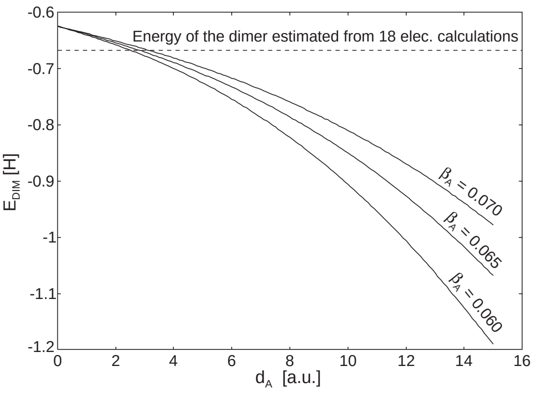

Figure 7.44: Influence of d_A on the dimer's energy for fixed values of β_A.

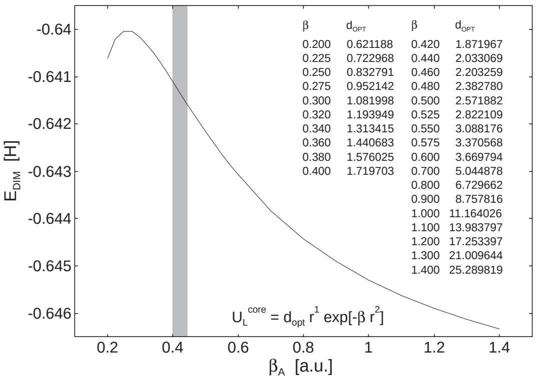

β	d_OPT	β	d_OPT
0.200	0.621188	0.420	1.871967
0.225	0.722968	0.440	2.033069
0.250	0.832791	0.460	2.203259
0.275	0.952142	0.480	2.382780
0.300	1.081998	0.500	2.571882
0.320	1.193949	0.525	2.822109
0.340	1.313415	0.550	3.088176
0.360	1.440683	0.575	3.370568
0.380	1.576025	0.600	3.669794
0.400	1.719703	0.700	5.044878
		0.800	6.729662
		0.900	8.757816
		1.000	11.164026
		1.100	13.983797
		1.200	17.253397
		1.300	21.009644
		1.400	25.289819

Figure 7.45: Order 3: Optimized bond length is 2.3578 Å.

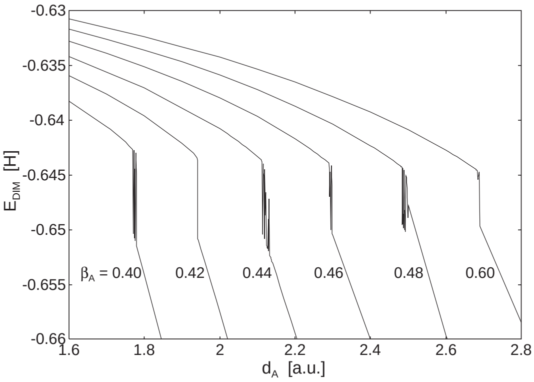

Figure 7.46: Influence of d_A on the optimized bond length

.

The original ECP form from Hay and Wadt (equation 2.64) suggests that the spherically symmetric part U_L^{core} represents the main structure of the core potential. As indicated in the figures 7.37 and 7.38 the attractive part of U_L^{core} should have the form $d_A \cdot r \cdot \exp[-\beta_A r^2]$ with 0.4 $\leq \beta_A \leq$ 0.44 (grey shaded area in figure 7.45). Such a function is of third order in the G94 input section and so close to the limits of the program's numerical capacities. The geometry optimisation module does not work any more due to a malfunction in the calculation of the energy derivatives. The bond length was therefore optimised by a hand-made code basing on the Newton optimisation algorithm and d_{OPT} optimized to yield so a bond length of 2.3575 Å. The results are shown in figure 7.45.

Although it is possible to reproduce the bond length of the LanL2DZ dimer (2.3575 Å) over a wide range, it was not possible to reproduce the dimersation energy (requires $E_{DIM} = -0.6675$ H) with the first set of computations. The calculations with zero order function (figure 7.43) showed, that in certain range for d_A two solutions are possible. In the next step we therefore calculated the optimised bond length for defined values of β_A as a function of d_A (figure 7.46).

The optimised dimer energy and the bond length do not change steadily with increasing values for d_A and fixed values for β_A (figure 7.46). During the calculation of every curve a point was reached, where the optimisation started to oscillate wildly. Figure 7.47 shows, how the properties

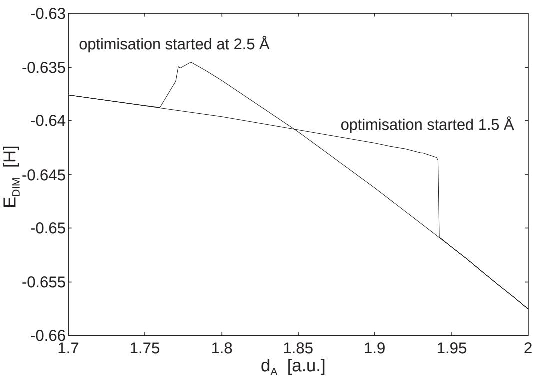

Figure 7.47: Two energy discontinuities observed for $\beta = 0.42$ a.u..

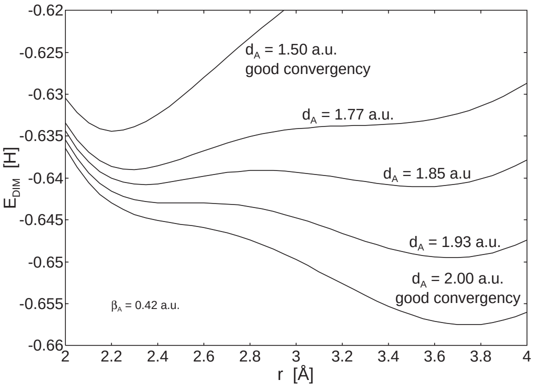

Figure 7.48: Influence of U_L^{core} on the potential energy surface ($\beta = 0.42$).

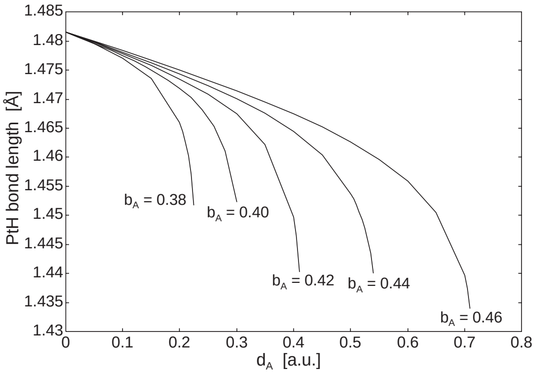

Figure 7.49: PtH bond length.

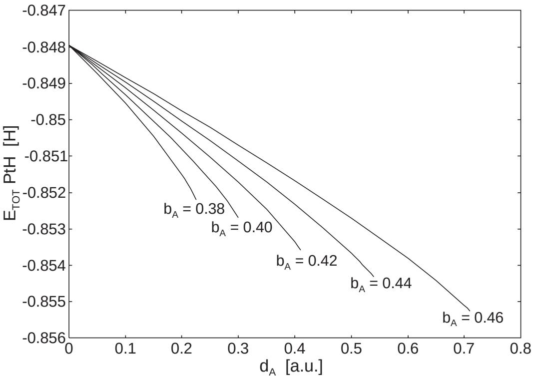

Figure 7.50: Total energy E_{TOT} of PtH.

of the optimized dimer change with the starting point of the optimisation. An explanation for this behaviour is shown in figure 7.48. The increase of d_A causes a second minimum with a longer bond length while the first minimum becomes more shallow until it finally vanishes ($d_A = 2.00$ a.u.). Within this development a region exists with two independent minima separated by a small maximum. In this region the optimisation algorithm can converge to any of these minima and oscillation is likely.

This observation leads to another requirement for an useful ECP: The ECP has not only to reproduce certain points of a given potential energy surface, but also has to reproduce the main features of the surface itself such as the number of stationary points.

7.3.4 How strong is the influence of U_L^{core} on the PtH bond?

The influence of U_L^{core} on the Pt-Pt bond in the platinum dimer is very strong, because both atoms use U_L^{core}. In this subsection we focus on the influence of U_L^{core} on bonds with only one ECP atom: PtH.

Figures 7.49 and 7.50 show the bond length and the total energy of PtH as a function of U_L^{core} (third order G94 input, attractive $U_L^{core} < 0$). With increasing strength of U_L^{core} the bond becomes shorter and stronger. This behaviour becomes more prominent as β_A moves into a chemical range ($0.44 \leq \beta_A \leq 0.44$). The end points of the curves in figure 7.49 and 7.50 are marked by the point,

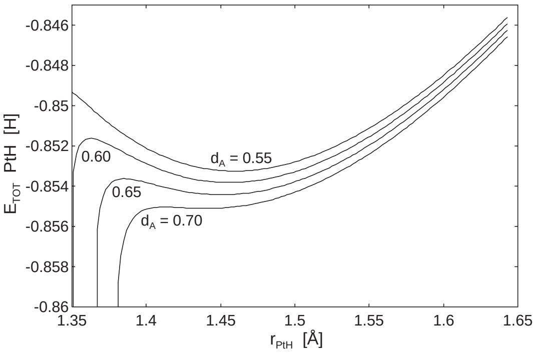

Figure 7.51 Collaps of PtH (β_A = 0.46).

d_A	0.13	0.01	0.0
6s	0.6065	0.582	0.5809
6p	1.1227	0.3969	0.3726
6d	0.1120	−0.0472	−0.0413

optimized PtPt distance, β = 0.42, triplet state (a_1^2 e e), 3rd order

Table 7.11 Mulliken population at the top in Pt_5^+.

where the hydrogen atom drops into the platinum. Figure 7.51 shows this development for β_A = 0.46. All graphs in this subsection show, that U_L^{core} is important for the bond between an ECP atom and an all-electron atom and the construction of a working ECP has therefore to focus also on the interaction between the ECP atom and 'normal' atoms.

The core-core repulsion (equation 7.1, page 204) is a repulsive function preventing two atoms to collide during a geometry optimisation. Figure 7.51 demonstrates, that it is possible to prevent such a collision with a well chosen function for U_L^{core} ($d_A < 0.60$) and therefore to simulate the core-core repulsion with U_L^{core}.

7.3.5 How does U_L^{core} change the electronic structure of Pt_5?

U_L^{core} has a strong influence on the bond between two atoms (subsections 7.3.3 and 7.3.4). During these calculations the ionisation energies of the 6spd orbitals did not change due to the construction of the G94 input file (subsection 7.3.3). The valence ionisation energy α in the pure Hückel theory is proportional to the ionisation energy of the orbital and this parameter did not change during the last calculations on Pt_2 and PTH. During these calculations changed the length and the energy of the bond. These two parameters depend on the bond energy integral β. It is therefore likely to assume, that the influence of U_L^{core} in the binding energy of the cluster can be described with the bond energy integral β.

According to pure Hückel theory the energy of the bonding orbitals in Pt_5^+ change with the value of β, but the charge distribution does not[8]. In this section we therefore analyse the influence of U_L^{core} on the electronic structure of Pt_5^+. Figures 7.52 and 7.53 show the results of these calculations. For these specific calculations we used a third order function in the input file. The ECP exponent β_A was chosen to be 0.42. As observed before for the platinum dimer, both the bond length and the total energy decrease with increasing values for d_A (figure 7.52) until the cluster finally collapses (not shown) long before the dimer values are reached (figure 7.45). Figure 7.53 shows the charge at the top of the platinum pyramid and the dipole moment of the cluster. In contrast to pure

---

[8] All Hückel energy eigenvalues have the same structure: $\alpha + k_i \cdot \beta$, k_i is a constant value. The replacement of ϵ_i in the secular determinant |D| during the calcualtion of the coefficients (c_i) eliminates α from the diagonal element and every element of |D| has then the form $k'_{ij} \cdot \beta$, k'_{ij} is another constant. It is now possible to take β out of the matrix: $|D| = \beta \cdot |\mathbf{k}'|$. The HMO coefficients (equation 5.4, page 118) are therefore independent of β and so is the charge distribution. $\mathbf{D}\,\mathbf{c} = \beta\,\mathbf{k}'\,\mathbf{c} = 0$

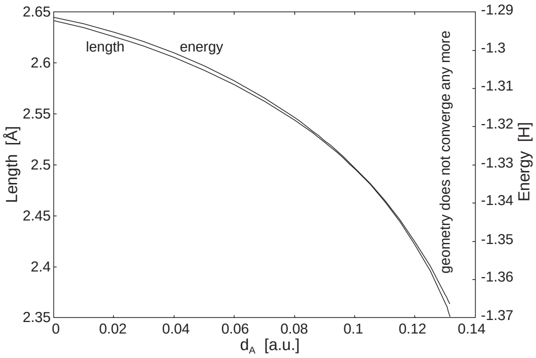

Figure 7.52: Bond length and E_{TOT} in Pt_5^+.

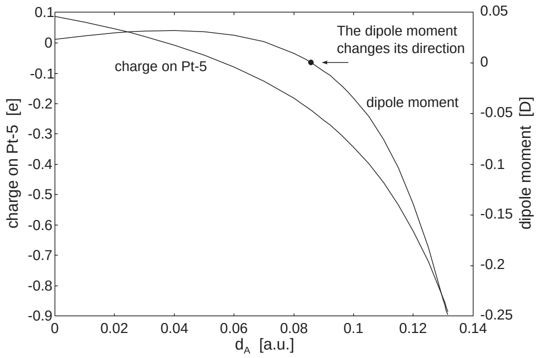

Figure 7.53: Charge on the top platinum and dipole moment in Pt_5^+.

β_A a.u.	d_A a.u.	r_{OPT} [Å]	E_{TOT} [H]	ϵ(a1) [H]	ϵ(e) [H]	ϵ(e) [H]
0.01	0.403607	3.9044	−2.929759	−0.86225	−0.81099	−0.81099
0.015	0.518808	3.6136	−2.808681	−0.85265	−0.78326	−0.78326
0.02	0.664460	3.0321	−2.765852	−0.89179	−0.84875	−0.84875
0.025	0.849058	2.8793	−2.832524	−0.91736	−0.88854	−0.88854
0.03	1.083997	2.7358	−2.964312	−0.95609	−0.95228	−0.95228
0.035	1.385072	2.5759	−3.169891	−1.01049	−1.05104	−1.05104
0.04	1.775204	2.2637	−3.484548	−1.08847	−1.26340	−1.26340

Table 7.12: Pt_5^+ properties calculated with a second order ECP function (triplett wave function).

Hückel theory these values change dramatically with increasing strength of U_L^{core}. The electrons accumulate at the pyramid's top (table 7.11) until finally the dipole moment changes its direction. U_L^{core} does not only control β but changes the ability of the core to attract electrons. The top platinum forms four bonds while a basal atoms are bonded thrice. It is therefore more easy for the top platinum to attract electrons then for a basal atom. These extra electrons stay mostly in the 6p and 6d orbitals (table 5.26). The 6s electrons obey the Hückel predictions while the 6p and 6d orbitals become more populated. This extra population indicates a major change in the metallic bonds and U_L^{core} can be used to manipulate the electronic structure of the cluster significantly. This has been observed with a set of second order ECP functions (table 7.12). The values for β_A and d_A have been taken from the corresponding dimer optimisations (table shown in figure 7.42). During these calculations change the $1a_1$ and the two 1e orbitals their relative energy order and the singlet cluster becomes more stable (not shown in table 7.12).

7.3.6 What happens if two different ECPs interact with each other?

A water molecule interacts with the platinum surface via the platinum 5d orbitals. It is therefore necessary to construct the surface with two different ECPs. The first ECP (1-valence electron) for bulk and passive surface atoms and the second for the active site (10 or 18 valence electrons). The analysis of this interface in the platinum pyramid was done in two steps: first, we sat U_L^{core} equal to nought and used different ECPs at the top and in the second step we changed U_L^{core} with a fixed

		LanL1MB	LanL1DZ	LanL2MB	LanL2DZ
q_5	[e]	−0.176	0.458	−0.090	0.413
q_1	[e]	0.044	−0.114	0.022	−0.103
q_2	[e]	0.044	−0.114	0.022	−0.103
μ	[D]	0.3464	−0.630	−0.1886	−0.6041
6s pop. Pt(5)		0.4769	0.09992	0.36828	0.13683
6s pop. Pt(1)		0.9006	0.93725	0.89082	0.92686
6s pop. Pt(2)		0.9006	0.93725	0.89082	0.92686
MOP Pt(1)-Pt(2)		0.069	0.1601	0.082	0.1576
MOP Pt(1)-Pt(5)		0.1546	0.0189	0.1438	0.019
ϵ(e)	[H]	−0.24179	−0.23596	−0.23779	−0.23494
$\epsilon(a_1')$ (6s)	[H]	−0.39312	−0.39356	−0.39193	−0.39338
$\epsilon(a_1'')$ (5d)	[H]	−0.36398	−0.36432	−0.36228	−0.36338

Table 7.13: Pt_5 pyramide with different ECP at the top.

ECP at the top.

Table 7.13 compiles the results for the first step. For all calculations the platinum-platinum bond length was set to the bulk value of 2.77 Å and a triplet wave function to simulate the combination of 4 ^{3}D platinums with 1 ^{1}S platinum.

The calculations with the LanL2DZ potential on all platinum atoms (chapter 6, page 145) showed, that a 6s population different form zero is necessary to describe the bond between water and platinum correctly. The top of the platinum pyramid (subsection 6.4.2, page 187) is negatively charged (−0.2 e) and the 6s population at the top platinum (0.734) is close to the value for a ^{3}D platinum interacting with water (1.010). The Hückel calculations on Pt_5 showed, that in an ideal pyramid the charge at the pyramid's top should be close to −0.55 e caused by a 6s population about 0.44 (subsection 5.3.1, page 122). This value is seldom reached due to the 5d-6s interaction as shown in subsection 5.3.3 (page 125).

Only the simple basis sets (MB) create a negative charge at the top, while the double zeta basis sets (DZ) cause a positive charge. The charge distribution depends stronger on the quality of basis sets then on the chosen ECPs (LanL1: 10 e^- , LanL2: 18 e^-) and the BSSE seems to be important for the metal-metal interaction at this theory level. The analysis of the Mulliken overlap population (MOP) demonstrates, that double zeta basis sets favour the bonds in the basis of the pyramid while the simple basis sets favour the bonds between the basis and the top. This difference in the metallic bonds explains the difference in the inner cluster charge distribution.

Both clusters with a simple basis set differ significantly in the charge at the pyramid's top (LanL1MB: −0.176 e, LanL2MB: −0.090 e). This difference cannot be explained with the 6s population alone. For both clusters the 6s population is close to the value predicted by pure Hückel theory. The 6s population is 0.1086 electrons higher in the LanL1MB cluster than in the LanL2MB cluster. The difference in the 6s poulation by 0.1086 should be visible in a charge difference of the same amount, but a smaller difference of 0.086 e can be observed. This discrepancy can be explained with the 5d-6s interaction in the clusters. The 5d population in the LanL1MB cluster is 9.4055 while the LanL2MB cluster has a 5d population of 9.4296. These numbers indicate, that the 5d-6s interaction in the LanL1MB clusters is stronger than in the LanL2MB clusters leading to an extra charge flow of 0.0241 electrons from top to the base in the LanL1MB cluster. The extra 6s

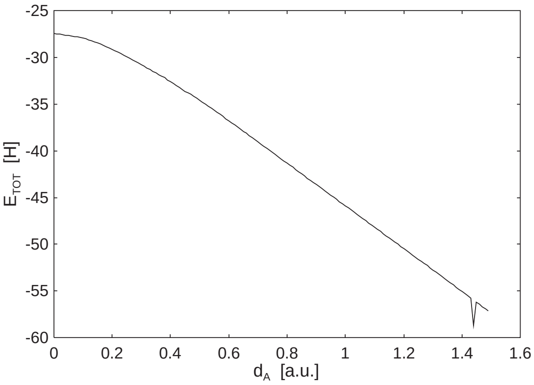

Figure 7.54: E_{TOT} of the LanL1MB cluster.

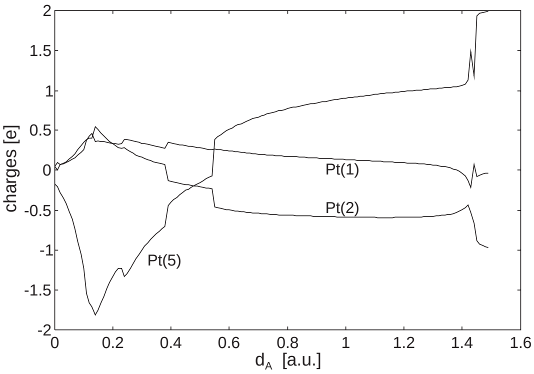

Figure 7.55: Charges on the LanL1MB cluster.

ECP	orb.	6s basis	6s top	$5d_{z^2}$ top	ϵ [H]
LanL2MB	a_1'	0.27838	0.14131	0.48018	−0.39193
	a_1''	−0.16517	−0.10936	0.86576	−0.36228
LanL1MB	a_1'	0.23717	0.19200	0.64613	−0.39312
	a_1''	−0.22202	−0.16556	0.75035	−0.36398

Table 7.14: Orbital coefficients in Pt_5.

electron flow of 0.1086 electrons in the LanL1MB cluster to the top has therefore to be corrected by the 0.0241 electrons leaving the top platinum via the 5d orbitals. This correction results in a net difference of 0.0845 electrons in the innermolecular charge transfer between the LanL1MB and the LanL2MB cluster, which agrees very well with the charge difference of 0.086 electrons at the top platinums. Table 7.13 is so a perfect confirmation of the 5d-6s interaction mechanism developed from Hückel calculations in subsection 5.3.3 (page 125). Figure 5.6 (page 126) shows both electron flows in the cluster.

The dipole moments of both clusters (LanL1MB and LanL2MB) reflect this mechanism. In the LanL1MB clusters the dipole moment points from the bottom of the pyramid to its top. Two topics can be used to explain this orientation: First; 3.60 6s electrons at the bottom of the pyramid face only 0.48 electrons at the top. Second; the 5d-6s interaction moves additional 5d electron density from the top to the base. The dipole moment has therefore to point upwards. The 5d-6s interaction is smaller in the LanL2MB cluster than in the LanL1MB (table 7.14) and charge transfer from tho top base of the pyramid is therefore smaller. The electrons accumulate at the top and the dipole moment changes its direction.

Two totally symmetric orbitals can be observed in the MB-clusters: the a_1' orbital and the a_1'' orbital. They are the products of the 5d-6s interaction. Table 7.14 lists the coefficients of these two orbitals. The a_1' orbital is the bonding combination of the 6s-a_1 orbital and the $5d_{z^2}$ platinum orbital. This MO is dominated by the 6s orbitals, while the antibonding combination (a_1'') is dominated by the $5d_{z^2}$ orbital. The advanced 5d-6s interaction deduced from the 5d population is reflected in the coefficients for the $5d_{z^2}$ orbital. In the LanL1MB cluster is the $5d_{z^2}$ coefficient in the a_1' orbital much stronger than in the LanL2MB case. Table 7.14 is so a good example for the second pathway for the 5d-6s interaction proposed in subsection 5.3.3 (page 125). The first pathway, with small 5s-6s overlap has been observed for calculations with badly chosen parameters

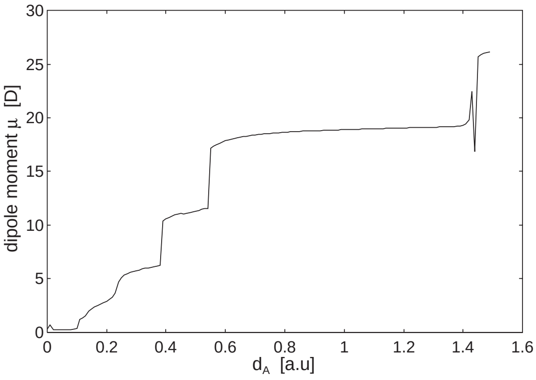

Figure 7.56: Dipole moment the LanL1MB cluster.

for the 6p orbital, but examples are not given for the sake of brevity. In all calculations in this subsection the 6p orbitals interact only weakly with the nonbonding e-orbitals and direct charge transfer is not observed.

So far U_L^{core} has been set equal to zero for all calculations. In the next step we changed U_L^{core} systematically to test the influence of U_L^{core} on the surface model. U_L^{core} was modelled with a third order function and β_A was chosen to be 0.42. Figure 7.54 displays the total energy of the cluster a function of d_A. With increasing values of d_A the total energy of the cluster becomes more negative. The same behaviour was observed before for Pt_5^+ (figure 7.52), but the development of the charge distribution in the cluster is different (figure 7.55 and 7.53). Now the charge at the top becomes more negative at the beginning of the curve but later the charge decreases and at the top becomes finally positively charged. During this electron movement loses the wavefunction its symmetry and the platinums one and two at the base carry now different charges.

The decrease of the total energy agrees well with the Hückel predictions (subsection 5.3.2, page 123). In contradiction to Hückel theory (equation 5.16, page 124) the nonbonding orbitals also decrease their energy and not only the totally symmetric. The charge flow within the cluster observed for values of $d_A \leq 0.14$ a.u. agrees well with predictions from the Hückel theory (equation 5.18, page 125). Hückel theory predicts, that with increasing bond strength between platinum atoms at the pyramid's bottom electron density flows from the top into the basal plane. With increasing values of d_A the negative charge at the top becomes smaller. The analysis of the eigenvectors showed, that with increasing values of d_A the contribution of the 6p orbitals becomes larger. This increase can be used to explain the discontinuities of the dipole moment of the cluster shown in figure 7.56.

7.3.7 Is the LanL1MB cluster a suitable surface model?

All calculations in the section 7.3.3 to 7.3.6 showed, that U_L^{core} has a strong influence on the properties of the metal cluster and via the 6s population also a strong influence on the platinum-water bond. The safest bet on U_L^{core} would be $U_L^{core} = 0$ for the following reasons:

1. According to HAY and WADT U_L^{core} describes the general shape of the ECP for $l \geq l_{max}$ and modifies so the characteristics of the Coulomb term (equation 2.65). Setting U_L^{core} equal to zero is therefore equivalent to the assumption, that the core for the new ECP is similar to a bare hydrogen nucleus.

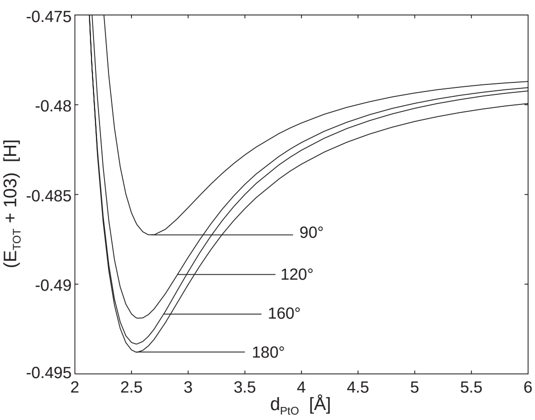

Figure 7.57: Dissociation curves.

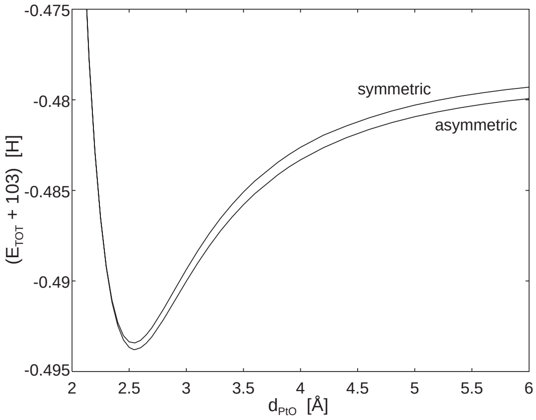

Figure 7.58: Influence of the symmetry.

2. If U_L^{core} represents the general shape of the ECP, it is likely to assume, that U_L^{core} has a similar shape than the pure functions for U_S^{core} and U_P^{core}. Both functions have an attractive third order part with an exponent β_A between 0.40 and 0.44 and repulsive second order function (subsection 7.3.2). A third order function for U_P^{core} is close to the numerical limits of Gaussian 94 and these jobs are difficult to handle. Setting U_L^{core} equal to zero spares us all numerical problems.

3. For $U_L^{core} = 0$ we observed a potential energy surface for the platinum dimer with one minimum (subsection 7.3.3) and the platin-hydrogen bond length in PtH was in a chemically reasonable range (subsection 7.3.4). Setting U_L^{core} equal to nought simulates the core-core repulsion reasonably well for PtH and creates the correct number of stationary points on the Pt_2 potential energy surface.

4. Reliable parameters for U_L^{core} are difficult to extract from the original paper by Hay and Wadt. Useful target properties to be reproduced by the new ECP are therefore properties of small platinum clusters (subsections 7.3.3 and 7.3.5). The calculations on these small clusters (Pt_2 and Pt_5) showed, that no simple set of parameters for U_L^{core} exists, which works as well on Pt_2 as on Pt_5. Only $U_L^{core} = 0$ resulted in reliable values for both clusters.

5. U_L^{core} has a very strong influence on the electronic structure of the nucleus and any potential, which cannot justify the chosen parameters for U_L^{core} in a strict manner remains therefore questionable. From the ethical point of view it is therefore better to stay with the simple hydrogen nucleus than to change to set of phoney parameters for U_L^{core}.

For these reasons we continue the analysis of the water-platinum interface with a bulk ECP according to subsection 7.3.2 with U_L^{core} equal to zero and the LanL1MB ECP for the active site. The water molecule will be described with the DZP basis set, which was used before, because test calculations on $Pt-H_2O$ using the LanL1MB basis set yielded in incorrect geometries, as the water-platinum bond was formed via the hydrogens.

The first set of calculations was very promising. Figure 7.57 shows the dissociation curves of Pt_5-H_2O with different orientations of the molecular plane of the water molecule relative to the

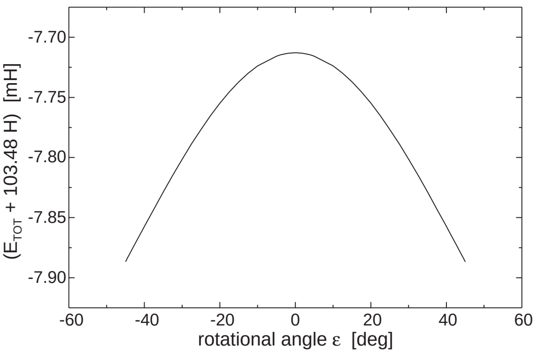

Figure 7.59: Rotational barriere - unsymmetric case.

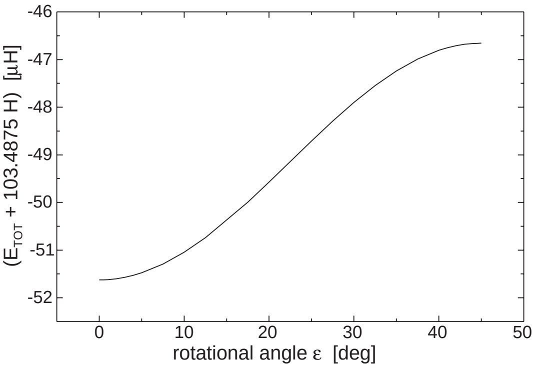

Figure 7.60: Rotational barriere - symmetric case.

surface[9]. On HF level the two hydrogens point upwards and the bonding energy of the water molecule is 9.492 kcal/mol. All curves finally converge to the same point. The energy to move the water molecule from the horizontal position into a vertical is 3.88 kcal/mol. The value of d_{PtO} was not optimized but taken directly from the curve. The true value is therefore likely to be a little larger. 3.88 kcal/mol is a much larger value than 0.26 kcal/mol found with LanL2DZ potential (subsection 6.4.2.3, page 191), but still reasonable regarding other values found in chapter 6.

The symmetry problem still exist if 1-valence ECPs are placed on the bulk atoms. Figure 7.58 shows the dissociation curves $\gamma = 180°$. The curve derived from the symmetric wavefunction has a slightly higher energy than the unsymmetrical curve. It is interesting to note, that both curves end at the same point. The symmetric curve is the same as the curve we calculated for $\gamma = 173°$. At this point also stopped the geometry optimisation. This symmetry error is small compared with the energy discontinuities observed before for Pt_2-H_2O, but the rotational problem of unsymmetrical curves still exists (subsections 5.3.4, page 126 and 6.4.2.2, page 190). Figure 6.75 shows the total energy of the cluster as a function of the rotational angle ϵ. The curve has the correct shape in the centre ($\epsilon = 0°$), but fails at the turning points ($\epsilon = \pm 45°$). Figure 7.60 displays the same movement for the symmetric case. The curve is smooth at the turning points ($\epsilon = 0°$, $45°$) and the energy difference is much smaller (unsymmetric: 200 μH, symmetric: 6 μH). It was impossible to model the rotation correctly with an unsymmetrical wavefunction.

The dissociation of the symmetric wavefunctions, which form the basis of the plot shown in figure 7.60, is interesting. The minimum is shifted away from the surface ($d_{\mathrm{PtO}} = 2.60$ Å) and consequently is the bond much weaker (approx. 6.4 kcal/mol, bond length not optimised). 2.6 Å is very large value for the platinum-water bond and the hydrogens interact only weakly with the metal atoms. The energy necessary to change γ from 135° to 180° is very small, nearly non existent (0.04 kcal/mol). This value is closer to that observed in pure LanL2DZ calculations (0.26 kal/mol).

In the next step we took the checkpoint files from the calculations with symmetric wavefunctions to start with MP2 calculations (figures 7.61 and 7.62). Despite the known disadvantages of this method, we hoped to get so a first estimate of the influence of correlation effects on this surface model. At MP2 level the water molecule moves closer to the surface ($d_{\mathrm{PtO}} = 2.4192$ Å, $\gamma =$

---

[9] For the ease of reading all variables are the same as in subsection 6.4.2 (page 187)

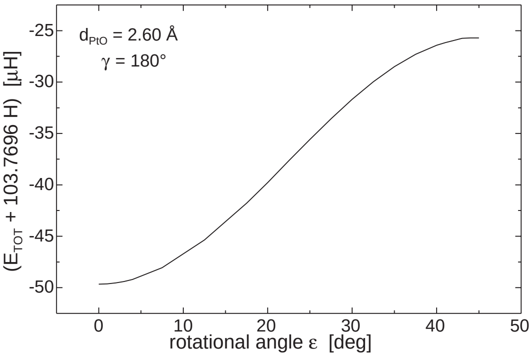

Figure 7.61: Rotational barriere at MP2 level.

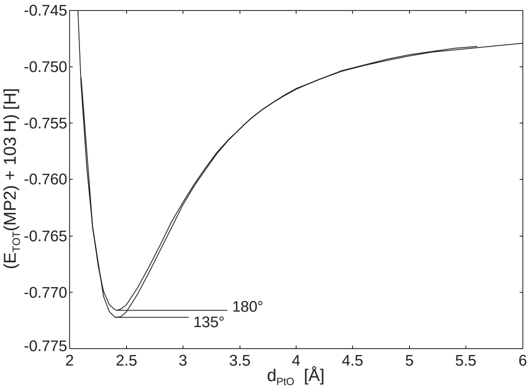

Figure 7.62: Dissociation at MP2 level.

135.18°) and becomes more strongly bonded (15.25 kcal/mol). This is a perfect reproduction of the experimental value. The neighbourhood to the metal cluster increases the metal-hydrogen interaction and moves the hydrogens closer to the surface. This movement increases the energy to reorientate the water molecule. The energy to lift the water molecule up ($\gamma = 135° \rightarrow \gamma = 180°$, d_{PtO} optimized for both angles) is 0.41 kcal/mol and so 10 times bigger than on HF level.

Figure 7.61 shows the rotation of the water molecule. The rotation is smooth and the curve has the correct shape. d_{PtO} has not the optimised value but the HF value of 2.6 Å. At this distance is the energy change caused by the rotational small (0.015 kcal/mol) and negligible.

All calculations in this subsection showed, that it is possible to construct a working surface model with an 1-valence electron ECP for the bulk atoms. The results obtained with this model agree very well with 18 valence electrons calculations and experimental results. One major problem during the calculation potential energy surfaces cannot be avoided: the break-down of symmetry as the water molecule changes its position. It is still vital to check, if the chosen wavefunction can used to describe all movements without sudden symmetry induced energy discontinuities. These checks are still boring and tedious, but can be done much faster now. A complete scan of the Pt_5-H_2O potential energy surface is straight forward is a matter of further research.

7.4 Conlusions from the analysis of the 1 valence electron ECP

1. In section 7.1 we extracted a set of target properties for a new 1-valence electron ECP from the LanL2DZ ECP. These values form the basis for the calculations in sections 7.2 and 7.3. The results for the 6s and 6p orbital are physically reasonable, while the positive energy eigenvalue for the 6d orbital is physically unreasonable. A positive energy eigenvalue for the 6d electron is physically not reasonable, since a positive energy eigenvalue implies dissociation.

2. A simple and naive approach towards a new ECP, which tries to reproduce all results from atomic calculations, failed. The problems were caused by the 6d orbital, which has a positive energy eigenvalue. An ECP, which reproduces the positive 6d energy eigenvalue, is therefore physically useless, but guarantees at least a smooth transition between both ECPs, since calculations in subsection 7.3.6 showed, that the electronic properties of the platinum cluster depend critically on the interface between different ECPs.

3. A positive energy eigenvalue $\epsilon_{6\mathrm{d}}$ without dissociation demands a local or global minimum in the $\epsilon_{6\mathrm{d}}(\alpha)$ curve. α is the gaussian exponent of the wavefunction and controls the distance of the electron density maximum from the nucleus. All calculations in the subsections 7.2.3 to 7.2.9 showed, that such a minimum and so a smooth transition between the ECPs is impossible to create with any number ECP functions.

4. Zurita et al. used a 1 valence electron successfully to model platinum clusters [318]. Both ECPs, Zurita and Hay and Wadt, use different forms for the ECP functions. This difference makes it impossible to use Zurita's ECP directly within the Gaussian 94 program suite. The most challenging problem is $\mathrm{U}_{\mathrm{L}}^{\mathrm{core}}$, which has a strong influence of polyatomic calculations.

5. In the next step we combined a simple representation of the 6s and 6p orbitals, which agree with the simplified functions of the subsections 7.1.1 and 7.1.2, with Zurita's 6d orbital and ECP. This combination reduced the number of indeterminate parameters to one: $\mathrm{U}_{\mathrm{L}}^{\mathrm{core}}$. The following calculations were used to analyse the influence of $\mathrm{U}_{\mathrm{L}}^{\mathrm{core}}$ on polyatomic calculations.

6. $\mathrm{U}_{\mathrm{L}}^{\mathrm{core}}$ has a dramatic influence on the platinum dimer. The calculation showed, that it is possible to tune the dimer's properties with $\mathrm{U}_{\mathrm{L}}^{\mathrm{core}}$. It was possible to reproduce the properties of the LanL2DZ dimer with a second order function in the G94 input file. This ECP stretches too far to be physically reasonable. The third order function allows us to reproduce the optimised bond length of the LanL2DZ dimer, but fails to reproduce the binding energy.

   $\mathrm{U}_{\mathrm{L}}^{\mathrm{core}}$ has a tremendous influence on the dimer's total energy as function of the interatomic distance r. The original curve ($\mathrm{U}_{\mathrm{L}}^{\mathrm{core}} = 0$) has a single, global minimum. With the increasing strength of $\mathrm{U}_{\mathrm{L}}^{\mathrm{core}}$ develops a second minimum. Geometry optimisations oscillate between these two minima and small changes of $\mathrm{U}_{\mathrm{L}}^{\mathrm{core}}$ have a very strong influence on the dimer. For very strong attractive functions dominates the second minimum and becomes global. This minimum moves to longer bond lengths until finally the dimer dissociates and the calculation becomes physically unreasonable.

7. A totally different behaviour has been observed for PtH. With increasing strength of $\mathrm{U}_{\mathrm{L}}^{\mathrm{core}}$ the bond becomes shorter until finally both atoms collide. $\mathrm{U}_{\mathrm{L}}^{\mathrm{core}}$ changes the potential energy curve of PtH from a single minimum curve into a function with now minimum in a chemically reasonable region.

8. $\mathrm{U}_{\mathrm{L}}^{\mathrm{core}}$ does not only change the strength of a chemical bond, but also changes the electron density within the cluster. Calculations on Pt_5^+ showed, that $\mathrm{U}_{\mathrm{L}}^{\mathrm{core}}$ also changes the orientation of the dipole moment. It is not possible to reproduce the properties of the LanL2DZ dimer and the LanL2DZ platinum pyramid with the same set of parameters for $\mathrm{U}_{\mathrm{L}}^{\mathrm{core}}$.

9. Suitable surface models contain at least one bonding platinum atom while the majority of the atoms are 1-valence electron ECPs to simulate bulk and passive surface atoms. In these clusters different ECPs get into contact and each ECP has its own set of parameters for $\mathrm{U}_{\mathrm{L}}^{\mathrm{core}}$. The calculations in subsection 7.3.6 showed, that the interface between both ECPs has a very strong influence on the electron distribution in the platinum cluster. The LanL1MB potential from Hay and Wadt gave the best results and we continued the work with this ECP. Since $\mathrm{U}_{\mathrm{L}}^{\mathrm{core}}$ of the bulk atoms is part of the controlling interface $\mathrm{U}_{\mathrm{L}}^{\mathrm{core}}$ can be used to manipulate the charge distribution in the cluster. The results of these calculations agree reasonably well (dipole moment) with the prediction from Hückel calculations.

All calculations so far showed, that it is possible to create nearly any wanted electronic property of the metal cluster with a suitable set of parameters for U_L^{core}. To avoid any future problems we set U_L^{core} equal to zero for all calculations in the last part of this chapter. This approximation is equal to a bare hydrogen nucleus at the core. We neglect so the spatial extension of the core, which we do not know. This procdure seems to be philosophically much better than working with unproved assumptions.

10. In large clusters interact the hydrogen atoms of the water molecule with passive surface atoms. The new 1-valence electron ECP ($U_L^{core} = 0$) describes the platinum-hydrogen interaction reasonably well (figures 7.49 and 7.50 in comparison with table 6.8, page 157), and successful calculations on larger clusters should therefore be possible.

11. The electronic structure of the Pt_5 pyramid with a LanL1MB platinum at the top shows a strong 5d6s interaction as precisely predicted by the Hückel calculations. This interaction changes the charge at the top platinum, since electron density flows away from the platinum via the 5d orbitals.

    Calculations on Pt_9-H_2O with the LanL2DZ potential indicated (section 6.5, page 192), that an extended 5d electron flow within the cluster is possible. This flow is beyond the possibilities of a simple 1-valence electron ECP. Since this 5d electron flow increases with cluster size is the credibility of the 1-valence electron ECP approach towards the adsorption of water on platinum limited by the cluster size. The extend of this limitation will be subject of future research.

12. The Pt_5 pyramid with a LanL1MB platinum at the top serves as good surface model. The pyramid carries a small negative charge at the top (-0.18 e), which repels the oxygen. The 6s population (0.48) is close to the Hückel prediction (0.44). Both, the negative charge at the top and the 6s population, repel the oxygen atom, while the 5d electron charge flow from the top atom to base creates a hole, which can be filled with electrons from the oxygen lone pair.

    This Pt_5-H_2O cluster with a LanL1MB ECP at the top allowed us to compute a working potential energy surface for the water-platinum interaction. The simplicity and speed of these calculations justify the chosen approximations, but the symmetry of the wavefunction is still the biggest problem. As the symmetry changes during the movement of the water molecule, the electron distribution also can change. A careful construction of the wavefunction allows us to describe all movements of the water molecule.

    The bond between the water molecule and the platinum atom is too weak on Hartree-Fock level. With the introduction of electron correlation on MP2 level the bond becomes stronger. The cluster is now a physically reasonable model of the surface ($\Delta E_{BOND} = 15.25$ kcal/mol). The molecule can rotate freely ($\Delta E_{ROT} = 0.015$ kcal/mol) at a distance of 2.6 Å, and nothing indicates a major rotational barrier for smaller distances. The water molecule is slightly tilted ($\gamma = 135°$) and the energy to lift the molecule up is also small ($\Delta E_{UP} = 0.41$ kcal/mol). Such a small energy reflects the weak interaction of the hydrogens with the surface. Calculations on Pt_9-H_2O will help to analyse the importance of the hydrogen-platinum interaction on the orientation of the water molecule.

13. The succesful calculations on Pt_5-H_2O showed, that the new 1-valence electron ECP can

be used on bulk and passive surface atoms, but the number of assumptions made, suggests that the applictaion of this ECP should be restricted to small surface modells with the experimentaly observed PtPt bond length of 2.77 Å.

14. The platinum-water interface is difficult to model and the analysis of the Hartree-Fock results was only possible with the results from the Hückel calculation and the 1-valence elctron ECP. The Hückel calculations are the link between the calculations with 18 valence electrons and calculations with the 1-valence electron ECP. Without any of the three parts (18 valence electron calculations, Hückel calculations, 1-valence electron ECP calculations) it would have been impossible to analyse the platinum-water interface.

Chapter 8

Water Clusters on the Platinum Surface

The first two chapters 3 and 4 focused on water clusters while the next two chapters 6 and 7 analysed the interaction of a single water molecule with the platinum surface. Now we concentrate on the interaction between extended water clusters and the metal surface. In this chapter we use the results of these initial four chapters and together with additional calculations we focus on a more realistic description of the platinum-water interface.

The first section (8.1) investigates the bond between small water clusters and simple platinum clusters: $\mathrm{Pt_n - (H_2O)_m}$ with $1 \leqq \mathrm{n} \leqq 3$ and $2 \leqq \mathrm{m} \leqq 3$. Cooperative forces have a strong influence of the structure of the water cluster. These effects can be used to explain experimental TDS data, which have been a matter of discussion so far. We published these new results already in "Langmuir"[42] to comment directly to the publication by Ogasawara et al., who collected the experimental data [56]. Section 8.1 is therefore a reprint of the manuscript.

In the second section (8.2) we use the new water-water interaction potential of chapter 4 to investigate the structure and the energy of the water hexamer on a virtual metal surface. The metal surface is purely described by geometrical constraints on the water cluster's geometry. All results, which have been checked quantum chemically, indicate that the molecular plane of the water molecule can be orientated parallel to the metal surface and the growth of ice is still possible. These new results can used to settle the dispute on the orientation of the water molecule and will be published as soon as possible [59].

Chapter 8 is compilation of two complete manuscripts submitted for publiclation, both containing a introductory subsection. Repetions regarding chapter 1 are therefore unavoidable and the subsections 8.1.1 and 8.2.1 may be skipped, but the author did not want to destroy the logical unity of the essays.

8.1 Influence of Cooperative Effects on the Formation of Water Trimers on Pt(111)

Abstract

Calculations on small platinum-water clusters demonstrate the importance of cooperative effects on the formation of a water bilayer structure on the platinum(111) surface. If the orientation of the bridging water molecule is allowed to relax during the simulation of this bilayer, one hydrogen bond is broken in favour of the other. The desorption energy of water from the relaxed model cluster is found to be in better agreement with published thermal desorption spectra (TDS) data than desorption energies arising from an ideal ice-like bilayer structure.

8.1.1 Introduction

Early work [36, 37] on the adsorption of water on the platinum(111) surface reported a $(\sqrt{3} \times \sqrt{3})$ R30° surface structure of adsorbed water molecules and suggested the formation of ice ordered in domains of 30 to 40 in length.

A water bilayer structure [38, 39] has been proposed as the basis of the growth of ice on hexagonal platinum lattices. In the initial stages of growth, a water molecule has two possible adsorption sites: attached either directly above a platinum on the surface or to a water molecule already bound to the surface [46, 48]. The smallest water cluster deduced from UHV experiments is a three dimensional water trimer [45].

Thermal desorption spectra [38, 43, 46, 48, 50–54, 56] of water from the platinum(111) surface remain controversial. The most recent data from Ogasawara et al. [56] shows three prominent peaks at 155 K, 165 K and 200 K. The first peak (at 155 K) was assigned to ice sublimation, the second (at 165 K) to water in the second adsorption layer and the third (at 200 K) to water directly bound to the surface. While the first two peaks have been positively identified, the origin of the third remains a matter of discussion [53, 54]. The formation of the second peak at 165 K can be observed at coverages as low as 0.13 to 0.27 monolayer (ML), where 1 ML refers to an ideal bilayer [39]. These TDS results are consistent with other experimental results [43, 45, 46, 48, 57, 58], which also support the formation of water clusters at low surface coverage.

The coexistence of both species (i.e. a water molecule directly bound to the surface and a water molecule attached to another water molecule) is commonly explained in terms of the energy of isolated bonds, although the importance of cooperative forces has been suggested previously [45, 49]. The strength of the platinum-water bond corresponds to that of two to three hydrogen bonds, so either type of bonding is possible. The structure of water cluster at metal surfaces is generally explained in terms of an extension to surfaces [39] of the Bernal-Fowler-Pauling (BFP) rules [9, 13]. Specifically [39], each water molecule is assumed bound by at least two bonds (which may be hydrogen bonds to other water molecules, or oxygen lone pair bonds to the surface) while maintaining a tetrahedral bonding configuration. The water is assumed bound to the surface via one lone pair orbital on the oxygen, all free lone pair orbitals on oxygen lying nearly perpendicular to the surface. In an ideal infinite bilayer, all water molecules have their dipole moments pointing away from the surface ("flip up"), whereas, in a finite cluster, water molecules whose dipole moments point towards the surface ("flop down") may occur at the edges of the cluster [39, 41]. Experimental results [43] suggest that the edges of ice-like clusters on Pt(111) are constructed from flip up

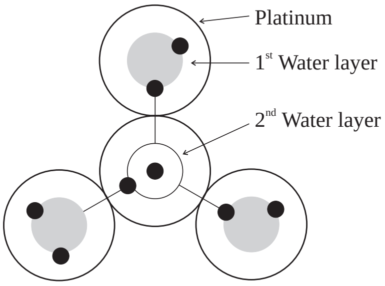

Figure 8.1: Fragment of the Pt(111) surface with water bilayer.

molecules together with water molecules with one OH bond parallel to the metal surface, in contrast to the flop down geometry predicted at the edges by the BFP rules. Such a water species has been observed on Pt(100) [44] and experimental evidence suggests that such a species may also exist on Pt(111) [45, 46]. It has not been possible to rule out such a structure by application of ultraviolet photoelectron spectroscopy (UPS) to Pt [6(111)×(100)] [37].

The metal-water interface has been examined previously by quantum chemical calculations [54, 60–72] and work on the platinum-water interface [54, 63–65, 68] suggests that the molecular plane of the water lies parallel to the surface [54, 63, 68]. These results agree with workfunction measurements [45, 52, 58, 73] on water-covered platinum surfaces, which show that that a contribution of about 0.2 D of the water dipole moment (single molecule 1.84 D) is normal to surface [58]. Theory and experiment agree that the water molecule is only slightly disturbed upon adsorption on Pt(111) [41, 45, 46, 48, 58, 73–75] and dissociation has so far only been observed experimentally on pre-covered surfaces [76–79].

The significance of hydrogen bonding and polarisation effects has been discussed previously [45, 56, 64, 75], but, to our knowledge, has not been studied in great detail. This work provides a theoretical analysis of the effects of cooperative water-metal interactions on the orientation of the water molecules in the second layer.

8.1.2 Computational Procedure

All calculations were carried out using Gaussian 94. The platinum atoms were described by the effective (18 valence electron) core potential of Hay and Wadt [189] using a double-zeta basis set[1]. The double-zeta plus polarization (DZP) basis sets of Dunning [355] were used to describe hydrogen and oxygen. Open shell species were treated by the unrestricted Hartree Fock (UHF) approach and charges determined according to the Mulliken scheme. Electron correlation was incorporated at the Møller-Plesset (MP2) level.

The structure of all platinum clusters corresponds to the top layer of the platinum(111) surface (figure 8.1) with a platinum-platinum distance of 2.77 Å. This value, which corresponds to the experimental platinum-platinum distance, has been used in previous quantum mechanical calculations [65]. In the case of Pt_3, the cluster corresponds to an isosceles triangle. For calculations on a Pt2 model cluster, the central platinum atom in Pt_3 was replaced by a dummy atom in order to represent a dumbbell with a platinum-platinum distance of 4.7978 Å.

---

[1] LanL2DZ, table 6.1, page 146

	Pt(^{1}S)	Pt(^{3}D)
r(PtO) [Å]	2.0986	2.4952
γ^a [deg]	116.43	123.2
q_{Pt} [e]	−0.162	−0.103
E[Pt(^{1}S)] + E[H_2O] − E[Pt−H_2O] [kJ mol^{-1}]	94.440	89.212
E[Pt(^{3}D)] + E[H_2O] − E[Pt−H_2O] [kJ mol^{-1}]	38.243	33.086

[a] γ is the angle between the symmetry plane of the water molecule and the Pt−O bond.

Table 8.1: Selected results for Pt−H_2O.

The OH bond of the water molecule was constrained at the experimental value of 0.9572 Å and the HOH angle at 104.52° [16]. During geometry optimisations the water molecule was not allowed to relax, since previous experimental and theoretical results had suggested that the monomer geometry was only slightly disturbed upon adsorption. The initial water clusters were constructed as ideal tetrahedra in accordance with the BFP rules, as was the platinum-water bond. The angle between the molecular plane of the water molecule and that containing the platinum-water bond was constrained at 125.29° assuming that the lone pair electrons point towards the edge of a tetrahedron. The first layer of water molecules was placed on top of the terminal platinum atoms at the base of the triangle, while the second layer of water molecules was placed on top of the central platinum atom.

During geometry optimisation, only the platinum-oxygen bonds were allowed to relax, while the remainder of the cluster was constrained in position. During these optimisation calculations the ideal geometry of the cluster was broken, and since the bond angles were not allowed to relax, the hydrogen bond became bent.

Deviations from this standard procedure are identified in the text.

8.1.3 Results and Discussion

The analysis of polarisation effects in small water clusters attached to a platinum surface commenced with the smallest possible clusters, Pt−H_2O and Pt−$(H_2O)_2$. The interaction energy of water and a platinum atom (Table 8.1) depends strongly on the electronic state of the platinum. The energy of Pt(^{1}S) H_2O lies 94.4 kJ/mol below that of Pt(^{1}S) and free water, and 38.2 kJ/mol below that of Pt(^{3}D) and free water, whereas the energy of Pt(^{3}D)−H_2O lies 33.1 kJ/mol lower than that of Pt(^{3}D) and free water. Comparison of Pt(^{3}D) (with electron configuration $5d^9 6s$) with Pt(^{1}S) (with electron configuration $5d^{10}$) shows that occupation of a 6s rather than a 5d orbital will result in movement of electron density away from the nucleus, increasing the Coulomb repulsion between platinum and oxygen and thereby weakening the bond.

Table 8.2 shows the results for the hydrogen bond in Pt−$(H_2O)_2$. The geometries B and C differ from that of A (figure 8.2) in the role of the second water molecule. In geometries B and C the second molecule acts as an electron donor whereas in geometry A it acts as an electron acceptor. The arrows in figure 8.2 show the direction of charge transfer during the formation of the cluster.

In geometry A the terminal water molecule acts as an electron acceptor. As in the formation of a hydrogen bond, bond formation between platinum and water is accompanied by charge transfer

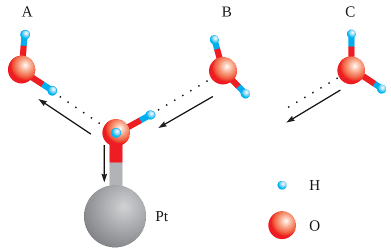

Figure 8.2: Platinum and a water dimer - principal geometries.

	state	A	C	B
r_{OO} [Å]	^{1}S-Pt	3.1190	2.7429	2.7009
	^{3}D-Pt	3.0504	2.8248	2.7876
r_{PtO} [Å]	^{1}S-Pt	2.1021	2.0758	2.0706
	^{3}D-Pt	2.4427	2.4354	2.4208
E_{HBOND} [kJ mol^{-1}]	^{1}S-Pt	8.096	38.850	49.558
	^{3}D-Pt	11.880	32.659	40.232
q_{Pt} [e]	^{1}S-Pt	−0.129	−0.177	−0.185
	^{3}D-Pt	−0.104	−0.123	−0.129
$q_{H_2O-CENT}$ [e]	^{1}S-Pt	0.134	0.128	0.136
	^{3}D-Pt	0.114	0.083	0.089
$q_{H_2O-TERM}$ [e]	^{1}S-Pt	−0.0004	0.049	0.050
	^{3}D-Pt	−0.010	0.040	0.041

Table 8.2: Results for $Pt-(H_2O)_2$.

from the water molecule to the platinum atom. Both bonding partners pull electron density away from the central water molecule. The charges on the fragments therefore become lower than on the free molecules ($q_{Pt} = 0.129$ e vs. 0.162 e in $Pt-H_2O$) and the hydrogen bond becomes weaker (free $(H_2O)_2$: $r_{OO} = 1.95$ Å, $E_{HBOND} = -26.1$ kJ/mol).

Different behaviour is observed when the second water molecule acts as an electron donor (figure 8.2, cases B and C). The dissociation energy of the hydrogen bond between the water molecules in $Pt-(H_2O)_2$ is much higher than that of the free water dimer. Charges on the terminal water molecules are also higher than for the free water dimer (0.028 e) and the dissociation energy of the hydrogen bond increases with the charge on the platinum atom. The strength of the hydrogen bond is related to the intramolecular charge transfer.

Charge transfer from the terminal water molecule to the platinum atom maintains a low charge on the central water molecule and simultaneously strengthens the hydrogen bond between the water molecules and the bond between platinum and the central water molecule. If the terminal water molecule acts as an electron acceptor, charge accumulates on the central water molecule and the platinum-water bond is weakened by the reduced ability of the central water molecule to transfer electron density to the platinum atom via its free electron pair.

The role of intramolecular charge transfer can be observed by a comparison of the results for geometries B and C, where, in both cases, the second water molecule acts as an electron donor. Geometry C forms part of an ideal infinite water bilayer structure as proposed by Thiel and

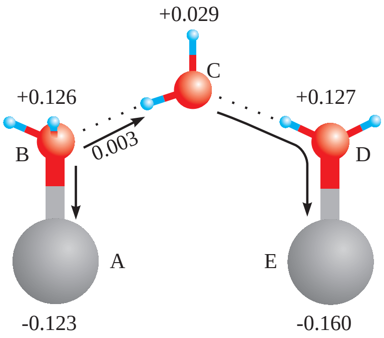

Figure 8.3: Cluster I: $Pt_2-(H_2O)_3$ cut from an ideal infinite bilayer structure.

Madey [38], while geometry B is constructed from an ideal water dimer. These geometries do not differ in the extent of charge transfer from the hydrogen acceptor to the hydrogen donor (Δq_{AD}) associated with the hydrogen bond (free water dimer from cluster B with fixed optimized geometry: $E_{HBOND} = -22.6$ kJ/mol, $\Delta q_{AD} = 0.035$ e; free water dimer from cluster C with fixed optimized geometry: $E_{HBOND} = -18.3$ kJ/mol, $\Delta q_{AD} = 0.034$ e) and the terminal water molecules are equally charged. The difference in hydrogen bond energies for these platinum clusters ($\Delta E_{HBOND} = -10.7$ kJ/mol) is more than twice that expected from the free dimers ($\Delta E_{HBOND} = -4.4$ kJ/mol). The reduced steric and Coulomb repulsions in the ideal dimer structure permits a shorter oxygen-oxygen distance, thereby enhancing orbital overlap. The improved orbital overlap stabilizes the charge on the central water molecule. The ideal dimer geometry facilitates the charge transfer between platinum and water and enhances cooperativity, yielding a stronger bond.

Table 8.2 shows the results for platinum-water clusters for both ^3D and ^1S platinum. The geometries of B and C are consistently longer in the case of Pt(^{3}D). In complexes based on ^{3}D platinum, the platinum water interaction energy is weaker and cooperative effects smaller (E_{COOP} for geometry B: -22.2 kJ/mol for the ^{1}A state and -11.3 kJ/mol for the ^{3}A state). The electron pull from the platinum atom is reduced and the charges on the water molecules therefore decrease. In agreement with this reduction in charge transfer, the hydrogen bond weakened. In the case of geometry A, the hydrogen bond is stronger, since the electron pull of the platinum atom is weaker. The charge on the platinum atom is reduced and charge transfer along the hydrogen bond is improved. The strength of the hydrogen bond is directly related to the negative charge on the platinum atom.

Similar cooperative effects are well known in water trimers [107, 145]. In the most stable trimers, the net charge on the water molecules is small and as many molecules as possible act simultaneously as electron donor and electron acceptor. The platinum atom is a strong electron acceptor and a strong hydrogen bond is formed only if the second water molecule acts as an electron donor.

These results suggest that cooperativity is important in the formation of small water clusters on metal surfaces. As the metal cluster size is increased so as to simulate the surface, the electronic state of the metal cluster becomes more significant. In this early stage of our work we chose to construct the platinum cluster purely from ^{1}S platinum atoms. The results for $Pt-H_2O$ and $Pt-(H_2O)_2$ suggest that this approach will include clusters with the strongest platinum-water interactions.

More closely related to the real bilayer structure is the $Pt_2-(H_2O)_3$ cluster (cluster I in figure 8.3), which forms a segment of an ideal, infinite bilayer structure. Both platinum-water bonds are

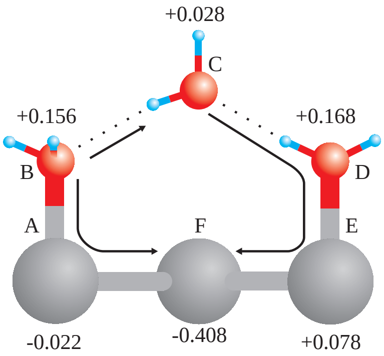

Figure 8.4: Cluster II: $Pt_3-(H_2O)_3$ as part of an ideal infinite bilayer structure.

of equal length, since previous results for $Pt-(H_2O)_2$ showed (Table 8.2) that the bond lengths differ only slightly with the geometry of the hydrogen bond. The bridging water molecule is slightly more strongly bound (E_{CENT} = 47.3 kJ/mol) in the water cluster than in the corresponding free water trimer (E_{CENT} = 44.2 kJ/mol). The bridging water molecule acts simultaneously as electron donor and electron acceptor. Since the molecule is more strongly bound than the free water dimer void of any platinum, the hydrogen bond enforcing cooperative forces on the C−D−E side will dominate the weaker forces on the C−B−A side. Charges on the left C−B−A side of the molecule are similar to those in the free $Pt-(H_2O)_2$ cluster, while the charges on the C−D−E side differ markedly from the free case. Although the charge transfer from the right is assisted by an additional 0.003 e from the left, the charge on platinum E is smaller than in the free cluster. This is caused by the extension of the hydrogen bond C−D (2.92 Å vs. 2.74 Å in $Pt-(H_2O)_2$ cluster C). The B−C hydrogen bond is shorter than the optimized bond length (3.12 Å in $Pt-(H_2O)_2$ cluster A) by the same amount.

Cluster II (Figure 8.4) forms part of an ideal bilayer structure. It differs from cluster I in that the central platinum atom lies directly below the central water molecule. This central water molecule is more weakly bound (E_{CENT} = 31.1 kJ/mol) than in cluster I or in the free trimer and the charges on the water molecules are larger than in cluster I. The C−D hydrogen bond is much weaker than in cluster I but still stronger than in the free water dimer, because the hydrogen bond is further extended. (Mulliken overlap populations (MOP) O_CH_D cluster II : 0.027, cluster I : 0.033, free water dimer : 0.010). The B−C hydrogen bond is slightly stronger (MOP O_BH_C cluster II : 0.006, cluster I : 0.005), because the bond length approaches the optimal hydrogen bond length for an electron accepting water molecule. The weak bond may be attributed to the Coulomb repulsion between the negative charge on platinum F and the oxygen electrons on the central water molecule, as shown previously for $Pt-H_2O$.

The Coulomb interaction is the driving force for the relaxation of the central water molecule (cluster III, Figure 8.5). The hydrogen bond involving the weakest cooperative forces is broken (MOP O_BH_C cluster III : 0.008, cluster II : 0.006) in favour of a strong Coulomb interaction between the hydrogen of water molecule C with platinum F (MOP H_CPt_F cluster III : 0.051, cluster II : 0.003) and a stronger C−D hydrogen bond (MOP O_CH_D cluster III : 0.044, cluster II : 0.027). Breaking the B−C hydrogen bond releases electron density from water molecule B, which is transferred via platinum A directly to the central platinum atom F. The charge on water molecule B is increased and platinum A becomes positively charged. Although the charges on water

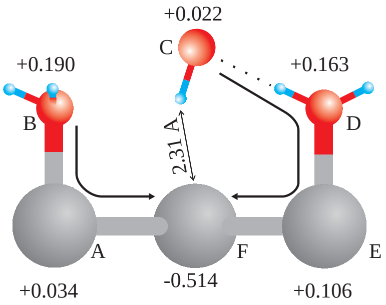

Figure 8.5: Cluster III: $Pt_3-(H_2O)_3$ with a relaxed central water molecule.

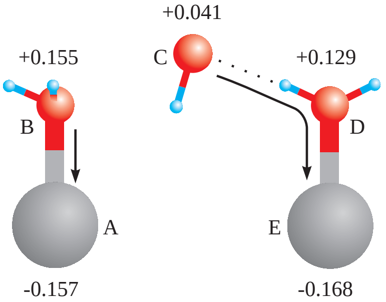

Figure 8.6: Cluster IV: $Pt_2-(H_2O)_3$ central water molecule in the same position as in cluster III.

molecules C and D decrease during this relaxation process, the total charge transfer from the right (C−D−E) side of the cluster is increased (cluster II : 0.274 e, cluster III : 0.291 e). The central water molecule now lies closer in geometry to that of the optimal dimer, but in an unfavourable trimer position. The binding energy of the central water molecule in the corresponding free water trimer is 28.3 kJ/mol, about two-thirds of the corresponding energy for the free water trimer in cluster II.

Figure 8.6 (cluster IV) shows the results of a single point calculation for cluster III in the absence of the central platinum atom. The B−C hydrogen bond is broken (MOP O_BH_C cluster IV : −0.003, cluster I : 0.005), the charge distribution in the A−B fragment is nearly the same as that in the free $Pt-H_2O$ cluster, and the charge distribution is close to that of $Pt-(H_2O)_2$, case C. The former hydrogen bond O_BH_C is broken and H_C now bonds weakly to platinum A (MOP H_CPt_A cluster IV : 0.004, cluster I : −0.004) via an overlap involving Pt(6s) and H(1s). In summary, the charges on the A−B side shows that 0.002 e must have been transferred from the C−D−E side. Since the water molecule D and the platinum atom are too far apart, the most likely donor water molecule is C. The platinum-platinum interaction is not affected by the geometry of the water cluster (MOP Pt_APt_E case IV: 0.028, case I: 0.029). Again, an unfavourable water trimer is stabilized by the presence of the platinum cluster below.

The total relaxation of the central water molecule in cluster IV yields a structure containing a strongly bound water molecule (cluster IVa, E_{CENT} = 71.9 kJ/mol). The central water molecule is bound via two hydrogen bonds to the water molecules B and D and via the free hydrogen atom to the platinum cluster. The distance between O_C and the platinum surface is only 2.26 Å while the distance between platinum and the linking water molecules B and D is 2.9 Å. The absence of platinum F allows the bridging water molecule to lie closer to the platinum atoms A and E,

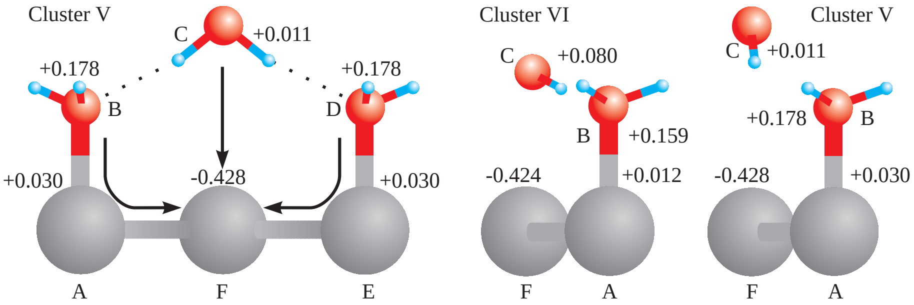

Figure 8.7: Cluster V and cluster VI: flop down structures.

forming the third bond.

Figure 8.7 shows the result (cluster V) of a geometry optimisation (platinum-oxygen distances and tilt of the bridging water molecule's molecular plane) of a water trimer on platinum with flop down geometry. The flop down arrangement for a bridging water molecule has been postulated at the fringes of the ice domains or in small water clusters [39]. According to the BFP rules, an electron lone pair of a second layer water molecule lies perpendicular to the surface, so the geometry optimisation commenced with such a structure (cluster VI).

The binding energy (41.2 kJ/mol) of the central water molecule in cluster V is higher than that for ideal coordination (as shown in Figure 8.3) but much smaller than that of a water molecule in a relaxed position (cluster III). During the optimisation, the BFP rules were violated. At the beginning (cluster VI) of the optimisation the central water molecule acts as a double electron acceptor and therefore weakens the platinum-oxygen bonds (MOP $\mathrm{Pt_AO_B}$: 0.036). The unfavourable hydrogen bonds $\mathrm{H_BO_C}$ and $\mathrm{H_DO_C}$ (MOP $\mathrm{H_BO_C}$: -0.019) break during the optimisation procedure (MOP $\mathrm{H_BO_C}$: -0.003) and the hydrogen atoms $\mathrm{H_C}$ bind directly to the central platinum atom (MOP $\mathrm{Pt_FH_C}$: 0.009). During the rotation of the bridging water molecules the platinum-oxygen bond increases and the hydrogen atoms turn towards platinum F. This reorganisation brings the central water molecule into a position in which it is unable to to pull electrons from its neighbours. As the electron pull diminishes, the bonds between the linking water molecules B and D with platinum atoms A and E become stronger (MOP $\mathrm{Pt_AO_B}$ cluster VI : 0.036, cluster V : 0.045). As before the system tries to relax by breaking an unfavourable hydrogen bond in the water cluster and establishing a direct interaction between a second layer hydrogen and platinum atoms on the surface.

Special care must be taken with the analysis of the charges. Contrary to expectation and the results for $\mathrm{Pt-(H_2O)_2}$ (Figure 8.2, geometry A) the bridging water molecule is positively charged (cluster V : +0.011 e, cluster VI : +0.080 e). The initial geometry for the optimisation (cluster VI) reflects the highest charge on the central water molecule so the analysis was carried out at this geometry. Initially, the geometry of the bridging water molecule is close to that found for an indivial water molecule with its molecular plane parallel to the metal surface. The platinum-oxygen bond is elongated as one expects from the orientation of hydrogen atoms. In this position charge flow from the water molecule to the surface is possible. To answer the question of how much charge flows from the central water molecule to the platinum cluster the calculations were repeated in the absence of the central platinum atom F (cluster VIa), when no charge was found on the central water molecule. The platinum atoms bind the electrons so strongly to the linking

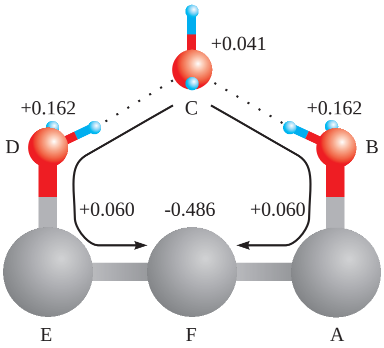

Figure 8.8: Cluster VII: flip-up structure, double electron donor.

water molecules B and D that no net charge flow is possible, as is shown by comparison with the corresponding free water trimer ($q_{\mathrm{H2Ocent}} = -0.048$ e). The binding of the electrons to the linking water molecules B and D weakens the binding energy of the bridging water molecule in cluster VIa (25 kJ/mol) in comparison with that of the free water trimer (43.3 kJ/mol). Since water molecule C is positively charged in clusters V and VI and no charge was found on the central water molecule in cluster VIa, it is reasonable to assume that no charge has been transferred from the bridging water molecules to compensate for the electron withdrawal. The binding energy of the central water molecule reinforces this assumption. Removal of the central platinum atom F from cluster VI increases the binding energy of the bridging water molecule (E_{CENT}) from -5.3 kJ/mol to 25.0 kJ/mol. The electron attraction between water C and platinum F produced a charge on water C and so created a repulsion between the positively charged water molecules B, C and D. With the removal of platinum F this repulsion vanishes and weak hydrogen bonds are formed between the water molecules.

Figure 8.8 shows the results of a geometry optimisation where the central water molecule acts as a double electron donor. During the first optimisation (cluster VII) the positions of the hydrogen atoms were fixed (One O_CH_C bond was maintained normal to platinum surface.) to avoid a direct platinum-hydrogen bond. In this geometry, two weak hydrogen bonds are formed between the water molecules (MOP H_CO_B : 0.018). The sum of the populations of these bonds (0.037) is slightly higher than in the other clusters. The number of electrons available for hydrogen bonding between the water molecules seems to be constant at about 0.036 (table 8.3). The platinum-water bond is also strong (MOP Pt_AO_B : 0.045). The charge on the water molecule C (0.41 e) is nearly twice that on the bridging water molecule in cluster III (0.022 e) and the charges on the water molecules B and D (0.162 e) are the same as those on the first layer water molecule D (0.163 e) in cluster III, which is the bridging molecule in the C−D−E bond which displays cooperative characteristics. Therefore one might assume that two strong cooperative bonds are formed and the binding energy of the bridging water molecule should therefore be high, but the opposite was found. Despite possessing two strong bonds, the binding energy of the central water molecule (E_{CENT} = 59.9 kJ/mol) remains smaller than in cluster III. This contradiction can be explained by a lower charge transfer within this platinum cluster than in cluster III. The total charge on the bridging platinum atoms A and E (0.120 e) is smaller than that in cluster III (0.140 e); a similar result applies to the central platinum atom F (cluster VII : -0.486 e, cluster III : -0.514 e). The large distance (3.06 Å) between platinum F and the bonding hydrogen atom H_C destabilises the charge

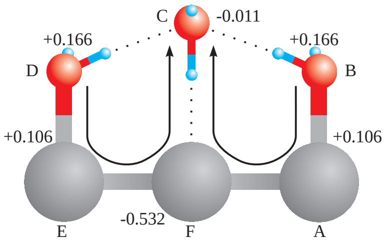

Figure 8.9: Cluster VIII: relaxed flip-up geometry.

accumulation on the central platinum atom and the interaction between both atoms is consequently reduced (MOP Pt_FH_C cluster VI : 0.011, cluster III : 0.051).

If the hydrogen atoms of the bridging water molecule C are allowed to relax without breaking the C_S symmetry (cluster VIII, Figure 8.9) H_C moves closer to Pt_F (2.16 AA). The hydrogen bonds between the water molecules are reinforced (MOP H_BO_C : 0.035) and a very strong bond between hydrogen H_C and platinum Pt_F is formed (MOP Pt_FH_C : 0.082). Since this water molecule is the most strongly bound in the whole set of clusters (98.1 kJ/mol), it is of interest to analyse its charge distribution. Bridging water molecules B and D have similar charges (0.166 e), while the charge on the bridging platinum atoms A and E (0.106 e) is close to that found in the presence of cooperative forces (cluster III, C-D-E triple bond). The charge on the central platinum is the highest in the series which suggests a strong platinum-water interaction. Surprisingly, the bridging water molecule is negatively charged, with electron flow from the central platinum atom to the water molecule. Charge transfer from the bridging water molecules B and D is unlikely, since the electron flow in a hydrogen bond between water molecules is along the lone pair on the oxygen and electrons are usually accepted via hydrogen atoms. In this Pt_FH_C bond the platinum d-orbitals contribute more strongly to the platinum water bond, and these electrons account for the strong hydrogen bond despite its unfavourable geometry: The hydrogen atoms of the bridging water molecules B and D point towards the negative charge on the central water molecule, which permits a strong Coulomb interaction and compensates for the small orbital overlap. The bridging water molecule is therefore triply bound - by two strong hydrogen bonds and one strong platinum-hydrogen bond.

The interaction between the water molecules in the second layer and the platinum surface occurs via highly charged surface atoms. The charge accumulation on these atoms is likely to be dependent upon cluster size. In a real extended metal surface, the electrons associated with the binding of the first layer of water molecules may move into the bulk or spread evenly across the surface. With such small clusters, it is virtually impossible to describe such electron rearrangements. Since the strength of the surface interactions with the second layer is proportional to the charge on platinum F, it is reasonable to assume that such interactions still exist on an extended metal surface but are reduced in magnitude. The platinum surface will still appear as a strong electron acceptor to first layer of water molecules. Hydrogen bonding to second layer molecules will therefore be strongly asymmetric depending upon whether the second layer molecule acts as electron donor or electron acceptor. It is reasonable to assume that the co-operative forces described here could be found on an extended surface, but would be reduced in size. The results for $Pt-(H_2O)_2$ provide clear evidence for the dependency of the cooperative forces on the electronic state of the platinum atoms. The electron configuration of the ground state is also strongly dependent upon cluster size. Extended Hückel calculations on platinum clusters have shown [285] that, with increasing cluster size, the 6s population on surface atoms converges to a population 0.1 - 0.2 lower than those in the layers below. Our results suggest that a 6s population of 0.8 would be appropriate for surface atoms. These results support our assumption that cooperativity on an extended surface will be reduced but will not fall to zero, as cooperativity is still observed in the $Pt-(H_2O)_2$ cluster with a ^{3}D platinum atom (with 6s population equal to 1).

8.1.4 Conclusions

The most recent TDS spectrum [56] of water on the Pt(111) surface shows three prominent peaks at 155 K, 165 K and 200 K. The first peak is the multilayer peak and commonly assigned to ice sublimation [38, 48] (40 kJ/mol) which is close to the sublimation energy of pure ice [48] (50 kJ/mol). Additional infrared reflection absorption energy spectroscopy (IRAS) data by OGASAWARA [56] showed that the third peak should be assigned to water directly attached to the surface and the second to indirectly bound water, forming the second layer of the bilayer. We used the Redhead equation [356, 357] and an ice sublimation energy of 44.4 kJ/mol, assuming zero-order desorption kinetics [48] and a pre-exponential factor [358] of 10^{15} s^{-1}, to estimate the binding energy of the other two water species from the TDS spectrum [56]. These calculations suggest that the binding energy of water directly bound to the surface is 58 kJ/mol. The binding energy of water in the second adsorption layer was calculated to be 47 kcal/mol. A suitable representation of the second layer in our model should therefore yield binding energies higher than the ice sublimation energy and lower then the direct interaction energy.

To estimate the ice sublimation energy within the model, we calculated the energy of formation of a linear water trimer constructed from ideal water dimers, since the ice sublimation energy is close to that of two hydrogen bonds [38, 359]. The energy of formation of the trimer from three water molecules was calculated as 59.4 kJ/mol and the binding energy of the central water molecule as 56.4 kJ/mol. For consistency, a successful candidate for the second layer structure should therefore yield a binding energy higher than 56 kJ/mol. An upper limit was found with a test calculation for Pt_3-H_2O in which the water molecule was attached to platinum A. The binding energy of this water molecule was found to be high, at 116.9 kJ/mol, caused by a low occupancy of the platinum 6s orbitals. A more reliable result would appear to be a binding energy of 63.4 kJ/mol for a single water molecule for Pt_9-H_2O, representing water on the Pt(100) surface.

Cluster II is not a suitable candidate, although its geometry agrees with the BFP rules, since its binding energy is only 31.1 kJ/mol. The BFP rules require a flop down structure for a water molecule at the edge of a finite bilayer structure. The binding energy of cluster III (75.5 kJ/mol) is sufficiently high for the cluster to constitute a possible model for the second layer, but the cluster violates the BFP rules since it is only bound to the surface via a single hydrogen bond. The interaction between the positive charge on the hydrogen and the electron concentration at a metal surface is not included in the BFP rule set. A flop down geometry with a double electron receiving water molecule has not proved to be a useful model for second layer water molecules, since the binding energy of the central water molecule was found to be smaller than 56 kJ/mol. On the other hand, the binding energy of the central water molecule in cluster VII ("flip up") is sufficiently high to be suitable as a candidate. During geometry optimisation, the binding energy of the central water molecule increases and the geometry changes from flip up to flop down. A flop down water molecule in a small water cluster would therefore have a geometry similar to that shown in Figure 8.9 rather than the BFP consistent geometry shown in Figure 8.7.

		cluster I	cluster II	cluster III	cluster IV	cluster V	cluster VI	cluster VII	cluster VIII
E_{CENT}	[kJ/mol]	47.35	31.06	75.57	51.01	41.2	−5.3	59.9	98.1
$d(Pt_AO_B)$	[Å]	2.0941	2.0878	2.0878	2.0878	2.0857	2.1	2.0712	2.0789
$d(Pt_FO_C)$	[Å]		3.3391	3.2034		3.4707	2.75	4.3718	3.0576
d_{OO}	[Å]	2.9146	3.0395	2.9862	2.9862	3.0971	2.8452	3.06457	2.9378
$d(O_BH_C)$	[Å]	1.9603	2.1026	2.5180	2.5180	2.2634	1.8957		
$d(H_BO_C)$	[Å]	1.9589	2.0851	2.0293	2.0293			2.1119	1.9810
$d(Pt_AH_C)$	[Å]	3.3197	3.6059	3.3969	2.3969	3.5797	3.0827	4.5795	3.6161
$d(Pt_FH_C)$	[Å]		3.2347	2.3063		2.9849	2.6206	3.2760	2.1568
$MOP(O_BH_C)$		0.005385	0.005865	−0.007866	−0.003105	−0.002850	−0.019404		
$MOP(Pt_AH_C)$		−0.003787	−0.000301	0.000497	0.004084	−0.000174	−0.004990	−0.000174	0.002733
$MOP(Pt_FH_C)$			−0.003053	0.051214		0.009069	−0.003356	0.011241	0.082056
$MOP(O_CH_D)$		0.032723	0.026679	0.044396	0.039424			0.018511	0.034919
$MOP(Pt_AO_B)$		0.033481	0.024016	0.050707	0.054635	0.045175	0.035941	0.045138	0.054989
$MOP(Pt_EO_D)$		0.059895	0.058430	0.064688	0.060741	0.045175	0.035941	0.045138	0.054989
$MOP(Pt_APt_F)$			0.118540	0.097850		0.103790	0.104580	0.107483	0.090507
$MOP(Pt_EPt_F)$			0.113012	0.099208		0.103790	0.104580	0.107483	0.069838
MOP(HBOND)		0.038108	0.032544	0.03653	0.036319	−0.000227	−0.038808	0.037022	0.069838

Table 8.3: Selected Values for larger platinum-water clusters

The binding of water to a metal surface via its hydrogen atoms has previously been observed for Pt(100) [44] and the observation of free hydroxyl groups suggests cleavage of the water molecule. IBACH and LEHWALD [44] propose the presence of water molecules as part of a larger water cluster, which binds directly to the surface via a single hydrogen atom. The observed rearrangements of water clusters during geometry optimisation leads to the same conclusion. The charge transfer from the platinum to the water molecule as observed for cluster VIII provides a possible explanation for a dissociation pathway similar to that for the dissociation of water on Pt(111) surfaces previously covered with potassium [63, 68, 73].

The binding energies of the bridging water molecules are higher than the binding energy of a single water molecule (63.4 kJ/mol) with the notable exception of the flip up geometry. The increase in binding energy is caused by a strong interaction of the second layer water molecule with the platinum surface below. The charge concentration on the central platinum atom F is likely to be a consequence of the limited cluster size. We are now calculating with larger clusters similar to that shown in figure 8.1. The binding energy ($E_{\text{CENT}} = 61.9$ kJ/mol) of the second layer water molecule in such a $Pt_4-(H_2O)_4$ cluster is higher than the ice sublimation energy but smaller than the binding energy of an isolated water molecule. This central water molecule is triply hydrogen bonded to the first adsorbate layer, but the binding energy of the central water molecule is lower than that expected for three individual hydrogen bonds (about 75 kJ/mol) due to the repulsive platinum-water interaction. To study the influence of platinum F on the binding energy of the central water molecule, the calculation was repeated in the absence of the central platinum F, when a binding energy of 83.2 kJ/mol was found, demonstrating once again the repulsive influence of the central platinum atom and the importance of cooperativity for the water bilayer structure. This interaction between the platinum surface and second layer water molecules might stabilize distorted water cluster as suggested by WAGNER and MOYLAN [43].

Our results suggest that the formation of the water bilayer structure on the Pt(111) surface is not determined solely by direct bonds. Polarisation effects and the interaction of the hydrogen atoms in water with the platinum surface contribute significantly to the binding energy of water molecules in the second adsorbate layer. Those additional forces allow the formation of small water clusters on the platinum surface, whose structures violate the BFP rule set. The strength of these cooperative forces depends on the size and the electronic structure of the platinum cluster. Preliminary results on larger platinum clusters indicate that the interaction between platinum and water in the second layer remains important.

Acknowlegements

T.L. would like to thank the "Studienstiftung des Deutschen Volkes"and the "Hansischen Universittsstiftung"for their financial support. He would also like to thank W. Hoffman for his help with the calculation [356] of the bonding energies from the TDS spectrum by published Ogasawara [56].

8.2 $(H_2O)_6$ on a Virtual Metal Surface: Testing the Ice Rules

Abstract

The water hexamer has been studied with a classical water-water interaction potential and quantum chemically at both RHF and MP2 levels. The influence of a virtual metal surface on $(H_2O)_6$ has been modeled through geometry constaints on the cluster. Additional data on $(H_2O)_2$ and $(H_2O)_3$ are presented to assist the interpretation of the results obtained for the hexamer.

These calculations suggest that water molecules in the first layer with their hydrogens pointing away from the surface ('flip up') only occur for a small range of values of surface lattice constant. In all other cases the dipole moment of the water molecules is found to lie nearly parallel to the metal surface.

8.2.1 Introduction

The problem of the orientation of hydrogen atoms in the first layer of water molecules arose during our studies of the water-platinum-vacuum system. Experiment suggests that the hydrogen atoms in the first layer of water on the metal point either slightly upwards as expected for water bonded to metal via the oxygen lone pair [38] or lie parallel to the metal surface [58, 360]. Theoretical calculations on the other hand, cannot unambiguously determine the orientation of the hydrogen atoms, since the orientation of the water molecule depends strongly on cluster size and the chosen method of calculation.

Since we are interested in the platinum-water-vacuum system the following discussion concentrates on the water-platinum interaction. An extensive review of water-metal interactions has been given by Thiel and Madey [38].

Early work [36, 37] on the adsorption of water on Pt(111) reported a $(\sqrt{3} \times \sqrt{3})$ R30° surface structure of adsorbed water molecules and suggested the formation of ice ordered in domains of 30 − 40 Å in length.

A water bilayer structure [38, 39] has been proposed as the basis of the growth of ice on hexagonal metal latices. The structure of this water bilayer is generally explained in terms of an extension to surfaces [39] of the Bernal-Fowler-Pauling rules (ice rules) [9, 13]. Specifically [39], each water molecule is bound by at least two bonds (which may be hydrogen bonds to other water molecules or oxygen lone pair bonds to the surface) while maintaining a tetrahedral configuration. Each water molecule in the lower layer is bound to the surface via a lone pair orbital on the oxygen and all free lone pair orbitals on oxygen remain nearly perpendicular to the surface. In an ideal infinite bilayer, all water molecules have their dipole moments pointing away from the surface ("flip up"), whereas in a finite cluster, water molecules whose dipole moments point toward the surface ("flip down") may occur at the edge of the cluster [39, 41, 42]. Doering and Madey [39], using the surface extended ice rule set, concluded that the smallest stable water cluster on a hexagonal metal surface should be the water nonamer. Such an $(H_2O)_9$ cluster has been observed on Ru(0001) within an $(6\sqrt{3} \times 6\sqrt{3})$ R0° superstructure [39, 47], whereas experimental results suggest, that the smallest cluster possible on platinum(111) is a three-dimensional water trimer [45].

The metal-water interface has been examined previously by quantum chemical calculations [54, 60–72] and work on the platinum-water interface [54, 63–65, 68] suggests that the molecular plane of the water lies parallel to the surface [54, 63, 68]. These results agree with workfunction measurements [45, 52, 58, 73] on water-covered platinum surfaces, which show that a contribution of about 0.2 D of the water dipole moment (single molecule 1.84 D) lies normal to surface [58]. Theory and experiment agree that the water molecule is only slightly distorted upon adsorption on Pt(111) [41, 45, 46, 48, 58, 73–75] and dissociation has so far only been observed experimentally on pre-covered surfaces [76–79].

The ice rules [9, 13] have been postulated for the structure of ice and the surface extension [39] assumes a seamless transition between water directly attached to the surface and crystalline ice. Experiment and theory suggest, on the other hand, that the surface of an ice crystal has a different structure than that of the bulk. Snowflakes have have been reported to be covered by a Quasi Liquid Layer (QLL), with a higher density than ice [361, 362]. Molecular dynamics simulation [363] of an ice crystal suggests the existence of molten ice on the crystall surface below the freezing point of water and scanning tunneling microscopy (STM) [54] provides evidence for three solid and one liquid ice phase on platinum(111). MORGENSTERN et al. concluded from their STM experiments, that the fourth, liquid 2-D water phase on Pt(111) has a higher density than the solid 2D ice phases as observed in three dimensional water and ice. DOSCH et al. [361] suggest that the formation of a quasi liquid layer can be induced by a surface-induced distortion of the hydrogen bonding network and LEED experiments of ultrathin water films on Pt(111) suggest a disordered ice layer [360].

The link between water adsorption on metal surfaces at low coverages and extended ice layers is formed via water clusters on a metal surface and in vacuum. The water dimer is the most widely analysed water cluster, not only the first water cluster to be treated by *ab initio* calculations [104] but is also commonly used as benchmark test for new calculations, and includes nearly every possible level of theory [105–131]. The global minimum corresponds to a linear geometry with C_S symmetry in which the nonbonding hydrogen atoms lie on opposite sites of the oxygen-oxygen bond. The optimized oxygen-oxygen distance is around 2.97 Å and the binding energy is around 4.8 kcal/mol (A review of the water dimer is provided in [125]).

SCHÜTZ et al. suggested a scheme for referring to the non-bonding hydrogen atoms in the cyclic water trimer, which fully describes the geometry of the cluster [132]: The nonbonding hydrogen can be either above (up, "u"), parallel to (planar, "p") or under (down, "d") the plane of oxygen atoms, while the bonding hydrogens lie in the plane of the oxygen atoms. When this plane bisects a water molecule, the geometry is marked with a "b". The global minimum of the potential energy surface of the water trimer corresponds to a ring structure. Early calculations suggested that the {uuu} water trimer is less stable and the {ppp} trimer is more stable than the ideal linear structure [133]. The linear trimer transforms smoothly into a {uud} ring structure, which defines the global minimum [128, 131, 132, 139–150]. The geometry of the water trimer is flexible and tunneling facilitates rapid changes among the 96 isoenergetic isomers ($2^n \times n! \times 2$, where n is the number of water molecules in the cluster) [103, 150–154, 156].

The potential energy surface of the water trimer [142, 145] is found to display 18 stationary points. The {ppp} trimer has a slightly smaller binding energy than the {uud} trimer ($\Delta^{\{ppp\}}_{\{uud\}}E_{TRIM} < 0.5$ kcal/mol) [132] and is a stationary point with a Hessian index of 3. Most calculations refer to the {uud} trimer and only a few treat the {ppp} trimer [132, 140, 142, 144, 157–159], despite the fact that {ppp} and {udp} trimers form possible intermediates in the rearrangement of the hydrogens [132].

The computational analysis of water clusters has gained interest recently, because such microcrystals can be used to investigate phase transitions [160]. However, the transition from small to large water clusters is not straightforward and the water hexamer separates two types of clusters.

The structure of water clusters is characterised by the number of hydrogen bondsbeing a maximum and repulsive interactions between nonbonding hydrogens and geometrical strains within the water rings being simultaneously a minimum. Small water clusters ($(H_2O)_n$ with $n \leqq 5$) are therefore commonly assumed to be cyclic and planar [103, 128, 133, 161–167], while larger clusters with $n \geqq 7$ have three-dimensional structures [160, 171–178]. The water hexamer delineates these regimes and is the smallest water cluster with a three-dimensional equilibrium structure. Several stable geometries with similar energies ($\Delta_{HEX}E < 1$ kcal/mol) have been found for the water hexamer [128, 148, 149, 179–182]. The multitude of energetically similar isomers makes the water hexamer a new benchmark system for those methods to be applied to larger clusters.

Although the cyclic water hexamer forms the basis of the ice structure [183] and has been observed as a structural element in liquid water [185], the most stable water hexamer in the gas phase has a cage structure [186, 187]. The energy difference between the cyclic hexamer and the cage hexamer is small and the free hexamer has been observed experimentally only recently [187].

Quantum calculations [128, 148, 149, 179–182, 188] on the cyclic water hexamer are in reasonable agreement regarding geometry, but disagree on energy. The most stable ring has a "chair"conformation (S_6 symmetry) with linear hydrogen bonds and an oxygen-oxygen distance between nearest neighbours which varies between 2.708 Å and 2.855 Å. The geometrical features of the cluster can be reproduced by simple treatments, whereas reliable energy calculations require more sophisticated treatments. With one exception (66.66 kcal/mol [181]) published values for the binding energy of the cyclic water hexamer vary between 37.99 kcal/mol and 56.00 kcal/mol depending on the level of computation [128, 148, 149, 179, 180, 182, 188].

Structural elements of the water dimer and trimer can be observed within the water hexamer. Since a description of the water hexamer is difficult without referring to these structures, we summarize here our results for $(H_2O)_2$ (section 8.2.3) and $(H_2O)_3$ (section 8.2.4). Section 8.2.5, which concentrates on the water hexamer, has been subdivided into five subsection: Subsection 8.2.5.1 describes the geometry of the water hexamer and gives additional information about the model used for our calculations, complementing section 8.2.2 which summarizes the computational methods applied in general to all water clusters. Subsection 8.2.5.2 describes the free hexamer and subsection 8.2.5.3 considers geometrical constraints imposed on the water hexamer to simulate a virtual metal surface. This procedure allows us to analyze the metal-water interface independently of the nature of the metal. In subsection 8.2.5.4 the surface constant of the virtual surface is varied systematically, allowing us to correlate the orientaion of the hydrogen atoms close to the surface with the geometry of the interface. Subsection 8.2.6 considers the water hexamer as part an ice bilayer and relates our results to experiment. Section 8.2.7 provides an summary.

8.2.2 Computational Procedure

The classical analysis of water clusters is based on a water-water interaction potential similar to that of Kistenmacher and Popkie [119, 120]. The water molecule has a rigid geometry based on experimental data, with an OH bond length of 0.9572 Å and an HOH bond angle of 104.52°, while the centre of negative charge M (-1.40 e) lies 0.24 Å along the symetry axis towards the hydrogens [16].

In addition to the Coulomb forces the repulsive forces between the atoms are taken into account. Equation 8.1 summarizes (in atomic units) the potentials beween the different centres on the water

parameter	value
r_{OH} (Å)	0.9572
$\angle_{HOH}$ (deg)	104.52
r_{OM} (Å)	0.2382
q (e)	−1.398323
a_1 (kcal/mol)	653.7789
a_2 (kcal/mol)	3457.857
b_1 (Å^{-1})	3.189600
b_2 (Å^{-1})	3.545410
f (kcal Å mol^{-1} e^{-2})	332.17752

Table 8.4: Water-Water interaction parameters.

molecules, where M denotes to the centre of negative charge. The positive charges are located at the positions of the hydrogen atoms.

$$V_{HH} = \frac{f\,q^2}{4\,r} + a_1\,e^{-b_1 r} \quad V_{OH} = a_2\,e^{-b_2 r} \quad V_{HM} = \frac{-f\,q^2}{2\,r} \quad V_{MM} = \frac{f\,q^2}{r} \tag{8.1}$$

The original parameters of Kistenmacher and Popkie were optimized to reproduce the results of a set of quantum chemical calculations (GAMESS UK, DZP basis set [355], MP3, full BSSE counterpoise correction of Boys and Bernadi [204]) for 120 dimers and 4 trimers. During parameter optimisation a higher weight was placed on the trimers so as to partially include cooperative effects into the new force field. These new parameters (Table 8.4) are used entirely in this work[2].

The quantum chemical calculations were performed with the same fixed geometry as the classical calculations. For this set of calculations we used Gaussian 94 with the DZP basis set[3] at HF and MP2 levels, without BSSE correction.

8.2.3 Water Dimer

Figure 8.10 displays the most stable water dimer and Table 8.5 lists its geometrical parameters calculated at various levels of theory. With the introduction of electron correlation the oxygen-oxygen distance decreases ($\Delta_{\mathrm{HF}}^{\mathrm{MP2}}\mathrm{r}_{\mathrm{OO}} = -0.0805$ Å) and the hydrogen bond becomes stronger ($\Delta_{\mathrm{HF}}^{\mathrm{MP2}}\mathrm{E}_{\mathrm{DIM}} = -1.151$ kcal/mol). As the level of correlation increases from MP2 to MP3 the length of the hydrogen bond increases ($\Delta_{\mathrm{MP2}}^{\mathrm{MP3}}\mathrm{r}_{\mathrm{OO}} = +0.0238$ Å) and the binding energy is reduced ($\Delta_{\mathrm{MP2}}^{\mathrm{MP3}}\mathrm{E}_{\mathrm{DIM}} = +0.333$ kcal/mol). The MP2 approach appears to overestimate electron correlation whereas MP3 appears to compensate this effect [125]. The final correction was a full BSSE correction to the binding energy and the geometry. The BSSE in the geometry was eliminated manually. A fine mesh

---

[2] During the optimisation of the force field parameters, the contribution of the oxygen-oxygen repulsion to the binding energy of the clusters close to equilibrium geometries was found to be neglible, while a strong oxygen-hydrogen repulsion was necessary to avoid physically unrealistic structures. Therefore, our classical potential does not contain an oxygen-oxygen repulsion term. Currently we are considering the importance of the oxygen-oxygen repulsion for water cluster geometries far from equilibrium.

[3] GAMES UK uses six cartesian d-functions whereas Gaussian 94 uses the five d-functions (l=2). The difference between these basis sets was found to be neglible.

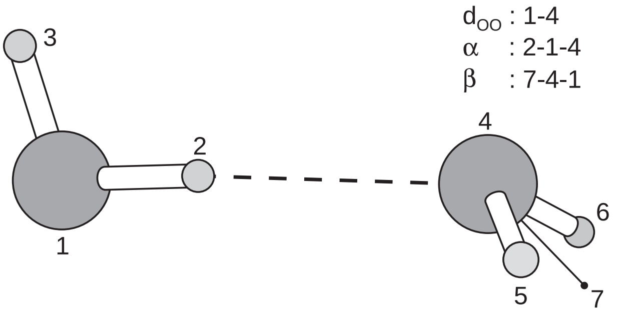

Figure 8.10: Water dimer.

	r_{OO} [Å]	α [deg]	β [deg]	$-E_{DIM}$ [kcal/mol]
Pot	2.9834	8.55	123.40	4.903
MP3[B]	2.9926	2.44	135.47	4.914
MP3	2.9354	3.28	125.43	5.949
MP2	2.9116	3.79	124.06	6.282
RHF	2.9921	1.99	132.03	5.131
experiment[*]	2.98 ± 0.04	0 ± 10	120 ± 10	5.4 ± 0.7

[B] BSSE corrected [*]references [118, 239, 364]

Table 8.5: Calculated properties of the water dimer.

of points was calculated with a BSSE corrected energy around the MP3 optimal geometry and the minimum of this energy surface was computed numerically. The BSSE correction produces an extended oxygen-oxygen distance ($\Delta^{\mathrm{BSSE}}_{\mathrm{MP3}} \mathrm{r}_{\mathrm{OO}} = +0.0572$ Å) and reduces the binding energy ($\Delta^{\mathrm{BSSE}}_{\mathrm{MP3}} \mathrm{E}_{\mathrm{DIM}} = +1.035$ kcal/mol). Due to the BSSE correction the oxygen-oxygen distance is now longer than that for the HF case and the binding energy is even lower. A value of -5 kcal/mol for $\mathrm{E}_{\mathrm{DIM}}$ appears reasonable, since our calculations with other basis sets and a full BSSE correction also yielded binding energies of about -5 kcal/mol at all levels of theory. Also, large scale calculations on the water dimer by KLOPPER et al. reported BSSE-corrected interaction energies below -5 kcal/mol [144].

The BSSE-corrected values agree well with experiment and previous quantum chemical calculations ($\mathrm{r}_{\mathrm{OO}} = 2.73$ Å - 3.04 Å, $\alpha = -7.2°$- 5.1°, $\beta = 150°$- 120°, $-\mathrm{E}_{\mathrm{DIM}} = 3.6$ kcal/mol - 7.2 kcal/mol, $-\mathrm{E}_{\mathrm{DIM}} = 3.7$ kcal/mol - 5.0 kcal/mol BSSE corrected) [105–108, 110, 112–115, 118–125, 127, 128, 130, 131]. The BSSE-corrected MP3 data were used to create a classical water-water interaction potential dedicated to the analysis of small water clusters at equilibrium geometry, since calculations with previously published classical interaction potentials yielded similar geometries but high binding energies (5.7 kcal/mol to 7.2 kcal/mol) [109, 116, 117, 126]. The dimer calculated with our classical potential reproduces the quantum chemical values (MP3, BSSE corrected) reasonably well: r_{OO} is shorter than in the quantum chemical case ($\Delta^{\mathrm{Pot}}_{\mathrm{MP3}} \mathrm{r}_{\mathrm{OO}} = -0.0092$ Å) whereas the binding energy is well reproduced ($\Delta^{\mathrm{Pot}}_{\mathrm{MP3}} \mathrm{E}_{\mathrm{DIM}} = -0.011$ kcal/mol). Only the bending angle of the new hydrogen bond ($\alpha = 8.55°$) is larger than the calculated quantum chemical value, following the inclusion of the trimers into the optimisation of the force field paramters, but is still in reasonable agreement with experiment.

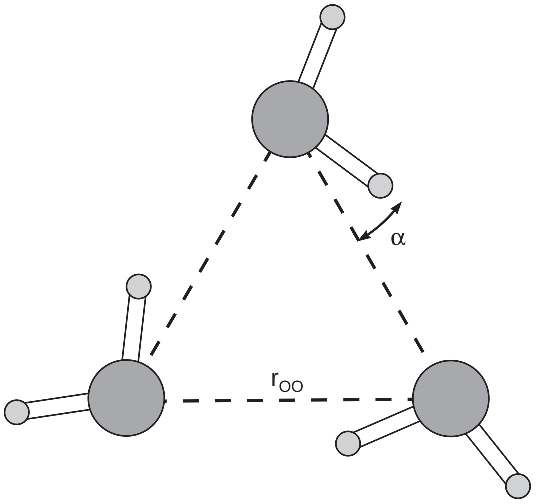

Figure 8.11: C_{3h} Water trimer.

8.2.4 Water Trimer

Figure 8.11 shows the planar water trimer with C_{3h} symmetry and Table 8.6 displays the geometrical parameters calculated at variouslevels of theory. A BSSE correction to the geometry of the trimer at MP3 level was not carried out due to to the computational effort required.

The predicted oxygen-oxygen distance r_{OO} is shorter than that in the dimer at all levels of theory. Even the calculation with the classical potential shows a shortening of the bond by 2.4%, which is close to that found at Hartree Fock level (2.9%). A similar effect has been observed in other trimers with varous geometries.

An analysis of the results shows that the shortening of the bonds is due to strong cooperative effects in the water cluster. In the planar {ppp} trimer these interactions account for 21% of the total (BSSE corrected) energy. The classical potential does not contain terms which take cooperative effects directly into account, but the bonds are still shorter than in the free dimer. This reduction is caused through interaction with the second nearest neighbour in the cluster. These energies are generally more binding than in the quantum chemical calculations. Repulsive interactions with the second nearest neighbour were reduced by 78% in the classical calculation, while attractive interactions were increased by 26%. Interactions between nearest neighbours are similar in both the quantum and classical calculations. For a fixed hydrogen bond geometry these energies differ by about 0.9%. The second nearest neighbour interactions in the classical model tend to reproduce attractive many body forces reasonably well, but give poorer results for repulsive forces.

The angle α of the hydrogen bond was found to be similar at all levels of theory (about 23°), suggesting that stable water clusters are possible with severely distorted hydrogen bonds. A positive value for the coupling constant between r_{OO} and α (classical potential: $\left(\frac{\partial^2 E_{TRIM}}{\partial \alpha \; \partial d_{OO}}\right) = 0.44\,\mathrm{kcal\,mol^{-1}\,deg^{-1}\,\AA^{-1}}$) indicates that as r_{OO} increases, α tends to zero and the bonding hydrogen atom lies on the line joining the two oxygen atoms.

The classical energy of formation for the trimer (E_{TRIM}) appears to be rather small compared with the MP3 result, but the BSSE correction to the MP3 energy (−13.789 kcal/mol) shows that the classical calculation matches the binding energy for the planar water trimer reasonably well.

	r_{OO} [Å]	α [deg]	$-E_{TRIM}$ [kcal/mol]
Pot	2.9135	24.18	13.685
MP3	2.8014	23.54	16.213^{B}
MP2	2.7782	23.55	17.020
RHF	2.8830	23.27	13.916

^{B} BSSE corrected 13.789 kcal/mol

Table 8.6: Calculated properties of the planar {ppp} water trimer.

The value of E_{TRIM} (−13.685 kcal/mol) for the {ppp} trimer is close to that found for the global minimum (−14.035 kcal/mol) using the classical potential. The global minimum has C_1 symmetry and a {uud} geometry. The two hydrogen atoms which point upwards move out of plane (dihedral angle HOOH = 23°), reducing their repulsion.

Our quantum results for the {ppp} water trimer are in reasonable agreement with previously published values (r_{OO} = 2.80 Å to 2.88 Å, α = 20° to 25°, $-E_{TRIM}$ = 13.0 kcal/mol and 16.7 kcal/mol) [132, 140, 142, 144, 157–159, references 157–159 being optimized with a fixed value for r_{OO}]. XANTHEAS [147] and VAN DUIJNEVELDT [140] reported three-body terms of about 2.3 kcal/mol and 2.0 kcal/mol for the global minimum structure (C_1 symetry) of the water trimer, while DEL BENE [108] found a value of 2.94 kcal/mol for the planar trimer, which is in better agreement with our findings (2.87 kcal/mol).

Cooperative effects are important for the structure of the water trimer at the quantum level. The analysis of our classical calculations showed that the reduction in repulsive forces between non-bonding hydrogen atoms and the interaction between second nearest neighbours are critical to the geometry of the trimer when calculated with a classical potential.

8.2.5 Water Hexamer

8.2.5.1 The Model

The structure of the metal-water interface is dominated both by the interaction between the surface atoms and the water molecules in the first layer and by the interactions among the water molecules within the ice cluster. To distinguish between these two effects, the surface was replaced by a mesh of auxiliary geometrical points, and the water cluster was maintained close to the ideal bilayer geometry proposed by DOERING and MADEY [39]. In effect, we asume a Lewis acid-base bond between the oxygen lone pair and the surface atom as starting point for the geometry optimisation. No other electronic effects of the surface are taken into account by the model. Use of the water hexamer as a model for the bilayer structure allows us to study the influence of geometrical constraints on the bilayer structure as water adsorbs on to the surface independently of the nature of the surface.

Figure 8.12a shows the water hexamer bound to a virtual metal surface together with its geometrical parameters. A hexagonal mesh of seven auxiliary geometrical points (d1 is the unit length of the mesh.) was placed below the cluster to model the metal surface. The water hexamer is assumed to have the same structure as a six-membered water ring in the ideal, infinite bilayer structure. Each water molecule rests on top of a virtual metal atom / auxiliary point. The water

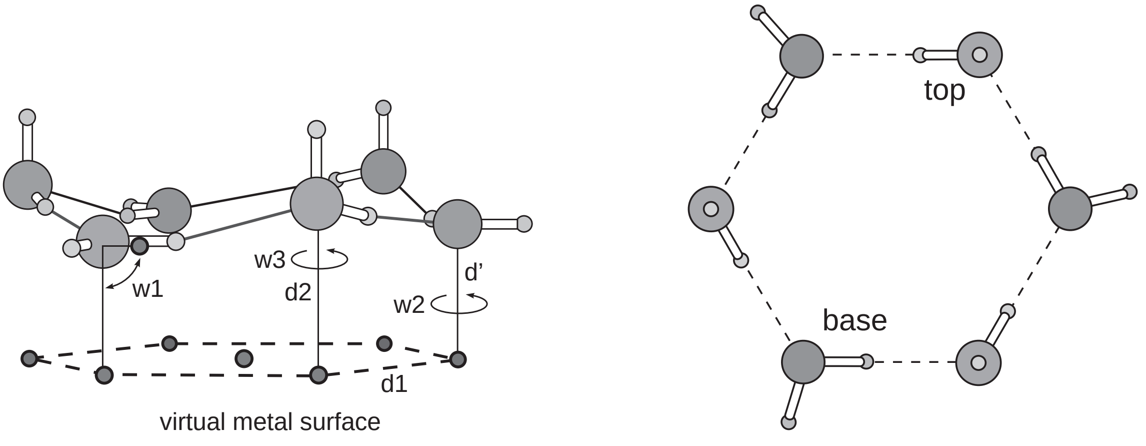

(a) Sideview (b) Topview

Figure 8.12: Water Hexamer on the virtual Surface (d1 = 2.8Å).

molecules in the first layer (base plane) lie at fixed distance (d′ = 1 Å) from the virtual surface while the distance d2 between the virtual surface and a second layer water molecule (top plane) is allowed to vary during the calculations. The difference, h = d2 - d′, is a measure of the height of the oxygen ring.

Both hydrogen atoms of a water molecule in the base plane lie the same distance from the surface, one hydrogen being used to form the hydrogen bond to the top plane. The angle w1 between the bond to the virtual surface and the molecular plane of the water molecule is allowed to vary during geometry optimisation so as to compensate for different heights (d2) of the ring or to break the metal-oxygen bond via the lone electron pair if necessary.

The water molecules in the base plane are also allowed to rotate around their bond to the virtual metal surface (w2). This rotation is required to describe the interaction between second nearest neighbours, since it allows the water molecules to form new hydrogen bonds.

One hydrogen-oxygen bond in the top plane water of molecules is initially chosen perpendicular to the virtual metal surface (see Section 8.2.5.3) while the second is used for the hydrogen bond to the base plane. This arrangement, following from the surface ice rules, simulates the interaction to the next water layer in an extended ice cluster. A water molecule in the top layer is allowed to rotate around the bond to the virtual surface (w3) and has two degress of freedom, as does a water molecule in the base plane. The angles w1 to w3 are defined with respect to the symmetry axis of the water molecule and an auxilary point, which lies between the hydrogen atoms (Figure 8.12a).

Figure 8.12b shows a topview of the water hexamer. The oxygen-oxygen bonds lie on top of the metal-metal bonds. This hexagon (dotted line in figure 8.12b) designates the ideal orientation of a hydrogen bond. As the angles w2 and w3 are allowed to vary during geometry optimization the bonding hydrogen atom can deviate from this ideal direction. For values of w2 > $-52°$ or w3 > $-60°$ the bonding hydrogen atoms lie within the hexagon. Rotations around the surface-oxygen bond, which result in one of these values, are described as 'inwards'.

Since the hexagonal symmetry of the surface is not allowed to change during the calculations, each surface is defined by the lattice unit d1. The geometrical constraints caused by different metal

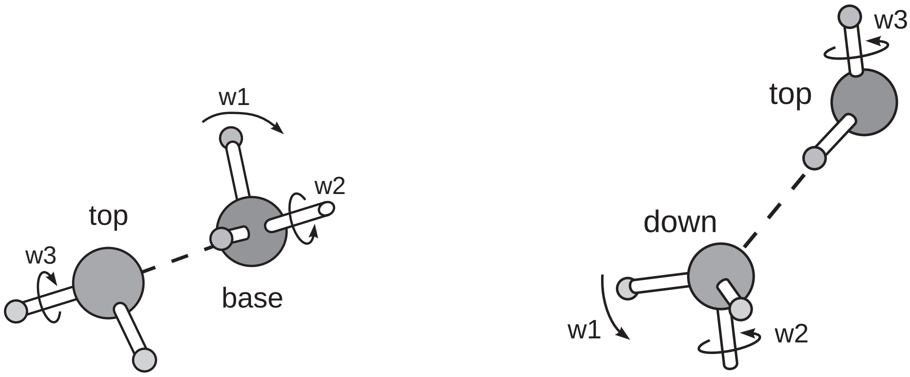

(a) base→top water dimer

(b) top→base water dimer

Figure 8.13: Water dimers in the surface-constrained hexamer. The arrows indicate the direction of motion as w1 decreases, w2 increases and w3 increases.

surfaces are simulated by variation of d1.

8.2.5.2 The free water hexamer

Geometry optimization of the free water hexamer, shown in figure 8.14, yields a structure comprising six nearly ideal hydrogen bonds ($E_{\mathrm{DIM}} = -4.774$ kcal/mol): the oxygen-oxygen distance (2.9539 Å) is smaller than in the dimer (2.9834 Å) but larger than in the trimer (2.9135 Å); the hydrogen atoms are located on the oxygen-oxygen line ($\alpha = 0.57°$); the angle β of 148.89° between the molecular plane of the hydrogen acceptor and the oxygen-oxygen bond is larger than in the dimer (figure 8.10, table 8.5) and the bond itself is slightly twisted, with $\gamma = 11.42°$ (ideal value $\gamma = 0°$).

The strong bonds between nearest neighbours ($\sum E^{\mathrm{1st}}_{\mathrm{DIM}} = -28.644$ kcal/mol) account for 81% of the total energy (-35.397 kcal/mol) and the interactions between second nearest neighbours account for an additional 14%. Both the geometry and the energy of formation appear to be determined by these forces.

The quantum chemical geometry optimization of the free water hexamer resulted in a similar structure: The hydrogen bonds were also linear ($\alpha = 0.57°$) but, as expected, shorter (2.73 Å), in agreement with that reported by Tsai and Jordan (2.725 Å) [182] and Xantheas (2.714 Å) [149]. The binding energy of -53.88 kcal/mol reproduces that found by Mhin et al. -53.94 kcal/mol (MP2/DZP HF optimized geometry) [180] and is close to that of Kim et al. (-56.00 kcal/mol (MP2/DZP)) [179].

This agreement shows that the results obtained with the clasical potential for the water hexamer are reasonable, although producing systematically an extended oxygen-oxygen separation.

8.2.5.3 The constrained hexamer

In calculations of the water hexamer on a virtual surface (Pt(111), d1 = 2.77Å), the hydrogen bonds of the hexamer lie directly above the metal-metal bonds of the virtual surface. Figure 8.12 shows the result of the geometry optimisation. The binding energy of the hexamer decreased

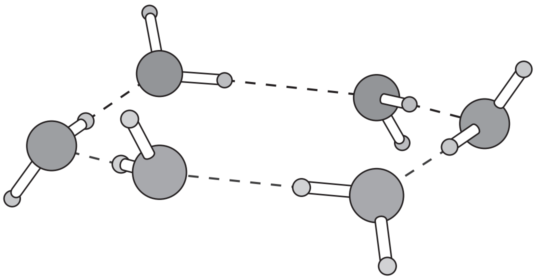

Figure 8.14: Free water hexamer.

by 2.754 kcal/mol. The interactions between nearest and second nearest neighbours account for 95.2% of the total energy (−32.643 kcal/mol). The analysis of the binding energy with the classical potential showed that the energies of the direct hydrogen bonds (top→base and base→top, figure 8.13) differ by 0.337 kcal/mol and are generally weaker ($\overline{\Delta^{\mathrm{free}}_{\mathrm{surf.}} \mathrm{E}^{\mathrm{1st}}_{\mathrm{DIM}}} = 0.464$ kcal/mol) as the symmetry changes from S_6 to C_3. The weakening of these direct hydrogen bonds can be accounted for by an increase in repulsion between the hydrogen atoms. This increase is partially compensated by an increase in interaction between second nearest neighbours of 2%, accounting for the relief of stress necessary to compensate for mechanical distorsions induced by the surface.

The water hexamer under surface conditions was nearly planar ($h = 0.7377$ Å); the base hydrogen atoms were slightly tilted towards the surface ($w1 = 89.17°$) while the oxygen-oxygen distance was reduced (2.8665 Å) from that observed in the free hexamer. To check whether this result was an artefact of the chosen input geometry the calculations were repeated with fewer geometrical constraints.

Geometrical constraints for the water cluster were lifted except that the hydrogen atoms of the base water molecule remained at the same height from the surface and the oxygen atoms were placed at the corners of the virtual metal hexagon ($d1 = 2.77$ Å). Geometry optimization then lowered the total energy by about 0.362 kcal/mol, but the water cluster retained its basic shape. The base hydrogens moved slightly upwards ($\Delta w1 = 4.32°$) as the ring became higher ($\Delta h = 0.078$ Å). The non-bonding hydrogen atoms of the top water molecules moved slightly away from the vertical axis (7.03° measured between the vertical and the OH bond of the top hydrogen), still allowing for the formation of an ice cluster, while both types of bonding hydrogen atoms (base→top and top→base hydrogen bonds) moved out of the metal hexagon ($w2 = -52.3°$, $w3 = -65.17°$).

The movement of the non-bonding hydrogens in the top layer is in agreement with the surface ice rules, which require these hydrogens to lie nearly perpendicular to the metal surface. The non-bonding top hydrogens point slightly into the hexagon and form the basis for the epitaxial growth of further ice layers. With each additional water layer the ring contracts until finally the bulk value for ice Ih is reached ($d1 = 2.6$ Å). This would imply that, with increasing water coverage, a single water molecule should become more strongly bound to the water cluster already on the surface. OGASAWARA et al. [56] observed a high-temperature shift of the ice peak on Pt(111) with increasing water coverage in their TDS (Temperature Controlled Desorption Spectroscopy) experiment. They suggested this shift to be due to zero-order desorption kinetics and to further stabilisation of water in the ice overlayer. This stabilisation may be correlated with the orientation of the non bonding hydrogens at the top of the water hexamer observed here.

BRUDERMANN et al. [365] concluded from their He atom scattering from large water clusters

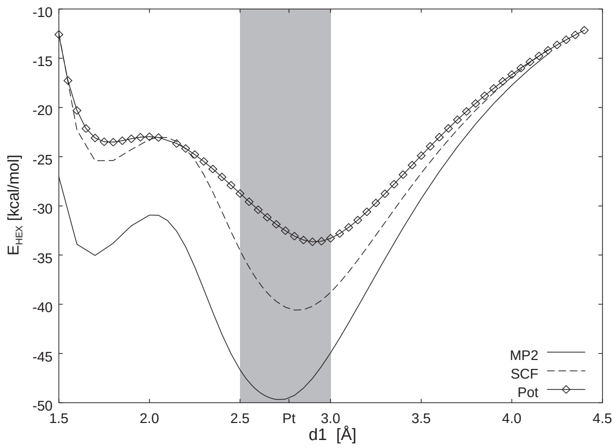

Figure 8.15: Energy of Formation E_{HEX} of the water hexamer under surface constraints.

that the water molecules becomes more strongly bound with increasing cluster size. Supported by theoretical calculations, they argue that the strain in the hydrogen bond network in small clusters reduces the O-O-O bending force constant. Our calculations suggest that a similar effect should apply to water clusters on Pt(111) where the strain in the hydrogen bond network is induced by the surface and becomes smaller as the cluster grows in size.

To confirm the physical relevance of such data the calculations of the second step above were repeated at MP2 level. The energy necessary to constrain the free water hexamer at the surface was similar (MP2: 4.3 kcal/mol, Pot: 2.7 kcal/mol) and in both sets of calculations the hydrogens of the base water molecules pointed towards the virtual surface (w1 MP2: 83.5°, Pot: 89.2°). In addition, the oxygen-oxygen bond lengths agreed reasonably well (MP2: 2.78 Å, Pot: 2.87 Å).

8.2.5.4 Variation of the surface lattice constant

Our results suggest that the water molecules in the first layer on Pt(111) can lie parallel to the surface and that the growth of ice crystals remains possible. To analyze the influence of the surface lattice constant d1, the calculation was repeated for various values of d1. For d1 = 2.77 Å (Pt(111)) the orientation of the non-bonding top hydrogen atoms has a minor effect on total energy (1% of the total energy -33.005 kcal/mol). In the following calculations these hydrogens were constrained to lie vertically for convenience, but the water molecules were still allowed to rotate around the bond to the virtual metal surface.

Figure 8.15 shows the energy of formation E_{HEX} at various levels of theory as a function of the surface lattice constant d1. The curves are very similar, each displaying two minima. The second, global, minimum represents a distorted water hexamer (Table 8.7, SCF optimum in figure 8.12), while the first shallow minimum represents two loosely bound water trimers which will dissociate as d1 is reduced.

Both the binding energy of the hexamer and the oxygen-oxygen distance r_{OO} behave similarly to the water trimer: With increasing level of theory, the global minimum moves to smaller values of d1 and corresponds to higher binding energies. As d1 is reduced, the oxygen-oxygen bond length becomes shorter, because the height of the ring (h) changes slightly ($\Delta h = 0.05$ Å).

The oxygen-oxygen distance decreases with increasing cluster size in the quantum calculations (at MP2 level: $\Delta_{trim}^{hex} r_{OO}$ = -0.052 Å) whereas it increases in the classical calculations ($\Delta_{trim}^{hex} r_{OO}$

	d_1 [Å]	d_2 [Å]	r_{OO} [Å]	w_1 [deg]	w_2 [deg]	w_3 [deg]	$-E_{HEX}$ [kcal/mol]	$-\Delta E_{TOP}$ [**] [kcal/mol]
Pot	2.90	1.44	2.93	80.72	−52.44	−63.24	33.66	10.862
SCF	2.80	1.39	2.83	86.12	−51.97	−64.51	40.59	14.558 [***]
MP2	2.70	1.44	2.74	90.78	−52.19	−64.15	49.67	18.199 [***]
ideal [*]	2.6	1.9	2.76	125	−52	−60		10.56

[*] approximate values for ice Ih

[***] calculated at the global optimum

[**] binding energy of a top plane water molecule

Table 8.7: Global minima of the potential energy curves for the constrained water hexamer (figure 8.15).

= +0.017 Å) as the number of water molecules is increased from 3 to 6. Quantum calculations take cooperative forces directly into account, whereas classical calculations simulate these forces via strong interactions between second nearest neighbours (see section 8.2.4). Such a mechanism cannot compensate fully for the cooperative effects. The oxygen-oxygen distance in the classical hexamer is therefore shorter than in the dimer but longer than in the trimer.

With increasing level of theory the global minimum of the potential energy curve moves into the range predicted by THIEL and MADEY for the existence of bilayer structures (2.48 Å (Ni) < d1 < 2.89 Å (Ag), grey shaded in figure 8.15) [38, 366], indicating the formation of ice-like water clusters on metal surfaces in agreement with the surface ice rules (see 8.2.5.1). Figure 8.15 also suggests that the range of suitable surfaces may be larger than expected.

The formation of water trimers within the hexamer for small values of d1 can be seen in Figure 8.16, which shows selected pair interaction energies calculated with the classical potential. The strength of the hydrogen bond between nearest neighbours (E_{DIM}^{1st}) decreases as d1 decreases, while the strength of the interaction between second nearest neighbours (E_{DIM}^{2nd}) increases. These interactions form the basis for the formation of water trimers, since, as d1 becomes smaller, the hexamer breaks into two trimers. This cleavage eliminates the repulsive forces between the base plane and the top layer and the total energy of the cluster is controlled by the repulsive forces within the newly formed water trimers.

We note that interactions between second nearest neighbours in the base plane are as strong as those between nearest neighbours. These interactions between second nearest neighbours influence the geometry of the cluster even at large values of d1. For d1 = 1.7 Å the total interaction energy between second nearest neighbours (E_{DIM}^{2nd}) in the base plane is 13.56 kcal/mol, a value close to the binding energy of the free {ppp} water trimer (13.68 kcal/mol). In the top plane the interactions between second nearest neighbours are small and do not extend as far as in the base plane.

The strengh of the hydrogen bond between nearest neighbours does not depend significantly on orientation; a top or a base plane water molecule may donate a hydrogen atom to the bond. Both curves in Figure 8.16 have similar shapes over the given interval for d1. At large values of d1 the top→base hydrogen bond is slightly more favourable than the base→top hydrogen bond, because the former is closer to the optimal hydrogen bond of the free water dimer. In the physically important region (2.5 Å $\leqq$ d1 $\leqq$ 3.0 Å) the base→top hydrogen bond is stronger than the top-base hydrogen bond. In this range, the basal hydrogen atoms move upwards and strengthen the hydrogen bonds.

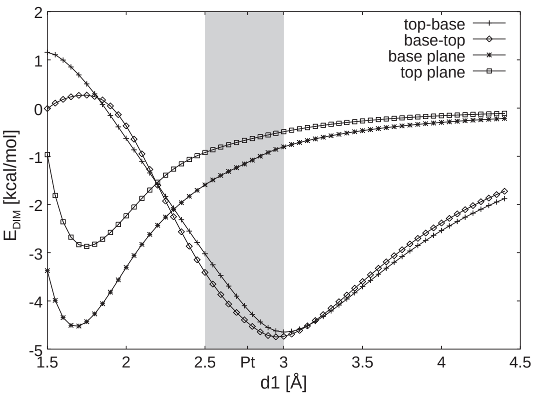

Figure 8.16: Pair interaction energies E_{DIM} in the water hexamer (classical potential).

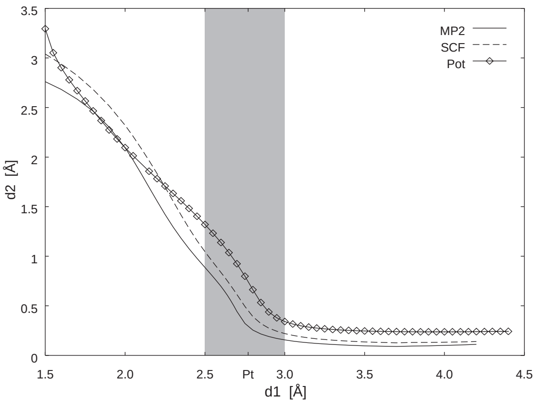

Figure 8.17: Height (h) of ring as function of surface lattice constant d1.

The maximum in the total energy (Figure 8.15) can be accounted for via Figure 8.16. The interactions between nearest neighbours become antibonding more readily than those between second nearest neighbours become bonding, causing a maximum in total energy. The dissociation of the water hexamer is controlled by interactions between nearest and second nearest neighbours.

Figure 8.16 shows, that both the top→base and base→top hydrogen bonds have the same strength despite their different geometries (Figure 8.13). Significant differences can be observed only for interactions between second nearest neighbours. In the base plane ($E^{2nd}_{MIN} = -4.52$ kcal/mol) these interactions are much stronger than in the top plane ($E^{2nd}_{MIN} = -2.87$ kcal/mol). This difference has a strong influence on the geometry, because the second nearest neighbour interactions in the base plane contribute significantly to the total energy whereas contributions in the top layer are negligible over a wide range of values for d1.

Figure 8.17 displays the height of the water ring ($h = d2 - d'$) as a function of d1. Again all three curves display similar features. As d1 is reduced the height remains close to zero until around 2.7 Å to 3 Å when it increases linearly with d1. A further change, not shown in figure 8.17, can be observed for $d1 < 1.5$ Å, when the hexamer breaks in two trimers as h tends to infinity.

Within the range of validity of the surface ice rules the height of the ring decreases to zero. It is therefore probable that the water hexamer lies flat on heavy metal surfaces and ideal ice-like structures ($h > 0$) can be expected only for values of d1 smaller than 2.6 Å (e.g. Fe, Co, Ni, Cu [366]).

As the water ring tends to planarity, the hydrogen atoms on water in the base plane move closer to the surface. Figure 8.18 shows w1 varies with d1. Again all three curves show similar behaviour. For values of $d1 \gtrsim 2.7$ Å the hydrogen atoms in the basal water molecules point towards the surface until w1 reaches a constant at 75°. This motion stablizes the base→top hydrogen bond (Figure 8.13a), since the geometry of the base→top water dimer approaches the ideal dimer geometry with C_S symmetry (to be compared with the basal plane of the free water hexamer, Figure 8.14). At a value of 75° two opposing effects compensate : the hydrogen atoms of the water molecules in the base plane move as far down as possible to reduce repulsion among the nonbonding hydrogen atoms without significantly distorting the base→top hydrogen bond, since the bonding hydrogen atom moves out of its ideal position as w1 decreases.

Values of w1 smaller than 90° are unlikely to be observed in practice, since the water molecule binds to most metal surfaces via a lone pair and an orientation of the water molecule with the

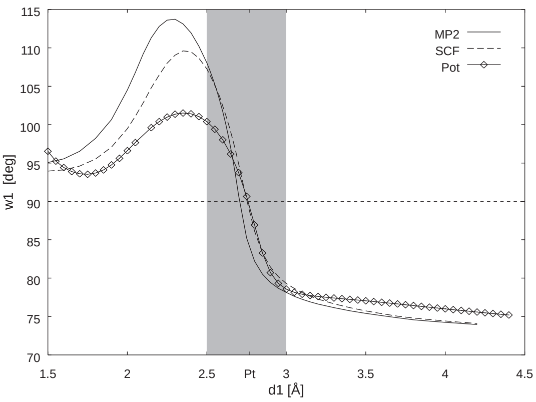

Figure 8.18: Angle w1 as a function of surface lattice constant d1.

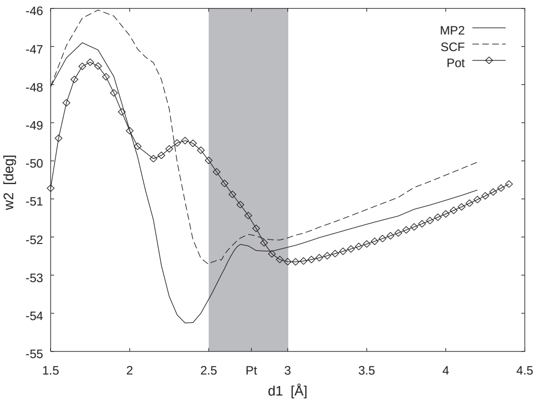

Figure 8.19: Angle w2 as a function of surface lattice constant d1.

hydrogens pointing downwards would require cleavage of the metal-oxygen bond.

For d1 < 2.7 Å, w1 increases until it reaches a maximum. In this region the changes of w1 and d2 are coupled. As the width of the ring increases the basal hydrogen atoms move upwards to maintain a strong base→top hydrogen bond. With increasing levels of theory, the maximum value of w1 increases, but fails to reach the value of 125.26° for ideal tetrahedra, the closest being at MP2 level (113.74°), when, at d1 $= 2.3$ Å, (r_{OO}) reaches its minimum of 2.64 Å. This is smaller than the value of 2.76 Å found for the ideal ice structure. The structure closest to the ideal ice structure can be observed only outside the range proposed by THIEL and MADEY.

As d1 is further reduced w1 again decreases, when the hexamer splits into two trimers. The optimal structure for a trimer in the base plane of the water hexamer is nearly planar (d1 $= 1.8$ Å, $r_{OO} = 3.05$ Å, $\alpha = 25.29°$, w1 $= 93.70°$) and the hydrogen atoms in the basal water molecules move downwards to bind to second nearest neighbours.

The splitting of the hexamer into two trimers can also be inferred from Figure 8.19 which displays w2 as a function of d1. For w2 $> -52°$ the bonding hydrogen atoms of the basal water molecules rotate into the water hexagon and point towards the second nearest neighbour.

For both small and large values of d1 quantum and classical results for w2 agree except in the central region ($\Delta^{\mathrm{Pot}}_{\mathrm{MP2}}\mathrm{w2} \approx 5°$). Figure 8.16 shows that for d1 ≈ 2.3 Å the interaction between nearest and second nearest neighbours in the base plane are similar in magnitude. At d1 $= 3$ Å the interactions between second nearest neighbours contribute 7.2% of the total energy and this contribution increases rapidly as d1 decreases. Since the interaction between the second nearest neighbours in the base plane increases with w2, the bonding hydrogen atoms of the base molecules turn into the hexagon. This slightly weakens the base→top hydrogen bonds, which are still similar in magnitude to the top→base bonds in this region. The classical potential, which is based on pairwise interactions, cannot compensate for the distortion of the dimer through cooperative effects. To balance the individual bonds in the hexamer the rotation of the base water molecules ceases when d1 $= 2.35$ Å and the bonding hydrogens turn back to reinforce the top→base hydrogen bonds until the interactions between second nearest neighbours dominate the total energy. Figure 8.16 shows how the top→base hydrogen bonds become more favourable than the base→top bonds in this region.

Quantum calculations include cooperative effects and these effects are likely to compensate for the distortion of hydrogen bonds between nearest neighbours. Artificially high interactions between second nearest neighbours as observed in classical calculations are therefore not necessary to compensate for the distortion. The bonding hydrogen atoms of the base water molecules can move out of the hexagon to form strong top→base dimer bonds and only for small values of d1 do the hydrogens move back into the hexagon to form trimers.

The first maximum (classical potential d1 = 1.8Å) in Figure 8.19 suggests the formation of a planar water trimer (classical potential: r_{OO} = 3.05 Å, $\alpha = 25.29°$) in the base plane. Both the r_{OO} and α are close to the free {ppp} water trimer values (r_{OO} = 2.91 Å, $\alpha = 24.18°$). The hydrogen bonds in the free C_{3h} water trimer are bent and the formation of such a trimer on a metal surface is likely for small values of d1. At d1 = 1.75 Å the binding energy curve (Figure 8.15) displays a local minimum, suggesting the formation of a flat trimer in the base plane, in agreement with the maximum in figure 8.19.

Calculations on the free water trimer showed that with increasing values of r_{OO}, α becomes smaller and the bonding hydrogen atoms turn back onto the oxygen-oxygen line. Such an effect is not observed in the water hexamer. As d1 increses, the bonding hydrogen atoms move away from the oxygen triangle in the base plane to form hydrogen bonds between nearest neighbours and w2 becomes more negative. The rotation of the bonding hydrogens in the base plane does not cease at $-52°$, when they move out of the water hexagon to minimize repulsions within the top→base bond (figure 8.13b), while the base→top hydrogen bond becomes stronger as the bonding hydrogen atoms move into the oxygen-oxygen line (figure 8.13a). As d1 increases, the repulsive forces decrease and the bonding hydrogen atoms in the basal water molecules turn back towards the oxygen-oxygen line. At the minimum of the total energy (d1 ≈ 2.8 Å), w2 ≈ 52° at all levels of theory.

For w1 $< 90°$ (d1 $>$ 2.7 Å), w2 must be smaller than $-52.26°$. Such a rotation moves the bonding hydrogen of a basal water molecule back towards the oxygen-oxygen line between direct neighbours and enhances the strength of the base→top hydrogen bond. This motion accounts for the shallow local minima around 3 Å.

For d1 $>$ 3 Å the hydrogen bonds between nearest neighbours rapidly weaken, while interactions between second next neighbours change slowly (Figure 8.16). For d1 = 4.4 Å (the final point chosen) the interactions between second nearest neighbours in the base plane still account for 5.3% of the total energy. The bonding hydrogen atoms of the basal water molecules turn back into the water hexagon to reinforce the bonding interactions between second nearest neighbours in the base plane. Classical calculations at d1 = 4.4 Å showed that forcing the bonding hydrogen atoms back on to the oxygen-oxygen line (w2 = $-52.54°$, taken from the global minimum structure) has only a small effect on the total binding energy ($\Delta^{52.45°}_{50.61°}E_{HEX} = +0.011$ kcal/mol). The average binding energy between nearest neighbours increases by only 0.002 kcal/mol but the binding energy between second nearest neighbours in the base plane decreases by 0.007 kcal/mol.

Figure 8.20 shows w3 as a function of d1. Once again all three curves are in reasonable agreement. The location of the first maximum suggests the formation of a water trimer in the top plane. The bonding hydrogen atoms turn into the water hexagon to form hydrogen bonds to second nearest neighbours. As d1 increases, the bonding hydrogen atoms move out of the hexagon and for d1 ≈ 2.2 Å w3 reaches its theoretical optimum of $-60°$, when the bonding hydrogen atoms lie directly above the oxygen-oxygen lines and point towards the centre oxygen atoms of the base molecule. As d1 increases further the bonding hydrogen atom moves outside the hexagon. An analysis of the classical curve shows that this motion strengthens both base→top and top→base hydrogen bonds by reducing the hydrogen-hydrogen repulsion. At the minimum of the classical curve (d1 = 2.5 Å,

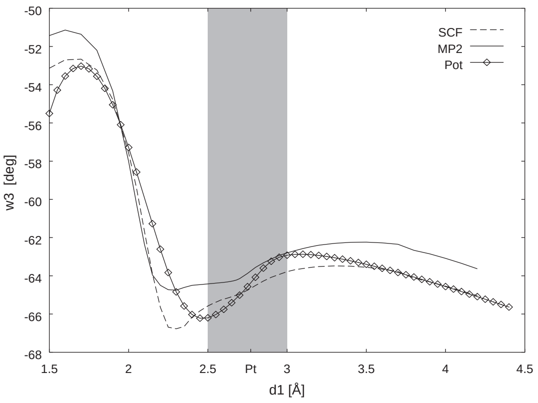

Figure 8.20: Angle w3 as a function of surface lattice constant d1.

w3 = −66.2°) the rotation of w3 back towards the oxygen-oxygen line reduces the total energy by about 0.45 kcal/mol. The increase in binding energy of 30.64 kcal/mol within the cluster is counteracted by an increase in the repulsive energy of 31.09 kcal/mol. Only the interactions between second nearest (and further) neighbours benefit from this rotation, while the hydrogen bonds between nearest neighbours weaken due to repulsions between the hydrogens. A similar distortion has been observed at the global minimum of the water trimer, where the repulsions between non-bonding hydrogens on the same side of the oxygen triangle force the non-bonding hydrogen atoms out of the plane.

As d1 increases further, the hydrogen atoms move back inside the hexagon until the direct hydrogen bonds become strongest at d1 = 3 Å (Figure 8.16), when w3 decreases again, strengthening the hydrogen bonds between nearest neighbours.

8.2.6 Discussion

In all calculations, moving from the classical potential to MP2 via RHF shortened the bond length and tightened the bond. The changes in the quantum calculations are a result of the inclusion of electron correlation, while the results of the clasical potential depend heavily on the parametrization of the potential, which was parametrized using the BSSE corrected MP3 results, extends the hydrogen bond and reduces the binding energy. To detect differences between classical and quantum calculations, we analyzed the sequence $(H_2O)_2 \rightarrow (H_2O)_3 \rightarrow (H_2O)_6$ instead of the sequence classical potential → RHF → MP2.

With increasing cluster size the quantum calculations produce shorter oxygen-oxygen distances in the free water cluster (MP2: 2.91 Å, 2.78 Å, 2.73 Å). XANTHEAS [128, 149] reported an exponential decrease of r_{OO} with cluster size, but showed also that the parameters of the exponential function depend on the method of calculation. The value of r_{OO} calculated with the classical potential showed little change with cluster size (2.98 Å, 2.91 Å, 2.95 Å). TSAI and JORDAN [182] observed similar behaviour in TIP4P calculations on water hexamers, with bond lengths ranging between 2.72 Å and 2.76 Å. These values are close to those calculated for the water dimer (2.75 Å) [116, 249, 250]. The reported binding energy of the cyclic hexamer (−44.4 kcal/mol) disagrees with our result of −35.4 kcal/mol. This difference may be explained through different strengths for an individual hydrogen bond (TIP4P: −6.24 kcal/mol, our potential: −4.90 kcal/mol). Taking a scaling factor $F_{Pot}^{TIPS}(E) = (E_{DIM}^{TIPS4})/(E_{DIM}^{Pot}) = 1.27$ for an individual hydrogen bond into account yields a binding energy of −45.1 kcal/mol, in reasonable agreement with the published value.

Results based on the classical potential depend critically on the parametrization of the interaction potential. Using table 8.5 calculated scaling factors for the bond length ($F_{Pot}^{MP2}(r_{OO})$ = 0.97) and the binding energy ($F_{Pot}^{MP2}(E)$ = 1.28) provide an indication of cooperative effects within the cyclic hexamer at MP2 level, leading to an oxygen-oxygen bond length of 2.86 Å and a binding energy of −45.3 kcal/mol. These results suggest that many body-body effects account for −8.6 kcal/mol (16% of the total binding energy)[4]. PEDULLA et al. [188] reported a value of −13.48 kcal/mol (32%) for the 3-, 4-, 5- and 6-body forces in the cyclic water hexamer, which is similar in size but twice as large as its contribution to the total energy. For the cage and prism structures many body forces account for 22% of the total binding energy (−9.5 kcal/mol). These results can be accounted for by the higher number of hydrogen bonds in the three-dimensional clusters (cage: 8, prism: 9).

The calculations on the water hexamer agree reasonably well for all levels of theory, allowing us to rule out further systematic errors. Energy differences between different configurations and the geometry of the cluster itself appear to be well defined.

As can be seen from Table 8.7, which contains data for the water hexamer as part of ice Ih, our calculations fail to reproduce the value of the surface lattice constant d1 of ice. Although d1 does decline at incresing levels of theory, the limiting value of 2.6 Å is never reached. Since d1 is large, the corresponding values of d2 and w1 are small in order to create strong direct hydrogen bonds with optimal oxygen-oxygen separations.

In an extended ice crystal, w1 is controlled by the water layer below the hexamer. This basic hydrogen bond raises the hydrogens of the base molecules, thereby increasing the height of the ring. Our model does not contain such directional forces and the water hexamer becomes more compressed than in bulk ice Ih. The oxygen-oxygen distance calculated at the MP2 level (2.74 Å) is close to that found in ice (2.76 Å). To maintain this value, an upward motion of the basal hydrogens would result in smaller values for d1. The inability of our model to reproduce d1 seems to be more a product of the finite spatial extent of the ice micro-crystal than of the chosen method of computation.

Our quantum calculations on the platinum-water interface showed that the reorientational energy $\Delta_{UP}E$ of the hydrogens to be very small ($\Delta_{UP}E < 0.5$ kcal/mol). A model with no directional forces would appear to be more realistic as a first approximation than one with strong directional forces as in ice.

Our calculations indicate that the formation of planar hexamers on hexagonal metal surfaces is feasible for a wide range of surface lattice constants and, by implication, of metals. As the value of surface lattice constant d1 approaches to 2.7 Å the ring becomes planar ($h \approx 0$, Figure 8.17) and the nonbonding hydrogens in the top layer were forced to point upwards. A planar water hexamer in the first bilayer does not prohibit the growth of ice clusters on any surface.

As h decreases, the basal hydrogens move closer to the surface. For $d1 \approx 2.7$Å, w1 equals 90° and tends to 75° as d1 increases. Values of w1 smaller than 90° are unlikely to be observed in practice, as the water-metal bond is generally formed through the lone pair of the water molecule [38, 70].

---

[4] RHF calculations of multi-center forces within the constrained hexamer showed that cooperative forces account for 20% of E_{HEX} at the global minimum (d1 = 2.80 Å).

The energy required to reorientate the water molecule in the interval $90^\circ \leqq \mathrm{w1} \leqq 180^\circ$ is small ($\Delta_{\mathrm{UP}}\mathrm{E} = 0.26$ kcal/mol for $\mathrm{Pt_5 - H_2O}$), while it is energetically unfavourable to bring $\mathrm{w1} < 90^\circ$, when $\Delta_{\mathrm{DOWN}}\mathrm{E} = 35.29$ kcal/mol. This energy reflects the breaking of the platinum-oxygen bond, which does not form part of our surface model. A more elaborate surface model to account for $\Delta\mathrm{E}_{\mathrm{DOWN}}$ should yield a value of 90° for w1 for d1 around 2.6 Å, since the energy gain within the water hexamer caused by the downwards motion of the hydrogens is compensated by the energy necessary to distort the surface-water bond.

The possibilty of the water molecules pointing downwards depends on $\Delta\mathrm{E}_{\mathrm{DOWN}}$ and therefore on the chosen model of computation. SPOHR [100, 101] published Molecular Dynamics Simulations on the Pt(100)- and Hg(111)-water interface. According to his simulations the moleculear planes of the water molecules in the first layer lie parallel to the metal surface, which agrees well with our results. In the Hg(111)-water interface system the oxygen-hydrogen bonds are pointing downwards to the metal surface. Our calculations suggest that for values of $\mathrm{d1} \geq 2.7$ Å the dipole moment vector of the water molecule should point downwards to the surface. The mercury-mercury distance is about 3.0 Å and the orientation of the hydrogen atoms agrees well with our results. The Molecular Dynamics simulations confirm so our assumptions, that the structure of the water-metal interface is controlled by the surface lattice constant d1.

The large value for $\Delta_{\mathrm{DOWN}}\mathrm{E}$ suggests $\mathrm{w1} \geqq 90^\circ$, whereas the value of w1 for a single water molecule depends on the choice of metal cluster and the method of calculation (Pt: $93.7^\circ \leqq \mathrm{w1} \leqq 180^\circ$, 90° [54], 180° [64], 90° (coadsorbed with K) [63], 180° [65], 90° [68], 180° [60]; Ni: 155° [72], 180° [62]; Cu: 120° [71]; Ru: 180° [66], Al: 125° [70]). The energy to move the hydrogens upwards $\Delta_{\mathrm{UP}}\mathrm{E}$ is usually small with the exception of $\mathrm{Pt_{10}}$ ($\Delta_{\mathrm{UP}}\mathrm{E} < 0.5$ kcal/mol, $\mathrm{Pt_{10}}$: ≈ 4 kcal/mol [63, 68], Ni: 0.9 kcal/mol [72], 1.5 - 0.07 kcal/mol [62], Al: 2.3 kcal/mol [70]).

Two different mechanisms are possible for the formation of extended water clusters on metal surfaces with large values for d1:

1. The molecular plane of the water molecule lies parallel to the metal surface even at low surface coverage (e.g. Pt). The planar water hexamer can grow unhindered.

2. A single water molecule adsorbs with $\mathrm{w1} > 90^\circ$ (e.g. Ru [66], Ni [72]). The structure of the hexamer is now determined by the energy required to distort the surface-water bond ($-\Delta_{\mathrm{UP}}\mathrm{E}$) and the energy gained by the downwards motion of the hydrogen in the basal plane. The small values for $\Delta_{\mathrm{UP}}\mathrm{E}$ and the large energies for conformational changes within the water cluster reported here suggest that the water hexamer will dominate the structure of the interface and force the hydrogens down towards the surface.

Both cases generate a flat water hexamer on the surface and seems likely ion a hexagonal metal surface irrespective of the values of w1 found in geometry optimisations of small clusters.

Our results suggest that the direct formation of a metal-ice interface can be observed for metals with strong metal-water bonds resulting in large values for $\Delta_{\mathrm{UP}}\mathrm{E}$, which force the base water molecules into a suitable orientation, or for small surface lattice constants.

The influence of the surface lattice constant d1 on the binding energy of the water molecule can be seen in a plot [38, 47] of the lattice mismatch ltm (distance between second nearest neighbours, $\mathrm{ltm} = \Delta\mathrm{d1} \cdot \sqrt{3}$) versus the highest desorption temperature of water from metal surfaces (multilayer peak). From table 8.8, the highest desorption temperature is found for Ru(0001) ($\mathrm{ltm} = -0.19$ Å, $\mathrm{d1} = 2.71$ Å) lying between 212 K and 220 K [47]. If ice is assumed to grow epitaxially on a metal

surface	d1 [Å]	ltm [Å]	T [K]	E_{HEX}^{MP2*} [kcal/mol]
Ni(111)	2.49	+0.19	170	−46.525
Cu(111)	2.56	+0.08	150	−48.128
Rh(111)	2.69	−0.16	190	−49.530
Ru(0001)	2.71	−0.19	212 - 220	−49.662
Re(0001)	2.76	−0.28	180	−49.562
Pt(111)	2.77	−0.30	170	−49.484
Ag(111)	2.89	−0.50	150	−47.721

* extrapolated from the MP2 potential energy curve (figure 8.15)

Table 8.8: Multilayer Peaks data from refs. [38, 47, 366]

surface, the highest desorption temperature for the multilayer peak should be found for copper (d1 = 2,56 Å, ltm = +0.08 Å), which is closest to the bulk ice surface lattice value (d1 = 2.6 Å). The experimental multi layer desorption temperature on Cu(111) is exceptionally low (150 K). Table 8.8 shows that E_{HEX}^{MP2} correlates with desorption reasonably well for all values of surface lattice constant, suggesting that the real bilayer structure lies closer to the constrained hexamer reported here than to bulk ice Ih.

We find that the water hexamer remains planar ($h \approx 0$) at d1 = 2.7 Å, in agreement with experiment [360] and suggests that the orientational forces of ruthenium on the water molecule are smaller than those of the stretched water ring. This experimental value for h [360] suggests that our simple model seems to reproduce both, the energy and the structure of the water bilayer.

The binding energy of a single water molecule to metal surfaces (e.g. Pt, Rh, Re, Ni, Ru [38]) is similar to the ice sublimation energy (≈ 14 kcal/mol) [38, 42, 56], which corresponds to two to three hydrogen bonds (table 8.5). A total binding energy of approximately 42 kcal/mol for three water-metal bonds can compensate for any hexamer conformation calculated here (Figure 8.15), but the experimentally observed range is much smaller.

In the intial stage of growth, a water molecule has two possible adsorption sites: one attached directly above a platinum, another to a water molecule already bound to the surface [46, 48]. The coexistence of both species is commonly explained in terms of the energy of isolated bonds, although the importance of cooperative forces has been suggested [42, 45, 49]. The strenghth of the platinum-water bond corresponds to that of two to three hydrogen bonds, so either type of bonding should be possible.

The analysis of the classical binding energy showed that the strongest bond between a top water molecule and the remaining water pentamer (ΔE_{TOP}) can be observed close to the global maximum of the total energy (d1 = 2.95 Å, $\Delta E_{TOP} = -10.862$ kcal/mol). This value is smaller than the energy of water bound directly to the surface and two dimensional growth of the water layer on metals should be more favourable than the formation of three dimensional islands. Quantum chemical calculations on $Pt_3-(H_2O)_3$ [42] have shown on the other hand, that cooperative effects play an important role in the formation of small water clusters on platinum(111) and the binding energy of a top water molecule should therefore be higher than that calculated with the classical potential.

The importance of cooperative effects and electron correlation can be inferred from the binding energies of a top water molecule (ΔE_{TOP}) at the global minima of the RHF (14.558 kcal/mol) and MP2 (18.199 kcal/mol) potential energy curves. Whereas the classical potential does not support the formation of three dimensional clusters, the formation of such clusters is predicted by the quantum calculations.

The binding energy ΔE_{TOP} decreases rapidly as the lattice constant d1 varies. The formation of three-dimensional water clusters as observed for Pt(111) [56] is therefore limited to a small range around the global minimum. Outside this region, two-dimensional growth will dominate and water molecules in the second layer will be observed only at higher surface coverage.

The existence of the planar water hexamer suggests that the structure of the metal-water interface is not continuous as suggested by the surface ice rules, but has its own structure. This structure is closer to ice Ih and therefore closer to the QLL than to the two-dimensional ice structures reported by KOGA et al. [367, 368] and ODELIUS et al. [369], which have similar oxygen-framework ($r_{OO} = 2.73 \pm 0.02$ Å, $h \approx 0$ [367]) but differ in the orientation of the hydrogen bonds.

8.2.7 Final Conclusions

The interface phase has its origin in the ending of the ice crystal. Quantum chemical calculations suggest that a single water molecule is bound more strongly to the metal surface ($\approx$ 15 kcal/mol) than to the ice cluster, but the platinum-water bond has a small influence on the orientation of the base water molecules ($\Delta E_{UP} \approx 0.5$ kcal/mol). The absence of these orientating forces allows the hydrogens of the water molecules directly attached to the metal to move freely. This free motion of the hydrogens makes the interfacial region similar to the ice-vacuum interface. The value of the lattice constant d1 seems to control the properties of the interfacial phase. As d1 increases the water hexamer becomes flatter and the molecular plane of the base water molecules lies parallel to the metal surface. We therefore asume the formation of an interfacial layer as the basis for ice growth on metals other than platinum with weak orientating forces and large interatomic distances.

Acknowledgement

Timm Lankau would like to thank K. Nagorny for his support and students who participated on the project: Axel Wichman, Sonja Staack and Ingo Reulecke. He would also like to thank the "Studienstiftung des Deutschen Volkes"and the "Hansische Universitätsstiftung"for financial support.

Chapter 9

Final Conclusions and Further Proceedings

The computational analysis of the platinum-water-vacuum interface started with an investigation of small water cluster as benchmark test. Our results obtained with MP3/DZP calculations for $(H_2O)_n$ and $n \leqq 3$ agree well with values (theoretical and experimental) previously published by other groups. Further improvement was achieved by a BSSE correction according to the full counter poise method by BOYS and BERNARDI of the bonding energy and the dimers geometry. These results agree even better with the experimental values.

The most stable water dimer has C_S symmetry, a oxygen-oxygen distance of 2.9926 Å, the hydrogen bond is slightly bent ($\alpha = 2.4°$) and the hydrogen acceptor moved out of his ideal tetrahedral geometry ($\beta = 44.5°$). The dimerisation energy calculated for this dimer is −4.914 kcal/mol, which is close to the experimental value of −5.44 ± 0.7 kcal/mol. High level quantum chemical calculations on the other hand suggest an interaction energy about −5.0 kcal/mol and it is commonly believed, that the true value for the strength of the hydrogen bond has to found at the lower part of the experimental range.

The experimental oxygen-oxygen distance is 2.97 ± 0.03 Å. Since the oxygen-oxygen distance dominates the interaction energy, this work, like others before, concentrates on its correct reproduction. The experimental uncertainty for the angles is 10° ($\alpha = 1°$, $\beta = 57°$). Although an increase of α will break the hydrogen bond, is the hydrogen bond bent to minimize exchange repulsion between the two monomers. Both angles α and β have only a small influence on the total interaction energy and the potential energy surface of the water dimer is therefore extremely flat around the global minimum.

The quantum chemical calculations showed, that the relaxation of the monomers geometries has only a small influence on the cluster formation. The energy difference between calculations with a rigid water molecules (experimental values: $r_{OH} = 0.9572$ Å, $\sphericalangle_{HOH} = 104.52°$) and flexible monomers can be neglected safely. This simplification allows us to scan vast areas of the $(H_2O)_2$ potential surface and to continue with larger clusters.

Due to computational restrictions when we were doing the MP3/DZP calculations it was impossible to calculate the energy of the cyclic {uud} trimer, which is the global minimum of the $(H_2O)_3$ potential energy surface. The most stable water trimer analyzed on the MP3/DZP level was the cyclic {ppp} trimer (C_{3h} symmetry) with a bonding energy of 13.8 kcal/mol, while the linear trimers were all higher in energy. Two of them, with a double hydrogen donor or acceptor, are energetically disfavoured as the cooperative effects are antibonding.

The analysis of the interaction between to water molecules showed, that the hydrogen bond is not formed by an overlap of frontier orbitals, but by a rearrangement of the inner orbitals and charge transfer is therefore small. The electric field of the second monomer induces a small energy shift of the first monomer's orbitals, which greatly enhances orbital overlap. Such a mechanism is part of the quantum chemical representation of polarisation, but an energy decomposition according to MOROKUMA showed, that the interaction is still dominated by electrostatic and exchange repulsive forces and polarisation plays only a minor role.

The possibilities of the quantum mechanical calculations are limited by three points despite their general utility:

1. The computational costs are so high that it is nearly impossible to do calculations at MP3/DZP level on the water trimer or bigger cluster with the available computational equipment.
2. The influence of the hydrogen atoms on the total energy is so small, that the geometry optimisation algorithm has problems to find the minimum and it takes more steps to optimize a given geometry.
3. With increasing cluster size the number of local minima becomes also larger, which increases the numerical efforts necessary to locate the global one.

Classical water-water potentials are easier to compute than the quantum chemical and offer so a possibility to extended the analysis of water clusters beyond the given limits. The comparison of cuts through the $(H_2O)_2$ potential energy surface curves calculated both quantum chemically and with classical potential energy functions showed, that none of the widely used potentials fits to the quantum mechanical results. Most of them also yield poor values for dimerisation energy and the dimer's equilibrium structure and even worse values for the water trimers.

The development of a new improved model started from the well-studied TIPS2 model by JORGENSEN. Since the energy decomposition according to MOROKUMA showed that the interaction between the monomers is controlled by electrostatic and exchange repulsive forces, the search for a better potential started with modifications of the van der Waals forces between two oxygen atoms and not with the inclusion of many-body energy terms. Most useful was an exponential function for the oxygen-oxygen interaction (potential E).

$$V_{OO}(r) = A \cdot e^{-b(r-c)} \tag{9.1}$$

Further improvement was achievement by the introduction of a set of repulsive functions for the different types of interactions, namely V_{OO}, V_{HH} and V_{OH}. The standard deviations of the curves calculated with newly fitted potential were better than the ones originally published. The fitting of this potential (originally suggested by KISTENMACHER and POPKIE) to the quantum mechanical calculated values yielded a potential, which describes the quantum mechanical curves very good (potential N) and gives also good values for the water trimers. The global minimum ($d_{OO} = 2.98$ Å, $\alpha = 8.5°$, $\beta = 56.6°$, $\Delta E = -4.883$ kcal/mol) for the water dimer of this potential agrees very well with experimental found values, despite the large value for α caused by the inclusion of the trimers into the optimisation of the potentials parameters.

A detailed analysis of the parameters of potential N showed, that the repulsive forces between the oxygen-oxygen atoms are very strong, but do not reach far. The contribution of V_{OO} to the total energy was equal to nought for all geometries. The analysis showed also, that V_{OH} is the most important function for the correct reproduction of the quantum chemical geometries and energies. This effect can be explained with chosen dimer geometries for the optimisation of the parameters. All geometries have been close to the equilibrium structure and mechanical stress on the hydrogen bond was more important than the oxygen-oxygen repulsion. The application of potential N is therefore limited to small water clusters close to their equilibrium structure.

Both potentials E and N have a third, shallow minimum in the potential energy surface of the water dimer with C_S symmetry. This minimum is caused by the dislocation of the center of charge from the oxygen atom. The set of repulsive functions in combination with the longer oxygen-oxygen distance in the water dimer buffers the effect. The well depth of this minimum is shallower for potential N than for potential E. Quantum chemical test calculations of selected points from this surface showed, that potential N allows the correct prediction of energy differences and geometries for the water dimer.

Potential N as a simple point charge model cannot describe any cooperative effects by definition. The fitting of the potential's parameters to the quantum mechanical values gave a potential, which describes both the dimers and the trimers well. Potential N has to simulate therefore attractive cooperative forces. The analysis of the water trimer and hexamer showed, that this is done with repulsive forces between non-bonding hydrogens and weak, but far reaching, interactions between second next neighbours. Despite the problems with many-body forces in potential N, potential N is suited for the simulation of large water clusters, as the investigation on the water hexamer showed.

We used potential N, which correctly predicts the {uud} geometry for the global minimum, to simulate the ring closure of the water trimer starting form the linear trimer. The calculated energy barriers are small enough to allow a transition between stable conformers by tunneling.

Next we started the quantum chemical investigation of the platinum-water bond at a series of Pt_n-H_2O clusters with n = 1, 2, 3, 5, and 9 on the MP2/DZP level. The platinum atoms in chapter 6 were described with HW18 ECP using a DZ basis set, while the water molecule was described as before with a DZP basis set.

First calculations on $Pt-H_2O$ showed, that the strength of the Pt-O bond depends on the electronic state of the platinum atom. Water is more strongly bonded to a ^1S platinum than to a ^3D atom, despite a higher electronic energy of the ^1S platimum. The dependency of the bond strength on the electronic state is one of the major problems in the computational analysis of the interface. With increasing cluster size becomes the number of electronic states with energies similar to the ground state rapidly larger and each electronic state creates a different bonding energy.

Figure 9.1 shows a simplified model of the platinum water interaction. The free electron pair of the water molecule, a linear combination of the water $3a_1$ and $1b_1$ orbitals, overlaps with a platinum 5d orbital. A strong bond between the metal and the water molecule is accompanied with charge transfer from the water molecule to the metal and a hole in the 5d band is therefore necessary to put up the electron density from the water molecule. The formation of a hole for the water electrons forces electrons from the 5d band into the 6s orbitals. An equivalent description of the bond can be given using the quantum chemical definition of polarisation (figure 2.3, page 28). The water molecule polarizes the metal cluster and causes so an occupation of the 6s orbitals. These new orbitals are than used for the formation of the bond resulting in a netto 6s density increasement during the formation of the platinum-water bond.

A second mechanism controls the 6s population: The 6s orbitals are wider spreading than the 5d

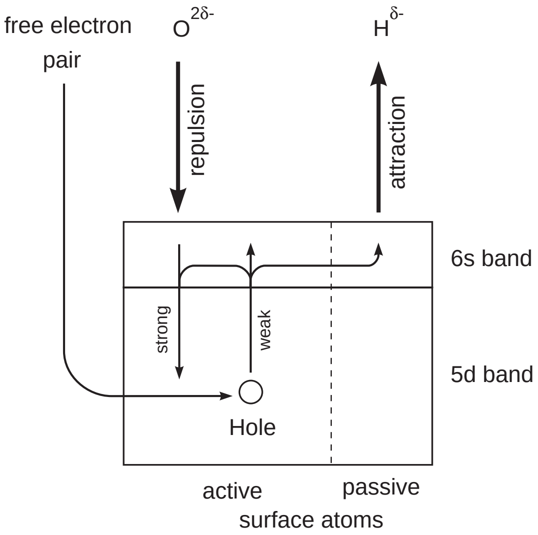

Figure 9.1: Model for the platinum-water interaction.

orbitals and the population of the 6s band increases the Coulomb repulsion between the platinum cluster and the water molecule. This repulsion forces electron density back into the cluster into the 5d orbitals.

The second mechanism forcing the electrons back into the cluster dominates the platinum-water bond for small values of the platinum-oxygen bond length. As the 6s electron density is forced back into the 5d orbitals by the water molecule, the hole in the 5d band cannot be large enough to put up two electrons from the free electron pair of the water molecule. The bond between water and a platimum surface is therefore not like the bond observed in inorganic complex ions, which can be described with the valence bond theory, but is more like the bond between water molecules, which bases on the interaction between fully occupied orbitals: The $3a_1$ and the $1b_1$ of the water molecule interact individually with occupied platinum 5d orbitals and the selection of the 5d orbitals used for the bond is entirely controlled by symmetry. The 6s orbitals of the metal cluster contribute only little to the bond. This small contribution is the origin of charge transfer form the 5d band into the 6s orbitals during the formation of the platinum-water bond. Polarization and cooperative effects similar to the effects observed in small water clusters have been observed also for the platinum-water bond.

The dominant role of the Coulomb repulsion for the selection of the electronic state of the platinum cluster has been demonstrated with a single platinum and a negative test charge of -0.6 e (charge on the oxygen atom in free water). As the charge gets closer to the platinum becomes the ^1S platinum more stable the ^3D atom. It is possible, that polarisation effects caused by the dipole moment of the water molecule can change the electronic state of the metal cluster.

The intermetallic bond among the platinums is formed via the 6s orbitals and a strong platinum-platinum bond demands therefore a high 6s population. Two each other opposing forces control so the 6s electron density. A stable metal cluster demands a high 6s population, but a high 6s population weakens the platinum-water bond. A very low 6s population on the other hand causes very strong platinum-water bonds, but weak platinum clusters. Such a platinum-water bond, caused by a very low 6s population, can be much stronger than the experimental observed bonds. The key element for a successful simulation of the platinum-water interface is the correct

6s population in the metal cluster and the 6s population again is controlled by electrostatic field of the water molecule and so a function of the platinum-water distance.

BIGOT and MINOT concluded form their Extended Hückel calculations, that a 6s population between 0.7 and 0.8 per platinum should be observed for surface atoms forming so a natural hole in the 5d band for the lone electron pair of the water molecule. This observed value is smaller than a value of 1.0 suggested for a cluster made purely from ^{3}D platinums. Our own calculations on Pt_5-H_2O gave good results for the platinum-water bond strength ($\Delta E_{BOND} = -17.23$ kcal/mol) at a 6s population of 0.714. These results suggest, that two possibilities for a working surface model exist: Either a large platinum cluster, which naturally creates the correct surface 6s population, or a small cluster with the correct 6s population in an excited state.

A platinum-platinum bond is much stronger than a platinum-water bond and a change of the 6s population causes so large changes of the total energy of the platinum-water cluster. A scan of the potential energy surface of a Pt_n-H_2O cluster is therefore difficult:

- A surface model, which reproduces correctly the binding energy, has necessarily a smaller 6s population than the most stable platinum cluster and is therefore an excited state of the Pt_n-H_2O cluster.
- Small changes the in orientation of the water molecule can cause sudden changes of the total energy for two reasons.
  - As the water molecule changes its position relative to the cluster changes also the electric field at the cluster and this change can force a new electronic state on the cluster. The strength $\vec{E}_\mu$ of an electric dipole field scales with r^{-3} and as the water molecule moves away from the platinum cluster the repulsive Coulomb forces become rapidly weaker and the electron density spills out off the cluster's core. This electron spill causes then a change of the cluster's electronic state.
  - A change in the position of the water molecule also can be a change of the symmetry in the Pt_n-H_2O cluster and orbitals, which have been separated well by symmetry can mix now. This mixing again can cause a sudden change of the cluster's electronic state. This mechanism can be observed in rotations around the platinum-oxygen bond, where changes about 0.001° can cause energy jumps about 2.4 kcal/mol and more.

The cluster size is very important for the quality of the surface model for three reasons and demands special consideration:

1. The hydrogen atoms of the water molecules interact with the surface via the platinum 6s orbitals. This interaction can be modeled sufficiently with a 1 valence electron ECP on the platinum, which covers only the the 6spd valence space. Larger platinum clusters are therefore likely to give higher values for the orientational energies of the water molecule.
2. Calculations on Pt_2-H_2O showed, that the 6s electron density flows away from the platinum-oxygen bond and cumulates at the atoms without a platinum-oxygen bond. The negative charge at these atoms interact with the positively charged hydrogens of the water molecule and increase so the energy necessary to reorientate the water molecule.
3. First results for Pt_9-H_2O showed, that the 6s electron flow is linked with a movement of the 5d electrons in larger clusters.

Complete surface model therefore need at least two slabs of platinum with a surface large enough to interact with the hydrogens. With increasing cluster size increases the number of nearly degenerated electronic states of the metal cluster and sudden energy discontinuities during the scanning of the potential energy surface more likely. To avoid these jumps more elaborate methods such as MCSCF are necessary for the calculation. The numerical efforts rise therefore in two ways: First, the cluster itself becomes bigger and second, more elaborate methods are needed for a suitable description of the platinum-water bond.

The calculations in chapter 6 showed, that the platinum-platinum bond is controlled by the 6s electrons. For the identification of the orbitals necessary for the construction of suitable electronic states of the metal cluster Hückel calculations proofed to be most helpful. The assumption of a perfect 1-valence electron ECP allows us to use the original Hückel theory on the platinum 6s orbitals and to calculate principal properties of the platinum clusters such as the multiplicity of the electronic ground state and the charge distribution in the cluster.

Hückel calculations give correct results for the symmetry and the relative energies of the 6s orbitals, which was used for the analysis of small platinum clusters (Pt_3). The indentification and construction of suitable electronic states and geometries for the platinum cluster was more complicated:

1. The active surface atom, which forms the bond to the water molecule, should have a $5d^{10}6s^0$ configuration (^1S), since the HF calculations easily home into this state and the low 6s population guarantees also a strong platinum-water bond.

2. The remaining platinums, passive surface and bulk atoms, may have a higher 6s population. ^3D platinums with a 6s population of 1 are suitable candidates, because they create strong platinum-platinum bonds with a low total energies.

3. After the Hückel calculation on a given geometry the bonding 6s orbitals are filled with electrons until a symmetric 6s population is reached. The Hückel calculations on Pt_5 suggested so a stable cluster with four 6s electrons. Such an electron configuration is possible with the combination of four ^3D platinums and one ^1S resulting in a triplet state for the metal cluster.

4. The 6s charge distribution was calculated using the approximation of orthogonal orbitals to test the active surface atom. This atom should carry a small negative charge, since previous calculations showed, that a neutral or positive charge on the active surface atom results in too strong platinum-water bonds.

   If the calculation of the 6s charge distribution failed to give a negative charge at the active site, the calculation was repeated with another electronic state.

5. The Hückel MO were then used to identify the relevant orbitals in the LanL2 calculations and to construct a surface model with a suitable 6s population. Two methods were used for the construction of the 6s population:

   (a) The informations of the symmetry and the relative energies of the 6s orbitals from the Hückel calculation were used to pick up the correct suitable orbitals from an initial HF run on the Pt_n-H_2O job and to swap orbital populations.

   (b) As the 6s population is a function of the platinum-oxygen distance we repeated the calculations from the last step for several values of the bond length. As the water molecule reached a certain distance from the metal cluster a sudden change in the 6s population was observed in some cases. The calculation with the correct 6s population was picked up and their eigenvectors used as initial guess for all following calculations.

The charge distribution in the metal cluster is very important for the surface model and Hückel calculations give valuable insight into the movement of the electrons. As mentioned above, the charge on the active surface atom is very important the surface model. Hückel calculation on Pt_5, Pt_9 and Pt_{17} showed, that the active surface atoms acts as an 6s electron sink. 6s electron density is transfered so from the base of the cluster to the active site and creates so the Coulomb repulsion necessary for the correct description of the platinum-water bond. A second electron flow from the top back to the base counter balances the 6s electron flow. This second flow is caused by a strong 6s5d interaction and two main pathways have been identified:

1. Partially filled 6sp molecular orbitals have orbital energies lower or equal to the 5d orbitals and these orbitals are populated instead of the 5d orbitals causing so a charge transfer from the 5d orbitals into the 6s band.
2. 6sp molecular orbitals have their energies in the range of the 5d orbitals. The 5d orbitals can overlap with these 6s orbitals correct symmetry provided. This overlap leads to an electron flow away from the central atom and the charge transfer depends so on the energy difference of the overlaping orbitals.

The Hückel calculations are the logical first step towards an 1-valence electron ECP for the passive surface and the bulk atoms. The transformation of ZURITA's ECP potential was not possible due to the special form of ECPs in Gaussian 94. Gaussian 94 demands the ECP in a form originally proposed by KAHN, BAYBUTT and TRUHLAR. These ECPs contain a term U_L^{core}, which describes the principal shape of the ECP, and the other potential functions for the orbitals with angular quantum numbers $l \leqq L$ are created from U_L^{core}. ZURITA's ECP does not contain U_L^{core} but individual potential functions for every value of l.

The potential finally used for this work is a combination of both methods: By setting $U_L^{core} = 0$ we assume, that the 5d electrons together with the other core electrons form a hydrogen like nucleus with no spatial extension. From the LanL2DZ ECP by HAY and WADT we extracted new radial functions for the 6s and 6p electrons in a hydrogen like environment and created an ECP to reproduce correctly the shape of the radial functions and the orbital energies. Finally, we copied the 6d ECP from ZURITA into the new ECP. The application of this new ECP is strictly limited to bulk and passive surface atoms in small platinum clusters.

A working surface model needs an active site with 5d orbitals for the bond to the water molecule. We were able to track these problems down to principal features of the used ECPs and to analyse their origin again with a Hückel model. It was possible to link the relative values of the valence ionistation energy α with U_l^{core} and the values of the bond strength integrals β with U_L^{core}. The Hückel calculations showed, that the observed problems in the interface region between the bulk and the active surface atoms are mainly caused by different properties of U_L^{core} at neighbouring pltinums.

First calculation on Pt_5^+ and Pt_5 showed, that the properties of the metal cluster depend strongly on the ECP chosen for the active site. The best results were obtained with LanL1MB potential. The 6s population (0.48) at the top is close to the value predicted by Hückel calculations (0.44) and the electron flow observed in the cluster is the same seen in the Hückel calculations: 6s electron density flows to the top cumulating to a negative charge for the repulsion of the oxygen atom, while the 5d6s interaction creates a hole in the 5d orbitals at the top for the free electron pair of the water molecule.

The cluster with the new ECP was tested as a surface model. Table 9.1 shows a comparison of both MP2 calculation with different ECPs for the bulk atoms. Changing to a simple model increases the bond length about 5% and reduces the binding energy about 13%. The new value for the bonding energy (15.25 kcal/mol) is a very good reproduction of the experimental value, which is commonly assumed to be close to 15 kcal/mol[1]. Both calculations suggest, that the energy to reorientate (E_{UP} and E_{ROT} the water molecule is negligible small. The water molecule seems to rotate freely on the surface. These small energy values also indicate, that the orientational energy, specially E_{UP} is not controlled by the platinum-oxygen bond, but the interactions between the hydrogens and passive surface atoms. Both clusters are too small to take these additional forces into account and it is therefore likely, that with increasing cluster-size (Pt_9) become the orientational energies also larger.

bulk ECP		$18\ e^-$	$1\ e^-$
ECP at the top		LanL2DZ	LanL1MB
d_{PtO}	Å	2.2973	2.4192
γ	deg	141.77	135.18
ΔE_{BOND}	kcal/mol	17.23	15.25
ΔE_{UP}	kcal/mol	0.26	0.41
ΔE_{ROT}	kcal/mol	0.03	0.015*
q_{TOP}	e	−0.203	−0.159
6sPop		0.734	0.534
time**	min	66.0	3.0

* $d_{PtO} = 2.6$ Å

** CPU time of a single point calculation

Table 9.1: $Pt_n - H_2O$ with different ECPs.

Table 9.1 shows, that the 6s population is in the cluster with the new 1 valence electron ECP smaller than the cluster with the LanL2MB ECP at the all platinums. Despite the lower 6s population at the top the platinum-oxygen bond is smaller in the cluster with the new ECP. This exception from the rule can be explained with the different ECPs at the active site. The different ECPs cause different bonds between the metal atoms and the water molecule.

So far only one water molecule was attached to the metal cluster, but our quantum chemical results on $(H_2O)_n$ in chapter 3 showed the dominant role of cooperative forces in the formation of water clusters. The analysis of the platinum-water bond in chapter 6 demonstrated the similarities between the water-water bond and the platinum-water bond, as both bonds are formed by the interaction of fully occupied orbitals and similar effects are therefore likely.

In chapter 8 we focus on large water clusters on metal surfaces to examine these effects. The calculations on $Pt_3 - (H_2O)_3$ showed, that far reaching cooperative forces control the structure of water on Pt(111) surfaces. The classical bilayer model from DOERING and MADEY assumes a seamless transition between the metal and the ice crystal. This plausible model demands hydrogens in the very first water bilayer to point away from the surface ("flip up") and distorsions of this ideal structure are only possible at the edge of the water cluster.

Our calculations on $Pt - (H_2O)_2$ and $Pt_3 - (H_2O)_3$ showed, that these distorsions are essential for the geometry of small water clusters on platinum surfaces. The bonding energy of such misaligned a water molecule in the second layer is therefore increased by two effects:

1. Initial calculations on $Pt - (H_2O)_2$ proofed the existence of strong cooperative forces. The bond between platinum and water is accompanied by a charge transfer from the water

---

[1] Our own rough estimate from the TDS spectrum published a OGASAWRA is 13.7 kcal/mol

molecule to the metal. The second water hydrogen bonding to the first can either pull electrons away from the first or support the first with additional hydrogens. This is the same mechanism observed before in water trimers, which were stabilized by water molecules which accept and donate electrons simultaneously.

2. Our calculations on $Pt_3-(H_2O)_3$ showed, that water molecules with their dipole moment pointig towards the surface are possible at very low water coverages. Electron density flows from the bridging water molecules in the second part of the bilayer via the direct bonding water molecules into the metal cluster. This extra charge cumulates underneath the hydrogens of the bridging water molecule at a passive surface atom. Strong Coulomb interactions between the passive surface atom and the hydrogens of the bridging water molecule can turn the bridging water molecule out of its ideal position.

The bonding energy of a second layer water molecule is stronger than the bonding energy of a water molecule in a surface-ice cluster, but still weaker than the bonding energy of water directly attached to the surface. Cooperative effects as suggested above can explain so the origin of the three peaks observed in TDS experiments.

The second simulation of the large water clusters looked at the cyclic water hexamer on a virtual metal surface. Our calculations agree well on all levels of theory (classical water-water interaction potential from chapter 4, HF and MP2), that the water molecule direct attached to the virtual surface has its molecular plane parallel to the Pt(111) surface. During these calculations were the non-bonding hydrogens of the second layer water molecules forced to stay perpendicular to the virtual metal surface. The formation of ice-like water clusters on metal surfaces is therefore still possible with the molecular planes of the first layer molecules parallel to the surface.

The systematic variation of the surface lattice constant showed, that the orientation of the molecular plane of the water molecule depends very much on the size of the surface lattice constant d_1. In the physically important region $2.5\ \text{Å} \leqq d_1 \leqq 3.0\ \text{Å}$ becomes the water hexamer flater with increasing values of d_1 until the height of the ring levels close to zero for values of d_1 larger than 2.7 Å. Ideal, ice-like clusters are therefore only possible for small surface lattice constants.

Theoretical calculations and experimental results disagree on the orientation of the water molecule on platinum. Any value for γ, the angle between the platinum-oxygen bond and the molecular plane of the water molecule, between 90° and 180° is possible. Our results from the chapters 6 and 7 indicate, that the orientational energies of the water molecule are very small and regardless of the orientation of a single water molecule the water hexamer will orientate the water molecules in the very first layer parallel to the surface.

It is a win-win scenario: Either the water molecule is already parallel to the surface, as extended calculations by MÜLLER suggest, or the water ring of the ice structure will orientate the water molecule parallel to the surface. The water molecule lies always flat on the surface and this orientation does not prohibit the epitaxial growth of more ice layers.

The work on the platinum-water interface does not stop with the end of this thesis and several questions arize from this work, which will be subject of future research subjects.

- The analysis of the water-water interaction potential showed, that the oxygen-oxygen repulsion function $V_{OO}(r)$ is unimportant for the chosen set of dimer geometries. The set of quantum chemical dimer and trimer calculations, which forms the basis for the development of the potential functions, will be enlarged to investigate the role of $V_{OO}(r)$ in equilibrium geometries.

- The size of the platinum clusters used as surface models will be extended to get a better estimate of the influence of the platinum-hydrogen interaction on the adsorption geometry and to analyze the charge transfer in the cluster.
- The water cluster on the virtual metal surface will be extended to ensure, that the parallel water molecules in the first layer are not an artefact of the limited cluster size.
- The research on the cyclic water hexamer showed, the strong cooperative forces can be expected in the water hexamer as part of a water bilayer on a metal surface. In the next step we are going to analyze these forces as a function of the surface lattice constant d_1.
- If possible, we would like to embed quantum chemical calculations on cooperative effects in the water hexamer into a force field to simulate the metal surface. These calculations will hopefully give a first estimate on the influence of the metal cluster on the many-body forces in the water cluster.

The End

Chapter 10

Bibliography

10.1 Cited literature

[1] N. N. Greenwood, A. Earnshaw; Chemie der Elemente; 1^{st} german edition; VCH; Weinheim 1988

  a) page 1196

  b) page 813

  c) page 66

[2] S. Völkening, K. Bedürftig, K. Jacobi, J. Witterlin, G. Ertl; submitted to Phys. Rev. Lett.

[3] K. Bedürftig, S. Völkening, Y. Wang, J. Witterlin, K. Jacobi, G. Ertl; submitted to J. Chem. Phys.

[4] A. T. Capitano, A. M. Gabelnick, J. L. Gland; Surf. Sci. **419** (1999) 104 - 113

[5] G. E. Mitchel, J. M. White; Chem. Phys. Lett. **135** (1987) 84 - 88

[6] H. R. Christen; Grundlagen der allgemeinen und anorganischen Chemie; 9^{th} edition; Salle 1988; page 529

[7] H. Kita, Y. Gao, K. Ohnishi; Chem. Lett. (1994) 73 - 76

[8] G. B. Fisher; Monolayer and Multilayer Adsorption of Water on the Pt(111) Surface; Physical Chemistry Department - General Motors Research Laboratories Warren, Michigan 48090; GMR-4007 PCP-171

[9] J. D. Bernal, R. H. Fowler; J. Chem. Phys. **1** (1933) 515 - 546

[10] R. J. Gillespie, E. A. Robinson; Angew. Chem. **108** (1996) 539 - 560

[11] R. J. Gillespie, I. Bytheway, T.-H. Tang, R. F. W. Bader; Inorg. Chem. **35** (1996) 3954 - 3963

[12] U. Müller; Anorganische Struktur Chemie; Teubener Studienbcher; Stuttgart 1992

[13] L. Pauling; J. Am. Chem. Soc. **57** (1935) 2680 - 2684

[14] E. D. Isaacs, A. Shukula, P. M. Platzman, D. R. Haman, B. Barbiellini, C. A. Tulk; Phys. Rev. Lett. **82** (1999) 600 - 603; Erratum: **83** (1999) 4445

[15] Handbook of Chemistry and Physics; 72nd edition; CRC Press 1991

[16] W. S. Benedict, N. Gailar, E. K. Plyer; J. Chem. Phys. **24** (1956) 1139 - 1165

[17] H. Haken, H. C. Wolf; Molekülphysik und Quantenchemie; Springer Verlag; Berlin 1992

  a) page 60
  b) page 23

[18] H. Engelhardt; Homepage of the Caltech Glaciology Group
http://skua.gps.caltech.edu/hermann/ice.htm

[19] J. P. Cowin, M. J. Iedma; J. Phys. Chem. B. **103** (1999) 8194 - 8194
As a reply to R. W. Whitworth; J. Chem. Phys. B. **103** (1998) 8192 - 8193

[20] M. J. Idema, M. J. Dresser, D. L. Doering, J. B. Rowland, W. P. Hess, A. A. Tsekouras, J. P. Cowin; J. Phys. Chem. B **102** (1998) 9203 - 9214

[21] A. R. West; Solid State Chemistry and its Application; 5th edition; John Wiley & Sons; Chichester 1992; section 15.4 page 540

[22] X. Su, L. Lianos, Y. R. Shen, G. A. Somorjai; Phys. Rev. Lett. **80** (1998) 1533 - 1536

[23] G. M. Barrow; Physikalische Chemie; 6st edition; Friedrich Vieweg & Sohn; Braunschweig 1984

[24] C. H. Haman, W. Vielstich; Elektrochemie I; 2nd edition; VCH Weinheim 1985

  a) section 2.3.5, page 42
  b) section 8.0 - 8.4, pages 149 - 160

[25] J. P. Cowin, A. A. Tsekouras, M. J. Idema, K. Wu, G. B. Ellison; Nature **398** (1999) 405 - 407

[26] H. Witek, V. Buch; J. Chem. Phys. **110** (1999) 3168 - 3175

[27] N. H. Fletcher; Phil. Mag. **7** (1962) 255 - 269
FLETCHER's ice rules are essentially the same as those proposed by BERNAL, FOWLER and PAULING [9, 13]. He also assumed that any orientaion of surface molecules is transmitted through the crystal, which is enegetically unfavourable and that orientated surface molecules are only possible with a thin water film ontop of the ice. WITEK et al. [26] showed that an orientad water molecules et the surface do not orientate all water molecules within the ice crystal.

[28] A. F. Hollemann, E. Wiberg; Lehrbuch der Anorganischen Chemie; 33rd edition; Verlag Walter de Gruyter; Berlin 1985

  a) page 976
  b) page 1208

[29] F. A. Cotton, G. Wilkinson; Advanced Inorganic Chemistry; 5th edition; John Wiley & Sons; New York 1988; page 94

[30] J. K. Sass, K. Kretzschmar, S. Holloway; Vacuum **31** (1981) 483 - 486

[31] E. Spohr; Chem. Phys. Lett. **207** (1993) 214 - 219

[32] S. Trasatti; Electrochim. Acta **36** (1991) 1659 - 1667; and literature cited therein

[33] G. Valettes; J. Electroanal. Chem. **122** (1982) 285 - 301

[34] S.-C. Chang, M. J. Weaver; J. Phys. Chem. **95** (1991) 5391 - 5400

[35] N. Kizhakevarim, X. Jiang, M. J. Weaver; J. Chem. Phys. **100** (1994) 6750 - 6764

[36] L. E. Firment, G.A. Somorjai; J. Chem. Phys. **63** (1975) 1037 - 1038

[37] L. E. Firment, G.A. Somorjai; Surf. Sci. **55** (1976) 413 - 426

[38] P. A. Thiel, T. E. Madey; Surf. Sci. Rep. **7** (1987) 211 - 385

[39] D.L. Doering, T.E. Madey; Surf. Sci. **123** (1982) 305 - 337

[40] L. E. Firment, G. A. Somorjai; Surf. Sci. **84** (1979) 275 - 294

[41] P. A. Thiel, F. M. Hoffmann, W. H. Weinberg; J. Chem. Phys. **75** (1981) 5556 - 5572

[42] T. Lankau, K. Nagorny, I. L. Cooper; Langmuir **15** (1999) 7308 - 7315

[43] F. T. Wagner, T. E. Moylan; Surf. Sci. **191** (1987) 121 - 146

[44] H. Ibach, S. Lehwald; Surf. Sci. **91** (1980) 187 - 197

[45] E. Langenbach, A. Spitzer, H. Lüth; Surf. Sci. **147** (1984) 179 - 190

[46] B. A. Sexton; Surf. Sci. **94** (1980) 435 - 445

[47] W. Hoffmann; Wasseradsorptionsstrukturen auf Ru(0001) und vizinalen Rutheniumoberflächen; Dissertation; University of Hamburg 1999

[48] G. B Fisher, J. L. Gland; Surf. Sci. **94** (1980) 446 - 455

[49] J. N. Miller, D. T. Ling, P. M. Stefan, D. L. Weissman, M. L. Shek, I. Lindau, W. E. Spicer; Phys. Rev, B **24** (1981) 1917 - 1926

[50] D. M. Collins, J. B. Lee, W. E. Spicer; J. Vac. Sci. Technol. **13** (1976) 266 - 268

[51] G. B. Fisher; Chem. Phys. Lett. **79** (1981) 452 - 458

[52] K. Griffiths, D. Bonnet; Surf. Sci. **177** (1986) 169 - 190

[53] M. Morgenstern, T. Michely, G. Cosma; Phys. Rev. Lett. **77** (1996) 703 - 706

[54] M. Morgenstern, J. Müller, T. Michely, G. Cosma; Zeit. f. Phys. Chem. **198** (1997) 43 - 72

[55] G. A. Garwood Jr., A. T. Hubbard; Surf. Sci. **118** (1982) 223 - 247
The authors were not able to observe the adsorption of water on Pt(111) in their experiments with polar solvents, because the temperature was too high (300 K).

[56] H. Ogasawara, J. Yoshinobu, M. Kawai; Chem. Phys. Lett. **231** (1994) 188 - 192

[57] U. Starke, N. Matere, A. Barbieri, R. Dll, K. Heinz, M. A. Van Hove, G. A. Somoja; Surf. Sci. **287/288** (1993) 432 - 437

[58] W. Ranke; Surf. Sci. **209** (1989) 57 - 76

[59] T. Lankau, I. L. Cooper; submitted to J. Phys. Chem.

[60] A. B. Anderson; Surf. Sci. **105** (1981) 159 - 176

[61] A. B. Anderson, N. K. Ray; J. Phys. Chem. **86** (1982) 488 - 494

[62] C. W. Bauchlicher; J. Chem. Phys. **83** (1985) 3129 - 3133

[63] H. P. Bonzel, G. Pirug, J. E. Müller; Phys. Rev. Lett. **58** (1987) 2138 - 2141

[64] S. Holloway, K.H. Bennemann; Surf. Sci. **101** (1980) 327 - 333

[65] G. Estiu, S. A. Maluendes, E. A. Castro, A. J. Arvia; J. Phys. Chem. **92** (1988) 2512 - 2516

[66] B. C. Khanra; Chem. Phys. Lett. **84** (1981) 107 - 110

[67] An. M. Kuznetsov, R. R. Nazmutdinov, M. S. Shapnik; Electrochimica Acta **34** (1989) 1821 - 1828

[68] J. E. Müller; Appl. Phys. A **49** (1989) 681 - 690

[69] J. E. Müller, J. Harris; Phys. Rev. Lett. **53** (1984) 2493 - 2496

[70] J. E. Müller; Surf. Sci. **178** (1986) 589 - 607

[71] M. W. Ribarsky, W. D. Luedtke, U. Landman; Phys. Rev. B **32** (1985) 1430 - 1433

[72] H. Yang, J. L. Whitten; Surf. Sci. **123** (1989) 131 - 150

[73] M. Kiskinova, G. Pirug, H. P. Bonzel; Surf. Sci. **150** (1985) 319 - 338

[74] T. E. Madey, J. T. Yates, Jr.; Chem. Phys. Lett. **51** (1977) 77 - 83

[75] J. N. Miller, I. Lindau, W. E. Spicer; Surf. Sci. **111** (1981) 595 - 608

[76] J. R. Creighton, J. M. White; Surf. Sci. **122** (1982) L648 - L652

[77] J. R. Creighton, J. M. White; Surf. Sci. **136** (1984) 449 - 462

[78] G. B. Fischer, B. A. Sexton; Phys. Rev. Lett. **44** (1980) 683 - 686

[79] C. E. Mooney, L. C. Anderson, J. H. Lunsford; J. Phys. Chem. **97** (1993) 2505 - 2506

[80] N. G. Parsonage, D. Nicholson; J. Chem. Soc. Faraday Trans. 2 **82** (1986) 1521 - 1535

[81] N. G. Parsonage, D. Nicholson; J. Chem. Soc. Faraday Trans. 2 **83** (1987) 663 - 673

[82] J. P. Valleau, A. A. Gardner; J. Chem. Phys. **86** (1987) 4162 - 4170
This article provides the background for ref. 83.

[83] A. A. Gardner, J. P. Valleau; J. Chem. Phys. **86** (1987) 4171 - 4176

[84] A. Kohlmeyer, W. Witschel, E. Spohr; Chem. Phys. **213** (1996) 211 - 216

[85] K. C. Foster; "Molecular Dynamics Simulation of Water between Platinum Walls" Dissertation; Ann Abor, University Microfilms Internamional MI 1991

[86] J. Böcker, E. Spohr, K. Heinzinger; Z. Naturforsch. **50a** (1995) 611 - 612

[87] G. Nagy, K. Heinzinger; J. Electroanl. Chem. **296** (1990) 549 - 558

[88] G. Nagy, K. Heinzinger; J. Electroanl. Chem. **327** (1992) 25 - 30

[89] O. Pecina, W. Schmickler, E. Spohr; J. Electroanl. Chem. **394** (1995) 29 - 34

[90] E. Spohr, G. Tóth, K. Heinzinger; Electrochim. Acta **41** (1996) 2131 - 2144

[91] J. Hautman, J. W. Halley, Y.-J. Rhee; J. Chem. Phys. **91** (1989) 467 - 472

[92] S.-B. Zhu, G. W. Robinson; J. Chem. Phys; **94** (1991) 1403 - 1410

[93] S.-B. Zhu, M. R. Philpott; J. Chem. Phys. **100** (1994) 6961 - 6968

[94] K. Heinzinger, E. Spohr; Electrochim. Acta **34** (1989) 1849 - 1856

[95] E. Spohr, K. Heinzinger; Ber. Bunsenges. Phys. Chem. **92** (1988) 1358 - 1363

[96] E. Spohr; J. Phys. Chem. **93** (1993) 6171 - 6180

[97] K. Foster, K. Raghavan, M. Berkowitz; Chem. Phys. Lett. **162** (1989) 32 - 38

[98] K. Raghavan, K. Foster, K. Motakabbir, M. Berkowitz; J. Chem. Phys. **94** (1991) 2110 - 2117

[99] E. Spohr; Acta. Chim. Scand. **49** (1995) 189 - 202

[100] E. Spohr; Computer Simulation of the Structure and Dynamics of Water Near Metal Surfaces; ACS Symposium Series 656 Solid-Liquid Electrochemical Interfaces; chapter 3 pages 32 - 44

[101] E. Spohr; Computer Modelling of Aqueous/Metallic Interfaces; Habilitationsschrift University Ulm; 1995

[102] E. Spohr; Chem. Phys. **141** (1990) 87 - 94

[103] K. Liu, J. D. Cruzan, R. J. Saykally; Science **271** (1996) 929 - 933

[104] Morokuma, L. Pedersen; J. Chem. Phys. **48** (1968) 3275 - 3282

[105] G. Alagona, C. Ghio, R. Cammi, J. Tomasi; Int. J. Quant. Chem. **32** (1987) 207 - 226

[106] G. Alagona, C. Ghio, R. Cammi, J. Tomasi; Int. J. Quant. Chem. **32** (1987) 227 - 248

[107] J. Del Bene, J. A. Pople; J. Chem. Phys. **52** (1970) 4858 - 4866

[108] J. Del Bene, J. A. Pople; J. Chem. Phys. **58** (1973) 3605 - 3608

[109] H. J. C. Berendsen, J. R. Grigera, T. P. Straatsma; J. Phys. Chem. **91** (1987) 6269 - 6271

[110] S. J. Chakravotry, E. R. Davidson; J. Phys. Chem. **97** (1993) 6373 - 6383

[111] H.-Y. Chen, W.-S. Sheu; J. Chem. Phys. **110** (1999) 9032 - 9038

[112] J. G. C. M. van Duijneveldt-van de Ridjt, F. B. van Duijneveldt; J. Chem. Phys. **97** (1992) 5019 - 5030

[113] D. Feller; J. Chem. Phys. **96** (1992) 6104 - 6114

[114] M. J. Frisch, J. E. Del Bene, J. S. Binkley, H. F. Schaefer III; J. Chem. Phys. **84** (1986) 2279 - 2289

[115] D. Hankins, J. W. Moskowitz, F. H. Stillinger; J. Chem. Phys. 53 (1970) 4544 - 4554

[116] W. L. Jorgensen, J. Chandrasekhar, J. D. Madura, R. W. Impey, M. L. Klein; J. Chem. Phys. **79** (1983) 926 - 935

[117] W. L. Jorgensen; J. Chem. Phys. **77** (1982) 4156 - 4163

[118] K. S. Kim, B. J. Mhin, U-S. Choi, K. Lee; J. Chem. Phys. **97** (1992) 6649 - 6662

[119] H. Kistenmacher, G. C. Lie, H. Popkie, E. Clementi; J. Chem. Phys. **61** (1974) 546 - 561

[120] H. Popkie, H. Kistenmacher, E. Clementi; J. Chem. Phys. **59** (1973) 1325 - 1336

[121] O. Matsuoka, E. Clementi, M. Yoshimine; J. Chem. Phys. **64** (1976) 1351 - 1361

[122] M. D. Newton, N. R. Kestner; Chem. Phys. Lett. **94** (1983) 198 - 201

[123] S. Saebø, P. Pulay; J. Chem. Phys. **88** (1988) 914 - 922

[124] S. Saebø, W. Tong, P. Pulay; J. Chem. Phys. **98** (1993) 2170 - 2175

[125] S. Scheiner; Annu. Rev. Phys. Chem. **34** (1994) 23 - 56

[126] F. H. Stillinger, A. Rahman; J. Chem. Phys. **60** (1974) 1545 - 1557

[127] H. Umeyama, K. Morokuma; J. Am. Chem. Soc. **99** (1977) 1316 - 1332

[128] S. S. Xantheas, T. H. Dunning, Jr.; J. Chem. Phys. **99** (1993) 8774 - 8792

[129] S. Yamabe, K. Morokuma; J. Am. Chem. Soc. **97** (1975) 4458 - 4465

[130] B. J. Yoon, K. Morokuma, E. R. Davidson; J. Chem. Phys. **83** (1985) 1223 - 1231

[131] E. Honegger, S. Leutwyler; J. Chem. Phys. **88** (1988) 2582 - 2595

[132] M. Schütz, T. Bürgi, S. Leutwyler, H. B. Bürgi; J. Chem. Phys. **99** (1993) 5228 - 5238; Erratum: J. Chem. Phys. **100** (1994) 1780

[133] B. R. Lentz, H. A. Scheraga; J. Chem. Phys. **58** (1973) 5296 - 5308

[134] G. C. Groenenboom, E. M. Mas, R. Bukowski, K. Szalewicz, P. E. S. Wormer, A. v. d. Arvoid; Phys. Rev. Lett. **84** (2000) 4072 - 4075

[135] T. Bürgi, S. Graf, S. Leutwyler, W. Klopper; J. Chem. Phys. **103** (1995) 1077 - 1084

[136] D. Sabo, Z. Bačić, T. Bürgi, S. Leutwyler; Chem. Phys. Lett. **224** (1995) 283 - 294

[137] D. J. Wales; J. Am. Chem. Soc. **115** (1993) 11180 - 11190

[138] C. J. Tsai, K. D. Jordan; J. Phys. Chem. **97** (1993) 11227 - 11237

[139] D. F. Coker, R. E. Miller, R. O. Watts; J. Chem. Phys. **82** (1985) 3554 - 3562

[140] J. G. C. M. van Duijneveldt-van de Ridjt, F. B. van Duijneveldt; Chem. Phys. **175** (1993) 271 - 281

[141] A. Engdahl, B. Nelander; J. Chem. Phys. **86** (1987) 4831 - 4837

[142] J. E. Fowler, H. F. Schaefer; J. Am. Chem. Soc. **117** (1995) 446 - 452

[143] R. Fröchtenicht, M. Kaloudis, M. Koch, F. Huisken; J. Chem. Phys. **105** (1996) 6128 - 6140

[144] W. Klopper, M. Schütz, H. P. Lüthi, S. Leutwyler; J. Chem. Phys. **103** (1995) 1085 - 1098

[145] O. Mó, M. Yáñez, J. Elguero; J. Chem. Phys. **97** (1992) 6628 - 6638

[146] I. M. B. Nielsen, E. T. Seidl, C. L. Janssen; J. Chem. Phys. **110** (1999) 9435 - 9442

[147] S. S. Xantheas, T. H. Dunning, Jr.; J. Chem. Phys. **98** (1993) 8037 - 8040

[148] S. S. Xantheas; J. Chem. Phys. **100** (1994) 7523 - 7534

[149] S. S. Xantheas; J. Chem. Phys. **102** (1995) 4505 - 4517

[150] K. Liu, M. J. Elrod, J. G. Loesser, J. D. Cruzan, N. Pugliano, M. G. Brown, J. Rzepiela, R. J. Saykally; Farraday Discuss. **97** (1994) 35 - 41

[151] J. K. Gregory, D. C. Clary; J. Chem. Phys. **102** (1995) 7871 - 7829

[152] J. K. Gregory, D. C. Clary; J. Chem. Phys. **103** (1995) 8924 - 8930

[153] J. C. Owicki, L. L. Shipman, H. A. Sheraga; J. Phys. Chem. **79** (1994) 1794 - 1811

[154] N. Pugliano, R. J. Saykally; Science **257** (1992) 1937 - 1940

[155] M. R. Viant, M. G. Brown, J. D. Cruzan, R. J. Saykally, M. Geleijns, A. v. d. Arvoid; J. Chem. Phys. **110** (1999) 4369 - 4381

[156] D. J. Wales; Science **271** (1996) 925 - 929

[157] Chałasiński, M. M. Szczęśniak, P. Cieplak, S. Scheiner; J. Chem. Phys. **94** (1991) 2873 - 2883

[158] J. G. C. M. van Duijneveldt-van de Ridjt, F. B. van Duijneveldt; Chem. Phys. Let. **237** (1995) 560 - 567

[159] M. Tachikawa, K. Iguchi; J. Chem. Phys. **101** (1994) 3062 - 3072

[160] J. Rodriguez, D. Laria, E. J. Marceca, D. A. Estrin; J. Chem. Phys. **110** (1999) 9039 - 9047

[161] M. G. Brown, F. N. Keutsch, R. J. Saykally; J. Chem. Phys. **109** (1998) 9645 - 9647

[162] L. R. Corrales; J. Chem. Phys. **110** (1999) 9071 - 9080

[163] J. D. Cruzan, L. B. Braly, K. Liu, M. G. Brown, R. J. Saykally; Science **271** (1996) 59 - 62

[164] K. Liu, M. G. Brown, J. R. Saykally; **271** (1996) 62 - 64

[165] T. Loerting, K. R. Liedl, B. M. Rode; J. Chem. Phys. **109** (1998) 2672 - 2679

[166] G. N. Merrill, M. S. Gordon; J. Phys. Chem. A **102** (1998) 2650 - 2657

[167] D. J. Wales, T. R. Walsh; J. Chem. Phys. **106** (1997) 7193 - 7207

[168] F. Huiskens, M. Kaloudis, A. Kulcke; J. Chem. Phys. **104** (1996) 17 - 25

[169] J. B. Paul, R. A. Provencal, C. Chapo, A. Petterson, R. J. Saykally; J. Chem. Phys. **109** (1998) 10201 - 10206

[170] J. M. Ugalde, I. Alkorta, J. Elguero; Angew. Chem. **112** (2000) 733 - 737

[171] J. Brudermann, M. Melzer, U. Buck, J. K. Kazimirzki, J. Sadlej, V. Bush; J. Chem. Phys. **110** (1999) 10649 - 10652

[172] U. Buck, I. Ettischer, M. Melzer, V. Bush, J. Sadlej; Phys. Rev. Lett. **80** (1998) 2578 - 2581

[173] C. J. Burnham, J. Li, S. S. Xantheas, M. Leslie; J. Chem. Phys. **110** (1999) 4566 - 4581

[174] S. McDonald, L. Ojamäe, S. J. Singer; J. Phys. Chem. A **102** (1998) 2824 - 2831

[175] J. C. Jiang, J.-C. Chang, B.-C. Wang, S. H. Lin, Y. T. Lee, H.-C. Chang; Chem. Phys. Lett. **289** (1998) 373 - 382

[176] J. Kim, D. Majumdar, H. M. Lee, K. S. Kim; J. Chem. Phys. **110** (1999) 9128 - 9134

[177] P. Nigra, S. Kais; Chem. Phys. Lett. **305** (1999) 433 - 438

[178] D. J. Wales, M. P. Hodges; Chem. Phys. Lett. **286** (1998) 65 - 72

[179] J. Kim, K. S. Kim; J. Chem. Phys. **109** (1998) 5886 - 5895

[180] B. J. Mhin, J. Kim, S. Lee, J. Y. Lee, K. S. Kim; J. Chem. Phys. **100** (1993) 4484 - 4486

[181] B. J. Mhin, H. S. Kim, H. S. Kim, C. W. Yoon, K. S. Kim; Chem. Phys. Lett. **176** (1991) 41 - 45

[182] C. J. Tsai, K. D. Jordan; Chem. Phys. Lett. **213** (1993) 181 - 188

[183] E. M. Schulson; JOM **51** (1999) 21 - 27
http://www.tms.org/pub/journals/JOM/9902/Schulson-9902.html

[184] D. Belford, E. S. Campbell; J. Chem. Phys **80** (1984) 3288 - 3296

[185] A. C. Belch, S. A. Rice; J. Chem. Phys. **86** (1987) 5676 - 5682

[186] K. Liu, M. G. Brown, C. Carter, R. J. Saycally, J. K. Gregory, D. C. Clary; Nature (London) **381** (1969) 501 - 503

[187] K. Nauta, R. E. Miller; Science **287** (2000) 293 - 295

[188] J. M. Pedulla, K. Kim, K. D. Jordan; Chem. Phys. Lett. **291** (1998) 78 - 84

[189] P. J. Hay, W. R. Wadt; J. Chem. Phys. **82** (1985) 299 - 310

[190] D. M. Hirst; A Computational Approach to Chemistry; 1^{st} edition; Blackwell Scientific Publications; Oxford 1990

[191] L. Zülicke; Quantenchemie - Band 2; Dr. Alfred Hüthig Verlag; Heidelberg 1985

[192] L. Zülicke; Quantenchemie - Band 1; Dr. Alfred Hüthig Verlag; Heidelberg 1978

[193] M. W. Hanna; Quantenmechanik in der Chemie; 1^{st} edition; Steinkopf; Darmstadt 1976

[194] F. Schwabl; Quantenmechanik; Springer Verlag; 4^{th} edition; Berlin 1993

  a) page 227
  b) page 205
  c) page 263 and following pages
  d) page 65

[195] R. J. Bartlett; Ann. Rev. Phys. Chem. **32** (1981) 359 - 401

[196] Chr. Møller, M. S. Plesset; Phys. Rev. **46** (1934) 618 - 622

[197] R. E. Christoffersen; Basic Principles and Techniques of Molecular Quantum Mechanics; Springer; New York 1991

[198] R. J. Bartlett; J. Phys. Chem. **93** (1989) 1697 - 1708

[199] P. A. Christiansen, Y.S. Lee, K.S. Pitzer; J. Chem. Phys. **71** (1979) 4445 - 4450

[200] P. Saxe, H.F. Schaefer, N.C. Handy; Chem. Phys. Lett. **79** (1981) 202 - 204

[201] W. J. Hehre, L. Radon, P. v. R. Schleyer, J. A. Pople; Ab Initio Molecular Theory; John Wiley & Sons; New York 1986

[202] GAMESS UK manual
http://tc5.chem.ruu.nl/Gamess0Manual/Gamess-Manual.xmosaic/Gamess0index.html

[203] CHEMISTRY@osc.edu

[204] S. F. Boys, F. Bernardi; Mol. Phys. **19** (1970) 553 - 566

[205] J. P. Daudey, J. P. Malrieu, O. Rojas; Int. J. Quant. Chem. **8** (1974) 17 - 28

[206] N. S. Ostlund, D. L. Merrifield; Chem. Phys. Lett. **39** (1976) 612 - 614

[207] J. R. Collins, G. A. Gallup; Chem. Phys. Let. **123** (1986) 56 - 61

[208] S. Scheiner; Molecular Interactions - From van der Waals to Srongly Bound Complexes; Wiley; Cichester 1997

  a) F.B. van Duijneveldt; Basis Set Superposition Error; page 81 - 104
  b) A. Karpfen; Case Studies in Cooperativity in Hydrogen Bonded Clusters and Polymers; page 265 - 296
  c) K. Szalewicz, B. Jeziorski; Symmetry adapted perturbation theory of molecular interactions; page 3 - 44

d) M. M. Szczęśniak, Chałasiński; Ab Initio Studies of Nonadditive Interactions; page 45 - 79

e) J.E. Del Bene, I. Shavitt, The quest of reliability in calculated properties of hydrogen-bonded complexes; page 157 - 180

[209] M. J. Elrod, R. J. Saykally; Chem. Rev. **94** (1994) 1975 - 1997

[210] S. Iwata, K. Morokuma; J. Am. Chem. Soc. **95** (1973) 7563 - 7486

[211] K. Morokuma; J. Chem. Phys. **55** (1971) 1236 - 1244

[212] K. Kitaura, K. Morokuma; Int. J. Quant. Chem. **10** (1976) 325 - 340

[213] GAMESS US manual

[214] P. J. Hay, W. R. Wadt; J. Chem. Phys. **82** (1985) 270 - 283

[215] P. J. Hay, W. R. Wadt; J. Chem. Phys. **82** (1985) 284 - 298

[216] J.C. Phillips, L. Kleinman; Phys. Rev. **116** (1959) 287 - 294

[217] J. D. Weeks, A. Hazi, S.A. Rice; Adv. Chem. Phys. **16** (1969) 283 - 342

[218] J. D. Weeks, S. A. Rice; J. Chem. Phys. **49** (1968) 2741 - 2755

[219] L. R. Kahn, P. Baybutt, D.G. Truhlar; J. Chem. Phys. **65** (1976) 3828 - 3853

[220] P. J. Hay, W. R. Wadt, L.R. Kahn; J. Chem. Phys. **68** (1978) 3059 - 3066

[221] L. R. Kahn, P.J. Hay, R.D. Cowan; J. Chem. Phys. **68** (1978) 2386 - 2397

[222] Gaussian 94 manual supplied with the code

[223] A. Messiah; Quantenmechanik 1; de Gruyter; 2$^{\mathrm{nd}}$ edition; Berlin 1991

[224] A. Messiah; Quantenmechanik 2; de Gruyter; 3$^{\mathrm{rd}}$ edition; Berlin 1990

[225] W. C. Ermler, Y. S. Lee, K. S. Pitzner, N. W. Winter; J. Chem. Phys. **69** (1978) 976 - 983

[226] W. R. Wadt, P. J. Hay, L. R. Kahn; J. Chem. Phys. **68** (1978) 1752 - 1759

[227] P. J. Hay, W. R. Wadt, L. R. Kahn, F. W. Bobrowicz; J. Chem. Phys. **69** (1978) 984 - 997

[228] L. D. Landau, E. M. Lifshitz; Quantum Mechanics (Nonrelativistic Theory); 3$^{\mathrm{rd}}$ edition; Pergamon Press; Oxford 1977; §79

[229] A. Gilbert, J. Baggot; Essentials of Molecular Photochemistry; Blackwell Scientific Publications; Oxford 1991

[230] C. J. Böttcher; Theory of Electric Polarisation; Vol. I; 2 nd edition; Elsevier; Amsterdam 1973

[231] Ä. Heyl, P. Botschwina; Theoretische Untersuchungen an HCN-Dimeren; poster contribution to the Bunsentagung 1997 in Darmstadt

[232] D. A. Smith, M. E. Mura; J. Phys. Chem. **98** (1994) 6903 - 6905

[233] A. D. Buckingham; Adv. Chem. Phys. **12** (1967) 107 - 142

[234] T. H. Dunning Jr; J. Chem. Phys. **90** (1989) 1007 - 1023

[235] R. W. Kunz; Molecular Modeling fr Anwendner; 1st edition; Teubner Studienbcher; Stuttgart 1991

[236] M. Scholz, H.-J. Köhler; Quantenchemie - Band 3; Dr. Alfred Hüthig Verlag; Heidelberg 1981

[237] S. Scheiner; J. Mol. Struc. (Thoechem) **256** (1992) 1 - 16

[238] S. M. Cybulski, S. Scheiner; J. Phys. Chem. **93** (1989) 6565 - 6574

[239] L. A. Curtiss, D. J. Frurip, M. Blander; J. Chem. Phys. **71** (1979) 2703 - 2711

[240] D. Young, J. F. Harrison; Lone Pairs and Molecular Electrostatic Potentials of Water; http://www.auburn.edu/~yound2/water/lp3.html

[241] F. B. van Duijneveldt, J. G. C. M. van Duijneveldt-van de Ridjt, J. H. van Lenthe; Chem. Rev. **94** (1994) 1873 - 1885

[242] W. H. Press, B. P. Flannery, S. A. Teukolsky, W. T. Vetterling; Numerical Recipes in Pascal; Cambridge University Press; Cambridge 1989

[243] T. R. Dyke, J.S. Muenter; J. Chem. Phys. **57** (1972) 5011 - 5012

[244] S. Wuelfert, D. Herren, S. Leutwyler; J. Chem. Phys. **86** (1987) 3751 - 3753

[245] W. B. Bosma, L. E. Fried, S. Mukamel; J. Chem. Phys. **98** (1993) 4413 - 4421

[246] M. W. Evans, G. C. Lie, E. Clementi; J. Chem. Phys. **87** (1987) 6040 - 6045

[247] M. W. Evans, G. C. Lie, E. Clementi; J. Chem. Phys. **88** (1988) 5157 - 5165

[248] I. Ohmine, H. Tanaka, P. G. Wolynes; J. Chem. Phys. **89** (1988) 5852 - 5860

[249] M. A. Wilson, A. Pohorille, L. R. Pratt; J. Phys. Chem. **91** (1987) 4873 - 4878

[250] M. A. Wilson, A. Pohorille, L. R. Pratt; J. Phys. Chem. **88** (1988) 3281 - 3285

[251] F. H. Stillinger, A. Rahman; J. Chem. Phys. **68** (1978) 666 - 670

[252] J. Brodholt, M. Sampoli, R. Vallauri; Mol. Phys. **85** (1995) 81 - 90

[253] I. Borzák, P. T. Cummings; Chem. Phys. Lett. **300** (1999) 359 - 363

[254] M. Reddy, M. Berkowitz; Chem. Phys. Lett. **155** (1989) 173 - 176

[255] I. M. Svishchev, P. G. Kusalik; J. Phys. Chem. **98** (1994) 728 - 733

[256] W. L. Jorgensen; J. Am. Chem. Soc. **103** (1981) 335 - 340

[257] F. H. Stillinger, C. W. David; J. Chem. Phys. **69** (1978) 1473 - 1484

[258] E. Clementi, G. Corongiu, F. Sciortino; J. Mol. Struc. **296** (1993) 205 - 213

[259] U. Niesar, G. Corongiu, E. Clementi, G. R. Kneller, D. K. Bhattacharya; J. Phys. Chem. **94** (1990) 7949 - 7956

[260] G. Dueck, T. Scheuer, H.M. Wallmeier; Spektrum der Wissenschaft; Mar. 1993; page 42 - 51

[261] S. Kirkpatrik, K. D. Gelatt, M. P. Vecchi; Sience **220** (1983) 671 - 680

[262] T. Lankau; "Simulated Annealing zur Auswertung von Mößbauerspektren mit verteilten Parametern"; degree's dissertation; Hamburg 1994

[263] T. Lankau, S. Bieber, K. Nagorny; Ber. Bunsenges. Phys. Chem. **102** (1998) 775 - 779

[264] N. Metropolis, A. W. Rosenbluth, M. N. Rosenbluth, A. H. Teller; J. Chem. Phys. **21** (1953) 1087 - 1092

[265] T. Otto; c't; Jan. 1994; pages 188 - 194

[266] E. E. Tucker; Anal. Chem. **64** (1992) 1199 - 1200

[267] J. M. Sutter, J. H. Kalivas; Anal. Chem. **63** (1991) 2383 - 2386

[268] E. M. Corey, D. A. Young; Comp. in Phys. May/June (1989) 33 - 37

[269] J. Stoer; Numerische Mathematik I; 5th edition; Springer Lehrbuch; Berlin 1989

[270] V. Sreedhara Kao, A. K. Chandra; Chem. Phys. **214** (1997) 103-112

[271] L. C. Cusachs, J. W. Reynolds; J. Chem. Phys. **43** (1956) S160 - S164

[272] L. C. Cusachs; J. Chem. Phys. **43** (1956) S157 - S159

[273] E. Heilbronner, H. Bock; Das HMO-Modell und seine Anwendung - Grundlagen und Handhabung; Verlag Chemie; Weinheim 1968

[274] E. Heilbronner, H. Bock; Das HMO-Modell und seine Anwendung - Übungsbeispiele und Lösungen; Verlag Chemie; Weinheim 1968

[275] E. Heilbronner, H. Bock; Das HMO-Modell und seine Anwendung - HMO Tabellen; Verlag Chemie; Weinheim 1968

[276] F. Marschner; Quantenchemie mit Personal Computern; Verlag Walter der Gruyter; New York 1991

[277] M. Wolfsberg, L. Helmholtz; J. Chem. Phys. **20** (1952) 837 - 843

[278] W. Haberditzel; Quantenchemie - Band 4; Dr. Alfred Hüthig Verlag; Heidelberg 1979

[279] R. Hoffmann, W.N. Lipscomb; J. Chem. Phys. **37** (1962) 2872 - 2883

[280] R. Hoffmann, W.N. Lipscomb; J. Chem. Phys. **36** (1962) 3489 - 3493

[281] R. Hoffmann, W.N. Lipscomb; J. Chem. Phys. **36** (1962) 2179 - 2189

[282] A. B. Anderson, R. Hoffmann; J. Chem. Phys. **61** (1974) 4545 - 4549

[283] R. C. Baetzold; J. Chem. Phys. **55** (1971) 4355 - 4363

[284] R. C. Baetzold; J. Chem. Phys. **55** (1971) 4363 - 4370

[285] B. Bigot, C. Minot; J. Am. Chem. Soc. **106** (1984) 6601 - 6615

[286] C. Minot, M. A. van Hove, G. A. Somorjai; Surf. Sci. **127** (1982) 441 - 460

[287] A. Juan, R. Hoffmann; Surf. Sci. **421** (1999) 1 - 16

[288] R. S. Mulliken; J. Chem. Phys. **23** (1955) 1833 - 1840

[289] R. S. Mulliken; J. Chem. Phys. **23** (1955) 1841 - 1846

[290] R. S. Mulliken; J. Chem. Phys. **23** (1955) 2338 - 2342

[291] R. S. Mulliken; J. Chem. Phys. **23** (1955) 2343 - 2346

[292] K. M. Ervin, J. Ho, W. C. Lineberger; J. Chem. Phys. **89** (1988) 4514 - 4521

[293] F. A. Cotton; Chemical Application of Group Theory; 3rd edition; John Wiley & Sons; New York 1990

  a) chapter 9, 253 - 303
  b) chapter 6, 114 - 129

[294] I. B. Bersuker; Coord. Chem. Rev. **14** (1975) 357 - 412

[295] R. Mc Weeny; Coulsons chemische Bindung; 2nd edition; S. Hirzel Verlag 1984; chapter 9.6

[296] R. Ahlrichs, S. D. Elliot; Phys. Chem. Chem. Phys. **1** (1999) 13 - 21

[297] E. Clementi, D. L. Raimondi; J. Chem. Phys, **38** (1963) 2686 - 2689

[298] F. E. Harris, H. H. Michels; J. Chem. Phys. **43** (1965) S165 - S169

[299] J. L. Whitten, L. C. Allen; J. Chem. Phys. **43** (1965) S170 - S171

[300] H.-J. Glaeske, J. Reinhold, P. Volkmer; Quantenchemie - Band 5; Dr. Alfred Hüthig Verlag; Heidelberg 1987

[301] S. Wolfram; Mathenatica - A System for Doing Mathematics by Computer; 2nd edition; Addison-Wesley Publishing Company; Redwood City California 1991

[302] C. F. Mellius, T. H. Upton, W. A. Goddard III; Solid State Commun. **28** (1978) 501 - 504

[303] A. Gavezotti, G. F. Tandardini, H. Miesner; J. Phys. Chem. **92** (1988) 872 - 878

[304] G. Landrum; http://overlap.chem.cornell.edu:8080/yehmop.html (1997)

[305] B. A. Heß; Ber. Bunsenges. Phys. Chem. **101** (1997) 1 - 10

[306] C. McMichael Rohlfing, P.J. Hay, R.L. Martin; J. Chem. Phys. **85** (1986) 1447 - 1455

  a) C.E. Moore; Atomic Energy Levels; Natl. Bur. Stand. Circ. 467 (US, GPO, Washington, DC, (1952) according to [306]

[307] H. Basch, S. Topiol; J. Chem. Phys. **71** (1979) 802 - 814

[308] A. Gavezotti, G. F. Tandardini, M. Simonetta; Chem. Phys. Lett. **129** (1986) 577 - 581

[309] S. W. Wang, K. S. Pitzer; J. Chem. Phys. **79** (1983) 3851 - 3858

[310] W. J. Kaufmann, L. S. Smarr; Simulierte Welten; Spektrum Akademischer Verlag; 1st edition; Heidelberg 1994, page 125

[311] M. Reiher, P. A. Netz; Chemie in unserer Zeit **33** (1999) 177 - 185

[312] S. Roszak, K. Balasubramanian; J. Phys. Chem. **97** (1993) 11238 - 11241

[313] K. Balasubramanian; J. Chem. Phys. **87** (1987) 2800 - 2805

[314] K. Balasubramanian, P. Y. Feng; J. Chem. Phys. **92** (1990) 541 - 550

[315] K. G. Dyall; J. Chem. Phys. **98** (1993) 9678 - 9686

[316] T. Fleig, C. M. Marian; Chem. Phys. Lett. **222** (1994) 267 - 273

[317] L. Visscher, T. Saue, W. C. Nieuwpoort, K. Faegri, O. Gropen; J. Chem. Phys. **99** (1993) 6704 - 6715

[318] S. Zurita, J. Rubio, F. Illas, J. C. Barthelat; J. Chem. Phys. **104** (1996) 8500 - 8506

[319] P. Messmer, D. R. Salahub, K. H. Johnson, C. Y. Yang; Chem. Phys. Lett. **51** (1977) 84 - 89

[320] C. Minot, B. Bigot, A. Hariti; J. Am. Chem. Soc. **108** (1986) 196 - 206

[321] National Institut of Standards (NIST), Constant of Diatomic Molecules http://webbook.nist.gov/cgi/cbook (Querry for PtH)

[322] K. Christmann, G. Ertl, T. Pignet; Surf. Sci. **54** (1976) 365 - 392

[323] T. Kubota, K. Asakura, N. Ichikani, Y. Iwasawa; Chem. Phys. Lett. **256** (1996) 445 - 448

[324] K. Balasubramanian; J. Chem. Phys. **87** (1987) 6573 - 6578

[325] K. Balasubramanian; J. Chem. Phys. **94** (1991) 1253 - 1263

[326] S. Roszak, K. Balasubramanian; J. Chem. Phys. **103** (1995) 1043 - 1049

[327] F. Illas, S. Zurita, A. M. Márquez, J. Rubio; Surf. Sci. **376** (1997) 279 - 296

[328] F. Illas, S. Zurita, J. Rubio, A.M. Márquez; Phys. Rev. B **52** (1995) 12372 - 12379

[329] F. Illas, J. Rubio, J.M. Ricart, J.P. Daudey; J. Chem. Phys. **93** (1990) 2521 - 2529

[330] J. M. Ricart, A. Cloet, F. Illas, J. Rubio; J. Chem. Phys. **100** (1994) 1988 - 1994

[331] J. M. Ricart, J. Rubio, F. Illas, P.S. Bagus; Surf. Sci. **304** (1994) 335 - 342

[332] M. D. Morse; Chem. Rev. **86** (1986) 1049 - 1109

[333] W. Weltner Jr., R. J. Van Zee; Ann. Rev. Phys. Chem. **35** (1984) 291 - 327

[334] G. Ertl, J. Küppers; Low Energy Electrons and Surface Chemistry; 2nd edition; VCH Weinheim 1985

  a) section 4.4.1, 109 - 110

  b) approximate value read from figure 4.15, page 109

[335] J.E. Demuth; Surf. Sci. **65** (1977) 639 - 375

[336] B.O. Roos (Ed.); Lecture Notes in Quantum Chemistry; Springer Verlag; 1st edition; Berlin 1992

  a) B.O. Roos, The Multiconfigurational (MC) Self-Consistent Field (SCF) Theory; pp. 190 - 191

  b) B.O. Roos, The Multiconfigurational (MC) Self-Consistent Field (SCF) Theory; pp. 239 - 240

[337] H. Wang, E. A. Carter; J. Chem. Phys. **96** (1992) 1197 - 1204

[338] D. Dai, D. W. Liao, K. Balasubramanian; J. Chem. Phys. **102** (1995) 7530 - 7539

[339] D. Dai, K. Balasubramanian; J. Phys. Chem. **96** (1992) 3279 - 3282

[340] P. S. Bagus, C. W. Bauschlicher Jr., C. J. Nelin, B. C. Laskowski, M. Seel; J. Chem. Phys. **81** (1984) 3594 - 3602

[341] J. Sauer; Chem. Rev. **89** (1989) 199 - 255; section IV.C pp. 216 - 218

[342] P. S. Bagus, W. Müller; Chem. Phys. Lett. **115** (1985) 540 - 544

[343] K. Hermann, P. S. Bagus, C. J. Nelin; Phys. Rev. B **35** (1987) 9467 - 9473

[344] J. M. Ricart, J. Torras, F. Illas, J. Rubio; Surf. Sci. **307-309** (1994) 107 - 112

[345] J. Torras, J. M. Ricart, F. Illas, J. Rubio; Surf. Sci. **297** (1993) 57 - 65

[346] U. Wahlgren, L. G. M. Petterson, P. Siegbahn; J. Chem. Phys. **90** (1989) 4613 - 4616

[347] I. Panas, J. Schüle, P. Siegbahn, U. Wahlgren; Chem. Phys. Lett. **149** (1988) 265 - 272

[348] P. E. M. Siegbahn, L. G. M. Petterson, U. Wahlgren; J. Chem. Phys. **94** (1991) 4024 - 4030

[349] C. W. Bauschlicher Jr.; J. Chem. Phys. **84** (1986) 250 - 259

[350] W. Müller, J. Flesch, W. Meyer; J. Chem. Phys. **80** (1984) 3297 - 3310

[351] F. T. Wagner, P. N. Ross Jr.; Surf. Sci. **160** (1985) 305 - 330

[352] G. H. Grant, W. G. Richards; Computational Chemistry; Oxford Science Publications; 1st edition, Oxford 1995; reprinted 1998, page 18

[353] I. Cohen; J. Chem. Ed. **42** (1965) 397 - 308

[354] R. C. Johnson, R. R. Rettew; J. Chem. Ed. **42** (1966) 145 - 146
This article asumes erroneously that the shape of an atom is dertimened by the occupation of its orbitals and only atoms with filled or half filled shells are spherically symmetric. This fault was corrected by COHEN [353].

[355] T. H. Dunning Jr., J. Chem. Phys. **53** (1970) 2823 - 2833

[356] program Auger V 1.23 by Wolfram Luithardt, University Hamburg

[357] P. A. Redhead; Vacuum **12** (1962) 203 - 211

[358] W. Hoffmann, C. Benndorf; Surf. Sci. **377-379** (1997) 681 - 686

[359] L. Pauling, General Chemistry, W. H. Freeman & Co, 3rd edition, San Fransico 1970

[360] N. Materer, U. Starke, A. Barbieri, M. A. Van Hove, G. A. Somorjai, G.-J. Kroes, C. Minot; J. Phys. Chem. **99** (1995) 6267 - 6269

[361] H. Dosch, A. Lied, J. H. Bilgram; Surf. Sci. **327** (1995) 145 - 164

[362] Y. Furukawa; Chemie in unserer Zeit Mar. 1997 58 - 65

[363] G.-J. Kroes; Surf. Sci. **275** (1992) 365 - 382

[364] T. R. Dyke, J. S. Muenter; J. Chem. Phys. **60** (1974) 2929 - 2930

[365] J. Brudermann, P. Lohbrandt, U. Buck, V. Buch; Phys. Rev. Lett. **80** (1998) 2821 - 2824

[366] WebElements Pro - The periodic table on the WWW; www.webelements.com

[367] K. Koga, X. C. Zeng, H. Tanaka; Phys. Rev. Lett. **79** (1997) 5262 - 5265

[368] H. Tanaka, R. Yamamoto, K. Koga, X. C. Zeng; Chem. Phys. Lett. **304** (1999) 378 - 384

[369] M. Odelius, M. Bernasconi, M. Parinello; Phys. Rev. Lett. **78** (1997) 2855 - 2858

[370] Research done by students under the subpervision of T. Lankau

a) J. Franke, C. Clasen; Optimierung von $(H_2O)_3$; Hamburg 1997

b) R. Schröder, R. Töber; Geometrie eines zyklischen Wassertrimers mit C_1-Symmetry im Vakuum, Hamburg 1997

c) A. Wichmann; Erstellung eines Programms zur Umwandlung interner in kartesische Koordinaten; Hamburg 1998

d) A. Wichmann; Erstellung eines Programms zur Energieberechnung und Energieminimierung kleiner Wassercluster für die Untersuchung von H_2O-Hexameren unter Platin-Oberflächenbedingungen; Hamburg 1998

e) S. Staack, I. Reulecke; Computerchemie, Geometrieoptimierung an Wasserclustern; Hamburg 1999

10.2 Programs used for this work

1. GAMESS-UK is a package of ab initio programs written by M.F. Guest, J.H. van Lenthe, J. Kendrick, K. Schoffel, P. Sherwood, and R.J. Harrison, with contributions from R.D. Amos, R.J. Buenker, M. Dupuis, N.C. Handy, I.H. Hillier, P.J. Knowles, V. Bonacic-Koutecky, W. von Niessen, V.R. Saunders, and A.J. Stone. The package is derived from the original GAMESS code due to M. Dupuis, D. Spangler and J. Wendoloski, NRCC Software Catalog, Vol. 1, Program No. QG01 (GAMESS), 1980.
   Moeller-Plesset perturbation theory (MP2, MP3):
   J.E. Rice, R.D.Amos, N.C. Handy, T.J. Lee and H.F. Schaefer, J. Chem. Phys. 85 (1986) 963: J.D. Watts and M. Dupuis, J. Comput. Chem. 9 (1988) 158.

2. GAMESS US Version = 26 Jul 1995, From Iowa State University; M.W. Schmidt, K.K. Baldridge, J.A. Boatz, S.T. Elbert, M.S. Gordon, J.H. Jensen, S. Koseki, N. Matsunaga, K.A. Nguyen, S.J. Su, T.L. Windus, Together with M. Dupuis, J.A. Montgomery; J. Comput. Chem. 14 (1993) 1347-1363

3. Gaussian 94, Revision C.2, M.J. Frisch, G.W. Trucks, H.B. Schlegel, P.M.W. Gill, B.G. Johnson, M. A. Robb, J.R. Cheeseman, T. Keith, G.A. Petersson, J.A. Montgomery, K. Raghavachari, M.A. Al-Laham, V.G. Zakrzewski, J.V. Ortiz, J.B. Foresman, J. Cioslowski, B.B. Stefanov, A. Nanayakkara, M. Challacombe, C.Y. Peng, P.Y. Ayala, W. Chen, M.W. Wong, J.L. Andres, E.S. Replogle, R. Gomperts, R.L. Martin, D.J. Fox, J.S. Binkley, D.J. Defrees, J. Baker, J.P. Stewart, M. Head-Gordon, C. Gonzalez, and J.A. Pople; Gaussian, Inc., Pittsburgh PA, 1995.

4. YaEHMOP G. Landrum; http://overlap.chem.cornell.edu:8080/yehmop.html (1997)

5. molden http://www.caos.kun.nl/ shaft/molden/molden.html

6. Mathematic 2.0 for Windows 3.11 (Student Version) (c) 1988-91 Wolfram Reserch, Inc.

7. Micro Cal Origin 2.94; (c) 1991-1993 Micro Cal Software, Inc.; Northampton

8. xlC 3.1.2.0 IBM

9. xlf 3.2.3.0 IBM

10. gcc, whatever version was running

Chapter 11

Appendix

11.1 Abbriviations

6-311++G**	Pople basis set[1], wich uses a primitive STO-6G basis for the core orbitals and a triple-zeta-basis for the valence space (3, 1, 1 gaussian function used). The '**' indicates polarisation functions on the heavy and hydrogen atoms, while the '++' indicates diffuse functions on the heavy and hydrogen atoms.
aug	**aug**mented
aug ccp VDZ	**aug**mented **c**orrelation **c**onsistend **V**alence **p**olarisation **D**ouble **Z**eta
aug ccp VQZ	**aug**mented **c**orrelation **c**onsistend **V**alence **p**olarisation **Q**uadruple **Z**eta
BF	water-water interaction potential by **B**ernal and **F**owler
BFP	**B**ernal **F**owler **P**auling ice rules
BNS	water-water interaction potential by **B**en-**N**aim and **S**tillinger
BSSE	**B**asis **S**et **S**uperposition **E**rror
cc	**c**orrelation **c**onsistend
ccp	**c**orrelation **c**onsistend **p**olarisation
CASSCF	**C**omplete **A**ctive **Space** **S**elf **C**onsistent **F**ield calculation
CASMP2	**C**omplete **A**ctive **Space** self consistent field **M**øller **P**lesset **2** calculation
CFMS	**C**entral **F**orce **M**odel for water-water interaction by **S**tillinger and David
CI	**C**onfiguration **I**nteraction
CISD	Gaussian 94 keyword for **C**onfigurartion **I**nteraction calculations with **S**ingle and **D**ouble excitations
CNDO	**C**omplete **N**eglect of **D**ifferential **O**verlap

---

[1] split valence basis sets, which use the same radial functions for s- and p-orbitals [235]

CP	**C**ounter **P**oise method
CT	**C**harge **T**ransfer
D	Debye
DZ	**D**ouble **Z**eta basis set
DZP	**D**ouble **Z**eta + **P**olarisation basis set
ECP	**E**ffective **C**ore **P**otential
EHT	**E**xtended **H**ückel **T**heory
ES	**E**lectro**S**tatic
EX	**Ex**change repulsion
FCP	**F**ull **C**ounter **P**oise method
G94	Gaussian 94
H	**H**artree
HF	**H**artree **F**ock
HFD	**D**irac **H**artree **F**ock
HFR	**R**elativistic **H**artree **F**ock
HMO	**H**ückel **M**olecular **O**rbital
HO	**H**igh **O**rder coupling
HOMO	**H**ighest **O**ccupied **M**olecular **O**rbital
LanL1DZ	10 valence electrons ECP from Hay and Wadt, double zeta basis
LanL1MB	10 valence electrons ECP from Hay and Wadt, primitive basis
LanL2DZ	18 valence electrons ECP from Hay and Wadt, double zeta basis
LanL2MB	18 valence electrons ECP from Hay and Wadt, primitive basis
LCAO	**L**inear **C**ombination of **A**tomic **O**rbitals
LEED	**L**ow **E**nergy **E**lectron **D**iffraction
LUMO	**L**owest **U**noccupied **M**olecular **O**rbital
MBPT	**M**any **B**ody **P**erturbation **T**heory
MC	**M**onte **C**arlo
MCSCF	**M**ulti **C**onfiguration **S**elf **C**onsistent **F**ield calculation
MD	**M**olecular **D**ynamics
ML	**M**ono **L**ayer

MO	**M**olecular **O**rbital
MPx	**M**øller **P**lesset calculation of the order x=2, 3, 4
NCC	water-water interaction potential by **N**iesar, **C**orongiu and **C**lementi
NRECP	**N**on **R**elativistic **E**ffective **C**ore **P**otential
PL	**P**o**l**arisation
potential N	water-water interaction potential developed within this work
QLL	**q**uasi **l**iquid **l**ayer
rms	**r**oot **m**ean **s**quare
RECP	**R**elativistic **E**ffective **C**ore **P**otential
RHF	**R**estricted **H**artree **F**ock
RMPx	**R**estricted Hartree Fock calculation followed by **M**øller **P**lesset calculation of the order **x**
ROHF	**R**estricted **O**pen Shell **H**artree **F**ock
ROMP2	**R**estricted **O**pen Shell Hartree Fock calculation followed by a second order **M**øller **P**lesset calculation
ROW	water-water interaction potential by **Row**linson
SALC	**S**ymmetry **A**dapted **L**inear **C**ombination
SAPT	**S**ymmetry **A**dapted **P**erturbation **T**heory
SCF	**S**elf **C**onsistent **F**ield calculation
SD-CI	**C**onfiguration **I**nteraction calculation with **S**ingle and **D**ouble excitations
SO	**S**pin **O**rbit
SOMO	**S**ingle **O**ccupied **M**olecular **O**rbital
SPC	**S**imple **P**oint **C**harge model for the water-water interaction
SPC/E	**E**xtended **S**imple **P**oint **C**harge model for the water-water interaction
STO	**S**later **T**ype **O**rbital
STO-nG	**S**later **T**ype **O**rbital described with n gaussian functions
ST2	revised water-water interaction potential by **S**tillinger and Rahman
TIPnP	**T**ransferable **I**ntermolecular **P**otential for water, n indicates the level of **p**arametrisation
TIPSn	**T**ransferable **I**ntermolecular **P**otential function**S** for water, n indicates the level of revision

TDS	**T**hermal **D**esorption **S**pectroscopy
TZVP	**T**riple **Z**eta **V**alence **P**olarisation basis set
UHF	**U**nrestricted **H**artree **F**ock
UMP2	**UHF** calculation followed by a **MP2** calculation
UHV	**U**ltra **H**igh **V**acuum
VCP	**V**irtual **C**ounter **P**oise method
VSEPR	**V**alence **S**hell **E**lectron **P**air **R**repulsion

11.2 Basis set and ECPS used with in this work

All data were directly taken from the GAMESS UK printouts. The DZP basis set for water in the Gaussian 94 calculations was manually defined in the G94-input file.

atom	type	exponent	coefficient
H	s	19.2384	0.032828
		2.89872	0.231204
		0.653472	0.817226
	s	0.163064	1.0
	p	1.0	1.0
O	s	7816.54	0.002031
		1175.82	0.015436
		273.188	0.073771
		81.1696	0.247606
		27.1836	0.611832
		3.4136	0.241205
	s	9.8322	1.0
	s	0.9398	1.0
	s	0.2846	1.0
	p	35.1832	0.01958
		7.904	0.124189
		2.3051	0.394727
		0.7171	0.627375
	p	0.2137	1.0
	d	0.85	1.23849

Table 11.1: DZP basis set for H_2O.

atom	type	exponent	coefficient
H	s	33.64	0.025374
		5.058	0.189684
		1.147	0.852933
	s	0.3211	1.0
	s	0.1013	1.0
	p	1.0	1.0
O	s	18050.0	0.000757
		2660.0	0.006066
		585.7	0.032782
		160.9	0.132609
		51.16	0.396839
		17.9	0.542572
	s	17.9	0.262490
		6.639	0.769828
	s	2.077	1.0
	s	0.7736	1.0
	s	0.2558	1.0
	p	49.83	0.016358
		11.49	0.106453
		3.6090	0.349302
		1.321	0.657183
	p	1.0	1.0
	p	0.1651	1.0
	d	1.28	1.0

Table 11.2: TZVP basis set for H_2O.

type	exponent	coefficient
S	.2547D+01	−.1473918D+01
	.1614D+01	.1911572D+01
	.5167D+00	.3922319D+00
S	.2547D+01	.1438817D+01
	.1614D+01	−.2091182D+01
	.5167D+00	−.1092132D+01
	.2651D+00	.1342660D+01
S	.5800D−01	.1000000D+01
P	.2911D+01	−.5247438D+00
	.1836D+01	.9671884D+00
	.5982D+00	.5438632D+00
P	.6048D+00	−.1061438D+00
	.9960D−01	.1038310D+01
P	.2900D−01	.1000000D+01
D	.1243D+01	.5598150D+00
	.4271D+00	.5511090D+00
D	.1370D+00	.1000000D+01

Table 11.3: LanL2DZ Pt basis set.

type	exponent	coefficient
S	.3755D+00	−.11780900D+01
	.2651D+00	.12683001D+01
	.5800D−01	.78955790D+00
P	.6048D+00	−.44732700D−01
	.9960D−01	.43758020D+00
	.2900D−01	.67304240D+00
D	.1243D+01	.50381630D+00
	.4271D+00	.49790020D+00
	.1370D+00	.19761290D+00

Table 11.4: LanL1MB Pt basis set.

l	n	α	c	l	n	α	c
G	1	728.9394056	−0.1619268	D-G	0	249.5650763	2.9343678
	2	320.6567800	−1320.2873852		1	126.6678585	59.3306571
	2	52.8680174	−298.3178135		2	63.1430586	452.4445194
	2	12.0280128	−87.5837065		2	17.9059470	210.4769479
	2	3.5238913	−8.1493274		2	4.2239373	58.6254112
S-G	0	409.4437358	2.7334218	F-G	0	121.8158799	3.9534253
	1	274.5419231	59.7024329		1	60.8757030	53.8555182
	2	127.5658570	891.4589550		2	31.4767147	247.4305133
	2	32.9036631	368.4467656		2	9.8811751	127.8187976
	2	5.0593880	238.0263090		2	2.7319874	15.3772046
	2	4.1506556	−107.0556454				
P-G	0	466.1728892	1.8878568				
	1	120.7888259	76.0138629				
	2	36.4118791	343.5511116				
	2	5.6985408	119.4911786				

Table 11.5: LanL2DZ Pt ECP.

l	n	α	c	l	n	α	c
G	0	415.2990463	-0.1619268	D-G	0	92.3112664	2.9343678
	1	117.9901046	-44.1056601		1	39.3772891	52.8691101
	2	41.2716533	-225.8208289		2	14.6918292	170.6411111
	2	11.8572771	-99.3462061		2	3.0234056	99.8353949
	2	3.5452121	-20.9272244		2	2.5666981	-54.3170702
	2	1.2031453	-2.7509383		2	0.4019102	-0.2872878
S-G	0	118.3123634	2.7334218	F-G	0	1.6524570	3.9534253
	1	40.2269849	76.8788294		1	23.2155161	44.9889323
	2	13.6420645	208.3220582		2	6.7336889	85.3111945
	2	3.9884442	60.0312229		2	1.4985371	28.7619037
	2	0.9246716	25.9812187		2	0.3567339	6.8855706
	2	0.7260083	-8.6418215		2	0.2699638	-2.6742821
P-G	0	111.7931938	1.8878568				
	1	36.4526949	57.1033025				
	2	11.9271531	150.6780890				
	2	3.2553879	37.2985110				
	2	0.7783811	12.3081605				

Table 11.6: LanL1MB Pt ECP.

type	exponent	coefficient
S	$0.148323D+01$	$0.22934D+00$
	$0.174646D+01$	$-0.90460D-01$
	$0.756591D+00$	$-0.52713D+00$
	$0.249017D+00$	$0.50171D+00$
	$0.580000D-01$	$0.79308D+00$
P	$0.582569D+00$	$0.22546D+00$
	$0.879439D+00$	$0.23282D+00$
	$0.724914D+00$	$-0.50879D+00$
	$0.301446D-01$	$0.68090D+00$
	$0.106229D+00$	$0.42878D+00$
D	$0.574860D-01$	$0.42750D-01$
	$0.317090D-01$	$0.21724D+00$
	$0.139180D-01$	$0.55726D+00$
	$0.613100D-02$	$0.31975D+00$

Table 11.7: New basis set for Pt.

l	n	α	c
F	3	0.4200000	0.00000000
S-F	2	1.5630487	12.72241997
	3	0.4053396	-0.78658492
P-F	2	0.7830368	9.14667910
	3	0.4365853	-1.41522900
D-F	4	0.2637440	0.13266900

Table 11.8: New ECP for Pt.

11.3 Selected Water Monomer Data

file	h2o_1.out	h2o_13.out	h2o_16.out	h2o_3.out	h2o_14.out
method	RHF	RHF	RHF	RHF	RMP2
basis set	STO-3G	DZ	DZP	TZVP	DZ
$\sphericalangle_{HOH}$ [°]	100.05	112.61	106.71	107.12	110.68
d_{OH} [Å]	0.9895	0.9509	0.9440	0.9407	0.9782
dipol. [D]	1.7088	2.5340	2.1869	2.2477	2.5167
q_H [e]	+0.165	+0.40	+0.34	+0.305	+0.38
q_O [e]	−0.33	−0.80	−0.68	−0.61	−0.76
E_{ELEC} [H]	−83.8712	−85.2490	−85.3657	−85.4060	−84.9938
E_{NUC} [H]	+8.9053	+9.2380	+9.3188	+9.3500	+8.9842
E_{RHF} [H]	−74.9659	−76.0110	−76.0469	−76.0560	−76.0095
E_{MP2} [H]					−0.1397
E_{TOTAL} [H]	−74.9659	−76.0110	−76.0469	−76.0560	−76.1492

file	h2o_17.out	h2o_9.out	h2o_15.out	h2o_18.out	h2o_12.out
method	RMP2	RMP2	RMP3	RMP3	RMP3
basis set	DZP	TZVP	DZ	DZP	TZVP
$\sphericalangle_{HOH}$ [°]	104.71	104.84	110.79	104.89	105.21
d_{OH} [Å]	0.9621	0.9576	0.9747	0.9590	0.9532
dipol. [D]	2.1653	2.2354	2.5041	2.1512	2.2085
q_O [e]	−0.66	−0.58	−0.75	−0.65	−0.57
q_H [e]	+0.33	+0.29	+0.375	+0.325	+0.285
E_{ELEC} [H]	−85.1935	−85.2457	−85.0263	−85.2228	−85.2872
E_{NUC} [H]	+9.1474	+9.1904	+9.0165	+9.1765	+9.2316
E_{RHF} [H]	−76.0461	−76.0553	−76.0099	−76.0463	−76.0556
E_{MP2} [H]	−0.2110	−0.2356	−0.1394	−0.2107	−0.2353
E_{MP3} [H]			−0.0013	−0.0063	−0.0036
E_{TOTAL} [H]	−76.2571	−76.2910	−76.1506	−76.2634	−76.2945

Table 11.9: GAMESS UK results for the water monomer.

file	experiment	Kim	difference	h2o_27	h2o_28
method		RMP2		RHF	RMP2
basis set		DZP[b]		6-311++G**	3-311++G**
$\sphericalangle_{HOH}$ [°]	104.5	104.7	0.01	106.21	104.05
d_{OH} [Å]	0.957	0.963	−0.0009	0.9407	0.9588
dipol. [D]	1.85	2.161	0.0043	1.9677	1.8988
q_O [e]	−0.66[a]	−0.65[c]	−0.01	−0.62	−0.57

file		experiment	Kim	difference	h2o_27	h2o_28
q_{H}	[e]	+0.33[a]	+0.32[c]	+0.01	+0.31	+0.29
E_{ELEC}	[H]				−85.4126	−85.2399
E_{NUC}	[H]				+9.3522	+9.1802
E_{RHF}	[H]				−76.0604	−76.0596
E_{MP2}	[H]					−0.3054
E_{TOTAL}	[H]	−76.4802	−76.25484	−0.00859	−76.0604	−76.3650

difference	difference between GAMESS UK results and KIM's.
KIM	KIM et al., J. Chem. Phys. **97** (1992) 6648
a	Charges calculated from the eperimental dipolmoment (model of pointcharges)
b	KIM does not use a kartesian basis set. So he has one basis function less than GAMESS UK.
c	KIM did not mention the method of calculation.

Table 11.10: GAMESS UK results for water in comparrison with other works.

11.4 Results from Single Point Calculations for the Water Dimer

file		dim_2	dim_3	dim_4	dim_5	dim_6
method		RHF	RHF	RHF	RHF	RMP2
basis set		STO-3G	DZ	DZP	TZVP	DZ
L1	[Å]	0.9880	0.9497	0.9432	0.9398	0.9762
L2	[Å]	0.9895	0.9587	0.9484	0.9453	0.9868
L3	[Å]	1.7517	1.8773	2.0350	2.0170	1.8473
L4	[Å]	0.9870	0.9512	0.9447	0.9412	0.9777
W1	[deg]	100.39	112.84	106.49	106.92	111.22
W2	[deg]	110.98	120.76	115.41	119.27	120.69
D1	[deg]	124.33	104.19	117.20	112.40	106.60
$\sphericalangle_{546}$	[deg]	100.89	112.84	106.9	107.50	110.98
d_{OO}	[Å]	2.7412	2.8360	2.9834	2.9624	2.8340
α	[deg]	0.00	0.00	0.00	0.00	0.00
β	[deg]	55.79	22.39	43.9	34.21	25.71
q_{O1}	[e]	−0.38	−0.86	−0.71	−0.64	−0.81
q_{H2}	[e]	+0.14	+0.38	+0.33	+0.30	+0.36
q_{H3}	[e]	+0.20	+0.47	+0.37	+0.34	+0.43
q_{O4}	[e]	−0.33	−0.84	−0.69	−0.64	−0.79
$q_{\mathrm{H5/6}}$	[e]	+0.19	+0.43	+0.35	+0.33	+0.40
charge trans.	[e]	0.045	0.010	0.015	0.007	0.025
dipole	[D]	2.8328	4.4168	3.3515	3.6466	4.4462

file		dim_2	dim_3	dim_4	dim_5	dim_6
E_{ELEC}	[H]	−187.2964	−187.1143	−188.5014	−188.6663	−188.6477
E_{NUC}	[H]	+37.3552	+37.0801	+36.3997	+36.5460	+36.6163
E_{RHF}	[H]	−149.9412	−152.0342	−152.1018	−152.1203	−152.0313
E_{MP2}	[H]					−0.2808
E_{TOTAL}	[H]	−149.9412	−152.0342	−152.1018	−152.1203	−152.3121

file		dim_7	dim_8	dim_9	dim_10	dim_11
method		RMP2	RMP2	RMP3	RMP3	RMP3
basis set		DZP	TZVP	DZ	DZP	TZVP
L1	[Å]	0.9613	0.9565	0.9730	0.9584	0.9527
L2	[Å]	0.9686	0.9638	0.9812	0.9638	0.9584
L3	[Å]	1.9452	1.9197	1.8738	1.9717	1.9364
L4	[Å]	0.9635	0.9583	0.9741	0.9601	0.9541
W1	[deg]	104.38	104.87	111.23	104.89	105.23
W2	[deg]	111.66	118.56	120.92	114.07	119.12
W3	[deg]	90.00	90.00	90.00	90.00	90.00
D1	[deg]	121.42	115.00	105.94	119.43	114.11
$\sphericalangle_{546}$	[deg]	104.95	105.51	111.15	105.34	105.76
d_{OO}	[Å]	2.9138	2.8836	2.8550	2.9355	2.8948
α	[deg]	0.00	0.00	0.00	0.00	0.00
β	[deg]	52.71	37.82	24.63	47.73	37.26
q_{O1}	[e]	−0.70	−0.61	−0.80	−0.69	−0.61
q_{H2}	[e]	+0.32	+0.28	+0.35	+0.32	+0.28
q_{H3}	[e]	+0.35	+0.32	+0.43	+0.36	+0.32
q_{O4}	[e]	−0.66	−0.61	−0.78	−0.67	−0.61
$q_{\mathrm{H5/6}}$	[e]	+0.35	+0.31	+0.40	+0.34	+0.31
charge trans.	[e]	0.028	0.014	0.020	0.021	0.011
dipole	[D]	3.2353	3.6552	4.4072	3.3082	3.6427
E_{ELEC}	[H]	−188.6435	−188.8640	−188.5752	−188.5366	−188.8626
E_{NUC}	[H]	+36.5336	+36.7452	+36.5431	+36.4360	+36.7433
E_{RHF}	[H]	−152.1000	−152.1187	−152.0321	−152.1006	−152.1193
E_{MP2}	[H]	−0.4243	−0.4732	−0.2799	−0.4236	−0.4725
E_{MP3}	[H]			−0.0021	−0.0122	−0.0067
E_{TOTAL}	[H]	−152.5243	−152.5919	−152.3141	−152.5364	−152.5985

Table 11.11: Dimer with a straight hydrogen bond (W3 = 90°).

file		dim_16	dim_19	dim_17	dim_22	dim_21
method		RMP3	RMP2	RHF	RHF	RHF
basis set		DZP	TZVP	6-311++G**	DZP	TZVP
L1	[Å]	0.9584	0.9564	0.9400	0.9432	0.9398
L2	[Å]	0.9640	0.9637	0.9447	0.9485	0.9452
L3	[Å]	1.9685	1.9194	2.1012	2.0345	2.0179
L4	[Å]	0.9600	0.9582	0.9414	0.9447	0.9412
W1	[deg]	105.02	104.96	106.27	106.53	106.88
W2	[deg]	114.00	118.68	113.88	112.88	119.69
W3	[deg]	93.85	89.90	94.53	94.66	89.02
D1	[deg]	119.48	114.84	118.87	119.26	111.8
$\sphericalangle_{546}$	[deg]	105.36	105.53	106.40	106.98	107.53
d_{OO}	[Å]	2.9311	2.8832	3.0439	2.9809	2.9631
α	[deg]	2.59	0.07	3.12	3.18	0.67
β	[deg]	49.13	37.49	48.88	50.67	32.77
q_{O1}	[e]	−0.69	−0.61	−0.65	−0.71	−0.64
q_{H2}	[e]	+0.32	+0.28	+0.30	+0.33	+0.30
q_{H3}	[e]	+0.36	+0.32	+0.38	+0.37	+0.34
q_{O4}	[e]	−0.67	−0.61	−0.71	−0.69	−0.64
$q_{H5/6}$	[e]	+0.34	+0.32	+0.34	+0.35	+0.33
charge trans.	[e]	0.021	0.015	0.028	0.016	0.006
dipole	[D]	3.1879	3.6634	2.8246	3.0538	3.7031
E_{ELEC}	[H]	−188.5545	−188.8657	−188.2380	−188.5305	−188.6608
E_{NUC}	[H]	+36.4518	+36.7470	+36.1120	+36.4287	+36.5405
E_{RHF}	[H]	−152.1006	−152.1187	−152.1270	−152.1018	−152.1203
E_{MP2}	[H]	−0.4236	−0.4732			
E_{MP3}	[H]	−0.0122				
E_{TOTAL}	[H]	−152.5364	−152.5919	−152.1270	−152.1018	−152.1203

Table 11.12: Dimers with a bended hydrogen bond.

file		dim_28	dim_29	dim_30	dim_31	dim_32
method		RHF	RMP2	RMP3	RHF	RMP2
basis set		DZP	DZP	DZP	TZVP	TZVP
r_{OH}	[Å]	0.9572	0.9572	0.9572	0.9572	0.9572
$\sphericalangle_{HOH}$	[deg]	104.52	104.52	104.52	104.52	104.52
d_{OO}	[Å]	2.9684	2.9116	2.9354	2.9706	2.8844
W3	[deg]	92.95	95.64	94.87	88.04	89.40
L2(O_4H_3)	[Å]	2.0301	1.9575	1.9805	2.0137	1.9273
α	[deg]	2.01	3.79	3.28	1.32	−0.40
β	[deg]	47.8	55.94	54.57	35.96	38.04
q_{O1}	[e]	−0.71	−0.69	−0.69	−0.63	−0.61

file		dim_28	dim_29	dim_30	dim_31	dim_32
q_{H2}	[e]	+0.33	+0.32	+0.32	+0.30	+0.28
q_{H3}	[e]	+0.37	+0.35	+0.35	+0.34	+0.32
q_{O4}	[e]	−0.69	−0.66	−0.66	−0.64	−0.61
$q_{H5/6}$	[e]	+0.36	+0.35	+0.34	+0.33	+0.31
charge trans.	[e]	0.016	0.028	0.022	0.007	0.014
dipole	[D]	3.2571	2.9265	3.0018	3.7883	3.6670
E_{ELEC}	[H]	−188.2742	−188.7865	−188.6169	−188.3447	−188.8928
E_{NUC}	[H]	36.1733	36.6857	36.5160	36.2257	36.7739
E_{RHF}	[H]	−152.1010	−152.1008	−152.1009	−152.1190	−152.1188
E_{MP2}	[H]		−0.4233	−0.4232		−0.4730
E_{MP3}	[H]			−0.0122		
E_{TOTAL}	[H]	−152.1010	−152.5241	−152.5363	−152.1190	−152.5918

Table 11.13: Dimer with a fixed water geometry ($r_{OH} = 0.9572$ Å, $\sphericalangle_{HOH} = 104.52°$).

11.5 Influence of the BSSE on the Monomer's Geometry

file			h2o_18	h2o_30	h2o_33	h2o_31
method		experiment	RMP3	RMP3	RMP3	RMP3
basis			DZP	DZP	DZP	DZP
geometry			optimized	rigid	optimized	rigid
kink				no	no	yes
type		monomer	monomer	donor	donor	donor
matrix[b]			MP3	SCF	MP3	SCF
$\sphericalangle_{HOH}$	[deg]	104.5	104.89	104.89	104.92	104.89
d_{OHn}	[Å]	0.957	0.9590	0.9590	0.9591	0.9590
d_{OHb}	[Å]	0.957	0.9590	0.9590	0.9588	0.9590
dipole	[D]	1.85	2.1512	2.2282	2.1436	2.2282
q_O	[e]	−0.66[a]	−0.649	−0.678	−0.648	−0.678
q_{Hn}	[e]	+0.33[a]	+0.325	+0.338	+0.323	+0.338
q_{Hb}	[e]	+0.33[a]	+0.325	+0.343	+0.328	+0.342
E_{ELEC}	[H]		−85.2228	−85.2230	−85.2234	−85.2230
E_{NUC}	[H]		9.1765	9.1765	9.1769	9.1765
E_{RHF}	[H]		−76.0463	−76.0465	−76.0465	−76.0465
E_{MP2}	[H]		−0.2107	−0.2110	−0.2110	−0.2110

file	h2o_18	h2o_30	h2o_33	h2o_31
E_{MP3} [H]	−0.0063	−0.0063	−0.0063	−0.0063
E_{TOTAL} [H]	−76.2634	−76.2639	−76.2639	−76.2638

[a] calculated from the experimetal dipolmoment

[b] density, on which the calculation of the dipolmoment bases

Table 11.14: Influence of the BSSE on the monomer's geometry (I).

file	h2o_34	h2o_36	h2o_39	h2o_37	h2o_40
method	RMP3	RMP3	RMP3	RMP3	RMP3
basis	DZP	DZP	DZP	DZP	DZP
geometry	optimized	rigid	optimized	rigid	optimized
kink	yes	no	no	yes	yes
type	donor	acceptor	acceptor	acceptor	acceptor
matrix[b]	MP3	SCF	MP3	SCF	MP3
$\sphericalangle_{\mathrm{HOH}}$ [deg]	104.92	104.89	104.92	104.89	104.92
d_{OHn} [Å]	0.9591	0.9590	0.9592	0.9590	0.9592
d_{OHb} [Å]	0.9589	0.9590	0.9592	0.9590	0.9592
dipole [D]	2.1453	2.2462	2.1729	2.2460	2.1727
q_{O} [e]	−0.6481	−0.674	−0.641	−0.674	−0.641
q_{Hn} [e]	+0.323	+0.340	+0.325	+0.340	+0.325
q_{Hb} [e]	+0.327	+0.340	+0.325	+0.340	+0.325
E_{ELEC} [H]	−85.2233	−85.2233	−85.2216	−85.2233	−85.2216
E_{NUC} [H]	9.1768	9.1765	9.1748	9.1765	9.1748
E_{RHF} [H]	−76.0465	−76.0468	−76.0468	−76.0468	−76.0468
E_{MP2} [H]	−0.2110	−0.2117	−0.2117	−0.2117	−0.2117
E_{MP3} [H]	−0.0063	−0.0062	−0.0063	−0.0062	−0.0062
E_{TOTAL} [H]	−76.2638	−76.2647	−76.2647	−76.2648	−76.2648

[b] density, on which the calculation of the dipolmoment bases

Table 11.15: Influence of the BSSE on the monomer's geometry (II).

file	h2o_9	h2o_32	h2o_35	h2o_38	h2o_41
method	RMP2	RMP2	RMP2	RMP2	RMP2
basis	TZVP	TZVP	TZVP	TZVP	TZVP
geometry	optimized	rigid	optimized	rigid	optimized
kink		no	no	no	no
type	monomer	donor	donor	acceptor	acceptor
matrix[b]	MP2	SCF	MP2	SCF	MP2
$\sphericalangle_{\mathrm{HOH}}$ [deg]	104.84	104.84	104.93	104.84	104.91

file		h2o_9	h2o_32	h2o_35	h2o_38	h2o_41
d_{OHn}	[Å]	0.9576	0.9576	0.9576	0.9576	0.9577
d_{OHb}	[Å]	0.9576	0.9576	0.9573	0.9576	0.9577
dipole	[D]	2.2354	2.2913	2.2181	2.2688	2.2044
q_{O}	[e]	−0.584	−0.600	−0.573	−0.618	−0.589
q_{Hn}	[e]	+0.292	+0.299	+0.292	+0.307	+0.295
q_{Hb}	[e]	+0.292	+0.304	+0.286	+0.307	+0.295
E_{ELEC}	[H]	−85.2457	−85.2460	−85.2475	−85.2462	−85.2455
E_{NUC}	[H]	9.1904	9.1904	9.1919	9.1904	9.1896
E_{RHF}	[H]	−76.0553	−76.0556	−76.0556	−76.0558	−76.0558
E_{MP2}	[H]	−0.2356	−0.2360	−0.2360	−0.2366	−0.2366
E_{TOTAL}	[H]	−76.2910	−76.2916	−76.2916	−76.2924	−76.2925

[b] density, on which the calculation of the dipolmoment bases

Table 11.16: Influence of the BSSE on the monomer's geometry (III).

file		h2o_17	h2o_42	h2o_43	h2o_44	h2o_45
method		RMP2	RMP2	RMP2	RMP2	RMP2
basis		DZP	DZP	DZP	DZP	DZP
geometry		optimized	rigid	optimized	rigid	optimized
kink			yes	yes	yes	yes
Typ		monomer	donor	donor	acceptor	acceptor
matrix[b]		MP2	SCF	MP2	SCF	MP2
$\sphericalangle_{\mathrm{HOH}}$	[deg]	104.71	104.71	104.71	104.71	104.71
d_{OHn}	[Å]	0.9621	0.9621	0.9621	0.9621	0.9621
d_{OHb}	[Å]	0.9621	0.9621	0.9621	0.9621	0.9621
dipole	[D]	2.1653	2.2576	2.1576	2.1919	2.1933
q_{O}	[e]	−0.66	−0.679	−0.657	−0.673	−0.645
q_{Hn}	[e]	+0.33	+0.338	+0.328	+0.340	+0.329
q_{Hb}	[e]	+0.33	+0.342	+0.332	+0.340	+0.329
E_{ELEC}	[H]	−85.1935	−85.1937	−85.1937	−85.1940	−85.1940
E_{NUC}	[H]	9.1474	9.1474	9.1474	9.1474	9.1474
E_{RHF}	[H]	−76.0461	−76.0463	−76.0463	−76.0467	−76.0467
E_{MP2}	[H]	−0.2110	−0.2113	−0.2113	−0.2120	−0.2120
E_{TOTAL}	[H]	−76.2571	−76.2576	−76.2576	−76.2586	−76.2586

[b] density, on which the calculation of the dipolmoment bases

Table 11.17: Influence of the BSSE on the monomer's geometry (IV).

11.6 Changing W3 and Bending the Hydrogen Bond

W3 was used for the geometry optimisations of the water dimer to avoid problems with the Z-matrix definition (linear bonds, definition of angles). W3 is a badly chosen variable for analytic purposes, since the oxygen-oxygen distance d_{OO} and bond angle α of the hydrogen bond (figure 11.1) change simultaneously.

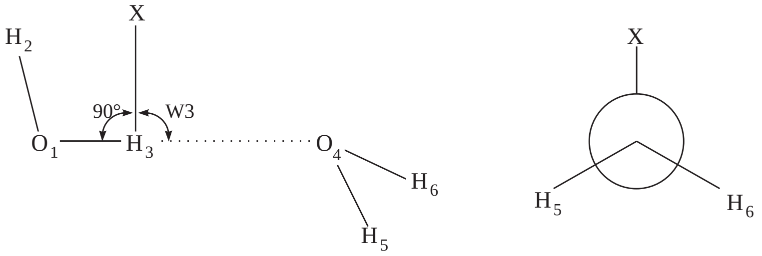

Figure 11.1: Variables of the water dimer.

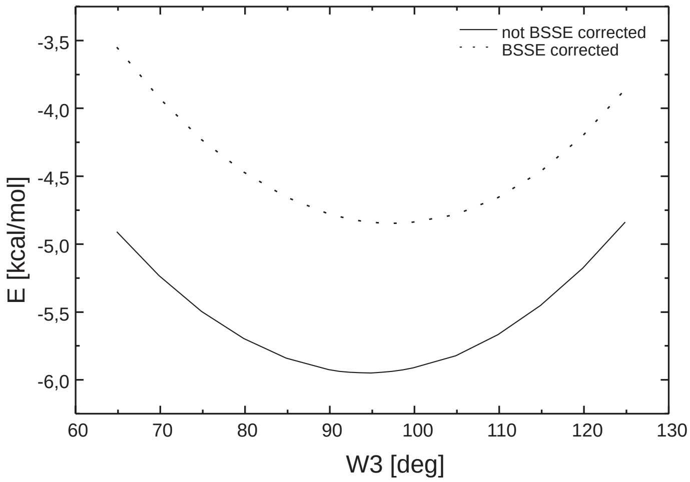

Figure 11.2: Bending of W3.

11.7 Energies of the Morokuma Energy Decompostion for the Water Dimer

The following abbriviations are going to be used:

ES : electrostatic energy
EX : exchange repulsion energy
CT : charge transfer energy
PL : polarisation energy
HO : high order coupling energy
ΔE : total ineraction energy

d_{OO} [Å]	ES	EX	CT	PL	HO	ΔE
2.2570	−35.40	70.01	−23.33	−10.89	14.82	15.21
2.3569	−28.30	48.79	−14.00	−6.05	6.93	7.37
2.4567	−22.72	33.92	−8.56	−3.57	3.17	2.23

d_{OO} [Å]	ES	EX	CT	PL	HO	ΔE
2.5564	−18.36	23.51	−5.40	−2.25	1.43	−1.06
2.6560	−14.93	16.24	−3.54	−1.51	0.65	−3.09
2.7054	−13.53	13.53	−2.94	−1.26	0.44	−3.76
2.7552	−12.26	11.21	−2.46	−1.07	0.31	−4.27
2.8049	−11.15	9.32	−2.09	−0.91	0.21	−4.62
2.8549	−10.13	7.69	−1.79	−0.79	0.15	−4.87
2.9049	−9.24	6.33	−1.54	−0.69	0.12	−5.02
2.9354	−8.74	5.62	−1.42	−0.64	0.10	−5.08
2.9549	−8.45	5.21	−1.35	−0.61	0.09	−5.10
3.0049	−7.75	4.28	−1.19	−0.54	0.07	−5.11
3.0548	−7.13	3.52	−1.06	−0.48	0.06	−5.08
3.1048	−6.57	2.89	−0.95	−0.43	0.05	−5.01
3.1548	−6.08	2.37	−0.86	−0.38	0.05	−4.91
3.2048	−5.64	1.94	−0.78	−0.34	0.04	−4.79
3.2569	−5.24	1.60	−0.73	−0.30	0.03	−4.64
3.3569	−4.57	1.07	−0.62	−0.25	0.03	−4.34
3.4569	−4.02	0.71	−0.54	−0.20	0.02	−4.03
3.5569	−3.57	0.47	−0.47	−0.17	0.02	−3.71
3.7571	−2.88	0.20	−0.35	−0.12	0.01	−3.14
3.9571	−2.37	0.09	−0.28	−0.08	0.00	−2.64
4.2071	−1.89	0.03	−0.20	−0.05	0.00	−2.12
4.4546	−1.53	0.01	−0.14	−0.03	0.00	−1.69
4.7046	−1.26	0.00	−0.08	−0.02	0.00	−1.36
4.9548	−1.05	0.00	−0.04	−0.02	0.00	−1.11
5.2044	−0.89	0.00	−0.02	−0.01	0.00	−0.92
5.4544	−0.76	0.00	−0.01	−0.01	0.00	−0.77
5.7044	−0.65	0.00	0.00	−0.01	0.00	−0.66
5.9543	−0.56	0.00	0.00	0.00	0.00	−0.57
6.4543	−0.43	0.00	0.00	0.00	0.00	−0.43
6.9543	−0.34	0.00	0.00	0.00	0.00	−0.34
7.4542	−0.27	0.00	0.00	0.00	0.00	−0.27
7.9542	−0.22	0.00	0.00	0.00	0.00	−0.22
8.9542	−0.15	0.00	0.00	0.00	0.00	−0.15
9.9541	−0.11	0.00	0.00	0.00	0.00	−0.11
10.9541	−0.08	0.00	0.00	0.00	0.00	−0.08

Table 11.18: MOROKUMA energy decomposition (d_{OO}) - all energies in kcal/mol.

$(\alpha + 52.26^\circ)$	ES	EX	CT	PL	HO	ΔE
40.54	−13.056	8.785	−2.085	−0.883	0.029	−7.210
41.54	−13.192	8.861	−2.114	−0.900	0.035	−7.310
42.54	−13.320	8.929	−2.142	−0.915	0.042	−7.406
43.54	−13.438	8.989	−2.167	−0.930	0.050	−7.496
44.54	−13.545	9.039	−2.190	−0.943	0.058	−7.582
45.54	−13.642	9.081	−2.210	−0.956	0.066	−7.661
46.54	−13.727	9.114	−2.228	−0.968	0.074	−7.735
47.54	−13.801	9.136	−2.243	−0.978	0.083	−7.803
48.54	−13.863	9.149	−2.256	−0.988	0.092	−7.864
49.54	−13.912	9.152	−2.265	−0.996	0.102	−7.919
50.54	−13.948	9.145	−2.271	−1.002	0.111	−7.966
51.54	−13.972	9.128	−2.275	−1.008	0.121	−8.006
52.54	−13.982	9.101	−2.275	−1.012	0.130	−8.038
53.54	−13.979	9.064	−2.272	−1.015	0.140	−8.063
54.54	−13.963	9.016	−2.267	−1.016	0.149	−8.080
55.54	−13.933	8.960	−2.258	−1.016	0.158	−8.090
56.54	−13.890	8.893	−2.246	−1.015	0.167	−8.091
57.54	−13.834	8.817	−2.231	−1.012	0.175	−8.085
58.54	−13.765	8.733	−2.214	−1.008	0.183	−8.071
59.54	−13.683	8.639	−2.193	−1.003	0.191	−8.049
60.54	−13.588	8.538	−2.170	−0.996	0.198	−8.019
61.54	−13.481	8.428	−2.144	−0.989	0.204	−7.982
62.54	−13.362	8.311	−2.116	−0.980	0.210	−7.937
63.54	−13.231	8.187	−2.086	−0.969	0.215	−7.884
64.54	−13.089	8.056	−2.054	−0.958	0.220	−7.825
65.54	−12.936	7.920	−2.020	−0.946	0.224	−7.758
66.54	−12.773	7.778	−1.983	−0.933	0.227	−7.685
67.54	−12.600	7.631	−1.946	−0.919	0.229	−7.604
68.54	−12.418	7.479	−1.907	−0.904	0.231	−7.518
69.54	−12.227	7.324	−1.866	−0.888	0.232	−7.425
70.54	−12.027	7.165	−1.825	−0.872	0.233	−7.326

Table 11.19: Morokuma energy decomposition (α) - all energies in 10^{-3} Hartree.

$(180^\circ - \beta)$	ES	EX	CT	PL	HO	ΔE
110.43	−13.810	9.356	−2.463	−0.950	0.107	−7.760
111.43	−13.836	9.332	−2.449	−0.955	0.110	−7.798
112.43	−13.859	9.307	−2.435	−0.960	0.113	−7.834
113.43	−13.879	9.282	−2.421	−0.965	0.117	−7.867
114.43	−13.897	9.256	−2.408	−0.970	0.120	−7.898

$(180° - \beta)$	ES	EX	CT	PL	HO	ΔE
115.43	−13.912	9.231	−2.394	−0.975	0.123	−7.926
116.43	−13.924	9.205	−2.380	−0.979	0.127	−7.952
117.43	−13.934	9.179	−2.367	−0.984	0.130	−7.976
118.43	−13.942	9.152	−2.353	−0.988	0.134	−7.997
119.43	−13.947	9.126	−2.339	−0.992	0.137	−8.016
120.43	−13.950	9.099	−2.326	−0.997	0.140	−8.034
121.43	−13.951	9.071	−2.312	−1.001	0.144	−8.049
122.43	−13.950	9.044	−2.298	−1.005	0.148	−8.062
123.43	−13.947	9.016	−2.285	−1.009	0.151	−8.073
124.43	−13.941	8.988	−2.271	−1.013	0.155	−8.082
125.43	−13.934	8.960	−2.258	−1.016	0.158	−8.090
126.43	−13.925	8.932	−2.245	−1.020	0.162	−8.096
127.43	−13.914	8.904	−2.231	−1.024	0.165	−8.100
128.43	−13.901	8.875	−2.218	−1.027	0.169	−8.102
129.43	−13.887	8.847	−2.205	−1.030	0.172	−8.103
130.43	−13.871	8.818	−2.192	−1.034	0.175	−8.103
131.43	−13.854	8.790	−2.179	−1.037	0.179	−8.101
132.43	−13.835	8.761	−2.166	−1.040	0.182	−8.098
133.43	−13.815	8.732	−2.153	−1.043	0.185	−8.094
134.43	−13.794	8.703	−2.141	−1.046	0.189	−8.088
135.43	−13.771	8.675	−2.128	−1.049	0.192	−8.081
136.43	−13.748	8.646	−2.116	−1.051	0.195	−8.074
137.43	−13.723	8.618	−2.104	−1.054	0.198	−8.065
138.43	−13.698	8.590	−2.092	−1.056	0.201	−8.055
139.43	−13.671	8.562	−2.080	−1.059	0.204	−8.044
140.43	−13.644	8.534	−2.068	−1.061	0.207	−8.032

Table 11.20: MOROKUMA energy decomposition (β) - all energies in 10^{-3} Hartree.

11.8 Different water-water interaction potentials from the literature

This section contains the plots of different classical water-water interaction potentials from the literature in comparison with the quantum chemical (DZP, MP3, fixed monomer geometry) calculated curves.

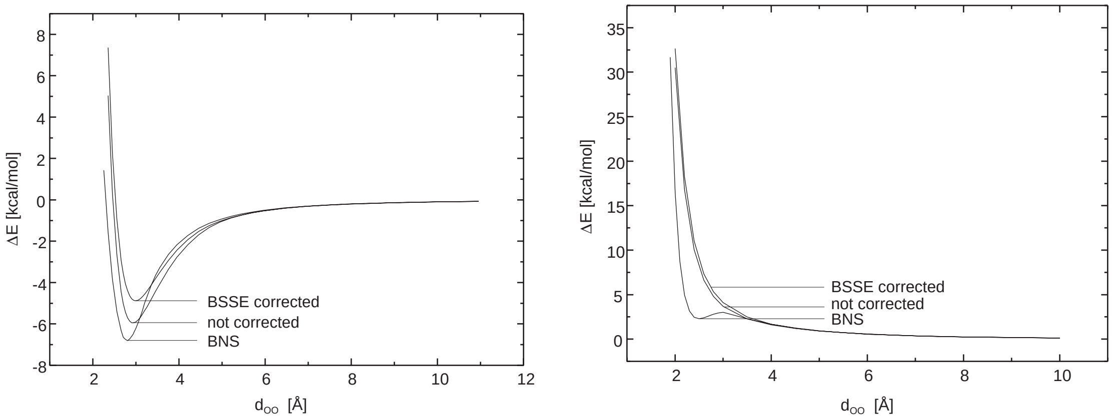

(a) Dimerisation (b) OO repulsion

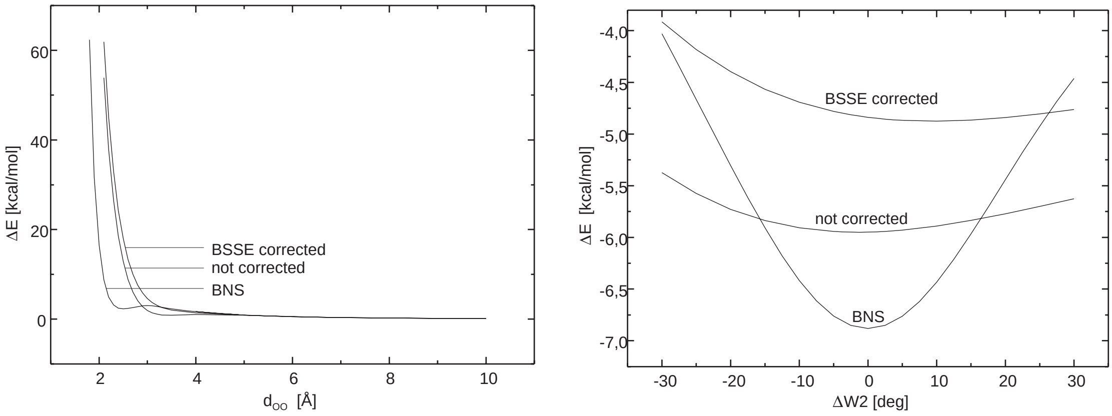

(c) HH repulsion (d) Variation of β

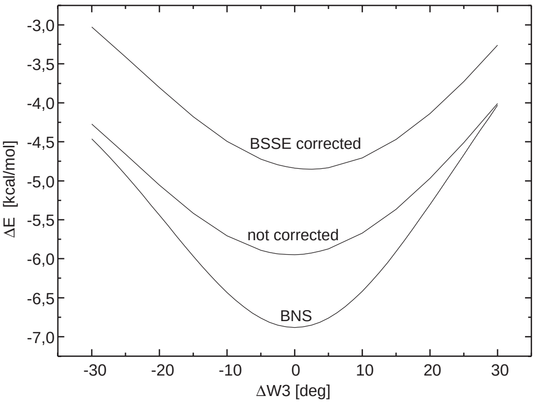

(e) Variation of α

Figure 11.3: Test of the BNS water-water interaction potential.

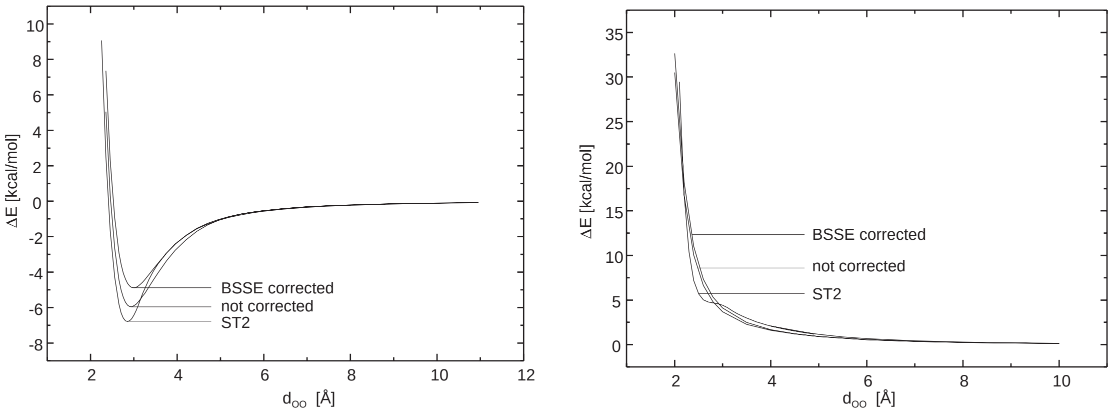

(a) Dimerisation (b) OO repulsion

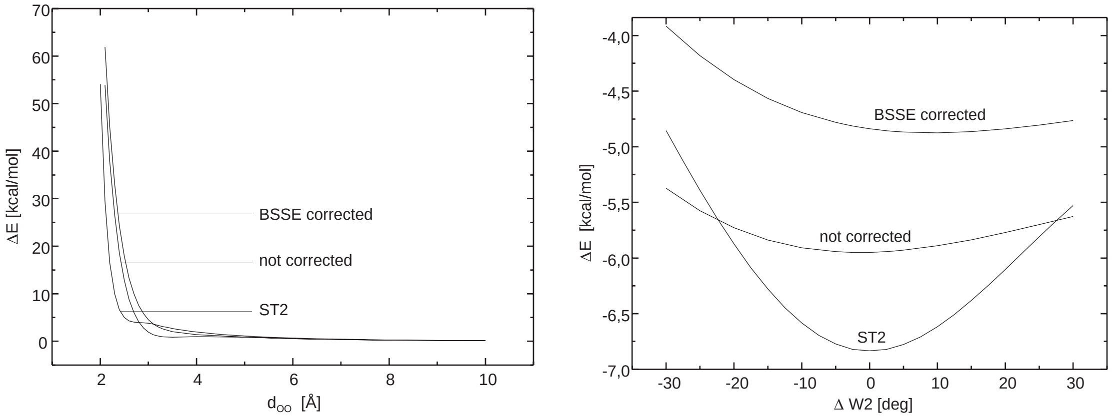

(c) HH repulsion (d) Variation of β

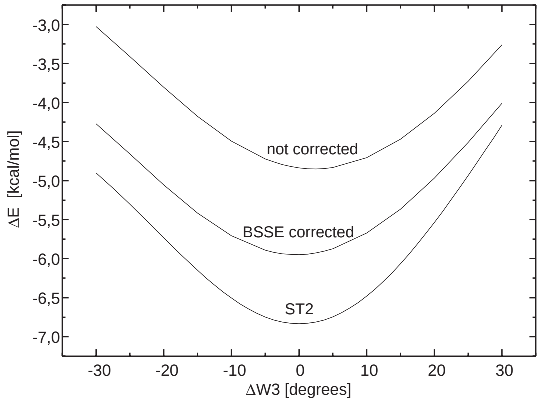

(e) Variation of α

Figure 11.4: Test of the ST2 water-water interaction potential.

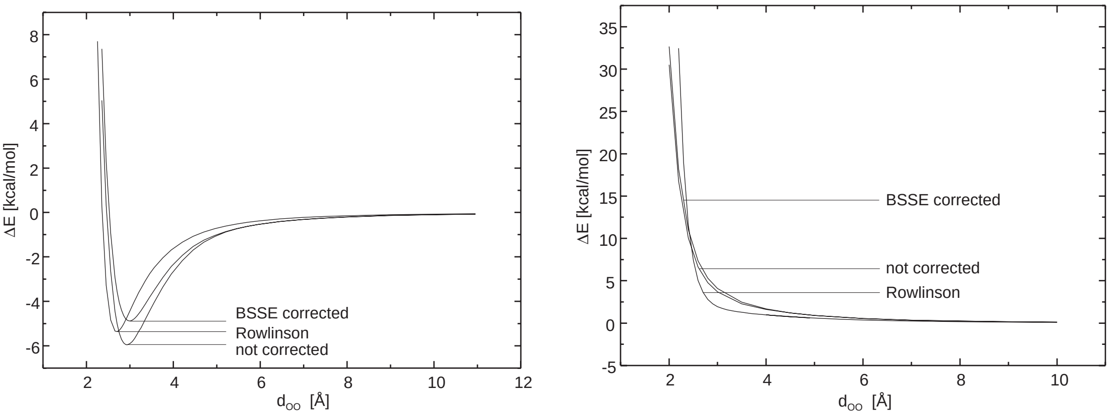

(a) Dimerisation (b) OO repulsion

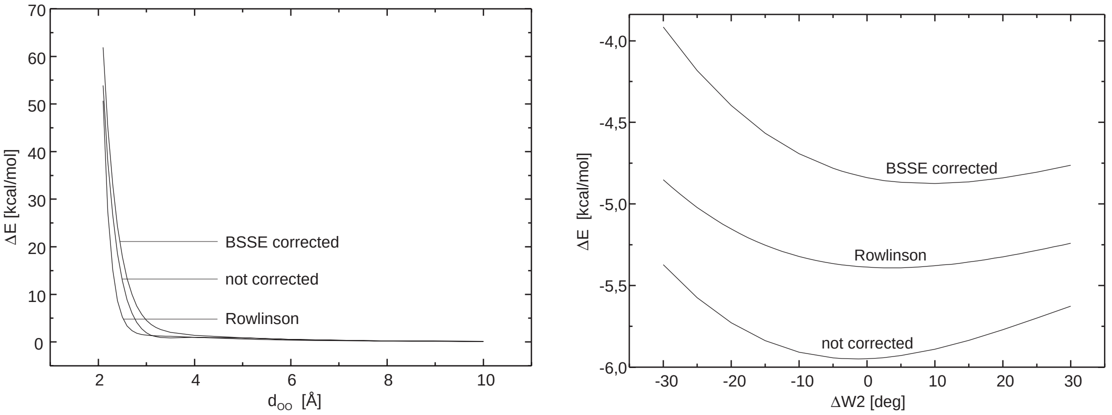

(c) HH repulsion (d) Variation of β

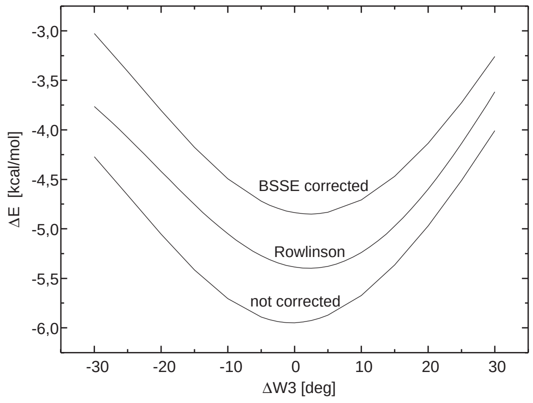

(e) Variation of α

Figure 11.5: Test of the ROWLINSON water-water interaction potential.

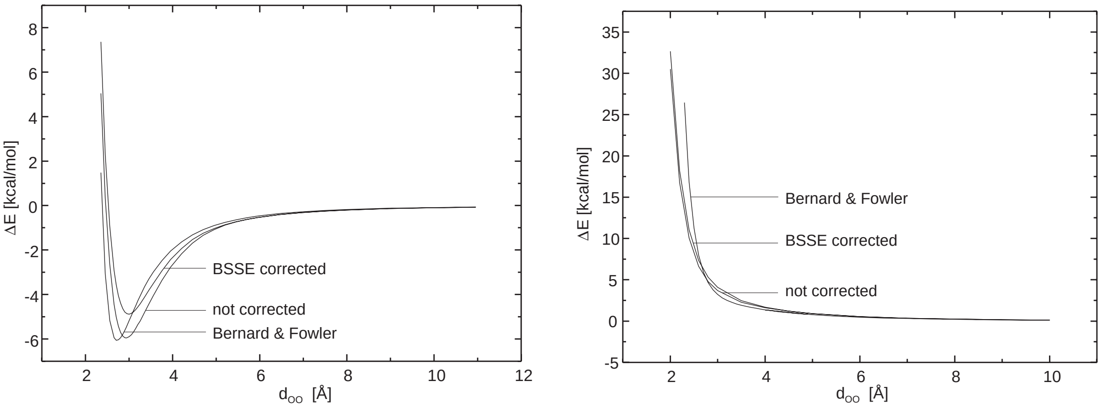

(a) Dimerisation (b) OO repulsion

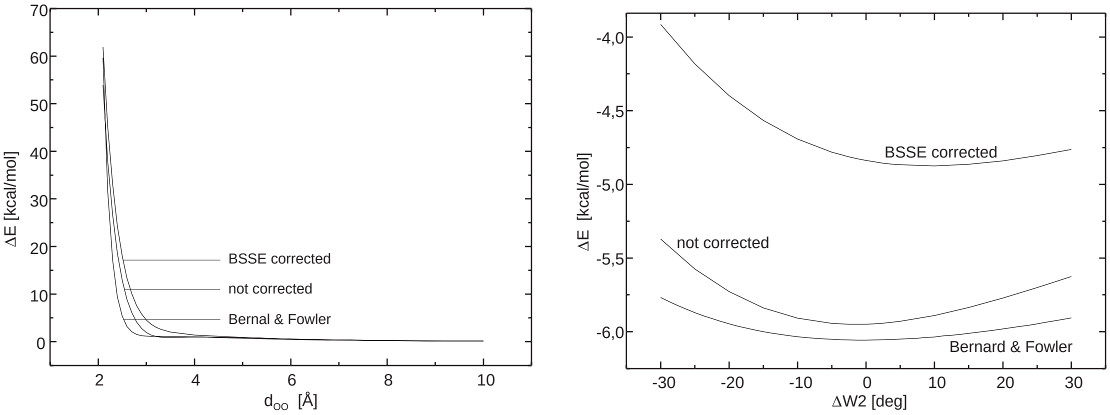

(c) HH repulsion (d) Variation of β

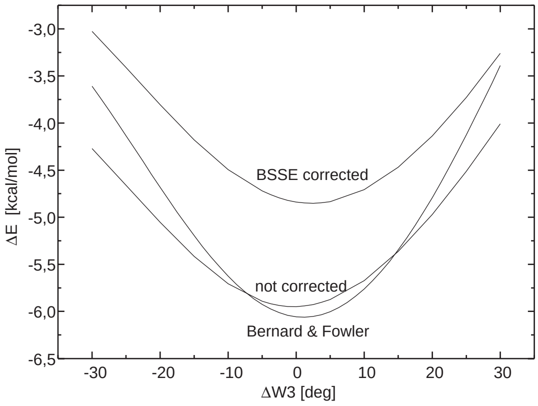

(e) Variation of α

Figure 11.6: Test of the Dernal and Fowler water-water interaction potential.

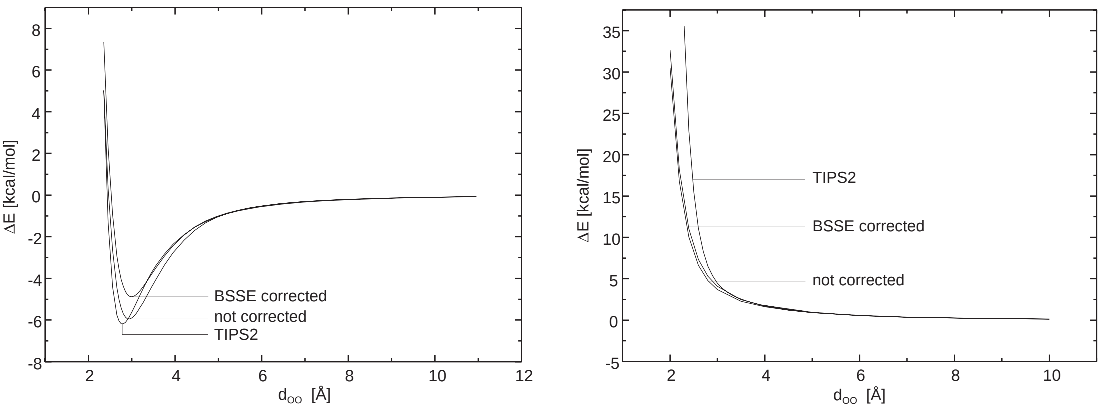

(a) Dimerisation (b) OO repulsion

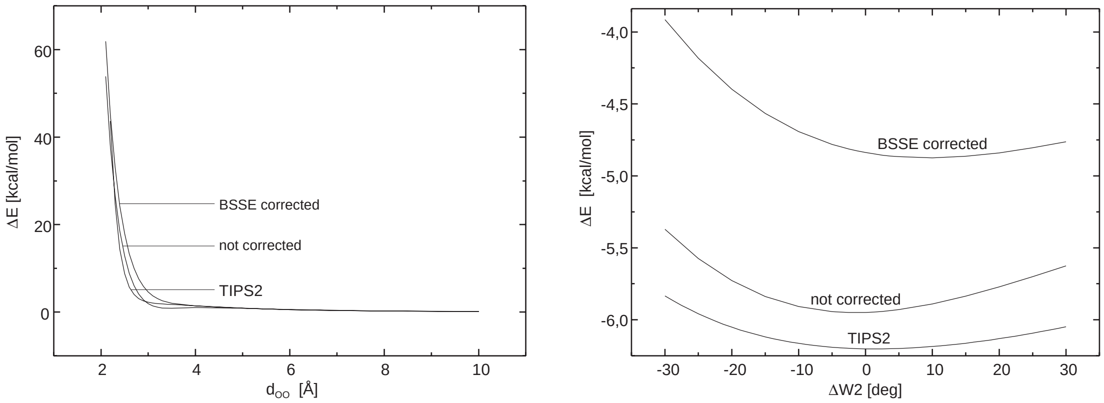

(c) HH repulsion (d) Variation of β

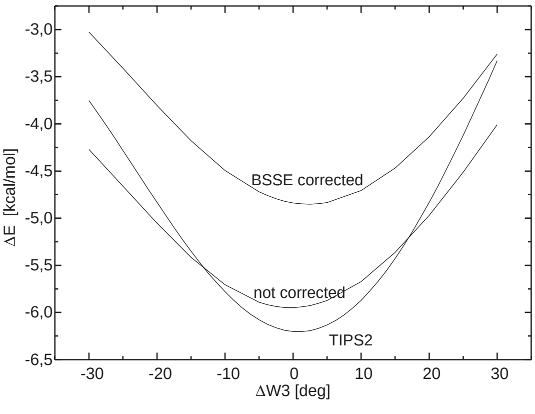

(e) Variation of α

Figure 11.7: Test of the TIPS2 water-water interaction potential.

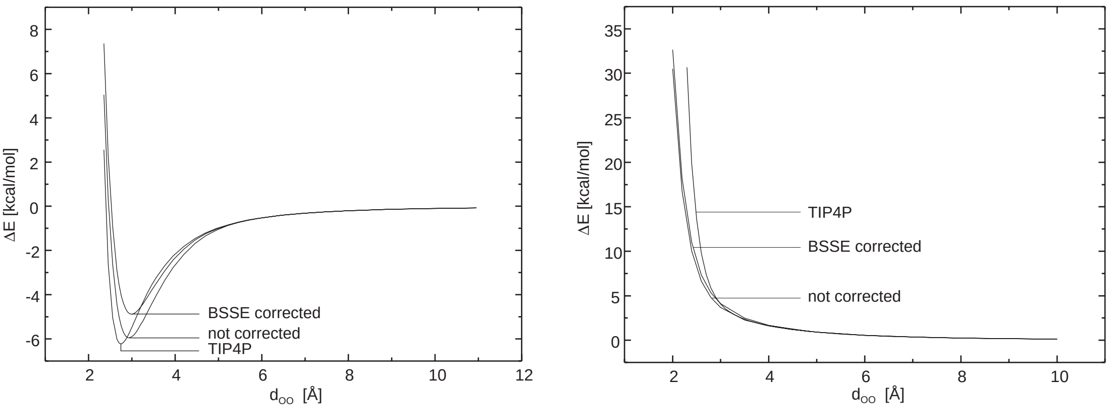

(a) Dimerisation (b) OO repulsion

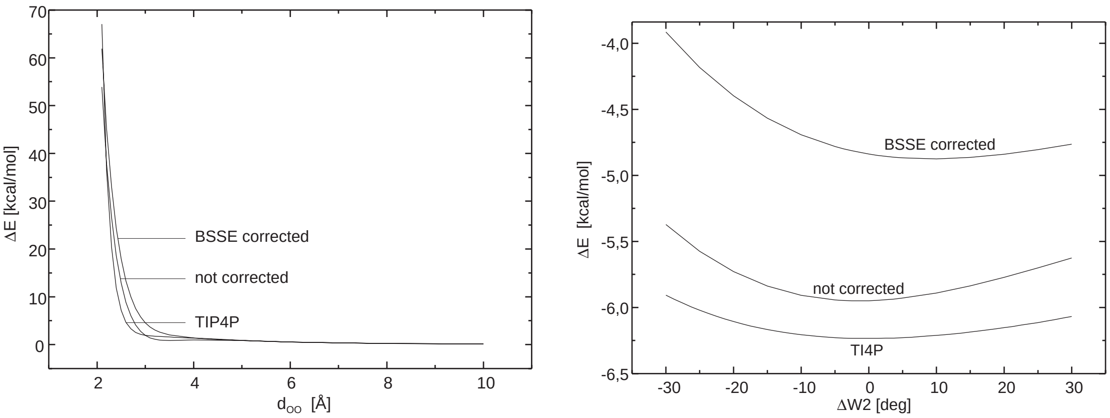

(c) HH repulsion (d) Variation of β

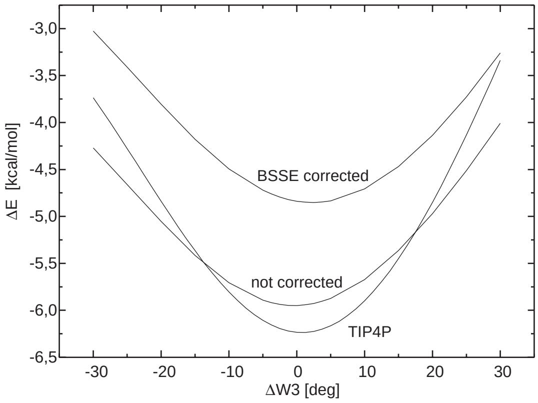

(e) Variation of α

Figure 11.8: Test of the TIP4P water-water interaction potential.

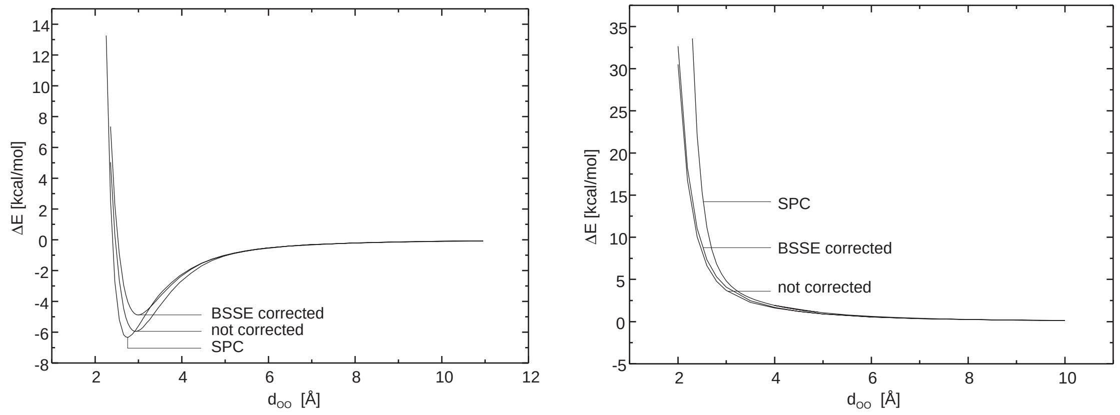

(a) Dimerisation (b) OO repulsion

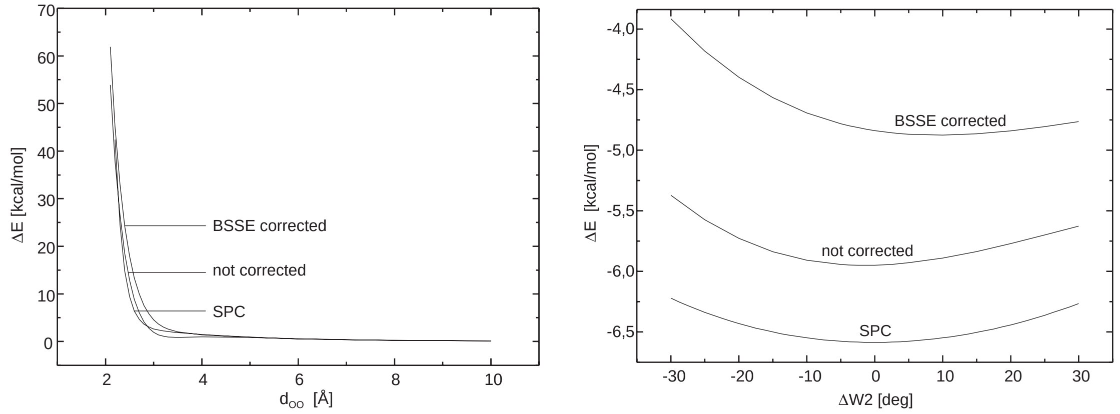

(c) HH repulsion (d) Variation of β

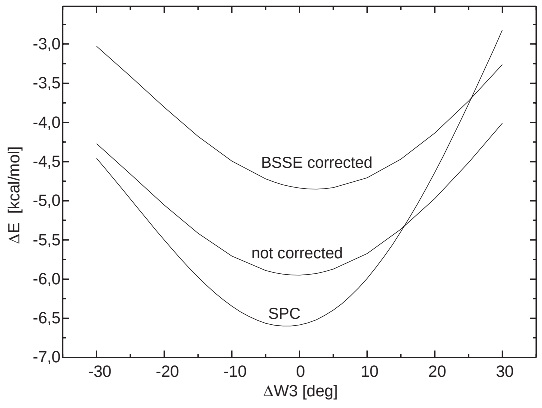

(e) Variation of α

Figure 11.9: Test of the SPC water-water interaction potential.

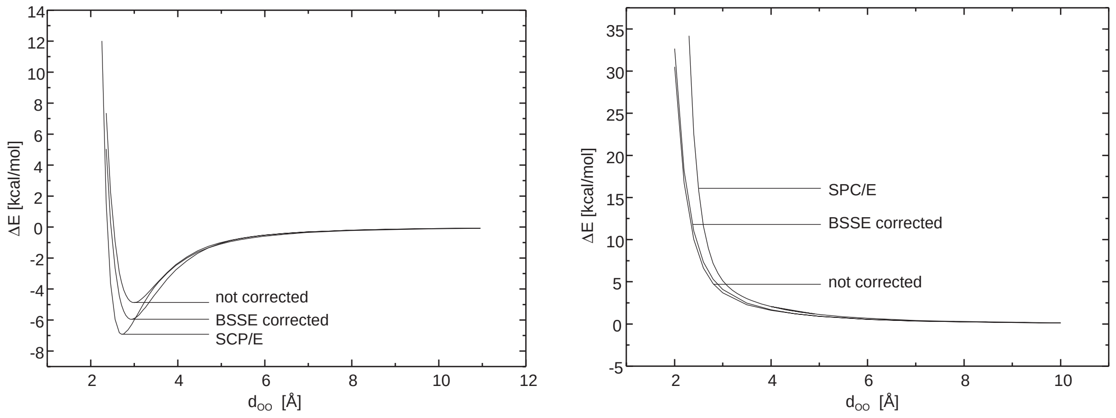

(a) Dimerisation (b) OO repulsion

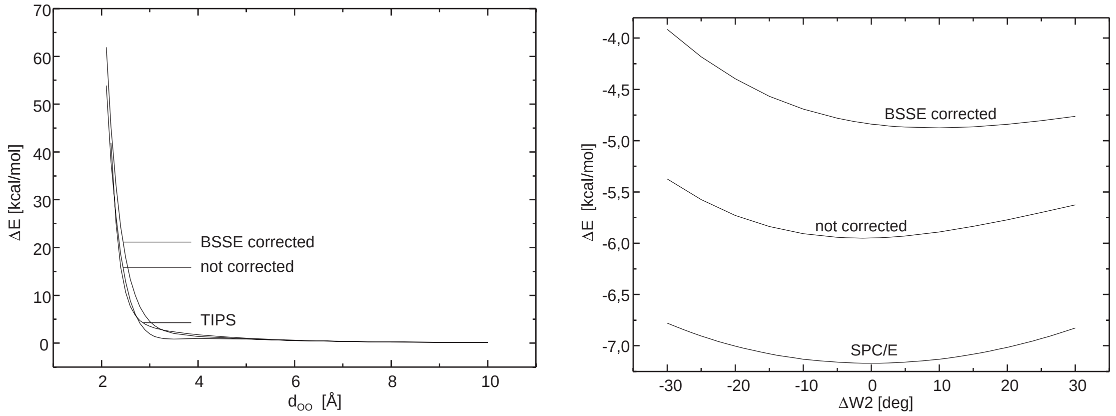

(c) HH repulsion (d) Variation of β

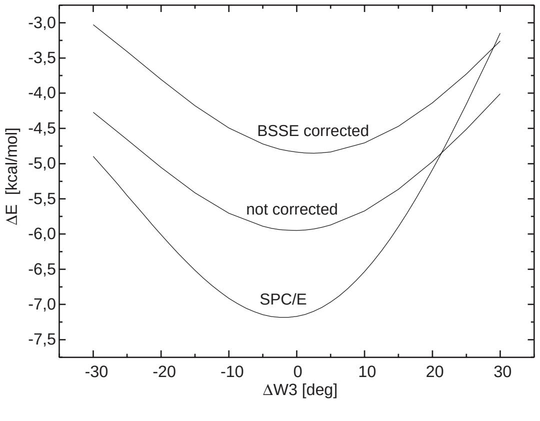

(e) Variation of α

Figure 11.10: Test of the SPC/E water-water interaction potential.

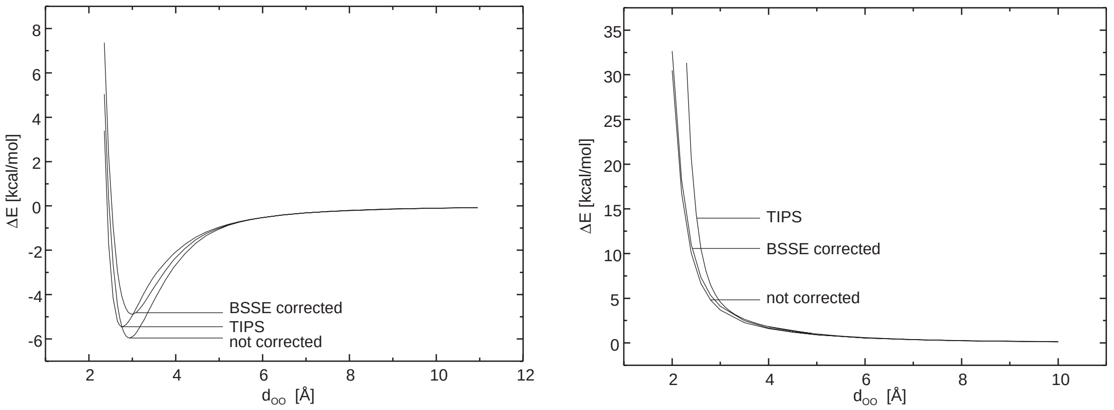

(a) Dimerisation (b) OO repulsion

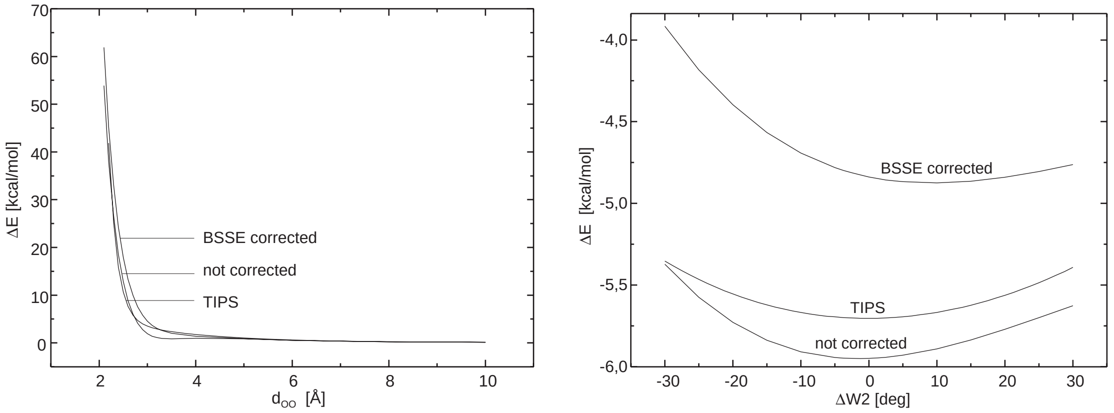

(c) HH repulsion (d) Variation of β

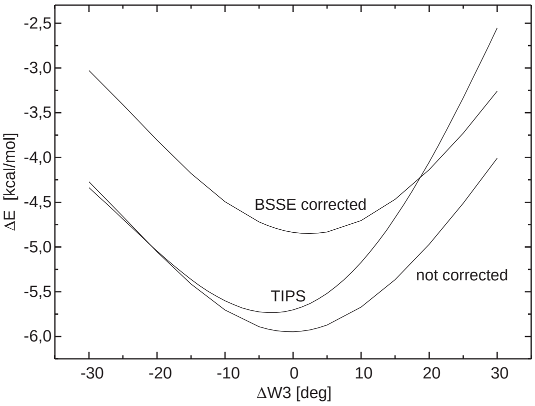

(e) Variation of α

Figure 11.11: Test of the TIPS water-water interaction potential.

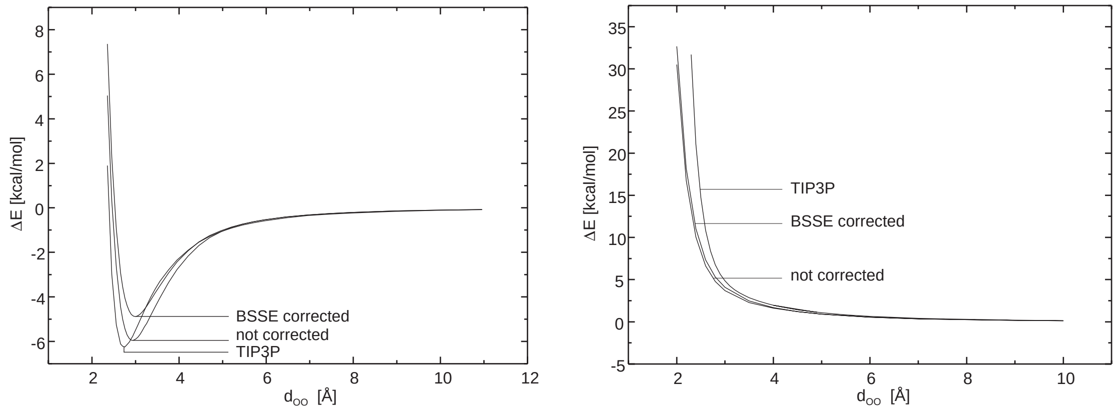

(a) Dimerisation (b) OO repulsion

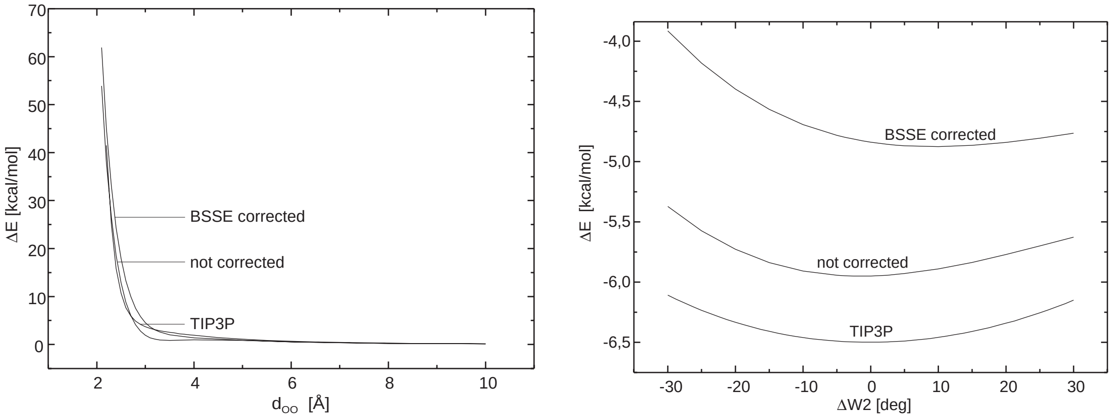

(c) HH repulsion (d) Variation of β

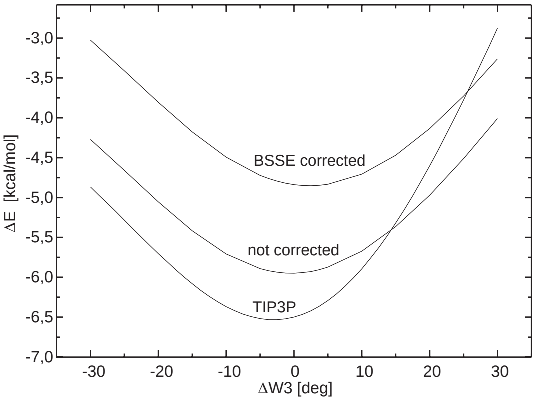

(e) Variation of α

Figure 11.12: Test of the TIP3P water-water interaction potential.

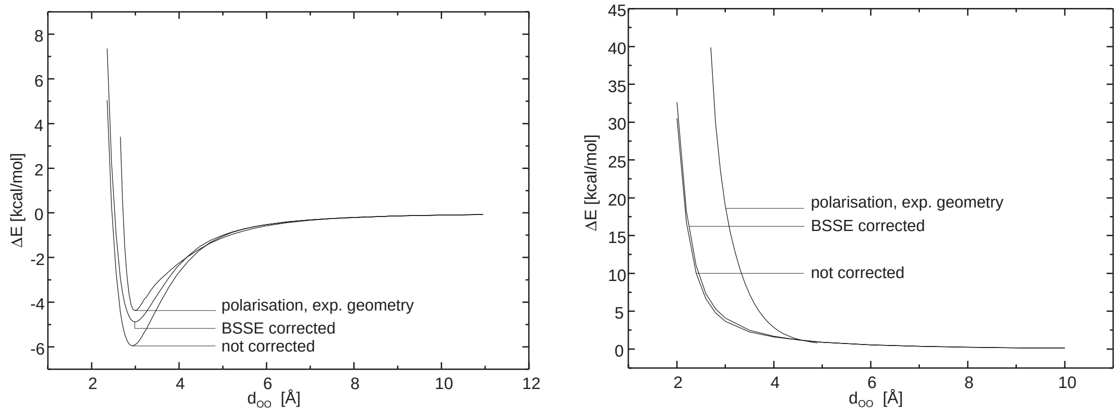

(a) Dimerisation, exp. H_2O geometry

(b) OO repulsion, exp. H_2O geometry

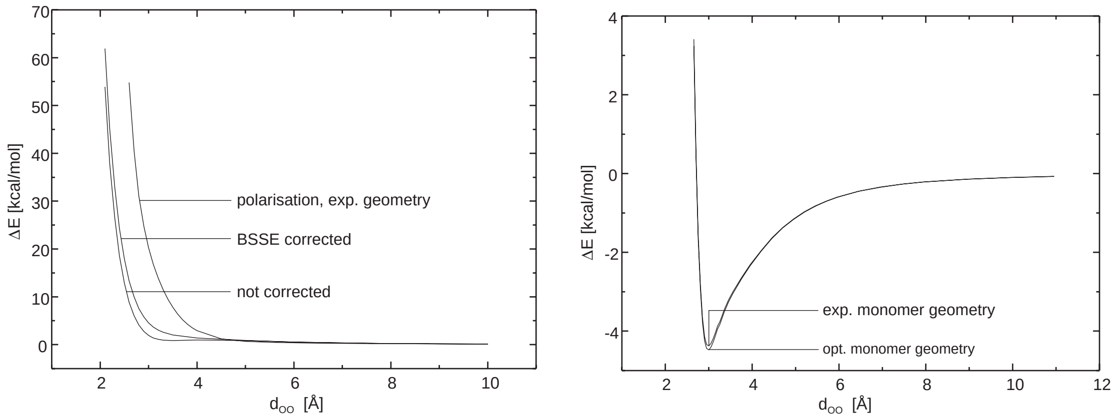

(c) HH repulsion, exp. H_2O geometry

(d) Influence of the monomer geometry

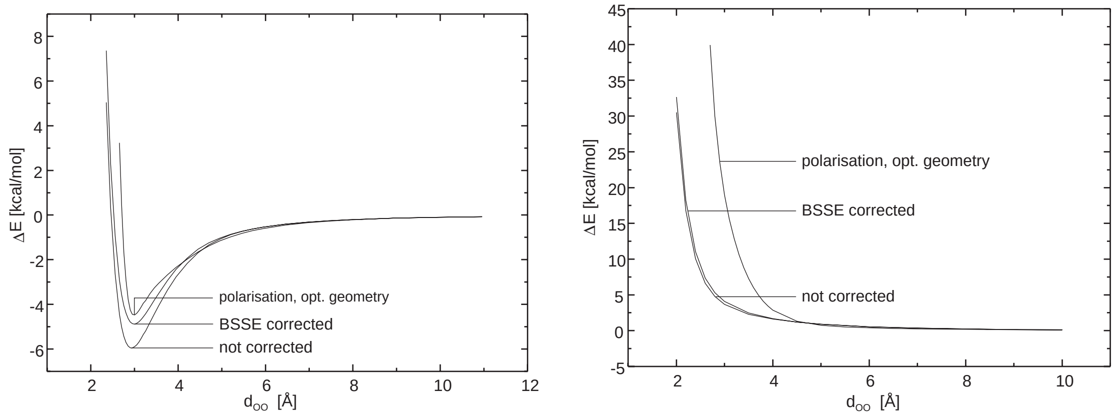

(e) Dimerisation, opt. H_2O geometry

(f) OO repulsion, opt. H_2O geometry

Figure 11.13: Test of the CFMS water-water interaction potential (I).

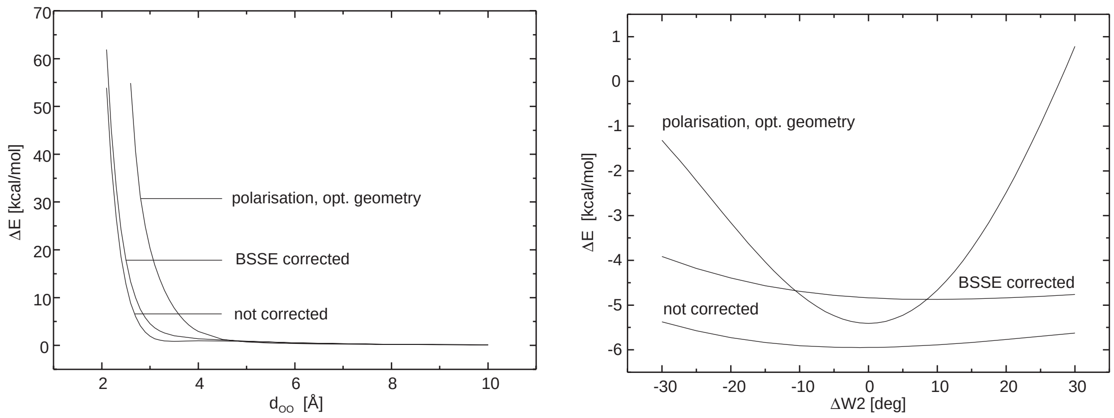

(a) HH repulsion, opt. H_2O geometry (b) Variation of β, opt. H_2O geometry

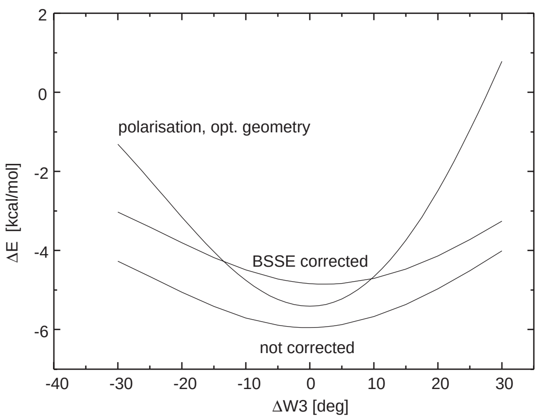

(c) Variation of α, opt. H_2O geometry

Figure 11.14: Test of the CFMS water-water interaction potential (II).

The equilibrium structure of water in the CMFS model ((opt.) $r_{\mathrm{OH}} = 0.99584$ Å, $\sphericalangle_{\mathrm{HOH}} = 104.45°$) differs from the one, which is usually regarded as the experimental structure ((exp.) $r_{\mathrm{OH}} = 0.5721$ Å, $\sphericalangle_{\mathrm{HOH}} = 104.42°$). Figure 11.13(d) displays the difference between both geometries for the dimerisation curve.

11.9 Geometry optimisation of water clusters within potential N

The optimisation of small water clusters within potential N has been subject of research work done by students of the university Hamburg under the supervision of T. Lankau. Details of the calculations are given in their reports [370].

11.9.1 Direct conversion

First [370a], we calculated the cartesian coordinates of the water molecules directly form from $\mathrm{d_{OO}}$, α and β (section 3.4, page 74 figures 3.35 to 3.38 and table 3.21). $\mathrm{r_{OH}}$ and ω describe the water molecule.

11.9.1.1 Trimer I

Water molecule 1:

$$\begin{aligned} O_1 &= \begin{pmatrix} -\frac{d_{OO}}{2} \\ 0 \\ 0 \end{pmatrix} \\ H_{1,1} &= \begin{pmatrix} -\frac{d_{OO}}{2} + r_{OH}\ \cos(60^\circ + \alpha) \\ r_{OH}\ \sin(60^\circ + \alpha) \\ 0 \end{pmatrix} \\ H_{1,2} &= \begin{pmatrix} -\frac{d_{OO}}{2} + r_{OH}\ \cos(60^\circ + \alpha + \omega) \\ r_{OH}\ \sin(60^\circ + \alpha + \omega) \\ 0 \end{pmatrix} \end{aligned} \tag{11.1}$$

Water molecule 2:

$$\begin{aligned} O_2 &= \begin{pmatrix} 0 \\ \frac{d_{OO}}{2}\sqrt{3} \\ 0 \end{pmatrix} \\ H_{2,1} &= \begin{pmatrix} r_{OH}\ \sin(30^\circ + \alpha) \\ \frac{d_{OO}}{2}\sqrt{3} - r_{OH}\ \cos(30^\circ + \alpha) \\ 0 \end{pmatrix} \\ H_{2,2} &= \begin{pmatrix} r_{OH}\ \sin(30^\circ + \alpha + \omega) \\ \frac{d_{OO}}{2}\sqrt{3} - r_{OH}\ \cos(30^\circ + \alpha + \omega) \\ 0 \end{pmatrix} \end{aligned} \tag{11.2}$$

Water molecule 3:

$$\begin{aligned} O_3 &= \begin{pmatrix} \frac{d_{OO}}{2} \\ 0 \\ 0 \end{pmatrix} \\ H_{3,1} &= \begin{pmatrix} \frac{d_{OO}}{2} - r_{OH}\ \cos(\alpha) \\ -r_{OH}\ \sin(\alpha) \\ 0 \end{pmatrix} \\ H_{3,2} &= \begin{pmatrix} \frac{d_{OO}}{2} - r_{OH}\ \cos(\alpha + \omega) \\ r_{OH}\ \sin(\alpha + \omega) \\ 0 \end{pmatrix} \end{aligned} \tag{11.3}$$

11.9.1.2 Trimer II

Water molecule 1:

$$\begin{aligned}
O_1 &= \begin{pmatrix} 0 \\ 0 \\ 0 \end{pmatrix} \\
H_{1,1} &= \begin{pmatrix} r_{OH}\ \sin(\tfrac{\omega}{2}) \\ r_{OH}\ \cos(\tfrac{\omega}{2}) \\ 0 \end{pmatrix} \\
H_{1,2} &= \begin{pmatrix} -r_{OH}\ \sin(\tfrac{\omega}{2}) \\ r_{OH}\ \cos(\tfrac{\omega}{2}) \\ 0 \end{pmatrix}
\end{aligned} \tag{11.4}$$

Water molecule 2:

$$\begin{aligned}
O_2 &= \begin{pmatrix} d_{OO}\ \sin(\tfrac{\omega}{2}+\alpha) \\ d_{OO}\ \cos(\tfrac{\omega}{2}+\alpha) \\ 0 \end{pmatrix} \\
H_{2,1} &= \begin{pmatrix} d_{OO}\ \sin(\tfrac{\omega}{2}+\alpha) + r_{OH}\ \cos(\tfrac{\omega}{2}) \cdot \sin(180^\circ - \tfrac{\omega}{2} - \alpha - \beta) \\ d_{OO}\ \cos(\tfrac{\omega}{2}+\alpha) - r_{OH}\ \cos(\tfrac{\omega}{2}) \cdot \cos(180^\circ - \tfrac{\omega}{2} - \alpha - \beta) \\ r_{OH}\ \sin(\tfrac{\omega}{2}) \end{pmatrix} \\
H_{2,2} &= \begin{pmatrix} d_{OO}\ \sin(\tfrac{\omega}{2}+\alpha) + r_{OH}\ \cos(\tfrac{\omega}{2}) \cdot \sin(180^\circ - \tfrac{\omega}{2} - \alpha - \beta) \\ d_{OO}\ \cos(\tfrac{\omega}{2}+\alpha) - r_{OH}\ \cos(\tfrac{\omega}{2}) \cdot \cos(180^\circ - \tfrac{\omega}{2} - \alpha - \beta) \\ -r_{OH}\ \sin(\tfrac{\omega}{2}) \end{pmatrix}
\end{aligned} \tag{11.5}$$

Water molecule 3:

$$\begin{aligned}
O_3 &= \begin{pmatrix} -d_{OO}\ \sin(\tfrac{\omega}{2}+\alpha) \\ d_{OO}\ \cos(\tfrac{\omega}{2}+\alpha) \\ 0 \end{pmatrix} \\
H_{3,1} &= \begin{pmatrix} -d_{OO}\ \sin(\tfrac{\omega}{2}+\alpha) - r_{OH}\ \cos(\tfrac{\omega}{2}) \cdot \sin(180^\circ - \tfrac{\omega}{2} - \alpha - \beta) \\ d_{OO}\ \cos(\tfrac{\omega}{2}+\alpha) - r_{OH}\ \cos(\tfrac{\omega}{2}) \cdot \cos(180^\circ - \tfrac{\omega}{2} - \alpha - \beta) \\ r_{OH}\ \sin(\tfrac{\omega}{2}) \end{pmatrix} \\
H_{3,2} &= \begin{pmatrix} -d_{OO}\ \sin(\tfrac{\omega}{2}+\alpha) - r_{OH}\ \cos(\tfrac{\omega}{2}) \cdot \sin(180^\circ - \tfrac{\omega}{2} - \alpha - \beta) \\ d_{OO}\ \cos(\tfrac{\omega}{2}+\alpha) - r_{OH}\ \cos(\tfrac{\omega}{2}) \cdot \cos(180^\circ - \tfrac{\omega}{2} - \alpha - \beta) \\ -r_{OH}\ \sin(\tfrac{\omega}{2}) \end{pmatrix}
\end{aligned} \tag{11.6}$$

11.9.1.3 Trimer III

Water molecule 1:

$$\begin{aligned} O_1 &= \begin{pmatrix} 0 \\ 0 \\ 0 \end{pmatrix} \\ H_{1,1} &= \begin{pmatrix} 0 \\ -r_{OH}\ \cos(\frac{\omega}{2}) \\ -r_{OH}\ \sin(\frac{\omega}{2}) \end{pmatrix} \\ H_{1,2} &= \begin{pmatrix} 0 \\ -r_{OH}\ \cos(\frac{\omega}{2}) \\ r_{OH}\ \sin(\frac{\omega}{2}) \end{pmatrix} \end{aligned} \tag{11.7}$$

Water molecule 2:

$$\begin{aligned} O_2 &= \begin{pmatrix} d_{OO}\ \sin(\beta) \\ d_{OO}\ \cos(\beta) \\ 0 \end{pmatrix} \\ H_{2,1} &= \begin{pmatrix} d_{OO}\ \sin(\beta) - r_{OH}\ \sin(\alpha+\beta) \\ d_{OO}\ \cos(\beta) - r_{OH}\ \cos(\alpha+\beta) \\ 0 \end{pmatrix} \\ H_{2,2} &= \begin{pmatrix} d_{OO}\ \sin(\beta) - r_{OH}\ \sin(\omega+\alpha+\beta) \\ d_{OO}\ \cos(\beta) - r_{OH}\ \cos(\omega+\alpha+\beta) \\ 0 \end{pmatrix} \end{aligned} \tag{11.8}$$

Water molecule 3:

$$\begin{aligned} O_3 &= \begin{pmatrix} -d_{OO}\ \sin(\beta) \\ d_{OO}\ \cos(\beta) \\ 0 \end{pmatrix} \\ H_{3,1} &= \begin{pmatrix} -d_{OO}\ \sin(\beta) + r_{OH}\ \sin(\alpha+\beta) \\ d_{OO}\ \cos(\beta) - r_{OH}\ \cos(\alpha+\beta) \\ 0 \end{pmatrix} \\ H_{3,2} &= \begin{pmatrix} -d_{OO}\ \sin(\beta) + r_{OH}\ \sin(\omega+\alpha+\beta) \\ d_{OO}\ \cos(\beta) - r_{OH}\ \cos(\omega+\alpha+\beta) \\ 0 \end{pmatrix} \end{aligned} \tag{11.9}$$

11.9.1.4 Trimer IV

Water molecule 1:

$$\begin{aligned}
O_1 &= \begin{pmatrix} 0 \\ 0 \\ 0 \end{pmatrix} \\
H_{1,1} &= \begin{pmatrix} -r_{OH}\ \cos(\frac{\omega}{2})\ \cos(\beta) \\ -r_{OH}\ \cos(\frac{\omega}{2})\ \sin(\beta) \\ r\ \sin(\frac{\omega}{2}) \end{pmatrix} \\
H_{1,2} &= \begin{pmatrix} -r_{OH}\ \cos(\frac{\omega}{2})\ \cos(\beta) \\ -r_{OH}\ \cos(\frac{\omega}{2})\ \sin(\beta) \\ -r\ \sin(\frac{\omega}{2}) \end{pmatrix}
\end{aligned} \tag{11.10}$$

Water molecule 2:

$$\begin{aligned}
O_2 &= \begin{pmatrix} d_{OO} \\ 0 \\ 0 \end{pmatrix} \\
H_{2,1} &= \begin{pmatrix} d_{OO} - r_{OH}\ \cos(\alpha) \\ r_{OH}\ \sin(\alpha) \\ 0 \end{pmatrix} \\
H_{2,2} &= \begin{pmatrix} d_{OO} - r_{OH}\ \cos(\omega + \alpha) \\ r_{OH}\ \sin(\omega + \alpha) \\ 0 \end{pmatrix}
\end{aligned} \tag{11.11}$$

Water molecule 3:

$$\begin{aligned}
O_3 &= \begin{pmatrix} -d_{OO}\ \cos(\frac{\omega}{2} + \alpha)\ \cos(\beta) \\ -d_{OO}\ \cos(\frac{\omega}{2} + \alpha)\ \sin(\beta) \\ -d_{OO}\ \sin(\frac{\omega}{2} + \alpha) \end{pmatrix} \\
H_{3,1} &= \begin{pmatrix} -\cos(\beta) \cdot \big[d_{OO}\ \cos(\frac{\omega}{2} + \alpha) + r_{OH}\ \cos(\frac{\omega}{2}) \cos(\frac{\omega}{2} + \alpha + \beta)\big] + r_{OH}\ \sin(\frac{\omega}{2}) \sin(\beta) \\ -\sin(\beta) \cdot \big[d_{OO}\ \cos(\frac{\omega}{2} + \alpha) + r_{OH}\ \cos(\frac{\omega}{2}) \cos(\frac{\omega}{2} + \alpha + \beta)\big] - r_{OH}\ \sin(\frac{\omega}{2}) \cos(\beta) \\ -d_{OO}\ \sin(\frac{\omega}{2} + \alpha) - r_{OH}\ \cos(\frac{\omega}{2}) \sin(\frac{\omega}{2} + \alpha + \beta) \end{pmatrix} \\
H_{3,2} &= \begin{pmatrix} -\cos(\beta) \cdot \big[d_{OO}\ \cos(\frac{\omega}{2} + \alpha) + r_{OH}\ \cos(\frac{\omega}{2}) \cos(\frac{\omega}{2} + \alpha + \beta)\big] - r_{OH}\ \sin(\frac{\omega}{2}) \sin(\beta) \\ -\sin(\beta) \cdot \big[d_{OO}\ \cos(\frac{\omega}{2} + \alpha) + r_{OH}\ \cos(\frac{\omega}{2}) \cos(\frac{\omega}{2} + \alpha + \beta)\big] + r_{OH}\ \sin(\frac{\omega}{2}) \cos(\beta) \\ -d_{OO}\ \sin(\frac{\omega}{2} + \alpha) - r_{OH}\ \cos(\frac{\omega}{2}) \sin(\frac{\omega}{2} + \alpha + \beta) \end{pmatrix}
\end{aligned} \tag{11.12}$$

Equations 11.1 to 11.12 have been used to optimize the geometry of the water trimers. For the optimisation we used a simplex algorithm [242].

11.9.2 Conversion of rotational into cartesian coordinates

The description of the ringclosure in the water trimer and the calculation of the tunneling probability (subsection 4.3.2, page 109) requested a change of the molecular symmetry during the calculation and it was not possible to use equations 11.1 to 11.12.

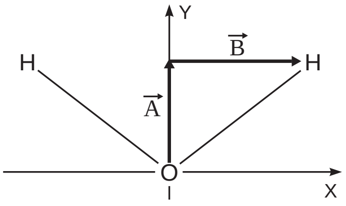

(a) Start orientation of a water molecule.

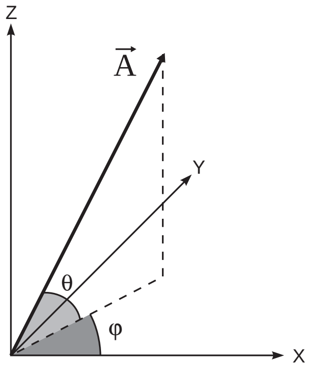

(b) Rotation of $\vec{A}$.

Position and orientation of an water molecule were described by 6 coordinates [370b]: The first three coordinates (x_O, y_O, z_O) are the cartesian coordinates of the oxygen atom while the last three (θ, φ, η) describe the rotation of the water molecule.

The calculation for the nine cartesian coordinates from the six rotational (x_O, y_O, z_O, θ, φ, η) coordinates was done in several steps:

1. Figure 11.15(a) shows the standard orienation of the water molecule. The cartesian coordinates of the water molecule in this oriantation are:

$$O = \begin{pmatrix} 0 \\ 0 \\ 0 \end{pmatrix} \qquad H_1 = \begin{pmatrix} r_{OH}\ \cos(\frac{\omega}{2}) \\ r_{OH}\ \sin(\frac{\omega}{2}) \\ 0 \end{pmatrix} \qquad H_2 = \begin{pmatrix} r_{OH}\ \cos(\frac{\omega}{2}) \\ -r_{OH}\ \sin(\frac{\omega}{2}) \\ 0 \end{pmatrix} \tag{11.13}$$

   The vectors $\vec{A}$ and $\vec{B}$ describe the position of the hydrogen atoms relative to the oxygen atom. $\vec{A}$ is placed on the C_2 axis of the molecule and $\vec{B}$ pointing to the hydogen atom stay perpendicular on $\vec{A}$.

$$\vec{A} = \begin{pmatrix} r_{OH}\ \cos(\frac{\omega}{2}) \\ 0 \\ 0 \end{pmatrix} \qquad \vec{B} = \begin{pmatrix} 0 \\ r_{OH}\ \sin(\frac{\omega}{2}) \\ 0 \end{pmatrix} \tag{11.14}$$

2. Figure 11.15(b) shows the orientation of $\vec{A}$ as a function of θ and φ. The new value of $\vec{A}$ is:

$$\vec{A} = \begin{pmatrix} |\vec{A}|\ \sin(\theta)\ \cos(\varphi) \\ |\vec{A}|\ \sin(\theta)\ \sin(\varphi) \\ |\vec{A}|\ \cos(\varphi) \end{pmatrix} \qquad |\vec{A}| = r_{OH}\ \cos(\tfrac{\omega}{2}) \tag{11.15}$$

   To calculate the cartesian coordinates of the hydrogen atoms a new value for $\vec{B}$ has to be found. The hydrogen atoms did not rotate around $\vec{A}$ so far and the $\vec{B}$ is therefore still parallel to the XY-plane ($B_Z = 0$). Now, we demand $\vec{B}$ to be orthogonal to $\vec{A}$:

$$A_X B_X + A_Y B_Y + A_Z B_Z = A_X B_X + A_Y B_Y = |\vec{A}||\vec{B}|\cos(90°) = 0 \tag{11.16}$$

   Since $\vec{B}$ is parallel to the XY-plane, we can replace B_Y by:

$$B_Y = \sqrt{|\vec{B}|^2 - B_X^2} \qquad |\vec{B}| = r_{OH}\ \sin(\tfrac{\omega}{2}) \tag{11.17}$$

The solution of 11.16 is so:

$$B_X = \pm \sqrt{\frac{|\vec{B}|^2}{\left(\frac{A_X}{A_Y}\right)^2 + 1}} \tag{11.18}$$

Two special cases have to be considered.

$$A_X = 0 \quad \rightarrow \quad \vec{B} = \begin{pmatrix} |\vec{B}| \\ 0 \\ 0 \end{pmatrix} \qquad\qquad A_Y = 0 \quad \rightarrow \quad \vec{B} = \begin{pmatrix} 0 \\ |\vec{B}| \\ 0 \end{pmatrix} \tag{11.19}$$

From equation 11.18 and $\mathrm{B_Y} = \pm\sqrt{|\vec{\mathrm{B}}|^2 - \mathrm{B_X^2}}$ follows that two pairs of vectors ($\vec{\mathrm{B}}$,-$\vec{\mathrm{B}}$) and ($\vec{\mathrm{B}}'$,-$\vec{\mathrm{B}}'$) are possible, but only one pair is orthogonal to $\vec{\mathrm{A}}$. This pair is used for the following calculation of the cartesian coordinates of the hydrogen atoms.

$$\vec{H}_1 = \vec{A} + \vec{B} \qquad\qquad \vec{H}_2 = \vec{A} - \vec{B} \tag{11.20}$$

3. Next, we consider the rotation of the hydrogen atoms around vector $\vec{\mathrm{A}}$. If two compononts of $\vec{\mathrm{A}}$ are equal to zero, $\vec{\mathrm{A}}$ lies on one of the axis of the coordinates system and the rotation around $\vec{\mathrm{A}}$ is equal to a rotation around one of the main axises ($\hat{\mathrm{R}}_\mathrm{X}$, $\hat{\mathrm{R}}_\mathrm{Y}$ and $\hat{\mathrm{R}}_\mathrm{Z}$).

$$\hat{R}_X = \begin{pmatrix} 1 & 0 & 0 \\ 0 & \cos\omega_X & \sin\omega_X \\ 0 & -\sin\omega_X & \cos\omega_X \end{pmatrix} \qquad \hat{R}_Y = \begin{pmatrix} \cos\omega_X & 0 & \sin\omega_X \\ 0 & 1 & 0 \\ -\sin\omega_X & 0 & \cos\omega_X \end{pmatrix}$$
$$\hat{R}_Z = \begin{pmatrix} \cos\omega_X & \sin\omega_X & 0 \\ -\sin\omega_X & \cos\omega_X & 0 \\ 0 & 0 & 1 \end{pmatrix} \tag{11.21}$$

   For every other case the rotation of the water molecule is done in three steps.

   (a) $\vec{\mathrm{A}}$ is normalized[2] and the values for ω_X and ω_Y are calculated, which rotate $\vec{\mathrm{A}}$ on the z-axis.

$$\hat{R}_X\ \hat{R}_Y\ \vec{A} = \begin{pmatrix} 1 & 0 & 0 \\ 0 & \cos\omega_X & \sin\omega_X \\ 0 & -\sin\omega_X & \cos\omega_X \end{pmatrix} \begin{pmatrix} \cos\omega_X & 0 & \sin\omega_X \\ 0 & 1 & 0 \\ -\sin\omega_X & 0 & \cos\omega_X \end{pmatrix} \vec{A} = \begin{pmatrix} 0 \\ 0 \\ 1 \end{pmatrix} \tag{11.22}$$

   The operators $\hat{\mathrm{R}}_\mathrm{X}$ and $\hat{\mathrm{R}}_\mathrm{Y}$ can be combined to one operator $\hat{\mathrm{R}}_\mathrm{XY}$, which simplifies the calculation:

$$\hat{R}_{XY} = \hat{R}_X\hat{R}_Y = \begin{pmatrix} a_2 & 0 & b_2 \\ -b_1b_2 & a_1 & a_2b_1 \\ -a_1b_2 & -b_1 & a_1a_2 \end{pmatrix} \qquad \begin{aligned} a_1 &= \cos\omega_X \\ a_2 &= \cos\omega_Y \\ b_1 &= \sin\omega_X \\ b_2 &= \sin\omega_Y \end{aligned} \tag{11.23}$$

---

[2] The normalisation can be spared, if insted of equation 11.22 the following equation is solved:

$$\hat{R}_X\ \hat{R}_Y\ \vec{A} = \begin{pmatrix} 0 \\ 0 \\ |\vec{A}| \end{pmatrix}$$

The combination of (11.22) and (11.23) allow us to calculate ω_X and ω_Y.

$$\begin{pmatrix} a_2 & 0 & b_2 \\ -b_1 b_2 & a_1 & a_2 b_1 \\ -a_1 b_2 & -b_1 & a_1 a_2 \end{pmatrix} \begin{pmatrix} A_X \\ A_Y \\ A_Z \end{pmatrix} = \begin{pmatrix} 0 \\ 0 \\ 1 \end{pmatrix} \tag{11.24}$$

The first line of equation 11.24 can be used to calculate ω_Y

$$\omega_Y = \arctan\left(\frac{-A_X}{A_Z}\right) \qquad \begin{array}{lcl} A_Y = 0 & \rightarrow & \omega_Y = 0^\circ \\ A_Z = 0 & \rightarrow & \omega_Y = -90^\circ \end{array} \tag{11.25}$$

Next we calculate ω_X form the second line of equation 11.24.

$$\omega_X = \arctan\left(\frac{-A_Y}{-b_2 A_X + a_2 A_Z}\right) = \arctan\left(\frac{-A_Y}{-A_X \sin\omega_Y + A_Z \cos\omega_Y}\right) \tag{11.26}$$

   (b) ω_X and ω_Y are used to turn the water molecule so that $\vec{\mathrm{A}}$ lies on the z-axis. By setting ω_Z equal to η it is now possible to describe the rotation around $\vec{\mathrm{A}}$ with $\hat{\mathrm{R}}_\mathrm{Z}$.

   (c) Finally, $-\omega_X$ and $-\omega_Y$ are used to move $\vec{\mathrm{A}}$ back into its original position and the hydrogen atom into their new.

4. In the last step we use the vector $(\mathrm{x_O, y_O, z_O})$ to move the water molecule into its final position. Water clusters, containing the $\mathrm{C_3}$ symmetry element were constructed using a $\hat{\mathrm{C}}_3$ operator similar to $\hat{\mathrm{R}}_\mathrm{Z}$.

11.9.3 Optimisation of $(\mathrm{H_2O})_6$

The optimisation of the water hexamers in section 8.2 (page 265) was done differently. We adapted [370c] the `int2cart.c` section of the `Babel` program by P. Walters and M. T. Stahl. This part of the code was written by P. Walters, who used code from `MOPAC 5`. The optimisation was done with a modified Newton-Rapson algorithm [370d]. This new program was finally used for the analysis of flat water hexamers on a virtual metal surface [370e].

11.10 The C++ Gaussian 94 interface

The interface between G94 and our own C++ programs is made from three parts. The first part are three short ASCII files (`blocka` to `blockc`), from wich the Gaussian 94 input file is made:

1. `blocka`

```
#!/sbin/csh

set jobname='geo'
cd /home4/fc/fc6a022/PYR_02
rm -f core

```

   The first file contains the begining of the input file with general commands.

2. <u>`blockb`</u>

```
set ba='0.420'
set da='0.099'
set na='3'
set dis='2.770000'
```

`blockb` contains the data for the variables, which are changed as the C++ program is executed. The C++ program writes `blockb` everytime G94 is called.

3. <u>`blockc`</u>

```

g94 << END > ${jobname}.out

%Mem=10000000
# GFInput
# UHF GEN Pseudo=Read
# SCF=(QC, TightLinEq, Tight)
# Pop=Full

Eigenschaften von Pt5, Polarisation?

0 3
Pt
Pt 1 a
Pt 2 a  1 90.0
Pt 3 a  2 90.0  1  0.0
Pt 1 a  2 60.0  4 60.0 +1
Variables:
a = ${dis}

1 2 3 4 0
 S  5  1.00
  1.4832274932   0.22934
  1.7464593543  -0.09046
  0.7565909320  -0.52713
  0.2490175212   0.50171
  0.0580000000   0.79308
 P  5  1.00
  0.5825687895   0.22546
  0.8794390610   0.23282
  0.7249140278  -0.50879
  0.0301445770   0.68090
  0.1062290255   0.42878
 D   4  1.00
```

```
  0.057486       0.04275
  0.031709       0.21724
  0.013918       0.55726
  0.006131       0.31975
 ****
5 0
LANL2MB
 ****

1 2 3 4 0
PT-ECP 3 77
f potential
1
${na}  ${ba}  -${da}
s-f potential
3
2  1.56304868  12.72241997
3  0.40533958  -0.78658492
${na}  ${ba}  ${da}
p-f potential
3
2  0.78303679   9.1466791
3  0.43658528  -1.4152290
${na}  ${ba}  ${da}
d-f
2
4  0.263744     0.132669
${na}  ${ba}  ${da}
5 0
LANL2MB

END

echo ${da} > ${jobname}.erg
echo ${dis} >> ${jobname}.erg
if (! -r core) then
  grep "SCF Done" ${jobname}.out | tail -n1 | cut -f1 -da |
  cut -f2 -d= >> ${jobname}.erg
endif
if (-r core) then
  echo "10.00" >> ${jobname}.erg
endif
grep "5  Pt" ${jobname}.out | tail -4 | head -1 |
cut -f2 -dt >> ${jobname}.erg
grep "1  Pt" ${jobname}.out | tail -4 | head -1 |
```

```
80  cut -f2 -dt >> ${jobname}.erg
81  grep "2  Pt" ${jobname}.out | tail -4 | head -1 |
82  cut -f2 -dt >> ${jobname}.erg
83  grep " Z=" ${jobname}.out | cut -f4 -d= | cut -f1 -dT >>
84  ${jobname}.erg
85  grep "Alpha  occ" ${jobname}.out | tail -1 | cut -c40-50 >>
86  ${jobname}.erg
87  rm -f core
88
89  cp geo.out ${da}.out
90  clearipc
91  exit
```

The third block (`blockc`) contains the rest of the G94 input file (line 1 to 66) and a small shell script, which extracts the important data from G94 output file (lines 68 to 87) and writes these data into the `${jobname}.erg` file.

The second part of the C++/G94 interface is the `${jobname}.erg` file, which contains the results of the quantum chemical calculation. The C++ program reads the processed data in the `${jobname}.erg` file and the quantum chemical data can be used by the program.

```
0.099
2.770000
  -119.621452442
  -1.580820
   0.532278
   0.258132
     0.5212
 -0.29436
```

The last part of the interface is the C++ code, which calls G94 and forms the link between quantum chemistry and the C++ code.

```
const double ba = 0.42;
const int na = 3;

long double func(double ba, double da, int na, double x) {
  ofstream datei1;
  ifstream datei2;
  char name[80], befehl[80];
  long double h1;

  datei1.setf(ios::showpoint);
  datei1.setf(ios::fixed);
  datei1.precision(3);
  strcpy(name, PFAD);
  strcat(name, "geob.blk");
```

```
15    datei1.open(name);
16    datei1 << "set ba='" << ba << "'" << endl;
17    datei1 << "set da='" << da << "'" << endl;
18    datei1 << "set na='" << na << "'" << endl;
19    datei1.precision(6);
20    datei1 << "set dis='" << x << "'" << endl;
21    datei1.close();
22    strcpy (befehl, "cd ");
23    strcat (befehl, PFAD);
24    strcat (befehl, "; cat geoa.blk geob.blk geoc.blk > geo.in");
25    system (befehl);
26    strcpy (befehl, "chmod a+x ");
27    strcat (befehl, PFAD);
28    strcat (befehl, "geo.in");
29    system (befehl);
30    strcpy (befehl, PFAD);
31    strcat (befehl, "geo.in");
32    system (befehl);
33    strcpy(name, PFAD);
34    strcat(name, "geo.erg");
35    datei2.open(name);
36    datei2 >> h1;        // da
37    datei2 >> h1;        // r
38    datei2 >> h1;        // Energie
39    datei2.close();
40    return(h1);}
```

Lines 15 to 21 create the `blockb` file, which contains data for the variables and lines 22 to 32 are used to create an G94 input file from the files `blocka` to `blockc`. In line 32 the `system` command is used to call G94 and to execute the input file. Finally, lines 33 to 39 are used to evaluate the `${jobname}.erg` file and to import the quantum chemical results into the C++ programm.

The next listing is not part of the interface, but gives an example for the application of the function `func` of the interface for the geometry optimisation of a Pt$_5$ pyramid.

```
double geo(double ba, double da, int na, double &start, double min, double max) {
  const int maxanz = 20;
  const double delta_min = 1E-5;
  const double max_step = 0.1;
  const double h = 0.0001;
  long double fx, fxph, fxmh, G, H;
  long double x1, x2;
  int notbremse;

  cout.precision(6);
  cout.setf(ios::showpoint);
  cout.setf(ios::fixed);
```

```
cout << "Start" << endl;
x1 = start;
fx = func(ba, da, na, x1);
cout.precision(6);
cout << "  Laenge  : " << x1 << endl;
cout.precision(12);
cout << "  Energie : " << fx << endl << endl;
notbremse = 1;
do{
  cout << "Schritt " << notbremse << " von " << maxanz << endl;
  cout << "  Berechne Energie 1" << endl;
  fxph = func(ba, da, na, x1+h);
  cout << "  Berechne Energie 2" << endl;
  fxmh = func(ba, da, na, x1-h);
  G = (fxph - fxmh)/2.0/h;
  H = (fxph + fxmh - 2.0*fx)/h/h;
  cout.precision(6);
  cout << "  G : " << G << endl;
  cout << "  H : " << H << endl;
  if (H > 0.0)
    x2 = -G/H;
    else x2 = -10.0*G;
  if (fabs(x2) > max_step)
    x2 *= max_step/fabs(x2);
  if (fabs(H) < 0.001)
    x2 = -10.0*G;
  cout << "  Schrittgroesse : " << x2 << endl;
  x1 += x2;
  fx = func(ba, da, na, x1);
  cout.precision(6);
  cout << "  neue Laenge    : " << x1 << endl;
  cout.precision(12);
  cout << "  neue Energie   : " << fx << endl << endl;
  if (x1 > max) {
    cout << "  Ueberschreiten der Obergrenze !" << endl;
    start = x1;
    return(fx);}
  if (x1 < min) {
    cout << "  Unterschreiten der Untergrenze !" << endl;
    start = x1;
    return(fx);}
  notbremse ++;
  }while (!((fabs(x2) <= delta_min) || (notbremse > maxanz)));
start = x1;
return(fx);}
```

1^{st} grp	SALC	$\left\langle \varphi_i \vert \hat{H} \vert \varphi_i \right\rangle$	symmetry	symbol	2^{nd} grp
1	χ_5	α	a_1	φ_2	A
2	$\frac{1}{2}(\chi_6 + \chi_7 + \chi_8 + \chi_9)$	α	a_1	φ_3	A
2	$\frac{1}{2}(\chi_6 - \chi_7 - \chi_8 + \chi_9)$	α	e	φ_5	B
2	$\frac{1}{2}(\chi_6 + \chi_7 - \chi_8 - \chi_9)$	α	e	φ_7	B
2	$\frac{1}{2}(\chi_6 - \chi_7 + \chi_8 - \chi_9)$	α	b_2	φ_9	C
3	$\frac{1}{2}(\chi_1 + \chi_2 + \chi_3 + \chi_4)$	$\alpha + 2\,\beta$	a_1	φ_1	A
3	$\frac{1}{2}(\chi_1 + \chi_2 - \chi_3 - \chi_4)$	α	e	φ_4	B
3	$\frac{1}{2}(\chi_1 - \chi_2 - \chi_3 + \chi_4)$	α	e	φ_6	B
3	$\frac{1}{2}(\chi_1 - \chi_2 + \chi_3 - \chi_4)$	$\alpha - 2\,\beta$	b_2	φ_8	C

Table 11.21: Basis set for the Pt$_9$ Hückel calculation.

11.11 Hückel calculations for Pt$_9$

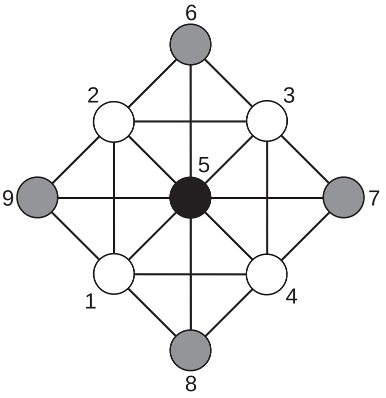

Figure 11.15: Pt$_9$ cluster, top view.

The secular determinant for this cluster is big (9 × 9) and therefore difficult to handle. The mathematical problem can be reduced by using SALC's as basis set for the calculation. This was done in three steps. In the first step were the atoms of the cluster divided into three groups. Each group contains all symmetric unique atoms, which interchange their places during the application of any symmetry operator. The first group contains just one atom; atom number 5 in the centre. The second group contains the surrounding atoms 6, 7, 8 and 9. The third finally contains the atoms at the bottom (1,2,3 and 4). In the next step SALCs were constructed from the orbitals in each group. In the last step were the orbitals regrouped according to their symmetry.

Since orbitals of different symmetry do not mix, the usage of the orbitals φ_1 to φ_9 simplifies the formation of the blocked secular determinant. The three blocks can be handled separately as before for the Pt$_5$ pyramid. The secular determinant[3] (equation 11.27) was then simplified as before.

$$\begin{vmatrix}
\alpha+2\beta-\epsilon & 2\beta & 2\beta & & & & & & \\
2\beta & \alpha-\epsilon & 2\beta & & & & & & \\
2\beta & 2\beta & \alpha-\epsilon & & & & & & \\
 & & & \alpha-\epsilon & \beta & 0 & -\beta & & \\
 & & & \beta & \alpha-\epsilon & -\beta & 0 & & \\
 & & & 0 & -\beta & \alpha-\epsilon & -\beta & & \\
 & & & -\beta & 0 & -\beta & \alpha-\epsilon & & \\
 & & & & & & & \alpha-2\beta-\epsilon & 0 \\
 & & & & & & & 0 & \alpha-\epsilon
\end{vmatrix} = 0 \qquad (11.27)$$

---

[3] The secular determinat was calculated with a small C++ program.

Group A:

$$\begin{vmatrix} -x+2 & 2 & 2 \\ 2 & -x & 2 \\ 2 & 2 & -x \end{vmatrix} = x^3 + 2\,x^2 - 12\,x + 8 = 0$$

$$\begin{aligned} x_1 &= -2 & \Rightarrow && \epsilon_1 &= \alpha - 2\,\beta \\ x_2 &= 2 - \sqrt{8} & \Rightarrow && \epsilon_2 &= \alpha + (2 - \sqrt{8})\,\beta \\ x_3 &= 2 + \sqrt{8} & \Rightarrow && \epsilon_2 &= \alpha + (2 + \sqrt{8})\,\beta \end{aligned} \tag{11.28}$$

Group B:

$$\begin{vmatrix} -x & 1 & 0 & -1 \\ 1 & -x & -1 & 0 \\ 0 & -1 & -x & -1 \\ -1 & 0 & -1 & -x \end{vmatrix} = (x^2 - 2)^2 = 0 \qquad \begin{aligned} x_4 &= \sqrt{2} & \Rightarrow && \epsilon_4 &= \alpha + \sqrt{2}\,\beta \\ x_5 &= \sqrt{2} & \Rightarrow && \epsilon_5 &= \alpha + \sqrt{2}\,\beta \\ x_6 &= -\sqrt{2} & \Rightarrow && \epsilon_6 &= \alpha - \sqrt{2}\,\beta \\ x_7 &= -\sqrt{2} & \Rightarrow && \epsilon_7 &= \alpha - \sqrt{2}\,\beta \end{aligned} \tag{11.29}$$

Group C:

$$\begin{vmatrix} \alpha - 2\,\beta - \epsilon & 0 \\ 0 & \alpha - \epsilon \end{vmatrix} = 0 \qquad \begin{aligned} \epsilon_8 &= \alpha - 2\,\beta \\ \epsilon_9 &= \alpha \end{aligned} \tag{11.30}$$

Although symmetrically allowed do the orbitals of group C not mix. The calculation of the coefficients is therefore very easy.

$$\Psi_8 = \varphi_8 = \frac{1}{2}(\chi_1 - \chi_2 + \chi_3 - \chi_4) \qquad \Psi_9 = \varphi_9 = \frac{1}{2}(\chi_6 - \chi_7 + \chi_8 - \chi_9) \tag{11.31}$$

For the other groups the usage of the blocks simplifies the calculation of the coefficients:
Group A:

$$\Psi_1 = \frac{1}{\sqrt{2}}\,(\varphi_2 - \varphi_3) \qquad \Psi_2 = \frac{1}{2}\,(-\sqrt{2}\,\varphi_1 + \varphi_2 + \varphi_3) \qquad \Psi_3 = \frac{1}{2}\,(\sqrt{2}\,\varphi_1 + \varphi_2 + \varphi_3) \tag{11.32}$$

Group B:

$$\begin{aligned} \Psi_4 &= \frac{1}{2}\,(\varphi_1 + \varphi_3 - \sqrt{2}\,\varphi_4) & \Psi_5 &= \frac{1}{2}\,(\varphi_1 - \varphi_3 + \sqrt{2}\,\varphi_4) \\ \Psi_6 &= \frac{1}{2}\,(\varphi_1 + \varphi_3 + \sqrt{2}\,\varphi_4) & \Psi_7 &= \frac{1}{2}\,(\varphi_1 - \varphi_3 - \sqrt{2}\,\varphi_4) \end{aligned} \tag{11.33}$$

The wavefunction Ψ_1 to Ψ_9 will be used for the discussion of the Pt_9 cluster (table 5.5 page 129).

11.12 Hückel calculations for Pt_{17}

As before for the calculation of the Pt_9 cluster symmetry adapted linear combinations (SALCS) [293b] were constructed from symmetrically equivalent 6s orbitals (I: χ_0, χ_1,χ_2, χ_3; II: χ_4, χ_5, χ_6, χ_7, χ_8, χ_9, χ_{10}, χ_{11}; III: χ_{12}, χ_{13}, χ_{14}, χ_{15}; IV: χ_{16}). These orbitals have been regrouped for the calculation of the energy eigenvalues. The results of this transformation are shown in table 11.22. Symmetry divides the basis set into 4 groups (A-D) and allows the calculation of the energy eigenvalues with small matrices. The different symmetries can be easily distinguished by the number of nodal planes in the orbital. The totally symmetric functions have no nodal plane, while the others have up to four planes (a_2).

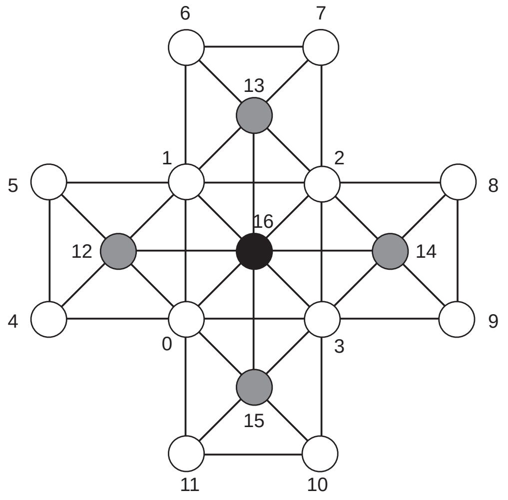

Figure 11.16: Pt_{17} cluster, top view.

Group A, totally symmetric, no nodal plane (a_1):

$$\begin{vmatrix} -x+2 & \sqrt{2} & 2 & 2 \\ \sqrt{2} & -x+1 & \sqrt{2} & 0 \\ 2 & \sqrt{2} & -x & 2 \\ 2 & 0 & 2 & -x \end{vmatrix} = x^4 - 3x^3 - 14x^2 + 8 = 0 \qquad \begin{aligned} x_{01} &= -2.3467 \\ x_{02} &= -0.8668 \\ x_{03} &= 0.7153 \\ x_{04} &= 5.4982 \end{aligned} \tag{11.34}$$

Group B, two nodal planes (b_1 and b_2):

$$\begin{vmatrix} -x-2 & 1 & -1 & 0 \\ 1 & -x & 1 & 1 \\ -1 & 1 & -x & 1 \\ 0 & 1 & 1 & -x \end{vmatrix} = x^4 + 2x^3 - 5x^2 - 6x = 0 \qquad \begin{aligned} x_{05} &= -3 \\ x_{06} &= -1 \\ x_{07} &= 0 \\ x_{08} &= 2 \end{aligned} \tag{11.35}$$

Group D, four nodal planes (a_2):

$$|-x-1| = 0 \qquad x_{16} = -1 \tag{11.36}$$

Group C, one nodel plane (e):

$$\begin{vmatrix} -x & 0 & \frac{1}{2} & a & -\frac{1}{2} & b & 1 & 1 \\ 0 & -x & -a & \frac{1}{2} & b & \frac{1}{2} & -1 & 1 \\ \frac{1}{2} & -a & -x+c & 0 & 0 & c & a & -\frac{1}{2} \\ a & \frac{1}{2} & 0 & -x+c & c & 0 & \frac{1}{2} & a \\ -\frac{1}{2} & b & 0 & c & -x-c & 0 & -b & \frac{1}{2} \\ b & \frac{1}{2} & c & 0 & 0 & -x-c & \frac{1}{2} & b \\ 1 & -1 & a & \frac{1}{2} & -b & \frac{1}{2} & -x & 0 \\ 1 & 1 & -\frac{1}{2} & a & \frac{1}{2} & b & 0 & -x \end{vmatrix} = 0 \quad \text{with} \quad \begin{aligned} a &= \frac{1}{2}\,(1+\sqrt{2}) \\ b &= \frac{1}{2}\,(1-\sqrt{2}) \\ c &= \frac{1}{2}\,\sqrt{2} \end{aligned}$$

$$0 = x^8 - 14x^6 - 12x^5 + 49x^4 + 84x^3 + 36x^2 \qquad \Rightarrow \qquad \begin{aligned} x_{08} = x_{09} &= -2 \\ x_{10} = x_{11} &= -1 \\ x_{12} = x_{13} &= 0 \\ x_{14} = x_{15} &= 3 \end{aligned} \tag{11.37}$$

1^{st} grp	SALC	$\left\langle \varphi_i \middle| \hat{H} \middle| \varphi_i \right\rangle$	sym	symbol	2^{nd} grp
I	$\frac{1}{2}\left(\chi_0 + \chi_1 + \chi_2 + \chi_3\right)$	$\alpha + 2\,\beta$	a_1	φ_0	A
I	$\frac{1}{2}\left(\chi_0 + \chi_1 - \chi_2 - \chi_3\right)$	α	e	φ_1	C
I	$\frac{1}{2}\left(\chi_0 - \chi_1 - \chi_2 + \chi_3\right)$	α	e	φ_2	C
I	$\frac{1}{2}\left(\chi_0 - \chi_1 + \chi_2 - \chi_3\right)$	$\alpha - 2\,\beta$	b_2	φ_3	B
II	$\frac{1}{\sqrt{8}}\left(\chi_4 + \chi_5 + \chi_6 + \chi_7 + \chi_8 + \chi_9 + \chi_{10} + \chi_{11}\right)$	$\alpha + \beta$	a_1	φ_4	A
II	$\frac{1}{\sqrt{8}}\left(\chi_5 + \sqrt{2}\,\chi_6 + \chi_7 - \chi_9 - \sqrt{2}\,\chi_{10} - \chi_{11}\right)$	$\alpha + \frac{1}{2}\sqrt{2}\,\beta$	e	φ_5	C
II	$\frac{1}{\sqrt{8}}\left(\sqrt{2}\,\chi_4 + \chi_5 - \chi_7 - \sqrt{2}\,\chi_8 - \chi_9 + \chi_{11}\right)$	$\alpha + \frac{1}{2}\sqrt{2}\,\beta$	e	φ_6	C
II	$\frac{1}{2}\left(\chi_4 - \chi_6 + \chi_8 - \chi_{10}\right)$	α	b_2	φ_7	B
II	$\frac{1}{2}\left(\chi_5 - \chi_7 + \chi_9 - \chi_{11}\right)$	α	b_2	φ_8	B
II	$\frac{1}{\sqrt{8}}\left(\chi_5 - \sqrt{2}\,\chi_6 + \chi_7 - \chi_9 + \sqrt{2}\,\chi_{10} - \chi_{11}\right)$	$\alpha - \frac{1}{2}\sqrt{2}\,\beta$	e	φ_9	C
II	$\frac{1}{\sqrt{8}}\left(\sqrt{2}\,\chi_4 - \chi_5 + \chi_7 - \sqrt{2}\,\chi_8 + \chi_9 - \chi_{11}\right)$	$\alpha - \frac{1}{2}\sqrt{2}\,\beta$	e	φ_{10}	C
II	$\frac{1}{\sqrt{8}}\left(\chi_4 - \chi_5 + \chi_6 - \chi_7 + \chi_8 - \chi_9 + \chi_{10} - \chi_{11}\right)$	$\alpha - \beta$	a_2	φ_{11}	D
III	$\frac{1}{2}\left(\chi_{12} + \chi_{13} + \chi_{14} + \chi_{15}\right)$	α	a_1	φ_{12}	A
III	$\frac{1}{2}\left(\chi_{12} + \chi_{13} - \chi_{14} - \chi_{15}\right)$	α	e	φ_{13}	C
III	$\frac{1}{2}\left(\chi_{12} - \chi_{13} - \chi_{14} + \chi_{15}\right)$	α	e	φ_{14}	C
III	$\frac{1}{2}\left(\chi_{12} - \chi_{13} + \chi_{14} - \chi_{15}\right)$	α	b_2	φ_{15}	B
IV	χ_{16}	α	a_1	φ_{16}	A

Table 11.22: Basis set for the Pt_{17} Hückel calculation.

11.13 Construction of figure 7.28

The construction of figure 7.28 was done in three steps. In the first step we calculated β_{R} as a function of β_{A} and d_{A}.

```
#include <fstream.h>
#include <iostream.h>
#include <math.h>
#include <stdlib.h>

const double pi = 3.141592654;

long double T(double a) {
  return(3.5*a);}

long double C(double a) {
  return(-16.0/15.0*sqrt(2.0*a/pi));}

long double E3(double a, double d, double b) {
  return(d*384.0/15.0*sqrt(2.0*pow(a,7)/pi/pow(2.0*a+b,8)));}

long double E4(double a, double d, double b) {
  return(d*28.0*sqrt(2.0*pow(a,7)/pow(2.0*a+b,9)));}

```

```
20  long double beta(int n, double a, double da, double ba, double dE) {
21    long double help;
22    help = E3(a,da,ba)/a;
23    help *= 3.5-8.0*a/(2.0*a+ba);
24    help += 8.0/15.0*sqrt(2.0/pi/a);
25    help -= 3.5;
26    help *= -a/dE;
27    help += 3.5;
28    help = 1.0/help;
29    help *= a;
30    help *= n+5;
31    help -= 2.0*a;
32    return(help);}
33
34  void main(void) {
35    long double da, ba, dE, dr, br;
36    const double da_max = 2.0;
37    const double ba_max = 0.5;
38    const double Et = 0.23842;
39    const double a = 0.1196;
40    int anz = 200;
41    ofstream datei;
42    datei.open("br_area.dat");
43    for (da=0.0; da<=da_max; da+=(da_max-0.0)/anz){
44           for (ba=0.0; ba<=ba_max; ba +=(ba_max-0.0)/anz){
45                  dE = Et - T(a) - C(a) - E3(a,-da,ba);
46                  br = beta(4,a,da,ba,dE);
47                  cout << da << "  " << ba << endl;
48                  datei << da << "  " << ba << "  " << br << endl;}
49           datei << endl;}
50    datei.close();
51    return;}
```

Table 11.23 shows the correlation between the functions in the program and the equations in section 7.2 (page 215). These functions are used in line 45 to calculate ΔE, which is used for the calculation of β_{R} in line 46. Finally, in line 48 the values of d_{A} (da), β_{A} (ba) and β_{R} (br) are written into the file `br_area.dat`, which is used for the plot.

`br_area.dat` is used to generate the 3D contour plot ($\beta_{\mathrm{R}}(\mathrm{d}_{\mathrm{A}},\beta_{\mathrm{A}})$) with `gnuplot`. The input file is listed below and the plot generated with this file is stored and used later for the final graph.

In the next step the same grid as before is used for the calculation of the second derivative of the total energy E(α) for $\alpha = 0.23842$ a.u..

```
set view 0,0,1
set parametric
set contour base
set cntrparam levels discrete 0.0, 0.02, 0.04, 0.06, 0.08, 0.1, 0.12, 0.14
```

function	variable	code line	equation	page
T	$\mathrm{T}(\alpha)$	8	7.29	218
C	$\mathrm{C}(\alpha)$	11	7.29	218
E3	$\bar{\mathrm{V}}_{\mathrm{D}}^{3}$	14	7.35	220
E4	$\bar{\mathrm{V}}_{\mathrm{D}}^{4}$	17	7.35	220
beta	β_{R}	20	7.54	227

Table 11.23: Functions used for the calculation of β_{R}.

```
5   set nosurface
6   splot 'br_area.dat' using 1:2:3 with lines
7   pause -1 "Hit return to continue"
```

```
1   #include <iostream.h>
2   #include <fstream.h>
3   #include <math.h>
4   #include <stdlib.h>
5
6   const double pi = 3.141592654;
7
8   long double T(double a) {
9     return(3.5*a);}
10
11  long double C(double a) {
12    return(-16.0/15.0*sqrt(2.0*a/pi));}
13
14  long double E3(double a, double d, double b) {
15    return(d*384.0/15.0*sqrt(2.0*pow(a,7)/pi/pow(2.0*a+b,8)));}
16
17  long double E4(double a, double d, double b) {
18    return(d*28.0*sqrt(2.0*pow(a,7)/pow(2.0*a+b,9)));}
19
20  long double beta(int n, double a, double da, double ba, double dE) {
21    long double help;
22    help = E3(a,da,ba)/a;
23    help *= 3.5-8.0*a/(2.0*a+ba);
24    help += 8.0/15.0*sqrt(2.0/pi/a);
25    help -= 3.5;
26    help *= -a/dE;
27    help += 3.5;
28    help = 1.0/help;
29    help *= a;
30    help *= n+5;
31    help -= 2.0*a;
32    return(help);}
```

```
33
34   long double E2(double a, double da, double ba, double dr, double br) {
35     long double h1, h2, h3;
36     h1  = 4.0/15.0*sqrt(2.0/pi/pow(a,3));
37     h2  = 12.0*a*a - 84.0*a*ba + 35.0*ba*ba;
38     h2 /= 4.0*(2.0*a+ba)*(2.0*a+ba);
39     h2 *= E3(a,-da,ba)/a/a;
40     h3  = 32.0*a*a - 112.0*a*br + 35.0*br*br;
41     h3 /= 4.0*(2.0*a+br)*(2.0*a+br);
42     h3 *= E4(a,dr,br)/a/a;
43     return(h1+h2+h3);}
44
45   void main(void) {
46     const double a = 0.1196;
47     const double Et = 0.23842;
48     const double da_max = 2.0;
49     const double ba_max = 0.5;
50
51     long double ba, da, dE, br, dr, E2a;
52     int anz=200;
53     ofstream datei;
54
55     datei.open("abl_area.dat");
56     for (da=0.0; da<=da_max; da+=(da_max-0.0)/anz){
57            for (ba=0.0; ba<=ba_max; ba +=(ba_max-0.0)/anz){
58                   dE = Et - T(a) - C(a) - E3(a,-da,ba);
59                   br = beta(4,a,da,ba,dE);
60                   dr = dE/E4(a,1.0,br);
61                   E2a = E2(a,da,ba,dr,br);
62                   cout << da << "  " << ba << endl;
63                   datei << da << "  " << ba << "  " << E2a << endl;}
64            datei << endl;}
65     datei.close();
66     return;}
```

Table 11.24 compiles the transformation of the equations in section 7.2 (page 215) into the C++ program. For every point (d_A, β_A) the energy difference ΔE is calculated (line 58). β_R and d_R are calculated in the lines 59 (br) and 60 (dr). In line 61 the the second derivative of the total energy is finally calculated. The result of this calculation is written into the `abl_area.dat` file, which is used for the plot.

The contour plot is done for only one value. E2a = 0 marks a saddle point and so the transition form a minimum to a maximum. The result of the gnuplot-run was stored. Finally both plots are combined with a graphics program and the plot shown in figure 7.28 created.

```
set view 0,0,1
set parametric
```

function	variable	code line	equation	page
T	$\mathrm{T}(\alpha)$	8	7.29	218
C	$\mathrm{C}(\alpha)$	11	7.29	218
E3	$\bar{\mathrm{V}}_{\mathrm{D}}^{3}$	14	7.35	220
E4	$\bar{\mathrm{V}}_{\mathrm{D}}^{4}$	17	7.35	220
beta	β_{R}	20	7.54	227
E2	$\partial^2\mathrm{E}/\partial\alpha^2$	34	7.60	229
dr	d_{R}	60	7.53b	226

Table 11.24: Functions used for the calculation of $\mathrm{E}''(\alpha)$.

```
set contour base
set cntrparam levels discrete 0
set nosurface
splot 'abl_area.dat' using 1:2:3 with lines
pause -1 "Hit return to continue"
```

Acknowledgements

In Hamburg, I would like to thank Prof. K. Nagorny for his support of the project. Without the freedom he gave me, there would not be such a project. I also would like to thank E. Kühl for the fruitful discussions and his patience proofreading this text. I also would like to thank S. Hirzberger for proofreading the text, specially checking equations and tables for typos. K. Kömpe has been the most helpfull ally in the struggle with computer hardware and administration.

During my dissertation project I had the pleasure to supervise several students. I would like to thank them all for their efforts for this project: J. Franke, C. Clasen, R. Schröder, R. Töber, A. Wichmann, S. Staack, I. Reulecke, O. Konrad and A. Steinmann.

I would like to thank Dr. I. L. Cooper in Newcastle upon Tyne. Without his efforts a start of this work would have been impossible. Also, I would like to thank Dr. M. Cortés Sack and Dr. M. Alcami for their help. Without them the start would have been much more difficult.

For financial support I have to thank the "Studienstiftung des deutschen Volkes", "Hansische Universitäts Stiftung" and my mother G. Lankau.

Eidesstattliche Erklärung

Ich versichere an Eides statt, daß ich die vorliegende Arbeit ohne unerlaubte fremde Hilfe und nur mit den angegebenen Mitteln angefertigt habe.
Ich versichere des weiteren, daß es keine früheren Promotionsversuche gibt.

Lebenslauf

Geboren	13.07.68	
in	Hamburg	
Wehrdienst	01.07.1987 bis 31.03.88	
Schule	1974 bis Sommer 1978	Birkenallee Schule in Uetersen
	Sommer 1978 bis 1987	Ludwig-Meyn-Gymnasium in Uetersen Schulabschluß Abitur
Studium	Okt. 1988	Beginn an der Iniversität Hamburg
	Okt. 1990	Vordiplom
	Aug. 1991	Aufnahme in die Studienstiftung des Deutschen Volkes
	1. Quartal 92	Studienaufenthalt in Newcastle upon Tyne mit ERASMUS - In der Arbeitsgruppe für physikalische organische Chemie von Dr. H. Maskill arbeitete ich an einem Project zur Solvolyse von Acetalen mit.
	Sommer 1992	Schwerpunktarbeit im Arbeitskreis von Prof. Förster: ”Quantenchemische Beschreibung der Adsorption von Z-Buten auf Zeolith A mit der SCC-Xα-Methode”
	Sep. 1993	Ende der mündlichen Prüfungen zum Hauptdiplom
	Sep. 1993	Sommerakademie der Studienstiftung (Französich)
	Okt. 1993	Beginn der Diplomarbeit bei Prof. Nagorny
	Jun. 1994	Ende der Förderung durch die Studienstiftung
	Aug. 1994	Abgabe der Diplomarbeit mit dem Titel: ”’Simulated Annealing’ zur Auswertung von Mößbauerspektren mit verteilten Parametern”
	Aug. 1994	Diplom
	Okt. 1994	Beginn der Doktorarbeit bei Prof. Nagorny zur Adsorption von Wasser auf Platinoberflächen
	Dez. 1994	eingeschränkte Sachkenntnisprüfung nach §5 der Chemikalien-Verbotsordnung vom 14. Oktober 1993
	1 Hälfte 95	Arbeit an der Dissertation in der Gruppe von Dr. I. Cooper an der Universität von Newcastle upon Tyne
	Juni 1995	Beginn der Promotionsförderung durch die Studienstiftung deutschen Volkes
	Juli 1996	Universität von Newcstle upon Tyne
	Juni 1997	Universität von Newcastle upon Tyne
	Okt. 1997	Ende der Promotionsförderung durch die Studienstiftung
Pyrotechnik	Mar. 1999	Sachkundeprüfung nach §36 der 1. SprengV Umgang mit pyrotechnischen Gegenständen …
	Mai 1999	Befähigungsschein nach §20 SprengG